International Journal of Alzheimer's Disease

Animal Models of Alzheimer's Disease

Guest Editors: Gemma Casadesus, Gary Arendash, Frank Laferla, and Mike McDonald

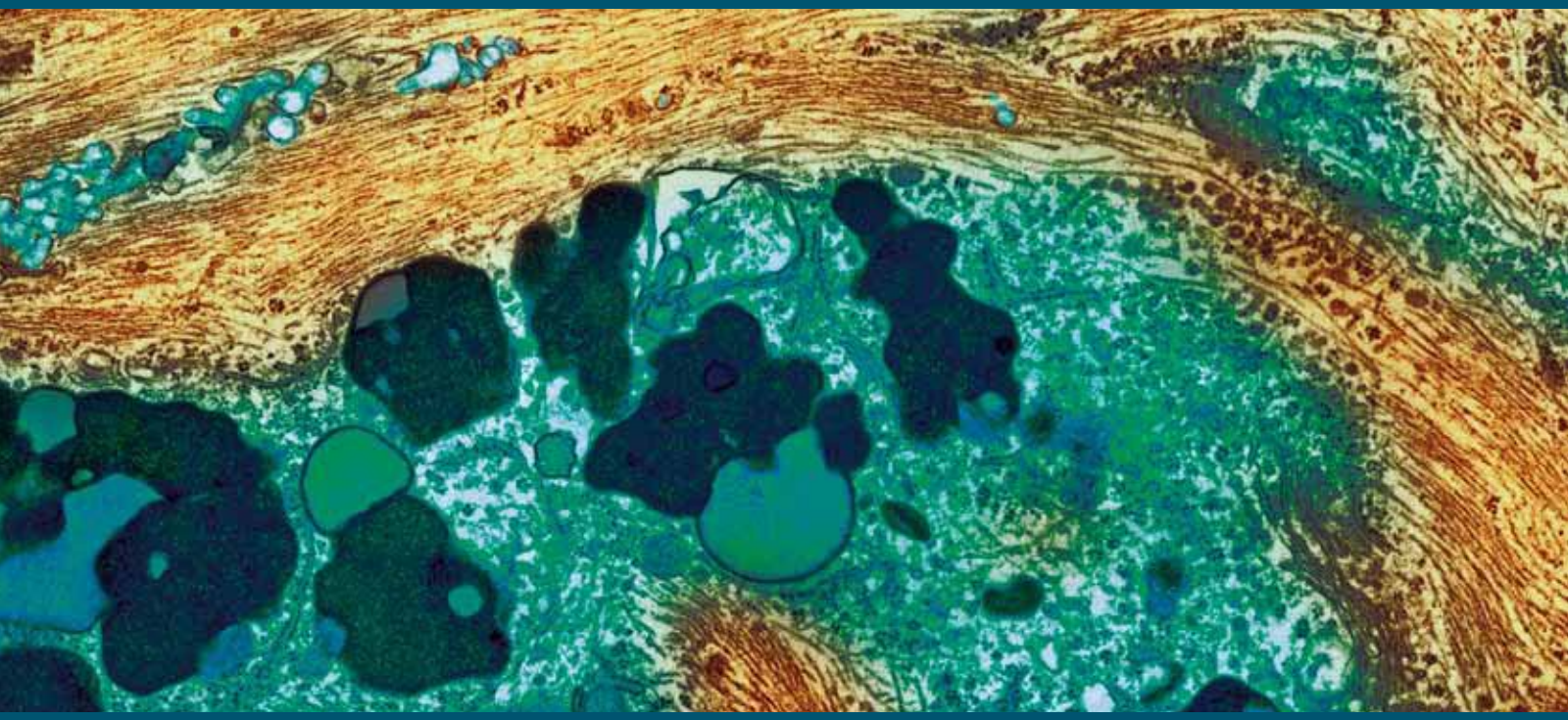

Animal Models of Alzheimer's Disease

International Journal of Alzheimer's Disease

Animal Models of Alzheimer's Disease

Guest Editors: Gemma Casadesus, Gary Arendash, Frank Laferla, and Mike McDonald

Editorial Board

Contents

SAGE-Hindawi Access to Research
International Journal of Alzheimer's Disease
Volume 2010, Article ID 606357, 2 pages
doi:10.4061/2010/606357

Editorial

Animal Models of Alzheimer's Disease

Gemma Casadesus,[1] Gary Arendash,[2] Frank Laferla,[3] and Mike McDonald[4]

[1] *Department of Neurosciences, School of Medicine, Case Western Reserve University, 2109 Adelbert Road, E-729, Cleveland, OH 44106, USA*
[2] *Department of Cell Biology, Microbiology and Molecular Biology, University of South Florida, USA*
[3] *School of Biological Sciences, Institute for Brain Aging and Dementia, Neurobiology and Behavior, UC Irvine, USA*
[4] *Department of Neurology, The University of Tennessee Health Science Center, USA*

Correspondence should be addressed to Gemma Casadesus, gxc40@case.edu

Received 31 December 2010; Accepted 31 December 2010

The necessity for a deeper understanding of neurological diseases such as Alzheimer's disease (AD) that increase in frequency as a function of age has become of paramount importance with the coming of age of the baby boom generation and the increasing social demands for individuals to perform better and longer. AD is characterized by a gradual decline in cognitive function and presence of pathological inclusions such as Aβ plaques and neurofibrillary tangles composed of hyper-phosphorylated tau in the brain. These are the main hallmarks of the disease and focus of most current therapeutic strategies. As such, the development of transgenic and non-transgenic models of AD over the last decade has primarily focused on these pathological markers. These models have become promising tools to decipher the mechanistic importance of tau phosphorylation and Aβ deposits, as well the relationship between each other, other pathological AD-related events, and cognitive loss. However, while seemingly obvious, it is important to remember that the validity of an animal model of disease is tightly linked to the ability of the animal to mimic the signs of the disease—which goes beyond the pathology and needs to include cognitive decline and neuronal loss. This special issue seeks to provide an updated and critical evaluation of the available animal models of AD with the primary goal to deepen our mechanistic understanding of AD and elucidate how the development of these models has led or can lead to novel therapies for AD patients.

The topics included in this special issue are the following:

(i) Development of novel transgenic or non-transgenic animal models of AD (rodents or other).

(ii) Mechanistic studies of AD-related pathology in animal models including but not limited to APP/Aβ and/or tau hyper-phosphorylation (i.e., oxidative stress, mitochondrial, inflammatory, cell cycle changes etc.)

(iii) Development of novel behavioral or translational methodologies to determine impairment in models of AD.

(iv) Novel therapeutic approaches to modulate AD pathology and cognitive impairment.

In the coming years, prevalence of Alzheimer's disease (AD) is said to overtake diseases such as AIDS or cardiovascular diseases (World Health Organization). The impact of this disease on millions of individuals, their families, and the health care system will be devastating. As such, the scientific community has strived to model AD in the hope that these models will provide the tools for effective and desperately needed therapeutic development and testing. At the forefront of the quest to decipher Alzheimer's disease are animal models. Developed through genetic, chemical, and/or lesions, animal models of AD try to faithfully mimic disease pathogenesis in a growing number of species ranging from invertebrates to higher mammals such as primates. The ultimate goal is to further our understanding of mechanisms associated with this plural and complex disease and allow us to test promising therapies to manage, prevent, and hopefully cure AD.

Novel animal models of AD are relentlessly being developed and existing ones fine-tuned; however, they face the challenges associated with the complexity of a neurodegenerative disease. For example, most animal models of AD do not

reproduce the full phenotypical disease spectrum. Also relevant is the fact that, like for most neurodegenerative diseases, the etiology of AD and the clinical presentation differs greatly across individuals. As such, while the current models are very well suited for the study of specific pathology-driven mechanisms, most notably amyloid-beta, pharmacological testing in animal models of neurodegenerative disease often translates into poor efficacy when applied to the clinical population. With these advances and challenges in mind, this special issue, written by experts in the field, provides a rich and updated overview of disease-related aspects modeled in several species, ranging from the established transgenic models but also including novel drosophila and chick models. A wide range of modeled disease-related events are discussed at all levels, from descriptive and mechanistic to technical in order to provide a full scope of this disease and additional techniques that may become useful to investigators in the field.

An important aim of this special issue is to provide an accurate picture of the plurality of this disease by presenting research that is not only focused on modeling primary pathology. This includes, the downstream impact of tau phosphorylation in both murine and drosophila models and presenilin-mediated signaling, and also disease-related events that go beyond classical pathology. This special issue includes primary research and review articles on oxidative stress and mitochondrial dysfunction, lipid raft alterations in the murine models of the disease, and attention to various enzymatic complexes including the 2-oxoglutarate dehydrogenase complex. Furthermore, classic neurotransmitter systems such as acetylcholine, and brain regions such as the locus coeruleus are also discussed in an attempt to highlight the importance of these alternate or additional processes in the disease and provide a breath of how AD can be modeled at different levels. In conjunction with these articles, this issue also includes in depth discussion of biomarkers, imaging, and behavioral techniques, and studies presenting gender differences in murine and nonmurine models of AD that provide additional insight to investigators in the field.

Taken together, the ultimate outcome of this exciting and plural special issue is to enrich current research on this devastating disease with the hope that it will help to get us a step closer to a much needed cure.

Gemma Casadesus
Gary Arendash
Frank Laferla
Mike McDonald

SAGE-Hindawi Access to Research
International Journal of Alzheimer's Disease
Volume 2010, Article ID 780102, 24 pages
doi:10.4061/2010/780102

Research Article

Staging of Alzheimer's Pathology in Triple Transgenic Mice: A Light and Electron Microscopic Analysis

Kwang-Jin Oh,[1] Sylvia E. Perez,[1] Sarita Lagalwar,[2] Laurel Vana,[2] Lester Binder,[2] and Elliott J. Mufson[1]

[1] *Department of Neurological Sciences, Rush University Medical Center, Chicago, IL 60612, USA*
[2] *Department of Cell and Molecular Biology, Feinberg School of Medicine, Northwestern University, Chicago, IL 60611, USA*

Correspondence should be addressed to Elliott J. Mufson, emufson@rush.edu

Received 5 February 2010; Accepted 24 May 2010

Academic Editor: Gemma Casadesus

The age-related pathological cascade underlying intraneuronal tau formation in 3xTg-AD mice, which harbor the human APP_{Swe}, $PS1_{M126V}$, and Tau_{P301L} gene mutations, remains unclear. At 3 weeks of age, AT180, Alz50, MC1, AT8, and PHF-1 intraneuronal immunoreactivity appeared in the amygdala and hippocampus and at later ages in the cortex of 3xTg-AD mice. AT8 and PHF-1 staining was fixation dependent in young mutant mice. 6E10 staining was seen at all ages. Fluorescent immunomicroscopy revealed CA1 neurons dual stained for 6E10 and Alz50 and single Alz50 immunoreactive neurons in the subiculum at 3 weeks and continuing to 20 months. Although electron microscopy confirmed intraneuronal cytoplasmic Alz50, AT8, and 6E10 reaction product in younger 3xTg-AD mice, straight filaments appeared at 23 months of age in female mice. The present data suggest that other age-related biochemical mechanisms in addition to early intraneuronal accumulation of 6E10 and tau underlie the formation of tau filaments in 3xTg-AD mice.

1. Introduction

During the last several years numerous transgenic animal models of Alzheimer's disease (AD) have been engineered to examine the effects of the two major AD neuropathological hallmarks, amyloid plaques, and neurofibrillary tangles (NFT) on neurodegeneration. The vast majority of these AD transgenic mice overexpress a mutant human amyloid-beta (Aβ) precursor protein (APP) gene alone or in combination with a mutated presenilin (PS) gene resulting in the presence of brain extracellular amyloid plaques, which are mainly formed by the accumulation of insoluble Aβ species [1–6]. Since overexpression of amyloid-beta peptide did not recapitulate all of the neuropathological features of AD, additional models were created adding mutant tau transgenes. For example, to further evaluate the pathogenic mechanisms underlying NFT formation, transgenic mouse models have been generated to harbor a mutant human tau gene found in frontotemporal dementia or Pick's disease (P301L or P301S). These mutant mouse models display NFT-like structures consisting of abnormal cytoskeletal tau protein aggregates in the central and peripheral nervous systems [4, 7–10]. Recently, a triple transgenic mouse (3xTg-AD) harboring the human APP_{Swe}, $PS1_{M146V}$, and Tau_{P301L} gene mutations was developed, displaying accumulation of both intracellular Aβ and tau in an age-dependent manner within the cortex, hippocampus, and amygdala [11–14], and to a lesser degree, in the brainstem [15].

Immunohistochemical studies using immersion-fixed 3xTg-AD mouse tissue have shown that intracellular Aβ precedes the appearance of tau pathology, developing Aβ deposits at 6 months and intraneuronal tau pathology at 9 months of age [11, 12, 14]. Recent reports have demonstrated that the development of Aβ plaques differed between 3xTg-AD mouse colonies as well as between male and female mice [16, 17]. Furthermore, rostral-caudal differences in the onset of tau pathology have been reported, but only in male 3xTg-AD mice [17]. Virtually no ultrastructural analysis of AD pathology in these mice has been described.

Therefore, in the present study we performed a systematic detailed evaluation of the evolution of tau conformation and phosphorylation events beginning at 3 weeks of

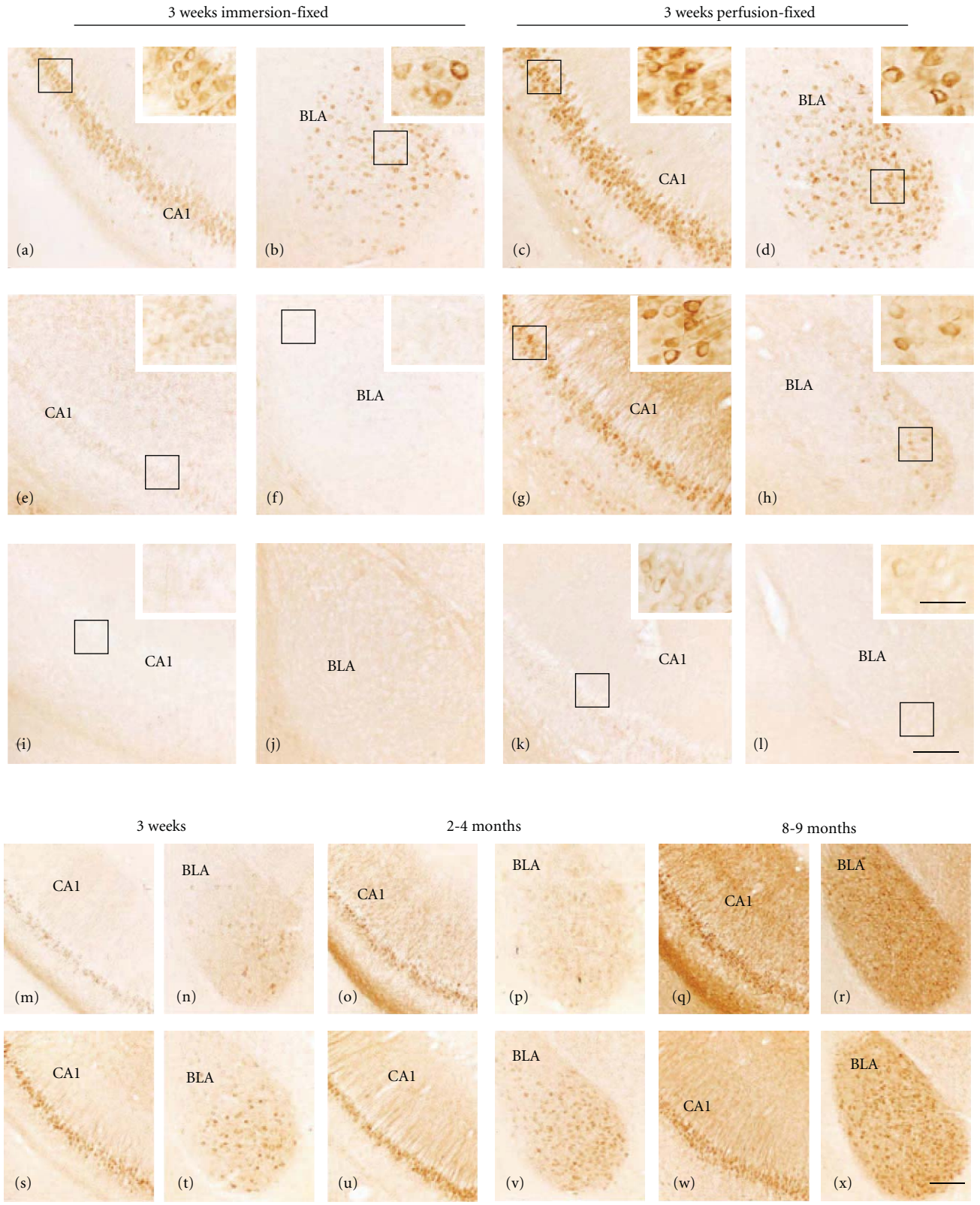

Figure 1: Photomicrographs of 6E10, AT8, PHF-1, Alz50, and AT180 intraneuronal and neuropil immunostaining in the CA1 field of the hippocampus and basolateral nucleus of the amygdala (BLA) at 3 weeks, 2–4-, and 8-9-month-old male 3xTg-AD mice. Note the differences in immunoreactivity between immersion and perfusion-fixed tissue in 3-week-old 3xTg-AD mice for 6E10 ((a)–(d)), AT8 ((e)–(h)), and PHF-1 ((i)–(l)). Alz50 ((m)–(r)) and AT180 ((s)–(x)) immunoreactivity was increased with age-dependent increases in the ventral hippocampus, ((m), (o), (q), and (s), (u), (w)) and basolateral amygdala, ((n), (p), (r) and (t), (v), (x)). Abbreviation: DG: dentate gyrus. Scale bar = 100 μm.

age using perfusion-fixed tissue at the light and electron microscopic level to more completely define the cascade of amyloid and tau pathology in male and female 3xTg-AD mice. The data derived from this study provide novel information underlying the temporal progression of amyloid and tau pathology within the cortex, hippocampal/subicular complex, and the amygdala that is pivotal in determining the selective vulnerability of neurons during the life span of male and female 3xTg-AD mice. This data is critical for the design of future experiments to address pharmacological, mechanistic, behavioral, and gender questions in studies using this widely used mouse model of AD.

2. Materials and Methods

2.1. Transgenic Mice. A colony of homozygous 3xTg-AD and nontransgenic (ntg) mice were generated from breeding pairs provided by Dr. Frank LaFerla, University of California Irvine. These transgenic mice harboring the human APP_{Swe}, $PS1_{M146V}$, and Tau_{P301L} mutations exhibit intraneuronal and extracellular amyloid pathology as well as tau pathology [12]. At least 4 male and 4 female juvenile (3 weeks), young (2-3 months), adult (4–6 months), middle-aged (8-9 months), and old (18–20 months) 3xTg-AD and *non-transgenic (ntg)* mice were examined. In addition young, middle-aged and old female 3xTg-AD mice were used for electron microscopic examination. Animal care and procedures were conducted according to the National Institutes of Health Guide for Care and Use of Laboratory Animals.

2.2. Fixation Protocol. Mice were anesthetized with an injection of ketamine/xylazine (100 mg/kg/5.0 mg/kg) and transcardially perfused for 2 minutes with 0.9% physiological saline followed by a solution containing 4% paraformaldehyde and 0.1% glutaraldehyde in 0.1 M phosphate buffer (PB) for 5 minutes (~50 ml) and then post-fixed in the same solution for 24 hours at 4°C. Since many transgenic mice studies use immersion-fixed brain tissue and considering that tau antigenicity is time and fixation sensitive [18–26], another group of mice was transcardially perfused with physiological saline and their brains hemisected and immersion-fixed for 24 hours in the same fixation solution. All brains were cryoprotected in 30% sucrose, sectioned on a sliding microtome at 40 micron thickness, and stored in a solution consisting of 30% glycerin, 30% ethylene glycol, in 0.1 M phosphate buffer at −20°C until processed for immunohistochemistry.

2.3. Immunohistochemistry. Tissues from immersion or perfusion fixed brains were processed as free-floating sections and immunostained for anti-hAPP/Aβ reactive amino acid residue 1–17 of beta-amyloid (6E10; 1 : 2,000 dilution, Covance, N.J.), the tau conformational antibodies Alz50 (66kD), MC1 (66kD) (1 : 10,000, 1 : 250 dilution, resp., both gifts from Dr. Peter Davies, Albert Einstein School of Medicine, N.Y.), and the phosphoepitope tau antibodies AT180 (~66 kD), AT8 (~66 kD) (both at 1 : 1000 dilution, Thermofisher, Waltham, MA) and PHF-1(57–67 kD) (1:10000 dilution; gift from Dr. Peter Davies, Albert Einstein College of Medicine) at each age examined. The specificity of each of the antibodies used in this study was previously characterized by western blot by others (6E10 (Covance), AT180 [27, 28], AT8 [29], PHF-1 [30–32], Alz50 [33–36], and MC1 [34, 35]). Prior to staining, sections were washed 3 × 10 min in phosphate buffer and 3 × 10 min in Tris-buffered saline (TBS) to remove cryoprotectant before a 20-minute incubation in 0.1 M sodium metaperiodate (Sigma, St. Louis, MO) in TBS to quench endogenous peroxidase activity. Tissue was then permeablized 3 × 10 minutes in TBS containing 0.25% Triton-X (Thermofisher, Waltham, MA) and blocked in the same solution containing 3% goat serum for 1 hour. Sections were incubated with appropriate antibody dilutions overnight on an orbital shaker at 45 RPM at room temperature in 0.25% Triton X-100, 1% goat serum solution. The next day, tissue was washed 3 × 10 min in TBS containing 1% goat serum prior to incubation with appropriate secondary antibody (see Table 1) at a 1 : 200 dilution for 1 hr. Following 3 × 10 minutes washes in TBS, sections were incubated in Vectastain ABC kit (Vector Labs, Burlingame, CA) in TBS for 1 hour. Tissue was then rinsed 3 × 10 minutes in 0.2 M sodium acetate, 1.0 M imidazol buffer, pH 7.4, and developed in acetate-imidazol buffer containing 0.05% 3,3'-diaminobenzidine tetrahydrochloride (DAB, Sigma, St Louis, MO). For comparison across ages sections from animals of different ages were immunostained at the same time and with the same duration of DAB reaction. The reaction was terminated in acetate-imidazol buffer, tissue mounted on glass slides, dehydrated through graded alcohols (70–95–100%, 3 × 5 min), cleared in xylenes (3 × 5 min), and coverslipped with DPX (Biochemica Fluka, Switzerland). Cytochemical control sections consisted of (1) tissue from ntg mice which were processed in a manner identical to the immunohistochemical procedures described above for 3xTg-AD animals, (2) tissue from 3xTg-AD as previously described with the exception of the primary antibody, and (3) a preadsorption control consisting of a 100 fold amount of $A\beta_{1\text{-}42}$ (US Peptides, Rancho Cucamonga, CA) incubated with 6E10 in TBS containing 0.25% Triton X-100, 1% goat serum overnight at room temperature. The preadsorbed serum was used in place of the 6E10 antibody in the immunohistochemistry protocol. Since the antigen used to create the tau monoclonal antibodies obtained from commercial sources was unavailable, only the 6E10 preadsorbtion control was performed. Brightfield images were acquired using a Nikon Optiphot microscope.

2.4. 6E10 and Alz50 Dual Immunofluorescent Staining. Selected sections were fluorescently double-labeled for 6E10 and Alz50 using the above protocol with the following modifications [15]. All steps prior to incubation of primary antibody were as described above with the exclusion of the quenching of endogenous peroxidase activity with 0.1 M sodium metaperiodate. Tissue was incubated with primary antibody overnight (6E10; 1 : 200 dilution). After rinsing 3 × 10 minutes in TBS, tissue was incubated with Cy3-conjugated goat antimouse IgG Fcγ Subclass 1 specific secondary antibody (Jackson Immunoresearch; West Grove,

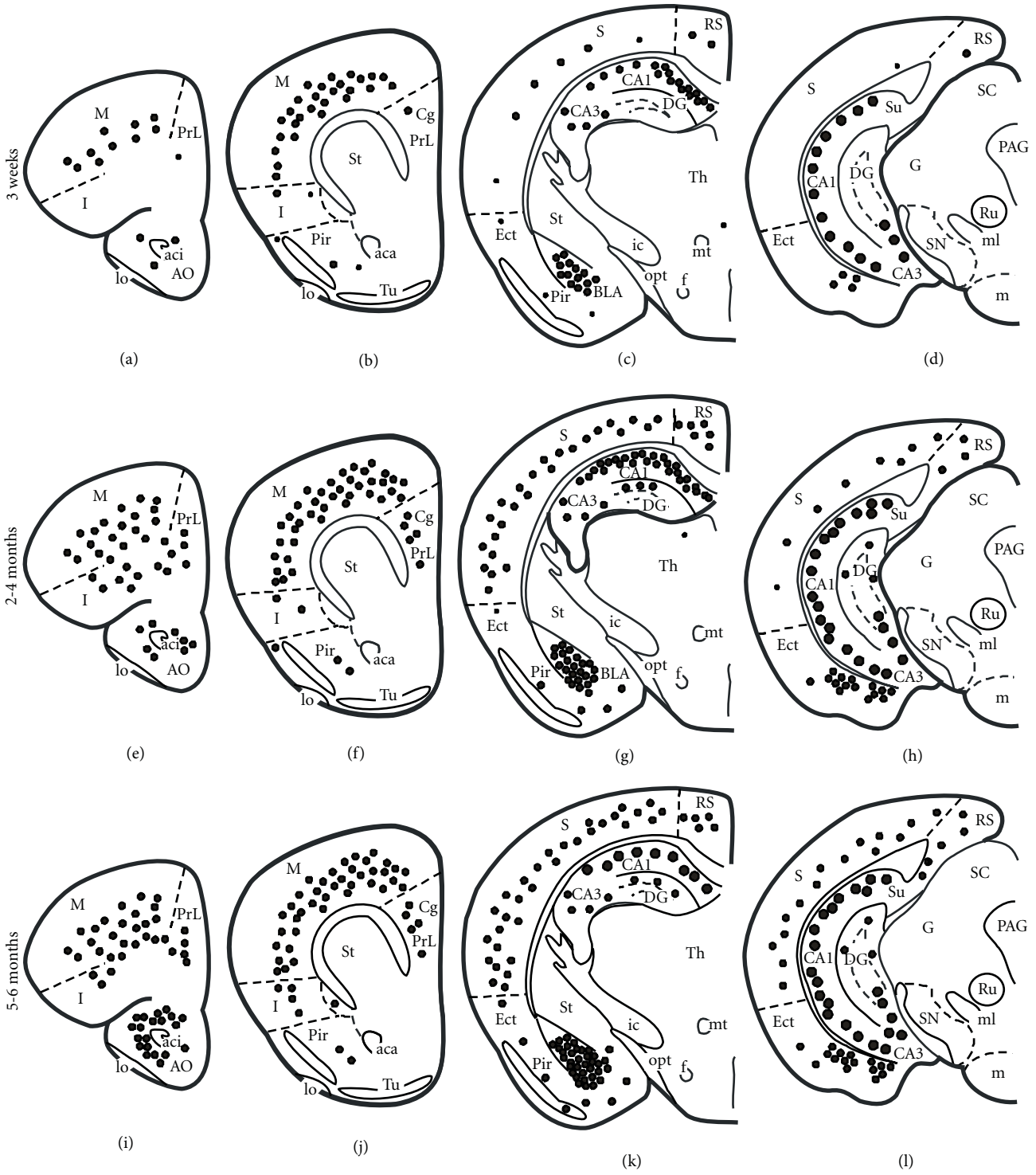

Figure 2: Schematic drawings representing the distribution of 6E10-ir neurons in 3-week, 2-, and 5-month-old perfusion-fixed 3xTg-AD transgenic mice. Note the age-related increase in the number of 6E10 positive neurons in the cortex, hippocampus, and amygdala. Abbreviations: Aca: anterior commissure, anterior; aci: anterior commissure, intrabulbar, A: amygdala; AO: anterior olfactory nucleus; BLA: basolateral nucleus of the amygdala; CA1: CA1 hippocampal subfield; CA3: CA3 hippocampal subfield; Cg: cingulate cortex; DG: dentate gyrus; Ect: ectorhinal cortex; F: fornix; G: geniculate nucleus; lo: lateral olfactory tract; I: insular cortex, ic: internal capsule; m: motor cortex; m: mammillary complex; ml: medial lemniscus; mt: mammillothalamic tract; opt: optic tract; PAG: periaqueductal gray, Pir: piriform cortex; Pr:L prelimbic cortex; Rn: red nucleus; RS: retrosplenial cortex; S: sensory cortex; SC: superior colliculus; SN: substantia nigra; St: striatum; Su: subiculum; th: thalamus; tu: olfactory tubercle. Small dots = 1–5 positive neurons, medium-size dots = 10–20 positive neurons, and large dots = 100 positive neurons.

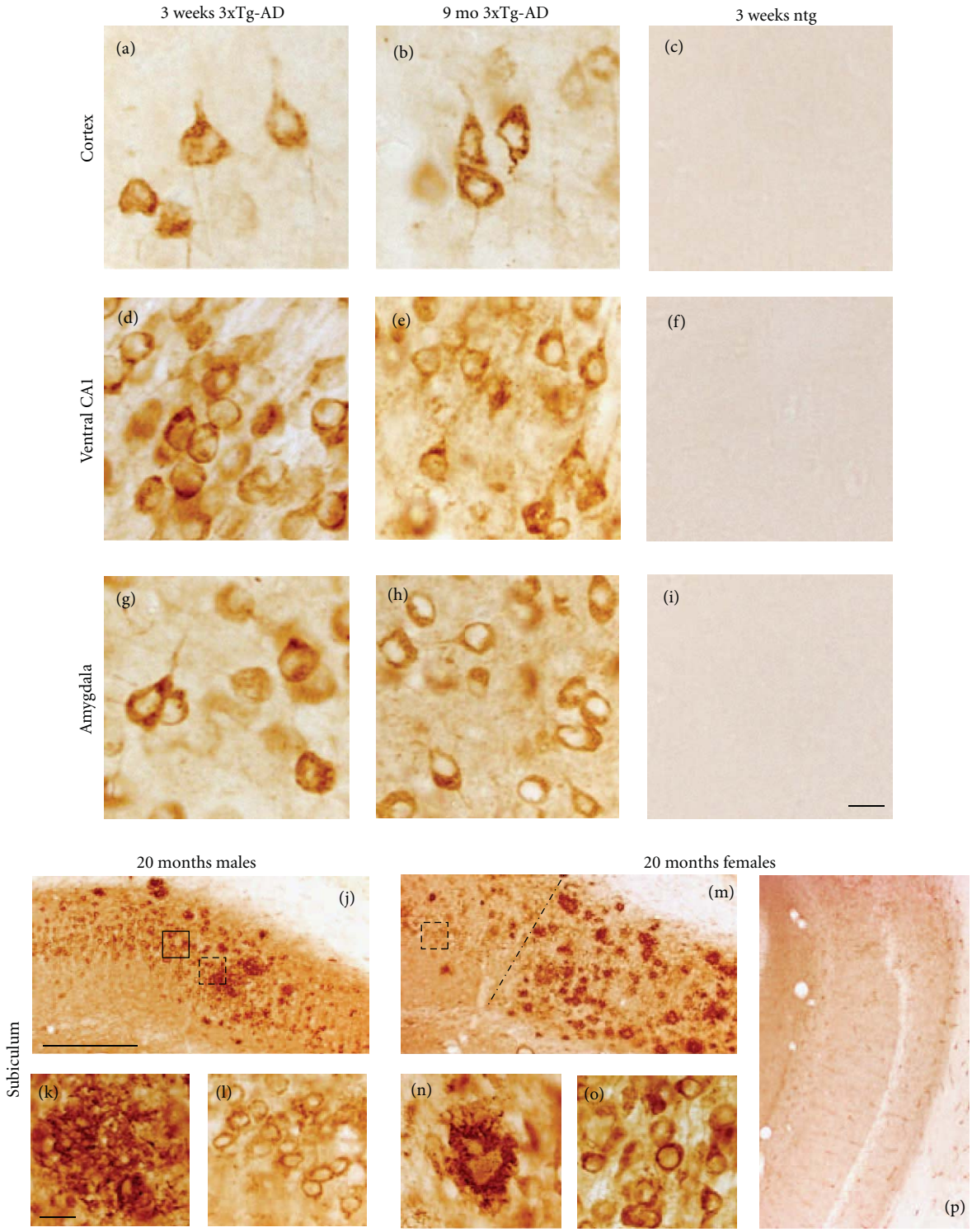

Figure 3: Photomicrographs showing 6E10 intraneuronal immnostaining in the cortex ((a)–(c)), ventral CA1 ((d)–(f)), BLA ((g)–(i)), and subiculum ((j)–(o)) in 3-week, 9- and 20-month-old 3xTg-AD mice. Round-or oval-shaped 6E10-ir neurons were found at the youngest age in all brain regions examined independent of fixation ((a), (d), (g)). At 9 months some 6E10 stained neurons appeared shrunken with a hollow center ((b), (e), (h)). 6E10 immunopositive plaques were found throughout the subiculum of female (j), and to a lesser extent in male mutant mice (m) at 20 months of age. Solid and dashed boxed areas in panels (j) and (m) outline a 6E10-ir plaque (k) and CA1-ir neurons shown at higher magnification in (l) and (o), respectively. Dashed line in panel m demarks the CA1 field from the subiculum. Higher-power photomicorgraph shows a posterior subicular 6E10 positive plaque in a female 20-month-old mutant mouse (n). Tissue processed following 6E10 antibody peptide preadsorbtion shows a lack of intra-or extraneuronal staining in CA1 or subiculum (P). Note the more diffuse compared to the compact nature of plaques found in male-versus female-aged mutant mice. Ntg mice failed to display 6E10 immunoreactivity (c, f, i) at 3 weeks of age. Scale bar in ((a)–(i)); ((k), ((l), (n), (o)) = 20 μm, ((j), (m)) = 100 μm.

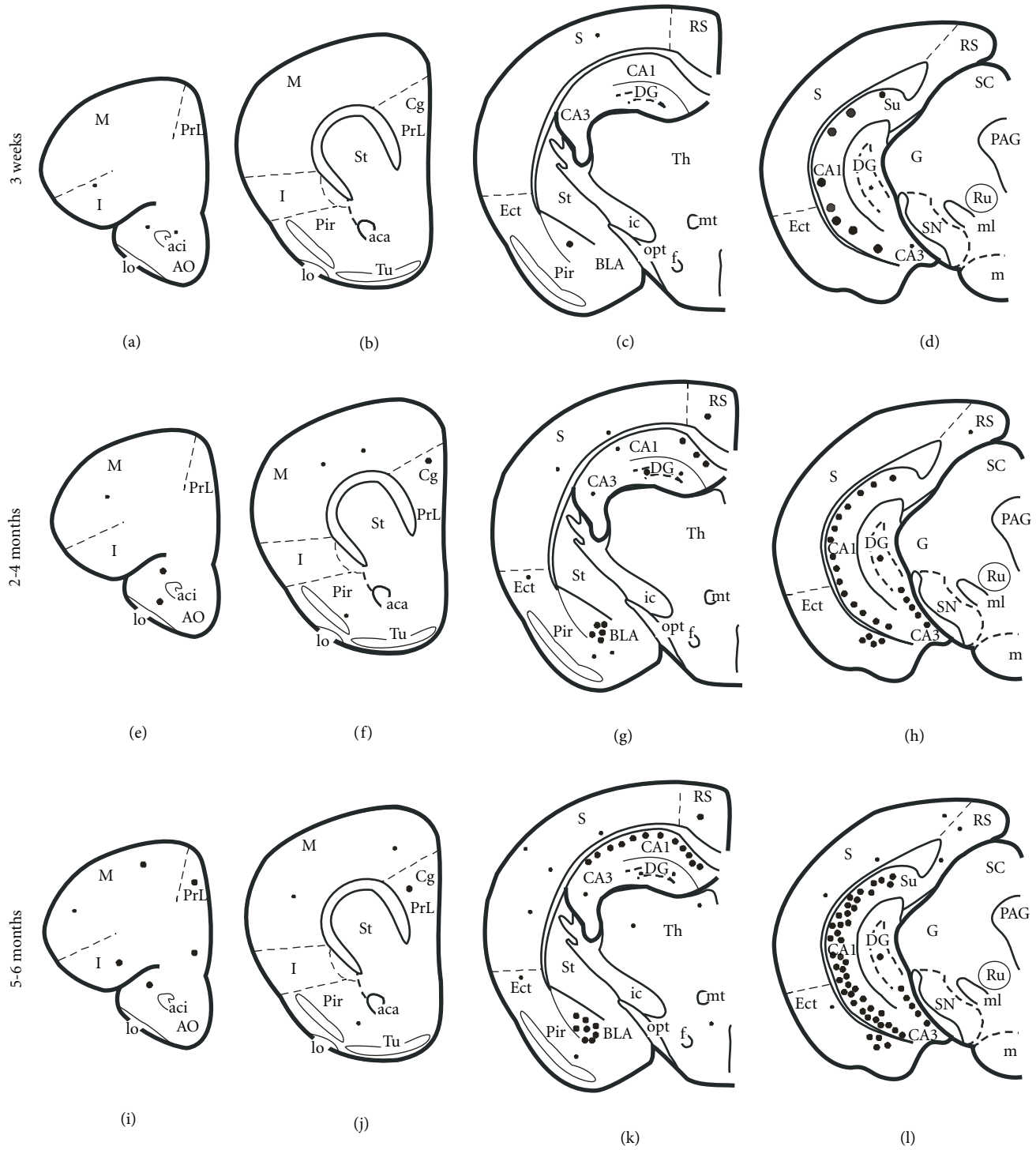

Figure 4: Schematic drawings showing the distribution of Alz50-ir neurons at 3-week, 2-, and 5-month-old transcardially-fixed 3xTg-AD mice. Alz50-ir neurons were found mainly in the CA1 ventral hippocampus at 3 weeks of age. Note the increase in the number of Alz50-ir hippocampal neurons in the 2- and 5-month old mutant mice. In addition there was an age-related increase in Alz-50 positive neurons within the BLA. Abbreviations are the same as in Figure 2. Small dots = 1–5 positive neurons, medium-size dots = 10–20 positive neurons, and large dots = 100 positive neurons.

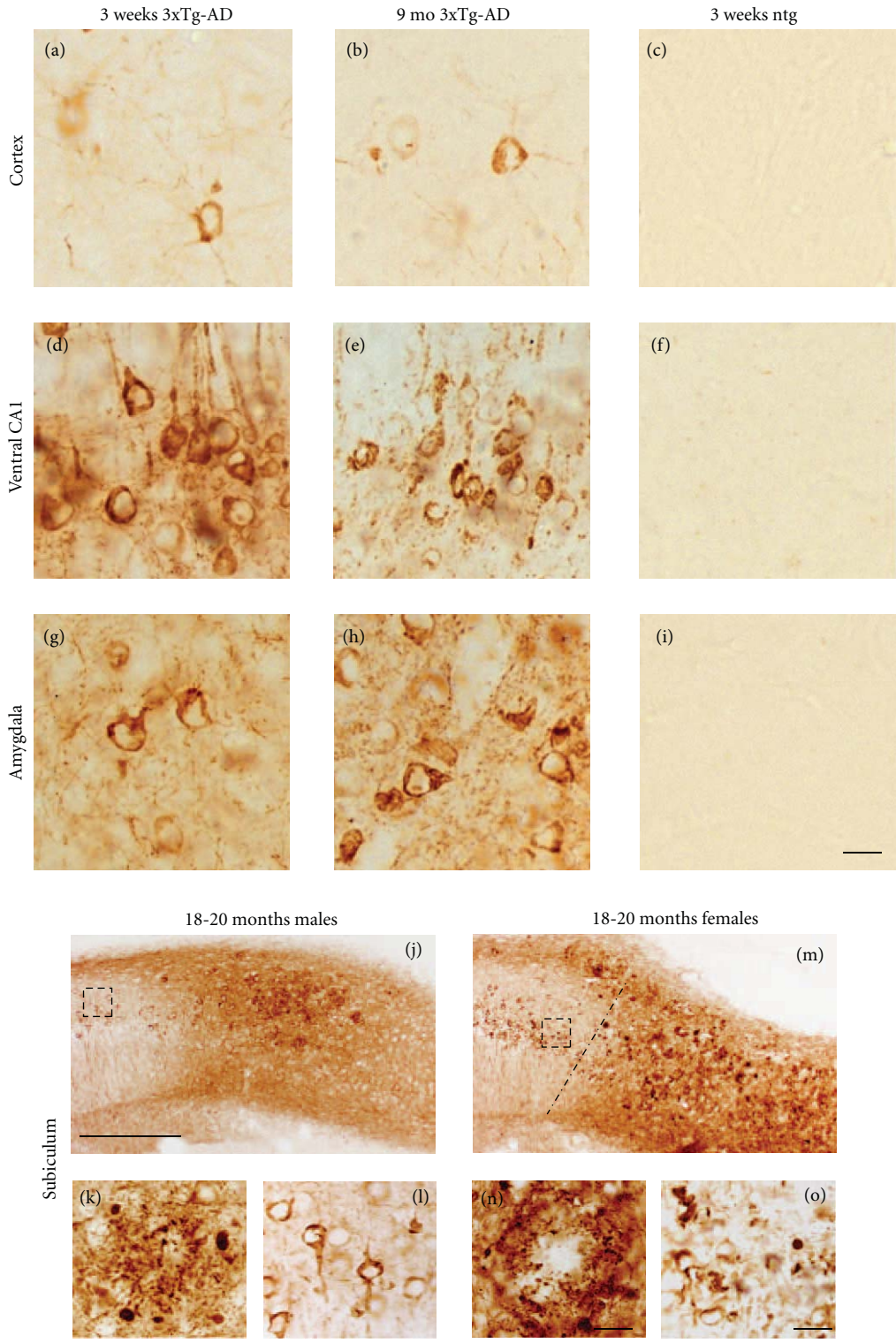

Figure 5: Photomicrographs of Alz50-ir neurons in 3-week, 9- and 18-20-month-old 3xTg-AD mice. At 3 weeks of age scattered neurons were found in the frontal parietal cortex (a) and BLA (g), whereas numerous Alz50-ir ventral hippocampal pyramidal cells were labeled (d). By 9 months of age, neurons in the BLA and ventral hippocampus appeared shrunken (e) compared to the cortex (b). Numerous Alz50-ir plaques and dystrophic neurites were found in the male ((j)-(k)) and female subiculum ((m)-(n)). Dashed boxes show higher magnification images of dystrophic Alz50-ir CA1 pyramidal neurons ((l), (o)). Dashed line in panel (m) demarks the CA1 field from the subiculum. Ntg mice failed to show Alz50 immunoreactivity ((c), (f), (i)). Scale bar in ((a)–(i)); ((k), (l), (o)) = 20 μm, ((j), (m)) = 100 μm, and (n) = 30 μm.

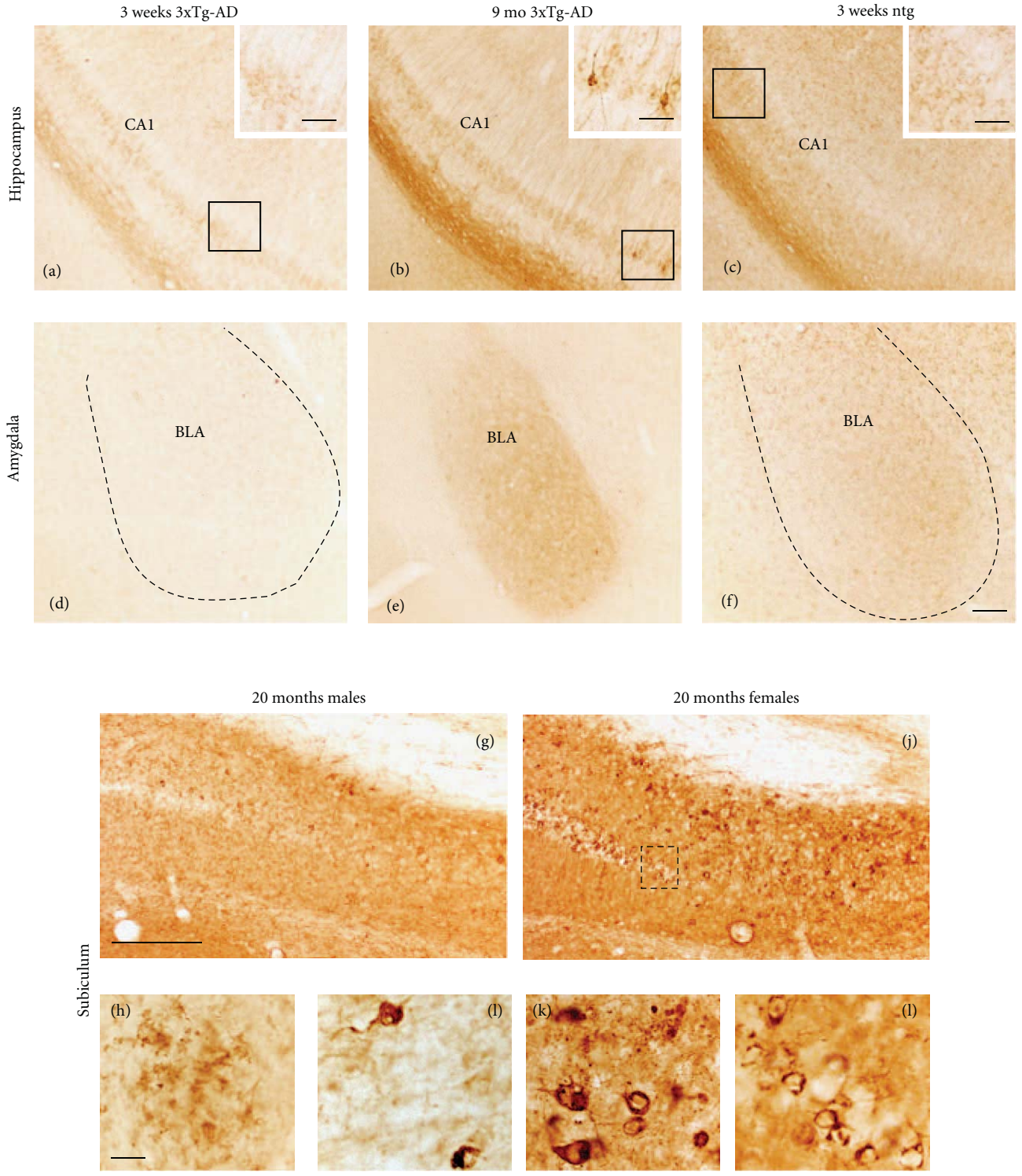

Figure 6: Photomicrographs showing MC1 immunoreactivity within the hippocampal CA1 field ((a)–(c)), BLA ((d)–(f)) and subiculum ((g)–(l)) at 3-week, 2–4-, 8-9-, and 20-month-old 3xTg-AD mice. Dashed line in (d) and (f) outlines the area containing the BLA. Note the increase in MC1 neuronal immunostaining in hippocampal CA1 neurons ((b), higher magnification shown in insert), the neuropil in the BLA (e) at 2–4 month and the reduction in reactivity in these areas in 9-month-old mutant mice ((c), higher magnification shown in insert and (f)). Low-magnification images of the subiculum from male (g) and female (j) 20 months of old 3xTg-AD mice. Example of MC1-ir neurites was observed in the subiculum of a male mutant mouse ((h)). Both male ((i)) and female ((j), higher magnification of boxed area shown in (l)) mutant mice displayed dystrophic subicular MC1-ir neurons. Scale bars: ((a)–(f)); ((g), (J)) =100 μm, insets = 35 μm, ((h), (i), (k), (l)) = 20 μm.

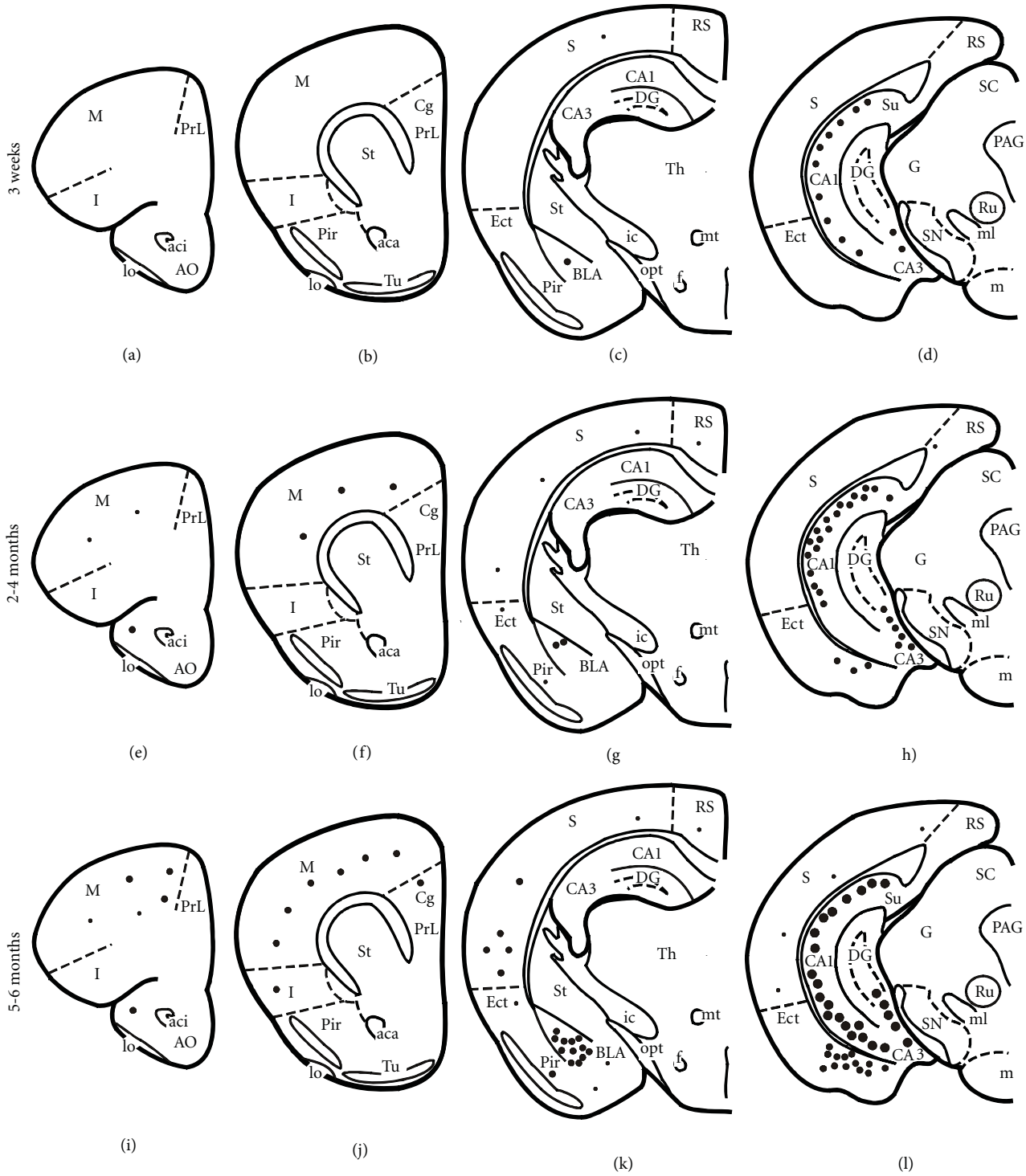

Figure 7: Schematic drawings showing the distribution of AT8-ir neurons in transcardially fixed 3-week, 3-, and 6-month-old 3xTg-AD mice. At 3 weeks, only scattered AT8-ir neurons were found in the cortex and basolateral amygdala compared to a greater number in the ventral hippocampus. Note that with increasing age, many more AT8-ir were found in the cortex, hippocampus, and amygdala. Abbreviations are the same as in Figure 2. Small dots = 1–5 positive neurons, medium-size dots = 10–20 positive neurons, and large dots = 100 positive neurons.

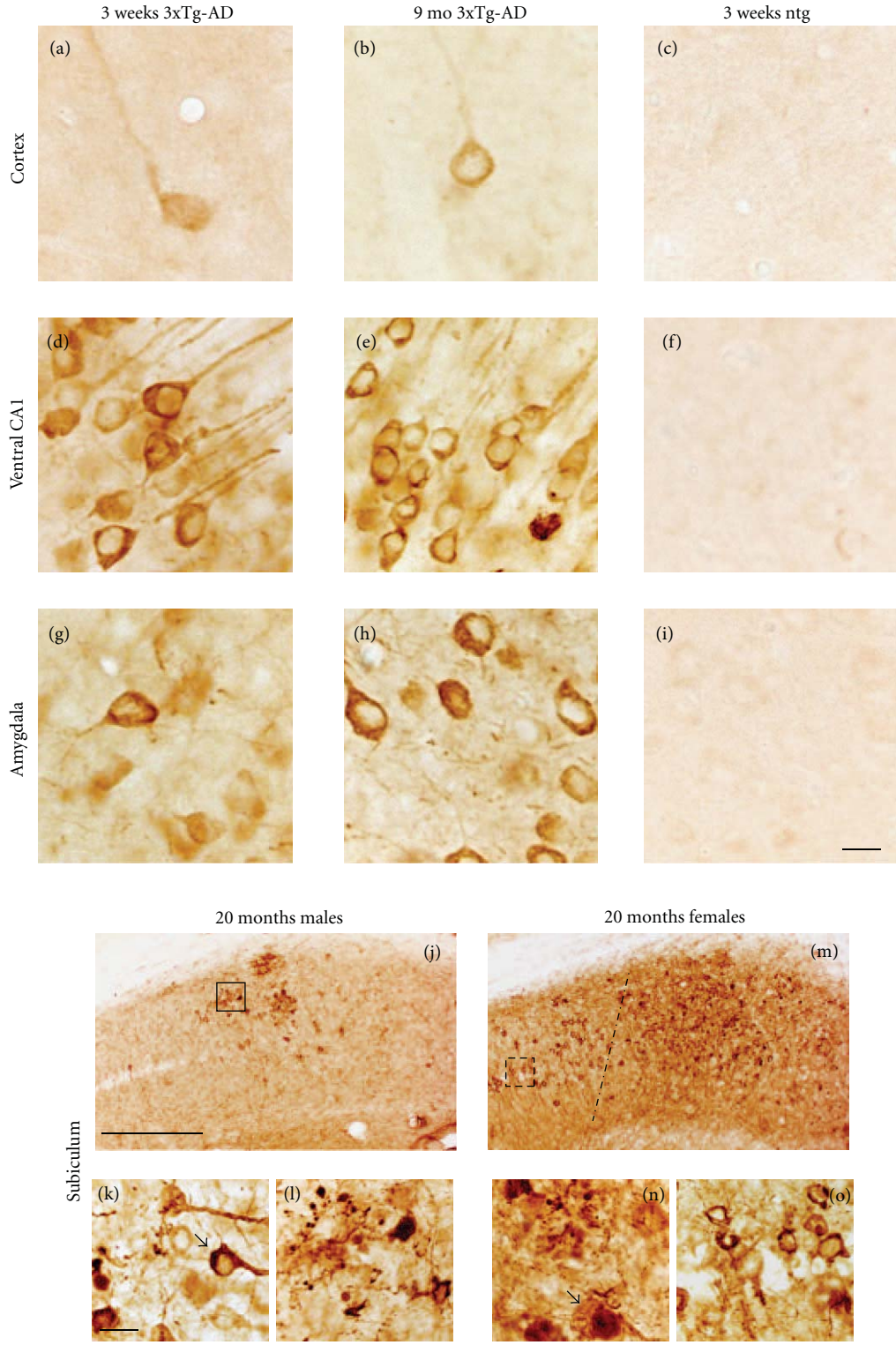

Figure 8: Photomicrographs showing AT8 immunoreactivity in the cortex ((a)–(c)), ventral CA1, ((d)–(f)), BLA ((g)–(i)), and subiculum ((j)–(o)) in 3-week, 9-, and 18–20-month-old 3xTg-AD mice. Transcardially fixed tissue revealed more AT8-ir neurons in the ventral hippocampus than either the neocortex or BLA in 3-week-old 3xTg-AD mice ((a), (d), (g)). Note that AT8-ir neurons within the hippocampus appeared shrunken with blunted dendrites at 9 months of age (e) when compared to younger (d) mutant mice. AT8 immunoreactive dystrophic neurons and plaques were observed in the subiculum of both male and female 20-month-old 3xTg-AD mice ((j)–(o)). Note the dystrophic neuronal morphology in male (k, arrow) and female (n, arrow) mice as well as the extent of tau pathology ((j), (m)). Dash line in m demarcates the boundary between the CA1 field and the subiculum. (l) and (o) represent higher magnification of boxed areas (j) and (m) respectively. Ntg 3-week-old mice displayed virtually no AT8 immunoreactivity ((c), (f), (i)). Scale bars: ((a)–(i)); ((k), (l), (n), (o)) = 20 μm and (j), (m) = 100 μm.

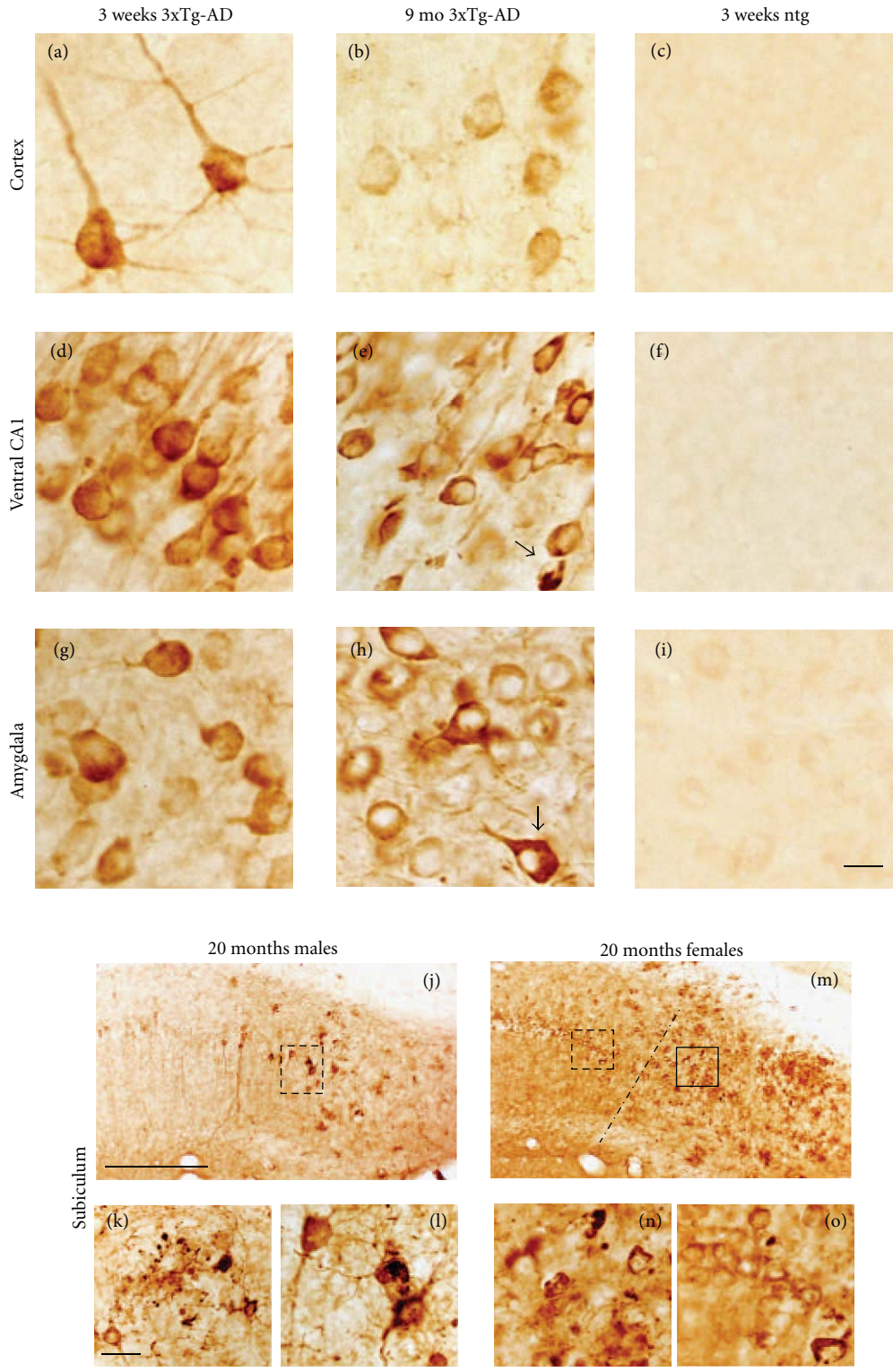

Figure 9: Photomicrographs showing AT180 immunoreactivity in the cortex ((a)–(c)), ventral CA1 ((d)–(F)), BLA ((g)–(i)), and subiculum ((j)–(o)) in 3xTg-AD mice. Note the more intense AT180-ir perinuclear staining (arrows), particularly in the BLA (h), and the shrunken appearance of ventral hippocampal neurons (e) at 9 months of age when compared to 3 weeks of age ((d), (g)). Greater AT180-ir tau pathology was observed in females than that in males at the CA1/subicular interface ((j), (m)). Higher magnification of dashed boxes in (j) and (m) are represented in (l) and (o), respectively, while (n) represents higher magnification of solid box in (m). Ntg mice showed only light background staining ((c), (f), (i)). Scale bars: ((a)–(i)); ((k), (l), (n), (o)) = 20 μm and (j, m) = 100 μm.

Table 1: Summary of Antibodies and Characterisitcs

Primary Antibody	Source	Epitope and Isotype	Secondary Antibody	Blocking Serum
Alz50	Dr. Peter Davies Albert Einstein College of Medicine, NY	aa's 5–15, 312–322;IgM	Goat-Anti mouse IgG, Vector Labs, Burlingame, CA	Goat; Gemini Bio-Products, West Sacramento, CA
MC1	Dr. Peter Davies Albert Einstein College of Medicine, NY	aa's 5–15, 312–322;IgG1	Goat-Anti mouse IgG, Vector Labs, Burlingame, CA	Goat; Gemini Bio-Products, West Sacramento, CA
AT180	ThermoFisher, Walthman, MA	Phosphothreonine 231; IgG 1K	Goat-Anti mouse IgG, Vector Labs, Burlingame, CA	Goat; Gemini Bio-Products, West Sacramento, CA
AT8	ThermoFisher, Walthman, MA	Phosphoserine 202/205; IgG 1	Goat-Anti mouse IgG, Vector Labs, Burlingame, CA	Goat; Gemini Bio-Products, West Sacramento, CA
PHF-1	Dr. Peter Davies Albert Einstein College of Medicine, NY	Phosphoserine 396/404; IgG1	Goat-Anti mouse IgG, Vector Labs, Burlingame, CA	Goat; Gemini Bio-Products, West Sacramento, CA
Aβ/APP (6E10)	Covance Princeton,NJ	aa's 3–8 of Aβ seqeunce; IgG 1		

PA) for 2 hours in the dark. Sections were washed 3 × 10 minutes in TBS and then incubated with Alz50 (1 : 1000) overnight in the dark. Tissue was again rinsed 3 × 10 minutes and then incubated in Cy2-conjugated goat antimouse IgM μ-chain specific secondary antibody (1 : 200 dilution) for 2 hours in the dark. Immunofluorescence was visualized using a Zeiss Axioplan 2 microscope using excitation filters at wavelengths 489 and 555 nm and emission filters at 505 and 570 nm for Cy2 and Cy3, respectively. Florescent images were stored on a computer and brightness and contrast was enhanced using GIMP Version 2.6.7. Double immunofluorescence staining for 6E10 and phosphotau markers were not successfully achieved using methods to block the cross reactivity between monoclonal IgG1 subclass primary antibodies (see Table 1).

2.5. Immunoelectron Microscopy. To determine ultrastructural localization of intraneuronal Aβ and tau immunoreactivity, we performed an immunoelectron microscopic analysis of hippocampal/subicular neurons obtained from female homozygous at 2- ($n = 2$), 9- ($n = 2$), and 23- ($n = 2$) month-old 3xTg-AD mice. Each animal was transcardially perfused with 4% paraformaldehyde/0.1% glutaraldehyde in phosphate buffer, brains were removed from the skull and immersion post-fixed in the same fixative overnight at 4°C and cut into 80 micron thick horizontal sections using a Vibratome-1500 (Vibratome, Saint-Louis, MO). Tissue containing the hippocampal/subicular complex was immunostained using the antibodies directed against Aβ/APP (6E10, 1 : 2000 dilution), the conformation specific tau antibody Alz50 (1 : 10,000 dilution), and the phospho-specific (Ser202/Thr205) antibody AT8 (1 : 1000 dilution). The chromogen DAB was used to visualize each antibody.

2.6. Transmission Electron Microscopy (TEM). Immunostained sections were post-fixed in 1% OsO_4 for 45–60 minutes, dehydrated and embedded in Epoxy resin. Immunoreactive profiles within the hippocampal/subicular complex were selected using light microscopy, ultrathin sections (50–70 nm) were cut using a Leica Ultracut UCT (Leica Microsystems Inc, Bannockburn, IL) microtome, and the majority of sections counter-stained with 2% uranyl acetate and lead citrate. TEM sections were viewed and photographed with a JEOL transmission electron microscope. Immunostaining appeared as an electron-dense precipitate (dark-black) in neurons and other profiles within hippocampal-subicular complex of mutant mice. Cortical brain tissue obtained at autopsy from an 82-year-old male AD patient was immersion fixed in 4% paraformaldehyde and processed for TEM without antibody staining to compare the ultrastructure of human AD pathology to that found in 3xTg-AD mice.

3. Results

3.1. General Considerations. In the present study forebrain sections from male and female 3-week, 2–4, 5-6, 8-9, and 18–20-month-old 3xTg-AD and age-matched ntg mice were immunostained using well-characterized antibodies directed against 6E10, tau conformational epitopes (Alz50

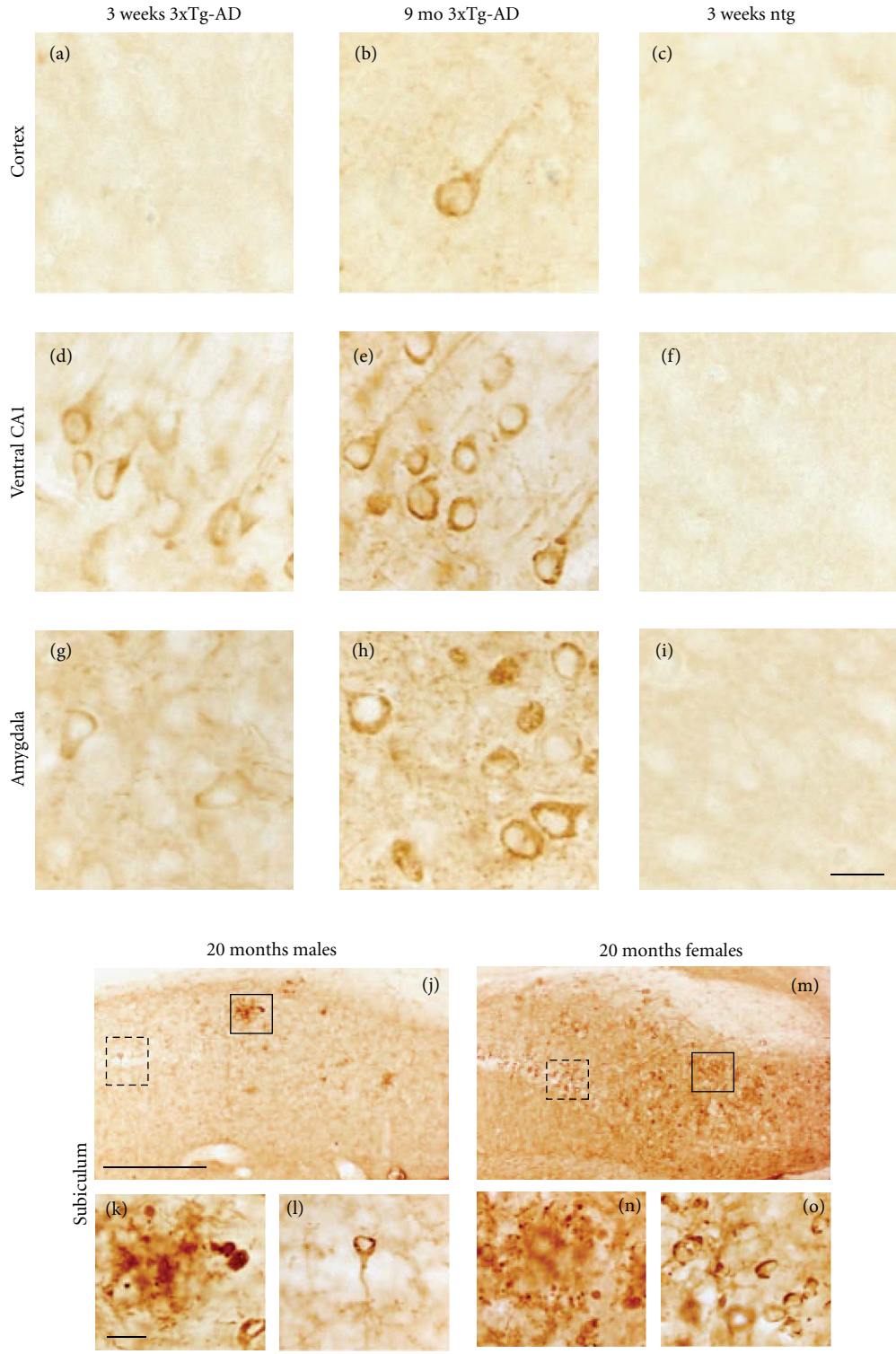

Figure 10: Photomicrographs showing PHF-1 immunostaining in cortex ((a)–(c)), hippocampus ((d)–(f)), BLA ((g)–(i)), and subiculum ((j)–(o)) in 3xTg-AD mice. PHF-1 immunostaining was seen almost exclusively in the ventral hippocampus of perfusion-fixed brains (d) compared to the cortex (a) and the BLA (g) at 3 weeks of age. By 8-9 months, many more PHF-1-ir neurons were apparent in the hippocampus and BLA ((e), (h)). Only scattered PHF-1-ir neurons were found in the neocortex at this age (b). Many more PHF-1 immunopositive neurons appeared in the dorsal anterior CA1 region of female mutant mice (area outline by dashed line in M and shown at higher magnification (o)) compared to males (area outline by dashed line in (j) and shown at higher magnification in (l)) at 18–20 months of age. PHF-1 immunopositive plaques were seen in the subiculum of male (solid boxed area in (j) and (k)) and female (solid boxed area in (m) and (o)) 3xTg-AD mice at 18–20 months of age. Note that the extent of PHF-1 immunoreactivity was greater in the subiculum in females (M) versus males (J). PHF-1-ir profiles were absent in ntg mice ((c), (f), (i)). Scale bars: (a)–(i); ((k), (l), (n), (o)) = 20 μm and ((j), (m)) = 100 μm.

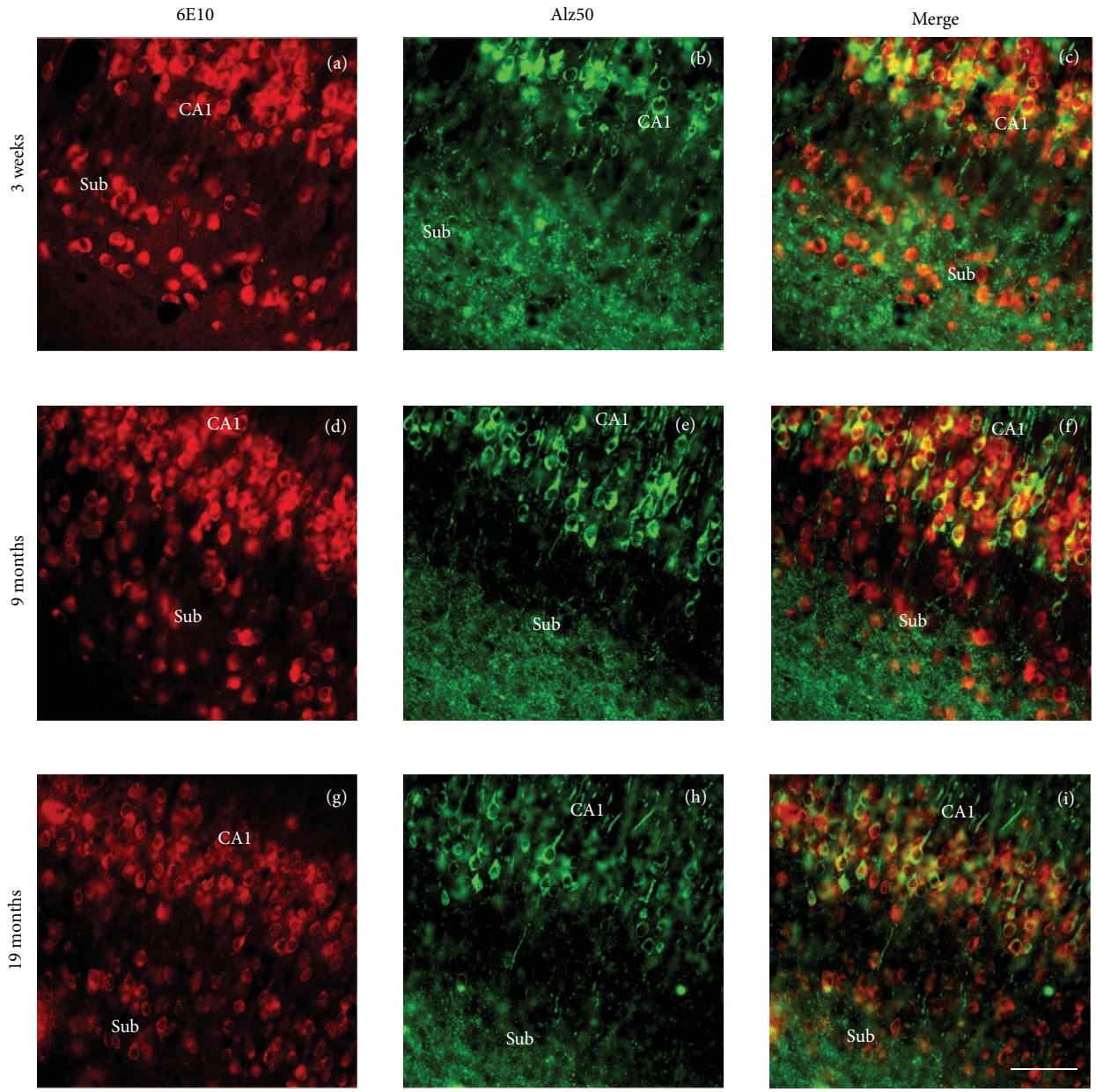

Figure 11: Immunofluorescent microscopic images showing single and dual 6E10 and Alz 50 staining in the hippocampal CA1 field and the subiculum of 3xTg-AD mice. Images of single 6E10 immunolabeled ((a), (d), and (g), red), (b), (e), (h) (Alz50, green) and merged (yellow, (c), (f), (i)) neurons at 3-week, 9- and 19-month-old 3xTg-AD mice. Note that 6E10 immunolabeled neurons are found in both the CA1 and subiculum but only Alz50 immunolabeled neurons were seen in CA1 at each age examined. The merged images show that many CA1 neurons contained both 6E10 and Alz50 immunoreactivity whereas the subicular neurons were only 6E10 positive at each age examined within Alz50-ir neuropil. Scale bar for (a)–(i) = 75 μm.

and MC1), and phosphotau epitopes AT180 (phosphothreonine 231), AT8 (phosphoserine 202/205), and PHF-1 (phosphoserine 396/404). In general, an age-related increase in intraneuronal and neuropil immunoreactivity in the hippocampal-subicular complex and amygdala were seen for all antibodies examined (Figure 1). The exception was MC1, where immunoreactivity decreased after 2–4 months of age (see Figure 6). Our findings revealed that transcardial but not immersion fixation dramatically enhanced the immunovisualization of AT8 (Figures 1(e)–1(h)) and PHF-1 (Figures 1(f)–1(l)) as early as 3 weeks of age. By contrast, AT180 and Alz50 immunoreactivity was not affected by the fixation procedure. Therefore all morphological analyses and photomicrographs subsequent to Figure 1 were derived from transcardially fixed tissue. The colocalization of 6E10 and tau antibodies using fluorescence was achieved successfully for 6E10 (IgG1) and Alz50 (IgM), but not for 6E10 and AT180 (IgG1) or AT8 (IgG1) due to the cross reactivity of their

primary antibodies. Therefore, the comparative analyses of the distribution of 6E10 and phosphotau markers were performed using DAB-reacted tissue sections at the light microscopic level. All immunohistochemical controls failed to display cellular or plaque reactivity beyond background levels for any tau antigen or 6E10 independent of fixation, age, and gender.

3.2. Staging 6E10 Immunoreactivity. The 6E10 antibody, which recognizes amino acids 3–8 of the Aβ sequence, revealed the greatest number and topographic distribution of immunoreactive (-ir) neurons in 3xTg-AD mice compared to the other antibodies we examined. There was an age-related increase in the extent of 6E10-ir neurons in all regions examined (Figure 2). Beginning at 3 weeks of age, intraneuronal 6E10-ir neurons were found in lamina 3 and 5 of the fronto-parietal cortex, deep layers of the cingulate cortex, CA fields of the hippocampus, subiculum, and the basolateral amygdala (BLA) in 3xTg-AD mice at each age independent of gender (Figure 2). 6E10-ir neurons, particularly in the hippocampal CA1 subfield, appeared round or oval in shape with many cells showing a thin ring of immunoreactivity located within the somatodendritic compartment (Figures 3(a), 3(d), and 3(g)). However, a number of cells in the cortex and amygdala had thickened perinuclear staining (Figures 3(d) and 3(a)), which became more prominent by 9 months of age (Figure 3(b) and 3(h)). Beginning at 9 months of age there was neuronal shrinkage of 6E10-ir neurons in 3xTg-AD mice (Figures 3(b), 3(e), and 3(h)), which continued at least until 18–20 months of age where many neurons displayed blunted dendrites, as well.

Although no dramatic gender differences in intraneuronal 6E10 staining were seen prior to 8-9 months, Aβ plaque deposits were visualized for the first time in the subiculum of 8-9-month-old female, but not male mutant mice (data not shown). By 18–20 months both genders displayed Aβ plaque deposits in the subiculum (Figures 3(j), 3(k), 3(m), and 3(n)) and hippocampus (data not shown). Aβ plaques appeared smaller and more diffuse in male than seen in the female subiculum of 3xTg-AD mice (Figures 3(j) and 3(k)). In fact, female CA1 neurons lost their dendritic 6E10-ir extensions into the substantia radiatum (Figure 3(o)) while similar processes remained present in male mutant mice (Figures 3(l) and 3(o)).

3.3. Staging of Tau Pathology

3.3.1. Alz50 Immunoreactivity. The Alz50 antibody recognizes an early stage conformational tau epitope that labels neurons undergoing early degenerative events associated with NFT formation but has also been shown to label neurons in normal brains [33–37]. Similar to 6E10 staining, the number of Alz50-ir neurons increased with age in all regions examined (Figure 4). As early as 3 weeks of age Alz50-ir staining was seen predominantly within the more caudal and ventral aspects of the hippocampal CA1 pyramidal and subicular neurons, whereas a few scattered Alz50-ir neurons were found in the neocortex and BLA (Figures 4(a)–4(d)). In addition, Alz50-ir neurons were also found in the septal but not temporal portions of the hippocampal formation (data not shown). Beginning at 2–4 months of age a few scattered Alz50-ir neurons were found in layers 3 and 5 of the fronto-parietal and the deep layers of the cingulate and retrosplenial cortex in 3xTg-AD mice (Figures 4(e)–4(h)). By 5-6 months of age there was an apparent increase in the number of Alz50-ir neurons in the ventral hippocampus and amygdala (Figures 4(i)-4(l)), as well as more intense neuropil staining (Figures 1(q) and 1(r)). However, unlike the continuous distribution of 6E10-ir pyramidal neurons in the hippocampal complex, the topographic distribution of labeled Alz50-ir CA1 pyramidal neurons spread in dorsal and anterior directions from the ventral and caudal regions of the brain (Figure 4). At 3 weeks of age Alz50-ir neurons in the cortex, hippocampus, and amygdala appeared round or oval and displayed a dense rim of perinuclear staining (Figures 5(a), 5(d), and 5(g)) with long dendrites extending into the neuropil. At 9 months of age many Alz50-ir neurons appeared shrunken with a distorted cellular morphology in the hippocampal complex and amygdala (Figures 5(e) and 5(h)). Interestingly, some cells no longer displayed perinuclear staining but became completely filled with Alz50 reaction product (Figure 5(h)) or were dystrophic (data not shown). While the presence of Alz50-ir dystrophic neurites appeared concomitantly with the onset of Aβ plaque deposition between 8 and 9 months of age in female mutant mice, dramatic differences between male and female Alz50 staining were only apparent by 18–20 months of age. The dorsal and anterior subicular region adjacent to the CA1 neurons was most affected with Alz50-ir dystrophic neurites in male and female 18–20-month-old 3xTg-AD mice (Figures 5(j) and 5(m)). In general, numerous large and globular dystrophic Alz50-ir neurites were seen surrounded by plaques in both male and female mice (Figures 5(m) and 5(n)). In female transgenic mice many plaques displayed a rim of dark Alz50-ir dystrophic neurites with a clear center (Figure 5(k)), while in males this neuritic organization was less obvious (Figure 5(n)). In addition, in 18–20-month-old female 3xTg-AD mice dark, swollen, Alz50-ir dystrophic neurons were found in abundance among more lightly stained CA1 pyramidal cells (Figures 5(m) and 5(o)). Furthermore, the amygdala displayed similar neuronal perinuclear staining in male and female transgenic mice with an occasional rim of Alz50-ir dystrophic neurites surrounding plaques only in female mutant mice (data not shown).

3.3.2. MC1 Immunoreactivity. The MC1 antibody recognizes early stage conformational epitopes similar to Alz50 but does not react with normal neuronal tau [34, 35, 37]. In contrast to Alz50 staining, lightly stained MC1-ir neurons were found only in the CA1 pyramidal cells of the ventral hippocampus in 3-week-old 3xTg-AD mice (Figure 6(a)). By 2–4 months, lightly stained MC1-ir neurons were seen throughout the CA1 subfield of the ventral hippocampus (Figure 6(b)). A few darkly stained MC1 neurons were seen, some of which appeared shrunken with blunted dendrites within the hippocampus. On the other hand, no MC1-ir neurons were seen in the BLA at 3 weeks of age (Figure 6(d)). In

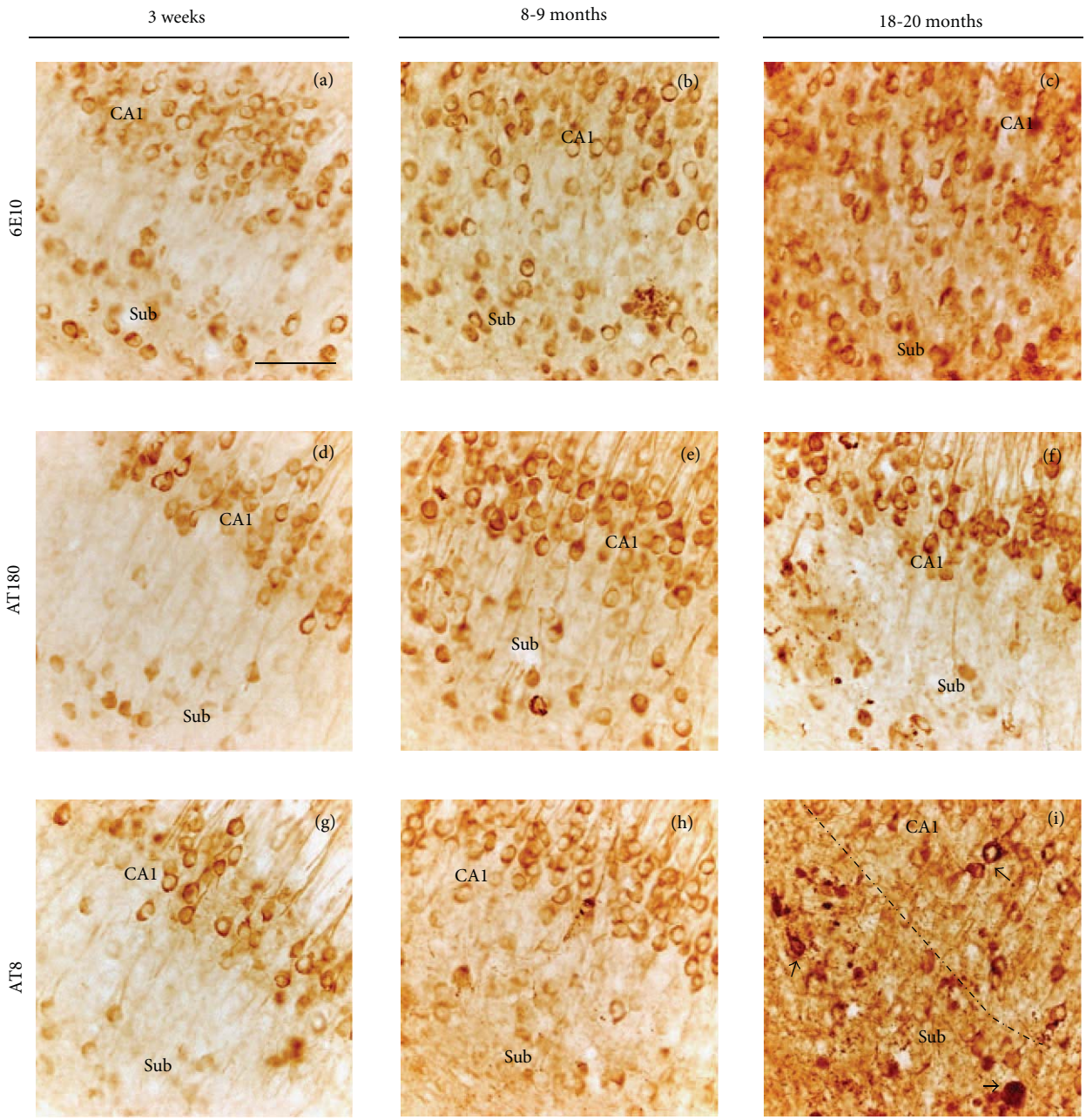

Figure 12: Light microscopic images of adjacent sections showing 6E10, AT180, and AT8 immunoreactive profiles in CA1 and subiculum in 3-week, 9-, and 18–20-months-old 3xTg-AD mice. AT180 and AT8 immunostained CA1 and subicular neurons were present at each age examined. This is in contrast to the Alz50, which only stained neurons in the CA1 field (see Figure 11). The arrows in F and I indicate dystrophic AT8 subicular neurons. Dashed line in (i) demarcates the CA1 field from the subiculum. Scale bar in (a) is the same for all panels = 50 μm.

2–4-month-old mutant mice, scattered round-or-oval shaped lightly stained MC1-ir neurons were found embedded within the MC1 immuopositive neuropil of the BLA. Interestingly, MC1-ir neuropil and neuronal labeling decreased in the hippocampus and BLA in 8-9-month-old mutant mice (Figures 6(c) and 6(f)). MC1-ir profiles were not detected in the neo- and limbic cortex up to 9 months of age. By 18–20 months, MC1 labeling matched Alz50 immunoreactivity in male and female 3xTg-AD mice. Although plaque-like structures were hard to detect, globular MC1-ir dystrophic neurites and neurons were found mainly throughout the female subiculum (Figures 6(j), 6(k), and 6(l)). Some dystrophic neurons appeared to have eccentrically located dark cytoplasmic neuronal inclusions (Figures 6(i), 6(k), and 6(l)).

3.3.3. AT8 Immunoreactivity. Hyperphosphorylated microtubule-associated protein tau is the major component of the

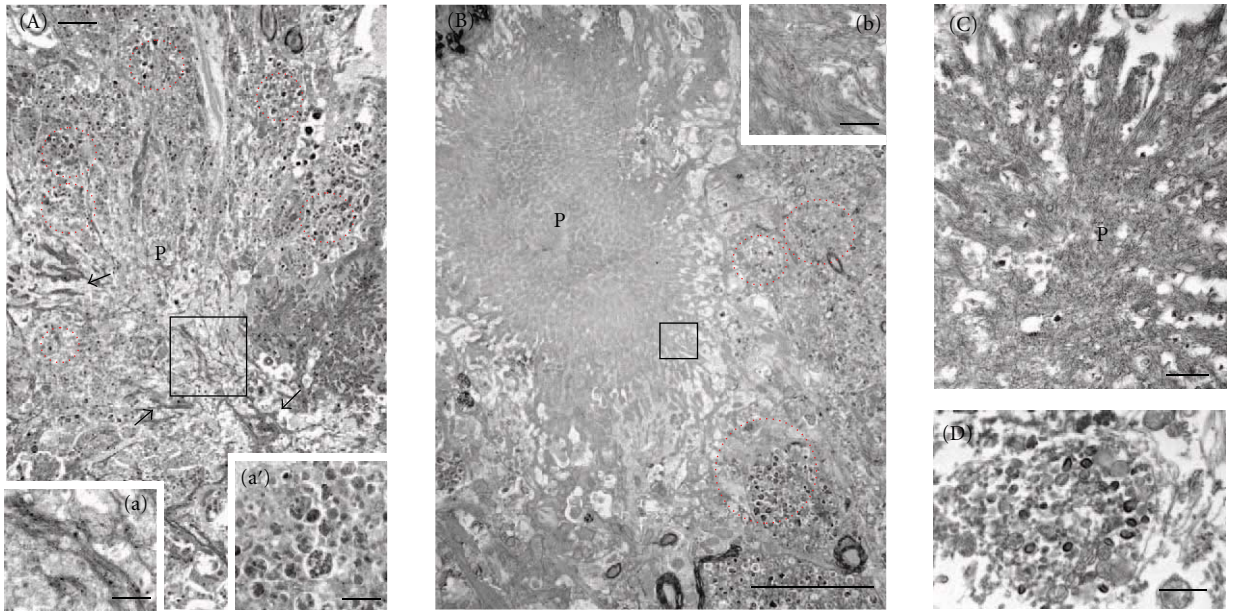

Figure 13: Electron microphotographs showing neuritic plaques (p) surrounded by numerous dystrophic neurites (dotted-red circles) in tissue sections through the hippocampal-subicular complex of a 9-(A) and 23-(B) month-old 3xTg-AD female mouse. Boxed area (a) shows details of the fibrillar material from amyloid plaque in A. a′ shows an example of a dystrophic neurite from a 9-month-old 3xTg-AD containing electron-dense multilaminar, multivesicular, and dense-core bodies similar to that seen in the cortex of a patient with AD (D). Note that at 23 months of age neuritic plaques show an electron dense center core (B) with numerous fibrillar branches (b) similar to a neuritic plaque seen in AD (c). Abbreviation: n: nucleus. Scale bars: A = 2 μm, B = 5 μm, C, a, b = 0.5 μm, and D, a′ =1 μm.

paired helical filament seen in the NFT. The monoclonal antibody AT8 marks tau phosphorylation at both serine 202 and threonine 205 [29]. AT8-ir neurons were found in the neocortex, amygdala, and hippocampal formation in both male and female 3xTg-AD mice at all ages examined (Figure 7). Like the distribution of Alz50-ir neurons, hippocampal and subicular regions contained the highest number of AT8-ir neurons compared to the cortex and amygdala in 3-week-old 3xTg-AD mice (Figures 7(a)–7(d)). A few AT8-ir neurons were observed in layer 5 of the fronto-parietal cortex and BLA (Figures 7(a)–7(c)). As mutant mice age, the extent of neuronal AT8 labeling in the hippocampal complex increased in a ventral to dorsal and posterior to anterior gradient (Figures 7(e)–7(l)), but unlike the Alz50-ir profiles at 5-6 months of age, anterior portions of the hippocampal complex did not appear to be affected (Figures 7(c), 7(g), and 7(k)). At 3 weeks of age, AT8-ir neurons displayed more diffuse cytoplasmic staining in the cortex, hippocampus, and BLA (Figures 8(a), 8(d), and 8(g)), rather than the dense perinuclear staining observed in Alz50-ir neurons in these regions. However by 9 months of age AT8-ir neurons appeared shrunken, distorted, and showed thicker perinuclear staining, especially in the amygdala (Figures 8(b), 8(e), and 8(h)). Some neurons in the hippocampus (Figure 8(e)), BLA (Figure 8(h)), and subiculum displayed blunted AT8-ir dendrites. AT8 dystrophic neurons were more abundant in the female subiculum and constituted the greatest difference between male and female pathology at 18–20 months of age (Figures 8(j)–8(o)). While the entire extent of the female subiculum showed numerous AT8-ir dystrophic neurites, the male subiculum contained less neuritic dystrophy (Figure 8(j) versus Figure 8(m)). AT8-ir pyramidal cells displayed an asymmetric accumulation of dense perinuclear staining (Figures 8(k) and 8(o)), and AT8-ir dystrophic neurites were associated with plaques (Figures 8(l), 8(n)).

3.3.4. AT180 Immunoreactivity. AT180 detects tau phosphorylation at the Thr231 site, an early event in the assembly of tau into filaments [27, 28]. AT180-ir neurons displayed the greatest number and spatial distribution of all tau antibodies examined at 3 weeks of age in 3xTg-AD mice. AT180-ir neurons were found in layer 5 of the fronto-parietal cortex, BLA, CA1 ventral hippocampus, and subiculum (Figures 9(a), 9(d), and 9(g)). Qualitatively there was an age-related increase in the number of AT180-ir neurons within each brain region examined as well as in the intensity of neuropil staining in the ventral hippocampus and BLA (Figures 1(s)–1(x)). At 3 weeks of age AT180 immunostaining appeared as diffuse cytoplasmic reactivity in round or oval pyramidal cells of the neocortex, hippocampus (Figures 9(a) and 9(d)) and BLA (Figure 9(g)) in 3xTg-AD mice. Some neurons embedded in the CA1 pyramidal cell layer, BLA, and subiculum displayed perinuclear staining (Figures 9(d) and 9(g)). By 9 months, AT180-ir hippocampal and BLA neurons revealed blunted staining in dendrites (Figure 9(e)). In the BLA, a number of neurons exhibited thickened perinuclear staining (Figure 9(h)). Differences between male and female AT180 staining occurred in the hippocampal CA1 neurons and the subiculum at older ages. Specifically, at 18–20

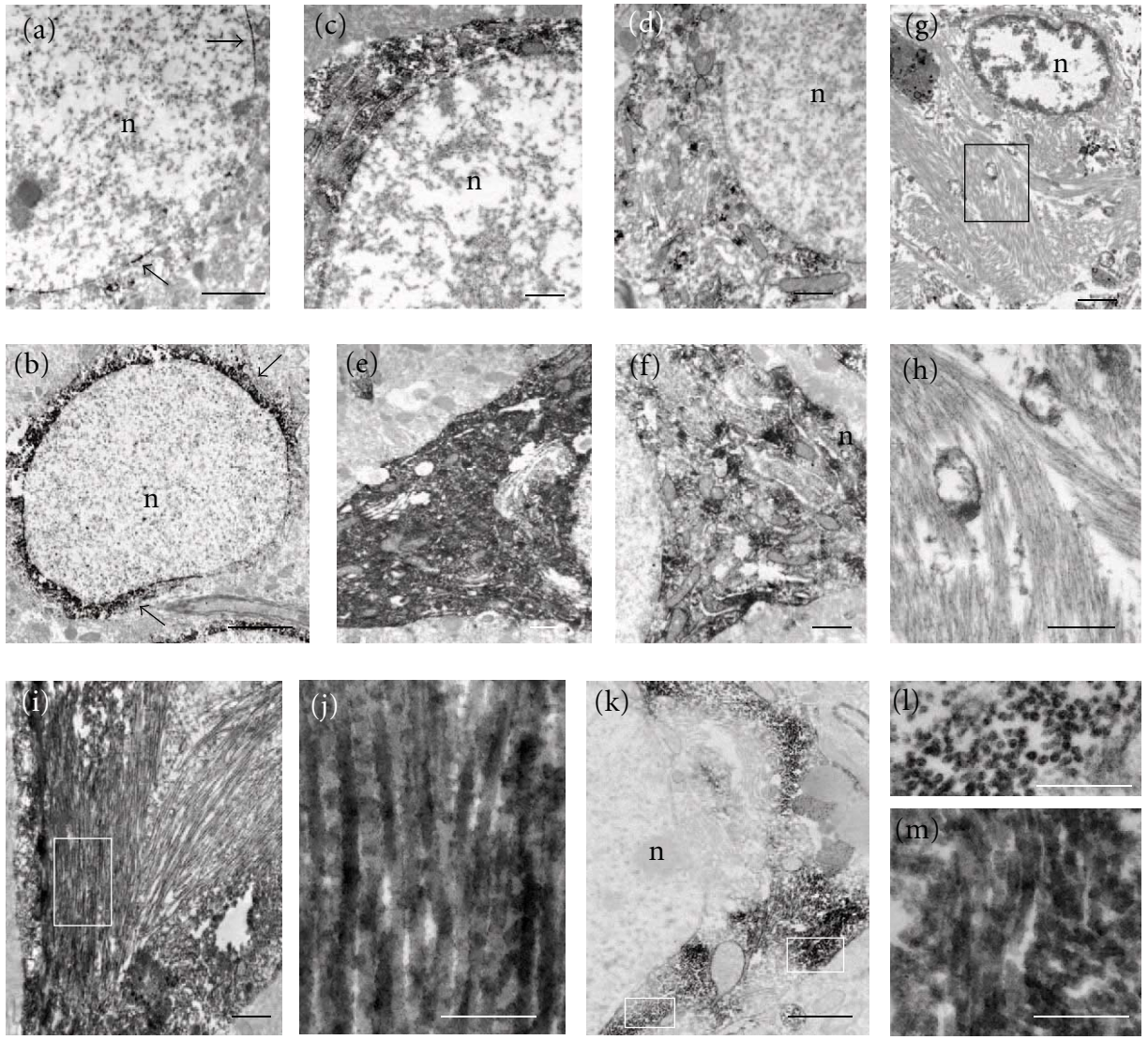

Figure 14: Electron photomicrographs showing perinuclear and cytoplasmic 6E10 immunoreactivity (black arrows) in hippocampal/subicular complex neurons at 2- (a) and 9- (b) month-old 3xTg-AD mice. Micrographs showing scattered Alz50 (c) and AT8 (d) immunoreactivity in hippocampal/subicular complex neurons in 2-month-old 3xTg-AD mice, whereas at 9 months Alz50 (e) and AT8 (f) immunoreactivity was increased, without the formation of filaments as seen in AD (g). Boxed area shows a higher-magnification photograph of the morphology of paired helical filaments in the AD brain (h). Photomicrographs of Alz50 ((i) and (j)) and AT8-ir ((k)–(m)) filaments in hippocampal/subicular complex neurons at 23 months in the 3xTg-AD mouse. J, Panel shows detail of straight Alz50-ir filaments from the white boxed area in (i). (l) and (m) areas containing AT8-ir filaments are outlined in white in panel k showing AT8 positive filaments in cross (l) and longitudinal (m) profile. Abbreviation: n: nucleus. Scale bars in (a), (b), (g) =2 μm, (c), (d), (f), (k) = 1 μm, (e), (i), (h) = 0.5 μm and (j), (l), (m) = 200 nm.

months of age AT180-ir dystrophic neurites were more widespread within the subiculum in female compared to male 3xTg-AD mice (Figures 9(j) and 9(m)). However, in male mice, AT180-ir dystrophic pathology was mainly found in the subiculum closest to the border with the CA1 pyramidal cell layer. In addition, CA1 pyramidal neurons displayed a dense perinuclear staining and blunted dendrites (Figures 9(l) and 9(o)).

3.3.5. PHF-1 Immunoreactivity. PHF-1 recognizes tau phosphorylated at serine residues 396 and 404 and is generally considered a late marker in the evolution of PHF positive NFTs [30–32]. At 3 weeks of age only a few lightly stained PHF-1-ir neurons were observed in the CA1 region of the ventral hippocampus and the BLA in perfusion fixed 3xTg-AD mice (Figures 10(d) and 10(g)). At 2-3 months, a few PHF-ir neurons were seen at the CA1/subicular interface of the dorsal hippocampus (data not shown). By 9 months, the number of PHF-1-ir ventral hippocampal CA1 pyramidal and BLA neurons increased (Figures 10(e) and 10(h)). The distribution of PHF-ir neurons in the hippocampal complex followed a ventral to dorsal gradient. Up to 9 months of age,

an occasional PHF-1-ir neuron was visible in the neocortex (Figure 10(b)). PHF-1 dystrophic neurons and neurites were more prevalent in the subiculum of aged females (Figures 10(m) and 10(n)) compared to aged males (Figures 10(j) and 10(k)). PHF-1-ir CA1 neurons displayed distorted cellular morphology, with broken, asymmetric, but strongly stained perinuclear staining in the female subiculum (Figure 10(o)). In contrast, PHF-1-ir neurons in the male subiculum showed similarly stained dark neurons but retained somatodendritic staining (Figure 10(l)).

3.4. Colocalization of 6E10 and Alz50 Immunoreactive Neurons. To evaluate whether neurons expressing 6E10 also contained tau epitopes we performed dual immunofluorescence and comparative light microscopic experiments on adjacent hippocampal subicular sections at 3-week, 9-, and 18–20-month old male and female 3xTg-AD mice. Although it would have been interesting to double stain for 6E10 and other tau makers (AT180 and AT8), all three antibodies are murine IgG1s. Therefore, dual immunofluorescence experiments were performed only for 6E10 and Alz50, an IgM. In these experiments we observed two bands of 6E10 immnoreactivity located within ventrally located within CA1 hippocampal and subiculum neurons of female mutant mice at all ages examined (Figures 11(a), 11(d), and 11(g)). By contrast, Alz50-ir neurons were only observed in the CA1 pyramidal cell layer, and as neuropil staining in the subiculum (Figures 11(b), 11(e), and 11(h)). In general, Alz50-ir neurons were found to be colocalized with 6E10-ir neurons at each age examined in the ventral hippocampus (Figures 11(c), 11(f), and 11(i)).

Because 6E10, AT180, or AT8 are all of the murine IgG1 subclass, adjacent sections through the CA1 and subicular fields were reacted with individual antibodies and visualized using peroxidase/DAB. In contrast to the single layer of Alz50-ir neurons in the CA1 pyramidal cell layer (Figures 12(b), 12(e), and 12(h)), numerous AT180, AT8, and 6E10 immunopositive neurons were seen in both CA1 and subicular fields in the ventral hippocampus at each age examined (Figure 12).

3.5. Ultrastructural Analysis of Amyloid and Tau Containing Structures in 3xTg-AD Mice. At the ultrastructural level, unstained tissue sections revealed plaques within the hippocampal/subicular complex that displayed numerous fibrillar branches, which were surrounded by dystrophic neurites in 9-month-old 3xTg-AD mice (Figure 13(a)). In 23-month-old female 3xTg-AD mice, the majority of neuritic plaques displayed a central core surrounded by many more fibrillar branches and dystrophic neurites, similar to that seen in human AD plaques (Figure 13(c)). The neuropil contained dystrophic neurites of different sizes displaying various accumulations of electron-dense cytoplasmic material, multilaminar, multivesiclular, and dense-core bodies in both 9- and 23-month-old 3xTg-AD mice (Figures 13(a) and 13(b)), similar to that seen in an AD plaque (Figure 13(d)). TEM analysis of intraneuronal 6E10 immunoreactivity revealed staining mainly confined to the periphery of the nucleus within CA1 hippocampal/subicular neurons in 2-month-old 3xTg-AD mice (Figure 14(a)). At 9 months of age this perinuclear 6E10 reaction product appeared more intense and extended into the cytoplasm (Figure 14(b)).

At the ultrastructural level, Alz50 and AT8-ir were seen in the soma and dendrites of CA1 neurons in female 2-month-old mutant mice (Figures 14(c) and 14(d)). Intraneuronal electron dense Alz50 and AT8-ir cytoplasmic staining was more widespread and increased in intensity in 9 month-old-mutant mice (Figures 14(e) and 14(f)). Interestingly, cytoplasmic Alz50-ir appeared more extensive than AT8 immunoreactivity in these neurons at both 2 and 9 months of age (Figures 14(c), 14(d), 14(e), and 14(f)). Despite the presence of AT8 and Alz50-ir cytoplasmic labeling within hippocampal/subicular CA1 neurons, TEM failed to reveal any type of filamentous aggregates in 2- or 9-month-old 3xTg-AD mice (Figures 14(c), 14(d), 14(e), 14(f), 14(l), and 14(m)). In contrast, at 23 months of age both male and female 3xTg-AD mice displayed Alz50 and AT8-ir straight filaments with a 19–20 nm diameter within the hippocampal-subicular complex (Figures 14(i)–14(m)).

4. Discussion

Previous studies have shown widespread amyloid but not tau pathology at 6 months of age in the hippocampus [3, 12, 13, 17], and behavioral studies using the Morris Water Maze have demonstrated memory retention deficits dependent upon the appearance of amyloid pathology at 6- but not 2-month-old 3xTg-AD mice [11]. Our study found that (1) the appearance of 6E10 immunoreactivity was concomitant with conformation (Alz50 and MC1) and phosphorylation (AT8, AT180, and PHF-1) events in the neurons of the hippocampal-subicular complex and amygdala as early as 3 weeks of age; (2) the detection of the two phospho-epitopes AT8 and PHF-1 was fixation dependent at all ages; (3) the number of Aβ plaques, as well as neuritic and neuronal dystrophy, increased with age in the cortex, hippocampus, and subicular area in 3xTg-AD mice; (4) aged female mice displayed more plaque and tau pathology than aged male 3xTg-AD mice; and finally (5) straight tau filaments were found only in 23-month-old female 3xTg-AD mice.

In the present study, 6E10-ir neurons were seen as early as 3 weeks of age in lamina 3 and 5 of the fronto-parietal cortex, deep layers of the cingulate cortex, CA1 pyramidal neurons of the hippocampus, subiculum, and BLA in 3xTg-AD mice independent of gender. These data indicate that intraneuronal 6E10 immunoreactivity occurs extremely early in the development of these mice (3 weeks) and are in contrast to previous investigations showing that 6E10 intraneuronal staining occurred between 3 and 6 months of age in the hippocampus of these mice [12, 17]. Because the 6E10 epitope resides in amino acids 3–8 of the N-terminal portion of the Aβ sequence, it does not preclude binding to full length APP or its amyloidgenic derivatives. Consequently, the exact amyloid species revealed within neurons at 3 weeks of age in 3xTg-AD mice and at other ages examined is unclear. Oligomeric Aβ species may, in part, underlie cellular degeneration [3, 11, 38–48].

We also observed many shrunken 6E10-ir neurons beginning at 8-9 month of age in each brain area examined in both male and female 3xTg-AD mice. This phenotype was most pronounced in CA1 hippocampal neurons of older female 3xTg-AD mice. These neurons exhibited loss of dendritic 6E10 immunoreactivity when compared to CA1 neurons in male mutant mice. These gender differences in Aβ intraneuronal pathology lend support to prior investigations showing that female 3xTg-AD mice display earlier and more severe plaque pathology [16], which may be related to progesterone and estrogen-mediated signaling [49]. However, other factors may contribute to the discrepancies in AD-like pathology reported in studies using different colonies of 3xTg-AD mice, including a loss of phenotype related to successive breeding, founder effects between colonies, or differential expression of transgenes [16]. Together or separately, variations in transgenic animal strain or amyloid species may affect both pathological and behavioral observations reported in studies using 3xTg-AD mice.

Of interest was the observation that the immunohistochemical localization of phosphospecific tau proteins AT8 and PHF-1 was fixation dependent, whereas Alz50, MC1, AT180, and 6E10 immunoreactivity was fixation independent in young, juvenile, and middle age 3xTg-AD mice. Notably, neurons containing the phospho-epitope AT8 were seen in layer 5 of frontoparietal cortex, ventral hippocampal pyramidal, and amygdala neurons, whereas PHF-1-ir intraneuronal staining was seen only in the ventral hippocampus in perfusion-fixed 3-week-old 3xTg-AD mice. Previous biochemical and immunohistochemical studies indicate that fixative composition affects the ability to detect various cytoskeletal proteins [18, 22, 23]. The process of aldehyde fixation relies upon a slow cross-linking of carbonyl aldehyde to functional protein groups. While perfusion fixation rapidly exposes proteins to fixative through the vasculature, immersion fixation relies upon a slow 1 mm per hour diffusion rate to penetrate tissue [20]. It is possible during immersion fixation that proteolysis or dephosphorylation of the tau phospho-epitopes recognized by AT8 and PHF-1 occurs prior to the full penetration of the fixative. Since immersion-fixed tissue reacts with C-terminal, N-terminal, and internal tau antibodies, proteoloysis of tau is unlikely [25, 50]. A more plausible possibility is the destruction of AT8 and PHF-1 epitopes by the action of endogenous phosphatases during slow immersion fixation [51–53]. However, AT180 immunoreactivity remained robust even in immersion-fixed tissue. Likely, phosphatases act differentially depending on the individual tau phosphoepitopes [54]; hence, it is possible that the AT180 phospho-epitope is less sensitive to phosphatase activity than either AT8 or PHF-1 phosphorylation sites, resulting in a more robust staining in immersion-fixed tissue. Although long postmortem intervals reduce phospho-tau antigenicity due to active phosphatases, [19, 50, 55], this was not a confounding variable in the present study since all animals were sacrificed and perfused with fixative within 5 minutes of anesthetization. The potential effect of fixation on the immunolocalization of tau and other proteins [56] represents an important caveat that may provide an explanation for the underlying differences in tau antigenicity reported in previous studies using the 3xTg-AD mouse model [3, 12–14, 16, 57, 58].

Although a previous report described intraneuronal MC1-ir CA1 dorsal hippocampal neurons only in 12–15-month-old 3xTg-AD mice [12], the present study displayed weak MC1 immunoreactive neurons in the ventral hippocampus even as early as 3 weeks of age. We also observed Alz50 immunoreactive CA1 pyramidal and subicular neurons in the ventral aspect of the hippocampal/subicular complex at 3 weeks of age. Although both MC1 and Alz50 antibodies recognize similar epitopes, they are not identical. Overall, Alz50 immunoreactivity was much more intense and labeled a greater distribution of immunoreactive neurons than with the MC1 antibody. While Alz50 immunoreactivity increased in an age dependent manner in the neocortex, hippocampus, and amygdala, MC1 immunoreactivity exhibited a biphasic response, peaking initially between 2 and 4 months, declining at 9 months and then peaking again at 18–20 months in numerous swollen, tangle-like appearing CA1 hippocampal and subicular neurons. Interestingly, both MC1 and Alz50-ir neurons were found in the CA1 pyramidal but not the subicular cell layer in the ventral hippocampal formation at the ages examined suggesting that Alz50 is labeling similar populations of neurons.

Unlike previous studies where various phosphotau epitopes were immunohistochemically detectable by 15 months of age in 3xTg-AD mice [12, 17, 49], we observed tau-ir neurons primarily in the ventral CA1 hippocampal pyramidal and subicular neurons at 3-weeks of age. This occurred well before the onset of plaque deposition in 8-9-month-old 3xTg-AD mice [17]. The current findings indicate that intraneuronal amyloid and tau co-occur or appear concurrent in the same neurons at least as early as 3 weeks of age suggesting that these mutant mice are born with the dual expression of these proteins within select populations of brain cells. The early appearance of tau-ir neurons in the forebrain of 3xTg-AD mice is not surprising since overexpression of mutant P301L four repeat tau and the APP_{swe} amyloid mutation together [59] or tau P301L alone [60] induces an age dependent onset of MC1, AT8, and PHF-ir neurofibrillary tangles (NFTs) in the telencephalon of mutant mice as young as 2.5 months of age [60].

However, it remains to be determined whether amyloid interacts with tau over time to induce the apparent age-related perikaryal degeneration seen in these mice. Studies are underway to test the hypothesis that depletion of intraneuronal amyloid at an early age would prevent or slow the degeneration of neurons in these mice. It is interesting to note that tau containing straight filaments were seen in 18–20-month-old mutant mice suggesting that late-stage tau neuronal aggregation also plays a key role in the ultimate demise of neurons in 3xTg-AD mice. Although no studies to date have shown frank neuronal cell loss, a recent report described a reduction in the number of neurons containing 6E10 and tau markers in the brainstem of these mutant mice [15].

To more fully understand the vulnerability of hippocampal complex neurons, we colocalized 6E10 and Alz50 using immunofluorescence. A previous study colocalized HT7,

a human specific pan tau antibody and M71/3 (oligomeric Aβ) in the dorsal hippocampus in 3xTg-AD mice [3]. However, at earlier ages conformation or phosphospecific tau antibodies were not evaluated. Our immunofluorescence colocalization experiments demonstrated that virtually all ventral CA1 pyramidal but not all subicular neurons contained both Alz50 and 6E10 from 3 weeks to at least 18–20 months of age, suggesting that CA1 neurons are more vulnerable to Alz50 pathology. Although we were unable to perform colocalization experiments between 6E10 and our tau antibodies, we performed a comparative light microscopic analysis of adjacent hippocampal sections. This study revealed AT180 and AT8-ir neurons in the caudal aspects of the subicular region where we failed to visualize Alz50-ir neurons across all ages examined. The reason for the selective appearance of AT180 and AT8 in the ventral subiculum remains unknown. One possibility is that neurofibrillary pathology proceeds according to a sequence of tau conformational and phosphorylation events [61–64], which may vary between neuronal populations. In AD, as tau transitions to a more hyperphosphorylated state, it undergoes a self-assembly process forming PHF structures reducing the microtubule stability of the neuronal cytoskeleton [65, 66]. More specifically, the evolution of NFTs in AD follows a progression of phosphorylated tau modifications from TG3 (phosphospecific at Thr231), found in preneurofibrillary tangles (preNFTs), to AT8 and PHF-1 in intraneuronal and extraneuronal NFTs [61]. This progression may be dynamic since intraneuronal AT180 and AT8 precedes Alz50 tau formation before the appearance of fibrillar tau [63, 64]. We suggest that the sequence of cellular tau conformation and phosphorylation events may also be dynamic in 3xTg-AD mice since Alz50-ir neurons were found only in CA1 neurons in the hippocampus but not in the underlying subiculum.

Despite differences in tau intraneuronal epitope expression, we found age-related changes in neuronal morphology in the 3xTg-AD mouse to be similar to the NFT neuronal phenotypes described in the human AD brain [67, 68]. Some AT8-ir neurons at 9 months of age displayed blunted dendrites (see Figure 8(e)) or tortuous proximal dendrites and thickened perinuclear staining reminiscent of Braak type 2 neurons [67]. In our aged mutant mice, proximal and distal dendrites lost AT8 immunoreactivity and neurons appeared more globose and dystrophic similar to Braak type 3 neurons, which accumulate fibrillar material in the human AD brain [67]. Furthermore, the present ultrastructural analysis revealed, for the first time, the presence of AT8 and Alz50 positive straight tau filamentous aggregates in female aged 23-month-old, but not in young or middle-age 3xTg-AD mice of the same gender, which are similar to those seen in tangle bearing neurons in the human AD brain. Similar tau filaments have been described in single transgenic mice overexpressing the mutant P301L human tau gene [10, 59] as well as in the double mutant (TAPP) mouse expressing APP_{swe} and P301L mutant forms of tau [59]. NFT formation was enhanced in young and middle age TAPP mutant mice with respect to single tau transgenic mice [59]. Although young and middle-aged 3xTg-AD mice carry the same APP_{swe}, and Tau_{P301L} mutations as the TAPP mouse, 3xTg-AD mice did not accumulate filamentous aggregates at younger ages. In this regard, mice overexpressing human genomic and cDNA tau genes also do not display intraneuronal filamentous structures at young ages [69]. These findings suggest that factors other than the accumulation of tau underlie the filamentous tangle bearing phenotype seen in human AD. Factors that may influence the formation of AD filaments include differences in the abundance or ratio of specific tau isotypes [70] in different cohorts of neurons and/or minor alterations in proteases, kinases, phosphatases that alter the structure of these proteins during the life span of the neuron [25], and/or the promoter system designed for specific transgene expression in particular brain regions. Since age is a major risk factor for AD, aging itself may be a crucial variable in the formation of intraneuronal filaments in 3xTg-AD mice. Despite differences in the evolution of tau biochemistry, there are morphological similarities between neurons containing tau in 3xTg-AD mice and human AD indicating the usefulness of these mice for studies of the mechanism(s) underlying select aspects of AD pathology.

Acknowledgments

This work is supported in part by AG10688 (EJM), AG014449 (LIB), Shapiro Foundation (EJM), and Rush University Medical Center Research Council (SEP). The authors thank Linda Juarez for her excellent electron microscopic work.

References

[1] J. L. Eriksen and C. G. Janus, "Plaques, tangles, and memory loss in mouse models of neurodegeneration," *Behavior Genetics*, vol. 37, no. 1, pp. 79–100, 2007.

[2] D. Games, D. Adams, R. Alessandrini et al., "Alzheimer-type neuropathology in transgenic mice overexpressing V717F β-amyloid precursor protein," *Nature*, vol. 373, no. 6514, pp. 523–527, 1995.

[3] S. Oddo, A. Caccamo, L. Tran et al., "Temporal profile of amyloid-β (Aβ) oligomerization in an in vivo model of Alzheimer disease: a link between Aβ and tau pathology," *Journal of Biological Chemistry*, vol. 281, no. 3, pp. 1599–1604, 2006.

[4] J. Götz, N. Deters, A. Doldissen et al., "A decade of tau transgenic animal models and beyond," *Brain Pathology*, vol. 17, no. 1, pp. 91–103, 2007.

[5] J. Götz, J. R. Streffer, D. David et al., "Transgenic animal models of Alzheimer's disease and related disorders: histopathology, behavior and therapy," *Molecular Psychiatry*, vol. 9, no. 7, pp. 664–683, 2004.

[6] T. L. Spires and B. T. Hyman, "Transgenic models of Alzheimer's disease: learning from animals," *NeuroRx*, vol. 2, no. 3, pp. 423–437, 2005.

[7] B. Allen, E. Ingram, M. Takao et al., "Abundant tau filaments and nonapoptotic neurodegeneration in transgenic mice expressing human P301s tau protein," *Journal of Neuroscience*, vol. 22, no. 21, pp. 9340–9351, 2002.

[8] J. Götz, F. Chen, R. Barmettler, and R. M. Nitsch, "Tau filament formation in transgenic mice expressing P301L tau," *Journal of Biological Chemistry*, vol. 276, no. 1, pp. 529–534, 2001.

[9] J. Lewis, E. McGowan, J. Rockwood et al., "Neurofibrillary tangles, amyotrophy and progressive motor disturbance in mice expressing mutant (P301L)tau protein," *Nature Genetics*, vol. 25, no. 4, pp. 402–405, 2000.

[10] W.-L. Lin, J. Lewis, S.-H. Yen, M. Hutton, and D. W. Dickson, "Ultrastructural neuronal pathology in transgenic mice expressing mutant (P301L) human tau," *Journal of Neurocytology*, vol. 32, no. 9, pp. 1091–1105, 2003.

[11] L. M. Billings, S. Oddo, K. N. Green, J. L. McGaugh, and F. M. LaFerla, "Intraneuronal Aβ causes the onset of early Alzheimer's disease-related cognitive deficits in transgenic mice," *Neuron*, vol. 45, no. 5, pp. 675–688, 2005.

[12] S. Oddo, A. Caccamo, M. Kitazawa, B. P. Tseng, and F. M. LaFerla, "Amyloid deposition precedes tangle formation in a triple transgenic model of Alzheimer's disease," *Neurobiology of Aging*, vol. 24, no. 8, pp. 1063–1070, 2003.

[13] S. Oddo, A. Caccamo, J. D. Shepherd et al., "Triple-transgenic model of Alzheimer's disease with plaques and tangles: intracellular Aβ and synaptic dysfunction," *Neuron*, vol. 39, no. 3, pp. 409–421, 2003.

[14] S. Oddo, A. Caccamo, I. F. Smith, K. N. Green, and F. M. LaFerla, "A dynamic relationship between intracellular and extracellular pools of Aβ," *American Journal of Pathology*, vol. 168, no. 1, pp. 184–194, 2006.

[15] C. R. Overk, C. M. Kelley, and E. J. Mufson, "Brainstem Alzheimer's-like pathology in the triple transgenic mouse model of Alzheimer's disease," *Neurobiology of Disease*, vol. 35, no. 3, pp. 415–425, 2009.

[16] C. Hirata-Fukae, H.-F. Li, H.-S. Hoe et al., "Females exhibit more extensive amyloid, but not tau, pathology in an Alzheimer transgenic model," *Brain Research*, vol. 1216, pp. 92–103, 2008.

[17] M. A. Mastrangelo and W. J. Bowers, "Detailed immunohistochemical characterization of temporal and spatial progression of Alzheimer's disease-related pathologies in male triple-transgenic mice," *BMC Neuroscience*, vol. 9, article 81, 2008.

[18] C. J. Conti, F. Larcher, J. Chesner, and C. M. Aldaz, "Polyacrylamide gel electrophoresis and immunoblotting of proteins extracted from paraffin-embedded tissue sections," *Journal of Histochemistry and Cytochemistry*, vol. 36, no. 5, pp. 547–550, 1988.

[19] E. S. Matsuo, R.-W. Shin, M. L. Billingsley et al., "Biopsy-derived adult human brain tau is phosphorylated at many of the same sites as Alzheimer's disease paired helical filament tau," *Neuron*, vol. 13, no. 4, pp. 989–1002, 1994.

[20] C. H. Fox, F. B. Johnson, J. Whiting, and P. P. Roller, "Formaldehyde fixation," *Journal of Histochemistry and Cytochemistry*, vol. 33, no. 8, pp. 845–853, 1985.

[21] N. J. Pollock and J. G. Wood, "Differential sensitivity of the microtubule-associated protein, tau, in Alzheimer's disease tissue to formalin fixation," *Journal of Histochemistry and Cytochemistry*, vol. 36, no. 9, pp. 1117–1121, 1988.

[22] B. M. Riederer, "Antigen preservation tests for immunocytochemical detection of cytoskeletal proteins: influence of aldehyde fixatives," *Journal of Histochemistry and Cytochemistry*, vol. 37, no. 5, pp. 675–681, 1989.

[23] B. M. Riederer, R. Porchet, R. A. Marugg, and L. I. Binder, "Solubility of cytoskeletal proteins in immunohistochemistry and the influence of fixation," *Journal of Histochemistry and Cytochemistry*, vol. 41, no. 4, pp. 609–616, 1993.

[24] J. Q. Trojanowski, M. A. Obrocka, and V. M.-Y. Lee, "Distribution of neurofilament subunits in neurons and neuronal processes: immunohistochemical studies of bovine cerebellum with subunit-specific monoclonal antibodies," *Journal of Histochemistry and Cytochemistry*, vol. 33, no. 6, pp. 557–563, 1985.

[25] J. Q. Trojanowski, T. Schuck, M. L. Schmidt, and V. M.-Y. Lee, "Distribution of tau proteins in the normal human central and peripheral nervous system," *Journal of Histochemistry and Cytochemistry*, vol. 37, no. 2, pp. 209–215, 1989.

[26] J. C. Vickers, B. M. Riederer, R. A. Marugg, et al., "Alterations in neurofilament protein immunoreactivity in human hippocampal neurons related to normal aging and Alzheimer's disease," *Neuroscience*, vol. 62, no. 1, pp. 1–13, 1994.

[27] M. Goedert, R. Jakes, R. A. Crowther et al., "Epitope mapping of monoclonal antibodies to the paired helical filaments of Alzheimer's disease: identification of phosphorylation sites in tau protein," *Biochemical Journal*, vol. 301, no. 3, pp. 871–877, 1994.

[28] M. Mercken, M. Vandermeeren, U. Lubke et al., "Monoclonal antibodies with selective specificity for Alzheimer Tau are directed against phosphatase-sensitive epitopes," *Acta Neuropathologica*, vol. 84, no. 3, pp. 265–272, 1992.

[29] M. Goedert, R. Jakes, and E. Vanmechelen, "Monoclonal antibody AT8 recognises tau protein phosphorylated at both serine 202 and threonine 205," *Neuroscience Letters*, vol. 189, no. 3, pp. 167–169, 1995.

[30] S. G. Greenberg and P. Davies, "A preparation of Alzheimer paired helical filaments that displays distinct τ proteins by polyacrylamide gel electrophoresis," *Proceedings of the National Academy of Sciences of the United States of America*, vol. 87, no. 15, pp. 5827–5831, 1990.

[31] E. Lang, G. I. Szendrei, V. M.-Y. Lee, and L. Otvos Jr., "Immunological and conformational characterization of a phosphorylated immunodominant epitope on the paired helical filaments found in Alzheimer's disease," *Biochemical and Biophysical Research Communications*, vol. 187, no. 2, pp. 783–790, 1992.

[32] L. Otvos Jr., L. Feiner, E. Lang, G. I. Szendrei, M. Goedert, and V. M.-Y. Lee, "Monoclonal antibody PHF-1 recognizes tau protein phosphorylated at serine residues 396 and 404," *Journal of Neuroscience Research*, vol. 39, no. 6, pp. 669–673, 1994.

[33] G. Carmel, E. M. Mager, L. I. Binder, and J. Kuret, "The structural basis of monoclonal antibody Alz50's selectivity for Alzheimer's disease pathology," *Journal of Biological Chemistry*, vol. 271, no. 51, pp. 32789–32795, 1996.

[34] G. A. Jicha, B. Berenfeld, and P. Davies, "Sequence requirements for formation of conformational variants of tau similar to those found in Alzheimer's disease," *Journal of Neuroscience Research*, vol. 55, no. 6, pp. 713–723, 1999.

[35] G. A. Jicha, R. Bowser, I. G. Kazam, and P. Davies, "Alz-50 and MC-1, a new monoclonal antibody raised to paired helical filaments, recognize conformational epitopes on recombinant tau," *Journal of Neuroscience Research*, vol. 48, no. 2, pp. 128–132, 1997.

[36] B. L. Wolozin, A. Pruchnicki, D. W. Dickson, and P. Davies, "A neuronal antigen in the brains of Alzheimer patients," *Science*, vol. 232, no. 4750, pp. 648–650, 1986.

[37] D. B. Rye, J. Leverenz, S. G. Greenberg, P. Davies, and C. B. Saper, "The distribution of Alz-50 immunoreactivity in the normal human brain," *Neuroscience*, vol. 56, no. 1, pp. 109–127, 1993.

[38] S. D. Yan, S. F. Yan, X. Chen et al., "Non-enzymatically glycated tau in Alzheimer's disease induces neuronal oxidant stress resulting in cytokine gene expression and release of amyloid β-peptide," *Nature Medicine*, vol. 1, no. 7, pp. 693–699, 1995.

[39] F. G. De Felice, P. T. Velasco, M. P. Lambert et al., "Aβ oligomers induce neuronal oxidative stress through an N-methyl-D-aspartate receptor-dependent mechanism that is blocked by the Alzheimer drug memantine," *Journal of Biological Chemistry*, vol. 282, no. 15, pp. 11590–11601, 2007.

[40] F. G. De Felice, D. Wu, M. P. Lambert et al., "Alzheimer's disease-type neuronal tau hyperphosphorylation induced by Aβ oligomers," *Neurobiology of Aging*, vol. 29, no. 9, pp. 1334–1347, 2008.

[41] S. T. Ferreira, M. N. N. Vieira, and F. G. De Felice, "Soluble protein oligomers as emerging toxins in Alzheimer's and other amyloid diseases," *IUBMB Life*, vol. 59, no. 4-5, pp. 332–345, 2007.

[42] C. G. Glabe, "Structural classification of toxic amyloid oligomers," *Journal of Biological Chemistry*, vol. 283, no. 44, pp. 29639–29643, 2008.

[43] P. N. Lacor, M. C. Buniel, P. W. Furlow et al., "Aβ oligomer-induced aberrations in synapse composition, shape, and density provide a molecular basis for loss of connectivity in Alzheimer's disease," *Journal of Neuroscience*, vol. 27, no. 4, pp. 796–807, 2007.

[44] M. P. Lambert, P. T. Velasco, L. Chang et al., "Monoclonal antibodies that target pathological assemblies of Aβ," *Journal of Neurochemistry*, vol. 100, no. 1, pp. 23–35, 2007.

[45] G. M. Shankar, B. L. Bloodgood, M. Townsend, D. M. Walsh, D. J. Selkoe, and B. L. Sabatini, "Natural oligomers of the Alzheimer amyloid-β protein induce reversible synapse loss by modulating an NMDA-type glutamate receptor-dependent signaling pathway," *Journal of Neuroscience*, vol. 27, no. 11, pp. 2866–2875, 2007.

[46] D. M. Walsh, D. M. Hartley, M. M. Condron, D. J. Selkoe, and D. B. Teplow, "In vitro studies of amyloid β-protein fibril assembly and toxicity provide clues to the aetiology of Flemish variant (Ala692 → Gly) Alzheimer's disease," *Biochemical Journal*, vol. 355, no. 3, pp. 869–877, 2001.

[47] D. M. Walsh and D. J. Selkoe, "Aβ oligomers—a decade of discovery," *Journal of Neurochemistry*, vol. 101, no. 5, pp. 1172–1184, 2007.

[48] C. Hirata-Fukae, H.-F. Li, L. Ma et al., "Levels of soluble and insoluble tau reflect overall status of tau phosphorylation in vivo," *Neuroscience Letters*, vol. 450, no. 1, pp. 51–55, 2009.

[49] J. C. Carroll, E. R. Rosario, L. Chang et al., "Progesterone and estrogen regulate Alzheimer-like neuropathology in female 3xTg-AD mice," *Journal of Neuroscience*, vol. 27, no. 48, pp. 13357–13365, 2007.

[50] T. D. Garver, K. A. Harris, R. A. W. Lehman, V. M.-Y. Lee, J. Q. Trojanowski, and M. L. Billingsley, "τ Phosphorylation in human, primate, and rat brain: evidence that a pool of τ is highly phosphorylated in vivo and is rapidly dephosphorylated in vitro," *Journal of Neurochemistry*, vol. 63, no. 6, pp. 2279–2287, 1994.

[51] J. Q. Trojanowski and V. M.-Y. Lee, "Phosphorylation of paired helical filament tau in Alzheimer's disease neurofibrillary lesions: focusing on phosphatases," *FASEB Journal*, vol. 9, no. 15, pp. 1570–1576, 1995.

[52] Z. Liang, F. Liu, K. Iqbal, I. Grundke-Iqbal, J. Wegiel, and C.-X. Gong, "Decrease of protein phosphatase 2A and its association with accumulation and hyperphosphorylation of tau in Down syndrome," *Journal of Alzheimer's Disease*, vol. 13, no. 3, pp. 295–302, 2008.

[53] J.-Z. Wang, I. Grundke-Iqbal, and K. Iqbal, "Kinases and phosphatases and tau sites involved in Alzheimer neurofibrillary degeneration," *European Journal of Neuroscience*, vol. 25, no. 1, pp. 59–68, 2007.

[54] F. Liu, I. Grundke-Iqbal, K. Iqbal, and C.-X. Gong, "Contributions of protein phosphatases PP1, PP2A, PP2B and PP5 to the regulation of tau phosphorylation," *European Journal of Neuroscience*, vol. 22, no. 8, pp. 1942–1950, 2005.

[55] C. Soulié, J. Lépagnol, A. Delacourte, and M. L. Caillet-Boudin, "Dephosphorylation studies of SKNSH-SY 5Y cell Tau proteins by endogenous phosphatase activity," *Neuroscience Letters*, vol. 206, no. 2-3, pp. 189–192, 1996.

[56] P. Lavenex, P. B. Lavenex, J. L. Bennett, and D. G. Amaral, "Postmortem changes in the neuroanatomical characteristics of the primate brain: hippocampal formation," *Journal of Comparative Neurology*, vol. 512, no. 1, pp. 27–51, 2009.

[57] N. Movsesyan, A. Ghochikyan, M. Mkrtichyan et al., "Reducing AD-like pathology in 3xTg-AD mouse model by DNA epitope vaccine—a novel immunotherapeutic strategy," *PLoS ONE*, vol. 3, no. 5, article e2124, 2008.

[58] S. Oddo, L. Billings, J. P. Kesslak, D. H. Cribbs, and F. M. LaFerla, "Aβ immunotherapy leads to clearance of early, but not late, hyperphosphorylated tau aggregates via the proteasome," *Neuron*, vol. 43, no. 3, pp. 321–332, 2004.

[59] J. Lewis, D. W. Dickson, W.-L. Lin et al., "Enhanced neurofibrillary degeneration in transgenic mice expressing mutant tau and APP," *Science*, vol. 293, no. 5534, pp. 1487–1491, 2001.

[60] M. Ramsden, L. Kotilinek, C. Forster et al., "Age-dependent neurofibrillary tangle formation, neuron loss, and memory impairment in a mouse model of human tauopathy (P301L)," *Journal of Neuroscience*, vol. 25, no. 46, pp. 10637–10647, 2005.

[61] J. C. Augustinack, A. Schneider, E.-M. Mandelkow, and B. T. Hyman, "Specific tau phosphorylation sites correlate with severity of neuronal cytopathology in Alzheimer's disease," *Acta Neuropathologica*, vol. 103, no. 1, pp. 26–35, 2002.

[62] L. I. Binder, A. L. Guillozet-Bongaarts, F. Garcia-Sierra, and R. W. Berry, "Tau, tangles, and Alzheimer's disease," *Biochimica et Biophysica Acta*, vol. 1739, no. 2, pp. 216–223, 2005.

[63] J. Luna-Muñoz, L. Chávez-Macías, F. García-Sierra, and R. Mena, "Earliest stages of tau conformational changes are related to the appearance of a sequence of specific phospho-dependent tau epitopes in Alzheimer's disease," *Journal of Alzheimer's Disease*, vol. 12, no. 4, pp. 365–375, 2007.

[64] J. Luna-Muñoz, F. García-Sierra, V. Falcón, I. Menéndez, L. Chávez-Macías, and R. Mena, "Regional conformational change involving phosphorylation of tau protein at the Thr231, precedes the structural change detected by Alz-50 antibody in Alzheimer's disease," *Journal of Alzheimer's Disease*, vol. 8, no. 1, pp. 29–41, 2005.

[65] A. D. C. Alonso, T. Zaidi, M. Novak, I. Grundke-Iqbal, and K. Iqbal, "Hyperphosphorylation induces self-assembly of τ into tangles of paired helical filaments/straight filaments," *Proceedings of the National Academy of Sciences of the United States of America*, vol. 98, no. 12, pp. 6923–6928, 2001.

[66] M. Goedert, "Tau gene mutations and their effects," *Movement Disorders*, vol. 20, no. 12, pp. S45–S52, 2005.

[67] E. Braak, H. Braak, and E.-M. Mandelkow, "A sequence of cytoskeleton changes related to the formation of neurofibrillary tangles and neuropil threads," *Acta Neuropathologica*, vol. 87, no. 6, pp. 554–567, 1994.

[68] I. Sassin, C. Schultz, D. R. Thal et al., "Evolution of Alzheimer's disease-related cytoskeletal changes in the basal nucleus of Meynert," *Acta Neuropathologica*, vol. 100, no. 3, pp. 259–269, 2000.

[69] K. Duff, H. Knight, L. M. Refolo et al., "Characterization of pathology in transgenic mice over-expressing human genomic and cDNA tau transgenes," *Neurobiology of Disease*, vol. 7, no. 2, pp. 87–98, 2000.

[70] S. D. Ginsberg, S. Che, S. E. Counts, and E. J. Mufson, "Shift in the ratio of three-repeat tau and four-repeat tau mRNAs in individual cholinergic basal forebrain neurons in mild cognitive impairment and Alzheimer's disease," *Journal of Neurochemistry*, vol. 96, no. 5, pp. 1401–1408, 2006.

SAGE-Hindawi Access to Research
International Journal of Alzheimer's Disease
Volume 2010, Article ID 604853, 11 pages
doi:10.4061/2010/604853

Review Article

In Vivo Imaging Biomarkers in Mouse Models of Alzheimer's Disease: Are We Lost in Translation or Breaking Through?

Benoît Delatour,[1] Stéphane Epelbaum,[1] Alexandra Petiet,[2] and Marc Dhenain[2,3,4]

[1] *CRICM—Team "Alzheimer's and Prion Diseases", UPMC/Inserm UMR-S 975, CNRS UMR 7225, G.H. Pitié Salpêtrière, 47-83 Boulevard de l'Hôpital, 75651 Paris Cedex 13, France*
[2] *NeuroSpin, Bâtiment 145, CEA Saclay, 91191 Gif-sur-Yvette, France*
[3] *CNRS, URA 2210, 18 route du Panorama, 92265 Fontenay aux Roses, France*
[4] *CEA, I2BM, MIRCen, 18 route du Panorama, 92265 Fontenay aux Roses, France*

Correspondence should be addressed to Benoît Delatour, benoit.delatour@upmc.fr

Received 15 May 2010; Accepted 27 July 2010

Academic Editor: Gemma Casadesus

Identification of biomarkers of Alzheimer's Disease (AD) is a critical priority to efficiently diagnose the patients, to stage the progression of neurodegeneration in living subjects, and to assess the effects of disease-modifier treatments. This paper addresses the development and usefulness of preclinical neuroimaging biomarkers of AD. It is today possible to image in vivo the brain of small rodents at high resolution and to detect the occurrence of macroscopic/microscopic lesions in these species, as well as of functional alterations reminiscent of AD pathology. We will outline three different types of imaging biomarkers that can be used in AD mouse models: biomarkers with clear translational potential, biomarkers that can serve as in vivo readouts (in particular in the context of drug discovery) exclusively for preclinical research, and finally biomarkers that constitute new tools for fundamental research on AD physiopathogeny.

1. Introduction

For more than a century, the primary criteria to diagnose Alzheimer's disease (AD) have been relying on clinical observations (development of progressive dementia with a rapid onset of episodic memory impairments). Thanks to the modern refinements of neuropsychological evaluation it is now possible to identify prodromal AD in patients with mild cognitive impairment (MCI) with a specificity of 90% [1]. However, the postmortem examination of brain tissues revealing the pathognomonic lesions of AD (neurofibrillary tangles and senile plaques) is currently the only way to perform a definite diagnosis of this neurodegenerative disease [2]. In vivo biomarkers are gaining ground in bridging the gap between clinical and neuropathological diagnosis of AD. The validation of new AD biomarkers has become a priority to allow an early diagnosis but also to better describe the natural history of the disease [3] and key physiopathological events associated with it [4]. In addition, it is crucial to identify surrogate markers allowing the evaluation of treatment effects and the dissociation between purely symptomatic treatments and disease-modifier actions of the therapies. Today, the most widely used AD markers are based on magnetic resonance imaging (MRI), positron emission tomography (PET), and biochemical exams of body fluids.

The evaluation of brain atrophy markers by structural MRI is the main approach to complement neuropsychological assessment. In particular, medial temporal lobe atrophy is considered to be an excellent criterion for the diagnosis of AD [5]. Volumetric analysis of brain tissues allows to predict conversion from MCI to incipient AD, to dissociate morphological anomalies between patients with early-onset versus late-onset forms of the disease [6, 7] and even to classify the various clinical subtypes of MCI [8]. Cortical hypometabolism quantified by functional MRI (fMRI) or PET is also constantly reported in AD patients, especially in the parietal-temporal regions [9, 10]. It is, however,

undoubtedly the direct imaging of AD brain lesions with PET radioligands [11] that has attracted the most successful research opportunities these last years. Various ligands derived from Congo red, thioflavin T, or other molecules showing affinity for aggregated Aβ have been engineered [12, 13]. The use of the PiB (Pittsburgh compound B) ligand described in the original work of Klunk and Engler [14] has received particular attention and has been validated through multicentric studies. This ligand allows the in vivo detection and quantification of brain amyloidosis. PiB has been used to follow the evolution of amyloidosis during disease progression, and to study its relationship with cognitive decline and with disease-modifier treatments [15, 16]. Despite its advantages, PiB presents several limitations: it can display high retention in the brain of aged nondemented subjects [17]; it does not readily detect soluble oligomeric Aβ conformations considered to be highly pathogenic [18]; it shows high affinity for vascular amyloid deposits that may vary from one patient to the other and can be observed in non-AD conditions [19, 20]. In humans, amyloid load, but also tau pathology, can concurrently be evaluated from peripheral markers, for instance, by means of protein dosages in cerebrospinal fluids (CSFs). The combination of various CSF markers (e.g., Aβ 42/Aβ 40 ratio [21], Aβ/tau ratio [22], or tau/phospho-tau ratio [23]) furthermore increases the sensitivity and specificity for AD diagnosis. Recent studies even suggest that amyloid load as detected by PiB-PET and Aβ concentrations measured in the CSF are intercorrelated [24, 25]. CSF dosages can thus be more cost-efficient alternatives to PET examination for the evaluation of amyloid load in patients.

Because of the multiple biomarkers available for the followup of AD brain pathology, recent consensus efforts have led to the conclusion that the diagnosis of AD should first rely on the evaluation of a core clinical criterion (gradual impairment of episodic memory) then on concurrent supportive features, including sets of biological markers (brain atrophy, CSF and plasmatic dosages, cortical hypometabolism, PiB retention, etc.) [26].

Preclinical research, mainly based on the use of mouse models of AD, is an emerging field in the area of biomarkers discovery and validation. Considering the studies performed in humans, the identification and validation of biomarkers in cohorts of patients ironically suffer from the lack of definite diagnosis of AD in the studied subjects. The vast majority of biomarker studies hence rely on the analysis of cognitively normal subjects compared with patients presenting a (high) suspicion of AD dementia. However, some of the controls included in the studied cohorts might present with a preclinical form of AD and display initial neuropathological alterations, albeit not declaring overt detectable cognitive symptoms. Also, the definite neuropathological confirmation of early AD diagnosis in the patients is nearly impossible to obtain in these populations (see however [27]). On the contrary, animal models are specifically engineered to homogeneously reproduce AD brain lesions. This allows to circumvent biases and limitations encountered in human studies that obviously slow down the discovery and validation of new biomarkers of the disease.

Here we will review the most widely used AD biomarkers and their associated techniques that can be studied or deployed in animal models (see Figure 1). We will focus on morphological and microscopic biomarkers of AD as well as on functional markers. The relevance/importance of the preclinical studies on AD biomarkers will be discussed. Many rationalizations will be explored in parallel throughout this paper.

(1) First, the discovery of new biomarkers in AD animal models can be implemented with a translational aim with the hope that it will ultimately pave new ways for practical applications in human patients. Indeed, we still need to refine the existing markers of AD and concurrently identify new biomarkers.

(2) In parallel, in vivo neuroimaging of biomarkers in AD animal models can provide crucial information to better understand the disease processes. For instance, the analysis of AD models might help disentangling the temporal relationship between the neuropathological lesions themselves and deciphering their impact on neuromorphology and on brain function. Advances in our knowledge of AD physiopathogeny have hence been associated with the development of new preclinical imaging techniques applied to AD transgenic mice, such as in vivo two-photon laser scanning microscopy [28].

(3) Finally, preclinical biomarkers can also be used to follow up animal models during drug evaluation.

2. Imaging of Brain Anatomy in AD Mouse Models

In humans, brain atrophy is one of the best-established markers for the diagnosis and prognosis of AD. Detecting and quantifying the process of atrophy in the rodent brain might be viewed as a challenge as the mouse brain is approximately 3000-fold smaller than the human cerebrum. The use of high-field MRI has nevertheless allowed bypassing these technical limits. In vivo analysis of brain morphology in preclinical models allows to longitudinally monitor the possible onset and progression of localized atrophies [29] and also to visualize the effects of disease-modifier treatments [30].

The preclinical study of brain atrophy in AD animal models has been mainly performed in transgenic mouse lines carrying familial AD mutations (APP and/or PS1-2 genes) and developing brain amyloidosis. The first reports were obtained in the PDAPP model and demonstrated that these transgenic mice overexpressing mutant APP display a severe atrophy of the medial temporal lobe with a focus on the hippocampus [31–36]. These original observations, derived from in vivo experiments and/or from postmortem analysis, suggested a similarity between morphological anomalies in AD patients and in mouse models; however, other data strongly argue against this initial statement.

(1) Brain atrophy as described in AD transgenic lines, have multiple foci and can involve brain areas that are

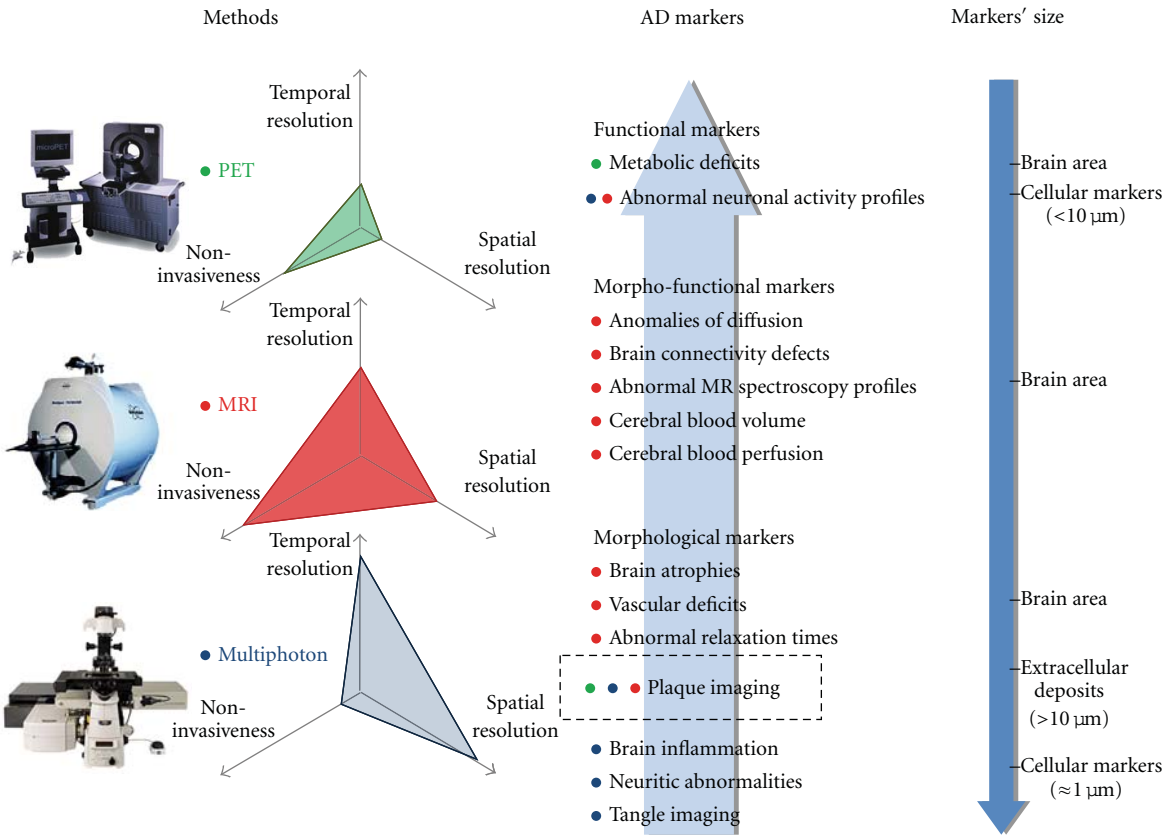

Figure 1: Summary of imaging techniques. This figure schematizes the principal methodologies and tools that can be used to image in vivo the brain lesions and functional alterations developed by mouse models of AD. Radioligands analyzed by PET (green dots) can be used to map brain metabolic deficits in APP(xPS1) transgenic mice. Their relevance for plaque detection in mouse models is more controversial. Applications derived from small animal MR-based imaging techniques (red dots) are more versatile. MRI allows the detection of pathological markers at the regional level (e.g., evaluation of brain atrophy) and also at a microscopic resolution (e.g., visualization of amyloid plaques). In vivo MRI is also a tool to assess functional markers of the pathology such as anomalies in brain perfusion. The recent development of manganese-enhanced MRI has opened new opportunities to map in vivo brain connectivity and neuronal activity with an exquisite spatial resolution. The detection of discrete markers at the (sub)cellular level relies today on the use of high resolution, but also more invasive, imaging techniques that require direct access to brain tissues through a craniotomy in anaesthetized animals: with multiphoton microscopy (blue dots) it is for instance possible to detect intraneuronal neurofibrillary tangles as well as dystrophic neurites in APP(xPS1) transgenic mice.

not usually atrophied in AD patients. For instance, posterior subcortical atrophy (mesencephalon) is displayed in APPxPS1 transgenic mice [37]. Also, white matter anomalies (including fiber tract atrophy in different regions: corpus callosum, anterior commissure, dorsal hippocampal commissure, fornix, corticospinal tract, etc.) have been described in various AD transgenic lines [37–39]. These neuropathological alterations encountered in AD mouse models, especially those affecting callosal fibers [33] are hardly evocative of human pathology, both in qualitative and in quantitative aspects.

(2) Moreover, in some mouse lines, the hippocampal atrophy of AD transgenics appears to have a very early onset during ontogenesis, which contrasts with the slow and gradual atrophy process depicted in AD patients. The data obtained in APP(xPS1) mice might thus underpin the occurrence of developmental abnormalities rather than of the true age-dependent AD-like brain atrophy [35]. Furthermore, the atrophy of the hippocampus is not constantly reported in AD transgenics. In a particular severely affected APPxPS1 model we demonstrated that there was no significant volume reduction of this brain area, even in the oldest animals [37]. In this study, the lack of hippocampal atrophy was further confirmed by postmortem histological assessment. In addition, two recent MRI studies performed on other APPxPS1 transgenic mice depicted a paradoxical accelerated growth of the hippocampus in the transgenics as compared to the wild-type animals [39, 40].

These puzzling data have to be reinterpreted in the context of the amyloid cascade hypothesis. The major tenet of this physiopathological hypothesis is that the deposition of Aβ in brain parenchyma precedes and triggers subsequent

brain anomalies including tissue loss and atrophy. Observations in APP(xPS1) transgenic mice somewhat dispute this belief: atrophy can be observed before the onset of brain amyloidosis or can concurrently be absent despite a heavy local amyloid burden. In addition, no correlations between amyloid load and overall brain volumes have been highlighted [37].

Brain volumetry, even when assessed in vivo, is thus a questionable biomarker in AD APP(xPS1) transgenic mice. Therefore, one has to be cautious when using brain volumes as morphological readouts for preclinical research as it has become clear that brain tissue atrophies are qualitatively and quantitatively different in mouse models of brain amyloidosis and in AD patients. This obviously constitutes a pitfall for subsequent translational efforts.

3. Imaging of Brain Microscopic Lesions in AD Mouse Models

3.1. Indirect Detection of Cerebral Amyloidosis. APP(xPS1) mouse lines are an adequate model to develop new imaging techniques in order to follow up onset and progression of amyloid burden. As a first step, global MR parameters expected to reflect Aβ deposition have been explored. For example, a reduction in T2 relaxation time has been depicted in APPxPS1 mouse lines [41, 42]. Such reduction in T2 is presumably explained by Aβ accumulation as stresses the correlation between T2 and histologically-assessed local amyloid load [43]. There is, however, an old controversy whether similar abnormal relaxation times can be depicted in human AD brains or not (see [44] but [45, 46]), which sheds some doubts on the possibility to extrapolate preclinical findings to the development of new valid diagnostic tools for human patients.

3.2. Direct Imaging of Plaques (and of Other Microscopic Lesions)

3.2.1. In Vivo Multiphoton Microscopy Imaging. In transgenic mice, in vivo multiphoton microscopy is a brain imaging modality that allows to image amyloid deposits and associated lesions in small tissue volumes at very high resolution (1 μm) (for reviews of the methods, see [28, 47]). After surgery involving local craniotomy [48] a fluorescent dye (e.g., thioflavin S or methoxy-X04) can be administered peripherally to label plaques and visualize them through the skull open window, using nondestructive multiphoton laser excitation. The field of view of the technique is limited, but images can be efficiently acquired from cortical surface up to 800 μm of depth. Visualization of vascular arborizations (intravenous injection of a fluorescent dye such as Texas red dextran) is generally performed simultaneously to provide constant landmarks for repeated imaging. Multiphoton imaging methods have also been successfully applied to visualize neurofibrillary lesions in vivo. For example, Spires-Jones and coworkers labeled in vivo the NFTs of rTg4510 mice, a model of taupathy, by application of thioflavin S on brain surface after dura resection [49, 50].

In vivo multiphoton microscopy has significantly increased our knowledge on AD physiopathogeny. Indeed, the method allows in vivo longitudinal studies (across weeks or months) of the kinetics of plaque progression [51, 52] and measurements of the effects of treatments (e.g., immunotherapies) on plaque clearance [53]. Using these methods, Meyer-Luehmann and colleagues [54] suggested that the initial formation of plaques might be an acute event (plaques were observed to form quickly within 24 hours). However, these observations have recently been challenged by another report indicating that amyloid plaques grow more slowly over periods of weeks [55]. Analysis of the role of brain inflammation in AD pathogeny has also been clarified by in vivo multiphoton imaging. For instance, the relationship between plaques (labeled with Methoxy-X04) and activated microglia (overexpressing GFP through an Iba-1 promoter) has recently been described in APPxPS1 transgenics [56]. In a smart-engineered model (GFP inserted in the CX3CR1 chemokine receptor of the 5xTg AD model, which also overexpressed Thy1-driven YFP), Fuhrman and colleagues were able to describe the live dialogue between microglia and neurons in the presence of AD lesions [57]. Finally, in vivo multiphoton microscopy studies have also allowed investigating the local toxicity of Aβ deposits on surrounding synapses and on neuritic processes. In direct support to the amyloid cascade hypothesis, Meyer-Luehmann et al. [54] demonstrated that plaques create a local microenvironment (a reservoir of bioactive molecules) that gradually promotes pathological changes in neighboring neurites within days. Koffie et al. [58] underlined that Aβ oligomers, the so-called "modern culprits" of AD, might be crucial players in these synaptic/neuritic alterations; in APPxPS1 mice they labeled plaques with Methoxy-XO4 and oligomers by infusing the antioligomers NAB61 antibody conjugated to a fluorescent dye on the cortex after dura opening. They were able to detect in vivo a hallo of oligomers surrounding senile plaques; subsequent histological analysis underlined that this peripheral hallo was associated with a severe synaptotoxic effect (loss of PSD75 immunoreactivity). AD-related neuritic anomalies detected by in vivo multiphoton microscopy might also serve to evaluate the impact of new therapies. For instance, it has been demonstrated that antioxidant treatments have a rescuing action on neuritic dystrophies (abnormal neurite curvature of fluorescently labeled neurons) while not reducing Aβ plaque size [59]. On the contrary, the same research group provided data showing that treatment with one γ-secretase inhibitor (LY-411575) does not affect the neuritic defects of APPxPS1 transgenics [60].

3.2.2. PET Imaging of Amyloid Plaques. Although in vivo multiphoton microscopy provided very interesting results on the physiopathogeny of AD, the method cannot be easily translated to patients. In humans, the best-established method to detect amyloid plaques relies on the use of the PiB radioligand. Although this compound was initially evaluated in transgenic mouse models of AD [61] to detect amyloid lesions by multiphoton imaging, it did not lead to conclusive results when used to detect amyloid plaques

by PET in APPxPS1 transgenic mice [62, 63]. Also, it has been evidenced that 18F-FDDNP, a good radioligand for amyloid plaques and tangles in humans, does not show good retention in the brain of Tg2576 mice [64]. Using ultrahigh specific-activity PiB (200 GBq/mole; injection of the tracer immediately after synthesis), Maeda and collaborators were nevertheless able to show increased retention of the ligand in APP transgenics. It is hence possible that paucity of high-affinity PiB binding sites in APP(xPS1) transgenic mice is the explanation for previous imaging failures. It might also be possible that the density of the high-affinity PiB binding sites varies from one transgenic line to the other (Maeda and collaborators used the APP23 line while previous works of Klunk and Tomaya were performed in Tg2576 APP mice and in APPxPS1 transgenics derived from the Tg2576 model). Interestingly, Rosen et al. recently demonstrated that PiB-binding is also reduced in aged rhesus macaques, chimpanzees, and squirrel monkeys despite the fact that the nonhuman primates they evaluated displayed heavy amyloid burden [65]. It can be tentatively concluded that PiB is an efficient probe only for human-specific molecular components of Aβ deposits. Despite differences between humans and animals, the development of new radioligands for AD brain lesions still strongly relies on preclinical tests in APP(xPS1) transgenic mice. For example, the recently-developed AV-45 ligand, which is expected to become a good substitute to PiB in the coming years, has first been tested in transgenic mice [66].

3.2.3. MR Imaging of Amyloid Plaques. Direct noninvasive in vivo imaging of plaques in APP(xPS1) transgenic mice is a very stimulating research area and the MRI-based detection of amyloid deposits is actively pursued as an alternative technique to PET imaging in preclinical research. Numerous studies performed in APP(xPS1) transgenic mice underlined that discrete aggregated Aβ deposits locally modify MR contrasts. These contrast anomalies can be detected in postmortem conditions (extracted brains) that favor the acquisition of high-resolution images [67–70] but they can also be detected in vivo in anaesthetized mice [71–73]. One mechanism that may explain the MRI spontaneous contrast of plaques is the accumulation of iron in amyloid deposits that locally alters the relaxation time of tissues [41, 74, 75]. The recent work of Meadowcroft and collaborators [76] emphasized that both the high iron concentrations and the interaction of water with dense aggregated amyloid mass can concomitantly modify transverse relaxation rates but that these two mechanisms might be differentially involved in human versus in mouse brain tissues.

MR imaging of plaques in rodents can also be performed using specific probes. For example, the amyloid-binding styrylbenzenes derived from the Congo red dye and complexed to 19F (fluorine) can pass through the blood-brain barrier (BBB). One publication suggested that these derivates can allow detection of Aβ deposits in living Tg2576 mice [77]. However, these results have not been replicated. Aβ conjugated to gadolinium or monocrystalline iron oxide nanoparticles (MIONs) are more robust methods for amyloid plaque visualization. When administered peripherally (intravenous or intracarotid injection), the peptide-contrast agent complexes have some tropism for amyloid plaques thanks to the binding affinity of Aβ peptides for other Aβ peptides. However, brain penetration of the conjugates often requires the opening of the BBB (using mannitol) or the complexion with polyamines (e.g., putrescin). These vectorized contrast agents can be used "in vivo" to detect amyloid plaques of AD transgenics [78, 79] and even to quantify amyloid load on a voxel-based analysis [80]. Recent studies emphasized the use of small-sized antibodies to build efficient MRI probes against Aβ deposits. For instance, Ramakrishnan and collaborators used polyamine-modified Fab fragments complexed to gadolinium to perform ex vivo amyloid plaque visualization by MRI in APPxPS1 mice [81]. Also, the group of Beka Solomon engineered anti-Aβ ScFv antibodies by phage display, mainly with a (immuno)therapeutical aim [82]. Interestingly, these small antibodies, when infused intranasally, have the capacity to penetrate into the brain and to reach the amyloid plaques, not only at the injection loci (olfactory bulbs) but also at long distances from the nose, for instance, in the hippocampi [83]. It might hence be predicted that complexing these phage-ScFv with an MRI contrast agent would allow in vivo plaque detection. Also, the small homodimeric antibodies of camelidae have been shown to be able to cross the BBB after intracarotid infusion and to reach their targets in brain parenchyma [84]. Some of these antibodies, much smaller than the classical IgGs, have been specifically produced to recognize Aβ epitopes [85, 86] and might be valuable tools to initiate new strategies for in vivo plaque detection.

The MRI-based methods implemented in rodents could find a first application in drug development as they offer a solution to monitor online the disease-modifier effects of treatment in animal models of AD. Up to now, it has been difficult to evaluate the translation from these preclinical data obtained in mice to valid MRI protocols utilizable in AD patients. However, the rising development of high-field MRI for clinical and research uses might accelerate the implementation of such noninvasive methods. Preliminary studies hence suggest that amyloid plaques will soon be detectable by MRI in humans [87, 88].

3.2.4. Other Imaging Approaches to Detect Amyloid Plaques. Alternative methods for plaque imaging are under scrutinization in APP(xPS1) mice (e.g., Near InfraRed Fluorescence (NIRF) in vivo imaging of new compounds that bind to plaques [89] or Diffraction Enhanced Imaging (DEI), a phase contrast X-ray imaging technique that provides high soft tissue contrast which allows Aβ plaque detection [90]). These methods might also find applications as preclinical tools to screen the effects of interventional therapies.

3.2.5. Relevance of Amyloid Plaque Detection. To conclude on amyloid plaque imaging, it is important to remind that while research efforts have contributed to implement various imaging techniques for the in vivo detection of amyloid plaques in animal models, the exact status of these lesions as

core biomarkers of AD is still obscure and largely discussed. It has been known for decades that Aβ accumulation can be observed in nondemented human individuals and this finding has recently been confirmed by PiB-PET scans that identified a subset of intellectually normal persons with a high PiB fixation indicating severe Aβ accumulation [17]. In addition there is, today, no conclusive evidence to support the hypothesis that reducing amyloid load by stimulating plaque clearance has any clinical effects in AD patients [91]. Hence, the relevance of imaging plaques as primary readouts for disease detection/progression as well as for the evaluation of disease-modifier therapies is challenged if not questionable. This urges the need for (1) better refining the status of amyloid plaques as in vivo gold standard markers of the disease, (2) stimulating new preclinical research efforts towards alternative biomarkers of AD.

3.3. Imaging of AD-Related Alterations of Brain Microstructure. Different imaging parameters are altered in animals developing cerebral amyloidosis but not necessarily as a direct consequence of Aβ accumulation. For example, anomalies of water diffusion detected by in vivo MRI have been described in AD transgenics accumulating amyloid plaques [92–94] (see however [95]). The exact origin of these diffusion defects is still uncertain (highly hydrophobic deposits might cause constraints on water diffusion but these defects might also come from loss or alterations of the white matter). MR spectroscopy shows a decrease of N-acetylaspartate (NAA) in the brains of APPxPS1 transgenics [96]. NAA is considered to be a good marker of neuronal viability; its decrease in APP(xPS1) mice might be caused by the intraparenchymal accumulation of Aβ; some reports indicated indeed a negative correlation between amyloid load and NAA levels [97]. Although of interest, these methods have not been used to followup disease progression in AD preclinical models, maybe because the tracked markers are not specific to AD condition and can be detected only in the oldest animals. It is uncertain whether therapeutical evaluation of disease-modifier treatments could rely on such markers.

4. Imaging of Brain Dysfunction in AD Mouse Models

Besides directly imaging the microscopic and macroscopic lesions of AD, it is also possible, even in animal models, to follow the evolution of the pathological process through the brain functional disorganizations it promotes (e.g., perfusion and neuronal activity impairments).

4.1. Vascular-Perfusion Anomalies. Since the initial observation of the occurrence of cerebral amyloid angiopathy in AD patients, it has been well established that vascular abnormalities are a major phenotype of the disease. Using dedicated postmortem morphological analysis (e.g., corrosion casts) similar vascular impairments have been described in AD transgenics under the form of eliminated/truncated brain vessels or dysmorphic vascular architecture [98, 99]. Importantly, such drastic changes in the morphology of brain vessels can also be visualized using in vivo magnetic resonance angiography (MRA) that allows the detailed detection of the vascular arborization in the brain. MRA has been successfully applied to APP [98] and APPxPS1 [100] mice that both demonstrate abnormal arterial voids. These methods are interesting tools to measure the preventive/curative effects of vascular-oriented therapies although the relationship between the incidence of vessels anomalies and Aβ brain deposition remains to be clarified.

In parallel, the cerebral blood volume (CBV) of AD transgenics has been observed to be reduced (for recent illustration in a triple APPxPS1xtau line, see [101]). Shrinking of the cerebrovascular space in rodents can be estimated in vivo using MR detection of susceptibility contrast agents such as gadolinium administered intraperitoneally [102] or monocrystalline iron oxide nanoparticles injected intravenously [103]. Restoration of normal CBV maps in AD transgenics has been demonstrated across therapeutic assays (e.g., long-term treatment with nonsteroidal anti-inflammatory drugs in Tg J20 mice [102]).

As a more functional consequence of vascular impairments in AD transgenics, blood perfusion is also decreased in different mouse models. This perfusion decrease can be assessed using standard autoradiographic methods [104], by laser Doppler [105], and by in vivo MRI (e.g., by means of spin-labeling techniques). For instance, MRI detection of perfusion impairments has been performed in APPxPS1-Ki mice [106] and in PS2APP mice [107].

4.2. Metabolic, Cellular, and Network Dysfunction. Recordings of cortical hypometabolism as measured by PET imaging and brain hypoactivities assessed by functional MRI are hallmarks classically described in AD patients. Similar anomalies can be observed in mouse models of AD. Thanks to their high spatial resolution, autoradiographic methods (e.g., of fluorodeoxyglucose-FDG or of 2-deoxy-D-glucose) have been applied to map brain metabolic activities in PDAPP mice [108, 109] and in APPxPS1 transgenics [110]. In these transgenic mice, hypometabolism was constantly evidenced in the association cortex (e.g., posterior cingulate cortex), evocative of findings obtained in AD patients. However, the relationship between these functional anomalies and amyloid burden is still questioned [109].

In vivo metabolic imaging in mice undergoes rapid development but it is technically challenging because PET imaging in rodents is limited by its low resolution, the cost of the ligands, and access to micro-PET devices. Also, recent data indicated no differences in FDG-PET between AD transgenics (Tg2576 mice) and control animals [64].

Alternative ways to visualize brain activity in living mice are available. The recent development of in vivo multiphoton calcium imaging techniques applied to AD mouse models [111–113] has provided us with remarkable new findings on the disease physiopathogeny but their use for therapeutic preclinical development is doubtful. Manganese-Enhanced MRI (MEMRI) is a better-established method to follow brain activity in rodents. It allows the in vivo detection of

active neuronal populations in rats, mice, and in nonhuman primates [114]. Manganese is an analog of calcium and after peripheral or stereotaxic administration it can penetrate into brain neurons via voltage-dependent Ca2+ channels. Paramagnetic properties of manganese allow its direct visualization by MRI. A raise in manganese concentrations has been described in selected brain regions following interoceptive/exteroceptive stimulations [115, 116]. We are not currently aware of any reports that have applied this pioneering method to map brain activities in APP or APPxPS1 mice. Kimura and collaborators conversely used MEMRI analysis in mice overexpressing tau and accumulating hyperphosphorylated tau in their brains [117]. The authors reported clear cortical hypoactivation in the tau mice, at the level of the postrhinal cortex (homologous to the parahippocampal area of primates, including humans) and in tight association with the occurrence of visuospatial cognitive deficits. In addition to being a good marker of activated neurons, manganese is also transported in axons via microtubules. It can therefore be used as an in vivo transsynaptic tracer to label brain networks in situ. Delays in manganese transport, assessing malfunction of brain connectivity, presumably as a response to synaptic/neuritic underlying pathologies, have recently been evidenced in APP and APPxPS1 transgenic mice [118, 119]. Interestingly, the analysis of transneuronal manganese transport can be used to screen the effects of therapies against AD (e.g., memantine [120]). Although associated with known putative toxic effects [114, 121], MEMRI might rapidly become a prominent method for the analysis of brain dysfunction in AD transgenic mice and of functional recovery after therapeutical intervention.

5. Conclusions

AD biomarkers have the opportunity to be developed, tested and validated in mouse models of the disease. In many cases, mice have allowed to produce the first proof of concept for biomarkers that have been then translated to humans. This is the case of radioligands that now allow the detection of amyloid plaques by PET in patients. MR biomarkers of amyloid plaques underwent a similar development pipeline (first tested in mice, then applied to humans). In the near future, one can predict that transgenic models will play a decisive role in the investigation of new biomarkers of AD pathology, such as, for example, markers of Tau pathology that are critically missing today.

Interestingly, major brain changes detected in AD patients (e.g., cerebral atrophy or reduced brain metabolism detected by FDG-PET) are not always replicated in animals. Such discrepancies can be explained by technical considerations but are also attributable to the intrinsic characteristics of the model and to its inability to mimic all aspects of the human pathology. On the other hand, a large range of biomarkers detecting AD brain alterations in humans is detectable in a similar way in transgenic mice. For instance, biomarkers of amyloid plaques, perfusion, and cerebral blood volume are all valid both in AD patients and in mouse models of the disease. These markers are critical to followup disease progression, to monitor the effects of treatments during preclinical studies, and to predict possible therapeutic effects in humans. They can thus be considered as good translational biomarkers of AD pathology. Finally, some markers and their associated methodologies have been implemented in animals and will probably be restricted to preclinical studies. These markers could be of importance to refine our understanding of the physiopathogeny of the disease or, alternatively, to detect the effects of new therapies initiated in animal models. This is particularly true for invasive approaches such as bi-photon imaging of amyloid plaques or for methods relying on potentially toxic contrast agents such as manganese-enhanced MRI.

To conclude, transgenic mouse models of AD can be used as tools to identify and validate new translational biomarkers of AD pathology. In parallel, the markers identified in these models might have a field of application restricted to the sole preclinical research but still with an interest for both fundamental and therapeutical investigations.

Acknowledgment

The authors are grateful to Dr. Ciobanu for her careful reading of the paper and her help with the English text.

References

[1] M. Sarazin, C. Berr, J. De Rotrou et al., "Amnestic syndrome of the medial temporal type identifies prodromal AD: a longitudinal study," *Neurology*, vol. 69, no. 19, pp. 1859–1867, 2007.

[2] M. Gearing, S. S. Mirra, J. C. Hedreen, S. M. Sumi, L. A. Hansen, and A. Heyman, "The Consortium to Establish a Registry for Alzheimer's Disease (CERAD)—part X: neuropathology confirmation of the clinical diagnosis of Alzheimer's disease," *Neurology*, vol. 45, no. 3, pp. 461–466, 1995.

[3] C. R. Jack Jr., D. S. Knopman, W. J. Jagust et al., "Hypothetical model of dynamic biomarkers of the Alzheimer's pathological cascade," *The Lancet Neurology*, vol. 9, no. 1, pp. 119–128, 2010.

[4] P. Edison, H. A. Archer, A. Gerhard et al., "Microglia, amyloid, and cognition in Alzheimer's disease: an [11C](R)PK11195-PET and [11C]PIB-PET study," *Neurobiology of Disease*, vol. 32, no. 3, pp. 412–419, 2008.

[5] P. Scheltens and E. S. C. Korf, "Contribution of neuroimaging in the diagnosis of Alzheimer's disease and other dementias," *Current Opinion in Neurology*, vol. 13, no. 4, pp. 391–396, 2000.

[6] T. Tapiola, C. Pennanen, M. Tapiola et al., "MRI of hippocampus and entorhinal cortex in mild cognitive impairment: a follow-up study," *Neurobiology of Aging*, vol. 29, no. 1, pp. 31–38, 2008.

[7] D. P. Devanand, G. Pradhaban, X. Liu et al., "Hippocampal and entorhinal atrophy in mild cognitive impairment: prediction of Alzheimer disease," *Neurology*, vol. 68, no. 11, pp. 828–836, 2007.

[8] S. W. Seo, K. Im, J.-M. Lee et al., "Cortical thickness in single- versus multiple-domain amnestic mild cognitive impairment," *NeuroImage*, vol. 36, no. 2, pp. 289–297, 2007.

[9] L. Mosconi, "Brain glucose metabolism in the early and specific diagnosis of Alzheimer's disease: FDG-PET studies in MCI and AD," *European Journal of Nuclear Medicine and Molecular Imaging*, vol. 32, no. 4, pp. 486–510, 2005.

[10] E. Salmon, B. Sadzot, P. Maquet et al., "Differential diagnosis of Alzheimer's disease with PET," *Journal of Nuclear Medicine*, vol. 35, no. 3, pp. 391–398, 1994.

[11] A. Nordberg, "Amyloid imaging in early detection of Alzheimer's disease," *Neurodegenerative Diseases*, vol. 7, no. 1–3, pp. 136–138, 2010.

[12] A. Nordberg, "Amyloid imaging in Alzheimer's disease," *Current Opinion in Neurology*, vol. 20, no. 4, pp. 398–402, 2007.

[13] E. K. Ryu and X. Chen, "Development of Alzheimer's disease imaging agents for clinical studies," *Frontiers in Bioscience*, vol. 13, no. 2, pp. 777–789, 2008.

[14] W. E. Klunk, H. Engler, A. Nordberg et al., "Imaging brain amyloid in Alzheimer's disease with Pittsburgh compound-B," *Annals of Neurology*, vol. 55, no. 3, pp. 306–319, 2004.

[15] K. E. Pike, G. Savage, V. L. Villemagne et al., "β-amyloid imaging and memory in non-demented individuals: evidence for preclinical Alzheimer's disease," *Brain*, vol. 130, no. 11, pp. 2837–2844, 2007.

[16] J. O. Rinne, D. J. Brooks, M. N. Rossor et al., "11C-PiB PET assessment of change in fibrillar amyloid-β load in patients with Alzheimer's disease treated with bapineuzumab: a phase 2, double-blind, placebo-controlled, ascending-dose study," *The Lancet Neurology*, vol. 9, no. 4, pp. 363–372, 2010.

[17] M. A. Mintun, G. N. Larossa, Y. I. Sheline et al., "[11C]PIB in a nondemented population: potential antecedent marker of Alzheimer disease," *Neurology*, vol. 67, no. 3, pp. 446–452, 2006.

[18] D. J. Selkoe, "Soluble oligomers of the amyloid β-protein impair synaptic plasticity and behavior," *Behavioural Brain Research*, vol. 192, no. 1, pp. 106–113, 2008.

[19] B. J. Bacskai, M. P. Frosch, S. H. Freeman et al., "Molecular imaging with Pittsburgh compound B confirmed at autopsy: a case report," *Archives of Neurology*, vol. 64, no. 3, pp. 431–434, 2007.

[20] A. Lockhart, J. R. Lamb, T. Osredkar et al., "PIB is a non-specific imaging marker of amyloid-beta (Aβ) peptide-related cerebral amyloidosis," *Brain*, vol. 130, no. 10, pp. 2607–2615, 2007.

[21] N. R. Graff-Radford, J. E. Crook, J. Lucas et al., "Association of low plasma Aβ42/Aβ40 ratios with increased imminent risk for mild cognitive impairment and Alzheimer disease," *Archives of Neurology*, vol. 64, no. 3, pp. 354–362, 2007.

[22] A. M. Fagan, C. M. Roe, C. Xiong, M. A. Mintun, J. C. Morris, and D. M. Holtzman, "Cerebrospinal fluid tau/β-amyloid42 ratio as a prediction of cognitive decline in nondemented older adults," *Archives of Neurology*, vol. 64, no. 3, pp. 343–349, 2007.

[23] K. Blennow and H. Hampel, "CSF markers for incipient Alzheimer's disease," *Lancet Neurology*, vol. 2, no. 10, pp. 605–613, 2003.

[24] W. J. Jagust, S. M. Landau, L. M. Shaw et al., "Relationships between biomarkers in aging and dementia," *Neurology*, vol. 73, no. 15, pp. 1193–1199, 2009.

[25] N. Tolboom, W. M. Van Der Flier, M. Yaqub et al., "Relationship of cerebrospinal fluid markers to 11C-PiB and 18F-FDDNP binding," *Journal of Nuclear Medicine*, vol. 50, no. 9, pp. 1464–1470, 2009.

[26] B. Dubois, H. H. Feldman, C. Jacova et al., "Research criteria for the diagnosis of Alzheimer's disease: revising the NINCDS-ADRDA criteria," *Lancet Neurology*, vol. 6, no. 8, pp. 734–746, 2007.

[27] T. Tapiola, I. Alafuzoff, S.-K. Herukka et al., "Cerebrospinal fluid β-amyloid 42 and tau proteins as biomarkers of Alzheimer-type pathologic changes in the brain," *Archives of Neurology*, vol. 66, no. 3, pp. 382–389, 2009.

[28] J. Dong, R. Revilla-Sanchez, S. Moss, and P. G. Haydon, "Multiphoton in vivo imaging of amyloid in animal models of Alzheimer's disease," *Neuropharmacology*, vol. 59, no. 4-5, pp. 268–275, 2010.

[29] B. McDaniel, H. Sheng, D. S. Warner, L. W. Hedlund, and H. Benveniste, "Tracking brain volume changes in C57BL/6J and ApoE-deficient mice in a model of neurodegeneration: a 5-week longitudinal micro-MRI study," *NeuroImage*, vol. 14, no. 6, pp. 1244–1255, 2001.

[30] G. Li, L. Zou, C. R. Jack Jr., Y. Yang, and E. S. Yang, "Neuroprotective effect of Coenzyme Q10 on ischemic hemisphere in aged mice with mutations in the amyloid precursor protein," *Neurobiology of Aging*, vol. 28, no. 6, pp. 877–882, 2007.

[31] J.-C. Dodart, C. Mathis, J. Saura, K. R. Bales, S. M. Paul, and A. Ungerer, "Neuroanatomical abnormalities in behaviorally characterized APP(V717F) transgenic mice," *Neurobiology of Disease*, vol. 7, no. 2, pp. 71–85, 2000.

[32] M. H. Donovan, U. Yazdani, R. D. Norris, D. Games, D. C. German, and A. J. Eisch, "Decreased adult hippocampal neurogenesis in the PDAPP mouse model of Alzheimer's disease," *Journal of Comparative Neurology*, vol. 495, no. 1, pp. 70–83, 2006.

[33] F. Gonzalez-Lima, J. D. Berndt, J. E. Valla, D. Games, and E. M. Reiman, "Reduced corpus callosum, fornix and hippocampus in PDAPP transgenic mouse model of Alzheimer's disease," *NeuroReport*, vol. 12, no. 11, pp. 2375–2379, 2001.

[34] J. M. Redwine, B. Kosofsky, R. E. Jacobs et al., "Dentate gyrus volume is reduced before onset of plaque formation in PDAPP mice: a magnetic resonance microscopy and stereologic analysis," *Proceedings of the National Academy of Sciences of the United States of America*, vol. 100, no. 3, pp. 1381–1386, 2003.

[35] J. Valla, L. E. Schneider, F. Gonzalez-Lima, and E. M. Reiman, "Nonprogressive transgene-related callosal and hippocampal changes in PDAPP mice," *NeuroReport*, vol. 17, no. 8, pp. 829–832, 2006.

[36] C. Weiss, P. N. Venkatasubramanian, A. S. Aguado et al., "Impaired eyeblink conditioning and decreased hippocampal volume in PDAPP V717F mice," *Neurobiology of Disease*, vol. 11, no. 3, pp. 425–433, 2002.

[37] B. Delatour, M. Guégan, A. Volk, and M. Dhenain, "In vivo MRI and histological evaluation of brain atrophy in APP/PS1 transgenic mice," *Neurobiology of Aging*, vol. 27, no. 6, pp. 835–847, 2006.

[38] J. C. Lau, J. P. Lerch, J. G. Sled, R. M. Henkelman, A. C. Evans, and B. J. Bedell, "Longitudinal neuroanatomical changes determined by deformation-based morphometry in a mouse model of Alzheimer's disease," *NeuroImage*, vol. 42, no. 1, pp. 19–27, 2008.

[39] S. Maheswaran, H. Barjat, D. Rueckert et al., "Longitudinal regional brain volume changes quantified in normal aging and Alzheimer's APP $\times$ PS1 mice using MRI," *Brain Research*, vol. 1270, pp. 19–32, 2009.

[40] S. Maheswaran, H. Barjat, S. T. Bate et al., "Analysis of serial magnetic resonance images of mouse brains using image registration," *NeuroImage*, vol. 44, no. 3, pp. 692–700, 2009.

[41] N. El Tannir El Tayara, B. Delatour, C. Le Cudennec, M. Guégan, A. Volk, and M. Dhenain, "Age-related evolution of amyloid burden, iron load, and MR relaxation times in a transgenic mouse model of Alzheimer's disease," *Neurobiology of Disease*, vol. 22, no. 1, pp. 199–208, 2006.

[42] J. A. Helpern, S.-P. Lee, M. F. Falangola et al., "MRI assessment of neuropathology in a transgenic mouse model of Alzheimer's disease," *Magnetic Resonance in Medicine*, vol. 51, no. 4, pp. 794–798, 2004.

[43] N. El Tannir El Tayara, A. Volk, M. Dhenain, and B. Delatour, "Transverse relaxation time reflects brain amyloidosis in young APP/PS1 transgenic mice," *Magnetic Resonance in Medicine*, vol. 58, no. 1, pp. 179–184, 2007.

[44] A. P. Haley, J. Knight-Scott, K. L. Fuchs, V. I. Simnad, and C. A. Manning, "Shortening of hippocampal spin-spin relaxation time in probable Alzheimer's disease: a 1H magnetic resonance spectroscopy study," *Neuroscience Letters*, vol. 362, no. 3, pp. 167–170, 2004.

[45] S. J. Kirsch, R. W. Jacobs, L. L. Butcher, and J. Beatty, "Prolongation of magnetic resonance T2 time in hippocampus of human patients marks the presence and severity of Alzheimer's disease," *Neuroscience Letters*, vol. 134, no. 2, pp. 187–190, 1992.

[46] M. P. Laakso, K. Partanen, H. Soininen et al., "MR T2 relaxometry in Alzheimer's disease and age-associated memory impairment," *Neurobiology of Aging*, vol. 17, no. 4, pp. 535–540, 1996.

[47] B. J. Bacskai and B. T. Hyman, "Alzheimer's disease: what multiphoton microscopy teaches us," *Neuroscientist*, vol. 8, no. 5, pp. 386–390, 2002.

[48] R. Mostany and C. Portera-Cailliau, "A craniotomy surgery procedure for chronic brain imaging," *Journal of Visualized Experiments*, no. 12, p. 680, 2008.

[49] A. De Calignon, L. M. Fox, R. Pitstick et al., "Caspase activation precedes and leads to tangles," *Nature*, vol. 464, no. 7292, pp. 1201–1204, 2010.

[50] T. L. Spires-Jones, A. De Calignon, T. Matsui et al., "In vivo imaging reveals dissociation between caspase activation and acute neuronal death in tangle-bearing neurons," *Journal of Neuroscience*, vol. 28, no. 4, pp. 862–867, 2008.

[51] R. H. Christie, B. J. Bacskai, W. R. Zipfel et al., "Growth arrest of individual senile plaques in a model of Alzheimer's disease observed by in vivo multiphoton microscopy," *Journal of Neuroscience*, vol. 21, no. 3, pp. 858–864, 2001.

[52] E. M. Robbins, R. A. Betensky, S. B. Domnitz et al., "Kinetics of cerebral amyloid angiopathy progression in a transgenic mouse model of Alzheimer disease," *Journal of Neuroscience*, vol. 26, no. 2, pp. 365–371, 2006.

[53] R. P. Brendza, B. J. Bacskai, J. R. Cirrito et al., "Anti-Aβ antibody treatment promotes the rapid recovery of amyloid-associated neuritic dystrophy in PDAPP transgenic mice," *Journal of Clinical Investigation*, vol. 115, no. 2, pp. 428–433, 2005.

[54] M. Meyer-Luehmann, T. L. Spires-Jones, C. Prada et al., "Rapid appearance and local toxicity of amyloid-β plaques in a mouse model of Alzheimer's disease," *Nature*, vol. 451, no. 7179, pp. 720–724, 2008.

[55] P. Yan, A. W. Bero, J. R. Cirrito et al., "Characterizing the appearance and growth of amyloid plaques in APP/PS1 mice," *Journal of Neuroscience*, vol. 29, no. 34, pp. 10706–10714, 2009.

[56] T. Bolmont, F. Haiss, D. Eicke et al., "Dynamics of the microglial/amyloid interaction indicate a role in plaque maintenance," *Journal of Neuroscience*, vol. 28, no. 16, pp. 4283–4292, 2008.

[57] M. Fuhrmann, T. Bittner, C. K. E. Jung et al., "Microglial Cx3cr1 knockout prevents neuron loss in a mouse model of Alzheimer's disease," *Nature Neuroscience*, vol. 13, no. 4, pp. 411–413, 2010.

[58] R. M. Koffie, M. Meyer-Luehmann, T. Hashimoto et al., "Oligomeric amyloid β associates with postsynaptic densities and correlates with excitatory synapse loss near senile plaques," *Proceedings of the National Academy of Sciences of the United States of America*, vol. 106, no. 10, pp. 4012–4017, 2009.

[59] M. Garcia-Alloza, L. A. Borrelli, B. T. Hyman, and B. J. Bacskai, "Antioxidants have a rapid and long-lasting effect on neuritic abnormalities in APP:PS1 mice," *Neurobiology of Aging*. In press.

[60] M. Garcia-Alloza, M. Subramanian, D. Thyssen et al., "Existing plaques and neuritic abnormalities in APP:PS1 mice are not affected by administration of the gamma-secretase inhibitor LY-411575," *Molecular Neurodegeneration*, vol. 4, no. 1, article 19, 2009.

[61] B. J. Bacskai, G. A. Hickey, J. Skoch et al., "Four-dimensional multiphoton imaging of brain entry, amyloid binding, and clearance of an amyloid-β ligand in transgenic mice," *Proceedings of the National Academy of Sciences of the United States of America*, vol. 100, no. 21, pp. 12462–12467, 2003.

[62] W. E. Klunk, B. J. Lopresti, M. D. Ikonomovic et al., "Binding of the positron emission tomography tracer Pittsburgh compound-B reflects the amount of amyloid-β in Alzheimer's disease brain but not in transgenic mouse brain," *Journal of Neuroscience*, vol. 25, no. 46, pp. 10598–10606, 2005.

[63] H. Toyama, D. Ye, M. Ichise et al., "PET imaging of brain with the β-amyloid probe, [11C]6-OH- BTA-1, in a transgenic mouse model of Alzheimer's disease," *European Journal of Nuclear Medicine and Molecular Imaging*, vol. 32, no. 5, pp. 593–600, 2005.

[64] C. Kuntner, A. L. Kesner, M. Bauer et al., "Limitations of small animal PET imaging with [18F]FDDNP and FDG for quantitative studies in a transgenic mouse model of alzheimer's disease," *Molecular Imaging and Biology*, vol. 11, no. 4, pp. 236–240, 2009.

[65] R. F. Rosen, L. C. Walker, and H. Levine III, "PIB binding in aged primate brain: enrichment of high-affinity sites in humans with Alzheimer's disease," *Neurobiology of Aging*. In press.

[66] S. R. Choi, G. Golding, Z. Zhuang et al., "Preclinical properties of 18F-AV-45: a PET agent for Aβ plaques in the brain," *Journal of Nuclear Medicine*, vol. 50, no. 11, pp. 1887–1894, 2009.

[67] M. Dhenain, B. Delatour, C. Walczak, and A. Volk, "Passive staining: a novel ex vivo MRI protocol to detect amyloid deposits in mouse models of Alzheimer's disease," *Magnetic Resonance in Medicine*, vol. 55, no. 3, pp. 687–693, 2006.

[68] S.-P. Lee, M. F. Falangola, R. A. Nixon, K. Duff, and J. A. Helpern, "Visualization of β-amyloid plaques in a transgenic mouse model of Alzheimer's disease using MR microscopy without contrast reagents," *Magnetic Resonance in Medicine*, vol. 52, no. 3, pp. 538–544, 2004.

[69] J. Zhang, P. Yarowsky, M. N. Gordon et al., "Detection of amyloid plaques in mouse models of Alzheimer's disease by magnetic resonance imaging," *Magnetic Resonance in Medicine*, vol. 51, no. 3, pp. 452–457, 2004.

[70] R. Chamberlain, D. Reyes, G. L. Curran et al., "Comparison of amyloid plaque contrast generated by T2-weighted, T2*-weighted, and susceptibility-weighted imaging methods in transgenic mouse models of Alzheimer's disease," *Magnetic Resonance in Medicine*, vol. 61, no. 5, pp. 1158–1164, 2009.

[71] M. Dhenain, N. El Tannir El Tayara, T.-D. Wu et al., "Characterization of in vivo MRI detectable thalamic amyloid plaques from APP/PS1 mice," *Neurobiology of Aging*, vol. 30, no. 1, pp. 41–53, 2009.

[72] C. R. Jack Jr., M. Garwood, T. M. Wengenack et al., "In vivo visualization of Alzheimer's amyloid plaques by magnetic resonance imaging in transgenic mice without a contrast agent," *Magnetic Resonance in Medicine*, vol. 52, no. 6, pp. 1263–1271, 2004.

[73] G. Vanhoutte, I. Dewachter, P. Borghgraef, F. Van Leuven, and A. Van Der Linden, "Noninvasive in vivo MRI detection of neuritic plaques associated with iron in APP[V717I] transgenic mice, a model for Alzheimer's disease," *Magnetic Resonance in Medicine*, vol. 53, no. 3, pp. 607–613, 2005.

[74] M. F. Falangola, S.-P. Lee, R. A. Nixon, K. Duff, and J. A. Helpern, "Histological co-localization of iron in Aβ plaques of PS/APP transgenic mice," *Neurochemical Research*, vol. 30, no. 2, pp. 201–205, 2005.

[75] C. Quintana, T. D. Wu, B. Delatour et al., "Morphological and chemical studies of pathological human and mice brain at the sub cellular level: correlation between light, electron and nanoSIMS microscopies," *Microscopy Research and Technique*, vol. 70, pp. 281–295, 2007.

[76] M. D. Meadowcroft, J. R. Connor, M. B. Smith, and Q. X. Yang, "MRI and histological analysis of beta-amyloid plaques in both human Alzheimer's disease and APP/PS1 transgenic mice," *Journal of Magnetic Resonance Imaging*, vol. 29, no. 5, pp. 997–1007, 2009.

[77] M. Higuchi, N. Iwata, Y. Matsuba, K. Sato, K. Sasamoto, and T. C. Saido, "19F and 1H MRI detection of amyloid β plaques in vivo," *Nature Neuroscience*, vol. 8, no. 4, pp. 527–533, 2005.

[78] J. F. Poduslo, T. M. Wengenack, G. L. Curran et al., "Molecular targeting of Alzheimer's amyloid plaques for contrast-enhanced magnetic resonance imaging," *Neurobiology of Disease*, vol. 11, no. 2, pp. 315–329, 2002.

[79] Y. Z. Wadghiri, E. M. Sigurdsson, M. Sadowski et al., "Detection of Alzheimer's amyloid in transgenic mice using magnetic resonance microimaging," *Magnetic Resonance in Medicine*, vol. 50, no. 2, pp. 293–302, 2003.

[80] E. M. Sigurdsson, Y. Z. Wadghiri, L. Mosconi et al., "A non-toxic ligand for voxel-based MRI analysis of plaques in AD transgenic mice," *Neurobiology of Aging*, vol. 29, no. 6, pp. 836–847, 2008.

[81] M. Ramakrishnan, T. M. Wengenack, K. K. Kandimalla et al., "Selective contrast enhancement of individual Alzheimer's disease amyloid plaques using a polyamine and Gd-DOTA conjugated antibody fragment against fibrillar Aβ42 for magnetic resonance molecular imaging," *Pharmaceutical Research*, vol. 25, no. 8, pp. 1861–1872, 2008.

[82] B. Solomon, "Filamentous bacteriophage as a novel therapeutic tool for Alzheimer's disease treatment," *Journal of Alzheimer's Disease*, vol. 15, no. 2, pp. 193–198, 2008.

[83] D. Frenkel and B. Solomon, "Filamentous phage as vector-mediated antibody delivery to the brain," *Proceedings of the National Academy of Sciences of the United States of America*, vol. 99, no. 8, pp. 5675–5679, 2002.

[84] C. Perruchini, F. Pecorari, J.-P. Bourgeois, C. Duyckaerts, F. Rougeon, and P. Lafaye, "Llama VHH antibody fragments against GFAP: better diffusion in fixed tissues than classical monoclonal antibodies," *Acta Neuropathologica*, vol. 118, no. 5, pp. 685–695, 2009.

[85] P. Lafaye, I. Achour, P. England, C. Duyckaerts, and F. Rougeon, "Single-domain antibodies recognize selectively small oligomeric forms of amyloid β, prevent Aβ-induced neurotoxicity and inhibit fibril formation," *Molecular Immunology*, vol. 46, no. 4, pp. 695–704, 2009.

[86] K. S. Rutgers, A. van Remoortere, M. A. van Buchem et al., "Differential recognition of vascular and parenchymal beta amyloid deposition," *Neurobiology of Aging*. In press.

[87] T. Nakada, H. Matsuzawa, H. Igarashi, Y. Fujii, and I. L. Kwee, "In vivo visualization of senile-plaque-like pathology in Alzheimer's disease patients by mr microscopy on a 7T system," *Journal of Neuroimaging*, vol. 18, no. 2, pp. 125–129, 2008.

[88] S. Van Rooden, M. L. C. Maat-Schieman, R. J. A. Nabuurs et al., "Cerebral amyloidosis: postmortem detection with human 7.0-T MR imaging system," *Radiology*, vol. 253, no. 3, pp. 788–796, 2009.

[89] M. Hintersteiner, A. Enz, P. Frey et al., "In vivo detection of amyloid-β deposits by near-infrared imaging using an oxazine-derivative probe," *Nature Biotechnology*, vol. 23, no. 5, pp. 577–583, 2005.

[90] D. M. Connor, H. Benveniste, F. A. Dilmanian, M. F. Kritzer, L. M. Miller, and Z. Zhong, "Computed tomography of amyloid plaques in a mouse model of Alzheimer's disease using diffraction enhanced imaging," *NeuroImage*, vol. 46, no. 4, pp. 908–914, 2009.

[91] C. Holmes, D. Boche, D. Wilkinson et al., "Long-term effects of Aβ42 immunisation in Alzheimer's disease: follow-up of a randomised, placebo-controlled phase I trial," *The Lancet*, vol. 372, no. 9634, pp. 216–223, 2008.

[92] T. Mueggler, M. Meyer-Luehmann, M. Rausch, M. Staufenbiel, M. Jucker, and M. Rudin, "Restricted diffusion in the brain of transgenic mice with cerebral amyloidosis," *European Journal of Neuroscience*, vol. 20, no. 3, pp. 811–817, 2004.

[93] S.-K. Song, J. H. Kim, S.-J. Lin, R. P. Brendza, and D. M. Holtzman, "Diffusion tensor imaging detects age-dependent white matter changes in a transgenic mouse model with amyloid deposition," *Neurobiology of Disease*, vol. 15, no. 3, pp. 640–647, 2004.

[94] S.-W. Sun, S.-K. Song, M. P. Harms et al., "Detection of age-dependent brain injury in a mouse model of brain amyloidosis associated with Alzheimer's disease using magnetic resonance diffusion tensor imaging," *Experimental Neurology*, vol. 191, no. 1, pp. 77–85, 2005.

[95] M. P. Harms, J. J. Kotyk, and K. M. Merchant, "Evaluation of white matter integrity in ex vivo brains of amyloid plaque-bearing APPsw transgenic mice using magnetic resonance diffusion tensor imaging," *Experimental Neurology*, vol. 199, no. 2, pp. 408–415, 2006.

[96] M. Marjanska, G. L. Curran, T. M. Wengenack et al., "Monitoring disease progression in transgenic mouse models of Alzheimer's disease with proton magnetic resonance spectroscopy," *Proceedings of the National Academy of Sciences of the United States of America*, vol. 102, no. 33, pp. 11906–11910, 2005.

[97] M. Von Kienlin, B. Künnecke, F. Metzger et al., "Altered metabolic profile in the frontal cortex of PS2APP transgenic mice, monitored throughout their life span," *Neurobiology of Disease*, vol. 18, no. 1, pp. 32–39, 2005.

[98] N. Beckmann, A. Schuler, T. Mueggler et al., "Age-dependent cerebrovascular abnormalities and blood flow disturbances

in APP23 mice modeling Alzheimer's disease," *Journal of Neuroscience*, vol. 23, no. 24, pp. 8453–8459, 2003.

[99] E. P. Meyer, A. Ulmann-Schuler, M. Staufenbiel, and T. Krucker, "Altered morphology and 3D architecture of brain vasculature in a mouse model for Alzheimer's disease," *Proceedings of the National Academy of Sciences of the United States of America*, vol. 105, no. 9, pp. 3587–3592, 2008.

[100] N. El Tannir El Tayara, B. Delatour, A. Volk, and M. Dhenain, "Detection of vascular alterations by in vivo magnetic resonance angiography and histology in APP/PS1 mouse model of Alzheimer's disease," *Magnetic Resonance Materials in Physics, Biology and Medicine*, vol. 23, no. 1, pp. 53–64, 2010.

[101] F. Bourasset, M. Ouellet, C. Tremblay et al., "Reduction of the cerebrovascular volume in a transgenic mouse model of Alzheimer's disease," *Neuropharmacology*, vol. 56, no. 4, pp. 808–813, 2009.

[102] H. Moreno, W. E. Wu, T. Lee et al., "Imaging the Aβ-related neurotoxicity of Alzheimer disease," *Archives of Neurology*, vol. 64, no. 10, pp. 1467–1477, 2007.

[103] E. X. Wu, H. Tang, T. Asai, and S. D. Yan, "Regional cerebral blood volume reduction in transgenic mutant APP (V717F, K670N/M671L) mice," *Neuroscience Letters*, vol. 365, no. 3, pp. 223–227, 2004.

[104] K. Niwa, K. Kazama, S. G. Younkin, G. A. Carlson, and C. Iadecola, "Alterations in cerebral blood flow and glucose utilization in mice overexpressing the amyloid precursor protein," *Neurobiology of Disease*, vol. 9, no. 1, pp. 61–68, 2002.

[105] K. Niwa, K. Kazama, L. Younkin, S. G. Younkin, G. A. Carlson, and C. Iadecola, "Cerebrovascular autoregulation is profoundly impaired in mice overexpressing amyloid precursor protein," *American Journal of Physiology*, vol. 283, no. 1, pp. H315–H323, 2002.

[106] A. Faure, L. Verret, B. Bozon et al., "Impaired neurogenesis, neuronal loss, and brain functional deficits in the APPxPS1-Ki mouse model of Alzheimer's disease," *Neurobiology of Aging*. In press.

[107] C. Weidensteiner, F. Metzger, A. Bruns, B. Bohrmann, B. Kuennecke, and M. Von Kienlin, "Cortical hypoperfusion in the B6.PS2APP mouse model for Alzheimer's disease: comprehensive phenotyping of vascular and tissular parameters by MRI," *Magnetic Resonance in Medicine*, vol. 62, no. 1, pp. 35–45, 2009.

[108] E. M. Reiman, A. Uecker, F. Gonzalez-Lima et al., "Tracking Alzheimer's disease in transgenic mice using fluorodeoxyglucose autoradiology," *NeuroReport*, vol. 11, no. 5, pp. 987–991, 2000.

[109] J. Valla, F. Gonzalez-Lima, and E. M. Reiman, "FDG autoradiography reveals developmental and pathological effects of mutant amyloid in PDAPP transgenic mice," *International Journal of Developmental Neuroscience*, vol. 26, no. 3-4, pp. 253–258, 2008.

[110] J. Valla, L. Schneider, and E. M. Reiman, "Age- and transgene-related changes in regional cerebral metabolism in PSAPP mice," *Brain Research*, vol. 1116, no. 1, pp. 194–200, 2006.

[111] M. A. Busche, G. Eichhoff, H. Adelsberger et al., "Clusters of hyperactive neurons near amyloid plaques in a mouse model of Alzheimer's disease," *Science*, vol. 321, no. 5896, pp. 1686–1689, 2008.

[112] K. V. Kuchibhotla, S. T. Goldman, C. R. Lattarulo, H.-Y. Wu, B. T. Hyman, and B. J. Bacskai, "Aβ plaques lead to aberrant regulation of calcium homeostasis in vivo resulting in structural and functional disruption of neuronal," *Neuron*, vol. 59, no. 2, pp. 214–225, 2008.

[113] K. V. Kuchibhotla, C. R. Lattarulo, B. T. Hyman, and B. J. Bacskai, "Synchronous hyperactivity and intercellular calcium waves in astrocytes in Alzheimer mice," *Science*, vol. 323, no. 5918, pp. 1211–1215, 2009.

[114] A. C. Silva, J. H. Lee, I. Aoki, and A. P. Koretsky, "Manganese-enhanced magnetic resonance imaging (MEMRI): methodological and practical considerations," *NMR in Biomedicine*, vol. 17, no. 8, pp. 532–543, 2004.

[115] H. Morita, T. Ogino, Y. Seo et al., "Detection of hypothalamic activation by manganese ion contrasted T1-weighted magnetic resonance imaging in rats," *Neuroscience Letters*, vol. 326, no. 2, pp. 101–104, 2002.

[116] X. Yu, Y. Z. Wadghiri, D. H. Sanes, and D. H. Turnbull, "In vivo auditory brain mapping in mice with Mn-enhanced MRI," *Nature Neuroscience*, vol. 8, no. 7, pp. 961–968, 2005.

[117] T. Kimura, S. Yamashita, T. Fukuda et al., "Hyperphosphorylated tau in parahippocampal cortex impairs place learning in aged mice expressing wild-type human tau," *EMBO Journal*, vol. 26, no. 24, pp. 5143–5152, 2007.

[118] S. Minoshima and D. Cross, "In vivo imaging of axonal transport using MRI: aging and Alzheimer's disease," *European Journal of Nuclear Medicine and Molecular Imaging*, vol. 35, no. 1, pp. S89–S92, 2008.

[119] K. D. B. Smith, V. Kallhoff, H. Zheng, and R. G. Pautler, "In vivo axonal transport rates decrease in a mouse model of Alzheimer's disease," *NeuroImage*, vol. 35, no. 4, pp. 1401–1408, 2007.

[120] F. Serrano, M. Deshazer, K. D. B. Smith, J. S. Ananta, L. J. Wilson, and R. G. Pautler, "Assessing transneuronal dysfunction utilizing manganese-enhanced MRI (MEMRI)," *Magnetic Resonance in Medicine*, vol. 60, no. 1, pp. 169–175, 2008.

[121] O. Eschenko, S. Canals, I. Simanova, and N. K. Logothetis, "Behavioral, electrophysiological and histopathological consequences of systemic manganese administration in MEMRI," *Magnetic Resonance Imaging*, vol. 28, no. 8, pp. 1165–1174, 2010.

SAGE-Hindawi Access to Research
International Journal of Alzheimer's Disease
Volume 2010, Article ID 621870, 11 pages
doi:10.4061/2010/621870

Review Article

Alzheimer's Proteins, Oxidative Stress, and Mitochondrial Dysfunction Interplay in a Neuronal Model of Alzheimer's Disease

Antonella Bobba, Vito A. Petragallo, Ersilia Marra, and Anna Atlante

Istituto di Biomembrane e Bioenergetica, CNR, Via Amendola 165/A, 70126 Bari, Italy

Correspondence should be addressed to Anna Atlante, a.atlante@ibbe.cnr.it

Received 14 April 2010; Revised 24 June 2010; Accepted 9 July 2010

Academic Editor: Gemma Casadesus

In this paper, we discuss the interplay between beta-amyloid (Aβ) peptide, Tau fragments, oxidative stress, and mitochondria in the neuronal model of cerebellar granule neurons (CGNs) in which the molecular events reminiscent of AD are activated. The identification of the death route and the cause/effect relationships between the events leading to death could be helpful to manage the progression of apoptosis in neurodegeneration and to define antiapoptotic treatments acting on precocious steps of the death process. Mitochondrial dysfunction is among the earliest events linked to AD and might play a causative role in disease onset and progression. Recent studies on CGNs have shown that adenine nucleotide translocator (ANT) impairment, due to interaction with toxic N-ter Tau fragment, contributes in a significant manner to bioenergetic failure and mitochondrial dysfunction. These findings open a window for new therapeutic strategies aimed at preserving and/or improving mitochondrial function.

1. Introduction

Alzheimer's disease (AD) is a common neurodegenerative disorder characterized by altered processing of specific proteins, formation of neurofibrillary tangles, imbalance of redox homeostasis, and degeneration of synapses and neurons. Although the mechanism of neurodegeneration in AD is not clearly understood, several studies presently indicate that apoptosis might occur and contribute to AD onset and progression [1–5]. Though it remains to be determined whether true apoptosis is a necessary event in neurodegeneration, a growing number of studies support the activation of apoptosis in general, and caspases specifically, as an early event that contributes to neurodegeneration and promote the pathological hallmarks associate with AD [6].

Transgenic animal models have been useful tools to study AD, but currently many of them do not fully replicate the cascade of amyloid deposition, neurofibrillary tangles, and neurodegeneration that characterize the human disease [7]. Thus, as far as the studies about AD are concerned, the lack of an animal model that sufficiently resembles this disease is the reason why research should still proceed along parallel lines: studies carried out in animal models should be integrated and correlated to ad hoc-devised neuronal models in which the identification of single molecular steps is made possible.

Rat cerebellar granule neurons (CGNs) are a neuronal model widely used to study events linking apoptosis and neurodegeneration [8, 9] due to the ease of CGN culture production, their high degree of cellular homogeneity, and the findings revealing that during the onset of apoptosis several molecular events reminiscent of AD are activated [10].

In this paper, the role of key players of the neuronal apoptotic process is discussed with particular attention to the results obtained in CGNs. The production, effect, and interplay of beta-amyloid (Aβ), Tau protein and its fragments are discussed together with the action of these proteins on mitochondria, and this is integrated in the scenario of CGN apoptosis.

2. The Experimental Model of CGNs: A Useful Model to Elucidate Neurodegenerative Mechanism(s)

CGNs survive and differentiate in vitro in the presence of depolarizing concentrations of KCl (25 mM) without additional need for neurotrophic factors [11]. The mechanism of action of KCl is still controversial but, generally, it is believed that the increase in intracellular Ca^{2+} concentration [12, 13] and the activation of mitogen-activated protein kinase (MAPK) [14] induced by depolarization are involved.

If the serum is removed, and the concentration of KCl is kept below depolarizing levels (K5), the majority of CGNs die by an apoptotic process [12]. Under these conditions, that are equivalent to in vivo deafferentation, neuronal death is initiated and follows a general scheme that has been extensively characterized in recent years (for a review see [15]). The production of reactive oxygen species (ROS) and nitric oxide (NO), the increase in proteasome, antioxidant enzyme, and nitric oxide synthase (NOS) activities, and release of cytochrome *c* (cyt *c*) into the cytosol are some of the main events taking place soon after apoptosis induction in CGNs and for which a cause-effect relationship has been defined. In the early phase of apoptosis, ROS, NO, and cGMP production increases as well as the activities of antioxidant enzymes and NOS [16–20], as the cell's attempt to counteract the ongoing oxidative stress [18]. However, due to superoxide production, cyt *c* is released into the cytosol where it carries out a triple function since it acts (i) as an antioxidant compound and an ROS scavenger, (ii) as a respiratory substrate which can generate the mitochondrial transmembrane potential, and (iii) as the activator of the caspase cascade [21–23]. As a consequence of both NO and superoxide anion production, an increase in the levels of nitrated proteins has been found in the late phase (ranging from 3 to 15 hours after apoptosis induction) [19]. With apoptosis progression, the oxidative damage proceeds, antioxidant enzymes are inactivated by caspases and proteasome [18, 24], and, at the mitochondrial level, the adenine nucleotide translocator (ANT) is progressively impaired thus contributing to the transition pore opening in the late phase of the death process [25, 26].

Furthermore, it has been demonstrated that during the onset of apoptosis of CGNs, several molecular events reminiscent of AD are induced. An amyloidogenic process is activated with an increased production of Aβ which initiates a sort of autocrine toxic loop [27]. Contextually to the increase in Aβ deposition, Tau protein, which is the main constituent of AD neurofibrillary tangles, is cleaved by the concerted action of calpain and caspases with the production of toxic fragments [28, 29]. The mechanism of action of a Tau toxic fragment has been elucidated, and ANT has been identified as the specific mitochondrial target of such fragment [30].

3. Formation of $A\beta$ and Tau Protein Fragments in AD

One of the central points in the physiopathology of AD is the altered function and/or structure of two "Alzheimer's proteins," namely the amyloid precursor protein (APP) and Tau.

APP is a membrane glycoprotein, which undergoes complex intracellular trafficking. The biological function of APP is still not fully clear. Roles in cell adhesion, neuronal migration, cell proliferation, neurite outgrowth, axonal transport, neuroprotection, and signal transduction have been proposed [31]. The abnormal cleavage of APP leads to the production of Aβ which is the main component of senile plaques in AD and *per se* can induce neuronal cell death.

Tau is a neuron-specific microtubule-associated protein and a critical component of the neuronal cytoskeleton which progressively disaggregates during apoptosis. The proper function of Tau depends upon a precise equilibrium between different isoforms and its state of phosphorylation. In AD, as well as in other human dementias, Tau undergoes a series of posttranslational changes including abnormal phosphorylation, glycosylation, glycation, and truncation (see [32]), which may render Tau more prone to form aggregated structures, the neurofibrillary tangles, which constitute a major hallmark of AD. Following such aggregation, the microtubules disintegrate, collapsing the neuron's transport system, with consequent altered communication between neurons, eventually ending in cell death.

Interestingly, in the experimental model of CGNs, it has been proposed that Tau and APP form a complex *in vivo* via the adaptor protein Fe65 [33] which is abundantly expressed in the central nervous system of mammals and in particular in the cerebellum and hippocampus [34]. As a consequence, the full-length Tau can play a role in regulating the proper localization of APP and of its partners. During apoptosis, the disruption of the Tau-Fe65 interaction leads to a mislocalization of the APP-Fe65 complex within the cell that in turn could induce a change in the proteolytic fate of both APP and Tau proteins (Figure 1).

As far as Aβ production is concerned, it has been reported that in the commitment phase (6 hours) of CGN apoptosis, an amyloidogenic process is activated which rapidly and irreversibly leads to increased production of Aβ [27]. Aβ may be released outside the cell and act as a soluble and diffusible apoptotic death mediator, affecting neighbouring healthy neurons and activating a toxic loop that further accelerates and propagates the process of neurodegeneration. Accordingly, it has been found that coincubation of CGN apoptotic cultures with antibodies directed against Aβ significantly slows down the extension of cell death and quantitatively increases the neuronal survival rate [27]. Studies carried out on CGNs as well as on various cell models indicate that both nonaggregated and, to a greater extent, aggregated Aβ peptides of the short toxic fragment Aβ25–35 can induce apoptosis when externally added to cell cultures [35, 36] and that different Aβ aggregation forms (monomers, protofibrillar intermediate, and mature fibrils) can have diverse effects [37–39].

In the same experimental model (i.e., CGNs), Aβ25–35-induced apoptosis has been found to be associated with the activation of multiple executioner caspases (caspases-2, -3, and -6) [40], and the shorter Aβ fragment (Aβ31–35) is able to induce neurodegeneration with an early increase in

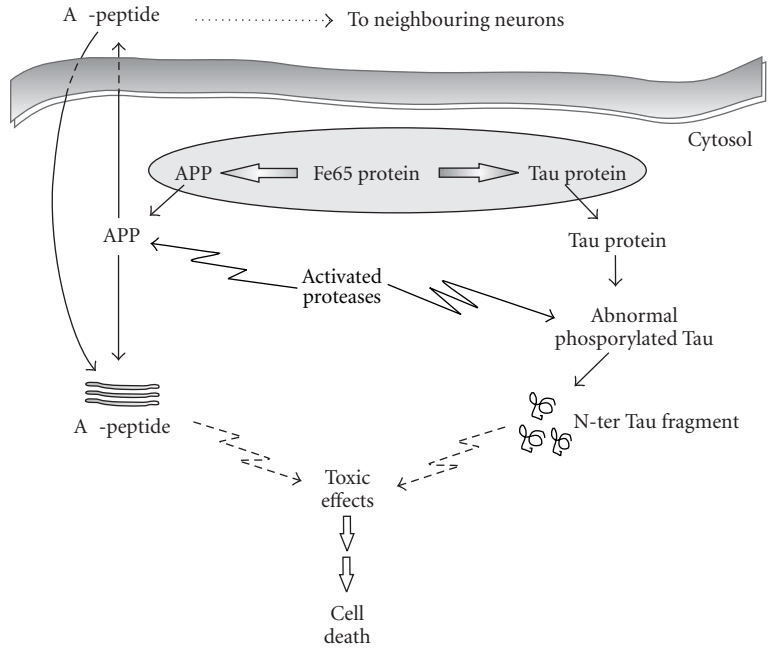

Figure 1: Schematic overview of Aβ peptide and Tau fragments production in CGNs. Aβ is produced intracellularly or taken up from extracellular sources and together with Tau fragments has various pathological effects on cell function.

bax mRNA level followed by delayed caspase-3 activation [41]. Finally, it has been reported that Aβ may interfere with K^+ channel trafficking [42, 43], altering K^+ currents and therefore causing an increase in cell death as a result of a decrease in cytoplasmic K^+ concentrations. Consistently, the selective upregulation of the expression of two voltage-dependent potassium channel subunits (Kv4.2 and Kv4.3) has been found in CGNs after Aβ25–35 exposure [44].

In CGNs, contextually to the significant increase in amyloidogenic metabolism of APP, Tau also undergoes posttranslational modifications. As soon as 6 hours after apoptosis induction, a change in Tau phosphorylation state occurs in concomitance with caspase and calpain-mediated cleavages (Figure 1). As a consequence, several fragments of Tau protein are produced during apoptosis, the most abundant of which is a 17 kDa residual fragment, probably located at the NH_2-terminus of Tau, which is unable to bind to microtubules and is diagnostic for the ongoing apoptotic process [28].

Truncated forms of Tau, besides being produced during apoptosis, can also be effectors of apoptosis by themselves and operate as toxic fragments that further induce cell death so contributing to the progression of neurodegeneration by an "autocatalytic process" [29, 45–47]. Both C-ter and N-ter Tau fragments have been analyzed for their neurotoxicity. While the microtubule-binding capacity of the C-ter fragment is well documented, relatively little is known about the function of the N-terminal domain. Transfection of neuronal cells with C-terminal Tau fragments induces cell death [46, 47] while exogenous overexpression of N-ter Tau fragments in CGNs can be either neuroprotective or neurotoxic depending on its length [29]. The long N-ter Tau fragment (1–230) is antiapoptotic and promotes the prosurvival effect of the AKT pathway. On the other hand, the short N-ter Tau fragment (1–44) exerts a toxic action involving glutamate receptors. Moreover, further analysis performed in the CGN model system further narrowed the extent of the aminoacid stretch which is toxic to the cells, and the N-ter-26–44 Tau fragment was found to be the minimal active moiety which retained a marked neurotoxic effect. On the other hand, the NH_2-1–25 Tau fragment was inactive [48].

4. $A\beta$ and N-ter Tau Fragments Interaction with Mitochondria

Mounting evidence indicates that mitochondrial dysfunction occurs early in AD, worsens with clinical deterioration, and is associated with impairment of energy homeostasis; deficit in the function of complexes of the respiratory chains reduced ATP synthesis as well as altered mitochondrial structure [49–51]. Consistently, a reduced activity of the cytochrome *c* oxidase (Complex IV of respiratory chain) has been reported in different brain regions [51] as well as in platelets [52] and fibroblasts [53] of AD patients, but the involvement of other mitochondrial oxidative phosphorylation complexes is less documented and more controversial. Cardoso and collaborators [54] found a decreased ATP level in AD cybrids, and other authors report that the activity of Complex IV, but not the activity of F1F0-ATPase (Complex V), decreases in the hippocampus and platelets of AD cases [55, 56]. Because mitochondria are the powerhouse of cells, damage to mitochondria, such as impairment of Complex IV activity, could have functional consequences on energy metabolism [56].

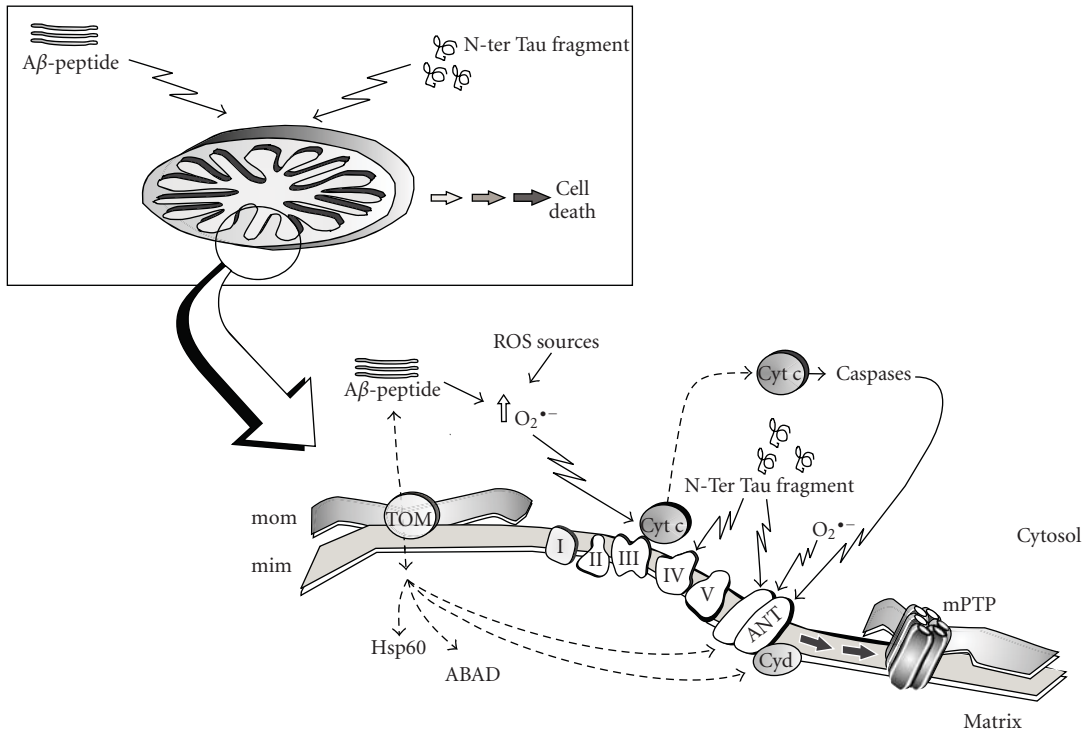

Figure 2: Proposed mechanism of Aβ peptide and N-ter Tau fragment interaction with mitochondria; for further details see text. *mom*, mitochondrial outer membrane; *mim*, mitochondrial inner membrane; *TOM*, translocase of the outer membrane; *I–V*, respiratory chain complexes; *cyt c*, cytochrome *c*; *ANT*, adenine nucleotide translocator; *CyD*, cyclophilin D; *mPTP*, mitochondrial permeability transition pore.

Furthermore, mitochondrial dysfunction has been proposed to be the link between the histopathological hallmarks of AD, caused by Aβ and Tau deposition, and neuronal and synaptic loss [57]. The emerging picture is one in which, at the level of mitochondria, both Alzheimer's proteins exhibit synergistic effects finally leading to the acceleration of neurodegenerative mechanisms (Figure 2).

As far as Aβ is concerned, although the classical view is that Aβ is deposited extracellularly, both cellular and biochemical studies carried out in different models of AD and aging have provided evidence that this peptide can also accumulate inside neurons, target mitochondria, and contribute to disease progression [58–61]. By using in vivo and in vitro approaches, it has been demonstrated that Aβ is transported into rat mitochondria via the translocase of the outer membrane (TOM) [62] and localizes within the mitochondrial cristae. A similar distribution pattern of Aβ in mitochondria has been shown by immunoelectron microscopy in human cortical brain biopsies [62].

Interaction of Aβ with mitochondria could be considered a general route common to different cell types since both in dividing cells (i.e., neuroblastoma cells) and in terminally differentiated neurons (i.e., primary neuronal cultures), either extracellulary applied or secreted *Aβ* can be internalized, and it colocalizes with mitochondrial markers [62, 63] (Figure 2). Interaction of Aβ with the matrix protein ABAD (amyloid-binding alcohol dehydrogenase) has been described [64], whereas Caspersen et al. [65] reported that in mouse and human brain samples from AD patients, Aβ colocalizes with the mitochondrial matrix protein Hsp60. Recent biochemical studies imply that the formation of the mitochondrial permeability transition pore (mPTP) is involved in Aβ-mediated mitochondrial dysfunction [66], and by using a computational approach and predictive analysis tools, it has been hypothesized that Aβ can strongly interact in the inner membrane with ANT and Cyclophilin D, two components of the mPTP [67].

A connection between Tau protein and mitochondria has recently been proposed; by overexpressing the N-ter Tau fragment truncated at Asp-421 to mimic caspase cleavage in immortalized neurons, it was possible to induce mitochondrial fragmentation and elevated oxidative stress levels [68].

To the best of our knowledge, the toxicity of N-ter Tau fragments on mitochondria has been deeply investigated only in the CGN model system and has been found to involve a mitochondrial dysfunction with impairment of oxidative phosphorylation [30] (Figure 2). Both Complex IV and ANT proved to be targets of the short NH_2-26–44 Tau fragment, but ANT is the only mitochondrial target responsible for the impairment of oxidative phosphorylation. Detailed biochemical studies have revealed that inhibition of ANT is noncompetitive, suggesting that the NH_2-26–44 Tau fragment does not interact with the catalytic site but with some other site of the enzyme which could distort the enzyme structure thus also affecting the catalytic binding site.

This finding is consistent with the picture of the apoptotic process in CGN that to date has been built up: in late apoptosis, a noncompetitive-like inhibition of ANT has been

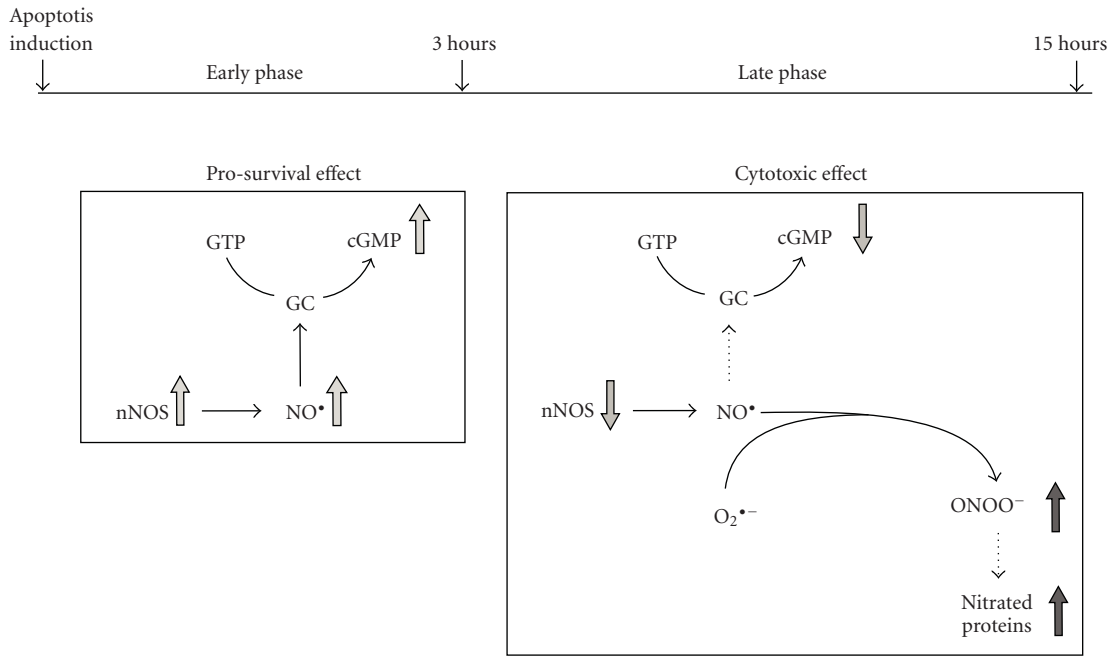

Figure 3: Schematic representation of the time-dependent, dual role of nitric oxide in CGN apoptosis; see text for details. *GC*, guanylil cyclase; *cGMP*, cyclic GMP; *nNOS*, neuronal nitric oxide synthase; $O_2^{\bullet -}$, superoxide anion; $ONOO^-$, peroxynitrite.

found, probably due to caspase activity [26], but it is not dependent on a direct caspase–ANT interaction. However since NH_2-26–44 Tau fragment is likely to be generated during apoptosis given that the N-terminal domain of Tau contains consensus sequences suitable for cleavage by caspase(s) [28, 45], which are activated in apoptotic degenerating neurons in AD [69, 70], the possibility exists that caspase(s) gradually inhibit/s ANT as a result of NH_2-Tau cleavage and the generation of toxic NH_2-26–44 Tau fragment. In this case, NH_2-26–44 Tau fragment should directly bind ANT.

5. Nitric Oxide and AD: Interplay between Alzheimer's Proteins, Nitrosative/Oxidative Stress, and Mitochondria

NO produced by NOS, is a molecule endowed with a double role acting as either a prosurvival or a toxic molecule. As a prosurvival molecule, NO plays a role in cell signaling in the nervous system and in synaptic plasticity [71, 72], and it may be involved in diverse biological functions acting through either cGMP-dependent or -independent pathways.

When the role of the NO/NOS system was investigated in CGNs, it was found that NO exerts its dual and opposite effects on the neurodegenerative process, depending on the time after induction of apoptosis (Figure 3). In an early phase, up to 3 h of apoptosis, there is an increase in the expression of the neuronal isoform of NOS (nNOS) as well as in the production of NO, which in turn supports the survival of CGNs through a cGMP-dependent mechanism.

Consistently with these results, it has also been reported that: (i) NO may be responsible for neuroprotection during Aβ-induced cell death [73, 74], (ii) low concentration of NO produced by a healthy cerebrovascular endothelium was found to influence the parenchymal brain cells in a protective way [75], and (iii) in cultured human neuroblastoma cells, low concentrations of NO upregulate the expression of alpha-secretase, while downregulating that of beta-secretase, suggesting that, in the relative absence of superoxide, cerebrovascular NO might act to suppress brain production of Aβ [76].

On the other hand, sustained generation of NO has been implicated in the cellular death occurring in different neurodegenerative diseases as well as in AD [77]. As far as the experimental system of CGNs is concerned (Figure 3), it was found that, in the late phase of the apoptotic program, after 3 h, nNOS expression and activity decreased, resulting in the shut down of NO and cGMP production, and the toxic role of nitric oxide prevailed due to the reaction with superoxide anions to produce peroxynitrite ($ONOO^-$) which in turn is able to induce neuronal injury mainly through nitration of tyrosine residues in cellular proteins, whose level increases. These events together with other apoptotic events already described in this cell model [15, 23, 25, 26] would commit these cells irreversibly to death.

Thus, it can be assumed that once accumulated inside the cell, NO can play different roles, depending on its level, cell context, and amount of superoxide anion. In Figure 4, a general picture is shown which takes into account the main findings on the involvement of nitrosative stress in the neurodegenerative process. In brains from AD patients, an early and striking upregulation of all three isoforms of NOS has been reported [78, 79]. This finding is further supported by experimental data obtained in different systems, ranging

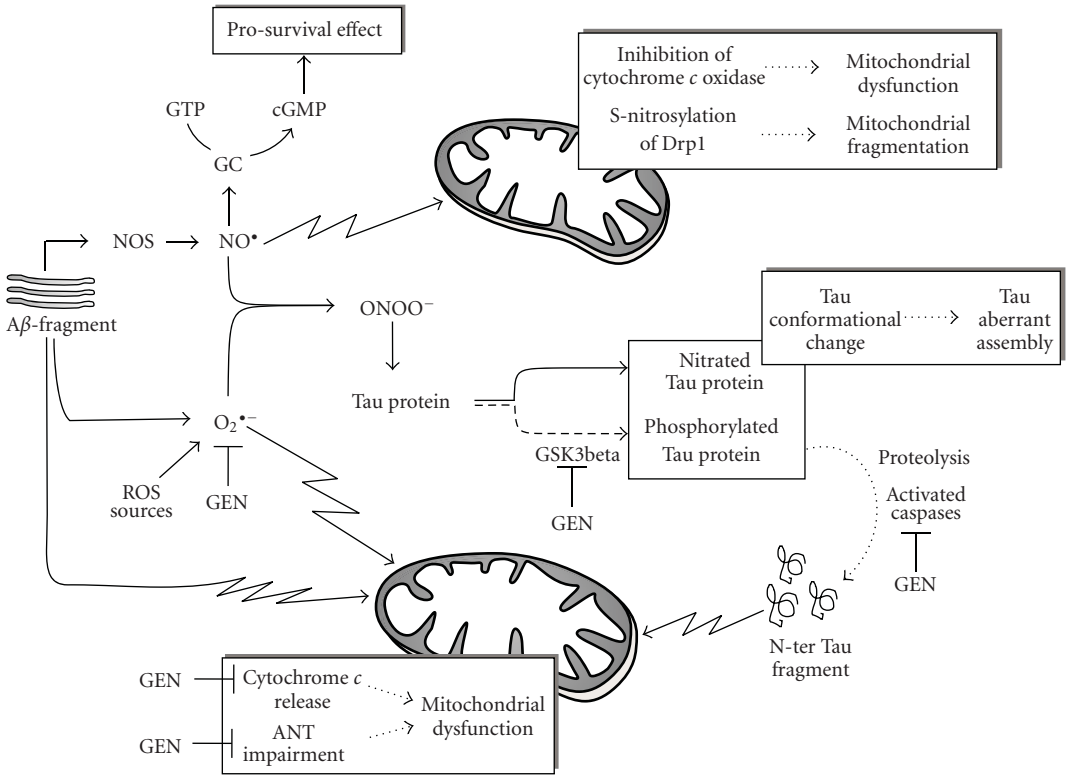

Figure 4: Schematic overview of the interplay between Aβ, Tau, oxidative/nitrosative stress, and mitochondria; see text for details. *GC*, guanylil cyclase; *cGMP*, cyclic GMP; *NOS*, nitric oxide synthase; $O_2^{\bullet -}$, superoxide anion; $ONOO^-$, peroxynitrite; *ANT*, adenine nucleotide translocator; *GSK3beta,* glycogen synthase kinase-3beta; *GEN*, Genistein.

from in vivo animals to cell lines, which indicates that NO is responsible for Aβ toxicity and highlights a link between NO/NOS level and Aβ-induced brain dysfunction [80, 81]. Activation of the neuronal isoform of NOS (nNOS) [82] and an increased production of NO [83] were also found in rat cerebral cortex and hippocampus after intracerebroventricular administration of Aβ25–30 and in APP-transfected cells, respectively.

In an early phase, NO could induce a cGMP-mediated prosurvival signaling pathway in an attempt to counteract the ongoing neurodegenerative process [19, 84]. However, NO can also directly trigger mitochondrial dysfunction, a process which is believed to play a causative role in AD onset and progression. Indeed it has been reported that NO both induces a bioenergetic failure, with impairment in the function of Complex IV [85], and triggers mitochondrial fission/fragmentation thus causing cell death in primary culture of cortical neurons [86, 87]. S-nitrosylation, a covalent redox reaction of NO with specific protein thiol groups, could be one mechanism contributing to the NO-induced mitochondrial fragmentation. Accordingly, it has been reported that in AD patients and animal model, NO induces S-nitrosylation of dynamin-related protein 1 (Drp1), a protein specifically involved in mitochondrial fission [88, 89]. On the other hand, Bossy et al. [90] found that NO can also induce Drp1 inactivation by increasing its phosphorylation. Although there are no data on the involvement of Drp1 in the CGN model, it has been recently reported that mitochondrial fragmentation occurs as an early event in response to injury in CGNs, and increased activation of mitofusin 2 (Mfn2), a protein involved in mitochondrial fusion, blocks mitochondrial fragmentation and protects neurons against cell death [91, 92].

In addition to NO, oxidative damage has been reported in aging and age-related neurodegenerative diseases, including AD [93, 94], and superoxide anion production has been induced by Aβ-treatment in neurons [95, 96]. It is known that in the course of neurodegeneration, the superoxide anion can act directly on mitochondria thus inducing cyt *c* release and precocious impairment of ANT (see [18] and references therein).

On the other hand, NO readily reacts with superoxide anions to form the strong oxidant $ONOO^-$ which in turn induces protein nitration. Consistently, an increase in protein nitration has been found in brain tissue from cases of AD which correlates with neurodegeneration [97]. Tau protein can also undergo a $ONOO^-$-mediated process, and nitration of the Tyr29 residue has been proposed as a specific disease-related event [98]. Furthermore, peroxynitrite can also induce AD-like Tau hyperphosphorylation via activation of both glycogen synthase kinase-3beta (GSK3beta) and p38 MAPKs [99].

Nitration, as well as phosphorylation, of Tau protein induces conformational changes that facilitate aberrant Tau

assembly. Consistently, it has been reported that nitrated Tau is colocalized with neurofibrillary tangle in AD brain, shows a significantly decreased binding activity to microtubules, and is involved in the formation of filamentous Tau inclusions [100]. In these conditions, Tau fragmentation might occur, and N-ter Tau fragments, together with Aβ and superoxide, can further decrease mitochondrial efficiency thus contributing to mitochondrial dysfunction.

6. Implication of Genistein on Preventing $A\beta$ and Tau Toxicity

The main goal in AD treatment is focused on a preventive approach. Treatment of declared AD with any compounds may have either a poor effect due to the severe neuronal death occurring in AD or a questionable risk/benefit ratio such as in the case of estrogen. In this regard, estrogen has been shown to block Aβ-induced neuronal cell death in several studies thus suggesting that estradiol replacement therapy should show improvement in patients with AD [101]. However, the efficiency of estradiol in the treatment of AD has been seriously questioned due to its fourth unwanted side effect, that is, proliferative and oncogenic effects on non-neuronal cells [102].

A clear point emerging from the bulk of studies dealing with AD etiopathology is that all factors involved in AD are associated with oxidative stress [103]. In the light of this, natural oxidants have recently received much attention as promising agents for reducing the risk of oxidative stress-related diseases. Among them genistein received a lot of attention.

Genistein (4′.5.7-trihydroxyisoflavone) is the most active compound of soy isoflavones, the one which reaches the highest concentration in human blood [104], possesses an antioxidant activity, shows an affinity to estrogen receptors, thus acting as an estrogen-like compound but without the negative effects of estrogens, and is able to cross the blood-brain barrier (see [105]).

There is considerable literature about the effect of genistein on the progression of neurodegeneration. It has been reported that in the nervous system, isoflavones attenuate primary neuronal apoptosis by activating estrogen receptors [106] and genistein is able both to suppress Aβ25–35-induced ROS overproduction in isolated rat brain synaptosomes [107] and to increase cell viability in cooperation with other trophic factor such as folic acid in cortical neurons [108]. Consistently, Zeng et al. [105] describe the protective effect of genistein on cultured hippocampal neurons against Aβ-induced apoptosis and have demonstrated that genistein inhibits the elevation of intracellular free Ca^{2+}, the production of oxidant free radicals caused by Aβ25–35, the DNA fragmentation, and the activation of caspase-3, thus suggesting that genistein acts upstream of caspase-3 to block apoptosis (Figure 4).

Genistein may also decrease the hyperphosphorylation of Tau protein by inactivating GSK3beta, the kinase involved in Tau phosphorylation in homocysteine-mediated neurodegeneration in SH-SY5Y human neuroblastoma cells [109].

Recently, in CGNs undergoing apoptosis, the effect of genistein was studied at subcellular level and for the first time at mitochondrial level [110]. Genistein and to a lesser extent its analogue daidzein, both used at dietary concentrations, can prevent low potassium-dependent apoptosis in CGNs by reducing the impairment of both aerobic glucose metabolism and mitochondrial uncoupling, two processes occurring in CGN apoptosis [16]. Furthermore, genistein is also able to prevent cyt *c* release, ANT alteration, and mPTP opening; that is, some steps of the mitochondrial pathway to apoptosis that are somehow related to the ROS production which takes place during apoptosis.

Thus, since both genistein and daidzein have been proved to decrease ROS levels, it has been suggested that the prevention of apoptosis is essentially due to the antioxidant properties of these flavonoids [110]. Nonetheless, the effect of genistein proved to be rather specific since other flavonoids such as catechin and epicatechin failed to prevent CGN death in spite of their shared antioxidant capability.

Consistently, genistein also abolishes neuronal ROS production induced by $A\beta$ administration to primary culture of cortical neurons [111] and enhances the activities of other antioxidant molecules and enzymes (superoxide dismutase, glutathione peroxidase and reductase) both in vitro and in vivo [112, 113].

7. Conclusions

The etiology of Alzheimer's disease is complex and not fully elucidated. On the other hand, it is important to develop a better understanding of the different biochemical pathways, their role, and their link with the amyloid hypothesis in AD, since it may lead to the development of more effective treatment strategies for this disease. It seems clear then that promising developments as for the prevention and/or delay of the onset of AD can be derived from definition of antiapoptotic treatments acting on the precocious steps of the death process, such as blockade of generation of reactive oxygen species and implementation of the NO prosurvival signaling pathway that, although not able to fully prevent the disease, can at least delay onset or reduce the severity of neurodegeneration. In this regard, genistein and its analogue daidzein may perhaps be of use in neuroprotection. Furthermore, the knowledge emerging from studies conducted on CGNs, that ANT impairment contributes in a significant manner to bioenergetic failure and mitochondrial dysfunction in the course of neurodegeneration, may open a window for new therapeutic strategies aimed at preserving and/or improving mitochondrial function, representing an exciting challenge for biochemists. More studies are required to determine whether phytoestrogens, protease inhibitors and mitochondrial-targeted compounds could fulfill these expectations.

Acknowledgment

The authors thank Mr. Richard Lusardi for linguistic consultation.

References

[1] M. P. Mattson, "Neuronal life-and-death signaling, apoptosis, and neurodegenerative disorders," *Antioxidants & Redox Signaling*, vol. 8, no. 11-12, pp. 1997–2006, 2006.

[2] C. Culmsee and S. Landshamer, "Molecular insights into mechanisms of the cell death programml: role in the progression of neurodegenerative disorders," *Current Alzheimer Research*, vol. 3, no. 4, pp. 269–283, 2006.

[3] A. Nunomura, P. I. Moreira, H. G. Lee et al., "Neuronal death and survival under oxidative stress in Alzheimer and Parkinson diseases," *CNS & Neurological Disorders—Drug Targets*, vol. 6, no. 6, pp. 411–423, 2007.

[4] L. S. Honig and R. N. Rosenberg, "Apoptosis and neurologic disease," *The American Journal of Medicine*, vol. 108, no. 4, pp. 317–330, 2000.

[5] A. Eckert, C. A. Marques, U. Keil, K. Schüssel, and W. E. Müller, "Increased apoptotic cell death in sporadic and genetic Alzheimer's Disease," *Annals of the New York Academy of Sciences*, vol. 1010, pp. 604–609, 2003.

[6] T. T. Rohn and E. Head, "Caspase activation in Alzheimer's disease: early to rise and late to bed," *Reviews in the Neurosciences*, vol. 19, no. 6, pp. 383–393, 2008.

[7] C. Schwab, M. Hosokawa, and P. L. McGeer, "Transgenic mice overexpressing amyloid beta protein are an incomplete model of Alzheimer disease," *Experimental Neurology*, vol. 188, no. 1, pp. 52–64, 2004.

[8] N. Canu and P. Calissano, "In vitro cultured neurons for molecular studies correlating apoptosis with events related to Alzheimer disease," *Cerebellum*, vol. 2, no. 4, pp. 270–278, 2003.

[9] P. Calissano, C. Matrone, and G. Amadoro, "Apoptosis and in vitro Alzheimer disease neuronal models," *Communitative & Integrative Biology*, vol. 2, no. 2, pp. 163–169, 2009.

[10] S. Cicconi, A. Gentile, M. T. Ciotti, T. Parasassi, A. Serafino, and P. Calissano, "Apoptotic death induces Aβ production and fibril formation to a much larger extent than necrotic-like death in CGNs," *Journal of Alzheimer's Disease*, vol. 12, no. 3, pp. 211–220, 2007.

[11] V. Gallo, M. T. Ciotti, F. Aloisi, and G. Levi, "Developmental features of rat cerebellar neural cells cultured in a chemically defined medium," *Journal of Neuroscience Research*, vol. 15, no. 3, pp. 289–301, 1986.

[12] S. R. D'Mello, C. Galli, T. Ciotti, and P. Calissano, "Induction of apoptosis in cerebellar granule neurons by low potassiumml: inhibition of death by insulin-like growth factor I and cAMP," *Proceedings of the National Academy of Sciences of the United States of America*, vol. 90, no. 23, pp. 10989–10993, 1993.

[13] C. Galli, O. Meucci, A. Scorziello, T. M. Werge, P. Calissano, and G. Schettini, "Apoptosis in cerebellar granule cells is blocked by high KCl, forskolin, and IGF-1 through distinct mechanisms of action: the involvement of intracellular calcium and RNA synthesis," *Journal of Neuroscience*, vol. 15, no. 2, pp. 1172–1179, 1995.

[14] L. B. Rosen, D. D. Ginty, M. J. Weber, and M. E. Greenberg, "Membrane depolarization and calcium influx stimulate MEK and MAP kinase via activation of Ras," *Neuron*, vol. 12, no. 6, pp. 1207–1221, 1994.

[15] A. Bobba, A. Atlante, L. de Bari, S. Passarella, and E. Marra, "Apoptosis and cytochrome *c* release in cerebellar granule cells," *In Vivo*, vol. 18, no. 3, pp. 335–344, 2004.

[16] A. Atlante, S. Gagliardi, E. Marra, and P. Calissano, "Neuronal apoptosis in rats is accompanied by rapid impairment of cellular respiration and is prevented by scavengers of reactive oxygen species," *Neuroscience Letters*, vol. 245, no. 3, pp. 127–130, 1998.

[17] A. Atlante and S. Passarella, "Detection of reactive oxygen species in primary cultures of cerebellar granule cells," *Brain Research Protocols*, vol. 4, no. 3, pp. 266–270, 1999.

[18] A. Atlante, A. Bobba, P. Calissano, S. Passarella, and E. Marra, "The apoptosis/necrosis transition in cerebellar granule cells depends on the mutual relationship of the antioxidant and the proteolytic systems which regulate ROS production and cytochrome *c* release en route to death," *Journal of Neurochemistry*, vol. 84, no. 5, pp. 960–971, 2003.

[19] A. Bobba, A. Atlante, L. Moro, P. Calissano, and E. Marra, "Nitric oxide has dual opposite roles during early and late phases of apoptosis in cerebellar granule neurons," *Apoptosis*, vol. 12, no. 9, pp. 1597–1610, 2007.

[20] A. Bobba, A. Atlante, V. A. Petragallo, and E. Marra, "Different sources of reactive oxygen species contribute to low potassium-induced apoptosis in cerebellar granule cells," *International Journal of Molecular Medicine*, vol. 21, no. 6, pp. 737–745, 2008.

[21] A. Atlante, P. Calissano, A. Bobba, A. Azzariti, E. Marra, and S. Passarella, "Cytochrome c is released from mitochondria in a reactive oxygen species (ROS)-dependent fashion and can operate as a ROS scavenger and as a respiratory substrate in cerebellar neurons undergoing excitotoxic death," *Journal of Biological Chemistry*, vol. 275, no. 47, pp. 37159–37166, 2000.

[22] A. Atlante, L. De Bari, A. Bobba, E. Marra, P. Calissano, and S. Passarella, "Cytochrome *c*, released from cerebellar granule cells undergoing apoptosis or excytotoxic death, can generate protonmotive force and drive ATP synthesis in isolated mitochondria," *Journal of Neurochemistry*, vol. 86, no. 3, pp. 591–604, 2003.

[23] A. Bobba, A. Atlante, S. Giannattasio, G. Sgaramella, P. Calissano, and E. Marra, "Early release and subsequent caspase-mediated degradation of cytochrome *c* in apoptotic cerebellar granule cells," *FEBS Letters*, vol. 457, no. 1, pp. 126–130, 1999.

[24] A. Bobba, N. Canu, A. Atlante, V. Petragallo, P. Calissano, and E. Marra, "Proteasome inhibitors prevent cytochrome c release during apoptosis but not in excitotoxic death of cerebellar granule neurons," *FEBS Letters*, vol. 515, no. 1–3, pp. 8–12, 2002.

[25] A. Atlante, S. Giannattasio, A. Bobba et al., "An increase in the ATP levels occurs in cerebellar granule cells en route to apoptosis in which ATP derives from both oxidative phosphorylation and anaerobic glycolysis," *Biochimica et Biophysica Acta*, vol. 1708, no. 1, pp. 50–62, 2005.

[26] A. Atlante, A. Bobba, L. de Bari et al., "Caspase-dependent alteration of the ADP/ATP translocator triggers the mitochondrial permeability transition which is not required for the low-potassium-dependent apoptosis of cerebellar granule cells," *Journal of Neurochemistry*, vol. 97, no. 4, pp. 1166–1181, 2006.

[27] C. Galli, A. Piccini, M. T. Ciotti et al., "Increased amyloidogenic secretion in cerebellar granule cells undergoing apoptosis," *Proceedings of the National Academy of Sciences of the United States of America*, vol. 95, no. 3, pp. 1247–1252, 1998.

[28] N. Canu, L. Dus, C. Barbato et al., "Tau cleavage and dephosphorylation in cerebellar granule neurons undergoing apoptosis," *Journal of Neuroscience*, vol. 18, no. 18, pp. 7061–7074, 1998.

[29] G. Amadoro, A. L. Serafino, C. Barbato et al., "Role of N-terminal tau domain integrity on the survival of cerebellar granule neurons," *Cell Death & Differentiation*, vol. 11, no. 2, pp. 217–230, 2004.

[30] A. Atlante, G. Amadoro, A. Bobba et al., "A peptide containing residues 26-44 of tau protein impairs mitochondrial oxidative phosphorylation acting at the level of the adenine nucleotide translocator," *Biochimica et Biophysica Acta*, vol. 1777, no. 10, pp. 1289–1300, 2008.

[31] E. H. Koo, "The β-amyloid precursor protein (APP) and alzheimer's disease: does the tail wag the dog?" *Traffic*, vol. 3, no. 11, pp. 763–770, 2002.

[32] M. Goedert, M. G. Spillantini, R. Jakes, D. Rutherford, and R. A. Crowther, "Multiple isoforms of human microtubule-associated protein tau: sequences and localization in neurofibrillary tangles of Alzheimer's disease," *Neuron*, vol. 3, no. 4, pp. 519–526, 1989.

[33] C. Barbato, N. Canu, N. Zambrano et al., "Interaction of Tau with Fe65 links tau to APP," *Neurobiology of Disease*, vol. 18, no. 2, pp. 399–408, 2005.

[34] S. Kesavapany, S. J. Banner, K.-F. Lau et al., "Expression of the Fe65 adapter protein in adult and developing mouse brain," *Neuroscience*, vol. 115, no. 3, pp. 951–960, 2002.

[35] A. Scorziello, O. Meucci, T. Florio et al., "β25-35 alters calcium homeostasis and induces neurotoxicity in cerebellar granule cells," *Journal of Neurochemistry*, vol. 66, no. 5, pp. 1995–2003, 1996.

[36] B. A. Yankner, L. R. Dawes, S. Fisher, L. Villa-Komaroff, M. L. Oster-Granite, and R. L. Neve, "Neurotixicity of a fragment of the amyloid precursor associated with Alzheimer's disease," *Science*, vol. 245, no. 4916, pp. 417–420, 1989.

[37] D. M. Hartley, D. M. Walsh, C. P. Ye et al., "Protofibrillar intermediates of amyloid β-protein induce acute electrophysiological changes and progressive neurotoxicity in cortical neurons," *Journal of Neuroscience*, vol. 19, no. 20, pp. 8876–8884, 1999.

[38] D. M. Walsh and D. J. Selkoe, "Deciphering the molecular basis of memory failure in Alzheimer's disease," *Neuron*, vol. 44, no. 1, pp. 181–193, 2004.

[39] G. M. Shankar, B. L. Bloodgood, M. Townsend, D. M. Walsh, D. J. Selkoe, and B. L. Sabatini, "Natural oligomers of the Alzheimer amyloid-β protein induce reversible synapse loss by modulating an NMDA-type glutamate receptor-dependent signaling pathway," *Journal of Neuroscience*, vol. 27, no. 11, pp. 2866–2875, 2007.

[40] J. W. Allen, B. A. Eldadah, X. Huang, et al., "Multiple caspases are involved in beta-amyloid-induced neuronal apoptosis," *Journal of Neuroscience Research*, vol. 65, no. 1, pp. 45–53, 2001.

[41] F. Misiti, M. E. Clementi, G. Tringali et al., "Fragment 31-35 of β-amyloid peptide induces neurodegeneration in rat cerebellar granule cells via bax gene expression and caspase-3 activation. A crucial role for the redox state of methionine-35 residue," *Neurochemistry International*, vol. 49, no. 5, pp. 525–532, 2006.

[42] A. Pannaccione, F. Boscia, A. Scorziello et al., "Up-regulation and increased activity of KV3.4 channels and their accessory subunit MinK-related peptide 2 induced by amyloid peptide are involved in apoptotic neuronal death," *Molecular Pharmacology*, vol. 72, no. 3, pp. 665–673, 2007.

[43] L. D. Plant, N. J. Webster, J. P. Boyle et al., "Amyloid β peptide as a physiological modulator of neuronal 'A'-type K^+ current," *Neurobiology of Aging*, vol. 27, no. 11, pp. 1673–1683, 2006.

[44] M. Pieri, G. Amadoro, I. Carunchio et al., "SP protects cerebellar granule cells against β-amyloid-induced apoptosis by down-regulation and reduced activity of Kv4 potassium channels," *Neuropharmacology*, vol. 58, no. 1, pp. 268–276, 2010.

[45] T. T. Rohn, R. A. Rissman, M. C. Davis, Y. E. Kim, C. W. Cotman, and E. Head, "Caspase-9 activation and caspase cleavage of tau in the Alzheimer's disease brain," *Neurobiology of Disease*, vol. 11, no. 2, pp. 341–354, 2002.

[46] L. Fasulo, G. Ugolini, M. Visintin et al., "The neuronal microtubule-associated protein tau is a substrate for caspase-3 and an effector of apoptosis," *Journal of Neurochemistry*, vol. 75, no. 2, pp. 624–633, 2000.

[47] C.-W. Chung, Y.-H. Song, I.-K. Kim et al., "Proapoptotic effects of tau cleavage product generated by caspase-3," *Neurobiology of Disease*, vol. 8, no. 1, pp. 162–172, 2001.

[48] G. Amadoro, M. T. Ciotti, M. Costanzi, V. Cestari, P. Calissano, and N. Canu, "NMDA receptor mediates tau-induced neurotoxicity by calpain and ERK/MAPK activation," *Proceedings of the National Academy of Sciences of the United States of America*, vol. 103, no. 8, pp. 2892–2897, 2006.

[49] K. Leuner, S. Hauptmann, R. Abdel-Kader et al., "Mitochondrial dysfunction: the first domino in brain aging and Alzheimer's disease?" *Antioxidants and Redox Signaling*, vol. 9, no. 10, pp. 1659–1675, 2007.

[50] V. Rhein, G. Baysang, S. Rao et al., "Amyloid-beta leads to impaired cellular respiration, energy production and mitochondrial electron chain complex activities in human neuroblastoma cells," *Cellular and Molecular Neurobiology*, vol. 29, no. 6-7, pp. 1063–1071, 2009.

[51] M. Mancuso, F. Coppedè, L. Murri, and G. Siciliano, "Mitochondrial cascade hypothesis of Alzheimer's disease: myth or reality?" *Antioxidants & Redox Signaling*, vol. 9, no. 10, pp. 1631–1646, 2007.

[52] W. D. Parker Jr., C. M. Filley, and J. K. Parks, "Cytochrome oxidase deficiency in Alzheimer's disease," *Neurology*, vol. 40, no. 8, pp. 1302–1303, 1990.

[53] K. Tieu, C. Perier, M. Vila et al., "L-3-hydroxyacyl-CoA dehydrogenase II protects in a model of Parkinson's disease," *Annals of Neurology*, vol. 56, no. 1, pp. 51–60, 2004.

[54] S. M. Cardoso, I. Santana, R. H. Swerdlow, and C. R. Oliveira, "Mitochondria dysfunction of Alzheimer's disease cybrids enhances Aβ toxicity," *Journal of Neurochemistry*, vol. 89, no. 6, pp. 1417–1426, 2004.

[55] F. Bosetti, F. Brizzi, S. Barogi et al., "Cytochrome c oxidase and mitochondrial F1F0-ATPase (ATP synthase) activities in platelets and brain from patients with Alzheimer's disease," *Neurobiology of Aging*, vol. 23, no. 3, pp. 371–376, 2002.

[56] M. Mancuso, M. Filosto, F. Bosetti et al., "Decreased platelet cytochrome *c* oxidase activity is accompanied by increased blood lactate concentration during exercise in patients with Alzheimer disease," *Experimental Neurology*, vol. 182, no. 2, pp. 421–426, 2003.

[57] A. Eckert, K .L. Schulz, V. Rhein, et al., "Convergence of amyloid-beta and tau pathologies on mitochondria in vivo," *Molecular Neurobiology*, vol. 41, no. 2-3, pp. 107–114, 2010.

[58] P. H. Reddy, "Mitochondrial dysfunction in aging and Alzheimer's disease: strategies to protect neurons," *Antioxidants & Redox Signaling*, vol. 9, no. 10, pp. 1647–1658, 2007.

[59] P. H. Reddy, "Amyloid beta, mitochondrial structural and functional dynamics in Alzheimer's disease," *Experimental Neurology*, vol. 218, no. 2, pp. 286–292, 2009.

[60] X. Chen and S. D. Yan, "Mitochondrial Aβ: a potential cause of metabolic dysfunction in Alzheimer's disease," *IUBMB Life*, vol. 58, no. 12, pp. 686–694, 2006.

[61] F. M. LaFerla, K. N. Green, and S. Oddo, "Intracellular amyloid-β in Alzheimer's disease," *Nature Reviews Neuroscience*, vol. 8, no. 7, pp. 499–509, 2007.

[62] C. A. Hansson Petersen, N. Alikhani, H. Behbahani et al., "The amyloid β-peptide is imported into mitochondria via the TOM import machinery and localized to mitochondrial cristae," *Proceedings of the National Academy of Sciences of the United States of America*, vol. 105, no. 35, pp. 13145–13150, 2008.

[63] L. Saavedra, A. Mohamed, V. Ma, S. Kar, and E. P. De Chaves, "Internalization of β-amyloid peptide by primary neurons in the absence of apolipoprotein E," *Journal of Biological Chemistry*, vol. 282, no. 49, pp. 35722–35732, 2007.

[64] K. E. Muirhead, E. Borger, L. Aitken, S. J. Conway, and F.J. Gunn-Moore, "The consequences of mitochondrial amyloid beta-peptide in Alzheimer's disease," *Biochemical Journal*, vol. 426, no. 3, pp. 255–270, 2010.

[65] C. Caspersen, N. Wang, J. Yao et al., "Mitochondrial Aβ: a potential focal point for neuronal metabolic dysfunction in Alzheimer's disease," *The FASEB Journal*, vol. 19, no. 14, pp. 2040–2041, 2005.

[66] H. Du and S. S. Yan, "Mitochondrial permeability transition pore in Alzheimer's disease: cyclophilin D and amyloid beta," *Biochimica et Biophysica Acta*, vol. 1802, no. 1, pp. 198–204, 2010.

[67] P. Singh, S. Suman, S. Chandna, et al., "Possible role of amyloid-beta, adenine nucleotide translocase and cyclophilin-D interaction in mitochondrial dysfunction of Alzheimer's disease," *Bioinformation*, vol. 3, no. 10, pp. 440–445, 2009.

[68] R. A. Quintanilla, T. A. Matthews-Roberson, P. J. Dolan, and G. V. W. Johnsion, "Caspase-cleaved tau expression induces mitochondrial dysfunction in immortalized cortical neurons: implications for the pathogenesis of alzheimer disease," *Journal of Biological Chemistry*, vol. 284, no. 28, pp. 18754–18766, 2009.

[69] T. T. Rohn, E. Head, J. H. Su et al., "Correlation between caspase activation and neurofibrillary tangle formation in Alzheimer's disease," *American Journal of Pathology*, vol. 158, no. 1, pp. 189–198, 2001.

[70] M. C. Gastard, J. C. Troncoso, and V. E. Koliatsos, "Caspase activation in the limbic cortex of subjects with early Alzheimer's disease," *Annals of Neurology*, vol. 54, no. 3, pp. 393–398, 2003.

[71] J. L. Dinerman, T. M. Dawson, M. J. Schell, A. Snowman, and S. H. Snyder, "Endothelial nitric oxide synthase localized to hippocampal pyramidal cells: implications for synaptic plasticity," *Proceedings of the National Academy of Sciences of the United States of America*, vol. 91, no. 10, pp. 4214–4218, 1994.

[72] M. Zhuo, E. R. Kandel, and R. D. Hawkins, "Nitric oxide and cGMP can produce either synaptic depression or potentiation depending on the frequency of presynaptic stimulation in the hippocampus," *Neuroreport*, vol. 5, no. 9, pp. 1033–1036, 1994.

[73] G. R. J. Thatcher, B. M. Bennett, and J. N. Reynolds, "NO chimeras as therapeutic agents in Alzheimer's disease," *Current Alzheimer Research*, vol. 3, no. 3, pp. 237–245, 2006.

[74] D. Puzzo, O. Vitolo, F. Trinchese, J. P. Jacob, A. Palmeri, and O. Arancio, "Amyloid-β peptide inhibits activation of the nitric oxide/cGMP/cAMP-responsive element-binding protein pathway during hippocampal synaptic plasticity," *Journal of Neuroscience*, vol. 25, no. 29, pp. 6887–6897, 2005.

[75] M. F. McCarty, "Toward prevention of alzheimers disease—potential nutraceutical strategies for suppressing the production of amyloid beta peptides," *Medical Hypotheses*, vol. 67, no. 4, pp. 682–697, 2006.

[76] T. Pak, P. Cadet, K. J. Mantione, and G. B. Stefano, "Morphine via nitric oxide modulates β-amyloid metabolismml: a novel protective mechanism for Alzheimer's disease," *Medical Science Monitor*, vol. 11, no. 10, pp. BR357–BR366, 2005.

[77] D. Seyidova, A. Aliyev, N. Rzayev et al., "The role of nitric oxide in the pathogenesis of brain lesions during the development of Alzheimer's disease," *In Vivo*, vol. 18, no. 3, pp. 325–334, 2004.

[78] H. J. Lüth, M. Holzer, H.-J. Gertz, and TH. Arendt, "Aberrant expression of nNOS in pyramidal neurons in Alzheimer's disease is highly co-localized with p21(ras) and p16(INK4a)," *Brain Research*, vol. 852, no. 1, pp. 45–55, 2000.

[79] S. M. de la Monte, B.-X. Lu, Y.-K. Sohn et al., "Aberrant expression of nitric oxide synthase III in Alzheimer's disease: relevance to cerebral vasculopathy and neurodegeneration," *Neurobiology of Aging*, vol. 21, no. 2, pp. 309–319, 2000.

[80] M. H. Tran, K. Yamada, A. Olariu, M. Mizuno, X. H. Ren, and T. Nabeshima, "Amyloid β-peptide induces nitric oxide production in rat hippocampus: association with cholinergic dysfunction and amelioration by inducible nitric oxide synthase inhibitors," *The FASEB Journal*, vol. 15, no. 8, pp. 1407–1409, 2001.

[81] J. Haas, B. Storch-Hagenlocher, A. Biessmann, and B. Wildemann, "Inducible nitric oxide synthase and argininosuccinate synthetase: co-induction in brain tissue of patients with Alzheimer's dementia and following stimulation with β-amyloid 1–42 in vitro," *Neuroscience Letters*, vol. 322, no. 2, pp. 121–125, 2002.

[82] M. YU. Stepanichev, M. V. Onufriev, A. A. Yakovlev et al., "Amyloid-β (25–35) increases activity of neuronal NO-synthase in rat brain," *Neurochemistry International*, vol. 52, no. 6, pp. 1114–1124, 2008.

[83] U. Keil, A. Bonert, C. A. Marques et al., "Amyloid β-induced changes in nitric oxide production and mitochondrial activity lead to apoptosis," *Journal of Biological Chemistry*, vol. 279, no. 48, pp. 50310–50320, 2004.

[84] K.-S. Ha, K.-M. Kim, Y.-G. Kwon et al., "Nitric oxide prevents 6-hydroxydopamine-induced apoptosis in PC12 cells through cGMP-dependent PI3 kinase/Akt activation," *The FASEB Journal*, vol. 17, no. 9, pp. 1036–1047, 2003.

[85] S. M. de la Monte and J. R. Wands, "Molecular indices of oxidative stress and mitochondrial dysfunction occur early and often progress with severity of Alzheimer's disease," *Journal of Alzheimer's Disease*, vol. 9, no. 2, pp. 167–181, 2006.

[86] H. Yuan, A. A. Gerencser, G. Liot et al., "Mitochondrial fission is an upstream and required event for bax foci formation in response to nitric oxide in cortical neurons," *Cell Death and Differentiation*, vol. 14, no. 3, pp. 462–471, 2007.

[87] M. J. Barsoum, H. Yuan, A. A. Gerencser et al., "Nitric oxide-induced mitochondrial fission is regulated by dynamin-related GTPases in neurons," *The EMBO Journal*, vol. 25, no. 16, pp. 3900–3911, 2006.

[88] D.-H. Cho, T. Nakamura, J. Fang et al., "S-nitrosylation of Drp1 mediates beta-amyloid-related mitochondrial fission and neuronal injury," *Science*, vol. 324, no. 5923, pp. 102–105, 2009.

[89] Z. Gu, T. Nakamura, and S. A. Lipton, "Redox reactions induced by nitrosative stress mediate protein misfolding and mitochondrial dysfunction in neurodegenerative diseases," *Molecular Neurobiology*, vol. 41, no. 2-3, pp. 55–72, 2010.

[90] B. Bossy, A. Petrilli, E. Klinglmayr, et al., "S-Nitrosylation of DRP1 does not affect enzymatic activity and is not specific to Alzheimer's disease," *Journal of Alzheimer's Disease*, vol. 20, no. 2, pp. 513–526, 2010.

[91] A. Jahani-Asl, E. C. C. Cheung, M. Neuspiel et al., "Mitofusin 2 protects cerebellar granule neurons against injury-induced cell death," *Journal of Biological Chemistry*, vol. 282, no. 33, pp. 23788–23798, 2007.

[92] B. Su, X. Wang, L. Zheng, G. Perry, M. A. Smith, and X. Zhu, "Abnormal mitochondrial dynamics and neurodegenerative diseases," *Biochimica et Biophysica Acta*, vol. 1802, no. 1, pp. 135–142, 2010.

[93] A. Nunomura, R. J. Castellani, X. Zhu, P. I. Moreira, G. Perry, and M. A. Smith, "Involvement of oxidative stress in Alzheimer disease," *Journal of Neuropathology and Experimental Neurology*, vol. 65, no. 7, pp. 631–641, 2006.

[94] B. Su, X. Wang, A. Nunomura et al., "Oxidative stress signaling in Alzheimer's disease," *Current Alzheimer Research*, vol. 5, no. 6, pp. 525–532, 2008.

[95] A. Jana and K. Pahan, "Fibrillar amyloid-β peptides kill human primary neurons via NADPH oxidase-mediated activation of neutral sphingomyelinase:implications for Alzheimer's disease," *Journal of Biological Chemistry*, vol. 279, no. 49, pp. 51451–51459, 2004.

[96] P. B. Shelat, M. Chalimoniuk, J.-H. Wang et al., "Amyloid beta peptide and NMDA induce ROS from NADPH oxidase and AA release from cytosolic phospholipase A2 in cortical neurons," *Journal of Neurochemistry*, vol. 106, no. 1, pp. 45–55, 2008.

[97] M. A. Smith, P. L. Richey Harris, L. M. Sayre, J. S. Beckman, and G. Perry, "Widespread peroxynitrite-mediated damage in Alzheimer's disease," *Journal of Neuroscience*, vol. 17, no. 8, pp. 2653–2657, 1997.

[98] M. R. Reynolds, J. F. Reyes, Y. Fu et al., "Tau nitration occurs at tyrosine 29 in the fibrillar lesions of Alzheimer's disease and other tauopathies," *Journal of Neuroscience*, vol. 26, no. 42, pp. 10636–10645, 2006.

[99] Y.-J. Zhang, Y.-F. Xu, Y.-H. Liu et al., "Peroxynitrite induces Alzheimer-like tau modifications and accumulation in rat brain and its underlying mechanisms," *The FASEB Journal*, vol. 20, no. 9, pp. 1431–1442, 2006.

[100] T. Horiguchi, K. Uryu, B. I. Giasson et al., "Nitration of tau protein is linked to neurodegeneration in tauopathies," *American Journal of Pathology*, vol. 163, no. 3, pp. 1021–1031, 2003.

[101] C. J. Pike, J. C. Carroll, E. R. Rosario, and A. M. Barron, "Protective actions of sex steroid hormones in Alzheimer's disease," *Frontiers in Neuroendocrinology*, vol. 30, no. 2, pp. 239–258, 2009.

[102] J. E. Rossouw, G. L. Anderson, R. L. Prentice et al., "Risks and benefits of estrogen plus progestin in healthy postmenopausal women: principal results from the women's health initiative randomized controlled trial," *Journal of the American Medical Association*, vol. 288, no. 3, pp. 321–333, 2002.

[103] G. Perry, A. D. Cash, and M. A. Smith, "Alzheimer disease and oxidative stress," *Journal of Biomedicine and Biotechnology*, vol. 2002, no. 3, pp. 120–123, 2002.

[104] O. Y. Bang, H. S. Hong, D. H. Kim et al., "Neuroprotective effect of genistein against beta amyloid-induced neurotoxicity," *Neurobiology of Disease*, vol. 16, no. 1, pp. 21–28, 2004.

[105] H. Zeng, Q. Chen, and B. Zhao, "Genistein ameliorates β-amyloid peptide (25-35)-induced hippocampal neuronal apoptosis," *Free Radical Biology and Medicine*, vol. 36, no. 2, pp. 180–188, 2004.

[106] N. J. Linford and D. M. Dorsa, "17β-Estradiol and the phytoestrogen genistein attenuate neuronal apoptosis induced by the endoplasmic reticulum calcium-ATPase inhibitor thapsigargin," *Steroids*, vol. 67, no. 13-14, pp. 1029–1040, 2002.

[107] J. M. Andersen, O. Myhre, and F. Fonnum, "Discussion of the role of the extracellular signal-regulated kinase-phospholipase A2 pathway in production of reactive oxygen species in Alzheimer's disease," *Neurochemical Research*, vol. 28, no. 2, pp. 319–326, 2003.

[108] H.-L. Yu, L. Li, X.-H. Zhang et al., "Neuroprotective effects of genistein and folic acid on apoptosis of rat cultured cortical neurons induced by beta-amyloid 31-35," *British Journal of Nutrition*, vol. 102, no. 5, pp. 655–662, 2009.

[109] Y.-J. Park, Y.-M. Jang, and Y. H. Kwon, "Isoflavones prevent endoplasmic reticulum stress-mediated neuronal degeneration by inhibiting tau hyperphosphorylation in SH-SY5Y Cells," *Journal of Medicinal Food*, vol. 12, no. 3, pp. 528–535, 2009.

[110] A. Atlante, A. Bobba, G. Paventi, R. Pizzuto, and S. Passarella, "Genistein and daidzein prevent low potassium-dependent apoptosis of cerebellar granule cells," *Biochemical Pharmacology*, vol. 79, no. 5, pp. 758–767, 2010.

[111] S. L. Vallés, C. Borrás, J. Gambini et al., "Oestradiol or genistein rescues neurons from amyloid beta-induced cell death by inhibiting activation of p38," *Aging Cell*, vol. 7, no. 1, pp. 112–118, 2008.

[112] Q. Cai and H. Wei, "Effect of dietary genistein on antioxidant enzyme activities in SENCAR mice," *Nutrition and Cancer*, vol. 25, no. 1, pp. 1–7, 1996.

[113] P. Foti, D. Erba, P. Riso, A. Spadafranca, F. Criscuoli, and G. Testolin, "Comparison between daidzein and genistein antioxidant activity in primary and cancer lymphocytes," *Archives of Biochemistry and Biophysics*, vol. 433, no. 2, pp. 421–427, 2005.

SAGE-Hindawi Access to Research
International Journal of Alzheimer's Disease
Volume 2010, Article ID 417314, 9 pages
doi:10.4061/2010/417314

Research Article

Pathological Hallmarks, Clinical Parallels, and Value for Drug Testing in Alzheimer's Disease of the APP[V717I] London Transgenic Mouse Model

An Tanghe,[1] Annelies Termont,[1] Pascal Merchiers,[2] Stephan Schilling,[3] Hans-Ulrich Demuth,[3] Louise Scrocchi,[4] Fred Van Leuven,[5] Gerard Griffioen,[1] and Tom Van Dooren[1]

[1] *reMYND NV, Gaston Geenslaan 1, 3001 Heverlee-Leuven, Belgium*
[2] *Ablynx NV, Technologiepark 214, 9052 Zwijnaarde-Gent, Belgium*
[3] *Probiodrug AG, Weinbergweg 22, 06120 Halle-Saale, Germany*
[4] *Amorfix Life Sciences Ltd., 3403 American Drive, Mississauga, ON, Canada L4V1T4*
[5] *Experimental Genetics Group LEGTEGG, KULeuven, Campus Gasthuisberg ON1, 3000 Leuven, Belgium*

Correspondence should be addressed to An Tanghe, an.tanghe@remynd.com

Received 14 May 2010; Accepted 9 July 2010

Academic Editor: Gemma Casadesus

The APP[V717I] London (APP-Ld) mouse model recapitulates important pathological and clinical hallmarks of Alzheimer's disease (AD) and is therefore a valuable paradigm for evaluating therapeutic candidates. Historically, both the parenchymal and vascular amyloid deposits, and more recently, truncated and pyroglutamate-modified Abeta$_{3(pE)–42}$ species, are perceived as important hallmarks of AD-pathology. Late stage symptoms are preceded by robust deficits in orientation and memory that correlate in time with Abeta oligomerization and GSK3β-mediated phosphorylation of endogenous murine Tau, all markers that have gained considerable interest during the last decade. Clinical parallels with AD patients and the value of the APP-Ld transgenic mouse model for preclinical *in vivo* testing of candidate drugs are discussed.

1. Introduction

Notwithstanding the vast amount of resources invested into discovery and development of new targets and treatments, Alzheimer's disease (AD) remains an indication with enormous unmet needs. One complicating factor for successful drug development is the unknown etiology of idiopathic AD. AD entails noxious aggregation of β-amyloid (Abeta) and Tau, representing fundamental processes in disease onset and progression [1–3]. The extracellular Abeta plaques and intracellular neurofibrillary tangles (NFTs) represent key pathological hallmarks, but are not necessarily the primary causes of neuronal toxicity. The underlying molecular mechanisms of plaque and tangle formation, and how they interact, remain largely elusive. It is generally accepted that these processes involve formation of misconfomers of the respective proteins with increased propensity to self-polymerize in a stepwise fashion. It is clear that the process of aggregation is toxic and triggers neuronal degeneration. However, no consensus exists as to the exact nature, composition, or conformation of the protein assemblies that trigger neuronal demise. This situation is reflected by the fact that no validated drug targets are known whose modulation provides a robust therapeutic response. However, given the fundamental involvement of Abeta in AD—which is hypothesized as an early instigator of toxic downstream processes in AD—pharmacological intervention of APP pathobiology (processing, clearance, and aggregation) received most interest from the pharma industry up to now.

The identification of the pathogenic variants of hAPP and hPS1 genes running in families with inheritable AD has enabled the generation of transgenic animal models, mainly rodents, for AD (for a recent review, see [4, 5]). In recent years, the value and limitations of AD rodent models, both in terms of providing a better understanding of disease pathogenesis and progression and aiding the development

of drugs for treating disease, have been a topic of intense and recurrent debate in the Alzheimer field, as is illustrated by numerous recent reviews and opinion papers [6, 7]. Although none of the current AD rodent models fully recapitulate all aspects of disease, that is, displaying a progressive development of all specific neuropathological and cognitive aspects of AD, some mouse models reproduce or recapitulate at least several of the most important characteristics [8].

In this paper, we review pathological read-outs and introduce two new neuropathological markers of the "APP London" (APP-Ld) mouse model, that is, early-onset aggregation of Abeta and subsequent appearance of truncated, pyroglutamate-modified Abeta3–42 ($\text{Abeta}_{3(\text{pE})-42}$) amyloid peptide species in the brain. Furthermore, we discuss clinical parallels with the human Alzheimer patient and the value of the model for preclinical *in vivo* testing of candidate Alzheimer drugs.

2. Experimental Procedures

2.1. Transgenic Mice. Female transgenic mice in mixed FVB/N × C57Bl/6J background expressing heterozygously hAPP[V717I] under control of the neuron-specific murine *thy1* gene promoter have been used in this study. The construction of the FVB/N background strain has been described earlier [1, 9, 10]. The F1-hybrid strain was a crossing of heterozygous APP[V717I] males in C57Bl/6J background with wild type FVB/N females. In addition, double transgenic mice overexpressing hAPP[V717I] and hPS1[A246E] were generated by crossbreeding the single hAPP[V717I] mutant with homozygous hPS1[A426E] mice [11]. Genotyping by two independent PCR assays per transgene at the age of three weeks and at the onset of the experiments on DNA extracted from tail biopsies confirmed the respective genotypes.

2.2. Animal Care and Handling. All treatments were approved by the Local Committee for Animal Use and were performed in accordance to state and federal regulations. During the time of study, mice had access to prefiltered sterile water and standard mouse chow (Ssniff Ms-H, Ssniff Spezialdiäten GmbH, Soest, Germany) ad libitum and were housed under a reversed day-night rhythm in individual ventilated macrolon T2 cages in accordance to local legislation on animal welfare.

2.3. Sacrifice, CSF Collection, and Brain Processing. The mice were anaesthetized with a mixture of Anesketin (Ketamin), Rompun (Xylazin 2%), Atropin and saline (1 : 1 : 1 : 1), and perfused transcardiacally with ice-cold saline. Cerebrospinal fluid (CSF) was collected via an incision in the neck muscles between the skull and the first cervical vertebrae. A puncture into the cisterna magna was given with a 26-gauge needle and 10–20 μL of CSF was collected with a fine glass pipette. The brain was excised from the cranium, and hindbrain and forebrain were separated at the coronal plane. The left and right hemispheres were separated. Routinely, one hemisphere was immersion fixed overnight in phosphate-buffered saline (PBS) containing 4% paraformaldehyde for (immuno) histology, and the other hemisphere was snap-frozen in liquid nitrogen and stored at −80°C until further use in biochemical assays.

2.4. Abeta40 and Abeta42 in CSF. Human Abeta40 and Abeta42 concentrations in CSF were measured using commercial ELISA kits according to the manufacturers protocol (Human Amyloid 40 or 42 HS ELISA, Millipore).

2.5. Abeta Immunohistochemistry. Sagittal free-floating sections (40 μm) were stored in PBS containing 0,01% (w/v) sodium azide at 4°C until staining. Sections were washed twice in PBS and quenched with 1.5% (v/v) hydrogen peroxide in PBS and methanol (1 : 1) for 15 minutes to remove endogenous peroxidase activity. After washing the sections three times in PBS containing 0,1% Triton X100 (PBST), sections were blocked for 30 minutes in 10% Fetal Calf Serum (FCS) in PBST and incubated overnight with a biotinylated anti-Abeta antibody in blocking buffer (proprietary anti-Abeta Nanobody against N-terminus of Abeta, reMYND/Ablynx). After rinsing, the sections were incubated in 0,01% trypsin in PBS for 15 minutes at room temperature, followed by incubation with avidin-biotin peroxidase complex (Vectastain Elite ABC, Vector Laboratories). The signal was developed with 3, 3′ diaminobenzidine tetrahydrochloride tablets (DAB, ICN). Sections were counterstained with Mayers hematoxylin, dehydrated and mounted in Depex (Depex mounting medium, VWR International). Microscopic images were recorded and digitalized with a 3 CCD color video camera and analyzed with dedicated software (Olympus BX41 microscope, Color view II—Olympus camera, Analysis Five—Cell^D software).

2.6. Abeta_{x-42} and $\text{Abeta}_{3(pE)-42}$ Levels in Brain. Brain tissue was homogenized in TBS (20 mM Tris-HCl pH 7.6, 137 mM NaCl) containing protease inhibitor cocktail (Complete Mini, Roche), followed by sequential extractions with 1% Triton X-100 in TBS (TBS fraction), 2% SDS in water (SDS fraction), and 70% formic acid (FA fraction). The FA fraction was neutralized with 3.5 M Tris and diluted 1 : 20 in EIA buffer (IBL International). Pyroglutamate-modified Abeta ($\text{Abeta}_{3(\text{pE})-42}$) and pan-Abeta42 ($\text{Abeta}_{x-42}$) were assessed using specific sandwich ELISAs (IBL International).

2.7. Aggregated Abeta in Brain. A 10% (w/v) brain homogenate was prepared from each brain sample in 2% (v/v) NP40 in PBS (NaCl 0.138 M, KCl 0.0027 M, pH 7.4) containing 1 mM PMSF and protease inhibitors (Complete Mini, Roche). The 10% brain homogenates were further diluted into buffer to a final concentration that would provide a signal within the linear range of the immunoassay. The concentration of aggregated Abeta was measured using a proprietary assay (Amorfix Aggregated Abeta Assay (A^4), Amorfix, Mississauga, Canada). Using a proprietary sample enrichment protocol, only the aggregated Abeta was isolated from each sample. Each sample was then disaggregated to

allow detection of monomeric Abeta using the Amorfix Abeta immunoassay based on an europium-fluorescent bead coupled to the 4G10 antibody (N-terminal) and magnetic beads coupled to the antibodies 1F8 and 2H12 (C-terminal) recognizing Abeta40 and Abeta42, respectively. The europium fluorescence intensity was measured using Time Resolved Fluorescence (TRF) on each sample in triplicate and is directly proportional to the concentration of Abeta within the sample. The current limit of detection is 50 fg/well. The S/N cutoff value for all experiments was 2.0, equaling two times the background signal from buffer alone.

3. Results and Discussion

3.1. The APP-Ld Transgenic Mouse Recapitulates Early and Late Hallmarks of Alzheimer's Disease. The APP[V717I] mutation is the most frequent in familial AD with 74 families known, *versus* only three with the APP Swedish mutation (AD&FTD Mutation Database—http://www.molgen.ua.ac.be/ADMutations). In the APP[V717I] mice, the London mutant allele is heterogeneously expressed under control of the neuron-specific murine *thy1* gene promoter, steering postnatal expression to a level 2 times higher than endogenous APP [9].

3.2. Late Stage Amyloid Plaque Pathology, the Object of Historical Focus

3.2.1. Increased Abeta Levels. In the APP-Ld mouse, an age-dependent progressive increase of both soluble and insoluble Abeta40 and Abeta42 levels was observed in brain extracts. Soluble Abeta42/40 ratios increased up to 1 with age, whereas insoluble Abeta42/40 ratios were 5–10 times higher ([11] and unpublished data). Thus, APP-Ld mice display a high relative concentration of Abeta42, the more fibrillogenic Abeta species, essential for amyloid deposition in the parenchyma and vessels [12]. The V717I substitution is located downstream of the gamma-secretase cleavage site and affects the processing of the APP protein causing a shift from Abeta40 to Abeta42 cleavage and thereby increasing the Abeta42/40 ratio. Since processing at the α-, β-, or γ-cleavage sites is not clearly affected by age, the production of Abeta *per se* is not thought to be the primary cause of the accumulation in the APP-Ld mouse brain [11]. Instead, the failure of Abeta clearance or degradation has been proposed as the underlying mechanism.

3.2.2. Parenchymal Amyloid Depositions. Parenchymal amyloid plaques arise at the age of 10–12 months in the entorhinal cortex and subiculum (Figure 1(a))—brain regions hierarchically involved in early stages of development of AD pathology in patients [13, 14]—and subsequently spread to the frontal cortex [9]. A proprietary anti-Abeta Nanobody recognizes fibrillar Abeta species with high specificity and affinity. Two types of Abeta depositions—resembling the pathology in AD brain—develop in the brain parenchyma of the APP-Ld mouse, that is, plaques bearing a diffuse character immunoreactive to Abeta antibodies and senile (Thioflavin S positive) plaques comprising an amyloid core surrounded by a halo and neuritic processes [9, 15]. The neuritic component contains hyperphosphorylated forms of protein Tau detected as dystrophic processes by mAb AT8 immunohistochemistry [9] attributed to early neurofibrillary changes in AD. In addition, plaque formation is accompanied by amyloid-associated neuroinflammation, that is, astrocytosis and gliosis, also typically found in AD patients [16], and can be readily detected with immunohistological markers GFAP for staining astrocytes and CD11b/CD45 for the total and activated microglia load, respectively.

3.2.3. Vascular Amyloid Depositions (Cerebral Amyloid Angiopathy, CAA). At old age, the deposition of amyloid in cerebral vessel walls is observed in the APP-Ld model, with from 10 to more than 50 vessels affected per coronal brain section [17]. Similar to parenchymal plaque formations, Abeta42 is the first peptide to be deposited in vessels, and as such entrapping massive amounts of soluble Abeta40 peptide, the latter ultimately making up for the vast majority of amyloid in vascular plaques [17]. Cerebral amyloid angiopathy is frequent in AD [18] and the ratio of Abeta42/40 is lower in vascular than in parenchymal plaques [19]. The latter is explained by drainage of Abeta40 along the perivascular space because of its higher solubility. The morphological, ultrastructural, and biochemical aspects of the human vascular amyloid depositions, as well as the localization and the type of vessels affected, are reproduced in the APP-Ld model suggesting a similar underlying mechanism of Abeta deposition [17]. Vascular amyloid leads to progressive vessel wall damage and aneurism formation, predisposing the mice to hemorrhage and eventual microbleeds observed at very old age (25–30 months) reminiscent of vascular amyloidosis in a subset of AD patients.

3.2.4. $Abeta_{3(pE)–42}$ Accumulation in Plaques. The presence of C-truncated Abeta1-38 and N-truncated Abeta11–42 peptides in APP-Ld brain extracts was demonstrated previously in [20]. In addition, we show here that pyroglutamate-modified Abeta3–42 ($Abeta_{3(pE)–42}$), a dominant fraction of Abeta peptides in senile plaques of AD brain [21], is detected in the insoluble fraction of brain extracts of APP-Ld mice from the age of 12 months onwards (Figure 2). Although absolute levels are low in both extracts, an age-dependent increase was observed. These N-terminal truncated Abeta species are abundant in amyloid deposits in sporadic and familial AD [22]. They resist proteolysis, accelerate aggregation by seeding and thereby entrapping other Abeta forms, and are claimed to be neurotoxic [23]. Reduction of $Abeta_{3(pE)–42}$ by inhibition of glutaminyl cyclase (QC), the enzyme catalyzing the N-terminal pGlu modification, was therefore suggested as a new therapeutic target in AD [24].

3.2.5. Decreased CSF Abeta42/40 Ratio with Age. In parallel with what is observed in AD patients [25–27], the ratio of Abeta42/40 in CSF decreases in ageing APP-Ld mice (Figure 3), correlating in time with the appearance of abundant parenchymal and vascular plaque formation from

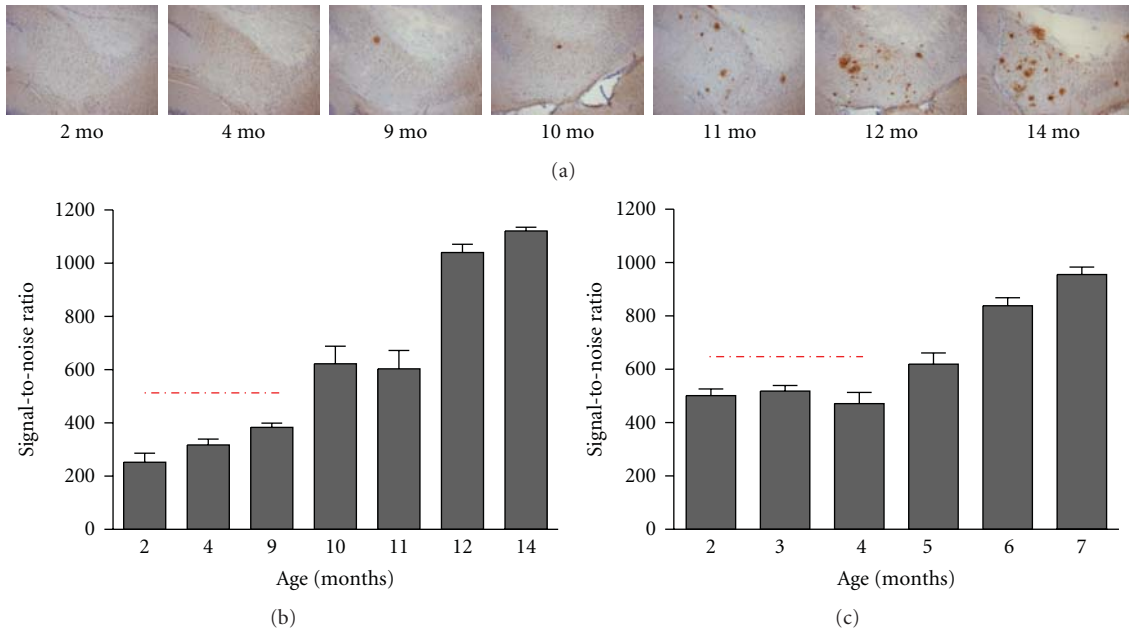

Figure 1: Abeta aggregation prior to plaque formation in APP[V717I] (APP-Ld) and APP[V717I] × PS1[A246E] mice. (a) Representative photo collection of anti-Abeta stained sections showing total plaque load in APP-Ld mice of different ages (proprietary anti-Abeta Nanobody, reMYND/Ablynx, Belgium). (b) Aggregated Abeta in APP-Ld mice of different ages, both in preplaque (indicated by the dashed line) and postplaque stages of the Alzheimer pathology (A^4-assay, Amorfix Life Sciences Ltd., Mississauga, Canada). The signal of nontransgenic mice was under the S/N cutoff value (data not shown). (c) As in B, for the APP[V717I] × PS1[A246E] model. The signal of nontransgenic mice was under the S/N cutoff value (data not shown).

the age of 15 months onwards. The ratio Abeta42/40 in CSF could be a more valuable diagnostic tool for early-stage AD and mild cognitive impairment (MCI) patients [25].

3.3. Early Stage Preplaque Pathology, the Object of More Recent Focus

3.3.1. Cognitive and Behavioral Impairment. From the age of three months onwards, robust and significant spatial and nonspatial orientation and memory deficits are observed in the APP-Ld model, which does not relate to the timing of plaque deposition [9]. Accordingly, impaired NMDA-dependent long-term potentiation and decreased NMDA-receptor activation in hippocampal CA1 region have been demonstrated at a preplaque age stadium. Inhibiting APP processing rescued this effect suggesting the dysfunction of the glutamate neurotransmitter system represents a pathologically relevant process secondary to Abeta toxicity involving synaptic plasticity and memory formation [9, 28, 29]. Also derangement of associative learning, hyperactivity, anxiety, and aggression develops independently of plaque formation [30]. Some of these have been shown to be alleviated by serotonergic drugs [31]. Premature death caused by epileptic seizures is an epiphenomenon observed in Alzheimer patients [32, 33] and is also found in the APP-Ld model [9].

The preplaque synaptic and cognitive demise and related behavioral deficits in the APP-Ld mouse dissociate the late fibrillar amyloid plaques from pathobiological processes at early age apparently elicited by specific soluble Abeta forms inducing neuronal toxicity (see also "Abeta aggregation prior to plaque formation").

A similar dissociation of amyloid plaque pathology and behavioral aspects was observed in mild cognitive impairment (MCI) patients [34]. In addition, occurrence of soluble aggregated Abeta forms—rather than the amyloid plaques—in AD brain correlates in time with the onset of cognitive decline in AD patients [35].

3.3.2. Brain Inflammation. In AD patients, neuroinflammation is recognized as an early defect in the pathogenesis [36]. In the APP-Ld model, early inflammation is evident as foci of activated microglia and astroglia randomly distributed throughout hippocampus and cortex, from the age of 3 months [37]. These foci have been proposed to represent the earliest sites of amyloid deposition, likely evolving into amyloid plaques. Moreover, these early and focal inflammatory events have been postulated to contribute to neuronal dysfunction at a young age and to the early cognitive impairment in the APP-Ld model. Interestingly, neuronal BACE1 expression was demonstrated to be upregulated in close proximity of activated microglia and astrocytes, strongly pointing to an interaction between neurodegenerative and neuroinflammatory events [37].

3.3.3. Abeta Aggregation Prior to Plaque Formation. Already at the age of two months, that is, long before the onset of amyloid deposition and plaque formation at 10–12 months,

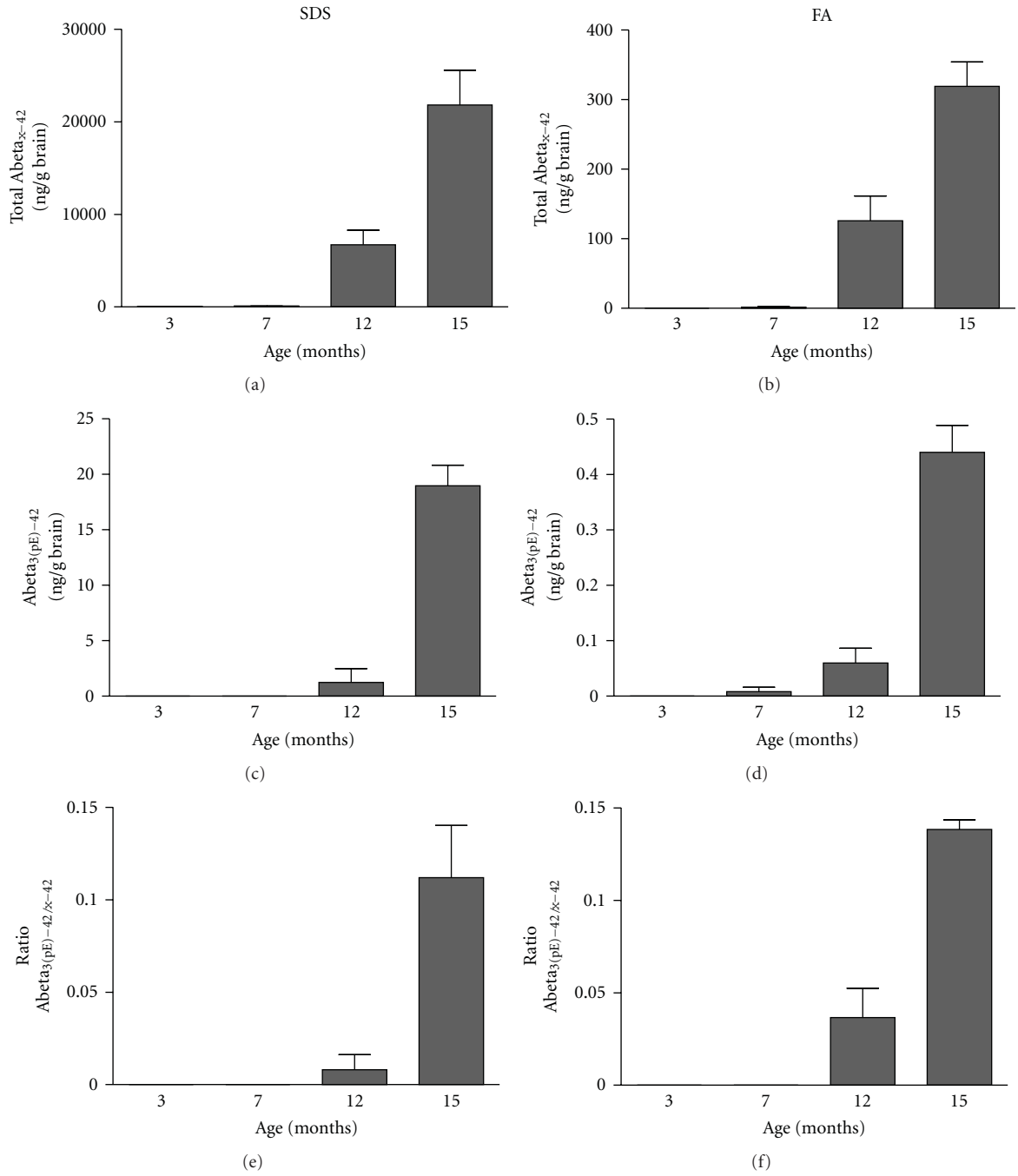

Figure 2: Abeta$_{3(pE)–42}$ determination in the SDS and FA extracts of APP-Ld brain. Pan-Abeta42 (a, b) and Abeta$_{3(pE)–42}$ (c,d) concentrations in SDS (a, c) and FA (b, d), as well as the corresponding Abeta$_{3(pE)–42}$ to pan-Abeta42 ratios (in %) (e, f).

soluble oligomeric Abeta is present in brain of APP-Ld mice and their levels gradually increase with age (Figure 1(b)). Determination of the exact nature of these aggregated Abeta species in the brain of APP-Ld mice, and their correlation with the significant cognitive deficits, is the subject of current investigations.

The coincidental timing with the onset of cognitive defects is intriguing, given that in diseased brains increases of soluble Abeta also correlate with cognitive decline and neuropathological hallmarks of AD [35]. A causal link of Abeta oligomers has also been suggested by a study where clearing of plaques, but not oligomers, did not mitigate cognitive decline [38]. The realization of Abeta oligomers representing noxious species has spurred research to find ways to inhibit their formation as a strategy for therapeutic intervention.

3.3.4. Tau Phosphorylation. In later stages of the pathology in APP-Ld mice, plaque-associated dystrophic neurites develop containing hyperphosphorylated murine Tau [9]. Recent

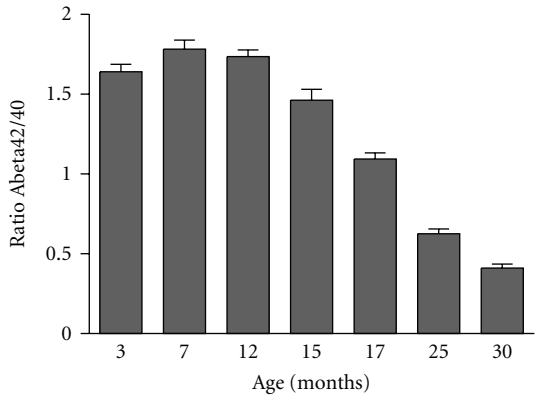

Figure 3: Progression of CSF Abeta42/40 ratios in ageing APP-Ld mice; from the age of 15 months onwards, the ratio of Abeta42/40 in CSF decreases.

data have demonstrated GSK3β-activation and mouse Tau phosphorylation in the hippocampus of the single APP-Ld model at a preplaque stadium ([1, 39] and unpublished data). These findings correlate with the presence of soluble Abeta aggregates and cognitive deficits suggesting an "instigator role" of Abeta in the downstream pathobiology mediated by kinases resulting in Tau phosphorylation. Although the exact nature of the responsible Abeta form(s) remain(s) elusive, an unspecified subset of soluble oligomeric species is hypothesized to be involved in the neurotoxicity cascade [38]. Relevant in this context, knockout of the murine Tau prevented decline of learning and memory as well as hypersensitivity to excitotoxicity in a independent APP transgenic mouse model [40]. The combined data support the hypothesis that endogenous Tau is required for Abeta-mediated neurotoxicity in mice, illustrating a pathobiological interplay between Abeta and Tau in transgenic APP mice.

3.4. The APP[V717I] × PS1[A246E] Model for Faster Ranking of Lead Molecules. Complementary to the late onset APP-Ld single transgenics, an APP[V717I] × PS1[A246E] bigenic model (APP*PS1) has been developed being a more aggressive model with accelerated amyloid pathology [11]. These mice carry additionally the human PS1[A246E] transgene, also under control of the murine *thy1* gene promoter, containing a clinical mutation in the region encoding the transmembrane (AD&FTD Mutation Database—http://www.molgen.ua.ac.be/ADMutations).

Whereas in ageing APP-Ld mice both Abeta42 and Abeta40 are increased, in the double transgenic APP[V717I] ×PS1[A246E] mice the more hydrophobic Abeta42 is preponderantly increased. Consequently, accelerated amyloid plaque pathology is observed, caused by the higher Abeta42/40 ratio (above 1), with amyloid plaque development at the age of 5–6 months [41].

Concomitant to the increased Abeta42 production in the APP*PS1 double transgenic model, soluble aggregated forms of Abeta during the preplaque stadium were found two-fold increased at the age of 2–4 months compared to the single APP-Ld model (Figure 1(c)). The aggravated Abeta pathobiology in the APP*PS1 double transgenic mouse recapitulates the effect of the early-onset familial Alzheimer disease (EOFAD) PS1 mutations on the metabolism of APP [42].

Practical advantage of the double APP*PS1 *versus* the single APP-Ld model involves the shorter time span between onset of amyloidosis and amyloid plaque development and thereby the relatively faster evaluation and prioritization of lead molecules before further drug development.

3.5. Combined and Age-Dependent Development of Amyloid Plaques and Neurofibrillary Tangles in APP[V717I] × TAU[P301L] Double Transgenic Mice. Tau mutations are linked with FTD in humans, evoking a tauopathy reminiscent of that in AD, including cognitive defects and neurodegeneration leading to dementia. In total, 32 families have been identified carrying this point mutation in exon 7 (AD&FTD Mutation Database—http://www.molgen.ua.ac.be/ADMutations).

In the single TAU[P301L] transgenics, the observed conformational change and age-dependent accumulation of AT8 and AT100 reactive insoluble Tau have been proposed to trigger an age-dependent tangle pathology (starting at age 8–9 months) [10, 43]. In parallel the TAU[P301L] mice develop motor deficits like limb clasping and impaired survival, that is, succumbing before age 12–13 months [10]. Although this model does not contain any amyloid-related hallmarks, it has been proven very suitable for therapeutic testing of candidate drugs aimed at Tau pathology ([10] and unpublished data).

To introduce Tau pathology in the APP-Ld mouse, the bigenic APP[V717I] × TAU[P301L] mouse line (APP*TAU) was created [1, 10]. Three important characteristics of AD are recapitulated in this model: intracellular neurofibrillary tangles (NFTs), extracellular amyloid plaques, and cognitive impairments. The amyloid pathology in these mice is more intense than in the single APP-Ld mouse, but similar in its aspects and timing [1]. NFT pathology is significantly enhanced in the hippocampus and cortex relative to the parental single TAU[P301L] model, developing in the same time frame as the amyloid plaques [1].

The bigenic APP*TAU model will be highly valuable for further investigating the molecular interplay between Abeta and protein Tau in causing neurodegeneration and as a tool to evaluate drug candidates.

4. Conclusions

During the past decades, a variety of rodent models have been developed and proven to be valuable tools for deciphering the complexity of AD and contributed to the discovery and development of diagnostic and therapeutic innovations. However, the current AD animal models have their limitations and may, at least partly, contribute to the high failure rates of AD drug candidates in clinical trials. Apart from the obvious gap between mice and men, the translational gap also stems from differences in etiological factors, spatiotemporal onset of pathology, and brain physiology [6].

Notwithstanding the above, the AD mouse models are of utmost importance for the exploration of novel therapeutic approaches. Given the particularities and limitations of the animal models, the single most important parameter for meaningful proof-of-concept studies is the selection of the most appropriate animal model which most faithfully recapitulates the key parameters of disease. In addition, preclinical proof-of-concept studies should ideally be performed in more than one model to capture as much disease pathology as possible and to discern animal and model specific artifacts. For instance, by analyzing two models with different APP mutations, compounds acting specific in the context of one particular mutation would be distinguished.

The APP-Ld mouse model for amyloid pathology represents a highly valuable model for drug testing, especially when targeting the amyloid cascade, but also for modulators of beginning Tau pathology. As summarized in this paper, the processing of human APP-Ld and production of Abeta in APP-Ld mice result in a plethora of pathological and behavioral effects modeling key disease parameters of AD.

Development of amyloyd plaque pathology in brain parenchyma and vasculature, and related inflammatory processes (astrocytosis, microgliosis) arise in an age-dependent way. Concomitant clearance of Abeta to CSF is affected as a presumed consequence of massive deposition of Abeta. Thus, the resultant decrease of Abeta CSF (in function of age) closely mimics the situation in AD patients and provides an efficacy biomarker in preclinical studies directed to evaluate Abeta-modulating drugs.

The novel data on the presence of insoluble pyroglutamate-modified Abeta3–42 in the brain of aged APP-Ld mice offer alternative therapeutic options. N-terminal truncated Abeta is highly abundant in AD brain and is believed to be an initiator of the Abeta aggregation cascade because of its exceptional physical properties. The conservation of the QC mediated posttranslational modification process provides unique opportunities to study the role of pyroglutamate-modified Abeta in AD and for testing novel QC inhibitors for therapeutic potential.

Early formed soluble aggregates of Abeta (as of 2 months) in brain of APP-Ld mice suggest that these Abeta misconformers are primary triggers of synaptic and neurotoxicity. The similarity with AD patients is striking, especially in light of recent findings demonstrating that soluble oligomers species were elevated in AD brain and appear to correlate with cognitive decline and neuropathological hallmarks [35]. Although the exact nature of the toxic Abeta species remains elusive, more than 25 years after their discovery, this finding can have an important impact on drug development strategies aimed at Abeta pathobiology.

Abeta-mediated activation of GSK3β-kinases and phosphorylation of endogenous mouse Tau in APP-Ld mouse brain reflect an intriguing and potentially very important connection between Abeta and Tau pathology [1]. Thus, the APP-Ld transgenics also model disease relevant Tau pathology [40] and would permit studies of Abeta effects on Tau pathology and assessing the therapeutic potential of Tau modulators.

Collectively, APP-Ld mice recapitulate the AD-related development and progression of Abeta pathobiology and its downstream effects on cognition and Tau most closely, however, without neurofibrillary tangles and massive neuronal loss. This positions the APP-Ld mouse model as a valuable tool for detecting and analyzing Abeta and Tau modulating AD drugs with the potential to fundamentally modify the course of the disease. By combining APP-Ld with mutant PS1, a further aggravated Abeta pathology is obtained providing practical advances for especially proof-of-concept studies of drug candidates. The APP-Ld*TAU-P301L double transgenics offer the advantage of a more complete pathology facilitating research and drug development focusing or addressing the interplay of Abeta and Tau in onset and progression of AD.

Acknowledgments

The authors express their sincere gratitude to all past and present collaborators of the Experimental Genetics Group—LEGTEGG—and the department of Human Genetics for their help and support. FvL is supported by FWO-Vlaanderen, KULeuven Research Fund, KULeuven-R&D, IWT, and EEC (FP5, FP6, FP7).

References

[1] D. Terwel, D. Muyllaert, I. Dewachter et al., "Amyloid activates GSK-3β to aggravate neuronal tauopathy in bigenic mice," *American Journal of Pathology*, vol. 172, no. 3, pp. 786–798, 2008.

[2] S. Oddo, A. Caccamo, M. Kitazawa, B. P. Tseng, and F. M. LaFerla, "Amyloid deposition precedes tangle formation in a triple transgenic model of Alzheimer's disease," *Neurobiology of Aging*, vol. 24, no. 8, pp. 1063–1070, 2003.

[3] J. Hardy, "The amyloid hypothesis for Alzheimer's disease: a critical reappraisal," *Journal of Neurochemistry*, vol. 110, no. 4, pp. 1129–1134, 2009.

[4] I. Torres-Aleman, "Mouse models of Alzheimer's dementia: current concepts and new trends," *Endocrinology*, vol. 149, no. 12, pp. 5952–5957, 2008.

[5] T. Jaworski, I. Dewachter, C. M. Seymour, et al., "Alzheimer's disease: old problem, new views from transgenic and viral models," *Biochimica et Biophysica Acta*, vol. 1802, no. 10, pp. 808–818, 2010.

[6] H. Geerts, "Of mice and men: bridging the translational disconnect in CNS drug discovery," *CNS Drugs*, vol. 23, no. 11, pp. 915–926, 2009.

[7] R. Epis, F. Gardoni, E. Marcello, A. Genazzani, P. L. Canonico, and M. Di Luca, "Searching for new animal models of Alzheimer's disease," *European Journal of Pharmacology*, vol. 626, no. 1, pp. 57–63, 2010.

[8] R. Radde, C. Duma, M. Goedert, and M. Jucker, "The value of incomplete mouse models of Alzheimer's disease," *European Journal of Nuclear Medicine and Molecular Imaging*, vol. 35, no. 1, pp. S70–S74, 2008.

[9] D. Moechars, I. Dewachter, K. Lorent et al., "Early phenotypic changes in transgenic mice that overexpress different mutants of amyloid precursor protein in brain," *Journal of Biological Chemistry*, vol. 274, no. 10, pp. 6483–6492, 1999.

[10] D. Terwel, R. Lasrado, J. Snauwaert et al., "Changed conformation of mutant tau-P301L underlies the moribund tauopathy, absent in progressive, nonlethal axonopathy of tau-4R/2N transgenic mice," *Journal of Biological Chemistry*, vol. 280, no. 5, pp. 3963–3973, 2005.

[11] I. Dewachter, J. Van Dorpe, L. Smeijers et al., "Aging increased amyloid peptide and caused amyloid plaques in brain of old APP/V717I transgenic mice by a different mechanism than mutant presenilin1," *Journal of Neuroscience*, vol. 20, no. 17, pp. 6452–6458, 2000.

[12] E. McGowan, F. Pickford, J. Kim et al., "Aβ42 is essential for parenchymal and vascular amyloid deposition in mice," *Neuron*, vol. 47, no. 2, pp. 191–199, 2005.

[13] H. Braak and E. Braak, "Neuropathological stageing of Alzheimer-related changes," *Acta Neuropathologica*, vol. 82, no. 4, pp. 239–259, 1991.

[14] D. R. Thal, U. Rüb, M. Orantes, and H. Braak, "Phases of Aβ-deposition in the human brain and its relevance for the development of AD," *Neurology*, vol. 58, no. 12, pp. 1791–1800, 2002.

[15] C. Duyckaerts, B. Delatour, and M.-C. Potier, "Classification and basic pathology of Alzheimer disease," *Acta Neuropathologica*, vol. 118, no. 1, pp. 5–36, 2009.

[16] P. Eikelenboom, R. Veerhuis, A. Familian, J. J. M. Hoozemans, W. A. Van Gool, and A. J. M. Rozemuller, "Neuroinflammation in plaque and vascular β-amyloid disorders: clinical and therapeutic implications," *Neurodegenerative Diseases*, vol. 5, no. 3-4, pp. 190–193, 2008.

[17] J. V. Dorpe, L. Smeijers, I. Dewachter et al., "Prominent cerebral amyloid angiopathy in transgenic mice overexpressing the London mutant of human APP in neurons," *American Journal of Pathology*, vol. 157, no. 4, pp. 1283–1298, 2000.

[18] J. J. Gilbert and H. V. Vinters, "Cerebral amyloid angiopathy: incidence and complications in the aging brain. I. Cerebral hemorrhage," *Stroke*, vol. 14, no. 6, pp. 915–923, 1983.

[19] F. Prelli, E. Castano, G. G. Glenner, and B. Frangione, "Differences between vascular and plaque core amyloid in Alzheimer's disease," *Journal of Neurochemistry*, vol. 51, no. 2, pp. 648–651, 1988.

[20] S. Pype, D. Moechars, L. Dillen, and M. Mercken, "Characterization of amyloid β peptides from brain extracts of transgenic mice overexpressing the London mutant of human amyloid precursor protein," *Journal of Neurochemistry*, vol. 84, no. 3, pp. 602–609, 2003.

[21] L. Miravalle, M. Calero, M. Takao, A. E. Roher, B. Ghetti, and R. Vidal, "Amino-terminally truncated Aβ peptide species are the main component of cotton wool plaques," *Biochemistry*, vol. 44, no. 32, pp. 10810–10821, 2005.

[22] T. C. Saido, T. Iwatsubo, D. M. A. Mann, H. Shimada, Y. Ihara, and S. Kawashima, "Dominant and differential deposition of distinct β-amyloid peptide species, AβN3(pE), in senile plaques," *Neuron*, vol. 14, no. 2, pp. 457–466, 1995.

[23] O. Wirths, H. Breyhan, H. Cynis, S. Schilling, H.-U. Demuth, and T. A. Bayer, "Intraneuronal pyroglutamate-Abeta 3-42 triggers neurodegeneration and lethal neurological deficits in a transgenic mouse model," *Acta Neuropathologica*, vol. 118, no. 4, pp. 487–496, 2009.

[24] S. Schilling, U. Zeitschel, T. Hoffmann et al., "Glutaminyl cyclase inhibition attenuates pyroglutamate Aβ and Alzheimer's disease-like pathology," *Nature Medicine*, vol. 14, no. 10, pp. 1106–1111, 2008.

[25] O. Hansson, H. Zetterberg, P. Buchhave et al., "Prediction of Alzheimer's disease using the CSF Aβ42/Aβ40 ratio in patients with mild cognitive impairment," *Dementia and Geriatric Cognitive Disorders*, vol. 23, no. 5, pp. 316–320, 2007.

[26] P. Lewczuk, H. Esselmann, M. Otto et al., "Neurochemical diagnosis of Alzheimer's dementia by CSF Aβ42, Aβ42/Aβ40 ratio and total tau," *Neurobiology of Aging*, vol. 25, no. 3, pp. 273–281, 2004.

[27] M. Shoji, M. Kanai, E. Matsubara et al., "The levels of cerebrospinal fluid Aβ40 and Aβ42(43) are regulated age-dependently," *Neurobiology of Aging*, vol. 22, no. 2, pp. 209–215, 2001.

[28] R. Postina, A. Schroeder, I. Dewachter et al., "A disintegrin-metalloproteinase prevents amyloid plaque formation and hippocampal defects in an Alzheimer disease mouse model," *Journal of Clinical Investigation*, vol. 113, no. 10, pp. 1456–1467, 2004.

[29] I. Dewachter, R. K. Filipkowski, C. Priller et al., "Deregulation of NMDA-receptor function and down-stream signaling in APP[V717I] transgenic mice," *Neurobiology of Aging*, vol. 30, no. 2, pp. 241–256, 2009.

[30] E. Domínguez-Del-Toro, A. Rodríguez-Moreno, E. Porras-García et al., "An in vitro and in vivo study of early deficits in associative learning in transgenic mice that over-express a mutant form of human APP associated with Alzheimer's disease," *European Journal of Neuroscience*, vol. 20, no. 7, pp. 1945–1952, 2004.

[31] D. Moechars, M. Gilis, C. Kuipéri, I. Laenen, and F. Van Leuven, "Aggressive behaviour in transgenic mice expressing APP is alleviated by serotonergic drugs," *Neuroreport*, vol. 9, no. 16, pp. 3561–3564, 1998.

[32] A. J. Larner, "Epileptic seizures in AD Patients," *Neuromolecular Medicine*, vol. 12, no. 1, pp. 71–77, 2010.

[33] J. J. Palop and L. Mucke, "Epilepsy and cognitive impairments in alzheimer disease," *Archives of Neurology*, vol. 66, no. 4, pp. 435–440, 2009.

[34] W. R. Markesbery, "Neuropathologic alterations in mild cognitive impairment: a review," *Journal of Alzheimer's Disease*, vol. 19, no. 1, pp. 221–228, 2010.

[35] J. L. Tomic, A. Pensalfini, E. Head, and C. G. Glabe, "Soluble fibrillar oligomer levels are elevated in Alzheimer's disease brain and correlate with cognitive dysfunction," *Neurobiology of Disease*, vol. 35, no. 3, pp. 352–358, 2009.

[36] P. Eikelenboom, E. van Exel, J. J.M. Hoozemans, R. Veerhuis, A. J.M. Rozemuller, and W. A. van Gool, "Neuroinflammation—an early event in both the history and pathogenesis of Alzheimer's disease," *Neurodegenerative Diseases*, vol. 7, no. 1–3, pp. 38–41, 2010.

[37] M. T. Heneka, M. Sastre, L. Dumitrescu-Ozimek et al., "Focal glial activation coincides with increased BACE1 activation and precedes amyloid plaque deposition in APP[V717I] transgenic mice," *Journal of Neuroinflammation*, vol. 2, article 22, 2005.

[38] W. J. Meilandt, M. Cisse, K. Ho et al., "Neprilysin overexpression inhibits plaque formation but fails to reduce pathogenic Aβ oligomers and associated cognitive deficits in human amyloid precursor protein transgenic mice," *Journal of Neuroscience*, vol. 29, no. 7, pp. 1977–1986, 2009.

[39] S.-H. Koh, M. Y. Noh, and S. H. Kim, "Amyloid-beta-induced neurotoxicity is reduced by inhibition of glycogen synthase kinase-3," *Brain Research*, vol. 1188, no. 1, pp. 254–262, 2008.

[40] E. D. Roberson, K. Scearce-Levie, J. J. Palop et al., "Reducing endogenous tau ameliorates amyloid β-induced deficits in an Alzheimer's disease mouse model," *Science*, vol. 316, no. 5825, pp. 750–754, 2007.

[41] I. Dewachter, D. Reversé, N. Caluwaerts et al., "Neuronal deficiency of presenilin 1 inhibits amyloid plaque formation

and corrects hippocampal long-term potentiation but not a cognitive defect of amyloid precursor protein [V717I] transgenic mice," *Journal of Neuroscience*, vol. 22, no. 9, pp. 3445–3453, 2002.

[42] M. Citron, C. B. Eckman, T. S. Diehl et al., "Additive effects of PS1 and APP mutations on secretion of the 42- residue amyloid β-protein," *Neurobiology of Disease*, vol. 5, no. 2, pp. 107–116, 1998.

[43] K. Spittaels, C. Van Den Haute, J. Van Dorpe et al., "Prominent axonopathy in the brain and spinal cord of transgenic mice overexpressing four-repeat human tau protein," *American Journal of Pathology*, vol. 155, no. 6, pp. 2153–2165, 1999.

SAGE-Hindawi Access to Research
International Journal of Alzheimer's Disease
Volume 2010, Article ID 825918, 11 pages
doi:10.4061/2010/825918

Review Article

Modeling Presenilin-Dependent Familial Alzheimer's Disease: Emphasis on Presenilin Substrate-Mediated Signaling and Synaptic Function

Angèle T. Parent[1] and Gopal Thinakaran[1,2]

[1] *Department of Neurobiology, The University of Chicago, 924 East 57th Street, Chicago, IL 60637, USA*
[2] *Department of Neurology, The University of Chicago, 924 East 57th Street, Chicago, IL 60637, USA*

Correspondence should be addressed to Angèle T. Parent, aparent@uchicago.edu and Gopal Thinakaran, gopal@uchicago.edu

Received 15 April 2010; Accepted 17 June 2010

Academic Editor: Gemma Casadesus

Mutations in *PSEN* genes, which encode presenilin proteins, cause familial early-onset Alzheimer's disease (AD). Transgenic mouse models based on coexpression of familial AD-associated presenilin and amyloid precursor protein variants successfully mimic characteristic pathological features of AD, including plaque formation, synaptic dysfunction, and loss of memory. Presenilins function as the catalytic subunit of γ-secretase, the enzyme that catalyzes intramembraneous proteolysis of amyloid precursor protein to release β-amyloid peptides. Familial AD-associated mutations in presenilins alter the site of γ-secretase cleavage in a manner that increases the generation of longer and highly fibrillogenic β-amyloid peptides. In addition to amyloid precursor protein, γ-secretase catalyzes intramembrane proteolysis of many other substrates known to be important for synaptic function. This paper focuses on how various animal models have enabled us to elucidate the physiological importance of diverse γ-secretase substrates, including amyloid precursor protein and discusses their roles in the context of cellular signaling and synaptic function.

1. Introduction

Mutations in *PSEN1* and *PSEN2* genes, which encode polytopic proteins termed presenilin 1 (PS1) and presenilin 2 (PS2), respectively, cause autosomal dominant early-onset familial Alzheimer's disease (FAD) [1]. Both PS1 and PS2 proteins (PS) share about 63% homology with the highest similarity in the transmembrane domains where most of the FAD-linked mutations are found [2, 3]. Since the first report of mutation in the *PSEN1* on chromosome 14, about 170 mutations have been identified, making mutations in *PSEN1* the most common cause of autosomal dominant early-onset AD [4]. In the case of *PSEN2*, 18 mutations have been reported so far, although not all have been confirmed to be pathogenic [2, 5]. As a probable explanation for the disparity between the two genes, defects in *PSEN2* function may be offset by the normal function of its homolog *PSEN1*. In support of this view, *PSEN2* null mice do not exhibit the phenotypic and functional defects seen in mice lacking *PSEN1* gene. *PSEN1* knockout (KO) mice are lethal, and disruption of *PSEN2* and *PSEN1* genes causes earlier embryonic lethality compared to *PSEN1* KO [6–10]. As supported by mouse model studies, it appears that PS1 contributes largely to total β-amyloid (Aβ) production in the brain [11, 12].

PS is the catalytic subunit of γ-secretase, the enzyme responsible for intramembraneous cleavage of amyloid precursor protein (APP) to generate peptides. FAD-linked PS variants enhance the production of highly fibrillogenic Aβ42 peptides that are deposited early in the brains of patients with AD [13]. PS is ubiquitously expressed in the nervous system and peripheral tissue and found localized in secretory and endocytic organelles in all cell types, as well as synaptic structures in neurons [14, 15]. As predicted from its broad pattern of expression, PS's function extends far beyond processing of APP and the pathogenesis of AD. For example, PS's catalytic function is required for intramembraneous γ-secretase cleavage of Notch receptors, which releases the Notch intracellular

domain (NICD). Nuclear signaling mediated by NICD is essential during mammalian development; mice with ablated *PSEN1* alleles die in late embryogenesis and exhibit phenotypes reminiscent of mice lacking *Notch 1* [6, 7]. Thus, PS-dependent activation of Notch signaling is essential for early development. Transgenic expression of FAD-linked mutant PS1 fully rescues the developmental phenotypes in mice with *PSEN1* deficiency [16, 17], supporting the notion that FAD-linked PS1 variants are functional, but acquired deleterious properties that have profound pathophysiological consequences. Candidate approaches and proteomic studies have identified a wide spectrum of type I membrane proteins that undergo γ-secretase cleavage, including Notch ligands, Deleted in Colorectal Cancer (DCC), and cadherins (reviewed in [13, 18–21]). Uniformly these substrates all undergo an ectodomain shedding by α-secretases, which in many cases is triggered by the binding of extracellular ligands. Interestingly, several noncatalytic γ-secretase-independent functions have been assigned to PS, such as its role in regulating intracellular calcium homeostasis (reviewed in [22]).

Synapses are continuously reconfigured, both structurally and functionally, during embryonic development and throughout adult life, forming the basis for learning and memory [23, 24]. Neuronal inability to exhibit such plastic changes has been proposed to be a root cause for various psychiatric and neurodegenerative disorders such as AD [23, 25, 26]. Not surprisingly, the duration and severity of cognitive impairments in AD patients closely parallels the extent of synaptic loss, leading to the notion that synaptic dysfunction is a critical element in the pathophysiology of AD [27]. Notably, memory and cognitive decline observed in AD patients correlate better with the synaptic pathology than either Aβ plaque load or tangle density, and synapse loss appears to precede neuronal degeneration. Details on how synaptic organization is altered in AD patients are beginning to emerge. Findings from several laboratories suggesting that Aβ might play a critical role in synaptic dysfunction have added significant information to the traditional amyloid cascade hypothesis of AD [28, 29]. Aβ can affect synaptic transmission [30–33], synaptic protein localization [34], AMPA and NMDA receptor trafficking [35, 36], and spine formation [35, 37–39].

FAD-linked mutations in PS1 were originally thought to enhance the production of Aβ42 peptides by a gain-of-function mechanism. However, it is becoming clear that FAD-linked PS1 variants also exhibit partial-loss-of-enzymatic-function observed as diminution of Aβ40 peptide production and defects in the extent of processing certain other transmembrane substrates (reviewed in [40, 41]). For example, FAD-linked PS1 mutations are thought to attenuate γ-secretase processing and generate reduced levels of the intracellular domains of APP, Notch, N-cadherin, EphB2, and EphA4 [42–45]. Taken together, it is plausible that FAD-linked mutations in PS1 exert pathophysiological effects on the synapses by elevating Aβ42 levels and by Aβ-independent mechanisms involving altered processing of γ-secretase substrates involved in synaptic function. This paper discusses findings from various animal models that reveal the role of PS and FAD-linked PS mutations in synapse formation and function.

2. PS Animal Models

Several mouse models (reviewed in [46]; see http://www.alzforum.org/res/com/tra/) and a few rat models [47–50] have been developed in order to recapitulate the main pathological features of AD and elucidate the mechanisms by which FAD-linked PS mutations contribute to AD pathogenesis. A variety of mouse models have been characterized such as mice expressing FAD-linked PS variants harboring point mutations or deletion mutation [51, 52], and FAD-linked *PSEN1* knock-in (KI) [M146V variant [53], I213T variant [54] and P264L variant [55]], and ΔE10 loop deletion KI [56]. These FAD-PS1 single transgenic or KI mouse models do not exhibit significant Aβ deposition in the brain. Therefore, the phenotypes described in these FAD-PS1 single transgenic mice are not due to classical Aβ pathology. In an attempt to reproduce more closely the human AD pathology, *PSEN1* KI coexpressing APP "Swedish" mutant and hyperphosphorylated tau mutants have been made [57].

In order to study the physiological function of PS, KO models of *PSEN1* and *PSEN2* [6–10], *PSEN1* conditional KO [58–60], as well as double *PSEN1* and *PSEN2* conditional KO [61] mice have also been created. In order to examine amyloid pathology, transgenic mice expressing APP mutants in a PS null background have been developed; such as *PSEN1* conditional KO coexpressing APP V717I variant [60] and APP V717F variant [62]. In these models, Aβ deposition is attenuated by the lack of PS1 expression and consequent loss of γ-secretase activity.

Besides their utility in examining proteolytic processing of APP into Aβ40 and Aβ42 peptides *in vivo* and phenocopying pathological hallmarks of AD (amyloid deposition and tau phosphorylation), these models have been extensively used to examine changes in synaptic transmission, synaptic plasticity, and associated signaling. In addition, several groups have generated *Drosophila* models (reviewed in [63]), and *Caenorhabditis elegans* models (reviewed in [64]) expressing human PS1 or PS2 bearing FAD-linked mutations, in an effort to understand mechanistic contribution of PS to AD pathology and neuronal dysfunction.

3. PS and Cellular Substrates of Memory

Synaptic transmission and long-term potentiation (LTP) contribute to several forms of memory storage. Using slice preparations from transgenic mice, we and others have demonstrated that expression of FAD-linked PS1 does not alter basal synaptic transmission, but leads to higher degree of LTP induction in the hippocampus ([57, 65–69] reviewed in [14]). However, one group has reported impairment of synaptic transmission associated with an increase of paired-pulse facilitation, an index of presynaptic release, in neurons of 6 month-old *PSEN1* M146V KI mice [57]. LTP induction by high-frequency stimulation in hippocampal CA1 area was also enlarged in this animal model [57]. Interestingly, in *PSEN1* M146V KI animal model, LTP induced by carbachol

(a muscarinic agonist) was reduced in CA1 hippocampal area, suggesting that FAD-linked PS1 variant might interfere with cholinergic cellular cascades as well [70]. The KI mouse models allow us to examine the functional properties of molecules associated with pathology when they are expressed at endogenous levels without any alteration in their spatial or temporal pattern of expression. Therefore, KI animal models give us the opportunity to rule out pathophysiological consequences (such as protein misfolding) associated with aberrant overexpression of proteins associated with human genetic disorders.

Interestingly, it has been described that the lack of PS function or overexpression of PS1 mutant was also associated with changes in presynaptic function. We have observed an increase of spontaneous miniature excitatory postsynaptic current in cortical neurons isolated from *PSEN1* KO mice [71], while others have reported that expression of mutant PS1 in cultured hippocampal neurons depresses synaptic transmission by reducing the number of synapses [72]. Another group has also observed that PS1 deficiency increases synaptic release and affects the number and docking of synaptic vesicles [69]. It was also shown that basal transmitter release was increased at the neuromuscular junction in Drosophila lacking PS expression [73]. However, even though basal synaptic transmission seems to be intensified in this later model, synaptic strength and plasticity were impaired after posttetanic potentiation [73]. As a likely consequence, associative learning ability was also impaired. In parallel, it has been reported that LTP induction declines more rapidly in CA1 hippocampal area of mice with only one allele of *PSEN1* [74]. In agreement with these observations, it has been recently found that a CA3-dependent presynaptic form of LTP in the hippocampus was attenuated in double *PSEN1* and *PSEN2* conditional KO mice [75]. Intriguingly, single *PSEN1* conditional KO mice do not show major changes in brain plasticity, suggesting that expression of PS2 might be sufficient to overcome the 60–80% loss of PS1 in the forebrain of these animals [59].

What can we learn from these animal models? First of all, it becomes apparent from these studies that PS is an essential element for the normal synapse function. Second, it becomes evident that PS dosage is a critical component for PS-dependent cellular function(s). Indeed, PS1 expression is developmentally regulated in rodent brain, reaching a peak of expression during the critical period of synaptogenesis between postnatal days 7 to 14 [76]. Accordingly, we can stipulate that PS-dependent substrates expressed during embryogenesis or early in development may significantly contribute to synaptic physiology. In this regard, it also remains to be established whether differences in PS-dependent proteolysis of developmentally regulated molecules might underlie changes in synaptic function later on in life. A well-known example is a condition where stress-induced early life biochemical events influence life-span changes in cognitive function and AD-associated abnormalities [77]. Accordingly, it has been proposed that age-related decline in cortical cholinergic function in AD patients might have developmental origins [78]. Finally, it has also been speculated that PS-dependent modulation of signaling pathways that are important in development may contribute to the neurodegenerative process [79]. Taken together, studies from various laboratories suggest that PS is specifically involved in cellular component(s) necessary for synaptic transmission and plasticity, and that FAD-linked mutations in PS1 may disrupt the normal cascade of synaptic events.

4. PS and Synapse Formation

A distinct feature of the nervous system is the intricate network of synaptic connections among neurons. The changes in the strength and efficacy of existing synapses, as well as remodeling of connectivity through the loss and gain of synapses in the neuronal network, are believed to be the basis of learning and memory in the brain. Interestingly, LTP has been associated with the increase in spine formation and spine head growth, whereas long-term depression (LTD) has been associated with spine shrinkage and retraction [80]. The morphology of dendritic spines is known to change in response to several factors including learning, age, hormones, and disease conditions [81]. In addition to their morphological plasticity, spine-like protrusions also display rapid motility, changing shape and size in a matter of seconds to minutes. This morphological plasticity suggests that long-term memory might be encoded by alterations in spiny structures and associated synaptic contacts [82]. Collectively, these events are critically important in synaptogenesis, in modulating of existing synapses, as well as in long-term synaptic plasticity [83, 84]. It has been reported that Aβ is closely associated with a decrease of spine formation and motility [35, 37, 85]. Overproduction of Aβ in PS mutant transgenic mice coexpressing the "Swedish" APP mutant causes age-associated decrease of synaptic excitability [57, 86, 87] and spine collapse [38, 88]. However, it has also been reported that acute Aβ application (less than 4 h) was associated with an increase of filopodia and growth cones in hippocampal cultures [89]. In support of this idea, it was shown that application of low levels of Aβ is associated with an increase of LTP, whereas higher concentration of Aβ reduced synaptic potentiation [32, 90]. Collectively, these observations suggest that Aβ might have dual roles on synapse formation. Conflicting results have also been observed in regard to spine morphology in neurons lacking PS expression. Treatment with Compound E, a γ-secretase inhibitor (10 nM; 24 h), produced an increase of spine-like protrusions in isolated neurons [71, 91]; whereas the density of spines was found to be decreased upon prolonged treatment with the same inhibitor (50 nM; seven days) [45]. In addition, neurons lacking both PS1 and PS2 expression have marked diminution in spine density [45]. To further support the effect of γ-secretase inhibition on dendritic spines, recent *in vivo* study showed that γ-secretase inhibitor treatment in wild-type mice significantly reduced the number of spine density in somatosensory cortex, while γ-secretase inhibitor treated APP null mice did not exhibit any effect [92]. These findings suggest that APP-dependent mechanism may underlie the PS-dependent morphological changes observed. The apparent discrepancy between inhibitor treatment and

loss of PS expression on spine density may be also due to differential effects of inhibitors that target mainly γ-secretase and genetic inactivation of PS that results in reduced γ-secretase-dependent and -independent function. All together, these observations support the idea that PS gene dosage and the level of expression may differentially influence synaptic morphology.

Although the molecular mechanisms that underlie these morphological changes are not completely understood, emerging evidence supports at least two important signaling pathways that have been linked to dendrite spine formation and AD etiology: (1) cAMP-dependent activation of PKA has been shown to be critical for the maintenance of the late phase of LTP, and downstream phosphorylation of CREB has been linked to formation of new spines [93]. Interestingly, it has been shown that Aβ inhibits PKA/CREB pathway [94], (2) the Rho family of small GTPases, well-known regulators of the actin cytoskeleton, has profound influence on spine formation. Among the members of this family Rac1, Cdc42, Rnd1, and Ras promote spine formation and growth, whereas Rap and RhoA induce shrinkage and loss of spines [80, 95]. p21-activated kinase (PAK) is a downstream signaling effector of the Rho/Rac family of small GTPases and has been shown to be associated to spine formation and memory consolidation [96]. A role of PAK in cognitive deficits of AD has also been reported [97].

A recent paper by Shuai and colleagues [98] suggests that the act of forgetting might also be linked to activation of the Rac pathway, using a simplistic model of olfactory learning in the fruit fly *Drosophila*. With the help of genetic manipulation, they were able to distinguish changes in Rac activity during passive memory decay, interference learning, and reversal learning, which are three different forms of forgetting events. In *Drosophila* olfactory memory model, it appears that cAMP/PKA and Rac/PAK-dependent memory acquisition and forgetting events are independent, as suggested by this group and others [98, 99]. In a more complex system, as it has been proposed in the mammals, it seems that memory consolidation might mechanistically require both pathways [96, 100, 101]. As demonstrated by several groups, Rac signaling cascade in the brain is directly linked to an increase of spine formation through subsequent activation of PAK leading to F-actin polymerization and changes in membrane morphology. Besides the known involvement of cAMP/PKA/CREB activation cascade, Rac/PAK-dependent cellular events also appear to be intimately associated with the process of memory consolidation, at least in rodents.

It is very exciting to think that perhaps similar cellular pathways as the one described above may be relevant to human disorders associated with memory dysfunction. One of the known hallmarks of AD is that patients do forget recent events, therefore, they are unable to consolidate their new memory. In our lab, we have shown that the lack of PS function or expression in cortical neurons produced an increase of steady-state levels of CREB and Rac/PAK cascade activation, which was also associated with an increase of spine-like protrusions [91]. Even though our study shows increase of phosphorylated CREB especially in dendritic area, transcriptional CREB activity was not directly determined in this experiment. More recently, Shen and collaborators have shown that CREB transcription was indeed reduced in PS deficient neuron through PS-independent mechanism [102]. Are these signaling events meaningful in the context of AD? Perhaps. As discussed above, recent studies support the idea that FAD-linked mutations in PS1 might cause a partial loss of function [40, 41]. It still remains to be determined whether Rac/PAK signaling is altered in neurons expressing FAD-linked PS1 variants. If this is the case, one might want to consider the possibility that changes in cAMP/PKA/CREB or Rac/PAK signaling in neurons might represent some of the earliest cellular dysfunctions that are relevant to synapse elimination and associated cognitive decline in AD.

5. PS-Dependent Substrate Signaling

γ-secretase-dependent PS function mediates transmembrane proteolysis of several substrates including APP, N- and E-cadherins, γ-protocadherin, CD44, DCC, ephrin/Eph receptors, leukocyte-common antigen related, nectin-1α, and syndecan (reviewed in [18, 20, 21]). Many of these substrates function as cell-adhesion molecules or cell surface receptors and are known for their diverse functions during development and are involved in axon guidance, neuronal outgrowth and synaptogenesis [103–113]. In addition, these molecules are also well known to be coupled to diverse intracellular signaling pathways [20, 44, 45, 108–110, 114–118]. It has been proposed that APP can affect synaptic function by its dual roles via its cell adhesive properties or through its putative receptor-like intracellular signaling components [112, 116, 117]. Indeed, it has been shown that accumulation of the APP intracellular domain can mediate a phosphoinositide-dependant calcium signaling [119]. Several other substrates of γ-secretase are also coupled with intracellular signaling events that can potentially influence synaptic function. For example, Eph receptors and N-cadherin are known to be coupled to Rac and CREB signaling, respectively [45, 115, 117, 120, 121]. Lack of EphB expression or kinase-defective EphB is associated with a reduction in glutamatergic synapses and abnormal spine development [120–122].

It has also been shown that three substrates of PS, namely ErbB4, γ-protocadherin, and leukocyte-common antigen related, are associated with PSD-95 clustering at the synapse [123, 124] and AMPA receptor function [125]. Consistent with these findings, we have previously reported that the lack of PS function increases axodendritic contacts, which was accompanied by increases of PSD-95 clusters, spine-like protrusions, and AMPA receptors-mediated synaptic transmission [71, 91]. Moreover, PS1 KO neurons and Wt neurons treated with γ-secretase inhibitors exhibited increases in the extent of cAMP/PKA activation [71, 91]. cAMP/PKA signaling plays a critical role in regulating short and long-term synaptic physiology [126]. It has been demonstrated that stimulus-induced activation of PKA pathway can also affect the synaptic morphology; therefore, it can indirectly affect basal synaptic transmission [127]. Thus, there exists a close relationship between increased phosphorylation of

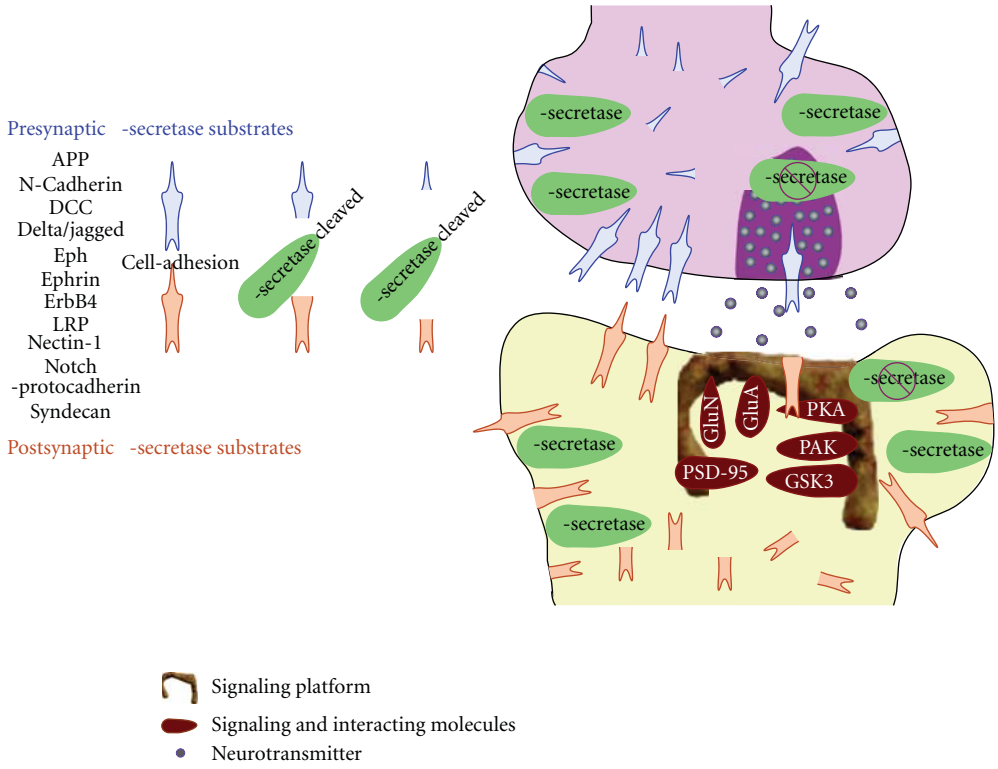

Figure 1: Schematic representation of PS-dependent processing of substrates and their role in synaptic function. Several γ-secretase substrates are located at the synapse where they influence the function of other synaptic proteins. Lack of γ-secretase-dependent cleavage of substrates could perturb presynaptic release and postsynaptic function of glutamate receptor-mediated events (NMDA-GluN and AMPA-GluA receptors). Synaptic contact could also be modulated through cell-adhesion properties of several γ-secretase substrates. Inefficient processing of these substrates will lead to sustained activation of signaling cascades capable of altering the postsynaptic morphology. How FAD-linked mutations in PS influence these processes and contribute to the disease progression has not been fully understood.

PKA substrates and enhanced synaptic transmission in neurons lacking PS function [71, 91].

Signaling downstream of DCC, the netrin receptor [105], is also modulated by γ-secretase activity [71]. Upon binding of the ligand netrin, DCC undergoes metalloprotease-dependent ectocomain shedding [128], which generates a membrane-tethered DCC C-terminal fragment (CTF) derivative, consisting of the transmembrane segment and the intracellular domain. DCC CTF undergoes intramembraneous proteolysis by γ-secretase, and accumulation of DCC CTF in neuroblastoma cells treated with γ-secretase inhibitors stimulates neurite outgrowth [71, 129]. γ-secretase processing of DCC attenuates cAMP-dependent signaling cascades associated with DCC CTF [71]. In this case, it is clear that γ-secretase terminates intracellular signaling associated with DCC. However, it remains to be determined if γ-secretase cleavage of other substrates would significantly impact cellular functions, especially pertaining to synaptic process, through termination of receptor-mediated signaling events (see our proposed model in Figure 1).

More recently, it was found that EphA4 undergoes PS-dependent endoproteolytic process, and EphA4 CTF accumulates following inhibition of γ-secretase activity or in cells lacking PS expression [45]. Accumulation of EphA4 CTF was found tightly linked to an increase of spine-like protrusions in hippocampal cultures. Overexpression of an inactive Rac form abolished the enhancement of dendritic spines in neurons and lamellipodia formation in NIH3T3 cell lines. In addition, this study showed that overexpression of membrane-tethered EphA4 intracellular domain was also associated with an increase of lamellipodia formation in NIH3T3 cell lines. All together, these results suggest that enhanced accumulation of EphA4 intracellular domain may induce Rac-dependent signaling events that regulate cell morphology.

It is clear that loss of intramembraneous proteolysis of γ-secretase substrates leads to the accumulation of their membrane-tethered cytosolic domains. The CTFs of certain substrates might serve as membrane anchors to facilitate the recruitment of signaling proteins in a manner that enhances phosphorylation of downstream signaling substrates. One of the signalings that have been implicated with PS function is GSK3β (reviewed in [130]). It is well established that PS1 can interact with the GSK3β/β-catenin complex [131–133]. However, besides this direct physical interaction with PS1, it is known that GSK3β is a ligand-receptor signaling molecule downstream of the activation of phosphatidylinositol-3-kinase pathway (reviewed in [134]).

Specifically, it has been shown that GSK3β signaling is important for axon specification and elongation during the establishment of neuronal polarity (review by [135]). In addition, it has been reported that decrease of GSK3β activity parallels LTP induction paradigms, whereas inhibition of phosphatidylinositol-3-kinase and subsequent activation of GSK3β lead to decrease of LTP ([136]; reviewed in [130, 137]). Decreased phosphorylation of GSK3β at the Ser 9 residue, indicative of an increase of GSK activity, was also observed in PS1-deficient neurons as well as in PS1 neurons carrying FAD-linked mutations [69, 138–141]. Alteration of phosphatidylinositol-3-kinase /Akt signaling cascade has been proposed to be the link between GSK3β activity and PS function [138, 140, 142]. Interestingly, increase of GSK3β activity also leads to hyperphosphorylation of tau protein, which underlies one of the known pathological hallmarks of AD, namely the tangle formation (reviewed in [130]).

It has been proposed that membrane microdomains rich in cholesterol and sphingolipids, termed lipid rafts, might influence γ-secretase activity and processing of substrates (reviewed in [143]). Lipid rafts play an important role in the maintenance of synapses through dendritic spine formation and AMPA receptor function [144]. Raft-dependent mechanisms facilitate trafficking of receptors in and out of the synapse and regulate synapse function (reviewed in [145]). Lipid rafts are known to serve as membrane platforms that compartmentalize diverse receptor-mediated signaling. Indeed, it was found that critical regulation of signaling associated with ErbB4, DCC, and EphA4, three γ-secretase substrates, involves their recruitment into lipid raft microdomains [45, 146, 147]. Based on the differences in spatiotemporal distribution of γ-secretase complexes and substrates [148, 149], different PS-dependent substrates might be subjected to different level of proteolysis depending on their membrane microdomain distribution at a given time during embryonic development and in adult life.

6. PS and Calcium Signaling

Besides a direct interaction of γ-secretase substrates with intracellular phosphorylation cascades, one of the key features of PS function is its role in intracellular Ca^{2+} homeostasis (reviewed in [22, 150, 151]). Ca^{2+} homeostasis is essential to maintain healthy cellular dynamics leading to proper physiological functions. Several studies have concluded that FAD-linked PS mutant expression in transfected cells and cultured neurons is associated with enhanced Ca^{2+} release from endoplasmic reticulum store. It has been reported that neurons generated from *PSEN1* M146V KI mice exhibit an increase of IP_3-evoked Ca^{2+} responses in brain slices as early as in one month old [152]. This Ca^{2+} dysregulation appears to be specific to intracellular endoplasmic reticulum store since it does not affect the voltage-gated Ca^{2+} entry. However, it has been shown that L-type Ca^{2+} channel may be involved after stress induction at the neuromuscular junction in drosophila larvae expressing FAD-linked PS1 mutant [153]. Accordingly, in this model system, the level of synaptic plasticity and memory paradigm was normal following heat shock stimulation or endoplasmic reticulum stress, but reduced after 24 h of stimulation recovery. These results suggest that mutation in PS might alter synaptic behavior following recovery of stress conditions. It has been also proposed that PS might serve as a passive Ca^{2+} leak channel in the endoplasmic reticulum and FAD-linked PS variants might fail to exhibit this property [154]. Using reconstituted planar lipid bilayers, Tu and collaborators demonstrated that PS by itself could form low-conductance divalent ion channels, which was not the case in several mutated forms of PS. It remains to be determined if results from these experimental conditions are applicable to *in vivo* situations that are relevant to the disease state.

More recently, Stutzmann and collaborators have established that the ryanodine receptor-evoked Ca^{2+} release (especially through RyR2 isoform) was increased in CA1 hippocampal slices of *PSEN1* M146V KI mice coexpressing Swedish APP and hyperphosphorylated tau mutants [155]. As a consequence, they observed an aberrant increase of ryanodine-dependent presynaptic neurotransmission, along with increases of long-term synaptic plasticity. Conversely, Shen and collaborators have observed a decrease of ryanodine-dependent presynaptic release in hippocampal neurons of PS-deficient mice [75]. All together, Stutzmann group concluded from their study that significant Ca^{2+} alterations are present at an early age even though Ca^{2+} homeostasis appears to be maintained. Compensatory mechanisms seem likely to take place in order to maintain normal synaptic function in early age. However, these subtle Ca^{2+}-mediated alterations may have profound impact later on that can affect synaptic and cognitive functions in disease states.

7. Conclusions

Production and deposition of Aβ peptides clearly have central role in AD pathogenesis. However, it is becoming clear that FAD-linked mutations in PS proteins affect diverse physiological processes in addition to promoting the production of highly fibrillogenic Aβ42 peptides. The identification and characterization of γ-secretase substrates and the mechanistic details on the successive cleavage of substrates by the γ-secretase have enhanced our understanding of how partial loss-of-function associated with FAD-linked PS mutations can in fact lead to a gain of activities with reference to intracellular signaling associated with certain substrates such as DCC, ErbB4, and EphA4. At least in some cases, lack of γ-secretase processing leads to profound changes in synaptic structure and functions as a consequence of sustained intracellular signaling by substrate CTFs. As details begin to emerge on additional γ-secretase substrates, it will be possible to determine whether γ-secretase cleavage of neuronal receptors is indeed a regulatory step that modulates physiological signaling downstream of ligand binding and ectodomain shedding. Still, the major task is to establish whether or not altered signaling directly contributes to AD pathogenesis and/or AD-related synaptic dysfunction.

Disclosure

The authors declare no competing interest.

Acknowledgments

Research in the author's laboratories is supported by the National Institutes of Health Grants (ATP: NS055223; GT: AG021495, and AG019070) and by grants from the Alzheimer's Association and American Health Assistance Foundation.

References

[1] R. E. Tanzi and L. Bertram, "New frontiers in Alzheimer's disease genetics," *Neuron*, vol. 32, no. 2, pp. 181–184, 2001.

[2] E. Levy-Lahad, W. Wasco, P. Poorkaj et al., "Candidate gene for the chromosome 1 familial Alzheimer's disease locus," *Science*, vol. 269, no. 5226, pp. 973–977, 1995.

[3] L. Bertram and R. E. Tanzi, "Thirty years of Alzheimer's disease genetics: the implications of systematic meta-analyses," *Nature Reviews Neuroscience*, vol. 9, no. 10, pp. 768–778, 2008.

[4] R. Sherrington, E. I. Rogaev, Y. Liang et al., "Cloning of a gene bearing missense mutations in early-onset familial Alzheimer's disease," *Nature*, vol. 375, no. 6534, pp. 754–760, 1995.

[5] E. I. Rogaev, R. Sherrington, E. A. Rogaeva et al., "Familial Alzheimer's disease in kindreds with missense mutations in a gene on chromosome 1 related to the Alzheimer's disease type 3 gene," *Nature*, vol. 376, no. 6543, pp. 775–778, 1995.

[6] P. C. Wong, H. Zheng, H. Chen et al., "Presenilin 1 is required for Notch 1 and Dll1 expression in the paraxial mesoderm," *Nature*, vol. 387, no. 6630, pp. 288–292, 1997.

[7] J. Shen, R. T. Bronson, D. F. Chen, W. Xia, D. J. Selkoe, and S. Tonegawa, "Skeletal and CNS defects in Presenilin-1-deficient mice," *Cell*, vol. 89, no. 4, pp. 629–639, 1997.

[8] D. B. Donoviel, A.-K. Hadjantonakis, M. Ikeda, H. Zheng, P. S. G. Hyslop, and A. Bernstein, "Mice lacking both presenilin genes exhibit early embryonic patterning defects," *Genes and Development*, vol. 13, no. 21, pp. 2801–2810, 1999.

[9] H. Steiner, K. Duff, A. Capell et al., "A loss of function mutation of presenilin-2 interferes with amyloid β- peptide production and Notch signaling," *The Journal of Biological Chemistry*, vol. 274, no. 40, pp. 28669–28673, 1999.

[10] A. Herreman, D. Hartmann, W. Annaert et al., "Presenilin 2 deficiency causes a mild pulmonary phenotype and no changes in amyloid precursor protein processing but enhances the embryonic lethal phenotype of presenilin 1 deficiency," *Proceedings of the National Academy of Sciences of the United States of America*, vol. 96, no. 21, pp. 11872–11877, 1999.

[11] B. De Strooper, P. Saftig, K. Craessaerts et al., "Deficiency of presenilin-1 inhibits the normal cleavage of amyloid precursor protein," *Nature*, vol. 391, no. 6665, pp. 387–390, 1998.

[12] S. Naruse, G. Thinakaran, J.-J. Luo et al., "Effects of PS1 deficiency on membrane protein trafficking in neurons," *Neuron*, vol. 21, no. 5, pp. 1213–1221, 1998.

[13] S. S. Sisodia and P. H. St George-Hyslop, "γ-secretase, Notch, Aβ and Alzheimer's disease: where do the presenilins fit in?" *Nature Reviews Neuroscience*, vol. 3, no. 4, pp. 281–290, 2002.

[14] G. Thinakaran and A. T. Parent, "Identification of the role of presenilins beyond Alzheimer's disease," *Pharmacological Research*, vol. 50, no. 4, pp. 411–418, 2004.

[15] S. Frykman, J.-Y. Hur, J. Frånberg et al., "Synaptic and endosomal localization of active γ-secretase in rat brain," *PLoS ONE*, vol. 5, no. 1, Article ID e8948, pp. 1–10, 2010.

[16] J. A. Davis, S. Naruse, H. Chen et al., "An Alzheimer's disease-linked PS1 variant rescues the developmental abnormalities of PS1-deficient embryos," *Neuron*, vol. 20, no. 3, pp. 603–609, 1998.

[17] S. Qian, P. Jiang, X.-M. Guan et al., "Mutant human presenilin 1 protects presenilin 1 null mouse against embryonic lethality and elevates Aβ1-42/43 expression," *Neuron*, vol. 20, no. 3, pp. 611–617, 1998.

[18] K. S. Vetrivel, Y.-W. Zhang, H. Xu, and G. Thinakaran, "Pathological and physiological functions of presenilins," *Molecular Neurodegeneration*, vol. 1, no. 1, article 4, 2006.

[19] R. Kopan and M. X. G. Ilagan, "γ-Secretase: proteasome of the membrane?" *Nature Reviews Molecular Cell Biology*, vol. 5, no. 6, pp. 499–504, 2004.

[20] A. L. Parks and D. Curtis, "Presenilin diversifies its portfolio," *Trends in Genetics*, vol. 23, no. 3, pp. 140–150, 2007.

[21] J. V. McCarthy, C. Twomey, and P. Wujek, "Presenilin-dependent regulated intramembrane proteolysis and γ-secretase activity," *Cellular and Molecular Life Sciences*, vol. 66, no. 9, pp. 1534–1555, 2009.

[22] G. Thinakaran and S. S. Sisodia, "Presenilins and Alzheimer disease: the calcium conspiracy," *Nature Neuroscience*, vol. 9, no. 11, pp. 1354–1355, 2006.

[23] C. L. Waites, A. M. Craig, and C. C. Garner, "Mechanisms of vertebrate synaptogenesis," *Annual Review of Neuroscience*, vol. 28, pp. 251–274, 2005.

[24] E. Bruel-Jungerman, S. Davis, and S. Laroche, "Brain plasticity mechanisms and memory: a party of four," *Neuroscientist*, vol. 13, no. 5, pp. 492–505, 2007.

[25] S. W. Scheff and D. A. Price, "Synaptic pathology in Alzheimer's disease: a review of ultrastructural studies," *Neurobiology of Aging*, vol. 24, no. 8, pp. 1029–1046, 2003.

[26] R. D. Terry, E. Masliah, D. P. Salmon et al., "Physical basis of cognitive alterations in Alzheimer's disease: synapse loss is the major correlate of cognitive impairment," *Annals of Neurology*, vol. 30, no. 4, pp. 572–580, 1991.

[27] D. J. Selkoe, "Alzheimer's disease is a synaptic failure," *Science*, vol. 298, no. 5594, pp. 789–791, 2002.

[28] R. E. Tanzi, "The synaptic Aβ hypothesis of Alzheimer disease," *Nature Neuroscience*, vol. 8, no. 8, pp. 977–979, 2005.

[29] G. M. Shankar and D. M. Walsh, "Alzheimer's disease: synaptic dysfunction and Aβ," *Molecular Neurodegeneration*, vol. 4, no. 1, article 48, 2009.

[30] F. Kamenetz, T. Tomita, H. Hsieh et al., "APP processing and synaptic function," *Neuron*, vol. 37, no. 6, pp. 925–937, 2003.

[31] E. Abramov, I. Dolev, H. Fogel, G. D. Ciccotosto, E. Ruff, and I. Slutsky, "Amyloid-β as a positive endogenous regulator of release probability at hippocampal synapses," *Nature Neuroscience*, vol. 12, no. 12, pp. 1567–1576, 2009.

[32] G. M. Shankar, S. Li, T. H. Mehta et al., "Amyloid-β protein dimers isolated directly from Alzheimer's brains impair synaptic plasticity and memory," *Nature Medicine*, vol. 14, no. 8, pp. 837–842, 2008.

[33] S. Li, S. Hong, N. E. Shepardson, D. M. Walsh, G. M. Shankar, and D. Selkoe, "Soluble oligomers of amyloid beta protein facilitate hippocampal long-term depression by disrupting neuronal glutamate uptake," *Neuron*, vol. 62, no. 6, pp. 788–801, 2009.

[34] C. G. Almeida, D. Tampellini, R. H. Takahashi et al., "Beta-amyloid accumulation in APP mutant neurons reduces PSD-95 and GluR1 in synapses," *Neurobiology of Disease*, vol. 20, no. 2, pp. 187–198, 2005.

[35] H. Hsieh, J. Boehm, C. Sato et al., "AMPAR removal underlies Aβ-induced synaptic depression and dendritic spine loss," *Neuron*, vol. 52, no. 5, pp. 831–843, 2006.

[36] E. M. Snyder, Y. Nong, C. G. Almeida et al., "Regulation of NMDA receptor trafficking by amyloid-β," *Nature Neuroscience*, vol. 8, no. 8, pp. 1051–1058, 2005.

[37] B. R. Shrestha, O. V. Vitolo, P. Joshi, T. Lordkipanidze, M. Shelanski, and A. Dunaevsky, "Amyloid β peptide adversely affects spine number and motility in hippocampal neurons," *Molecular and Cellular Neuroscience*, vol. 33, no. 3, pp. 274–282, 2006.

[38] J. Tsai, J. Grutzendler, K. Duff, and W.-B. Gan, "Fibrillar amyloid deposition leads to local synaptic abnormalities and breakage of neuronal branches," *Nature Neuroscience*, vol. 7, no. 11, pp. 1181–1183, 2004.

[39] W. Wei, L. N. Nguyen, H. W. Kessels, H. Hagiwara, S. Sisodia, and R. Malinow, "Amyloid beta from axons and dendrites reduces local spine number and plasticity," *Nature Neuroscience*, vol. 13, no. 2, pp. 190–196, 2010.

[40] B. De Strooper, "Loss-of-function presenilin mutations in Alzheimer disease. Talking Point on the role of presenilin mutations in Alzheimer disease," *EMBO Reports*, vol. 8, no. 2, pp. 141–146, 2007.

[41] M. S. Wolfe, "When loss is gain: reduced presenilin proteolytic function leads to increased Aβ42/Aβ40. Talking point on the role of presenilin mutations in Alzheimer disease," *EMBO Reports*, vol. 8, no. 2, pp. 136–140, 2007.

[42] X. Cao and T. C. Südhof, "A transcriptivety active complex of APP with Fe65 and histone acetyltransferase Tip60," *Science*, vol. 293, no. 5527, pp. 115–120, 2001.

[43] T. Moehlmann, E. Winkler, X. Xia et al., "Presenilin-1 mutations of leucine 166 equally affect the generation of the Notch and APP intracellular domains independent of their effect on Aβ42 production," *Proceedings of the National Academy of Sciences of the United States of America*, vol. 99, no. 12, pp. 8025–8030, 2002.

[44] C. Litterst, A. Georgakopoulos, J. Shioi et al., "Ligand binding and calcium influx induce distinct ectodomain/γ- secretase-processing pathways of EphB2 receptor," *The Journal of Biological Chemistry*, vol. 282, no. 22, pp. 16155–16163, 2007.

[45] E. Inoue, M. Deguchi-Tawarada, A. Togawa et al., "Synaptic activity prompts γ-secretase-mediated cleavage of EphA4 and dendritic spine formation," *Journal of Cell Biology*, vol. 185, no. 3, pp. 551–564, 2009.

[46] R. Radde, C. Duma, M. Goedert, and M. Jucker, "The value of incomplete mouse models of Alzheimer's disease," *European Journal of Nuclear Medicine and Molecular Imaging*, vol. 35, no. 1, supplement, pp. S70–S74, 2008.

[47] V. Echeverria, A. Ducatenzeiler, L. Alhonen et al., "Rat transgenic models with a phenotype of intracellular Aβ accumulation in hippocampus and cortex," *Journal of Alzheimer's Disease*, vol. 6, no. 3, pp. 209–219, 2004.

[48] V. Echeverria, A. Ducatenzeiler, E. Dowd et al., "Altered mitogen-activated protein kinase signaling, tau hyperphosphorylation and mild spatial learning dysfunction in transgenic rats expressing the β-amyloid peptide intracellularly in hippocampal and cortical neurons," *Neuroscience*, vol. 129, no. 3, pp. 583–592, 2004.

[49] D. G. Flood, Y.-G. Lin, D. M. Lang et al., "A transgenic rat model of Alzheimer's disease with extracellular Aβ deposition," *Neurobiology of Aging*, vol. 30, no. 7, pp. 1078–1090, 2009.

[50] W. C. Leon, F. Canneva, V. Partridge, et al., "A novel transgenic rat model with a full Alzheimer's-like amyloid pathology displays pre-plaque intracellular amyloid-beta-associated cognitive impairment," *Journal of Alzheimer's Disease*, vol. 20, no. 1, pp. 113–126, 2010.

[51] D. R. Borchelt, G. Thinakaran, C. B. Eckman et al., "Familial Alzheimer's disease-linked presenilin I variants elevate aβ1-42/1-40 ratio in vitro and in vivo," *Neuron*, vol. 17, no. 5, pp. 1005–1013, 1996.

[52] K. Duff, C. Eckman, C. Zehr et al., "Increased amyloid-β42(43) in brains of mice expressing mutant presenilin 1," *Nature*, vol. 383, no. 6602, pp. 710–713, 1996.

[53] Q. Guo, W. Fu, B. L. Sopher et al., "Increased vulnerability of hippocampal neurons to excitotoxic necrosis in presenilin-1 mutant knock-in mice," *Nature Medicine*, vol. 5, no. 1, pp. 101–106, 1999.

[54] Y. Nakano, G. Kondoh, T. Kudo et al., "Accumulation of murine amyloidβ42 in a gene-dosage-dependent manner in PS1 'knock-in' mice," *European Journal of Neuroscience*, vol. 11, no. 7, pp. 2577–2581, 1999.

[55] R. Siman, A. G. Reaume, M. J. Savage et al., "Presenilin-1 P264L knock-in mutation: differential effects on Aβ production, amyloid deposition, and neuronal vulnerability," *Journal of Neuroscience*, vol. 20, no. 23, pp. 8717–8726, 2000.

[56] Y. Deng, L. Tarassishin, V. Kallhoff et al., "Deletion of presenilin 1 hydrophilic loop sequence leads to impaired γ-secretase activity and exacerbated amyloid pathology," *Journal of Neuroscience*, vol. 26, no. 14, pp. 3845–3854, 2006.

[57] S. Oddo, A. Caccamo, J. D. Shepherd et al., "Triple-transgenic model of Alzheimer's Disease with plaques and tangles: intracellular Aβ and synaptic dysfunction," *Neuron*, vol. 39, no. 3, pp. 409–421, 2003.

[58] H. Yu, C. A. Saura, S.-Y. Choi et al., "APP processing and synaptic plasticity in presenilin-1 conditional knockout mice," *Neuron*, vol. 31, no. 5, pp. 713–726, 2001.

[59] R. Feng, C. Rampon, Y.-P. Tang et al., "Deficient neurogenesis in forebrain-specific presenilin-1 knockout mice is associated with reduced clearance of hippocampal memory traces," *Neuron*, vol. 32, no. 5, pp. 911–926, 2001.

[60] I. Dewachter, D. Reversé, N. Caluwaerts et al., "Neuronal deficiency of presenilin 1 inhibits amyloid plaque formation and corrects hippocampal long-term potentiation but not a cognitive defect of amyloid precursor protein [v717i] transgenic mice," *Journal of Neuroscience*, vol. 22, no. 9, pp. 3445–3453, 2002.

[61] C. A. Saura, S.-Y. Choi, V. Beglopoulos et al., "Loss of presenilin function causes impairments of memory and synaptic plasticity followed by age-dependent neurodegeneration," *Neuron*, vol. 42, no. 1, pp. 23–36, 2004.

[62] C. A. Saura, G. Chen, S. Malkani et al., "Conditional inactivation of presenilin 1 prevents amyloid accumulation and temporarily rescues contextual and spatial working memory impairments in amyloid precursor protein transgenic mice," *Journal of Neuroscience*, vol. 25, no. 29, pp. 6755–6764, 2005.

[63] G. A. Seidner, Y. Ye, M. M. Faraday, W. G. Alvord, and M. E. Fortini, "Modeling clinically heterogeneous presenilin mutations with transgenic Drosophila," *Current Biology*, vol. 16, no. 10, pp. 1026–1033, 2006.

[64] A. Smialowska and R. Baumeister, "Presenilin function in Caenorhabditis elegans," *Neurodegenerative Diseases*, vol. 3, no. 4-5, pp. 227–232, 2006.

[65] A. Parent, D. J. Linden, S. S. Sisodia, and D. R. Borchelt, "Synaptic transmission and hippocampal long-term potentiation in transgenic mice expressing FAD-linked presenilin 1," *Neurobiology of Disease*, vol. 6, no. 1, pp. 56–62, 1999.

[66] S. H. Zaman, A. Parent, A. Laskey et al., "Enhanced synaptic potentiation in transgenic mice expressing presenilin 1 familial Alzheimer's disease mutation is normalized with a benzodiazepine," *Neurobiology of Disease*, vol. 7, no. 1, pp. 54–63, 2000.

[67] P. A. Barrow, R. M. Empson, S. J. Gladwell et al., "Functional phenotype in transgenic mice expressing mutant human presenilin-1," *Neurobiology of Disease*, vol. 7, no. 2, pp. 119–126, 2000.

[68] I. Schneider, D. Reversé, I. Dewachter et al., "Mutant presenilins disturb neuronal calcium homeostasis in the brain of transgenic mice, decreasing the threshold for excitotoxicity and facilitating long-term potentiation," *The Journal of Biological Chemistry*, vol. 276, no. 15, pp. 11539–11544, 2001.

[69] I. Dewachter, L. Ris, S. Croes et al., "Modulation of synaptic plasticity and Tau phosphorylation by wild-type and mutant presenilin1," *Neurobiology of Aging*, vol. 29, no. 5, pp. 639–652, 2008.

[70] Y. Wang, N. H. Greig, Q.-S. Yu, and M. P. Mattson, "Presenilin-1 mutation impairs cholinergic modulation of synaptic plasticity and suppresses NMDA currents in hippocampus slices," *Neurobiology of Aging*, vol. 30, no. 7, pp. 1061–1068, 2009.

[71] A. T. Parent, N. Y. Barnes, Y. Taniguchi, G. Thinakaran, and S. S. Sisodia, "Presenilin attenuates receptor-mediated signaling and synaptic function," *Journal of Neuroscience*, vol. 25, no. 6, pp. 1540–1549, 2005.

[72] C. Priller, I. Dewachter, N. Vassallo et al., "Mutant presenilin 1 alters synaptic transmission in cultured hippocampal neurons," *The Journal of Biological Chemistry*, vol. 282, no. 2, pp. 1119–1127, 2007.

[73] D. Knight, K. Iliadi, M. P. Charlton, H. L. Atwood, and G. L. Boulianne, "Presynaptic plasticity and associative learning are impaired in a Drosophila presenilin null mutant," *Developmental Neurobiology*, vol. 67, no. 12, pp. 1598–1613, 2007.

[74] R. A. Morton, F. M. Kuenzi, S. M. Fitzjohn et al., "Impairment in hippocampal long-term potentiation in mice underexpressing the Alzheimer's disease related gene presenilin-1," *Neuroscience Letters*, vol. 319, no. 1, pp. 37–40, 2002.

[75] C. Zhang, B. Wu, V. Beglopoulos et al., "Presenilins are essential for regulating neurotransmitter release," *Nature*, vol. 460, no. 7255, pp. 632–636, 2009.

[76] X.-X. Yan, T. Li, C. M. Rominger et al., "Binding sites of gamma-secretase inhibitors in rodent brain: distribution, postnatal development, and effect of deafferentation," *Journal of Neuroscience*, vol. 24, no. 12, pp. 2942–2952, 2004.

[77] B. S. McEwen, "Early life influences on life-long patterns of behavior and health," *Mental Retardation and Developmental Disabilities Research Reviews*, vol. 9, no. 3, pp. 149–154, 2003.

[78] M. Sarter and J. P. Bruno, "Developmental origins of the age-related decline in cortical cholinergic function and associated cognitive abilities," *Neurobiology of Aging*, vol. 25, no. 9, pp. 1127–1139, 2004.

[79] E. H. Koo and R. Kopan, "Potential role of presenilin-regulated signaling pathways in sporadic neurodegeneration," *Nature Medicine*, vol. 10, pp. S26–S33, 2004.

[80] T. Tada and M. Sheng, "Molecular mechanisms of dendritic spine morphogenesis," *Current Opinion in Neurobiology*, vol. 16, no. 1, pp. 95–101, 2006.

[81] K. E. Sorra and K. M. Harris, "Overview on the structure, composition, function, development, and plasticity of hippocampal dendritic spines," *Hippocampus*, vol. 10, no. 5, pp. 501–511, 2000.

[82] C. Lüscher, R. A. Nicoll, R. C. Malenka, and D. Muller, "Synaptic plasticity and dynamic modulation of the postsynaptic membrane," *Nature Neuroscience*, vol. 3, no. 6, pp. 545–550, 2000.

[83] R. Yuste and T. Bonhoeffer, "Morphological changes in dendritic spines associated with long-term synaptic plasticity," *Annual Review of Neuroscience*, vol. 24, pp. 1071–1089, 2001.

[84] T. Bonhoeffer and R. Yuste, "Spine motility: phenomenology, mechanisms, and function," *Neuron*, vol. 35, no. 6, pp. 1019–1027, 2002.

[85] G. M. Shankar, B. L. Bloodgood, M. Townsend, D. M. Walsh, D. J. Selkoe, and B. L. Sabatini, "Natural oligomers of the Alzheimer amyloid-β protein induce reversible synapse loss by modulating an NMDA-type glutamate receptor-dependent signaling pathway," *Journal of Neuroscience*, vol. 27, no. 11, pp. 2866–2875, 2007.

[86] S. M. Fitzjohn, R. A. Morton, F. Kuenzi et al., "Age-related impairment of synaptic transmission but normal potentiation in transgenic mice that overexpress the human APP695SWE mutant form of amyloid precursor protein," *Journal of Neuroscience*, vol. 21, no. 13, pp. 4691–4698, 2001.

[87] E. H. Chang, M. J. Savage, D. G. Flood et al., "AMPA receptor downscaling at the onset of Alzheimer's disease pathology in double knockin mice," *Proceedings of the National Academy of Sciences of the United States of America*, vol. 103, no. 9, pp. 3410–3415, 2006.

[88] T. L. Spires, M. Meyer-Luehmann, E. A. Stern et al., "Dendritic spine abnormalities in amyloid precursor protein transgenic mice demonstrated by gene transfer and intravital multiphoton microscopy," *Journal of Neuroscience*, vol. 25, no. 31, pp. 7278–7287, 2005.

[89] A. Mendoza-Naranjo, C. Gonzalez-Billault, and R. B. Maccioni, "Aβ1-42 stimulates actin polymerization in hippocampal neurons through Rac1 and Cdc42 Rho GTPases," *Journal of Cell Science*, vol. 120, no. 2, pp. 279–288, 2007.

[90] D. Puzzo, L. Privitera, E. Leznik et al., "Picomolar amyloid-β positively modulates synaptic plasticity and memory in hippocampus," *Journal of Neuroscience*, vol. 28, no. 53, pp. 14537–14545, 2008.

[91] N. Y. Barnes, J. Shi, H. Yajima, G. Thinakaran, and A. T. Parent, "Steady-state increase of cAMP-response element binding protein, Rac, and PAK signaling in presenilin-deficient neurons," *Journal of Neurochemistry*, vol. 104, no. 6, pp. 1637–1648, 2008.

[92] T. Bittner, M. Fuhrmann, S. Burgold et al., "γ-secretase inhibition reduces spine density in vivo via an amyloid precursor protein-dependent pathway," *Journal of Neuroscience*, vol. 29, no. 33, pp. 10405–10409, 2009.

[93] D. D. Murphy and M. Segal, "Morphological plasticity of dendritic spines in central neurons is mediated by activation of cAMP response element binding protein," *Proceedings of the National Academy of Sciences of the United States of America*, vol. 94, no. 4, pp. 1482–1487, 1997.

[94] O. V. Vitolo, A. Sant'Angelo, V. Costanzo, F. Battaglia, O. Arancio, and M. Shelanski, "Amyloid β-peptide inhibition of the PKA/CREB pathway and long-term potentiation: reversibility by drugs that enhance cAMP signaling," *Proceedings of the National Academy of Sciences of the United States of America*, vol. 99, no. 20, pp. 13217–13221, 2002.

[95] M. Negishi and H. Katoh, "Rho family GTPases and dendrite plasticity," *Neuroscientist*, vol. 11, no. 3, pp. 187–191, 2005.

[96] M. L. Hayashi, S.-Y. Choi, B. S. Rao et al., "Altered cortical synaptic morphology and impaired memory consolidation in forebrain- specific dominant-negative PAK transgenic mice," *Neuron*, vol. 42, no. 5, pp. 773–787, 2004.

[97] L. Zhao, Q.-L. Ma, F. Calon et al., "Role of p21-activated kinase pathway defects in the cognitive deficits of Alzheimer disease," *Nature Neuroscience*, vol. 9, no. 2, pp. 234–242, 2006.

[98] Y. Shuai, B. Lu, Y. Hu, L. Wang, K. Sun, and Y. Zhong, "Forgetting is regulated through rac activity in Drosophila," *Cell*, vol. 140, no. 4, pp. 579–589, 2010.

[99] R. L. Davis, "Olfactory memory formation in Drosophila: from molecular to systems neuroscience," *Annual Review of Neuroscience*, vol. 28, pp. 275–302, 2005.

[100] Y. Fukazawa, Y. Saitoh, F. Ozawa, Y. Ohta, K. Mizuno, and K. Inokuchi, "Hippocampal LTP is accompanied by enhanced F-actin content within the dendritic spine that is essential for late LTP maintenance in vivo," *Neuron*, vol. 38, no. 3, pp. 447–460, 2003.

[101] E. R. Kandel, "The molecular biology of memory storage: a dialogue between genes and synapses," *Science*, vol. 294, no. 5544, pp. 1030–1038, 2001.

[102] H. Watanabe, M. J. Smith, E. Heilig, V. Beglopoulos, R. J. Kelleher III, and J. Shen, "Indirect regulation of presenilins in CREB-mediated transcription," *The Journal of Biological Chemistry*, vol. 284, no. 20, pp. 13705–13713, 2009.

[103] B. J. Dickson, "Molecular mechanisms of axon guidance," *Science*, vol. 298, no. 5600, pp. 1959–1964, 2002.

[104] S. J. Araújo and G. Tear, "Axon guidance mechanisms and molecules: lessons from invertebrates," *Nature Reviews Neuroscience*, vol. 4, no. 11, pp. 910–922, 2003.

[105] T. E. Kennedy, "Cellular mechanisms of netrin function: long-range and short-range actions," *Biochemistry and Cell Biology*, vol. 78, no. 5, pp. 569–575, 2000.

[106] M. Yamagata, J. R. Sanes, and J. A. Weiner, "Synaptic adhesion molecules," *Current Opinion in Cell Biology*, vol. 15, no. 5, pp. 621–632, 2003.

[107] Y. Goda, "Cadherins communicate structural plasticity of presynaptic and postsynaptic terminals," *Neuron*, vol. 35, no. 1, pp. 1–3, 2002.

[108] M. Ozaki, "Neuregulins and the shaping of synapses," *Neuroscientist*, vol. 7, no. 2, pp. 146–154, 2001.

[109] Y. Yamaguchi and E. B. Pasquale, "Eph receptors in the adult brain," *Current Opinion in Neurobiology*, vol. 14, no. 3, pp. 288–296, 2004.

[110] Y. Takai, K. Shimizu, and T. Ohtsuka, "The roles of cadherins and nectins in interneuronal synapse formation," *Current Opinion in Neurobiology*, vol. 13, no. 5, pp. 520–526, 2003.

[111] P. Washbourne, A. Dityatev, P. Scheiffele et al., "Cell adhesion molecules in synapse formation," *Journal of Neuroscience*, vol. 24, no. 42, pp. 9244–9249, 2004.

[112] M. Leyssen, D. Ayaz, S. S. Hébert, S. Reeve, B. De Strooper, and B. A. Hassan, "Amyloid precursor protein promotes post-developmental neurite arborization in the Drosophila brain," *EMBO Journal*, vol. 24, no. 16, pp. 2944–2955, 2005.

[113] C. Reinhard, S. S. Hébert, and B. De Strooper, "The amyloid-β precursor protein: integrating structure with biological function," *EMBO Journal*, vol. 24, no. 23, pp. 3996–4006, 2005.

[114] A. S. Yap and E. M. Kovacs, "Direct cadherin-activated cell signaling: a view from the plasma membrane," *Journal of Cell Biology*, vol. 160, no. 1, pp. 11–16, 2003.

[115] P. Marambaud, P. H. Wen, A. Dutt et al., "A CBP binding transcriptional repressor produced by the PS1/ε-cleavage of N-Cadherin is inhibited by PS1 FAD mutations," *Cell*, vol. 114, no. 5, pp. 635–645, 2003.

[116] P. Soba, S. Eggert, K. Wagner et al., "Homo- and heterodimerization of APP family members promotes intercellular adhesion," *EMBO Journal*, vol. 24, no. 20, pp. 3624–3634, 2005.

[117] J. L. Brusés, "N-cadherin signaling in synapse formation and neuronal physiology," *Molecular Neurobiology*, vol. 33, no. 3, pp. 237–252, 2006.

[118] A. Haapasalo, D. Y. Kim, B. W. Carey, M. K. Turunen, W. H. Pettingell, and D. M. Kovacs, "Presenilin/γ-secretase-mediated cleavage regulates association of Leukocyte-common Antigen-related (LAR) receptor tyrosine phosphatase with β-catenin," *The Journal of Biological Chemistry*, vol. 282, no. 12, pp. 9063–9072, 2007.

[119] M. A. Leissring, M. P. Murphy, T. R. Mead et al., "A physiologic signaling role for the γ-secretase-derived intracellular fragment of APP," *Proceedings of the National Academy of Sciences of the United States of America*, vol. 99, no. 7, pp. 4697–4702, 2002.

[120] P. Penzes, A. Beeser, J. Chernoff et al., "Rapid induction of dendritic spine morphogenesis by trans-synaptic ephrinB-EphB receptor activation of the Rho-GEF kalirin," *Neuron*, vol. 37, no. 2, pp. 263–274, 2003.

[121] M. B. Dalva, M. A. Takasu, M. Z. Lin et al., "EphB receptors interact with NMDA receptors and regulate excitatory synapse formation," *Cell*, vol. 103, no. 6, pp. 945–956, 2000.

[122] M. Henkemeyer, O. S. Itkis, M. Ngo, P. W. Hickmott, and I. M. Ethell, "Multiple EphB receptor tyrosine kinases shape dendritic spines in the hippocampus," *Journal of Cell Biology*, vol. 163, no. 6, pp. 1313–1326, 2003.

[123] R. A. G. Garcia, K. Vasudevan, and A. Buonanno, "The neuregulin receptor ErbB-4 interacts with PDZ-containing proteins at neuronal synapses," *Proceedings of the National Academy of Sciences of the United States of America*, vol. 97, no. 7, pp. 3596–3601, 2000.

[124] J. A. Weiner, X. Wang, J. C. Tapia, and J. R. Sanes, "Gamma protocadherins are required for synaptic development in the spinal cord," *Proceedings of the National Academy of Sciences of the United States of America*, vol. 102, no. 1, pp. 8–14, 2005.

[125] A. W. Dunah, E. Hueske, M. Wyszynski et al., "LAR receptor protein tyrosine phosphatases in the development and maintenance of excitatory synapses," *Nature Neuroscience*, vol. 8, no. 4, pp. 458–467, 2005.

[126] R. Malinow and R. C. Malenka, "AMPA receptor trafficking and synaptic plasticity," *Annual Review of Neuroscience*, vol. 25, pp. 103–126, 2002.

[127] H. Kasai, M. Matsuzaki, J. Noguchi, N. Yasumatsu, and H. Nakahara, "Structure-stability-function relationships of dendritic spines," *Trends in Neurosciences*, vol. 26, no. 7, pp. 360–368, 2003.

[128] M. J. Galko and M. Tessier-Lavigne, "Function of an axonal chemoattractant modulated by metalloprotease activity," *Science*, vol. 289, no. 5483, pp. 1365–1367, 2000.

[129] Y. Taniguchi, S.-H. Kim, and S. S. Sisodia, "Presenilin-dependent "γ-secretase" processing of deleted in colorectal cancer (DCC)," *The Journal of Biological Chemistry*, vol. 278, no. 33, pp. 30425–30428, 2003.

[130] C. Hooper, R. Killick, and S. Lovestone, "The GSK3 hypothesis of Alzheimer's disease," *Journal of Neurochemistry*, vol. 104, no. 6, pp. 1433–1439, 2008.

[131] A. Takashima, M. Murayama, O. Murayama et al., "Presenilin 1 associates with glycogen synthase kinase-3β and its substrate tau," *Proceedings of the National Academy of Sciences of the United States of America*, vol. 95, no. 16, pp. 9637–9641, 1998.

[132] Z. Zhang, H. Hartmann, V. M. Do et al., "Destabilization of β-catenin by mutations in presenilin-1 potentiates neuronal apoptosis," *Nature*, vol. 395, no. 6703, pp. 698–702, 1998.

[133] D. E. Kang, S. Soriano, X. Xia et al., "Presenilin couples the paired phosphorylation of β-catenin independent of axin: implications for β-catenin activation in tumorigenesis," *Cell*, vol. 110, no. 6, pp. 751–762, 2002.

[134] L. C. Cantley, "The phosphoinositide 3-kinase pathway," *Science*, vol. 296, no. 5573, pp. 1655–1657, 2002.

[135] T. Yoshimura, N. Arimura, and K. Kaibuchi, "Signaling networks in neuronal polarization," *Journal of Neuroscience*, vol. 26, no. 42, pp. 10626–10630, 2006.

[136] L.-Q. Zhu, S.-H. Wang, D. Liu et al., "Activation of glycogen synthase kinase-3 inhibits long-term potentiation with synapse-associated impairments," *Journal of Neuroscience*, vol. 27, no. 45, pp. 12211–12220, 2007.

[137] S. Peineau, C. Bradley, C. Taghibiglou et al., "The role of GSK-3 in synaptic plasticity," *British Journal of Pharmacology*, vol. 153, no. 1, pp. S428–S437, 2008.

[138] L. Baki, J. Shioi, P. Wen et al., "PS1 activates PI3K thus inhibiting GSK-3 activity and tau overphosphorylation: effects of FAD mutations," *EMBO Journal*, vol. 23, no. 13, pp. 2586–2596, 2004.

[139] G. Pigino, G. Morfini, A. Pelsman, M. P. Mattson, S. T. Brady, and J. Busciglio, "Alzheimer's presenilin 1 mutations impair kinesin-based axonal transport," *Journal of Neuroscience*, vol. 23, no. 11, pp. 4499–4508, 2003.

[140] L. Baki, R. L. Neve, Z. Shao, J. Shioi, A. Georgakopoulos, and N. K. Robakis, "Wild-type but not FAD mutant presenilin-1 prevents neuronal degeneration by promoting phosphatidylinositol 3-kinase neuroprotective signaling," *Journal of Neuroscience*, vol. 28, no. 2, pp. 483–490, 2008.

[141] K. Tanemura, D.-H. Chui, T. Fukuda et al., "Formation of tau inclusions in knock-in mice with familial Alzheimer disease (FAD) mutation of presenilin 1 (PS1)," *The Journal of Biological Chemistry*, vol. 281, no. 8, pp. 5037–5041, 2006.

[142] D. E. Kang, I. S. Yoon, E. Repetto et al., "Presenilins mediate phosphatidylinositol 3-kinase/AKT and ERK activation via select signaling receptors: selectivity of PS2 in platelet-derived growth factor signaling," *The Journal of Biological Chemistry*, vol. 280, no. 36, pp. 31537–31547, 2005.

[143] H. Cheng, K. S. Vetrivel, P. Gong, X. Meckler, A. Parent, and G. Thinakaran, "Mechanisms of disease: new therapeutic strategies for Alzheimer's disease—targeting APP processing in lipid rafts," *Nature Clinical Practice Neurology*, vol. 3, no. 7, pp. 374–382, 2007.

[144] H. Hering, C.-C. Lin, and M. Sheng, "Lipid rafts in the maintenance of synapses, dendritic spines, and surface AMPA receptor stability," *Journal of Neuroscience*, vol. 23, no. 8, pp. 3262–3271, 2003.

[145] T. Golub, S. Wacha, and P. Caroni, "Spatial and temporal control of signaling through lipid rafts," *Current Opinion in Neurobiology*, vol. 14, no. 5, pp. 542–550, 2004.

[146] L. Ma, Y. Z. Huang, G. M. Pitcher et al., "Ligand-dependent recruitment of the ErbB4 signaling complex into neuronal lipid rafts," *Journal of Neuroscience*, vol. 23, no. 8, pp. 3164–3175, 2003.

[147] Z. Hérincs, V. Corset, N. Cahuzac et al., "DCC association with lipid rafts is required for netrin-1-mediated axon guidance," *Journal of Cell Science*, vol. 118, no. 8, pp. 1687–1692, 2005.

[148] K. S. Vetrivel, H. Cheng, W. Lin et al., "Association of γ-secretase with lipid rafts in post-golgi and endosome membranes," *The Journal of Biological Chemistry*, vol. 279, no. 43, pp. 44945–44954, 2004.

[149] K. S. Vetrivel, H. Cheng, S.-H. Kim et al., "Spatial segregation of γ-secretase and substrates in distinct membrane domains," *The Journal of Biological Chemistry*, vol. 280, no. 27, pp. 25892–25900, 2005.

[150] G. E. Stutzmann, "The pathogenesis of Alzheimers disease—is it a lifelong "calciumopathy"?" *Neuroscientist*, vol. 13, no. 5, pp. 546–559, 2007.

[151] F. M. LaFerla, "Calcium dyshomeostasis and intracellular signalling in Alzheimer's disease," *Nature Reviews Neuroscience*, vol. 3, no. 11, pp. 862–872, 2002.

[152] G. E. Stutzmann, A. Caccamo, F. M. LaFerla, and I. Parker, "Dysregulated IP3 signaling in cortical neurons of knock-in mice expressing an Alzheimer's-linked mutation in presenilin1 results in exaggerated Ca^{2+} signals and altered membrane excitability," *Journal of Neuroscience*, vol. 24, no. 2, pp. 508–513, 2004.

[153] Y. Lu, Y. Lv, Y. Ye et al., "A role for presenilin in post-stress regulation: effects of presenilin mutations on Ca^{2+} currents in Drosophila," *FASEB Journal*, vol. 21, no. 10, pp. 2368–2378, 2007.

[154] H. Tu, O. Nelson, A. Bezprozvanny et al., "Presenilins form ER Ca^{2+} leak channels, a function disrupted by familial Alzheimer's disease-linked mutations," *Cell*, vol. 126, no. 5, pp. 981–993, 2006.

[155] S. Chakroborty, I. Goussakov, M. B. Miller, and G. E. Stutzmann, "Deviant ryanodine receptor-mediated calcium release resets synaptic homeostasis in presymptomatic 3xTg-AD mice," *Journal of Neuroscience*, vol. 29, no. 30, pp. 9458–9470, 2009.

SAGE-Hindawi Access to Research
International Journal of Alzheimer's Disease
Volume 2010, Article ID 723782, 6 pages
doi:10.4061/2010/723782

Review Article

Neuron Loss in Transgenic Mouse Models of Alzheimer's Disease

Oliver Wirths and Thomas A. Bayer

Division of Molecular Psychiatry and Alzheimer Ph.D. Graduate School, Department of Psychiatry, University of Goettingen, von-Siebold-Str. 5, 37075 Goettingen, Germany

Correspondence should be addressed to Oliver Wirths, owirths@gwdg.de

Received 3 May 2010; Revised 5 July 2010; Accepted 9 July 2010

Academic Editor: Gemma Casadesus

Since their initial generation in the mid 1990s, transgenic mouse models of Alzheimers's disease (AD) have been proven to be valuable model systems which are indispensable for modern AD research. Whereas most of these models are characterized by extensive amyloid plaque pathology, inflammatory changes and often behavioral deficits, modeling of neuron loss was much less successful. The present paper discusses the current achievements of modeling neuron loss in transgenic mouse models based on APP/Aβ and Tau overexpression and provides an overview of currently available AD mouse models showing these pathological alterations.

1. Introduction

Alzheimer's disease (AD) represents the most frequent form of dementia and is characterized by two major neuropathological hallmarks: (i) extracellular plaques composed of the 40–42 residues Aβ peptide [1] and (ii) neurofibrillary tangles (NFTs), consisting of abnormal phosphorylated Tau protein [2]. There is increasing evidence that, in addition to the well-known extracellular amyloid deposition in the parenchyma, Aβ peptides accumulate within neurons [3]. It has been hypothesized that this initial accumulation is one of the earliest pathological events, which is able to trigger the cascade leading to neurodegeneration [4]. Whereas the vast majority of AD cases occur sporadically, a small percentage (<2%) of all cases represents familial forms of AD with an autosomal dominant mode of inheritance. Identification of the underlying mutations opened manifold opportunities for the generation of transgenic mouse models. Since their initial generation in the mid 1990s, transgenic mice have been proven to represent valuable model systems reflecting various pathological aspects of AD including plaque deposition, inflammatory changes or behavioral abnormalities (reviewed in [5, 6]). In the present short paper, we summarize the current achievements of modeling neuron loss in transgenic mice based on APP/Aβ overexpression.

2. APP-/Aβ-Based Mouse Models with Neuron Loss

A variety of different transgenic AD mouse models have been developed during the last 15 years which can be categorized as either APP single transgenic mice (e.g., PDAPP [7], Tg2576 [8], APP/Ld [9], TgCRND8 [10], APP23 [11], tg APP_ArcSwe [12], APP-Au [13], or $APPE_{693\Delta}$ [14]), bigenic mice expressing both APP and PS1/PS2 or Tau (e.g., APPswe/PS1dE9 [15], APP/PS1 [16], PS2APP [17], APP/PS1KI [18], or APP/tau [19]), and triple transgenic mice expressing APP, PS1, and Tau (e.g., 3xTg [20] or TauPS2APP [21]). Whereas most of these models present abundant extracellular amyloid plaque pathology, several efforts modelling significant neuron loss remained less successful [22, 23].

First evidence for neurotoxic *in vivo* properties of Aβ came from a transgenic mouse model expressing murine Aβ under the control of the mouse Neurofilament-light gene (NF-L) promoter, ensuring neuronal expression. This resulted in abundant neurodegeneration, with biochemical and morphological evidence for an apoptotic mechanism [24]. Later, a transgenic mouse model expressing human APP with the Swedish mutation (APP23) under the control of the murine Thy1-promoter was reported, showing

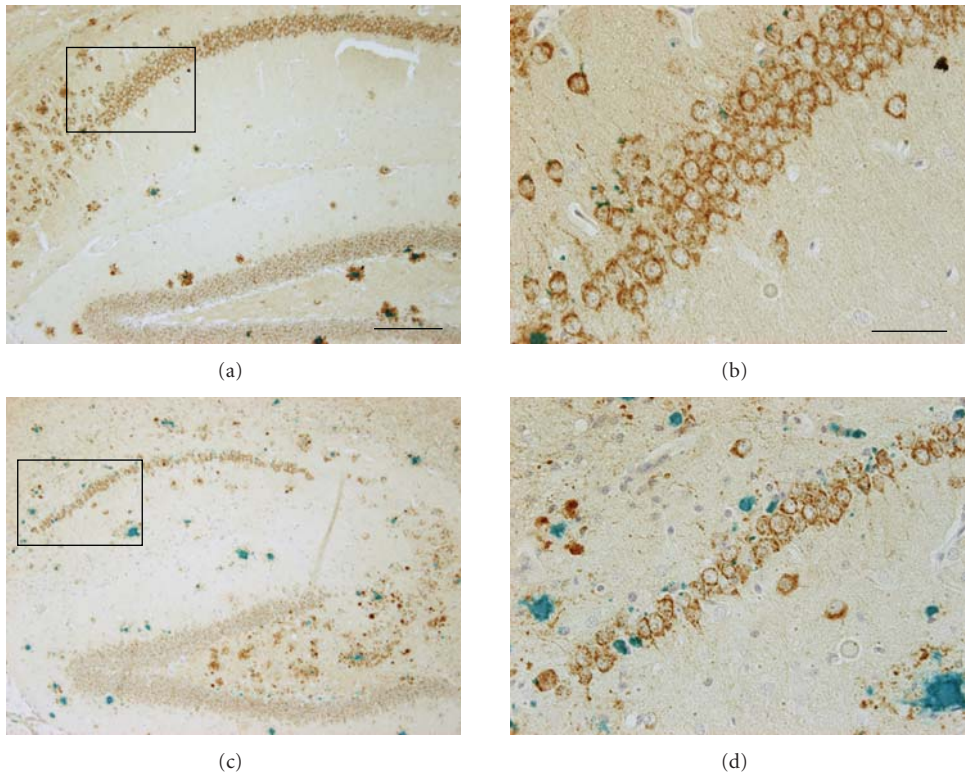

Figure 1: Hippocampal neuron loss in the APP/PS1KI mouse model of AD. (a) APP (brown) and Aβ staining (green) in the hippocampal formation of a 2-month-old and (c) a 10-month-old APP/PS1KI mouse. (b,d) Higher magnification of the CA1 granular cell layer of a 2-month-old (b) and a 10-month-old APP/PS1KI reveals profound neuron loss at the later time point. Scale bars: (a,c): 200 μm, (b,d): 50 μm.

significant hippocampal CA1 neuron loss (−14%) at the age of 14 to 18 months. These mice show an age-dependent extracellular plaque deposition primarily in neocortex and hippocampus, accompanied by severe gliosis. The number of CA1 neurons is inversely correlated with CA1 plaque load and neuron loss was observed primarily in the vicinity of extracellular plaques [25]. It has been shown that focal neuronal toxicity is associated with extracellular Aβ deposits when they occur in a fibrillar beta-pleated sheet confirmation [26]. Surprisingly, no differences in the neocortical synaptic bouton number as well as in synaptophysin protein levels were detected during aging or in comparison with age-matched nontransgenic control mice [27].

Analysis of 17-month-old APP_{751SL}/PS1M146L transgenic mice using unbiased stereologic methods revealed a loss of CA1-3 neurons in a magnitude of ∼30% compared to age-matched PS1 control animals. Interestingly, the plaque load was approximately 10% smaller than the level of hippocampal pyramidal cell loss in these mice, indicating a loss of neurons at sites of Aβ aggregation but also clearly observed in areas distant from extracellular Aβ deposits. This observation points to the potential involvement of more than one mechanism in hippocampal neuron loss in this mouse model [29]. A quantitative study of synaptophysin-immunoreactive presynaptic boutons (SIPBs) revealed an age-related loss in both APP_{751SL} and PS1M146L single transgenic mice within the stratum radiatum, which was most severe in APP751SL/PS1M146L mice extending also to plaque-free regions [30].

Another model showing a more severe hippocampal neuron loss is the APP/PS1KI mouse model [18]. At the age of 10 months an extensive neuron loss (>50%) in the hippocampus was reported, that correlated with the accumulation of intraneuronal Aβ and Thioflavin-S positive intracellular material [18] (Figure 1). Extending these studies to earlier ones revealed that this CA1 neuron loss is already detectable at the age of 6 months. At this time point, a loss of 33% of CA1 pyramidal neurons compared to PS1KI littermates could be demonstrated, together with a decrease in the CA1 volume (−30%), an atrophy of the entire hippocampus of 18% and synaptic alterations, including reduced levels of pre- (SNAP25, clathrin light chain) and post-synaptic markers (PSD-95). In addition, recordings of field excitatory postsynaptic potentials (fEPSPs) revealed a significant reduction of 6 months in APP/PS1KI compared to PS1KI or nontransgenic mice [31]. A detailed stereological comparison of neuronal numbers in frontal cortex and thalamus, representing brain areas with intra- and extracellular Aβ accumulation (frontal cortex) or with only extracellular Aβ pathology (thalamus), revealed an early loss of cortical neurons starting at the age of 6 months. This neuronal loss correlated with the transient intraneuronal

Table 1: Overview of transgenic AD mouse models in which neuronal loss and/or intraneuronal Aβ accumulation has been reported. In addition, information on the transgene, extracellular plaque onset, and intraneuronal Aβ accumulation are given. (n.d.: not determined).

Transgenic mouse model	Mutation APP	Mutation PS1	Promoter	Plaque onset	Intraneur. Aβ	Neuron loss	Synaptic dysfunction	Reference
NF-L-Aβ	—	—	NF-L (Aβ)	n.d.	√	√	n.d.	[24]
APP23	Swedish	—	Thy1 (APP)	6 m	n.d.	14–18 m	—	[25]
APP_{751SL}x PS1M146L	Swedish, London	M146L	Thy1 (APP) HMG-CoA (PS1)	3 m	√	17 m	√	[16]
APP_{751SL}/ PS1KI	Swedish, London	M233T, L235P	Thy1 (APP) PS1 knockin	2 m	√	6 m	√	[18]
5XFAD	Swedish, Florida, London	M146L, L286V	Thy1 (APP, PS1)	2 m	√	9 m	√	[28]
TBA2	—	—	Thy1 ($AbpE_{3-42}$)	2 m	√	2 m	n.d.	[42]
$APP_{E693\Delta}$	Japanese	—	Prp (APP)	—	√	24 m	√	[14]
3xTg	Swedish	M146V	Thy1 (APP, Tau) PS1 knockin	6 m	√	n.d.	√	[20]
APP/tau	Swedish	—	Prion Protein (APP) Thy1 (Tau)	9 m	n.d.	9 m	n.d.	[19]
TauPS2APP	Swedish	N141I (PS2)	Thy1 (APP, PS2, Tau)	4 m	n.d.	—	n.d.	[46]

Aβ accumulation. No neuron loss could be observed in the thalamus where on extracellular Aβ plaques, however, in a comparable amount as in the cortex were present [32]. A related observation was made in distinct cholinergic brain stem nuclei (Mo5, 7N) in this mouse model, where neuronal loss at 6 or 12 months of age correlated with the presence of intraneuronal Aβ peptides [33]. Interestingly, a significant loss of parvalbumin- (PV)-positive interneurons in CA1-2 (40%–50%) and calretinin- (CR)-immunoreactive interneurons in the hilus and dentate gyrus (37%–52%) has been recently reported in 10-month-old APP/PS1KI mice [34]. This is in the range of PV- and CR-positive interneuron losses in the dentate gyrus of postmortem brain specimen from AD patients. In addition, a significant neuron loss has been found in the granule cell layer of the dentate gyrus of 12-month-old APP/PS1KI mice, where abundant Aβ deposition is present. This loss is likely due to local extracellular plaque pathology [26], in combination with a complete loss of neurogenesis already at the age of 6 months [35, 36], which prevents any re-integration of new-born neurons in that particular cell layer.

A recently described mouse model expressing mutant APP and PS1 under the control of the murine Thy1 promoter (5XFAD mice) underscores the potential influence of intraneuronal Aβ accumulation on the loss of neurons. Analysis of cresyl violet stained sections in 9-month-old mice revealed a reduced number of cortical layer 5 neurons, a region with robust intracellular Aβ immunoreactivity. The same holds true for the subiculum where neurons where pale or entirely missing [28]. In a very recent report, cortical and hippocampal neuron numbers were analysed by design-based unbiased stereological methods in 12-month-old female mice, verifying the discrete layer 5 neuron loss. No reductions in neuron numbers and no intraneuronal Aβ immunoreactivity were detected in the CA1 layer of the hippocampus adding further evidence to the assumption that intraneuronal Aβ accumulation is closely associated with neuron loss [37]. These mice also show synaptic alterations demonstrated by a decline in synaptophysin levels already at 4 months of age as well as significantly reduced syntaxin and PSD-95 levels at the age of 9 months [28].

Besides full-length Aβ peptides ending at amino acid 40 or 42, N-terminally truncated peptides have recently gained in importance. One of the most abundant truncated peptides in AD brain is $A\beta_{pE3-42}$ carrying a pyroglutamate (pE) at position 3 [38]. It has been demonstrated that this peptide is characterized by a higher aggregation propensity [39], stability [40], and increased toxicity compared to full-length Aβ [41]. Recently *in vivo* toxicity of this peptide has been demonstrated in a mouse model expressing $A\beta_{pE3-42}$ in neurons under the control of the murine Thy1 promoter. Glutamate (E) at position three of Aβ has been mutated into glutamine (Q), as it is well established that glutamine becomes much faster converted into pyroglutamate. These mice showed a severe neurological phenotype with premature death and abundant loss of cerebellar Purkinje cells [42].

Very recently, a new transgenic mouse model expressing human APP with the $APP_{E693\Delta}$ mutation has been published [14]. This mutation has been initially described in a Japanese pedigree showing Alzheimer's-type dementia and is characterized by decreased total Aβ secretion but increased resistance to proteolytic degradation and enhanced oligomerization [43]. The resulting transgenic mice displayed intraneuronal accumulation of Ab oligomers staring at the age of 8 months, however, no extracellular Aβ plaque formation could be detected even at the age of 24 months. In addition, micro-and astroglial accumulation was observed,

as well as a significant decrease in the number of NeuN-positive cells in the hippocampal CA3 region at 24 months of age compared to age-matched nontransgenic littermates and transgenic mice expressing wild-type APP. Furthermore, an age-dependent decrease in synaptophysin levels was shown by means of immunohistochemistry starting at the age of 8 months, which coincides with impairments in synaptic plasticity as shown by *in vivo* electrophysiology [14] (see Table 1).

3. APP and Tau Transgenic Mouse Models

Recently a triple transgenic mouse model has been developed expressing both mutant APP (Swedish) and Tau (P301L) on a mutant PS1 knockin background (3xTg-AD mice) [20]. Intracellular Aβ is apparent between 3 and 4 months in these mice and precedes the deposition of extracellular Aβ peptides starting around the age of 6 months. At this time point synaptic plasticity was already strongly compromised in these mice, as shown by impaired long-term potentiation [20]. Behavioral analyses have suggested that intracellular Aβ accumulation is functionally linked to cognitive impairment in these mice, as they develop deficits in long-term retention at the age of 4 months, a time point prior to plaque deposition where only intracellular Aβ is present [44]. Morphological alterations of hippocampal synapses have been characterized in 13-month-old 3xTg-AD mice and age-matched PS1KI control mice. The numeric density of synapses, the average synaptic contact area as well as the synaptic surface density were not altered, however, 3xTg-AD mice showed a significant reduction in the fraction of perforated synapses, which is believed to represent a reliable indirect index of synaptic plasticity [45].

A double transgenic mouse line based on Tg2576 mice crossed with VLW mice (Tau G272V, P310L, R406W) showed increased amyloid deposition at the age of 16 months compared to APP single transgenic mice. In addition, APP/Tau mice revealed a significantly reduced neuron number in the entorhinal cortex at 9 months of age compared to APP single transgenic, Tau single transgenic, or wild-type mice, which were extended to the CA1 layer at the age of 16 months. It was further reported that cell death in these APP/Tau mice preceded overt amyloid plaque formation and NFT formation and did not correlate with amyloid burden in any of the regions examined [19].

Another new transgenic mouse line expressing mutant APP, Presenilin-2 (PS2), and Tau (TauPs2APP) has been recently described. It has been demonstrated that Aβ in these triple transgenic mice impacts on Tau pathology by increasing the phosphorylation of Tau at serine 422. However, despite of increased levels of phosphorylated Tau, no differences in neuron numbers were detected in hippocampal subregions comparing triple transgenic and wild-type mice. Quantitative receptor autoradiography revealed significantly reduced mGluR2 levels in aged triple transgenic mice, which were however not different from the PS2APP double transgenic control line, arguing against a prominent role of increased Tau phosphorylation [46].

4. Conclusion

In summary, there is no doubt that transgenic mice have been proven to be valuable model systems in modern AD research. There is accumulating evidence that significant neuron loss in APP/Aβ-related transgenic mice is linked to intraneuronal Aβ accumulation, as this pathological alteration precedes neurodegeneration in almost all the models where neuronal loss has been convincingly reported. If this is also true for the human situation is currently less clear, as intraneuronal Aβ seems to be a transient phenomenon which might not be adequately detected in end-stage AD patients. Although it has been shown that reductions in Tau levels prevented behavioral deficits in transgenic mice expressing human amyloid precursor protein and also protected both transgenic and nontransgenic mice against excitotoxicity [47], overexpression of mutant Tau in APP or APP/PS transgenic mice does not result in dramatic effects on neurodegeneration. One possibility might be that murine neurons could be devoid of the downstream pathways necessary for Aβ-induced toxicity leading to tau aggregation in NFTs in human AD brain.

Acknowledgment

Financial support of the Alzheimer Forschung Initiative e.V. (AFI) is gratefully acknowledged.

References

[1] J. Hardy and D. Allsop, "Amyloid deposition as the central event in the aetiology of Alzheimer's disease," *Trends in Pharmacological Sciences*, vol. 12, no. 10, pp. 383–388, 1991.

[2] H. Braak and E. Braak, "Neuropathological stageing of Alzheimer-related changes," *Acta Neuropathologica*, vol. 82, no. 4, pp. 239–259, 1991.

[3] G. K. Gouras, J. Tsai, J. Naslund et al., "Intraneuronal Aβ42 accumulation in human brain," *American Journal of Pathology*, vol. 156, no. 1, pp. 15–20, 2000.

[4] O. Wirths, G. Multhaup, and T. A. Bayer, "A modified β-amyloid hypothesis: intraneuronal accumulation of the β-amyloid peptide–the first step of a fatal cascade," *Journal of Neurochemistry*, vol. 91, no. 3, pp. 513–520, 2004.

[5] C. Duyckaerts, M.-C. Potier, and B. Delatour, "Alzheimer disease models and human neuropathology: similarities and differences," *Acta Neuropathologica*, vol. 115, no. 1, pp. 5–38, 2008.

[6] D. Games, M. Buttini, D. Kobayashi, D. Schenk, and P. Seubert, "Mice as models: transgenic approaches and Alzheimer's disease," *Journal of Alzheimer's Disease*, vol. 9, supplement 3, pp. 133–149, 2006.

[7] D. Games, D. Adams, R. Alessandrini et al., "Alzheimer-type neuropathology in transgenic mice overexpressing V717F β-amyloid precursor protein," *Nature*, vol. 373, no. 6514, pp. 523–527, 1995.

[8] K. K. Hsiao, P. Chapman, S. Nilsen et al., "Correlative memory deficits, Aβ elevation, and amyloid plaques in transgenic mice," *Science*, vol. 274, no. 5284, pp. 99–102, 1996.

[9] D. Moechars, I. Dewachter, K. Lorent et al., "Early phenotypic changes in transgenic mice that overexpress different mutants of amyloid precursor protein in brain," *The Journal of Biological Chemistry*, vol. 274, no. 10, pp. 6483–6492, 1999.

[10] M. A. Chishti, D.-S. Yang, C. Janus et al., "Early-onset amyloid deposition and cognitive deficits in transgenic mice expressing a double mutant form of amyloid precursor protein 695," *The Journal of Biological Chemistry*, vol. 276, no. 24, pp. 21562–21570, 2001.

[11] C. Sturchler-Pierrat, D. Abramowski, M. Duke et al., "Two amyloid precursor protein transgenic mouse models with Alzheimer disease-like pathology," *Proceedings of the National Academy of Sciences of the United States of America*, vol. 94, no. 24, pp. 13287–13292, 1997.

[12] A. Lord, H. Kalimo, C. Eckman, X.-Q. Zhang, L. Lannfelt, and L. N. G. Nilsson, "The Arctic Alzheimer mutation facilitates early intraneuronal Aβ aggregation and senile plaque formation in transgenic mice," *Neurobiology of Aging*, vol. 27, no. 1, pp. 67–77, 2006.

[13] B. Van Broeck, G. Vanhoutte, D. Pirici et al., "Intraneuronal amyloid β and reduced brain volume in a novel APP T714I mouse model for Alzheimer's disease," *Neurobiology of Aging*, vol. 29, no. 2, pp. 241–252, 2008.

[14] T. Tomiyama, S. Matsuyama, H. Iso, et al., "A mouse model of amyloid β oligomers: their contribution to synaptic alteration, abnormal Tau phosphorylation, glial activation, and neuronal loss in vivo," *Journal of Neuroscience*, vol. 30, no. 14, pp. 4845–4856, 2010.

[15] D. R. Borchelt, T. Ratovitski, J. van Lare et al., "Accelerated amyloid deposition in the brains of transgenic mice coexpressing mutant presenilin 1 and amyloid precursor proteins," *Neuron*, vol. 19, no. 4, pp. 939–945, 1997.

[16] V. Blanchard, S. Moussaoui, C. Czech et al., "Time sequence of maturation of dystrophic neurites associated with Aβ deposits in APP/PS1 transgenic mice," *Experimental Neurology*, vol. 184, no. 1, pp. 247–263, 2003.

[17] J. G. Richards, G. A. Higgins, A.-M. Ouagazzal et al., "PS2APP transgenic mice, coexpressing hPS2mut and hAPPswe, show age-related cognitive deficits associated with discrete brain amyloid deposition and inflammation," *Journal of Neuroscience*, vol. 23, no. 26, pp. 8989–9003, 2003.

[18] C. Casas, N. Sergeant, J.-M. Itier et al., "Massive CA1/2 neuronal loss with intraneuronal and N-terminal truncated Aβ42 accumulation in a novel Alzheimer transgenic model," *American Journal of Pathology*, vol. 165, no. 4, pp. 1289–1300, 2004.

[19] E. M. Ribé, M. Pérez, B. Puig et al., "Accelerated amyloid deposition, neurofibrillary degeneration and neuronal loss in double mutant APP/tau transgenic mice," *Neurobiology of Disease*, vol. 20, no. 3, pp. 814–822, 2005.

[20] S. Oddo, A. Caccamo, J. D. Shepherd et al., "Triple-transgenic model of Alzheimer's disease with plaques and tangles: intracellular Aβ and synaptic dysfunction," *Neuron*, vol. 39, no. 3, pp. 409–421, 2003.

[21] F. Grueninger, B. Bohrmann, C. Czech et al., "Phosphorylation of Tau at S422 is enhanced by Aβ in TauPS2APP triple transgenic mice," *Neurobiology of Disease*, vol. 37, no. 2, pp. 294–306, 2009.

[22] M. C. Irizarry, M. McNamara, K. Fedorchak, K. Hsiao, and B. T. Hyman, "APPSw transgenic mice develop age-related Aβ deposits and neuropil abnormalities, but no neuronal loss in CA1," *Journal of Neuropathology and Experimental Neurology*, vol. 56, no. 9, pp. 965–973, 1997.

[23] M. C. Irizarry, F. Soriano, M. McNamara et al., "Aβ deposition is associated with neuropil changes, but not with overt neuronal loss in the human amyloid precursor protein V717F (PDAPP) transgenic mouse," *Journal of Neuroscience*, vol. 17, no. 18, pp. 7053–7059, 1997.

[24] F. M. LaFerla, B. T. Tinkle, C. J. Bieberich, C. C. Haudenschild, and G. Jay, "The Alzheimer's Aβ peptide induces neurodegeneration and apoptotic cell death in transgenic mice," *Nature Genetics*, vol. 9, no. 1, pp. 21–30, 1995.

[25] M. E. Calhoun, K.-H. Wiederhold, D. Abramowski et al., "Neuron loss in APP transgenic mice," *Nature*, vol. 395, no. 6704, pp. 755–756, 1998.

[26] B. Urbanc, L. Cruz, R. Le et al., "Neurotoxic effects of thioflavin S-positive amyloid deposits in transgenic mice and Alzheimer's disease," *Proceedings of the National Academy of Sciences of the United States of America*, vol. 99, no. 22, pp. 13990–13995, 2002.

[27] S. Boncristiano, M. E. Calhoun, V. Howard et al., "Neocortical synaptic bouton number is maintained despite robust amyloid deposition in APP23 transgenic mice," *Neurobiology of Aging*, vol. 26, no. 5, pp. 607–613, 2005.

[28] H. Oakley, S. L. Cole, S. Logan et al., "Intraneuronal β-amyloid aggregates, neurodegeneration, and neuron loss in transgenic mice with five familial Alzheimer's disease mutations: potential factors in amyloid plaque formation," *Journal of Neuroscience*, vol. 26, no. 40, pp. 10129–10140, 2006.

[29] C. Schmitz, B. P. F. Rutten, A. Pielen et al., "Hippocampal neuron loss exceeds amyloid Plaque load in a transgenic mouse model of Alzheimer's disease," *American Journal of Pathology*, vol. 164, no. 4, pp. 1495–1502, 2004.

[30] B. P. F. Rutten, N. M. Van der Kolk, S. Schafer et al., "Age-related loss of synaptophysin immunoreactive presynaptic boutons within the hippocampus of APP751SL, PS1M146L, and APP751 SL/PS1M146L transgenic mice," *American Journal of Pathology*, vol. 167, no. 1, pp. 161–173, 2005.

[31] H. Breyhan, O. Wirths, K. Duan, A. Marcello, J. Rettig, and T. A. Bayer, "APP/PS1KI bigenic mice develop early synaptic deficits and hippocampus atrophy," *Acta Neuropathologica*, vol. 117, no. 6, pp. 677–685, 2009.

[32] D. Z. Christensen, S. L. Kraus, A. Flohr, M.-C. Cotel, O. Wirths, and T. A. Bayer, "Transient intraneuronal Aβ rather than extracellular plaque pathology correlates with neuron loss in the frontal cortex of APP/PS1KI mice," *Acta Neuropathologica*, vol. 116, no. 6, pp. 647–655, 2008.

[33] D. Z. Christensen, T. A. Bayer, and O. Wirths, "Intracellular Aβ triggers neuron loss in the cholinergic system of the APP/PS1KI mouse model of Alzheimer's disease," *Neurobiology of Aging*, vol. 31, no. 7, pp. 1153–1163, 2008.

[34] H. Takahashi, I. Brasnjevic, B. P. F. Rutten, et al., "Hippocampal interneuron loss in an APP/PS1 double mutant mouse and in Alzheimer's disease," *Brain Structure and Function*, vol. 214, no. 2-3, pp. 145–160, 2010.

[35] M. C. Cotel, S. Jawhar, D. Z. Christensen, et al., "Environmental enrichment fails to rescue working memory deficits, neuron loss, and neurogenesis in APP/PS1KI mice," *Neurobiology of Aging*. In press.

[36] A. Faure, L. Verret, B. Bozon, et al., "Impaired neurogenesis, neuronal loss, and brain functional deficits in the APPxPS1-Ki mouse model of Alzheimer's disease," *Neurobiology of Aging*. In press.

[37] S. Jawhar, A. Trawicka, C. Jenneckens, et al., "Motor deficits, neuron loss and reduced anxiety coinciding with axonal degeneration and intraneuronal Aβ aggregation in the 5XFAD mouse model of Alzheimer's disease," *Neurobiology of Aging*. In press.

[38] T. C. Saido, T. Iwatsubo, D. M. A. Mann, H. Shimada, Y. Ihara, and S. Kawashima, "Dominant and differential deposition of distinct β-amyloid peptide species, AβN3(pE), in senile plaques," *Neuron*, vol. 14, no. 2, pp. 457–466, 1995.

[39] S. Schilling, T. Lauber, M. Schaupp et al., "On the seeding and oligomerization of pGlu-amyloid peptides (in vitro)," *Biochemistry*, vol. 45, no. 41, pp. 12393–12399, 2006.

[40] Y.-M. Kuo, S. Webster, M. R. Emmerling, N. De Lima, and A. E. Roher, "Irreversible dimerization/tetramerization and post-translational modifications inhibit proteolytic degradation of Aβ peptides of Alzheimer's disease," *Biochimica et Biophysica Acta*, vol. 1406, no. 3, pp. 291–298, 1998.

[41] C. Russo, E. Violani, S. Salis et al., "Pyroglutamate-modified amyloid β-peptides—AβN3(pE)—strongly affect cultured neuron and astrocyte survival," *Journal of Neurochemistry*, vol. 82, no. 6, pp. 1480–1489, 2002.

[42] O. Wirths, H. Breyhan, H. Cynis, S. Schilling, H.-U. Demuth, and T. A. Bayer, "Intraneuronal pyroglutamate-Aβ 3-42 triggers neurodegeneration and lethal neurological deficits in a transgenic mouse model," *Acta Neuropathologica*, vol. 118, no. 4, pp. 487–496, 2009.

[43] T. Tomiyama, T. Nagata, H. Shimada et al., "A new amyloid β variant favoring oligomerization in Alzheimer's-type dementia," *Annals of Neurology*, vol. 63, no. 3, pp. 377–387, 2008.

[44] L. M. Billings, S. Oddo, K. N. Green, J. L. McGaugh, and F. M. LaFerla, "Intraneuronal Aβ causes the onset of early Alzheimer's disease-related cognitive deficits in transgenic mice," *Neuron*, vol. 45, no. 5, pp. 675–688, 2005.

[45] C. Bertoni-Freddari, S. L. Sensi, B. Giorgetti et al., "Decreased presence of perforated synapses in a triple-transgenic mouse model of Alzheimer's disease," *Rejuvenation Research*, vol. 11, no. 2, pp. 309–313, 2008.

[46] F. Grueninger, B. Bohrmann, C. Czech et al., "Phosphorylation of Tau at S422 is enhanced by Aβ in TauPS2APP triple transgenic mice," *Neurobiology of Disease*, vol. 37, no. 2, pp. 294–306, 2010.

[47] E. D. Roberson, K. Scearce-Levie, J. J. Palop et al., "Reducing endogenous Tau ameliorates amyloid β-induced deficits in an Alzheimer's disease mouse model," *Science*, vol. 316, no. 5825, pp. 750–754, 2007.

SAGE-Hindawi Access to Research
International Journal of Alzheimer's Disease
Volume 2010, Article ID 604792, 56 pages
doi:10.4061/2010/604792

Research Article

Complex and Multidimensional Lipid Raft Alterations in a Murine Model of Alzheimer's Disease

Wayne Chadwick,[1] Randall Brenneman,[1,2] Bronwen Martin,[3] and Stuart Maudsley[1]

[1] *Receptor Pharmacology Unit, National Institute on Aging, National Institutes of Health, 251 Bayview Boulevard, Suite 100, Baltimore, MD 21224, USA*
[2] *Miller School of Medicine, University of Miami, Miami, FL 33124, USA*
[3] *Metabolism Unit, National Institute on Aging, National Institutes of Health, 251 Bayview Boulevard, Suite 100, Baltimore, MD 21224, USA*

Correspondence should be addressed to Stuart Maudsley, maudsleyst@mail.nih.gov

Received 17 May 2010; Accepted 27 July 2010

Academic Editor: Gemma Casadesus

Various animal models of Alzheimer's disease (AD) have been created to assist our appreciation of AD pathophysiology, as well as aid development of novel therapeutic strategies. Despite the discovery of mutated proteins that predict the development of AD, there are likely to be many other proteins also involved in this disorder. Complex physiological processes are mediated by coherent interactions of clusters of functionally related proteins. Synaptic dysfunction is one of the hallmarks of AD. Synaptic proteins are organized into multiprotein complexes in high-density membrane structures, known as lipid rafts. These microdomains enable coherent clustering of synergistic signaling proteins. We have used mass analytical techniques and multiple bioinformatic approaches to better appreciate the intricate interactions of these multifunctional proteins in the 3xTgAD murine model of AD. Our results show that there are significant alterations in numerous receptor/cell signaling proteins in cortical lipid rafts isolated from 3xTgAD mice.

1. Introduction

Alzheimer's disease (AD) is one of the most prevalent neurodegenerative disorders amongst adults of advanced age, and it is the most common form of dementia and cognitive impairment [1, 2]. The behavioral abnormalities in AD result from dysfunction and death of neurons in brain regions involved in cognition and mood, such as the hippocampus, amygdala, and cortical regions. Progressive short-term and eventual long-term memory loss and reduced cognitive capacity are associated with two primary neurodegenerative lesions, that is, extra- and intracellular β-amyloid plaques, as well as neurofibrillary tangles (NFTs) composed of the microtubule protein tau [3–5]. In addition to the effects of amyloid plaques and NFTs, the lipid trafficking molecule, apolipoprotein E4 (apoE4), has also been demonstrated to be a genetic risk factor for AD [6, 7]. The AD characteristic extracellular plaques, found in both the hippocampus and cortex of AD patients, consist of 39–42 amino acid long amyloid-β (Aβ) peptides. These extracellular peptides are generated by digestion of a transmembrane amyloid precursor protein (APP). Proteolysis of the transmembrane APP by a set of intramembrane enzymes, β- (also known as BACE-1) and γ-secretases, is thought to be responsible for toxic Aβ creation [5]. The discovery of familial mutations in the APP gene that were strongly correlated with the presentation of AD reinforced the importance of Aβ processing in this disorder. A growing body of evidence indicates that changes in lipid and cholesterol homeostasis can influence AD progression and specifically Aβ production. One of the prime sub cellular regions of amyloidogenic APP processing is thought to be cholesterol-enriched membrane microdomains, termed lipid rafts [8]. Cellular organization of protein signaling complexes, to enhance the magnitude and fidelity of transmembrane signaling receptors, is facilitated by variations in the lipid constituents of the plasma membrane. Lipid rafts represent discontinuous regions of the plasma membrane that form functional microdomains,

which constrain the association of proteins in a coherent and advantageous manner with respect to neurotransmissive signaling [9]. Disruption of the correct stoichiometry of signaling complexes within lipid rafts may underpin the etiology of many different neurodegenerative disorders [10–12]. The hypothesis that changes in the lipid composition of rafts contribute to AD pathology has gained considerable support. For example, ApoE4 has been strongly correlated with the generation of AD symptomatology. Both of the amyloidogenic processing enzymes (β- and γ-secretase), as well as APP, are all enriched in lipid raft membranes [13, 14]. Reinforcing the connection between lipid density levels and Aβ production, increasing cholesterol levels elevate the activity of both β-secretase (BACE-1) and γ-secretase [14, 15]. In addition, ganglioside lipids, which are also enriched in lipid rafts, can control the assembly of amyloid-β proteins [16, 17]. Changes in ganglioside composition, similar to those noted in human AD patients, are also observed in different transgenic mouse models of AD [18]. In addition to a role of the lipid components of lipid rafts in controlling amyloidogenesis, these raft environments may also affect NFTs as well. It has been demonstrated that Aβ can induce activation of the tyrosine kinase Fyn in neuronal cells, that is then recruited to lipid rafts which catalyzes phosphorylation of tyrosine residue 18 on tau [19, 20]. Association of Aβ plaques to lipid rafts can mediate recruitment of excess Fyn to the rafts, as well as further recruitment and phosphorylation of tau. These activities are thought to induce neurotoxicity via the effects of tau-induced changes in the actin cytoskeleton and receptor/cellular signaling pathways [21]. Therefore, the potential changes in the lipid composition of lipid rafts, caused by exposure to cytotoxic activities characteristic to AD, can induce profound changes in cellular signal transduction and thereby induce intracellular changes that lead to the development of AD. The complexity of protein complexes within the lipid raft environments raises considerable challenges to understanding the molecular mechanisms of AD pathophysiology in both the hippocampus and cortex of animals. Therefore, we have employed a shotgun proteomics approach, allied to advanced bioinformatic functional profiling, to gain a broad and detailed appreciation of the alterations in signaling proteins in lipid rafts in the triple-transgenic (3xTgAD) model of AD [22]. Our study demonstrates that cortical lipid rafts are profoundly affected in the 3xTgAD mice and that many of the neurophysiological deficits characteristic of AD (impaired synaptic strength, impaired learning and memory, and increased oxidative stress) can be strongly linked to changes in receptor and cell signaling events in the lipid rafts in these animals. Therefore, the lipid raft environments can be seen as one of the most important pathophysiological loci of this disorder.

2. Methods

2.1. Animals and Morris Water Maze Testing. Animal care and experimental procedures followed NIH guidelines and were approved by the National Institute on Aging Animal Care, and Use Committee. Experiments were performed using male 3xTgAD [22–24] and control male C57-BL6 mice that were maintained under a 12-hour light/12-hour dark cycle with continuous access to food and water. Water maze testing took place using a modified version of the methodology described previously [25]. Briefly, animals (n = 10 per group, control male C57-BL6 or male 3xTgAD, on a C57-BL6 background) received 8 days of acquisition training using a nonvisible target platform, consisting of four trials per day, with an intertrial interval of approximately 10 minutes. Each trial lasted until the animal found the platform, or for a maximum of 60 seconds; animals that failed to find the platform within 60 seconds were guided there by the experimenter. On each trial, mice were placed into the pool, facing the wall, with start locations varied pseudorandomly. Distance swam to escape the water, escape time, and swim speed were measured for either control or 3xTgAD mice using a HVS2020 automated tracking system (HVS Image, UK).

2.2. Isolation of Lipid Raft Detergent-Resistant Membranes. The mice were anesthetized with isoflurane, decapitated, and the brain was microdissected on ice. After removal of the cortex, the tissue was split into left and right hemisphere, half for mass spectrometry raft analysis and half to prepare lipid raft tissues for Western blot analysis. The hemicortices were washed twice in ice-cold phosphate buffered saline (PBS) and then transferred into a Tris-saline buffer supplemented with a cocktail of protease and phosphatase inhibitors (50 mM Tris-HCl, 150 mM NaCl, 5 mM EDTA, and Roche Complete-Mini (Roche Diagnostics Inc.) protease and phosphatase inhibitor cocktail, pH 7.4). Crude tissue disruption was then rapidly achieved (at 4°C) using a sonic dismembrator (Fisher Scientific Model 100) followed by a brief centrifugation (4°C, 1000 × g, 10 minutes) to pellet cell nuclei and unbroken cells. The resultant supernatant was removed and Triton X-100 (Sigma Aldrich, USA) was added to the Tris-saline buffer to a final concentration of 1%. The supernatant membranes were then incubated at 4°C for 60 minutes in the Triton X-100 Tris-saline solution. After incubation, the supernatant solution was then added to a discontinuous gradient of 30% and 60% OptiPrep (Iodixanol, Sigma Aldrich, and U.S.A.) before centrifugation at 200 000 × g for 16 hours at 4°C. After centrifugation, a detergent-resistant lipid band was evident in the vertical solution column. Multiple fractions of 300 μl volumes were then removed from the vertical centrifugation column. Proteins were then extracted from these fractions using a proprietary ProteoExtract (EMD Biosciences) kit, according to the manufacturer's instructions. Isolated protein pellets were then prepared for mass spectrometric analysis.

2.3. Mass Spectrometric Protein Analysis. Protein pellets were dissolved into an ammonium bicarbonate buffer (100 mM, pH 8.5) and then reduced with dithiothreitol (500 mM: Pierce Biotechnology), alkylated with iodoacetamide (800 mM: Sigma Aldrich) and then digested with modified trypsin (5–10 μg) (Promega) at 37°C for 17 hours. Proteolysis was terminated by the addition of glacial acetic acid. Tryptic peptides were then loaded onto a desalting

column ($360 \times 200\,\mu$m fused silica packed with 15 cm of C18 beads (YMC ODS-AQ, Waters)), washed with 0.1% acetic acid and eluted into sample tubes with 80% acetonitrile in 0.1% acetic acid. Sample volume was reduced to usable volumes under vacuum on a Savant SpeedVac. Samples were then transferred onto a PicoFrit (75×100 mm) column packed with ProteoPep II C_{18}, 300 Å, 5 μm particles (New Objective) connected to a nanoliquid chromatography system (Dionex, Sunnyvale, CA) online with an LTQ ion trap mass spectrometer (Thermo Finnigan, San Jose, CA). The peptides were eluted using a linear gradient of 0–65% acetonitrile over 90 minutes at a flow rate of 250 nl/min directly into the mass spectrometer, which was operated to generate collision-induced dissociation spectra (data-dependent MS/MS mode). The resultant tandem mass spectrometry data were processed using the BioWorks suite, and multiple collected spectra were used to interrogate the NCBI nonredundant mouse and Swiss-Prot protein sequence databases, using the computer algorithm SEQUEST to generate accurate protein identities. Protein genpept accession identities were then converted to Official Gene Symbol terms using NIAID-DAVID v. 6.7 (http://david.abcc.ncifcrf.gov/). The statistical analysis and validation of the search results were performed using MASCOT (Matrix Science). For protein identification, a maximum of three missed tryptic cleavages was used, including fixed modification of carbamidomethylation and variable modifications of oxidized methionine and N-terminal glutamine conversion to pyroglutamic acid in the search. Only proteins with at least two validated peptides and a total score 25 and a confidence of identification of at least 95% were considered valid for reporting. Where required, additional spectral counting was performed to determine simplistic relative quantitation in conjunction with the reported number of identified unambiguous peptides per protein. Three lipid raft fraction samples (fractions 2, 3, and 4) from each three control (nontransgenic gender/age matched C57-BL6) or Alzheimer's disease (3xTgAD) were pooled and then run in an individual random order. Proteins identified based on two unambiguous peptides that were present in at least two out of the three individual animals were employed for further expression pattern analysis.

2.4. Lipid Raft Band Quantification. Digitized images of centrifugal vertical fluid columns were obtained using a Canon Digital camera and were converted from Joint Photographic Experts Group (JPG) files to a TIFF (Tagged Image File Format) form using L-Process v. 2.2 (image handling software: Fuji-Film). Image densitometry was then performed using Fuji-Film Image Gauge v. 4.2. Lipid raft band intensity was represented as a relative absorbance unit (AU) value with background (B) subtraction per square pixel (px^2) (AU-B/px^2).

2.5. Western Blotting Procedures. For the examination of specific proteins in cortical cell samples (both lipid raft and nonlipid raft), aliquots were removed from centrifugal fractions from Section 2.2 and their protein concentration was determined with a standard BCA protocol. Aliquot samples for western blotting analysis were then mixed with an equal volume of Laemmli sample buffer [26]. Samples were resolved using one-dimensional gel electrophoresis (SDS-PAGE), followed by electrotransfer to polyvinylenedifluoride (PVDF: PerkinElmer, Waltham, MA). PVDF membranes were blocked for one hour at room temperature in 4% nonfat milk (Santa Cruz; Santa Cruz, CA) before application of specific primary antisera in the same nonfat milk. The presence of primary antibody reactivity with the PVDF membrane was detected by the application of a 1 : 5000 dilution of a species-specific alkaline phosphatase-conjugated secondary antibody (Sigma, St. Louis, MO). PVDF-bound immune complexes of secondary and primary antibodies were subsequently detected using enzyme-linked chemifluorescence (ECF: GE Healthcare; Pittsburgh, PA). Chemifluorescent signals from the membranes were captured and quantified using a Typhoon 9410 phosphorimager (GE Healthcare, Pittsburgh, PA). Specific primary antisera used were obtained from the following sources: flotillin-1, proline-rich tyrosine kinase 2 (Pyk2), focal adhesion kinase (FAK), G protein-coupled receptor kinase interactor-1 (GIT-1), and paxilin antibodies were obtained from BD Bioscience, San Jose, CA; Janus kinase 2 (Jak2), v-Crk avian sarcoma virus CT10 oncogene homolog (Crk), and insulin receptor substrate-1 (IRS1) antibodies were obtained from Santa Cruz Biotechnology Corporation, CA; caspase-7, FKBP12-rapamycin complex-associated protein 1/mammalian target of rapamycin (FRAP1/mTOR), and Fyn and IGF-1 receptor beta antibodies were obtained from Cell Signaling Technology, Danvers, MA); G protein-regulated inducer of neurite outgrowth 2 (Grin2) antibody was obtained from Sigma Aldrich. For the identification of nonspecific total proteins in each sample the highly sensitive protein dye, SYPRO Ruby (Invitrogen Corporation) was employed. Fixed SDS-PAGE gels were immersed in SYPRO-Ruby for 1 hour and then washed in deionized water before scanning using a Typhoon 9410 phosphorimager (GE Healthcare, Pittsburgh, PA).

2.6. Bioinformatic Analyses. Protein identities were converted to standard gene symbol nomenclature for simplicity of usage with the batch conversion tool of NIH Bioinformatics Resources DAVID v. 6.7 (http://david.abcc.ncifcrf.gov/). Primary protein sets (containing consistently identified lipid raft extract proteins) were organized into functional signaling pathway groups and then analyzed for their differential significance of population of these canonical signaling pathways. To compare the relative degree of association of specific signaling pathways with the control or 3xTgAD protein sets, the difference between the signaling pathways "hybrid scores" was calculated (control subtracted from 3xTgAD). The magnitude of the "hybrid score" is indicative of strength and significance of association of the input protein set with the specific signaling pathway. Signaling pathway hybrid scores were generated using a process that takes into account the significant population and potential activation of that pathway by multiplying the pathway enrichment *ratio* (percentage of proteins in a designated pathway that were also found in the experimental dataset)

and the probability (P) that the respective pathway is significantly associated with the experimental dataset. However, to create a simple numerical value, the hybrid pathway score is calculated by multiplication of the *ratio* with the negative $\log -10$ of the P value. Each signaling pathway considered was required to contain at least two unique proteins from either control or 3xTgAD datasets and possess a P value of $\leq .05$. Unbiased network analysis was also performed on subsets of the primary protein sets that were specifically limited to transmembrane receptor proteins. The networks generated create predictions of the most likely functional interactions between proteins in a complex dataset [27]. Networks are created to indicate the most significant series of molecular interactions. The networks with the highest predictive "*scores*" possess the highest number of statistically significant "*focus molecules*": "*focus molecules*" are proteins that are present in the most statistically-likely predicted functional network and are present in the input experimental dataset. The network "*score*" is a numerical value used to rank networks according to their degree of relevance to the input dataset. The "*score*" accounts for the number of experimental focus molecules (proteins) in the network and its size, as well as the total number of proteins in the Ingenuity Knowledge Base that could potentially be included in the specific networks. The network "*score*" is based on the hypergeometric distribution and is calculated with the right-tailed Fisher's Exact Test. Specific scientific textual associations between filtered protein sets (transmembrane receptor proteins IPA analysis) and Alzheimer's disease processes were created using latent semantic indexing (LSI) algorithms using GeneIndexer (Computable Genomix, Incorporated: https://www.computablegenomix.com/geneindexer). GeneIndexer correlates the strength of association between specific factors (proteins) in a dataset with a user-defined interrogation term. GeneIndexer employs a 2010 murine or human database of over 1×10^6 scientific abstracts to perform text-protein correlation analysis. LSI facilitates the specific textual interrogation of an input dataset with a specific term, that is, Alzheimer's disease, to ascertain which of the input dataset proteins are explicitly associated with the interrogation term. Using LSI algorithms, not only is the direct interrogation term used to analyze the input dataset but also closely correlated additional terms, implicitly associated with the user-defined interrogation term, are also employed in the search patterns. A latent semantic indexing correlation score indicates the strength of association of the interrogation term and the specific proteins in the dataset. A highly relevant protein-term correlation yields a large number of explicitly/implicitly associated proteins with high LSI correlation scores. Therefore, a strong correlation between the proteins in a dataset and a specific user-defined interrogation term yields a large number of correlated proteins with high LSI correlation scores.

3. Statistical Analysis

Statistical analysis on multiple samples was performed using a standard nonparametric two-tailed Student's t-test using 95% confidence limits. Analyses were computed using built-in software in GraphPad Prism v. 3.0a (GraphPad Software Inc., La Jolla, CA). Results are expressed as means ± SE. $P \leq .05$ was considered statistically significant. For statistical analysis using Ingenuity Pathway Analysis v. 8.5 of signaling pathways and interaction network analysis, Fisher's Exact test was employed with a $P \leq .05$ cutoff. Network interaction scores were generated using a right-tailed Fisher's Exact Test.

4. Results

4.1. 3xTgAD Mice Demonstrate Impaired Learning and Memory Ability in the Morris Water Maze. Using the nonvisible Morris water maze trial and 16-month-old male control (C57-BL6) and 3xTgAD animals ($n = 10$ for both) we noted that the 3xTgAD mice demonstrated a significant reduction in their ability to find the location of the hidden platform (Figure 1). The 3xTgAD mice demonstrated significantly longer escape latencies and distances traveled compared to the control mice, while not showing any significant difference in calculated swim speed. Retention testing (three trials one week after the initial training) of these animals (control and 3xTgAD) also demonstrated a reduced cognitive capacity of the 3xTgAD mice compared to control (data not shown).

4.2. 3xTgAD Mice Demonstrate a Significant Alteration in Lipid Raft Density and Protein Marker Composition. Employment of the lipid raft isolation process described in the Methods section resulted in the clear visible isolation of a detergent-resistant lipid layer comprising centrifugal fractions 2–4 (Figure 1(a)). The lipid raft marker protein, flotillin-1, was demonstrated to be specifically enriched in these centrifugal fractions (2–4) (Figure 2(a)). The visual lipid density (absorbance units-background/square pixel) of the raft layers was quantified using Fuji-Film Image Gauge. Compared to control, both 8-month-old (Figure 2(c)) and 16-month-old (Figure 2(d)) 3xTgAD-derived centrifugal raft layers demonstrated a significant (8 months old $P = .027$, $n = 3$; 16 months old $P = .031$, $n = 3$) increase in buoyant detergent-insoluble density. This 3xTgAD increase in raft size, compared to control animals, demonstrated a strong association with a significant increase in expression of flotillin-1 in the raft fractions of 3xTgAD mice, especially in centrifugal fraction 2 (Figure 2(e), $P = .017$, $n = 3$). Equal levels of total protein (measured using BCA and also SYPRO gel staining) were employed for each Western blot of the raft extracts. Quantification of fraction 2 was chosen, as this reliably indicated the greatest enrichment of this lipid raft marker. Similar quantitative alterations in expression of flotillin-1 between control and 3xTgAD mice were also seen in the additional lipid raft centrifugal fractions, that is, 3 and 4. Qualitatively similar results, with respect to 3xTgAD mouse lipid raft density and flotillin-1 expression were noted in parallel experiments carried out with age-matched female mice. In addition we also noted a similar qualitative lipid raft expression of flotillin-1 trend in male human cortex tissue (data not shown). These latter data and their significance

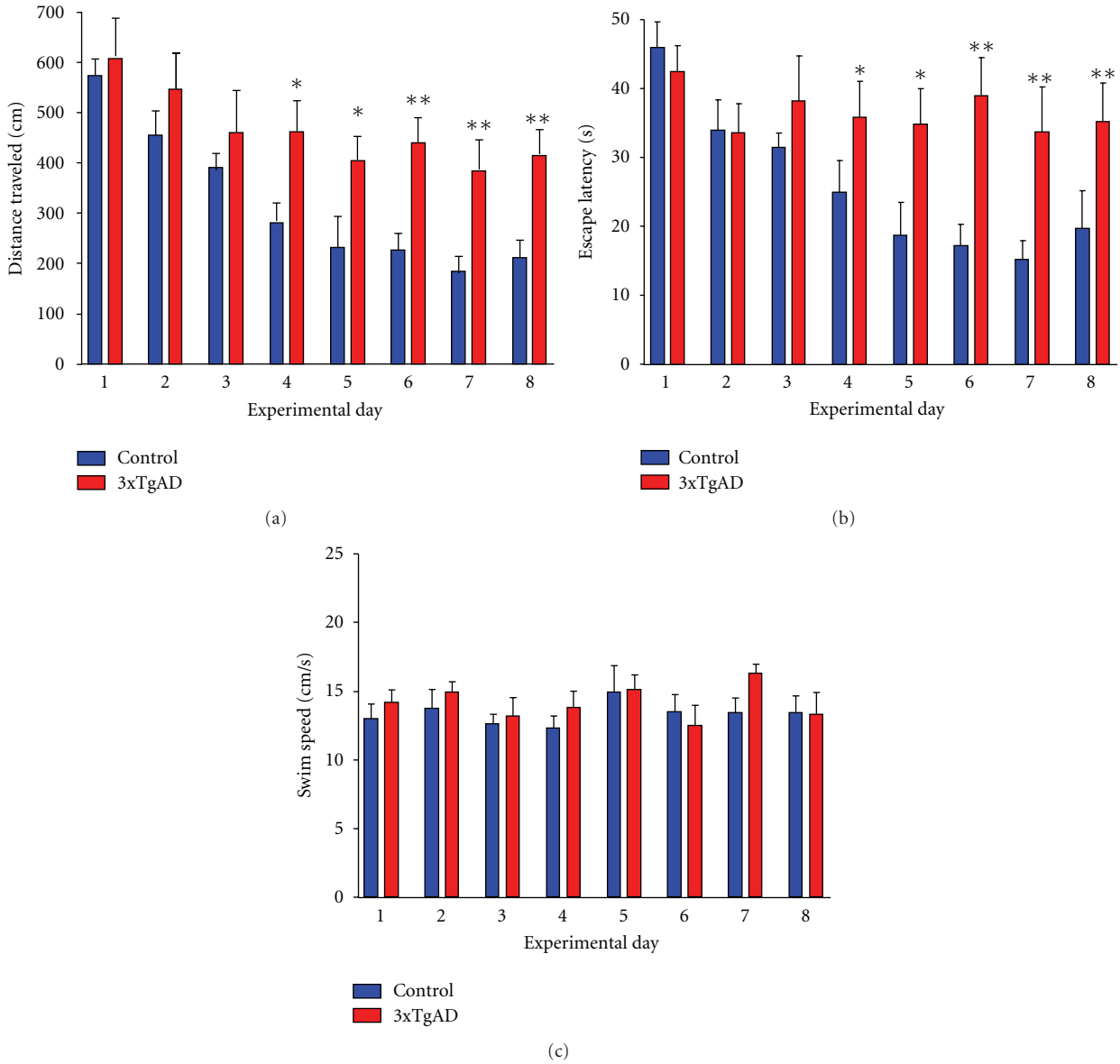

Figure 1: Morris Water Maze testing of control and 3xTgAD mice. (a) Distance travelled (cm) in the nonvisible probe target results for control ($n = 10$, blue bars) and 3xTgAD mice ($n = 10$, red bars) for 8 days of training. (b) Water maze escape latency (s) for days 1 to 8 of training in the nonvisible probe target. (c) Swim speed (cm/s) assessment of control and 3xTgAD animals during days 1–8 of training. $^{*}P < .05$; $^{**}P < .01$.

to our current data will be further addressed in subsequent manuscripts.

4.3. Differential Protein Expression in Lipid Rafts Isolated from 3xTgAD Mice Compared to Control Mice. Using an un-biased proteomic analysis of replicate lipid raft extracts, we were able to identify (from at least two individual nonambiguous peptides) multiple proteins in both control and 3xTgAD cortical extracts (control, Appendix A; 3xTgAD, Appendix B). When comparing the relative differences in lipid raft protein expression, only a small minority (17%: Figure 3(a)) of identified proteins were substantively identified in both control and 3xTgAD raft samples; however many of these common proteins identified were differentially detected (see Supplementary Table 1 in Supplementary Material available online at doi:10.4061/2010/604792). To verify the relative differential expression of multiple proteins in the control versus 3xTgAD lipid raft extracts, we also performed multiple Western blot analyses of raft centrifugal fraction-2 (F-2) samples. With loading of total equal protein quantities (50 μg: assessed in an unbiased manner with SYPRO-Ruby: Figure 3(b)) of either control or 3xTgAD F-2 samples, we assessed the relative differential expression of multiple proteins (Figures 3(c)–3(n)). From the Western blot analysis it was consistently demonstrated that

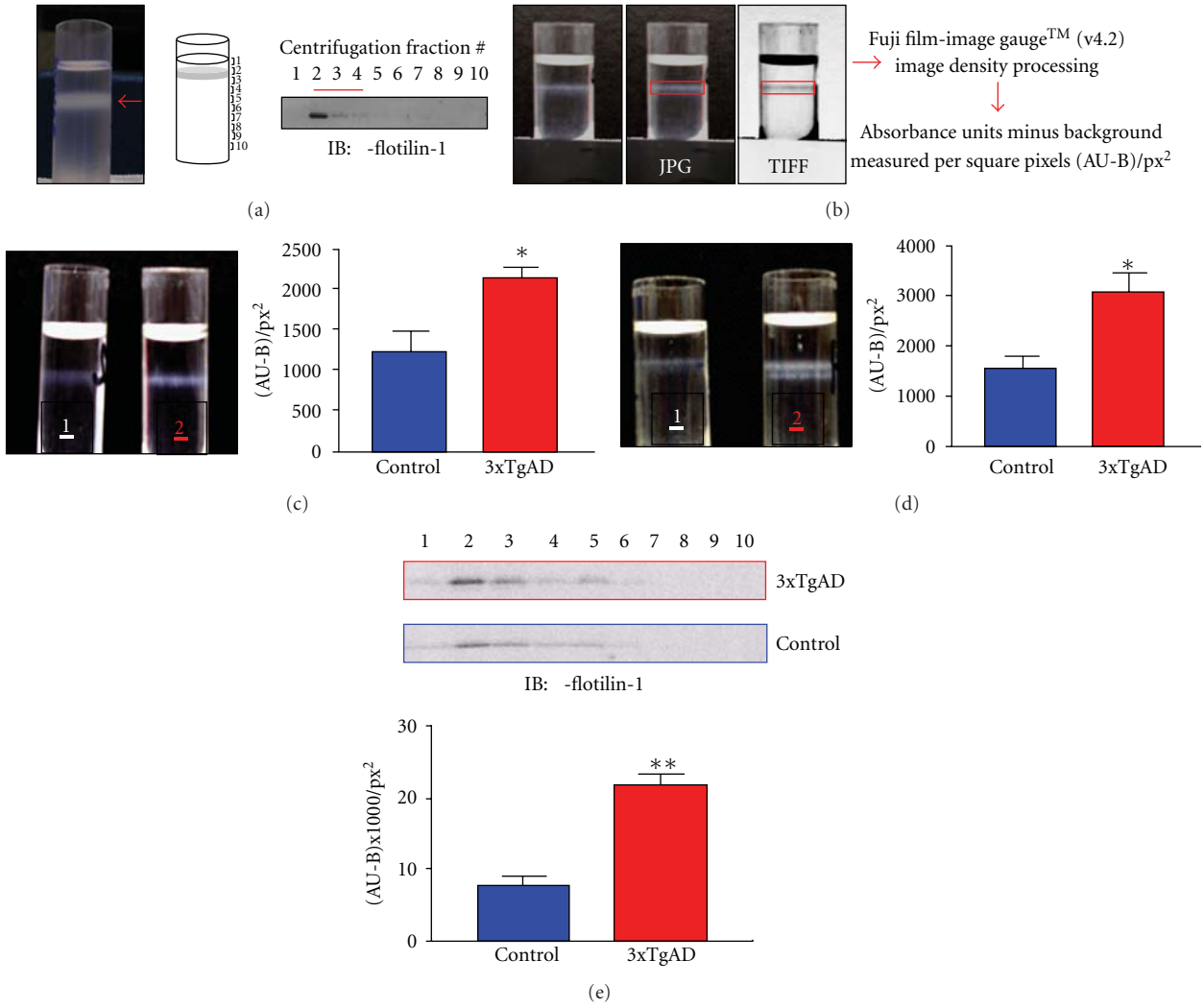

Figure 2: Quantification of detergent-resistant lipid rafts. (a) The pictorial panel depicts an image of iodixanol-separated detergent resistant membrane fractions (centered on red arrow), captured using a Nikon 3200 digital camera. The line diagram indicates the direction of collection of centrifugal fractions 1–10, and the associated Western blot for flotillin-1 demonstrates its enrichment in the raft fractions. (b) Captured Joint Photographic Expert Group (JPG) images were converted to a Tagged Image File Format (TIFF) version and imported to Image Gauge (v4.2) software and the specific area of interest (red box), that is, the detergent-resistant, flotillin-1-rich lipid raft band was quantified into absorbance units minus background absorbance per square pixel area ((AU-B)/px^2) values. (c) Representative set of male 8-month-old control (1) and 3xTgAD (2) mice detergent-resistant membranes isolated from plasma membrane fractions separated using an Iodixanol gradient. The associated histogram depicts mean ± s.e. (standard error) mean detergent-resistant membrane intensity ((AU-B)/px^2) from at least three separate control and 3xTgAD mice (P = .033, nonpaired, two-tailed t-test). (d) Representative set of male 16-month-old control (1) and 3xTgAD (2) mice detergent resistant membranes isolated from plasma membrane fractions separated using an Iodixanol gradient. The associated histogram depicts mean ± s.e. (standard error) mean detergent resistant membrane intensity ((AU-B)/px^2) from at least three separate C57-BL6 and 3xTgAD mice (P = .0224, non-paired, two-tailed t-test). (e) Representative flotillin-1 Western blot for the lipid raft fraction series for 3xTgAD (red outline) or control (C57-BL6: blue outline) mice. The associated histogram depicts mean ± s.e. (standard error) mean fraction 2 flotillin expression intensity ((AU-B)/px^2) from at least three separate C57-BL6 and 3xTgAD mice (P = .015, non-paired, two-tailed t-test).

differential qualitative protein detection in control versus 3xTgAD raft samples strongly correlated with differential semiquantitative protein expression. Hence, the absence of consistent MS-based detection of Pyk2 (Figure 3(d)), Jak2 (Figure 3(f)), Fyn (Figure 3(h)), paxilin (Figure 3(i)), IRS-1 (Figure 3(j)), caspase 7 (Figure 3(k)), mTOR/FRAP1 (Figure 3(l)) and IGF-1R (Figure 3(n)) in control raft sample correlated to their significantly lower expression in control raft F-2 samples, compared to that in 3xTgAD samples. Conversely, the absence of consistent MS-based detection of FAK (Figure 3(c)), GIT-1 (Figure 3(e)), Crk (Figure 3(g)), and Grin2 (Figure 3(m)), correlated to their significantly lower expression in 3xTgAD raft F-2 samples, compared to that in control samples.

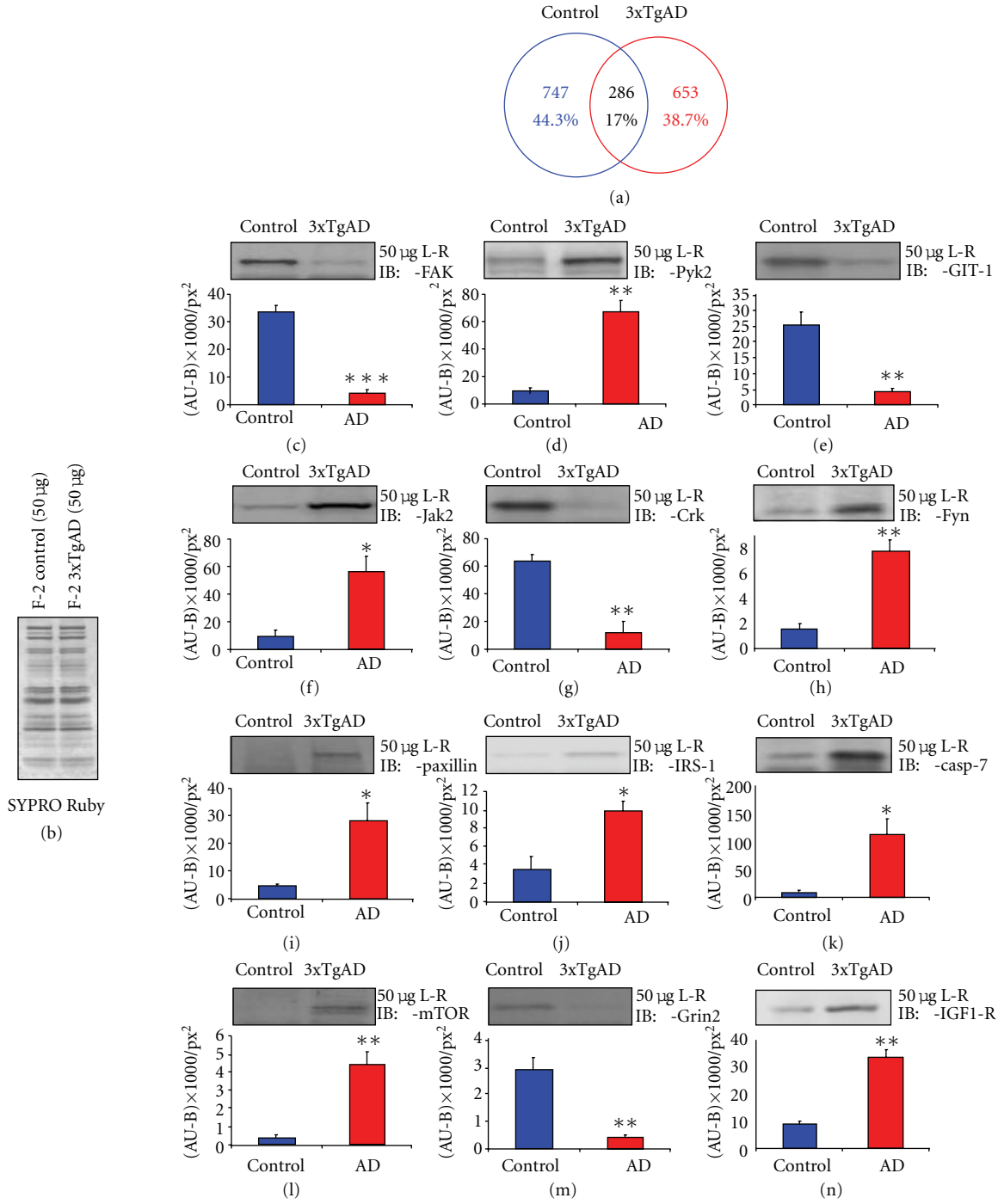

Figure 3: Differential protein expression in control versus 3xTgAD lipid raft extracts. (a) Proportionately drawn Venn diagram analysis of reliably identified proteins from control lipid rafts (blue line) and 3xTgAD rafts (red line). (b) Total protein loading control for centrifugal fraction 2. A total of 50 mg of fraction 2 protein was loaded and stained with SYPRO Ruby and scanned using a phosphorimager. (c)–(n). Representative western blots from multiple expression analysis experiments for differential presentation of proteins in fraction 2 extracts from control (blue) or 3xTgAD mice (red). Associated with each panel (c)–(n) the associated histograms represent the mean ± s.e. mean of protein expression intensity (measured in $((\text{AU-B})/\text{px}_2)$) from at least three separate experiments. $^*P < .05$; $^{**}P < .01$; $^{***}P < .001$. Protein abbreviations are as follows. FAK: focal adhesion kinase; Pyk2: proline-rich tyrosine kinase 2; GIT-1: GRK interactor-1; Jak2: Janus kinase 2; Crk: v-Crk avian sarcoma virus CT10 oncogene homolog; Fyn: Fyn tyrosine kinase; IRS-1: insulin receptor substrate-1; casp 7: caspase 7; mTOR: mammalian target of rapamycin; Grin2: G protein-regulated inducer of neurite outgrowth 2; IGF-1R: insulin-like growth factor-1 receptor.

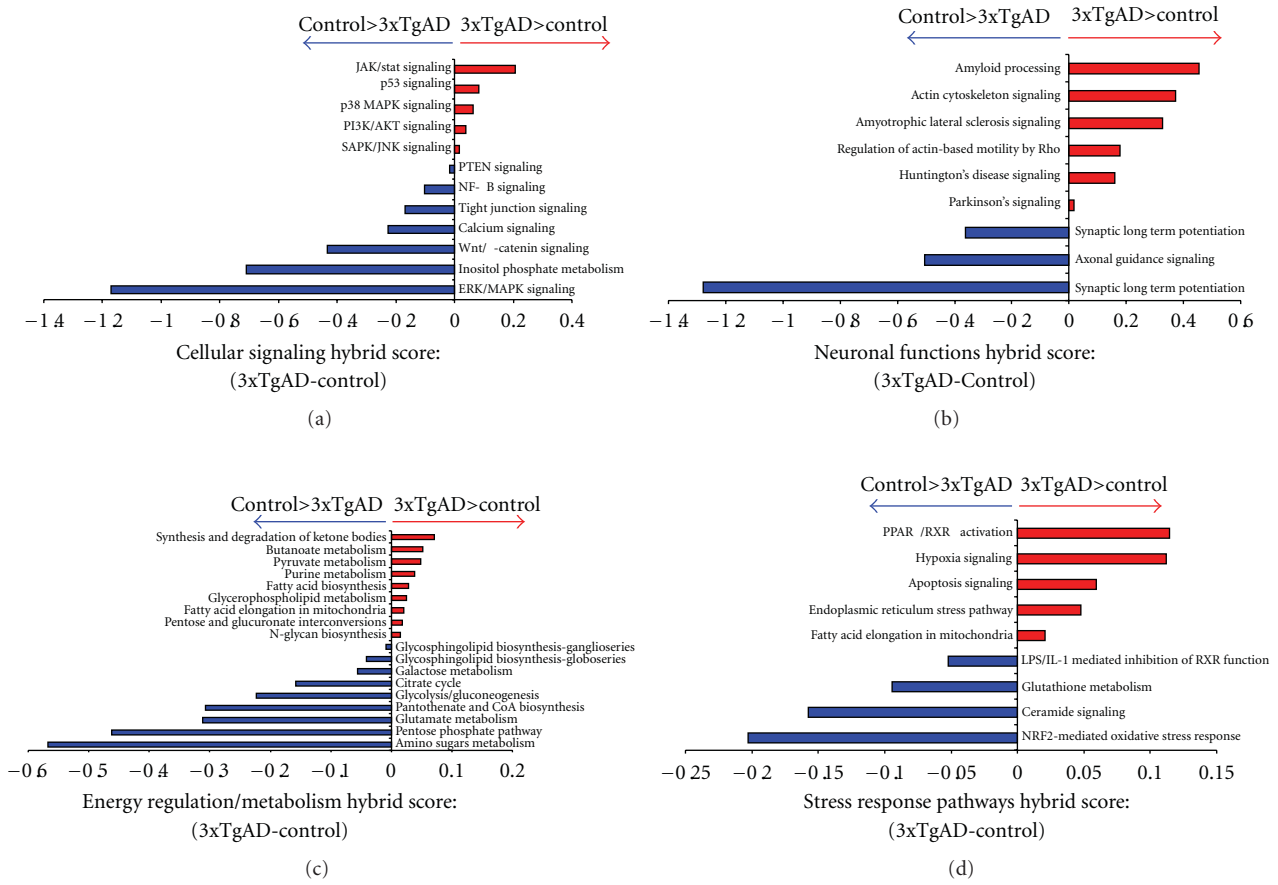

FIGURE 4: Functional pathway informatic clustering of control and 3xTgAD lipid raft proteins. (a) Subtractive representation of hybrid score generation after clustering of lipid raft proteins from control and 3xTgAD animal rafts into cellular signaling pathways. The hybrid scores were generated by multiplication of the protein enrichment ratio of the specific pathway with the negative $\log_{10}$ ($-\log_{10}$) of the probability of that enrichment (see Section 2). The data is presented as a numerical value of the control pathway hybrid score subtracted from the 3xTgAD pathway hybrid score. Pathways in which the score in 3xTgAD was greater than the control are denoted in red; pathways in which the control hybrid score is greater than the 3xTgAD hybrid score are denoted in blue. A similar depiction format is employed for differential analysis of control versus 3xTgAD Neuronal Function pathways (b), Energy Regulation/Metabolism pathways (c), and Stress Response pathways (d).

4.4. Functional Signaling Cluster Analysis of Control versus 3xTgAD Lipid Raft Proteomes. As our MS-based multidimensional protein identification process identified several hundred proteins from each control or 3xTgAD lipid raft sample, we employed a bioinformatic analysis process to assess the relative functionalities of both the control versus 3xTgAD raft protein lists. As the majority of cellular signaling processes are mediated and regulated by multiple groups of proteins interacting with each other, we clustered, in a statistically significant manner, proteins in control or 3xTgAD animal raft samples into functional signaling groups. To assess the relative changes in regulation of classical signaling pathways, we applied a subtractive approach for the pathway "*hybrid*" scores (indicative of the "activity" of the specific signaling pathway: calculated by significant expression enrichment ratio of proteins in that pathway multiplied by the negative $\log_{10}$ ($-\log_{10}$) of the probability of the pathway enrichment). For each specific common signaling pathway, our mathematical approach subtracted control pathway "hybrid" scores from the pathway "*hybrid*" scores generated from the 3xTgAD protein set. Hence, a positive result of this subtraction indicates a greater activity of this functional pathway in 3xTgAD animals, and a negative score indicates a greater activity of this functional pathway in the control animals. Analysis of pathways involved in cellular signaling (Figure 4(a): proteins and scores in associated Appendix C) demonstrated that pathways commonly associated with cell stress responses were highly activated in 3xTgAD rafts, for example "*p53 signaling*", "*p38 mitogen-activated protein kinase (MAPK) signaling*", and "*stress-activated protein kinase (SAPK)/JNK pathways*". In a stark contrast, prosurvival synaptic connectivity and neurotransmissive pathways were more profoundly activated in the control mice, for example, "*tight junction signaling*", "*calcium signaling*", "*PTEN signaling*", and "*Wnt/β-catenin signaling*". To investigate the specific neuronal functional effects of these disparate signaling activities, we next studied the significant clustering of raft proteins into neuron-functional pathways (Figure 4(b): Appendix D). As one would expect, the 3xTgAD mice raft protein clustering revealed a considerably

greater (relative to control) activation of multiple neurodegenerative neuronal processes including: "*amyloid processing*", "*Amyotrophic lateral sclerosis*", "*Huntington's disease signaling*" and "*Parkinson's signaling*". In addition to the greater activation of these degenerative processes, the 3xTgAD mice also demonstrated profound changes in the significant clustering of proteins into cytoskeletal remodeling groups ("*actin cytoskeleton signaling*", *regulation of actin-based motility by Rho*') compared to the control mice. In accordance with our demonstration of the significant diminution of the learning and memory ability of the 3xTgAD mice, it was striking to notice the profoundly greater activation of neuron-functional pathways that control synaptic learning-dependent processes (*i.e.,* "*synaptic long-term depression*", "*axonal guidance signaling*",and "*synaptic long-term potentiation*") in the control mice compared to the 3xTgAD mice. Considerable evidence from multiple experimental studies has recently underlined the importance of the regulation of energy metabolism in controlling the aging process and neurodegenerative disorders [28–30]. Upon inspection of the relative differences in the activation of energy-regulatory pathways created by clustering of control raft proteins versus 3xTgAD raft proteins, a profound functional distinction was noted (Figure 4(c): Appendix E). In control animals versus 3xTgAD, there was a considerably stronger activation of energy-generating pathways connected to the use of the primary metabolic substrate, that is, sugars ("*amino sugars metabolism*", "*glycolysis/gluconeogenesis*", and "*pentose phosphate pathway*"). In contrast, the energy regulatory pathways that were more strongly associated with the 3xTgAD animals involved energy derivation from alternative energy sources, for example, "*synthesis and degradation of ketone bodies*", "*butanoate metabolism*", and "*fatty acid biosynthesis*". Many of the alterations in energy regulation in aging and degenerative disorders are thought to be associated with adaptive responses to the induction of cellular stresses, potentially through toxic effects of Aβ, NFTs and accumulated oxidative damage [30]. When the raft proteins from control and 3xTgAD mice were clustered into functional stress response pathways, again a stark contrast in the control- or 3xTgAD-associated pathways was demonstrated (Figure 4(d): Appendix F). In the 3xTgAD mice raft clustering it was noted that the association of energy-associated stressful and neuronal damage-related pathways ("*PPARα/RXRα activation*", "*hypoxia signaling*", "*apoptosis signaling*", and "*endoplasmic reticulum stress pathway*") was considerably stronger than in the control mice. Indicating a correlated connection between stress response capacity and AD pathology, there was a considerably greater association of the "*Nrf2-mediated oxidative stress response pathway*" in control mice compared to the 3xTgAD. Therefore, the 3xTgAD mice may demonstrate excessive neuronal stress and damage due to the attenuated activation of such stress response pathways in lipid rafts of AD synapses.

4.5. Functional Receptor Signaling Cluster Analysis of Control versus 3xTgAD Lipid Raft Proteomes. As one of the most important functions of synaptic lipid rafts is to congregate transmembrane or juxtamembrane receptor systems [31], we next performed an in-depth investigation of the significant differential functional clustering of receptor signaling pathways between control and 3xTgAD rafts. Upon functional clustering of the raft proteins into receptor signaling pathways, strong differences in pathways association between control and 3xTgAD mice were noted (Figure 5: Appendix G). Some of the strongest differences were noted by the considerably poorer activation of growth factor-related signaling ("*PDGF signaling*", "*EGF signaling", and "FGF signaling*"), structural trans-synaptic receptor signaling ("*Neuregulin signaling*" and "*Ephrin receptor signaling*"), excitatory signaling (*glutamate receptor signaling*) and neurodevelopmental signaling (*Sonic hedgehog signaling*) pathways in the 3xTgAD mice, compared to the control mice. The receptor signaling profile of the 3xTgAD mice demonstrated a more profound association compared to control mice for pathways linked to inhibitory synaptic signaling ("*GABA receptor signaling*" and "*Aryl hydrocarbon receptor signaling":* [32]), amyloid processing ("*Notch signaling" and "Integrin signaling":* [33]), and neuronal stress (*glucocorticoid receptor signaling*). Transmembrane receptor signaling by systems including receptor tyrosine kinases or G protein-coupled receptors (GPCRs) represents one of the most important signaling mechanisms of neuronal synaptic regulation [34]. However, the activation of transmembrane receptor systems and the stimulation of their intracellular signaling cascades, especially for GPCRs, is now considered to be far more complex and intricate than initially proposed by two-state receptor models [34, 35]. Much of this additional signaling diversity is thought to arise from the additional complexity of receptor-accessory scaffolding protein modification of receptor signaling [35]. To appreciate the multiple connections between receptor (and GPCR in particular) activity and the presence of neurophysiological deficits in AD, we performed a multidimensional analysis of the proteins present in control or 3xTgAD mice. Using the novel, un-biased, bioinformatic GeneIndexer latent semantic indexing (LSI) process (https://www.computablegenomix.com/geneindexer.php), explicit correlations can be made between protein/gene factors from input datasets and their linkage (in over 1×10^6 curated scientific abstracts) to a specific interrogation term, for example, Alzheimer's. The semantic indexing algorithms of GeneIndexer also allow for multidimensional correlations to be measured for terms significantly related to the interrogation term, hence providing a flexible, intelligent query process. For the control and 3xTgAD datasets, we employed multiple interrogation terms targeted to demonstrate differences between control and 3xTgAD datasets. Using the following interrogation terms: Alzheimer's, oxidation, neurodegeneration, synaptic transmission, neurogenesis, scaffolding, and GPCR, we demonstrated that, at a multidimensional interactive level, there is minimal functional cross-over between control and 3xTgAD raft samples (Figure 6: Appendix H). Only proteins that demonstrated explicit correlations (latent semantic indexing score of ≥ 0.1) to at least two of the interrogation

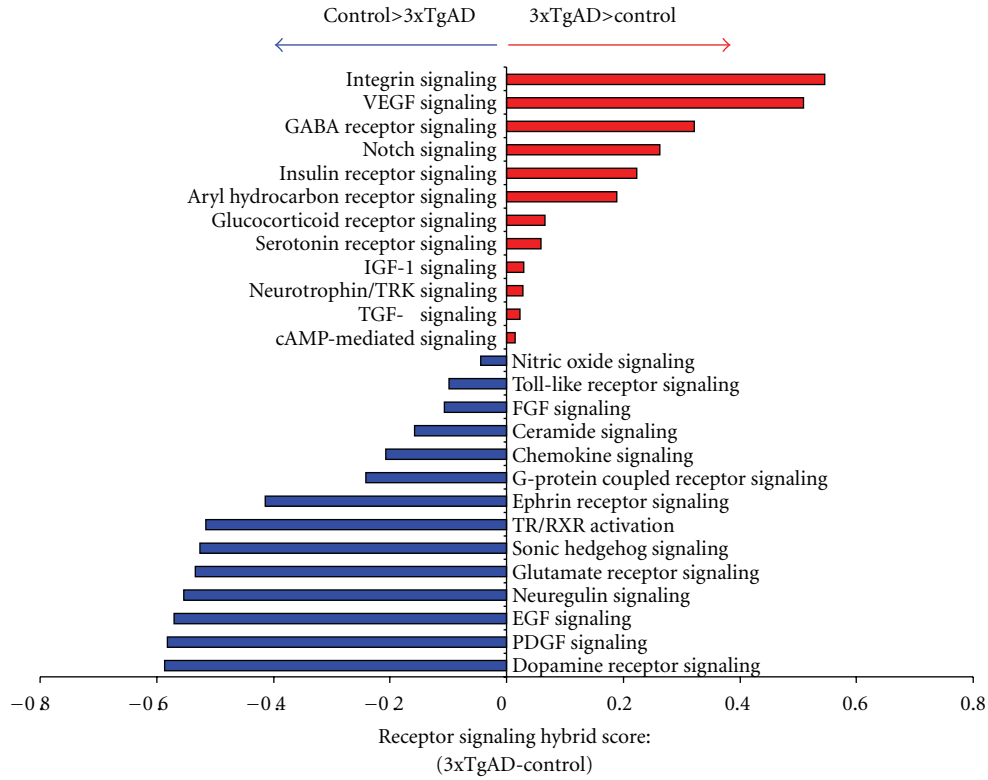

Figure 5: Functional receptor signaling pathway informatic clustering of control and 3xTgAD lipid raft proteins. Subtractive representation of hybrid score generation after clustering of raft proteins from control and 3xTgAD animal rafts into receptor signaling pathways. The data is presented as a numerical value of the control pathway hybrid score subtracted from the 3xTgAD pathway hybrid score. Pathways in which the score in 3xTgAD was greater than the control are denoted in red; pathways in which the control hybrid score was greater than the 3xTgAD hybrid score are denoted in blue.

terms are denoted in the multidimensional heatmap (Figure 6: Appendix H). Therefore, each of the proteins identified in the heatmap are strongly correlated with many of the connected interrogation terms and therefore show potential synergistic activity. Analysis of identified proteins in this manner, that is, selected specifically for multidimensional neurological roles, allows for an un-biased focusing on proteins that may possess keystone-like functions in the molecular signaling networks involved in neurodegeneration. With respect to specific interrogation terms, a strong validation of the technique is demonstrated by the fact that using the Alzheimer's interrogation term, 47 3xTgAD-unique multidimensional proteins were indicated while only 10 such multidimensional proteins were shown in control rafts (Figure 6). Confirming a strong role of oxidative damage, 21 3xTgAD-unique multidimensional proteins were present in the oxidation results while only 6 such control-unique were demonstrated. Interestingly and perhaps suggestive of a potential future line of AD research was the observation that considerably fewer multidimensional 3xTgAD-unique proteins were associated with the process of neurogenesis (15), compared to the 32 control-unique multidimensional proteins associated with this neuroprotective mechanism. In accordance with the important role of receptor systems in AD, we additionally noted that more 3xTgAD-unique proteins were associated with GPCRs (27) compared to control-unique GPCR-related multidimensional proteins (16).

4.6. Functional Interaction Networks of Receptor Signaling Proteins in Control versus 3xTgAD Lipid Raft Proteomes. From our investigation of the multidimensional nature of raft proteins with respect to neurodegenerative processes, it is clear that there are many factors that are highly likely to work together in complex and intricate functional networks. To investigate the nature of the most statistically likely functional network interactions, we employed IPA network analysis of a receptor-filtered (using IPA-knowledge base data filtering, IPA v. 8,5) subset of the control or 3xTgAD raft protein datasets (Tables 1 and 2, resp.). Using these datasets, un-biased network analysis is able to predict the most likely series of functional interactions (based on empirically derived experimental evidence) that take place between the receptor-associated raft proteins. The control and 3xTgAD receptor-specific filtered datasets demonstrated a relatively minimal overlap, that is, 11.6% commonality, indicating that substantial alterations of these proteins may occur in the rafts of 3xTgAD animals (Figure 7(a)). The most statistically likely interaction network that was predicted to occur in control mice centered on neuroprotective and neurotransmissive factors such as phosphoinositide-3-kinse

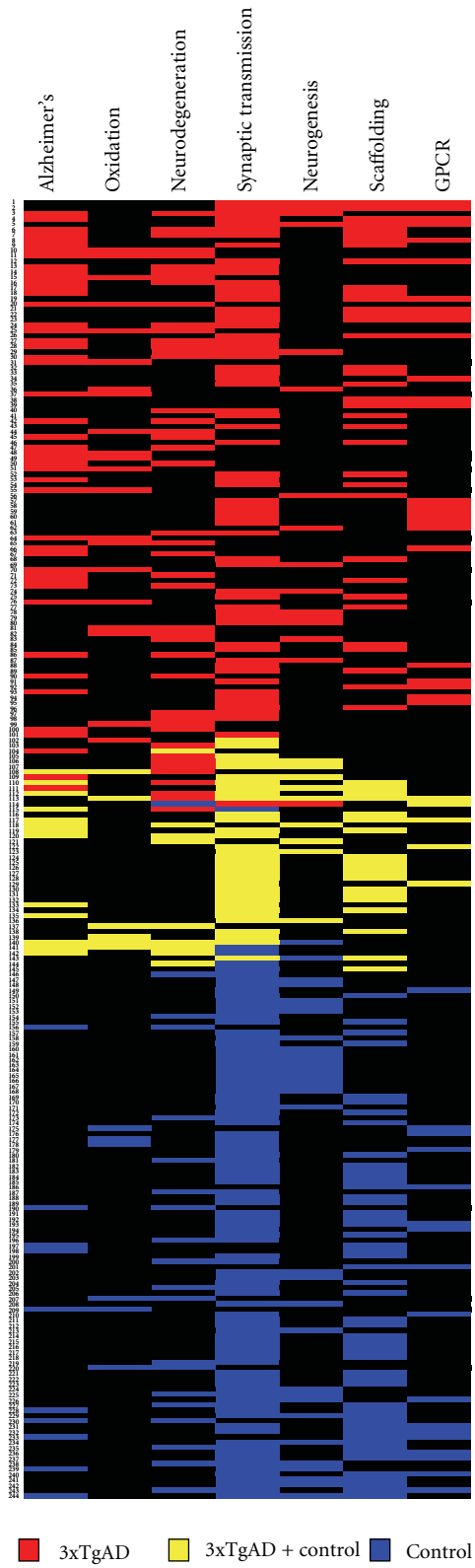

Figure 6: Multidimensional protein latent semantic indexing (LSI) analysis of proteins extracted from control and 3xTgAD lipid rafts. Proteins from the control or 3xTgAD extracted datasets that possessed an explicit latent semantic indexing (LSI, GeneIndexer, Computable Genomix) score in at least two of the multiple GeneIndexer interrogation terms (Alzheimer's, oxidation, neurodegeneration, synaptic transmission, neurogenesis, scaffolding, and GPCR) are represented in a heatmap format. Proteins are identified on the left side of the heatmap as an individual number (see Appendix H for key). The presence of a colored panel (3xTgAD, red: control, blue: 3xTgAD and control: yellow) on the same lateral as the numbered protein denotes explicit textual correlation of that protein with the specific vertical interrogation term.

Table 1: *Receptor-specific protein list from lipid raft extracts from control animals*. Primary protein lists of extracted lipid raft proteins were filtered for a specific receptor profile using IPA v. 8.5.

Symbol	Protein definition	Location	Protein type
Cd4	CD4 molecule	Plasma membrane	Transmembrane receptor
Celsr2	Cadherin, EGF LAG seven-pass G-type receptor 2	Plasma membrane	G-protein coupled receptor
Celsr3	Cadherin, EGF LAG seven-pass G-type receptor 3	Plasma membrane	G-protein coupled receptor
Chrm5	Cholinergic receptor, muscarinic 5	Plasma membrane	G-protein coupled receptor
Chrnb3	Cholinergic receptor, nicotinic, beta 3	Plasma membrane	Transmembrane receptor
Chrnb4	Cholinergic receptor, nicotinic, beta 4	Plasma membrane	Transmembrane receptor
Chrng	Cholinergic receptor, nicotinic, gamma	Plasma membrane	Transmembrane receptor
Cldn4	Claudin 4	Plasma membrane	Transmembrane receptor
Clecsf6	C-type lectin domain family 4, member A	Plasma membrane	Transmembrane receptor
Cnr1	Cannabinoid receptor 1 (brain)	Plasma membrane	G-protein coupled receptor
Cntfr	Ciliary neurotrophic factor receptor	Plasma membrane	Transmembrane receptor
Cxadr	Coxsackie virus and adenovirus receptor	Plasma membrane	Transmembrane receptor
Dag1	Dystroglycan 1 (dystrophin-associated glycoprotein 1)	Plasma membrane	Transmembrane receptor
Ednrb	Endothelin receptor type B	Plasma membrane	G-protein coupled receptor
Fshr	Follicle stimulating hormone receptor	Plasma membrane	G-protein coupled receptor
Fzd9	Frizzled homolog 9 (Drosophila)	Plasma membrane	G-protein coupled receptor
Gabbr1	Gamma-aminobutyric acid (GABA) B receptor, 1	Plasma membrane	G-protein coupled receptor
Gabrr3	Gamma-aminobutyric acid (GABA) receptor, rho 3	Plasma membrane	Transmembrane receptor
Gcgr	Glucagon receptor	Plasma membrane	G-protein coupled receptor
Gfra1	GDNF family receptor alpha 1	Plasma membrane	Transmembrane receptor
Gfra3	GDNF family receptor alpha 3	Plasma membrane	Transmembrane receptor
Gpr116	G protein-coupled receptor 116	Plasma membrane	G-protein coupled receptor
Gpr141	G protein-coupled receptor 141	Plasma membrane	G-protein coupled receptor
Gprc6a	G protein-coupled receptor, family C, group 6, member A	Plasma membrane	G-protein coupled receptor
Grm4	Glutamate receptor, metabotropic 4	Plasma membrane	G-protein coupled receptor
Grm5	Glutamate receptor, metabotropic 5	Plasma membrane	G-protein coupled receptor
Cbp	Opsin 1 (cone pigments), long-wave-sensitive	Plasma membrane	G-protein coupled receptor
Oprd1	Opioid receptor, delta 1	Plasma membrane	G-protein coupled receptor
Osmr	Oncostatin M receptor	Plasma membrane	Transmembrane receptor
Prom2	Prominin 2	Plasma membrane	Transmembrane receptor
Prph2	Peripherin 2 (retinal degeneration, slow)	Plasma membrane	Transmembrane receptor
Ptger2	Prostaglandin E receptor 2 (subtype EP2), 53kda	Plasma membrane	G-protein coupled receptor
Pthr2	Parathyroid hormone 2 receptor	Plasma membrane	G-protein coupled receptor
Sfrp4	Secreted frizzled-related protein 4	Plasma membrane	Transmembrane receptor
Smo	Smoothened homolog (Drosophila)	Plasma membrane	G-protein coupled receptor
Sstr2	Somatostatin receptor 2	Plasma membrane	G-protein coupled receptor
Tacr1	Tachykinin receptor 1	Plasma membrane	G-protein coupled receptor
Tas2r41	Taste receptor, type 2, member 41	Plasma membrane	G-protein coupled receptor
Thbd	Thrombomodulin	Plasma membrane	Transmembrane receptor
Tlr3	Toll-like receptor 3	Plasma membrane	Transmembrane receptor
Tlr4	Toll-like receptor 4	Plasma membrane	Transmembrane receptor
Tlr5	Toll-like receptor 5	Plasma membrane	Transmembrane receptor
Tlr6	Toll-like receptor 6	Plasma membrane	Transmembrane receptor
Tlr9	Toll-like receptor 9	Plasma membrane	Transmembrane receptor
Tshr	Thyroid stimulating hormone receptor	Plasma membrane	G-protein coupled receptor
Unc5b	Unc-5 homolog B (C. Elegans)	Plasma membrane	Transmembrane receptor
Vipr2	Vasoactive intestinal peptide receptor 2	Plasma membrane	G-protein coupled receptor

Table 2: *Receptor-specific protein list from lipid raft extracts from 3xTgAD animals*. Primary protein lists of extracted lipid raft proteins were filtered for a specific receptor profile using IPA v. 8.5.

Symbol	Protein definition	Location	Protein type
Adcyap1r1	Adenylate cyclase activating polypeptide 1 (pituitary) receptor type I	Plasma membrane	G-protein coupled receptor
Cd36	CD36 molecule (thrombospondin receptor)	Plasma membrane	Transmembrane receptor
Cd86	CD86 molecule	Plasma membrane	Transmembrane receptor
Cnr1	Cannabinoid receptor 1 (brain)	Plasma membrane	G-protein coupled receptor
Cxadr	Coxsackie virus and adenovirus receptor	Plasma membrane	Transmembrane receptor
Gabbr1	Gamma-aminobutyric acid (GABA) B receptor, 1	Plasma membrane	G-protein coupled receptor
Gpr1	G protein-coupled receptor 1	Plasma membrane	G-protein coupled receptor
Gpr141	G protein-coupled receptor 141	Plasma membrane	G-protein coupled receptor
Gpr56	G protein-coupled receptor 56	Plasma membrane	G-protein coupled receptor
Htr2c	5-hydroxytryptamine (serotonin) receptor 2C	Plasma membrane	G-protein coupled receptor
Htr4	5-hydroxytryptamine (serotonin) receptor 4	Plasma membrane	G-protein coupled receptor
Igf1r	Insulin-like growth factor 1 receptor	Plasma membrane	Transmembrane receptor
Igf2r	Insulin-like growth factor 2 receptor	Plasma membrane	Transmembrane receptor
Il1r2	Interleukin 1 receptor, type II	Plasma membrane	Transmembrane receptor
Il1rapl1	Interleukin 1 receptor accessory protein-like 1	Plasma membrane	Transmembrane receptor
Lifr	Leukemia inhibitory factor receptor alpha	Plasma membrane	Transmembrane receptor
Lphn1	Latrophilin 1	Plasma membrane	G-protein coupled receptor
Lphn2	Latrophilin 2	Plasma membrane	G-protein coupled receptor
Lrpap1	Low density lipoprotein receptor-related protein associated protein 1	Plasma membrane	Transmembrane receptor
Npr2	Natriuretic peptide receptor B/guanylate cyclase B	Plasma membrane	G-protein coupled receptor
Npy5r	Neuropeptide Y receptor Y5	Plasma membrane	G-protein coupled receptor
Omg	Oligodendrocyte myelin glycoprotein	Plasma membrane	G-protein coupled receptor
Cbp	Opsin 1 (cone pigments), long-wave-sensitive	Plasma membrane	G-protein coupled receptor
Ptch1	Patched homolog 1 (Drosophila)	Plasma membrane	Transmembrane receptor
Pthr2	Parathyroid hormone 2 receptor	Plasma membrane	G-protein coupled receptor
Robo1	Roundabout, axon guidance receptor, homolog 1 (Drosophila)	Plasma membrane	Transmembrane receptor
Lgr7	Relaxin/insulin-like family peptide receptor 1	Plasma membrane	G-protein coupled receptor
Tlr5	Toll-like receptor 5	Plasma membrane	Transmembrane receptor
Tnfrsf14	Tumor necrosis factor receptor superfamily, member 14	Plasma membrane	Transmembrane receptor
Tshr	Thyroid stimulating hormone receptor	Plasma membrane	G-protein coupled receptor

(PI3K), Akt-1, muscarinic GPCRs (Chrm5), and glutamate receptors (Grm5) (Figure 7(a): Appendix I). In contrast, the highest statistically scoring network from 3xTgAD receptor-specific proteins was centered on lipid-regulating factors and stress-related factors including: p38 MAPK; Jnk (c-jun N-terminal kinase), Lrpap1 (low-density lipoprotein receptor-related protein associated protein 1); LDL (low density lipoprotein), and NF-κB (Figure 7(b): Appendix J). Therefore, at the level of functional interaction of receptor-related proteins in the lipid rafts, it is clear that these membrane microdomains are a strong functional locus of this degenerative disease. Reinforcing this AD-relevant microcosm effect in the lipid rafts we analyzed, using latent semantic indexing (LSI) interrogation of these receptor-specific datasets (Table 2—control; Appendix I-3xTgAD), the Alzheimer's disease correlation of these receptor-specific proteins. In Figure 8, we demonstrate that almost twice as many proteins in the 3xTgAD dataset (21) explicitly correlated with the interrogation term Alzheimer's disease compared to the proteins in the control dataset (11). The degree of correlation of the interrogation term (Alzheimer's) to each specific protein is indicated by the LSI score. In Figure 8(b) the cumulated LSI score for the 3xTgAD Alzheimer's-related proteins was 2.92 while for the control proteins only 1.21 (Figure 8(b)), demonstrating that a much stronger correlation of receptor-associated proteins existed for the proteins in 3xTgAD rafts, compared to control. Upon comparison of the phylogenetic relationships of the receptor-specific proteins that form the most likely functional networks (from Figure 7(b)), it is clear that for the control-set proteins only three of these in this network are highly correlated to reports of Alzheimer's disease (27.2%: Figure 8(c)) while the most coherent interaction network of 3xTgAD raft proteins possessed a much higher percentage of Alzheimer's disease-related proteins (62%: Figure 8(d)). Therefore, this suggests that one of the important pathological loci of AD could be the disruption of interactivity of receptor-associated proteins in the lipid raft microdomains

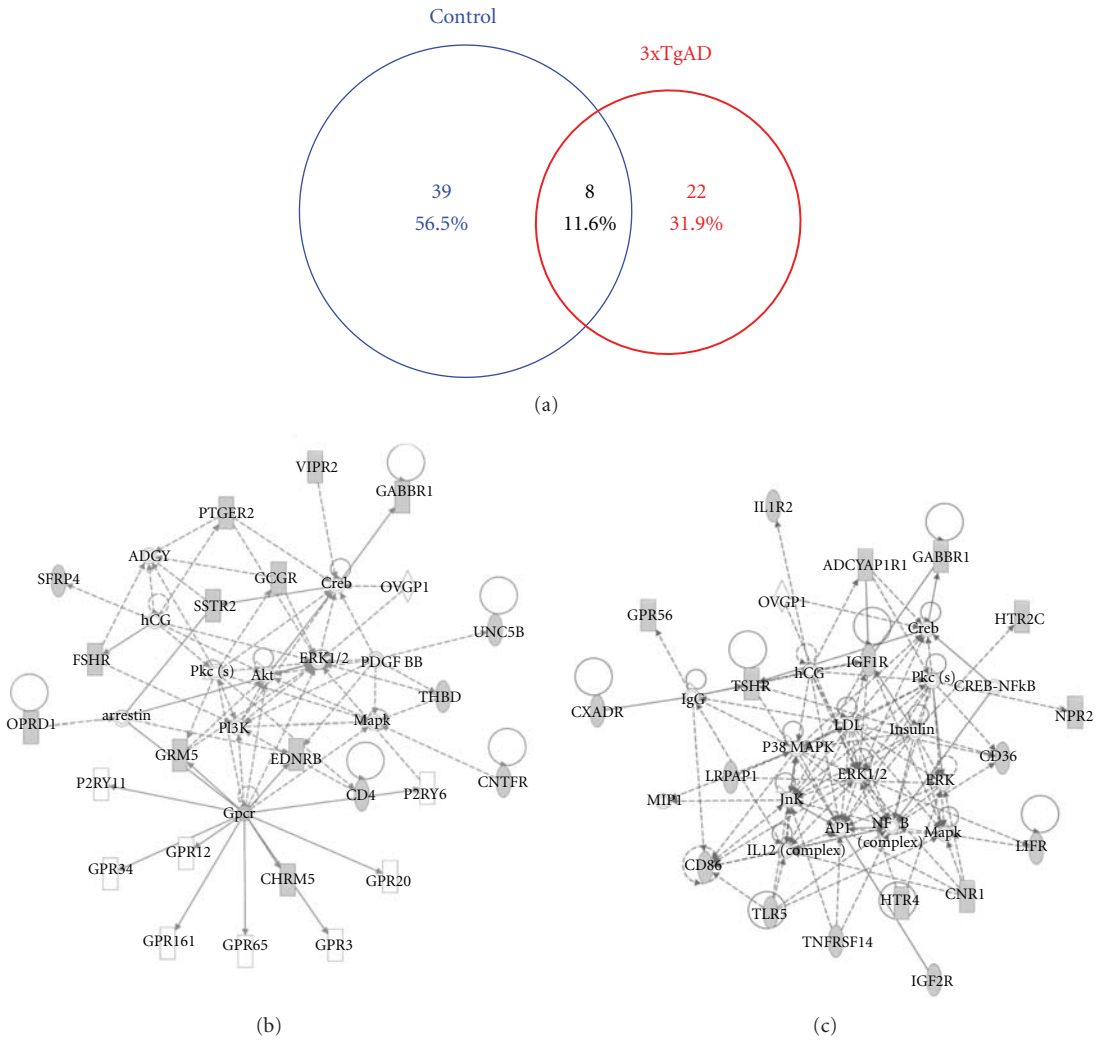

Figure 7: Receptor-restricted control and 3xTgAD network interaction analysis. (a) Proportionally drawn Venn diagram depicting the relative distribution between control or 3xTgAD raft samples of receptor-specific proteins filtered using IPA version 8.5 (control filtered protein list, Table 1; 3xTgAD filtered protein list, Table 2). (b) The highest scoring protein interaction network generated from IPA Network analysis (network scores and focus molecules are listed in Appendix I) of the receptor-specific control dataset. (c) The highest scoring protein interaction network generated from IPA Network analysis (network scores and focus molecules are listed in Appendix I) of the receptor-specific 3xTgAD dataset (Appendix J). A full description of the nature of interactions based on the connecting lines can be found at the following webpage linked to the IPA analysis module (https://analysis.ingenuity.com/pa/info/help/help.htm#ipa_help.htm). Dashed lines represent indirect gene interactions while solid lines represent empirically measured direct interactions. The two highest significantly scoring networks (B—control, C—3xTgAD) are based on the highest percentage of the network occupation by specific proteins (focus molecules) from the input receptor-specific datasets.

and that such a finding can be uncovered in a completely unbiased informatic format from extremely large and difficult to interpret datasets.

5. Discussion

Multiple informatic techniques were employed to investigate and elucidate the nature of functional protein interactions that occur differentially in the lipid raft microdomains of control versus 3xTgAD Alzheimer's disease mice. Cognitively impaired male 3xTgAD mice showed profound differences in the protein constituents of lipid raft extracts compared to age-matched control mice, that is, only 17% of raft proteins were similar between the two groups of mice. Our microdomain proteomic approach was able to specifically assist in the identification of altered proteins that are highly characteristic of AD-related raft pathophysiology, for example, the Src-family tyrosine kinase Fyn (Figure 3(h)) [19, 20].

Currently, biological scientists are often faced with complex biological issues concerning the interpretation of their results due to the development of facile mass data acquisition technologies, that is, extracting relevant and illuminating information from large datasets is often extremely challenging. However, with the application of multiple, sequential

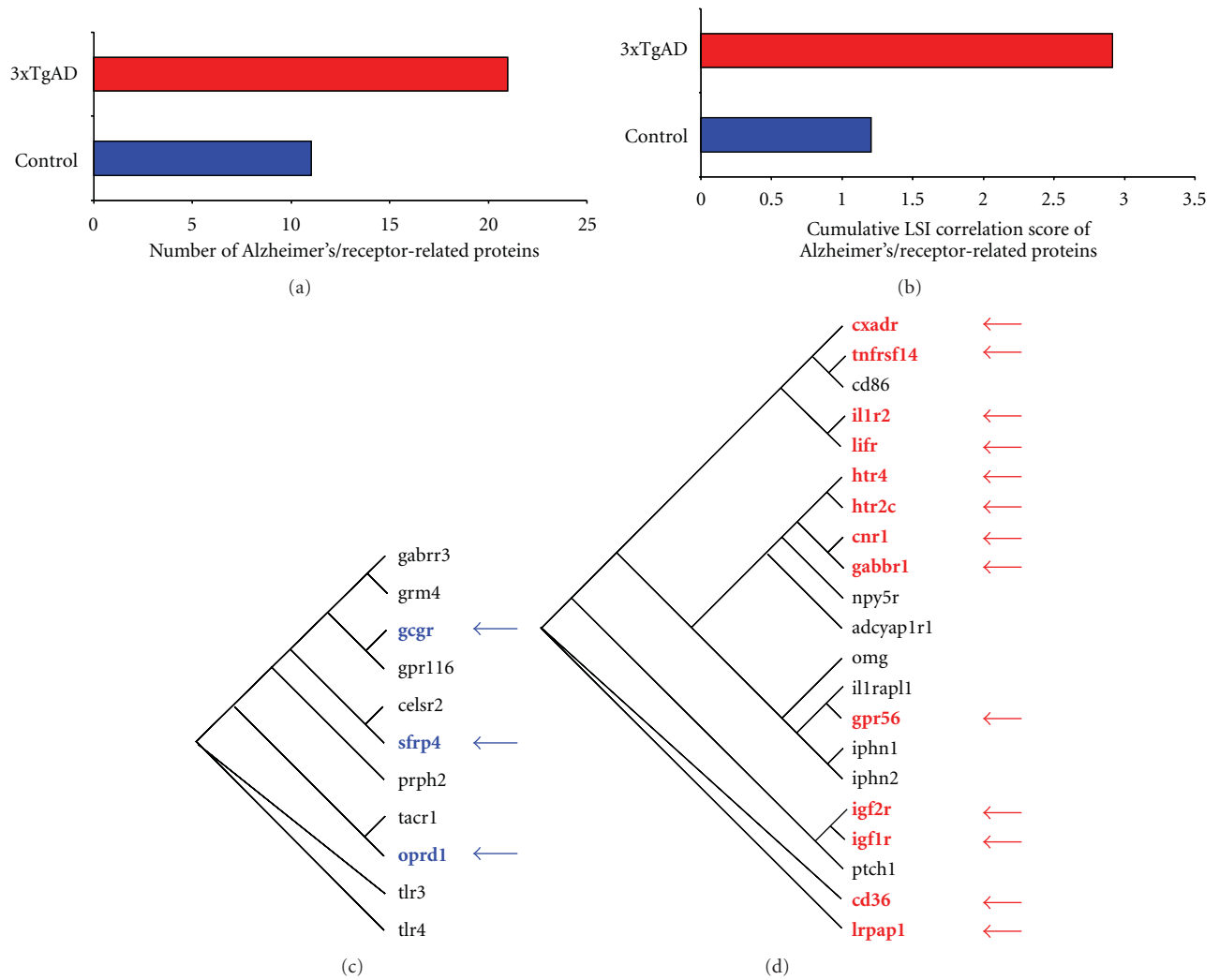

Figure 8: Alzheimer's disease correlation of control or 3xTgAD receptor-specific lipid raft proteins. (a) The histogram represents the number of receptor-specific raft proteins (Table 1: control, Table 2: 3xTgAD) that demonstrate an explicit LSI correlation to the term "Alzheimer's" for control (blue) or 3xTgAD (red) extracts. (b) The histogram depicts the cumulated LSI correlation scores for the Alzheimer's-related receptor-specific proteins identified in (a). panels (c) and (d) represent the phylogenetic dendrograms for the receptor-specific raft proteins linked to the interrogation term "Alzheimer's" from control (c) or 3xTgAD (d) datasets. The proteins highlighted in red or blue and indicated by an arrow were specifically clustered into the highest scoring protein interaction networks for control (Figure 7(b)) or 3xTgAD (Figure 7(c)) samples.

un-biased informatic processes, we were able to identify specific lipid raft involvement in altered pathways that can control multiple degenerative mechanisms, for example, attenuation of the Wnt/β-catenin signaling pathway, profound reduction of the important Nrf2 stress response pathway (Figure 4(d)), the loss of neurogenesis association, and the important involvement of synaptic GPCR-systems (Figure 6) in the 3xTgAD mice [36–38].

Elucidation of the crucial signaling relationships in this degenerative disorder, and the identity of the proteins that mediate them, could lead to the more rational development of novel therapeutics for Alzheimer's disease. Using our informatic receptor-targeted approach, we were also able to reinforce the validity of our discovery process by also identifying the importance of energy-related insulin/insulin-like growth factor (IGF) signaling in AD (Figures 3(j), 3(n), 5, and 8(d)) that has recently become more widely appreciated by other researchers [39–42]. In addition to IGF receptor activity, we noted a potential implication of the presynaptic latrophilins (lphn) in AD pathophysiology (Figure 8(d)). These unique receptors form the high affinity target of α-latrotoxin and may be able to integrate presynaptic calcium regulation with an ability to potentially physically interact with the postsynaptic neuron [43]. Another receptor signaling system that our analysis revealed to possess a potential role in AD is the Sonic Hedgehog (Shh) systems (Figures 5 and 8(d)). With a specific correlation to AD pathophysiology, it has been demonstrated that Shh can act in a synergistic manner with nerve growth factor to act on central nervous system cholinergic neurons [44], and cholinergic insufficiency has been strongly associated with cognitive decline and Alzheimer's-related pathophysiology [45].

6. Conclusions

The combined use of broad range proteomic analysis, with sequential multidimensional informatic analysis enables the determination of important correlations between pathophysiology and functional protein differences. Using discrete proteomes, that is, lipid raft extracts, versus whole-cell/tissue proteomes, facilitates an improved ability to understand the complex interactivity between transmembrane receptor protein systems in a disease setting. The appreciation and clustering of protein datasets into coherent groups greatly increases our capacity to focus upon potentially important therapeutic target networks. The knowledge gained of protein activity networks may greatly assist in the future development of network-targeting therapeutics that possess a multidimensional efficacy at several interacting proteins.

Appendices

A.

Lipid raft-derived extracted proteins from control mouse 16-month-old cortical tissue. Specific proteins isolated from control mouse cortex were identified with multidimensional protein identification technology (MudPIT) LC MS/MS. Each protein was identified in at least two out of three experimental replicate animals and from at least two isolated peptides per protein. The following are the protein symbol and its corresponding definitions.

Atm: ataxia telangiectasia mutated

Bcat1: branched chain aminotransferase 1, cytosolic

Bcl11a: B-cell CLL/lymphoma 11A (zinc finger protein)

Bnip1: BCL2/adenovirus E1B 19 kDa interacting protein 1

Brd2: bromodomain containing 2

Bteb1: Kruppel-like factor 9

Bzrap1: benzodiazepine receptor (peripheral) associated protein 1

C3: complement component 3

C5: complement component 5

Cacna1a: calcium channel, voltage-dependent, P/Q type, alpha 1A subunit

Cacna1c: calcium channel, voltage-dependent, L type, alpha 1C subunit

Cacna2d2: calcium channel, voltage-dependent, alpha 2/delta subunit 2

Cadps: Ca++-dependent secretion activator

Calb1: calbindin 1, 28 kDa

Calb2: calbindin 2

Calm2: calmodulin 2 (phosphorylase kinase, delta)

Camkk1: calcium/calmodulin-dependent protein kinase kinase 1, alpha

Camkk2: calcium/calmodulin-dependent protein kinase kinase 2, beta

Cap1: CAP, adenylate cyclase-associated protein 1 (yeast)

Cast: calpastatin

Cat: catalase

Catsper2: cation channel, sperm associated 2

Cav1: caveolin 1, caveolae protein, 22 kDa

Cblb: Cas-Br-M (murine) ecotropic retroviral transforming sequence b

Cbp: opsin 1 (cone pigments), long-wave-sensitive

Cbr1: carbonyl reductase 1

Cbwd1: COBW domain containing 1

Cbx5: chromobox homolog 5 (HP1 alpha homolog, Drosophila)

Ccbl1: cysteine conjugate-beta lyase, cytoplasmic

Ccin: calicin

Ccl28: chemokine (C-C motif) ligand 28

Ccl4: chemokine (C-C motif) ligand 4

ccnb1: cyclin B1

Ccnc: cyclin C

Cct2: chaperonin containing TCP1, subunit 2 (beta)

Cct3: chaperonin containing TCP1, subunit 3 (gamma)

Cct4: chaperonin containing TCP1, subunit 4 (delta)

Cct5: chaperonin containing TCP1, subunit 5 (epsilon)

Cct6a: chaperonin containing TCP1, subunit 6A (zeta 1)

Cd1: ribosomal protein L5

Cd151: CD151 molecule (Raph blood group)

Cd200: CD200 molecule

Cd276: CD276 molecule

Cd2ap: CD2-associated protein

Cd4: CD4 molecule

Cdc10: septin 7

Cdc25b: cell division cycle 25 homolog B (S. pombe)

Cdc42: cell division cycle 42 (GTP binding protein, 25 kDa)

Cdc42bpa: CDC42 binding protein kinase alpha (DMPK-like)

Cdc5l: CDC5 cell division cycle 5-like (S. pombe)

Cdh1: cadherin 1, type 1, E-cadherin (epithelial)

Cdh10: cadherin 10, type 2 (T2-cadherin)

Cdh2: cadherin 2, type 1, N-cadherin (neuronal)

Cdh4: cadherin 4, type 1, R-cadherin (retinal)

Cdk2: cyclin-dependent kinase 2

Cdk5rap2: CDK5 regulatory subunit associated protein 2

Cdk5rap3: CDK5 regulatory subunit associated protein 3

Cdk6: cyclin-dependent kinase 6

Cdk7: cyclin-dependent kinase 7

Cdkl2: cyclin-dependent kinase-like 2 (CDC2-related kinase)

Cdkl3: cyclin-dependent kinase-like 3

Cdkn1b: cyclin-dependent kinase inhibitor 1B (p27, Kip1)

Cds1: CDP-diacylglycerol synthase (phosphatidate cytidylyltransferase) 1

Cdv1: intraflagellar transport 81 homolog (Chlamydomonas)

Cebpe: CCAAT/enhancer binding protein (C/EBP), epsilon

Cebpz: CCAAT/enhancer binding protein (C/EBP), zeta

Celsr2: cadherin, EGF LAG seven-pass G-type receptor 2 (flamingo homolog, Drosophila)

Celsr3: cadherin, EGF LAG seven-pass G-type receptor 3 (flamingo homolog, Drosophila)

Cend1: cell cycle exit and neuronal differentiation 1

Cenpf: centromere protein F, 350/400ka (mitosin)

Centa1: ArfGAP with dual PH domains 1

Centg1: ArfGAP with GTPase domain, ankyrin repeat and PH domain 2

Cep350: centrosomal protein 350 kDa

Ces1: carboxylesterase 1 (monocyte/macrophage serine esterase 1)

Ces3: carboxylesterase 3

Cetn2: centrin, EF-hand protein, 2

Cetn3: centrin, EF-hand protein, 3 (CDC31 homolog, yeast)

Cfh: complement factor H

Cfl1: cofilin 1 (nonmuscle)

Chd3: chromodomain helicase DNA binding protein 3

Chd4: chromodomain helicase DNA binding protein 4

Chga: chromogranin A (parathyroid secretory protein 1)

Chl1: cell adhesion molecule with homology to L1CAM (close homolog of L1)

Chmp1a: chromatin modifying protein 1A

Chn2: chimerin (chimaerin) 2

Chrm5: cholinergic receptor, muscarinic 5

Chrnb3: cholinergic receptor, nicotinic, beta 3

Chrnb4: cholinergic receptor, nicotinic, beta 4

Chrng: cholinergic receptor, nicotinic, gamma

Chst7: carbohydrate (N-acetylglucosamine 6-O) sulfotransferase 7

Chx10: visual system homeobox 2

Cirbp: cold inducible RNA binding protein

Cit: citron (rho-interacting, serine/threonine kinase 21)

Cktsf1b1: gremlin 1, cysteine knot superfamily, homolog (Xenopus laevis)

Clasp2: cytoplasmic linker associated protein 2

Clcc1: chloride channel CLIC-like 1

Clcn7: chloride channel 7

Cldn1: claudin 1

Cldn19: claudin 19

Cldn4: claudin 4

CLEC10A: C-type lectin domain family 10, member A

Clecsf6: C-type lectin domain family 4, member A

Clic4: chloride intracellular channel 4

CLIP3: CAP-GLY domain containing linker protein 3

Clpb: ClpB caseinolytic peptidase B homolog (E. coli)

Clstn1: calsyntenin 1

Cltb: clathrin, light chain (Lcb)

Cndp2: CNDP dipeptidase 2 (metallopeptidase M20 family)

Cnga1: cyclic nucleotide gated channel alpha 1

Cnga4: cyclic nucleotide gated channel alpha 4

Cnksr2: connector enhancer of kinase suppressor of Ras 2

Cnot6: CCR4-NOT transcription complex, subunit 6

Cnp: 2′,3′-cyclic nucleotide 3′ phosphodiesterase

Cnr1: cannabinoid receptor 1 (brain)

Cntfr: ciliary neurotrophic factor receptor

Cntn1: contactin 1

Cog3: component of oligomeric golgi complex 3

Colm: gliomedin

Copa: coatomer protein complex, subunit alpha

Copb1: coatomer protein complex, subunit beta 1

COPB2: coatomer protein complex, subunit beta 2 (beta prime)

Cops4: COP9 constitutive photomorphogenic homolog subunit 4 (Arabidopsis)

Cops8: COP9 constitutive photomorphogenic homolog subunit 8 (Arabidopsis)

Coro1a: coronin, actin binding protein, 1A

Coro7: coronin 7

Cp: ceruloplasmin (ferroxidase)

Cpe: carboxypeptidase E

Cplx1: complexin 1

Cpt1a: carnitine palmitoyltransferase 1A (liver)

Cpt2: carnitine palmitoyltransferase 2

Crabp2: cellular retinoic acid binding protein 2

Crhbp: corticotropin releasing hormone binding protein

Crip2: cysteine-rich protein 2

Crk: v-crk sarcoma virus CT10 oncogene homolog (avian)

Crkl: v-crk sarcoma virus CT10 oncogene homolog (avian)-like

Crmp1: collapsin response mediator protein 1

Crnkl1: crooked neck pre-mRNA splicing factor-like 1 (Drosophila)

Crp: C-reactive protein, pentraxin-related

Cry1: cryptochrome 1 (photolyase-like)

Crygc: crystallin, gamma C

Crygs: crystallin, gamma S

Crym: crystallin, mu

Cs: citrate synthase

Csf1: colony stimulating factor 1 (macrophage)

Csnk1e: casein kinase 1, epsilon

Csnk1g2: casein kinase 1, gamma 2

Csnk2a1: casein kinase 2, alpha 1 polypeptide

Csnk2b: casein kinase 2, beta polypeptide

Cspg2: versican

Cspg3: neurocan

Cspg5: chondroitin sulfate proteoglycan 5 (neuroglycan C)

Cspg6: structural maintenance of chromosomes 3

Cst6: cystatin E/M

Cstb: cystatin B (stefin B)

Ctf1: cardiotrophin 1

Cthrc1: collagen triple helix repeat containing 1

Ctla4: cytotoxic T-lymphocyte-associated protein 4

Ctnnb1: catenin (cadherin-associated protein), beta 1, 88 kDa

Ctnnd2: catenin (cadherin-associated protein), delta 2 (neural plakophilin-related arm-repeat protein)

Ctrb: chymotrypsinogen B1

Ctrl: chymotrypsin-like

Ctsd: cathepsin D

Cttn: cortactin

Cttnbp2: cortactin binding protein 2

Cul1: cullin 1

Cul5: cullin 5

Cuta: cutA divalent cation tolerance homolog (E. coli)

Cutl1: cut-like homeobox 1

CX3CL1: chemokine (C-X3-C motif) ligand 1

Cxadr: coxsackie virus and adenovirus receptor

Cxcl2: chemokine (C-X-C motif) ligand 2

Cyb5: cytochrome b5 type A (microsomal)

Cyb5b: cytochrome b5 type B (outer mitochondrial membrane)

Cyb5r1: cytochrome b5 reductase 1

Cybb: cytochrome b-245, beta polypeptide

Cyln2: CAP-GLY domain containing linker protein 2

Cyp2s1: cytochrome P450, family 2, subfamily S, polypeptide 1

Cyr61: cysteine-rich, angiogenic inducer, 61

Dab2: disabled homolog 2, mitogen-responsive phosphoprotein (Drosophila)

Dab2ip: DAB2 interacting protein

Dad1: defender against cell death 1

Dag1: dystroglycan 1 (dystrophin-associated glycoprotein 1)

Dap: death-associated protein

Dapk3: death-associated protein kinase 3

Dbc1: deleted in bladder cancer 1

DBH: dopamine beta-hydroxylase (dopamine beta-monooxygenase)

Dbn1: drebrin 1

Dbndd2: dysbindin (dystrobrevin binding protein 1) domain containing 2

Dbnl: drebrin-like

Dcd: dermcidin

Dci: dodecenoyl-Coenzyme A delta isomerase (3,2 trans-enoyl-Coenzyme A isomerase)

Dclk2: doublecortin-like kinase 2

Dclre1c: DNA cross-link repair 1C (PSO2 homolog, S. cerevisiae)

Dctn2: dynactin 2 (p50)

Ddah2: dimethylarginine dimethylaminohydrolase 2

Ddb1: damage-specific DNA binding protein 1, 127 kDa

Ddn: dendrin

Ddost: dolichyl-diphosphooligosaccharide-protein glycosyltransferase

Ddr2: discoidin domain receptor tyrosine kinase 2

Ddt: D-dopachrome tautomerase

Ddx1: DEAD (Asp-Glu-Ala-Asp) box polypeptide 1

Ddx17: DEAD (Asp-Glu-Ala-Asp) box polypeptide 17

Ddx47: DEAD (Asp-Glu-Ala-Asp) box polypeptide 47

Ddx5: DEAD (Asp-Glu-Ala-Asp) box polypeptide 5

Decr1: 2,4-dienoyl CoA reductase 1, mitochondrial

Des: desmin

Dgcr14: DiGeorge syndrome critical region gene 14

Dgkb: diacylglycerol kinase, beta 90 kDa

Dgkg: diacylglycerol kinase, gamma 90 kDa

Dhcr7: 7-dehydrocholesterol reductase

Dhodh: dihydroorotate dehydrogenase

Dhrs8: hydroxysteroid (17-beta) dehydrogenase 11

Dhx16: DEAH (Asp-Glu-Ala-His) box polypeptide 16

Dhx30: DEAH (Asp-Glu-Ala-His) box polypeptide 30

Dia1: cytochrome b5 reductase 3

Dio1: deiodinase, iodothyronine, type I

Disc1: disrupted in schizophrenia 1

Dkc1: dyskeratosis congenita 1, dyskerin

Dlat: dihydrolipoamide S-acetyltransferase

Dlc1: deleted in liver cancer 1

Dld: dihydrolipoamide dehydrogenase

Dlgap1: discs, large (Drosophila) homolog-associated protein 1

Dlgap2: discs, large (Drosophila) homolog-associated protein 2

Dlgap4: discs, large (Drosophila) homolog-associated protein 4

Dll1: delta-like 1 (Drosophila)

Dll3: delta-like 3 (Drosophila)

Dlx5: distal-less homeobox 5

Dmd: dystrophin

Dmn: synemin, intermediate filament protein

Dmrt1: doublesex and mab-3 related transcription factor 1

Dnah6: dynein, axonemal, heavy chain 6

Dnaja2: DnaJ (Hsp40) homolog, subfamily A, member 2

Dnch1: dynein, cytoplasmic 1, heavy chain 1

Dncl2a: dynein, light chain, roadblock-type 1

Dntt: deoxynucleotidyltransferase, terminal

Dock9: dedicator of cytokinesis 9

Dpp3: dipeptidyl-peptidase 3

Dpyd: dihydropyrimidine dehydrogenase

Dpysl3: dihydropyrimidinase-like 3

Dpysl4: dihydropyrimidinase-like 4

Drd1ip: calcyon neuron-specific vesicular protein

Drg1: developmentally regulated GTP binding protein 1

Drpla: atrophin 1

Dscam: Down syndrome cell adhesion molecule

Dscr1l1: regulator of calcineurin 2

Dtnb: dystrobrevin, beta

Duox1: dual oxidase 1

Dusp12: dual specificity phosphatase 12

Dusp2: dual specificity phosphatase 2

Dvl1: dishevelled, dsh homolog 1 (Drosophila)

Dync1h1: dynein, cytoplasmic 1, heavy chain 1

Dync1li2: dynein, cytoplasmic 1, light intermediate chain 2

Dyx1c1: dyslexia susceptibility 1 candidate 1

Eaf2: ELL associated factor 2

Ecel1: endothelin converting enzyme-like 1

Echdc1: enoyl Coenzyme A hydratase domain containing 1

Ecm1: extracellular matrix protein 1

Ecm2: extracellular matrix protein 2, female organ and adipocyte specific

Edf1: endothelial differentiation-related factor 1

Ednrb: endothelin receptor type B

Eef2: eukaryotic translation elongation factor 2

Efcbp1: N-terminal EF-hand calcium binding protein 1

Efemp2: EGF-containing fibulin-like extracellular matrix protein 2

Efnb1: ephrin-B1

Egf: epidermal growth factor (beta-urogastrone)

Egfl3: multiple EGF-like-domains 6

Egfr: epidermal growth factor receptor (erythroblastic leukemia viral (v-erb-b) oncogene homolog, avian)

Ehd2: EH-domain containing 2

Ehd4: EH-domain containing 4

Eif2c2: eukaryotic translation initiation factor 2C, 2

Eif5b: eukaryotic translation initiation factor 5B

Elac2: elaC homolog 2 (E. coli)

Elavl3: ELAV (embryonic lethal, abnormal vision, Drosophila)-like 3 (Hu antigen C)

ELK1: ELK1, member of ETS oncogene family

Elmo1: engulfment and cell motility 1

Emb: embigin homolog (mouse)

Emd: emerin

Eml5: echinoderm microtubule associated protein like 5

Enah: enabled homolog (Drosophila)

Enc1: ectodermal-neural cortex (with BTB-like domain)

Eno2: enolase 2 (gamma, neuronal)

Eno3: enolase 3 (beta, muscle)

Enpp2: ectonucleotide pyrophosphatase/phosphodiesterase 2

Enpp3: ectonucleotide pyrophosphatase/phosphodiesterase 3

Enpp5: ectonucleotide pyrophosphatase/phosphodiesterase 5 (putative function)

Ensa: endosulfine alpha

Entpd2: ectonucleoside triphosphate diphosphohydrolase 2

Entpd8: ectonucleoside triphosphate diphosphohydrolase 8

Epha3: EPH receptor A3

Epha5: EPH receptor A5

Epha7: EPH receptor A7

Ephb3: EPH receptor B3

Ephx1: epoxide hydrolase 1, microsomal (xenobiotic)

Epn1: epsin 1

Eprs: glutamyl-prolyl-tRNA synthetase

Eps8l1: EPS8-like 1

Erap1: endoplasmic reticulum aminopeptidase 1

Erbb3: v-erb-b2 erythroblastic leukemia viral oncogene homolog 3 (avian)

Erbb4: v-erb-a erythroblastic leukemia viral oncogene homolog 4 (avian)

Ercc5: excision repair cross-complementing rodent repair deficiency, complementation group 5

Erp29: endoplasmic reticulum protein 29

Esd: esterase D/formylglutathione hydrolase

Esr2: estrogen receptor 2 (ER beta)

Etfb: electron-transfer-flavoprotein, beta polypeptide

Ets1: v-ets erythroblastosis virus E26 oncogene homolog 1 (avian)

Evl: Enah/Vasp-like

Exoc5: exocyst complex component 5

Exoc7: exocyst complex component 7

Ezr: ezrin

Fabp1: fatty acid binding protein 1, liver

Fabp2: fatty acid binding protein 2, intestinal

Fabp3: fatty acid binding protein 3, muscle and heart (mammary-derived growth inhibitor)

Fabp4: fatty acid binding protein 4, adipocyte

Fabp7: fatty acid binding protein 7, brain

Fads1: fatty acid desaturase 1

Fads2: fatty acid desaturase 2

Faim: Fas apoptotic inhibitory molecule

Fancd2: Fanconi anemia, complementation group D2

Faslg: Fas ligand (TNF superfamily, member 6)

Fasn: fatty acid synthase

Fat: FAT tumor suppressor homolog 1 (Drosophila)

Fat3: FAT tumor suppressor homolog 3 (Drosophila)

Fbn1: fibrillin 1

Fbn2: fibrillin 2

Fbxw11: F-box and WD repeat domain containing 11

Fetub: fetuin B

FGA: fibrinogen alpha chain

Fgb: fibrinogen beta chain

Fgf18: fibroblast growth factor 18

Fgf23: fibroblast growth factor 23

Fgfr1: fibroblast growth factor receptor 1

Fgfr1op2: FGFR1 oncogene partner 2

Fgfr2: fibroblast growth factor receptor 2

Fgfr3: fibroblast growth factor receptor 3

Fhl1: four and a half LIM domains 1

Fignl1: fidgetin-like 1

Fip1l1: FIP1 like 1 (S. cerevisiae)

Fkbp14: FK506 binding protein 14, 22 kDa

Fkbp1b: FK506 binding protein 1B, 12.6 kDa

Fkbp5: FK506 binding protein 5

Flg: filaggrin

Flii: flightless I homolog (Drosophila)

Fmo3: flavin containing monooxygenase 3

Fnta: farnesyltransferase, CAAX box, alpha

Fos: FBJ murine osteosarcoma viral oncogene homolog

Fpgt: fucose-1-phosphate guanylyltransferase

Freq: frequenin homolog (Drosophila)

Fshr: follicle stimulating hormone receptor

Fthfd: aldehyde dehydrogenase 1 family, member L1

Fuca1: fucosidase, alpha-L-1, tissue

fut10: fucosyltransferase 10 (alpha (1,3) fucosyltransferase)

Fxc1: fracture callus 1 homolog (rat)

Fxyd6: FXYD domain containing ion transport regulator 6

Fzd9: frizzled homolog 9 (Drosophila)

Gaa: glucosidase, alpha; acid

Gabarap: GABA(A) receptor-associated protein

Gabarapl2: GABA(A) receptor-associated protein-like 2

Gabbr1: gamma-aminobutyric acid (GABA) B receptor, 1

Gabra3: gamma-aminobutyric acid (GABA) A receptor, alpha 3

Gabrg2: gamma-aminobutyric acid (GABA) A receptor, gamma 2

Gabrr3: gamma-aminobutyric acid (GABA) receptor, rho 3

Gadd45a: growth arrest and DNA-damage-inducible, alpha

Galc: galactosylceramidase

Galk1: galactokinase 1

Galt: galactose-1-phosphate uridylyltransferase

Gapdh: glyceraldehyde-3-phosphate dehydrogenase

Gars: glycyl-tRNA synthetase

Gas6: growth arrest-specific 6

Gas7: growth arrest-specific 7

Gata2: GATA binding protein 2

Gata3: GATA binding protein 3

GC: group-specific component (vitamin D binding protein)

Gc: group-specific component (vitamin D binding protein)

Gcgr: glucagon receptor

Gckr: glucokinase (hexokinase 4) regulator

Gclc: glutamate-cysteine ligase, catalytic subunit

Gcnt3: glucosaminyl (N-acetyl) transferase 3, mucin type

Gdap2: ganglioside induced differentiation associated protein 2

Gdi1: GDP dissociation inhibitor 1

Gdi2: GDP dissociation inhibitor 2

Gfap: glial fibrillary acidic protein

Gfpt2: glutamine-fructose-6-phosphate transaminase 2

Gfra1: GDNF family receptor alpha 1

Gfra3: GDNF family receptor alpha 3

Ggt1: gamma-glutamyltransferase 1

Ggtl3: gamma-glutamyltransferase 7

Ggtla1: gamma-glutamyltransferase 5

Ghitm: growth hormone inducible transmembrane protein

Gif: gastric intrinsic factor (vitamin B synthesis)

Gipc1: GIPC PDZ domain containing family, member 1

Git1: G protein-coupled receptor kinase interacting ArfGAP 1

Gja1: gap junction protein, alpha 1, 43 kDa

Gja10: gap junction protein, alpha 10, 62 kDa

Gja4: gap junction protein, alpha 4, 37 kDa

Gjb6: gap junction protein, beta 6, 30 kDa

Gla: galactosidase, alpha

Gldc: glycine dehydrogenase (decarboxylating)

Glg1: golgi apparatus protein 1

Gli: GLI family zinc finger 1

Glo1: glyoxalase I

Glra2: glycine receptor, alpha 2

Glrx2: glutaredoxin 2

Glud1: glutamate dehydrogenase 1

Glul: glutamate-ammonia ligase (glutamine synthetase)

Gm2a: GM2 ganglioside activator

Gmcl1: germ cell-less homolog 1 (Drosophila)

Gmfb: glia maturation factor, beta

Gmfg: glia maturation factor, gamma

Gmpr2: guanosine monophosphate reductase 2

Gng7: guanine nucleotide binding protein (G protein), gamma 7

Gnpat: glyceronephosphate O-acyltransferase

Gns: glucosamine (N-acetyl)-6-sulfatase

Golga2: golgi autoantigen, golgin subfamily a, 2

Golgb1: golgin B1, golgi integral membrane protein

Golph3: golgi phosphoprotein 3 (coat-protein)

Golph4: golgi integral membrane protein 4

Gosr2: golgi SNAP receptor complex member 2

Got1: glutamic-oxaloacetic transaminase 1, soluble (aspartate aminotransferase 1)

Got2: glutamic-oxaloacetic transaminase 2, mitochondrial (aspartate aminotransferase 2)

Gpam: glycerol-3-phosphate acyltransferase, mitochondrial

Gpc2: glypican 2

Gpi: glucose phosphate isomerase

Gpm6a: glycoprotein M6A

Gpr116: G protein-coupled receptor 116

Gpr141: G protein-coupled receptor 141

Gprc6a: G protein-coupled receptor, family C, group 6, member A

Gpsm1: G-protein signaling modulator 1 (AGS3-like, C. elegans)

Gpt: glutamic-pyruvate transaminase (alanine aminotransferase)

Gramd1a: GRAM domain containing 1A

Grasp: GRP1 (general receptor for phosphoinositides 1)-associated scaffold protein

Grem1: gremlin 1, cysteine knot superfamily, homolog (Xenopus laevis)

Gria1: glutamate receptor, ionotropic, AMPA 1

Grid2: glutamate receptor, ionotropic, delta 2

Grik1: glutamate receptor, ionotropic, kainate 1

Grik4: glutamate receptor, ionotropic, kainate 4

Grin2a: glutamate receptor, ionotropic, N-methyl D-aspartate 2A

Grin2b: glutamate receptor, ionotropic, N-methyl D-aspartate 2B

Grip1: glutamate receptor interacting protein 1

Gripap1: GRIP1 associated protein 1

Grk4: G protein-coupled receptor kinase 4

Grk5: G protein-coupled receptor kinase 5

Grk6: G protein-coupled receptor kinase 6

Grm4: glutamate receptor, metabotropic 4

Grm5: glutamate receptor, metabotropic 5

Grpel1: GrpE-like 1, mitochondrial (E. coli)

Gstk1: glutathione S-transferase kappa 1

Gstm2: glutathione S-transferase mu 2 (muscle)

Gsto1: glutathione S-transferase omega 1

Gtf2ird1: GTF2I repeat domain containing 1

Gtpbp4: GTP binding protein 4

Gucy1a2: guanylate cyclase 1, soluble, alpha 2

Gucy1a3: guanylate cyclase 1, soluble, alpha 3

Gucy1b2: guanylate cyclase 1, soluble, beta 2

Gucy2d: guanylate cyclase 2D, membrane (retina-specific)

Gulp1: GULP, engulfment adaptor PTB domain containing 1

Haao: 3-hydroxyanthranilate 3,4-dioxygenase

Itpka: inositol 1,4,5-trisphosphate 3-kinase A

Khdrbs2: KH domain containing, RNA binding, signal transduction associated 2

Kpnb1: karyopherin (importin) beta 1

Lamp2: lysosomal-associated membrane protein 2

Ncstn: nicastrin

Nedd4l: neural precursor cell expressed, developmentally down-regulated 4-like

Nip7: nuclear import 7 homolog (S. cerevisiae)

Nnat: neuronatin

Nos1: nitric oxide synthase 1 (neuronal)

Nox1: NADPH oxidase 1

Npepps: aminopeptidase puromycin sensitive

Nr1h3: nuclear receptor subfamily 1, group H, member 3

Nr1i2: nuclear receptor subfamily 1, group I, member 2

Nr6a1: nuclear receptor subfamily 6, group A, member 1

Nrcam: neuronal cell adhesion molecule

Nrd1: nardilysin (N-arginine dibasic convertase)

Ntn1: netrin 1

Nucb2: nucleobindin 2

Nudc: nuclear distribution gene C homolog (A. nidulans)

Nup35: nucleoporin 35 kDa

Nup54: nucleoporin 54 kDa

Nup98: nucleoporin 98 kDa

Oaz1: ornithine decarboxylase antizyme 1

Ocrl: oculocerebrorenal syndrome of Lowe

Oit3: oncoprotein induced transcript 3

Olfm2: olfactomedin 2

Opa1: optic atrophy 1 (autosomal dominant)

Oplah: 5-oxoprolinase (ATP-hydrolysing)

Oprd1: opioid receptor, delta 1

Orc4l: origin recognition complex, subunit 4-like (yeast)

Osmr: oncostatin M receptor

Oxr1: oxidation resistance 1

P2rx7: purinergic receptor P2X, ligand-gated ion channel, 7

P4hb: prolyl 4-hydroxylase, beta polypeptide

Pa2g4: proliferation-associated 2G4, 38 kDa

Pabpc4: poly(A) binding protein, cytoplasmic 4 (inducible form)

Pace4: proprotein convertase subtilisin/kexin type 6

Pacs1: phosphofurin acidic cluster sorting protein 1

Pafah1b2: platelet-activating factor acetylhydrolase, isoform Ib, subunit 2 (30 kDa)

Pafah1b3: platelet-activating factor acetylhydrolase, isoform Ib, subunit 3 (29 kDa)

Pak1: p21 protein (Cdc42/Rac)-activated kinase 1

Pak2: p21 protein (Cdc42/Rac)-activated kinase 2

Pak3: p21 protein (Cdc42/Rac)-activated kinase 3

Palm: paralemmin

Pamci: Ras association (RalGDS/AF-6) domain family (N-terminal) member 9

Panx1: pannexin 1

Panx2: pannexin 2

Pard3: par-3 partitioning defective 3 homolog (C. elegans)

Parg: poly (ADP-ribose) glycohydrolase

Park7: Parkinson disease (autosomal recessive, early onset) 7

Pawr: PRKC, apoptosis, WT1, regulator

Pax3: paired box 3

Pbp: phosphatidylethanolamine binding protein 1

Pc: pyruvate carboxylase

Pcca: propionyl Coenzyme A carboxylase, alpha polypeptide

Pcdh21: protocadherin 21

Pcdh7: protocadherin 7

Pcdha3: protocadherin alpha 3

Pcdhb1: protocadherin beta 1

Pck1: phosphoenolpyruvate carboxykinase 1 (soluble)

Pclo: piccolo (presynaptic cytomatrix protein)

Pcm1: pericentriolar material 1

Pcmt1: protein-L-isoaspartate (D-aspartate) O-methyltransferase

PCNT: pericentrin

Pcnx: pecanex homolog (Drosophila)

Pcnxl3: pecanex-like 3 (Drosophila)

Pcsk1: proprotein convertase subtilisin/kexin type 1

Pcsk1n: proprotein convertase subtilisin/kexin type 1 inhibitor

Pcsk5: proprotein convertase subtilisin/kexin type 5

Pcyox1: prenylcysteine oxidase 1

Pcyt1b: phosphate cytidylyltransferase 1, choline, beta

Pdap1: PDGFA associated protein 1

Pdc: phosducin

Pdcd2: programmed cell death 2

Pdcl: phosducin-like

Pde10a: phosphodiesterase 10A

Pde1a: phosphodiesterase 1A, calmodulin-dependent

Pde1c: phosphodiesterase 1C, calmodulin-dependent 70 kDa

Pde4a: phosphodiesterase 4A, cAMP-specific (phosphodiesterase E2 dunce homolog, Drosophila)

Pde4b: phosphodiesterase 4B, cAMP-specific (phosphodiesterase E4 dunce homolog, Drosophila)

Pde4d: phosphodiesterase 4D, cAMP-specific (phosphodiesterase E3 dunce homolog, Drosophila)

Pde5a: phosphodiesterase 5A, cGMP-specific

Pde7a: phosphodiesterase 7A

Pde7b: phosphodiesterase 7B

Pdgfra: platelet-derived growth factor receptor, alpha polypeptide

Pdhb: pyruvate dehydrogenase (lipoamide) beta

Pdia3: protein disulfide isomerase family A, member 3

Pdia4: protein disulfide isomerase family A, member 4

Pdk4: pyruvate dehydrogenase kinase, isozyme 4

Pdlim7: PDZ and LIM domain 7 (enigma)

Pds5b: PDS5, regulator of cohesion maintenance, homolog B (S. cerevisiae)

Pdzd3: PDZ domain containing 3

Pepd: peptidase D

Per3: period homolog 3 (Drosophila)

Pex14: peroxisomal biogenesis factor 14

Pfkl: phosphofructokinase, liver

Pfkm: phosphofructokinase, muscle

Pfkp: phosphofructokinase, platelet

Pgam1: phosphoglycerate mutase 1 (brain)

PGAP1: post-GPI attachment to proteins 1

Pgd: phosphogluconate dehydrogenase

Pgf: placental growth factor

Pgk1: phosphoglycerate kinase 1

Pgm1: phosphoglucomutase 1

Pgr: progesterone receptor

Pgrmc1: progesterone receptor membrane component 1

Phactr1: phosphatase and actin regulator 1

Phactr3: phosphatase and actin regulator 3

Phb: prohibitin

Phex: phosphate regulating endopeptidase homolog, X-linked

Phgdh: phosphoglycerate dehydrogenase

Phip: pleckstrin homology domain interacting protein

Phtf1: putative homeodomain transcription factor 1

Phyhipl: phytanoyl-CoA 2-hydroxylase interacting protein-like

Pi4ka: phosphatidylinositol 4-kinase, catalytic, alpha

Picalm: phosphatidylinositol binding clathrin assembly protein

Pigq: phosphatidylinositol glycan anchor biosynthesis, class Q

Pigs: phosphatidylinositol glycan anchor biosynthesis, class S

Pik3cg: phosphoinositide-3-kinase, catalytic, gamma polypeptide

Pip5k1a: phosphatidylinositol-4-phosphate 5-kinase, type I, alpha

Pip5k1c: phosphatidylinositol-4-phosphate 5-kinase, type I, gamma

Pip5k2a: phosphatidylinositol-5-phosphate 4-kinase, type II, alpha

Pip5k2c: phosphatidylinositol-5-phosphate 4-kinase, type II, gamma

Pipox: pipecolic acid oxidase

Pitpn: phosphatidylinositol transfer protein, alpha

Pkd1: polycystic kidney disease 1 (autosomal dominant)

Pkia: protein kinase (cAMP-dependent, catalytic) inhibitor alpha

Pkm2: pyruvate kinase, muscle

Pla2g4c: phospholipase A2, group IVC (cytosolic, calcium-independent)

Plaa: phospholipase A2-activating protein

Plau: plasminogen activator, urokinase

Plcb1: phospholipase C, beta 1 (phosphoinositide-specific)

Plcl1: phospholipase C-like 1

Pld3: phospholipase D family, member 3

Plekha4: pleckstrin homology domain containing, family A (phosphoinositide binding specific) member 4

Plekhe1: PH domain and leucine rich repeat protein phosphatase 1

Plekhm1: pleckstrin homology domain containing, family M (with RUN domain) member 1

Plg: plasminogen

Plk1: polo-like kinase 1 (Drosophila)

Plrg1: pleiotropic regulator 1 (PRL1 homolog, Arabidopsis)

Plunc: palate, lung and nasal epithelium associated

Plvap: plasmalemma vesicle associated protein

Plxnb2: plexin B2

Pmpca: peptidase (mitochondrial processing) alpha

Pmvk: phosphomevalonate kinase

Pnliprp2: pancreatic lipase-related protein 2

Pnma1: paraneoplastic antigen MA1

Pno1: partner of NOB1 homolog (S. cerevisiae)

Pnpla2: patatin-like phospholipase domain containing 2

Pofut1: protein O-fucosyltransferase 1

Pon2: paraoxonase 2

Pon3: paraoxonase 3

Pop7: processing of precursor 7, ribonuclease P/MRP subunit (S. cerevisiae)

Por: P450 (cytochrome) oxidoreductase

Pou2f2: POU class 2 homeobox 2

Ppfia3: protein tyrosine phosphatase, receptor type, f polypeptide (PTPRF), interacting protein, alpha 3

Ppgb: cathepsin A

Ppib: peptidylprolyl isomerase B (cyclophilin B)

Ppid: peptidylprolyl isomerase D

Ppil3: peptidylprolyl isomerase (cyclophilin)-like 3

Ppm2c: pyruvate dehydrogenase phosphatase catalytic subunit 1

Ppp1r10: protein phosphatase 1, regulatory (inhibitor) subunit 10

Ppp1r14b: protein phosphatase 1, regulatory (inhibitor) subunit 14B

Ppp1r14d: protein phosphatase 1, regulatory (inhibitor) subunit 14D

Ppp1r1a: protein phosphatase 1, regulatory (inhibitor) subunit 1A

Ppp1r7: protein phosphatase 1, regulatory (inhibitor) subunit 7

Ppp1r8: protein phosphatase 1, regulatory (inhibitor) subunit 8

Ppp1r9a: protein phosphatase 1, regulatory (inhibitor) subunit 9A

Ppp1r9b: protein phosphatase 1, regulatory (inhibitor) subunit 9B

Ppp2cb: protein phosphatase 2 (formerly 2A), catalytic subunit, beta isoform

Ppp2r1a: protein phosphatase 2 (formerly 2A), regulatory subunit A, alpha isoform

Ppp2r1b: protein phosphatase 2 (formerly 2A), regulatory subunit A, beta isoform

Ppp2r2a: protein phosphatase 2 (formerly 2A), regulatory subunit B, alpha isoform

PPP2R2B: protein phosphatase 2 (formerly 2A), regulatory subunit B, beta isoform

Ppp2r5e: protein phosphatase 2, regulatory subunit B', epsilon isoform

Ppp3cc: protein phosphatase 3 (formerly 2B), catalytic subunit, gamma isoform

Ppp5c: protein phosphatase 5, catalytic subunit

Prdm4: PR domain containing 4

Prdx1: peroxiredoxin 1

Prep: prolyl endopeptidase

Prf1: perforin 1 (pore forming protein)

Prkaa2: protein kinase, AMP-activated, alpha 2 catalytic subunit

Prkaca: protein kinase, cAMP-dependent, catalytic, alpha

prkar1a: protein kinase, cAMP-dependent, regulatory, type I, alpha (tissue specific extinguisher 1)

Prkar1a: protein kinase, cAMP-dependent, regulatory, type I, alpha (tissue specific extinguisher 1)

Prkar2a: protein kinase, cAMP-dependent, regulatory, type II, alpha

Prkar2b: protein kinase, cAMP-dependent, regulatory, type II, beta

Prkca: protein kinase C, alpha

Prkcb1: protein kinase C, beta

Prkci: protein kinase C, iota

Prkcm: protein kinase D1

PRKCQ: protein kinase C, theta

Prkcz: protein kinase C, zeta

Prkwnk1: WNK lysine deficient protein kinase 1

Prmt3: protein arginine methyltransferase 3

Prnp: prion protein

Prom2: prominin 2

Prph2: peripherin 2 (retinal degeneration, slow)

Prpsap1: phosphoribosyl pyrophosphate synthetase-associated protein 1

Prpsap2: phosphoribosyl pyrophosphate synthetase-associated protein 2

Prr3: proline rich 3

Prrx2: paired related homeobox 2

Prrxl1: dorsal root ganglia homeobox

Prss1: protease, serine, 1 (trypsin 1)

Prss12: protease, serine, 12 (neurotrypsin, motopsin)

Prss15: lon peptidase 1, mitochondrial

Prtg: protogenin homolog (Gallus gallus)

Prx: periaxin

Psat1: phosphoserine aminotransferase 1

Psd: pleckstrin and Sec7 domain containing

Psd4: pleckstrin and Sec7 domain containing 4

Psmc1: proteasome (prosome, macropain) 26S subunit, ATPase, 1

Psmc3: proteasome (prosome, macropain) 26S subunit, ATPase, 3

Psmc5: proteasome (prosome, macropain) 26S subunit, ATPase, 5

Psmd1: proteasome (prosome, macropain) 26S subunit, non-ATPase, 1

Psme1: proteasome (prosome, macropain) activator subunit 1 (PA28 alpha)

Psme2: proteasome (prosome, macropain) activator subunit 2 (PA28 beta)

Psme3: proteasome (prosome, macropain) activator subunit 3 (PA28 gamma; Ki)

Psph: phosphoserine phosphatase

Ptbp1: polypyrimidine tract binding protein 1

Ptbp2: polypyrimidine tract binding protein 2

Ptger2: prostaglandin E receptor 2 (subtype EP2), 53 kDa

Ptgis: prostaglandin I2 (prostacyclin) synthase

Ptgs1: prostaglandin-endoperoxide synthase 1 (prostaglandin G/H synthase and cyclooxygenase)

Pth: parathyroid hormone

Pthr2: parathyroid hormone 2 receptor

Ptk2: PTK2 protein tyrosine kinase 2

Ptn: pleiotrophin

Ptov1: prostate tumor overexpressed 1

Ptp4a1: protein tyrosine phosphatase type IVA, member 1

Ptpn11: protein tyrosine phosphatase, non-receptor type 11

Rnmt: RNA (guanine-7-) methyltransferase

Rraga: Ras-related GTP binding A

Rtn4: reticulon 4

Ryr3: ryanodine receptor 3

Sca1: ataxin 1

Sca10: ataxin 10

Scfd1: sec1 family domain containing 1

Scgb3a2: secretoglobin, family 3A, member 2

Scn1a: sodium channel, voltage-gated, type I, alpha subunit

Scn2a1: sodium channel, voltage-gated, type II, alpha subunit

Scp2: sterol carrier protein 2

Sdad1: SDA1 domain containing 1

Sdc2: syndecan 2

Sdcbp: syndecan binding protein (syntenin)

Sdfr1: neuroplastin

Sdha: succinate dehydrogenase complex, subunit A, flavoprotein (Fp)

Sec11l3: SEC11 homolog C (S. cerevisiae)

Sec31l1: SEC31 homolog A (S. cerevisiae)

Sectm1: secreted and transmembrane 1

Sema6c: sema domain, transmembrane domain (TM), and cytoplasmic domain, (semaphorin) 6C

Sephs1: selenophosphate synthetase 1

Serinc3: serine incorporator 3

Serpinb3: serpin peptidase inhibitor, clade B (ovalbumin), member 3

Serpine2: serpin peptidase inhibitor, clade E (nexin, plasminogen activator inhibitor type 1), member 2

Sez6: seizure related 6 homolog (mouse)

Sf3b1: splicing factor 3b, subunit 1, 155 kDa

Sfpq: splicing factor proline/glutamine-rich (polypyrimidine tract binding protein associated)

Sfrp4: secreted frizzled-related protein 4

Sfrs10: transformer 2 beta homolog (Drosophila)

Sfrs8: splicing factor, arginine/serine-rich 8 (suppressor-of-white-apricot homolog, Drosophila)

Sfrs9: splicing factor, arginine/serine-rich 9

Sftpb: surfactant protein B

Sfxn3: sideroflexin 3

Sfxn5: sideroflexin 5

Sgca: sarcoglycan, alpha (50 kDa dystrophin-associated glycoprotein)

Sgtb: small glutamine-rich tetratricopeptide repeat (TPR)-containing, beta

Sh2d4a: SH2 domain containing 4A

Sh3bp4: SH3-domain binding protein 4

Sh3bp5: SH3-domain binding protein 5 (BTK-associated)

Sh3gl3: SH3-domain GRB2-like 3

Sh3glb2: SH3-domain GRB2-like endophilin B2

Shank1: SH3 and multiple ankyrin repeat domains 1

Shank2: SH3 and multiple ankyrin repeat domains 2

Shc1: SHC (Src homology 2 domain containing) transforming protein 1

Shh: sonic hedgehog homolog (Drosophila)

Shoc2: soc-2 suppressor of clear homolog (C. elegans)

Siat7A: ST6 (alpha-N-acetyl-neuraminyl-2,3-beta-galactosyl-1,3)-N-acetylgalactosaminide alpha-2,6-sialyltransferase 1

Sipa1: signal-induced proliferation-associated 1

Sipa1l2: signal-induced proliferation-associated 1 like 2

Sipa1l3: signal-induced proliferation-associated 1 like 3

Sirpa: signal-regulatory protein alpha

Sirt2: sirtuin (silent mating type information regulation 2 homolog) 2 (S. cerevisiae)

Sirt5: sirtuin (silent mating type information regulation 2 homolog) 5 (S. cerevisiae)

Slc11a2: solute carrier family 11 (proton-coupled divalent metal ion transporters), member 2

Slc12a1: solute carrier family 12 (sodium/potassium/chloride transporters), member 1

Slc12a5: solute carrier family 12 (potassium-chloride transporter), member 5

Slco3a1: solute carrier organic anion transporter family, member 3A1

Slit1: slit homolog 1 (Drosophila)

Slit2: slit homolog 2 (Drosophila)

Slit3: slit homolog 3 (Drosophila)

Slk: STE20-like kinase (yeast)

Slu7: SLU7 splicing factor homolog (S. cerevisiae)

Smad1: SMAD family member 1

Smarca2: SWI/SNF related, matrix associated, actin dependent regulator of chromatin, subfamily a, member 2

Smc1l1: structural maintenance of chromosomes 1A

Smo: smoothened homolog (Drosophila)

Smoc1: SPARC related modular calcium binding 1

Smu1: smu-1 suppressor of mec-8 and unc-52 homolog (C. elegans)

Sn: sialic acid binding Ig-like lectin 1, sialoadhesin

Snai1: snail homolog 1 (Drosophila)

Snai2: snail homolog 2 (Drosophila)

Snap23: synaptosomal-associated protein, 23 kDa

Snap25: synaptosomal-associated protein, 25 kDa

Snap91: synaptosomal-associated protein, 91 kDa homolog (mouse)

Snca: synuclein, alpha (non A4 component of amyloid precursor)

Sncb: synuclein, beta

Snd1: staphylococcal nuclease and tudor domain containing 1

Snph: syntaphilin

Snrk: SNF related kinase

Snx17: sorting nexin 17

Snx25: sorting nexin 25

Snx3: sorting nexin 3

Soat1: sterol O-acyltransferase 1

Socs1: suppressor of cytokine signaling 1

SOD1: superoxide dismutase 1, soluble

Sod2: superoxide dismutase 2, mitochondrial

Sord: sorbitol dehydrogenase

Sox10: SRY (sex determining region Y)-box 10

Sp2: Sp2 transcription factor

Sparc: secreted protein, acidic, cysteine-rich (osteonectin)

Spata20: spermatogenesis associated 20

Spint1: serine peptidase inhibitor, Kunitz type 1

Spp1: secreted phosphoprotein 1

Spsb4: splA/ryanodine receptor domain and SOCS box containing 4

Sqle: squalene epoxidase

Src: v-src sarcoma (Schmidt-Ruppin A-2) viral oncogene homolog (avian)

Srd5a2: steroid-5-alpha-reductase, alpha polypeptide 2

Srebf1: sterol regulatory element binding transcription factor 1

Srprb: signal recognition particle receptor, B subunit

Ssb: Sjogren syndrome antigen B (autoantigen La)

Ssr4: signal sequence receptor, delta (translocon-associated protein delta)

Ssrp1: structure specific recognition protein 1

Sstr2: somatostatin receptor 2

Ssx2ip: synovial sarcoma, X breakpoint 2 interacting protein

St14: suppression of tumorigenicity 14 (colon carcinoma)

St18: suppression of tumorigenicity 18 (breast carcinoma) (zinc finger protein)

St3gal1: ST3 beta-galactoside alpha-2,3-sialyltransferase 1

St6gal2: ST6 beta-galactosamide alpha-2,6-sialyltransferase 2

St7: suppression of tumorigenicity 7

St7l: suppression of tumorigenicity 7 like

Star: steroidogenic acute regulatory protein

Stard3nl: STARD3 N-terminal like

Stat1: signal transducer and activator of transcription 1, 91 kDa

Stat3: signal transducer and activator of transcription 3 (acute-phase response factor)

Stau1: staufen, RNA binding protein, homolog 1 (Drosophila)

Stch: heat shock protein 70 kDa family, member 13

Ste: sulfotransferase family 1E, estrogen-preferring, member 1

Stim2: stromal interaction molecule 2

Stip1: stress-induced-phosphoprotein 1

Stk10: serine/threonine kinase 10

Stk11: serine/threonine kinase 11

Stmn1: stathmin 1

Stmn2: stathmin-like 2

Stmn3: stathmin-like 3

Stmn4: stathmin-like 4

Stnl: eukaryotic translation elongation factor 1 alpha 2

Stom: stomatin

Strbp: spermatid perinuclear RNA binding protein

Strn: striatin, calmodulin binding protein

Stx12: syntaxin 12

Stx1a: syntaxin 1A (brain)

Stx4a: syntaxin 4

Stx5a: syntaxin 5

Stx6: syntaxin 6

Stx8: syntaxin 8

Stxbp3: syntaxin binding protein 3

Stxbp5: syntaxin binding protein 5 (tomosyn)

Suclg1: succinate-CoA ligase, alpha subunit

Sult1a1: sulfotransferase family, cytosolic, 1A, phenol-preferring, member 1

Sult1c1: sulfotransferase family, cytosolic, 1C, member 2

Sult1c2: sulfotransferase family, cytosolic, 1C, member 2

Sult1e1: sulfotransferase family 1E, estrogen-preferring, member 1

Sult4a1: sulfotransferase family 4A, member 1

Supv3l1: suppressor of var1, 3-like 1 (S. cerevisiae)

Surf6: surfeit 6

Suv420h2: suppressor of variegation 4-20 homolog 2 (Drosophila)

Sv2a: synaptic vesicle glycoprotein 2A

Sv2b: synaptic vesicle glycoprotein 2B

Sycp1: synaptonemal complex protein 1

Sycp2: synaptonemal complex protein 2

Syn1: synapsin I

Syn2: synapsin II

Syn3: synapsin III

Syngap1: synaptic Ras GTPase activating protein 1 homolog (rat)

Synj1: synaptojanin 1

Synj2: synaptojanin 2

Synj2bp: synaptojanin 2 binding protein

Synpo: synaptopodin

Sypl: synaptophysin-like 1

Syt11: synaptotagmin XI

Syt12: synaptotagmin XII

Syt5: synaptotagmin V

Syt6: synaptotagmin VI

Syt8: synaptotagmin VIII

Tacc1: transforming, acidic coiled-coil containing protein 1

Tacc2: transforming, acidic coiled-coil containing protein 2

Tacr1: tachykinin receptor 1

Taf1c: TATA box binding protein (TBP)-associated factor, RNA polymerase I, C, 110 kDa

Taf9l: TAF9B RNA polymerase II, TATA box binding protein (TBP)-associated factor, 31 kDa

Tagln: transgelin

Tagln3: transgelin 3

Taldo1: transaldolase 1

Taok1: TAO kinase 1

Tapbp: TAP binding protein (tapasin)

Tars: threonyl-tRNA synthetase

Tas2r41: taste receptor, type 2, member 41

Tat: tyrosine aminotransferase

Tax1bp1: Tax1 (human T-cell leukemia virus type I) binding protein 1

Tbc1d10b: TBC1 domain family, member 10B

Tbca: tubulin folding cofactor A

Tbx2: T-box 2

Tcirg1: T-cell, immune regulator 1, ATPase, H+ transporting, lysosomal V0 subunit A3

Tcn2: transcobalamin II; macrocytic anemia

Tcp1: t-complex 1

Tcra: T cell receptor alpha locus

Tdg: thymine-DNA glycosylase

Tdrd7: tudor domain containing 7

Tead1: TEA domain family member 1 (SV40 transcriptional enhancer factor)

Tegt: transmembrane BAX inhibitor motif containing 6

Tg: thyroglobulin

Tgfb1: transforming growth factor, beta 1

Tgfbr3: transforming growth factor, beta receptor III

Tgm1: transglutaminase 1 (K polypeptide epidermal type I, protein-glutamine-gamma-glutamyltransferase)

Tgm2: transglutaminase 2 (C polypeptide, protein-glutamine-gamma-glutamyltransferase)

Thbd: thrombomodulin

Thbs4: thrombospondin 4

Thpo: thrombopoietin

Thra: thyroid hormone receptor, alpha (erythroblastic leukemia viral (v-erb-a) oncogene homolog, avian)

Thrap3: thyroid hormone receptor associated protein 3

Thrb: thyroid hormone receptor, beta (erythroblastic leukemia viral (v-erb-a) oncogene homolog 2, avian)

Thy1: Thy-1 cell surface antigen ¡list-item¿¡label/¿

Tigd3: tigger transposable element derived 3

Timm44: translocase of inner mitochondrial membrane 44 homolog (yeast)

Timm8a: translocase of inner mitochondrial membrane 8 homolog A (yeast)

Tinag: tubulointerstitial nephritis antigen

Tjp1: tight junction protein 1 (zona occludens 1)

Tjp2: tight junction protein 2 (zona occludens 2)

Tkt: transketolase

Tle3: transducin-like enhancer of split 3 (E(sp1) homolog, Drosophila)

Tlr3: toll-like receptor 3

Tlr4: toll-like receptor 4

Tlr5: toll-like receptor 5

Tlr6: toll-like receptor 6

Tlr9: toll-like receptor 9

Tm4sf8: tetraspanin 3

Tm9sf2: transmembrane 9 superfamily member 2

Tm9sf3: transmembrane 9 superfamily member 3

Tmco1: transmembrane and coiled-coil domains 1

Tmeff1: transmembrane protein with EGF-like and two follistatin-like domains 1

Tmem27: transmembrane protein 27

Tmf1: TATA element modulatory factor 1

Tmpo: thymopoietin

Tmsb10: thymosin beta 10

Tnfaip1: tumor necrosis factor, alpha-induced protein 1 (endothelial)

Tnni1: troponin I type 1 (skeletal, slow)

Tnni2: troponin I type 2 (skeletal, fast)

Tnnt3: troponin T type 3 (skeletal, fast)

Tob1: transducer of ERBB2, 1

Tob2: transducer of ERBB2, 2

Tom1: target of myb1 (chicken)

Tor3a: torsin family 3, member A

Tpbg: trophoblast glycoprotein

Tpd52l2: tumor protein D52-like 2

Tph2: tryptophan hydroxylase 2

Tpm3: tropomyosin 3

Tpo: thyroid peroxidase

Tpst2: tyrosylprotein sulfotransferase 2

Tpt1: tumor protein, translationally-controlled 1

Tr4: nuclear receptor subfamily 2, group C, member 2

Traf3ip1: TNF receptor-associated factor 3 interacting protein 1

Trak2: trafficking protein, kinesin binding 2

Trap1: TNF receptor-associated protein 1

Trib3: tribbles homolog 3 (Drosophila)

Trim13: tripartite motif-containing 13

Trim54: tripartite motif-containing 54

Trip10: thyroid hormone receptor interactor 10

Trpc2: transient receptor potential cation channel, subfamily C, member 2 (pseudogene)

Trpc4: transient receptor potential cation channel, subfamily C, member 4

Trpc5: transient receptor potential cation channel, subfamily C, member 5

Trpc7: transient receptor potential cation channel, subfamily C, member 7

Trpv1: transient receptor potential cation channel, subfamily V, member 1

Trpv4: transient receptor potential cation channel, subfamily V, member 4

Tsc1: tuberous sclerosis 1

Tsc2: tuberous sclerosis 2

Tsg101: tumor susceptibility gene 101

Tsga10: testis specific, 10

Tsga10ip: testis specific, 10 interacting protein

Tshr: thyroid stimulating hormone receptor

Tsn: translin

Tsnax: translin-associated factor X

Tst: thiosulfate sulfurtransferase (rhodanese)

Ttc1: tetratricopeptide repeat domain 1

Ttn: titin

Tub: tubby homolog (mouse)

Tuba1a: tubulin, alpha 1a

Tubb2b: tubulin, beta 2B

Tubb2c: tubulin, beta 2C

Tubb3: tubulin, beta 3

Tusc3: tumor suppressor candidate 3

Txn: thioredoxin

Txn2: thioredoxin 2

Txndc4: endoplasmic reticulum protein 44

Txnip: thioredoxin interacting protein

Txnl2: glutaredoxin 3

Txnrd1: thioredoxin reductase 1

Txnrd2: thioredoxin reductase 2

Ubc: ubiquitin C

Ube2e2: ubiquitin-conjugating enzyme E2E 2 (UBC4/5 homolog, yeast)

Ubl3: ubiquitin-like 3

Ubqln1: ubiquilin 1

Ubxd3: UBX domain protein 10

Uchl1: ubiquitin carboxyl-terminal esterase L1 (ubiquitin thiolesterase)

Ucp1: uncoupling protein 1 (mitochondrial, proton carrier)

Ucp2: uncoupling protein 2 (mitochondrial, proton carrier)

Ugt1a1: UDP glucuronosyltransferase 1 family, polypeptide A1

Umod: uromodulin

Unc13a: unc-13 homolog A (C. elegans)

Unc13b: unc-13 homolog B (C. elegans)

Unc13c: unc-13 homolog C (C. elegans)

Unc5b: unc-5 homolog B (C. elegans)

Uqcrc2: ubiquinol-cytochrome c reductase core protein II

Uqcrfs1: ubiquinol-cytochrome c reductase, Rieske iron-sulfur polypeptide 1

Uso1: USO1 homolog, vesicle docking protein (yeast)

Usp11: ubiquitin specific peptidase 11

Vamp1: vesicle-associated membrane protein 1 (synaptobrevin 1)

Vamp2: vesicle-associated membrane protein 2 (synaptobrevin 2)

Vamp3: vesicle-associated membrane protein 3 (cellubrevin)

Vapa: VAMP (vesicle-associated membrane protein)-associated protein A, 33 kDa

Vapb: VAMP (vesicle-associated membrane protein)-associated protein B and C

VCAN: versican

Vcan: versican

Vcp: valosin-containing protein

Vcpip1: valosin containing protein (p97)/p47 complex interacting protein 1

Vdac1: voltage-dependent anion channel 1

Vdac2: voltage-dependent anion channel 2

Vegfa: vascular endothelial growth factor A

Vgcnl1: sodium leak channel, non-selective

Vgf: VGF nerve growth factor inducible

Vipr2: vasoactive intestinal peptide receptor 2

Vpreb1: pre-B lymphocyte 1

Vps33a: vacuolar protein sorting 33 homolog A (S. cerevisiae)

Vps33b: vacuolar protein sorting 33 homolog B (yeast)

Vps4a: vacuolar protein sorting 4 homolog A (S. cerevisiae)

Vsnl1: visinin-like 1

Vtn: vitronectin

Wars: tryptophanyl-tRNA synthetase

Wbp2: WW domain binding protein 2

Wdr10: intraflagellar transport 122 homolog (Chlamydomonas)

Wdr44: WD repeat domain 44

Wdr7: WD repeat domain 7

Wfs1: Wolfram syndrome 1 (wolframin)

Wif1: WNT inhibitory factor 1

Wipf1: WAS/WASL interacting protein family, member 1

Wnk4: WNK lysine deficient protein kinase 4

Wnt5a: wingless-type MMTV integration site family, member 5A

Wnt7a: wingless-type MMTV integration site family, member 7A

Xkr6: XK, Kell blood group complex subunit-related family, member 6

Xpnpep2: X-prolyl aminopeptidase (aminopeptidase P) 2, membrane-bound

Xpo1: exportin 1 (CRM1 homolog, yeast)

Xpo6: exportin 6

Xrcc1: X-ray repair complementing defective repair in Chinese hamster cells 1

Xrcc5: X-ray repair complementing defective repair in Chinese hamster cells 5

Xylt1: xylosyltransferase I

Yars2: tyrosyl-tRNA synthetase 2, mitochondrial

Yes1: v-yes-1 Yamaguchi sarcoma viral oncogene homolog 1

Ykt6: YKT6 v-SNARE homolog (S. cerevisiae)

Ywhab: tyrosine 3-monooxygenase/tryptophan 5-monooxygenase activation protein, beta polypeptide

Yy1: YY1 transcription factor

Znf382: zinc finger protein 382

Zranb1: zinc finger, RAN-binding domain containing 1

Zwint: ZW10 interactor.

B.

Lipid raft-derived extracted proteins from Alzheimer's disease (3xTgAD) mouse 16-month-old cortical tissue. Specific proteins isolated from 3xTgAD mouse cortex were identified with multidimensional protein identification technology (MudPIT) LC MS/MS. Each protein was identified in at least two out of three experimental replicate animals and from at least two isolated peptides per protein. The following are the protein symbol and its corresponding definition.

Abca1: ATP-binding cassette, sub-family A (ABC1), member 1

ABCA7: ATP-binding cassette, sub-family A (ABC1), member 7

Abcb4: ATP-binding cassette, sub-family B (MDR/TAP), member 4

Abcc1: ATP-binding cassette, sub-family C (CFTR/MRP), member 1

Abcc2: ATP-binding cassette, sub-family C (CFTR/MRP), member 2

Abcc4: ATP-binding cassette, sub-family C (CFTR/MRP), member 4

Abi1: abl-interactor 1

Acadl: acyl-Coenzyme A dehydrogenase, long chain

Acat1: acetyl-Coenzyme A acetyltransferase 1

Acin1: apoptotic chromatin condensation inducer 1

Acmsd: aminocarboxymuconate semialdehyde decarboxylase

Acp2: acid phosphatase 2, lysosomal

Acta1: actin, alpha 1, skeletal muscle

Actb: actin, beta

Actn4: actinin, alpha 4

Acvr1: activin A receptor, type I

Adam2: ADAM metallopeptidase domain 2

Adam6: ADAM metallopeptidase domain 6 (pseudogene)

Adcy1: adenylate cyclase 1 (brain)

Adcy5: adenylate cyclase 5

Adcy8: adenylate cyclase 8 (brain)

Adcyap1: adenylate cyclase activating polypeptide 1 (pituitary)

Adcyap1r1: adenylate cyclase activating polypeptide 1 (pituitary) receptor type I

Add1: adducin 1 (alpha)

Add2: adducin 2 (beta)

Adrbk1: adrenergic, beta, receptor kinase 1

Aes: amino-terminal enhancer of split

Agpat1: 1-acylglycerol-3-phosphate O-acyltransferase 1 (lysophosphatidic acid acyltransferase, alpha)

Agpat4: 1-acylglycerol-3-phosphate O-acyltransferase 4 (lysophosphatidic acid acyltransferase, delta)

Agrn: agrin

Ahi1: Abelson helper integration site 1

Ahr: aryl hydrocarbon receptor

Ahrr: aryl-hydrocarbon receptor repressor

Ak3: adenylate kinase 3

Akap12: A kinase (PRKA) anchor protein 12

Akap3: A kinase (PRKA) anchor protein 3

Akap4: A kinase (PRKA) anchor protein 4

Akap9: A kinase (PRKA) anchor protein (yotiao) 9

Alad: aminolevulinate, delta-, dehydratase

Aldh1a3: aldehyde dehydrogenase 1 family, member A3

Alox5: arachidonate 5-lipoxygenase

Ampd1: adenosine monophosphate deaminase 1 (isoform M)

Anxa3: annexin A3

Anxa6: annexin A6

Apex2: APEX nuclease (apurinic/apyrimidinic endonuclease) 2

Apob: apolipoprotein B (including Ag(x) antigen)

Apod: apolipoprotein D

App: amyloid beta (A4) precursor protein

Aps: kallikrein-related peptidase 3

Aqp3: aquaporin 3 (Gill blood group)

Aqp4: aquaporin 4

Aqp8: aquaporin 8

Arf1: ADP-ribosylation factor 1

Arf4: ADP-ribosylation factor 4

Arf6: ADP-ribosylation factor 6

Arfip1: ADP-ribosylation factor interacting protein 1

Arhgap20: Rho GTPase activating protein 20

Arhgap8: Rho GTPase activating protein 8

Arhgdia: Rho GDP dissociation inhibitor (GDI) alpha

Arhgef11: Rho guanine nucleotide exchange factor (GEF) 11

Arhgef12: Rho guanine nucleotide exchange factor (GEF) 12

Arhgef6: Rac/Cdc42 guanine nucleotide exchange factor (GEF) 6

Arnt: aryl hydrocarbon receptor nuclear translocator

Arntl: aryl hydrocarbon receptor nuclear translocator-like

Arpp19: cAMP-regulated phosphoprotein, 19 kDa

Ascc1: activating signal cointegrator 1 complex subunit 1

Asz1: ankyrin repeat, SAM and basic leucine zipper domain containing 1

Atcay: ataxia, cerebellar, Cayman type

Atf3: activating transcription factor 3

Atm: ataxia telangiectasia mutated

Atp1a1: ATPase, Na+/K+ transporting, alpha 1 polypeptide

Atp1a4: ATPase, Na+/K+ transporting, alpha 4 polypeptide

Atp1b1: ATPase, Na+/K+ transporting, beta 1 polypeptide

ATP2B1: ATPase, Ca++ transporting, plasma membrane 1

Atp2b1: ATPase, Ca++ transporting, plasma membrane 1

Atp2b2: ATPase, Ca++ transporting, plasma membrane 2

Atp5a1: ATP synthase, H+ transporting, mitochondrial F1 complex, alpha subunit 1, cardiac muscle

Atp5b: ATP synthase, H+ transporting, mitochondrial F1 complex, beta polypeptide

Atp5f1: ATP synthase, H+ transporting, mitochondrial F0 complex, subunit B1

Atp5h: ATP synthase, H+ transporting, mitochondrial F0 complex, subunit d

Atp5i: ATP synthase, H+ transporting, mitochondrial F0 complex, subunit E

Atp5j: ATP synthase, H+ transporting, mitochondrial F0 complex, subunit F6

Atp6b2: ATPase, H+ transporting, lysosomal 56/58 kDa, V1 subunit B2

Atp6l: ATPase, H+ transporting, lysosomal 16 kDa, V0 subunit c

Atp6v0a1: ATPase, H+ transporting, lysosomal V0 subunit a1

ATPBD1C: GPN-loop GTPase 3

Atxn3: ataxin 3

Avil: advillin

B3gat1: beta-1,3-glucuronyltransferase 1 (glucuronosyltransferase P)

Bace1: beta-site APP-cleaving enzyme 1

Basp1: brain abundant, membrane attached signal protein 1

Bat2: HLA-B associated transcript 2

Bat5: HLA-B associated transcript 5

Bax: BCL2-associated X protein

Bcl10: B-cell CLL/lymphoma 10

Begain: brain-enriched guanylate kinase-associated homolog (rat)

Bmp6: bone morphogenetic protein 6

Bnip1: BCL2/adenovirus E1B 19 kDa interacting protein 1

Bnip3: BCL2/adenovirus E1B 19 kDa interacting protein 3

Bpnt1: 3′(2′), 5′-bisphosphate nucleotidase 1

Brd2: bromodomain containing 2

Brd8: bromodomain containing 8

Bst1: bone marrow stromal cell antigen 1

Btg2: BTG family, member 2

Bzrap1: benzodiazepine receptor (peripheral) associated protein 1

c3orf6: coiled-coil domain containing 50

C4a: complement component 4A (Rodgers blood group)

c8b: complement component 8, beta polypeptide

Cabc1: chaperone, ABC1 activity of bc1 complex homolog (S. pombe)

Cabin1: calcineurin binding protein 1

Cacna1g: calcium channel, voltage-dependent, T type, alpha 1G subunit

Cacna2d1: calcium channel, voltage-dependent, alpha 2/delta subunit 1

Cacna2d2: calcium channel, voltage-dependent, alpha 2/delta subunit 2

Cacna2d3: calcium channel, voltage-dependent, alpha 2/delta subunit 3

Cacnb2: calcium channel, voltage-dependent, beta 2 subunit

Calb1: calbindin 1, 28 kDa

Calb2: calbindin 2

Cald1: caldesmon 1

calm2: calmodulin 2 (phosphorylase kinase, delta)

Calr: calreticulin

Camk2g: calcium/calmodulin-dependent protein kinase II gamma

Camkk1: calcium/calmodulin-dependent protein kinase kinase 1, alpha

Camkv: CaM kinase-like vesicle-associated

Canx: calnexin

Cap1: CAP, adenylate cyclase-associated protein 1 (yeast)

Capn1: calpain 1, (mu/l) large subunit

Capn5: calpain 5

Capn6: calpain 6

Capzb: capping protein (actin filament) muscle Z-line, beta

Card9: caspase recruitment domain family, member 9

Carhsp1: calcium regulated heat stable protein 1, 24 kDa

Caskin1: CASK interacting protein 1

Casp7: caspase 7, apoptosis-related cysteine peptidase

Cast: calpastatin

Cbp: opsin 1 (cone pigments), long-wave-sensitive

Cbx3: chromobox homolog 3 (HP1 gamma homolog, Drosophila)

Ccnd2: cyclin D2

Ccs: copper chaperone for superoxide dismutase

Cct2: chaperonin containing TCP1, subunit 2 (beta)

Cd2ap: CD2-associated protein

Cd36: CD36 molecule (thrombospondin receptor)

Cd86: CD86 molecule

Cdc25b: cell division cycle 25 homolog B (S. pombe)

Cdc42: cell division cycle 42 (GTP binding protein, 25 kDa)

Cdc5l: CDC5 cell division cycle 5-like (S. pombe)

Cdh1: cadherin 1, type 1, E-cadherin (epithelial)

Cdh10: cadherin 10, type 2 (T2-cadherin)

Cdh13: cadherin 13, H-cadherin (heart)

Cdh2: cadherin 2, type 1, N-cadherin (neuronal)

Cdk5rap2: CDK5 regulatory subunit associated protein 2

Cdkn1b: cyclin-dependent kinase inhibitor 1B (p27, Kip1)

Cds1: CDP-diacylglycerol synthase (phosphatidate cytidylyltransferase) 1

Cdv1: intraflagellar transport 81 homolog (Chlamydomonas)

Cebp: CCAAT/enhancer binding protein (C/EBP), alpha

Cend1: cell cycle exit and neuronal differentiation 1

Cenpc1: centromere protein C 1

Cenpi: centromere protein I

Centa1: ArfGAP with dual PH domains 1

Ces1: carboxylesterase 1 (monocyte/macrophage serine esterase 1)

Cetn2: centrin, EF-hand protein, 2

Cfd: complement factor D (adipsin)

Cfl1: cofilin 1 (nonmuscle)

Cftr: cystic fibrosis transmembrane conductance regulator (ATP-binding cassette sub-family C, member 7)

Chgb: chromogranin B (secretogranin 1)

Chka: choline kinase alpha

Chm: choroideremia (Rab escort protein 1)

Chst10: carbohydrate sulfotransferase 10

Chx10: visual system homeobox 2

Cktsf1b1: gremlin 1, cysteine knot superfamily, homolog (Xenopus laevis)

Clcf1: cardiotrophin-like cytokine factor 1

Cldn18: claudin 18

Clic4: chloride intracellular channel 4

Clip3: CAP-GLY domain containing linker protein 3

Clta: clathrin, light chain (Lca)

Cltb: clathrin, light chain (Lcb)

Cltc: clathrin, heavy chain (Hc)

Clu: clusterin

Cnga1: cyclic nucleotide gated channel alpha 1

Cngb1: cyclic nucleotide gated channel beta 1

Cnot4: CCR4-NOT transcription complex, subunit 4

Cnr1: cannabinoid receptor 1 (brain)

Col5a3: collagen, type V, alpha 3

Copb1: coatomer protein complex, subunit beta 1

Cops4: COP9 constitutive photomorphogenic homolog subunit 4 (Arabidopsis)

Coro1a: coronin, actin binding protein, 1A

Cp: ceruloplasmin (ferroxidase)

Cpa2: carboxypeptidase A2 (pancreatic)

Cpt2: carnitine palmitoyltransferase 2

Creb1: cAMP responsive element binding protein 1

Crhbp: corticotropin releasing hormone binding protein

Crip2: cysteine-rich protein 2

Cript: cysteine-rich PDZ-binding protein

Crmp1: collapsin response mediator protein 1

Cry2: cryptochrome 2 (photolyase-like)

Csf1: colony stimulating factor 1 (macrophage)

Csh1: chorionic somatomammotropin hormone 1 (placental lactogen)

Csnk1e: casein kinase 1, epsilon

Csnk1g1: casein kinase 1, gamma 1

Csnk1g3: casein kinase 1, gamma 3

Cspg6: structural maintenance of chromosomes 3

Cst6: cystatin E/M

Cstb: cystatin B (stefin B)

Ctnnb1: catenin (cadherin-associated protein), beta 1, 88 kDa

Cttn: cortactin

Cugbp2: CUG triplet repeat, RNA binding protein 2

Cul5: cullin 5

Cutl1: cut-like homeobox 1

Cxadr: coxsackie virus and adenovirus receptor

Cxcl10: chemokine (C-X-C motif) ligand 10

Cyb5r4: cytochrome b5 reductase 4

Cyln2: CAP-GLY domain containing linker protein 2

Cyp19a1: cytochrome P450, family 19, subfamily A, polypeptide 1

Cyp1a1: cytochrome P450, family 1, subfamily A, polypeptide 1

Cyp4x1: cytochrome P450, family 4, subfamily X, polypeptide 1

Dab2ip: DAB2 interacting protein

Dbn1: drebrin 1

Dctn1: dynactin 1 (p150, glued homolog, Drosophila)

Dctn2: dynactin 2 (p50)

Dctn4: dynactin 4 (p62)

Dcxr: dicarbonyl/L-xylulose reductase

Ddah2: dimethylarginine dimethylaminohydrolase 2

Ddb1: damage-specific DNA binding protein 1, 127 kDa

Ddt: D-dopachrome tautomerase

Ddx1: DEAD (Asp-Glu-Ala-Asp) box polypeptide 1

Ddx19: DEAD (Asp-Glu-Ala-As) box polypeptide 19B

Ddx27: DEAD (Asp-Glu-Ala-Asp) box polypeptide 27

Ddx5: DEAD (Asp-Glu-Ala-Asp) box polypeptide 5

Dedd: death effector domain containing

Degs1: degenerative spermatocyte homolog 1, lipid desaturase (Drosophila)

Des: desmin

Dgkg: diacylglycerol kinase, gamma 90 kDa

Dhcr7: 7-dehydrocholesterol reductase

Dhodh: dihydroorotate dehydrogenase

Dhx40: DEAH (Asp-Glu-Ala-His) box polypeptide 40

Dia1: cytochrome b5 reductase 3

Disc1: disrupted in schizophrenia 1

Dkc1: dyskeratosis congenita 1, dyskerin

Dlat: dihydrolipoamide S-acetyltransferase

Dlc1: deleted in liver cancer 1

Dlgap2: discs, large (Drosophila) homolog-associated protein 2

Dlgap4: discs, large (Drosophila) homolog-associated protein 4

Dll1: delta-like 1 (Drosophila)

Dnah7: dynein, axonemal, heavy chain 7

Dnah9: dynein, axonemal, heavy chain 9

Dnajc5: DnaJ (Hsp40) homolog, subfamily C, member 5

Dnch1: dynein, cytoplasmic 1, heavy chain 1

Dnch2: dynein, cytoplasmic 2, heavy chain 1

Dnm1: dynamin 1

Dnmt1: DNA (cytosine-5-)-methyltransferase 1

Dnmt3a: DNA (cytosine-5-)-methyltransferase 3 alpha

Dntt: deoxynucleotidyltransferase, terminal

Dpp3: dipeptidyl-peptidase 3

Dpp6: dipeptidyl-peptidase 6

Dpyd: dihydropyrimidine dehydrogenase

Drd1ip: calcyon neuron-specific vesicular protein

Drg1: developmentally regulated GTP binding protein 1

Dtnb: dystrobrevin, beta

Dtnbp1: dystrobrevin binding protein 1

Duox1: dual oxidase 1

Dvl1: dishevelled, dsh homolog 1 (Drosophila)

Dyx1c1: dyslexia susceptibility 1 candidate 1

Eaf2: ELL associated factor 2

Echs1: enoyl Coenzyme A hydratase, short chain, 1, mitochondrial

Eef1g: eukaryotic translation elongation factor 1 gamma

Eef2: eukaryotic translation elongation factor 2

Eef2k: eukaryotic elongation factor-2 kinase

Efemp2: EGF-containing fibulin-like extracellular matrix protein 2

Egfr: epidermal growth factor receptor (erythroblastic leukemia viral (v-erb-b) oncogene homolog, avian)

Eif2ak3: eukaryotic translation initiation factor 2-alpha kinase 3

Eif2b1: eukaryotic translation initiation factor 2B, subunit 1 alpha, 26 kDa

Eif2c2: eukaryotic translation initiation factor 2C, 2

Eif2s2: eukaryotic translation initiation factor 2, subunit 2 beta, 38 kDa

eif4a1: eukaryotic translation initiation factor 4A, isoform 1

Elavl3: ELAV (embryonic lethal, abnormal vision, Drosophila)-like 3 (Hu antigen C)

ELK1: ELK1, member of ETS oncogene family

Emd: emerin

Eno2: enolase 2 (gamma, neuronal)

Enpp2: ectonucleotide pyrophosphatase/phosphodiesterase 2

Entpd8: ectonucleoside triphosphate diphosphohydrolase 8

Ephx2: epoxide hydrolase 2, cytoplasmic

Epn1: epsin 1

Erp29: endoplasmic reticulum protein 29

Esd: esterase D/formylglutathione hydrolase

Espn: espin

Esrrb: estrogen-related receptor beta

Etfa: electron-transfer-flavoprotein, alpha polypeptide

Etfb: electron-transfer-flavoprotein, beta polypeptide

Exoc7: exocyst complex component 7

Ezr: ezrin

F5: coagulation factor V (proaccelerin, labile factor)

Fabp1: fatty acid binding protein 1, liver

Fancd2: Fanconi anemia, complementation group D2

Fat: FAT tumor suppressor homolog 1 (Drosophila)

Fat2: FAT tumor suppressor homolog 2 (Drosophila)

Fat3: FAT tumor suppressor homolog 3 (Drosophila)

Fbn1: fibrillin 1

Fdps: farnesyl diphosphate synthase

Fgfr1op2: FGFR1 oncogene partner 2

Filip1: filamin A interacting protein 1

Fkbp1b: FK506 binding protein 1B, 12.6 kDa

Flg: filaggrin

Flot1: flotillin 1

Flot2: flotillin 2

Fosl1: FOS-like antigen 1

Fosl2: FOS-like antigen 2

Fpgt: fucose-1-phosphate guanylyltransferase

Frap1: mechanistic target of rapamycin (serine/threonine kinase)

Freq: frequenin homolog (Drosophila)

Fyn: FYN oncogene related to SRC, FGR, YES

Gaa: glucosidase, alpha; acid

Gabbr1: gamma-aminobutyric acid (GABA) B receptor, 1

Gabra3: gamma-aminobutyric acid (GABA) A receptor, alpha 3

Gabre: gamma-aminobutyric acid (GABA) A receptor, epsilon

Gadd45a: growth arrest and DNA-damage-inducible, alpha

Galc: galactosylceramidase

Galk1: galactokinase 1

Galnt10: UDP-N-acetyl-alpha-D-galactosamine: polypeptide N-acetylgalactosaminyltransferase 10

Gars: glycyl-tRNA synthetase

Gas7: growth arrest-specific 7

Gc: group-specific component (vitamin D binding protein)

Gdi1: GDP dissociation inhibitor 1

Gdi2: GDP dissociation inhibitor 2

Gfap: glial fibrillary acidic protein

Gif: gastric intrinsic factor (vitamin B synthesis)

Gjb2: gap junction protein, beta 2, 26 kDa

Gla: galactosidase, alpha

Gldc: glycine dehydrogenase (decarboxylating)

Glra2: glycine receptor, alpha 2

Glut3: solute carrier family 2 (facilitated glucose transporter), member 3

Gmcl1: germ cell-less homolog 1 (Drosophila)

Gmfb: glia maturation factor, beta

Gna11: guanine nucleotide binding protein (G protein), alpha 11 (Gq class)

Gnai1: guanine nucleotide binding protein (G protein), alpha inhibiting activity polypeptide 1

Gnai2: guanine nucleotide binding protein (G protein), alpha inhibiting activity polypeptide 2

Gnao1: guanine nucleotide binding protein (G protein), alpha activating activity polypeptide O

Gnaq: guanine nucleotide binding protein (G protein), q polypeptide

Gnaz: guanine nucleotide binding protein (G protein), alpha z polypeptide

Gnb2l1: guanine nucleotide binding protein (G protein), beta polypeptide 2-like 1

Gnl3: guanine nucleotide binding protein-like 3 (nucleolar)

Gnpat: glyceronephosphate O-acyltransferase

Gpi: glucose phosphate isomerase

Gpm6a: glycoprotein M6A

Gpr1: G protein-coupled receptor 1

Gpr141: G protein-coupled receptor 141

Gpr56: G protein-coupled receptor 56

Gpsm1: G-protein signaling modulator 1 (AGS3-like, C. elegans)

Gpt2: glutamic pyruvate transaminase (alanine aminotransferase) 2

Grin1: glutamate receptor, ionotropic, N-methyl D-aspartate 1

Grpel1: GrpE-like 1, mitochondrial (E. coli)

Gstm2: glutathione S-transferase mu 2 (muscle)

Gstm3: glutathione S-transferase mu 3 (brain)

Gucy2d: guanylate cyclase 2D, membrane (retina-specific)

Gucy2f: guanylate cyclase 2F, retinal

H1f0: H1 histone family, member 0

H1f4: histone cluster 1, H1e

H2afy: H2A histone family, member Y

Haao: 3-hydroxyanthranilate 3,4-dioxygenase

Hap1: huntingtin-associated protein 1

Hapln3: hyaluronan and proteoglycan link protein 3

Hbld2: iron-sulfur cluster assembly 1 homolog (S. cerevisiae)

Hck: hemopoietic cell kinase

Hcn1: hyperpolarization activated cyclic nucleotide-gated potassium channel 1

Hdac6: histone deacetylase 6

Hdgf: hepatoma-derived growth factor (high-mobility group protein 1-like)

Hdlbp: high density lipoprotein binding protein

Hey1: hairy/enhancer-of-split related with YRPW motif 1

Hgf: hepatocyte growth factor (hepapoietin A; scatter factor)

Hip1r: huntingtin interacting protein 1 related

Hivep1: human immunodeficiency virus type I enhancer binding protein 1

Hk1: hexokinase 1

Hmga2: high mobility group AT-hook 2

Hmgcr: 3-hydroxy-3-methylglutaryl-Coenzyme A reductase

Hmgcs1: 3-hydroxy-3-methylglutaryl-Coenzyme A synthase 1 (soluble)

Hmgn3: high mobility group nucleosomal binding domain 3

Hn1: hematological and neurological expressed 1

Hnf4a: hepatocyte nuclear factor 4, alpha

Hnmt: histamine N-methyltransferase

Hnrnph1: heterogeneous nuclear ribonucleoprotein H1 (H)

Hnrpa1: heterogeneous nuclear ribonucleoprotein A1

Hnrpk: heterogeneous nuclear ribonucleoprotein K

Hnrpu: heterogeneous nuclear ribonucleoprotein U (scaffold attachment factor A)

hook3: hook homolog 3 (Drosophila)

Hps5: Hermansky-Pudlak syndrome 5

Hpse: heparanase

Hras1: v-Ha-ras Harvey rat sarcoma viral oncogene homolog

Hsd11b2: hydroxysteroid (11-beta) dehydrogenase 2

Hsd17B1: hydroxysteroid (17-beta) dehydrogenase 1

Hsf1: heat shock transcription factor 1

Hsp90ab1: heat shock protein 90 kDa alpha (cytosolic), class B member 1

Hspa14: heat shock 70 kDa protein 14

Hspe1: heat shock 10 kDa protein 1 (chaperonin 10)

Htr2c: 5-hydroxytryptamine (serotonin) receptor 2C

Htr3a: 5-hydroxytryptamine (serotonin) receptor 3A

Htr4: 5-hydroxytryptamine (serotonin) receptor 4

Hyou1: hypoxia up-regulated 1

Id2: inhibitor of DNA binding 2, dominant negative helix-loop-helix protein

Idh1: isocitrate dehydrogenase 1 (NADP+), soluble

Igf1r: insulin-like growth factor 1 receptor

Igf2r: insulin-like growth factor 2 receptor

Ikbkap: inhibitor of kappa light polypeptide gene enhancer in B-cells, kinase complex-associated protein

IL1b: interleukin 1, beta

Il1r2: interleukin 1 receptor, type II

Il1rapl1: interleukin 1 receptor accessory protein-like 1

Il6: interleukin 6 (interferon, beta 2)

Ilf3: interleukin enhancer binding factor 3, 90 kDa

Inhbc: inhibin, beta C

Inpp4a: inositol polyphosphate-4-phosphatase, type I, 107 kDa

Inpp4b: inositol polyphosphate-4-phosphatase, type II, 105 kDa

Inpp5d: inositol polyphosphate-5-phosphatase, 145 kDa

Irs1: insulin receptor substrate 1

Irs2: insulin receptor substrate 2

Isg20: interferon stimulated exonuclease gene 20 kDa

Itga6: integrin, alpha 6

Itm2c: integral membrane protein 2C

Itpr2: inositol 1,4,5-triphosphate receptor, type 2

Itpr3: inositol 1,4,5-triphosphate receptor, type 3

Ivl: involucrin

Jag1: jagged 1 (Alagille syndrome)

Jak1: Janus kinase 1

Jak2: Janus kinase 2

Junb: jun B proto-oncogene

Kalrn: kalirin, RhoGEF kinase

Katna1: katanin p60 (ATPase-containing) subunit A 1

Kcnh1: potassium voltage-gated channel, subfamily H (eag-related), member 1

Kcnh2: potassium voltage-gated channel, subfamily H (eag-related), member 2

Kcnk2: potassium channel, subfamily K, member 2

Kcns1: potassium voltage-gated channel, delayed-rectifier, subfamily S, member 1

Kcns3: potassium voltage-gated channel, delayed-rectifier, subfamily S, member 3

Kcnt1: potassium channel, subfamily T, member 1

Kif5a: kinesin family member 5A

Klc1: kinesin light chain 1

Klhl12: kelch-like 12 (Drosophila)

Kpnb1: karyopherin (importin) beta 1

Kras: v-Ki-ras2 Kirsten rat sarcoma viral oncogene homolog

Lama5: laminin, alpha 5

Lancl1: LanC lantibiotic synthetase component C-like 1 (bacterial)

Lars: leucyl-tRNA synthetase

Lbp: lipopolysaccharide binding protein

Lcmt1: leucine carboxyl methyltransferase 1

Letm1: leucine zipper-EF-hand containing transmembrane protein 1

Lgi1: leucine-rich, glioma inactivated 1

Lgr7: relaxin/insulin-like family peptide receptor 1

Lhfpl4: lipoma HMGIC fusion partner-like 4

Lhx3: LIM homeobox 3

Lifr: leukemia inhibitory factor receptor alpha

Lin10: chromosome 16 open reading frame 70

LMO7: LIM domain 7

Lphn1: latrophilin 1

Lphn2: latrophilin 2

Lpin1: lipin 1

Lrpap1: low density lipoprotein receptor-related protein associated protein 1

Lsamp: limbic system-associated membrane protein

Ltbp1: latent transforming growth factor beta binding protein 1

Luzp1: leucine zipper protein 1

Ly6g5b: lymphocyte antigen 6 complex, locus G5B

Lyar: Ly1 antibody reactive homolog (mouse)

LYL1: lymphoblastic leukemia derived sequence 1

Lyst: lysosomal trafficking regulator

Lzic: leucine zipper and CTNNBIP1 domain containing

M6pr: mannose-6-phosphate receptor (cation dependent)

Magi3: membrane associated guanylate kinase, WW and PDZ domain containing 3

Maoa: monoamine oxidase A

Map1lc3a: microtubule-associated protein 1 light chain 3 alpha

Map2: microtubule-associated protein 2

Map3k7ip2: mitogen-activated protein kinase kinase kinase 7 interacting protein 2

Map4: microtubule-associated protein 4

Mapk1: mitogen-activated protein kinase 1

Mapkapk2: mitogen-activated protein kinase-activated protein kinase 2

Mark1: MAP/microtubule affinity-regulating kinase 1

Mark3: MAP/microtubule affinity-regulating kinase 3

Matr3: matrin 3

Mcm7: minichromosome maintenance complex component 7

Mdga2: MAM domain containing glycosylphosphatidylinositol anchor 2

Mdh1: malate dehydrogenase 1, NAD (soluble)

Mecp2: methyl CpG binding protein 2 (Rett syndrome)

Mfap3: microfibrillar-associated protein 3

Mgat1: mannosyl (alpha-1,3-)-glycoprotein beta-1,2-N-acetylglucosaminyltransferase

Mgat5: mannosyl (alpha-1,6-)-glycoprotein beta-1,6-N-acetyl-glucosaminyltransferase

Mid1: midline 1 (Opitz/BBB syndrome)

Mkln1: muskelin 1, intracellular mediator containing kelch motifs

Mkrn2: makorin ring finger protein 2

Mlp: MARCKS-like 1

Mmp10: matrix metallopeptidase 10 (stromelysin 2)

Mnat1: ménage à trois homolog 1, cyclin H assembly factor (Xenopus laevis)

Mpdz: multiple PDZ domain protein

Mpi: mannose phosphate isomerase

Mpo: myeloperoxidase

mpp7: membrane protein, palmitoylated 7 (MAGUK p55 subfamily member 7)

mre11: MRE11 meiotic recombination 11 homolog A (S. cerevisiae)

Mrpl38: mitochondrial ribosomal protein L38

Mrpl9: mitochondrial ribosomal protein L9

Mrps9: mitochondrial ribosomal protein S9

Msn: moesin

Mtap: methylthioadenosine phosphorylase

Mtdh: metadherin

Mtmr3: myotubularin-related protein 3

Mtr: 5-methyltetrahydrofolate-homocysteine methyltransferase

Mtus1: microtubule-associated tumor suppressor 1

Mx1: myxovirus (influenza virus) resistance 1, interferon-inducible protein p78 (mouse)

Mybpc1: myosin binding protein C, slow type

myc: v-myc myelocytomatosis viral oncogene homolog (avian)

Mycbpap: MYCBP associated protein

Myh10: myosin, heavy chain 10, nonmuscle

Myh6: myosin, heavy chain 6, cardiac muscle, alpha

Myh9: myosin, heavy chain 9, nonmuscle

Myo1a: myosin IA

Myo1e: myosin IE

Myo5a: myosin VA (heavy chain 12, myoxin)

Myo5b: myosin VB

Myo7a: myosin VIIA

Myo9a: myosin IXA

Myom1: myomesin 1, 185 kDa

Nab1: NGFI-A binding protein 1 (EGR1 binding protein 1)

Nab2: NGFI-A binding protein 2 (EGR1 binding protein 2)

Naca: nascent polypeptide-associated complex alpha subunit

Naglu: N-acetylglucosaminidase, alpha-

Nap1l3: nucleosome assembly protein 1-like 3

Napepld: N-acyl phosphatidylethanolamine phospholipase D

Nasp: nuclear autoantigenic sperm protein (histone-binding)

Ncam1: neural cell adhesion molecule 1

Ncam2: neural cell adhesion molecule 2

Ncdn: neurochondrin

Ncl: nucleolin

Ncstn: nicastrin

Ndel1: nudE nuclear distribution gene E homolog (A. nidulans)-like 1

Ndufa9: NADH dehydrogenase (ubiquinone) 1 alpha subcomplex, 9, 39 kDa

Ndufc2: NADH dehydrogenase (ubiquinone) 1, subcomplex unknown, 2, 14.5 kDa

Ndufs1: NADH dehydrogenase (ubiquinone) Fe-S protein 1, 75 kDa (NADH-coenzyme Q reductase)

Ndufs6: NADH dehydrogenase (ubiquinone) Fe-S protein 6, 13 kDa (NADH-coenzyme Q reductase)

Ndufs7: NADH dehydrogenase (ubiquinone) Fe-S protein 7, 20 kDa (NADH-coenzyme Q reductase)

Nedd4: neural precursor cell expressed, developmentally down-regulated 4

Nef3: neurofilament, medium polypeptide

Nefh: neurofilament, heavy polypeptide

Negr1: neuronal growth regulator 1

Nell1: NEL-like 1 (chicken)

Neo1: neogenin homolog 1 (chicken)

Nes: nestin

Nexn: nexilin (F actin binding protein)

Nf2: neurofibromin 2 (merlin)

Nfix: nuclear factor I/X (CCAAT-binding transcription factor)

Nfkb1: nuclear factor of kappa light polypeptide gene enhancer in B-cells 1

Ninj1: ninjurin 1

Nlgn2: neuroligin 2

Nlgn3: neuroligin 3

Nme2: non-metastatic cells 2, protein (NM23B) expressed in

Nolc1: nucleolar and coiled-body phosphoprotein 1

Nos1: nitric oxide synthase 1 (neuronal)

Nos3: nitric oxide synthase 3 (endothelial cell)

Notch1: Notch homolog 1, translocation-associated (Drosophila)

Notch2: Notch homolog 2 (Drosophila)

Notch4: Notch homolog 4 (Drosophila)

Npc2: Niemann-Pick disease, type C2

Npdc1: neural proliferation, differentiation and control, 1

Npepps: aminopeptidase puromycin sensitive

Npm1: nucleophosmin (nucleolar phosphoprotein B23, numatrin)

Npr2: natriuretic peptide receptor B/guanylate cyclase B (atrionatriuretic peptide receptor B)

Npvf: neuropeptide VF precursor

Npy5r: neuropeptide Y receptor Y5

Nr1i2: nuclear receptor subfamily 1, group I, member 2

Nr5a2: nuclear receptor subfamily 5, group A, member 2

Nr6a1: nuclear receptor subfamily 6, group A, member 1

Nras: neuroblastoma RAS viral (v-ras) oncogene homolog

Nrbf2: nuclear receptor binding factor 2

Nrp2: neuropilin 2

Nsf: N-ethylmaleimide-sensitive factor

Ntrk2: neurotrophic tyrosine kinase, receptor, type 2

Nucb1: nucleobindin 1

Nucb2: nucleobindin 2

Nudc: nuclear distribution gene C homolog (A. nidulans)

Nup88: nucleoporin 88 kDa

Oas3: 2′-5′-oligoadenylate synthetase 3, 100 kDa

Obscn: obscurin, cytoskeletal calmodulin and titin-interacting RhoGEF

Ociad1: OCIA domain containing 1

Odc1: ornithine decarboxylase 1

Odf2: outer dense fiber of sperm tails 2

Ogfr: opioid growth factor receptor

Olfm2: olfactomedin 2

Olfm3: olfactomedin 3

Omg: oligodendrocyte myelin glycoprotein

Optn: optineurin

Osbp: oxysterol binding protein

Oxr1: oxidation resistance 1

P4hb: prolyl 4-hydroxylase, beta polypeptide

Pabpc1: poly(A) binding protein, cytoplasmic 1

Pabpc4: poly(A) binding protein, cytoplasmic 4 (inducible form)

Padi2: peptidyl arginine deiminase, type II

Pak3: p21 protein (Cdc42/Rac)-activated kinase 3

Palm: paralemmin

Panx1: pannexin 1

Pard3: par-3 partitioning defective 3 homolog (C. elegans)

Parg: poly (ADP-ribose) glycohydrolase

Park7: Parkinson disease (autosomal recessive, early onset) 7

Pbp: phosphatidylethanolamine binding protein 1

Pcca: propionyl Coenzyme A carboxylase, alpha polypeptide

Pcdh21: protocadherin 21

Pcdha3: protocadherin alpha 3

Pcdhb1: protocadherin beta 1

Pcdhb10: protocadherin beta 10

Pcdhga12: protocadherin gamma subfamily A, 12

Pclo: piccolo (presynaptic cytomatrix protein)

Pcolce: procollagen C-endopeptidase enhancer

Pcsk1n: proprotein convertase subtilisin/kexin type 1 inhibitor

Pcsk5: proprotein convertase subtilisin/kexin type 5

Pcyox1: prenylcysteine oxidase 1

Pdap1: PDGFA associated protein 1

Pdcd4: programmed cell death 4 (neoplastic transformation inhibitor)

Pdcl: phosducin-like

Pde10a: phosphodiesterase 10A

Pde4b: phosphodiesterase 4B, cAMP-specific (phosphodiesterase E4 dunce homolog, Drosophila)

Pdlim7: PDZ and LIM domain 7 (enigma)

Pea15: phosphoprotein enriched in astrocytes 15

Pecr: peroxisomal trans-2-enoyl-CoA reductase

Per1: period homolog 1 (Drosophila)

Per3: period homolog 3 (Drosophila)

Pfkl: phosphofructokinase, liver

PGAP1: post-GPI attachment to proteins 1

Phactr3: phosphatase and actin regulator 3

Phb: prohibitin

Phka1: phosphorylase kinase, alpha 1 (muscle)

Phkg2: phosphorylase kinase, gamma 2 (testis)

Pi4ka: phosphatidylinositol 4-kinase, catalytic, alpha

Picalm: phosphatidylinositol binding clathrin assembly protein

Pik3c3: phosphoinositide-3-kinase, class 3

Pik3cb: phosphoinositide-3-kinase, catalytic, beta polypeptide

Pik3r2: phosphoinositide-3-kinase, regulatory subunit 2 (beta)

Pim1: pim-1 oncogene

Pip5k2a: phosphatidylinositol-5-phosphate 4-kinase, type II, alpha

Pitpnm1: phosphatidylinositol transfer protein, membrane-associated 1

Pkia: protein kinase (cAMP-dependent, catalytic) inhibitor alpha

Pkm2: pyruvate kinase, muscle

Pla2g2a: phospholipase A2, group IIA (platelets, synovial fluid)

Plb1: phospholipase B1

Plcb4: phospholipase C, beta 4

Plcd4: phospholipase C, delta 4

Plec1: plectin 1, intermediate filament binding protein 500kDa

Plk1: polo-like kinase 1 (Drosophila)

Pnkp: polynucleotide kinase 3'-phosphatase

Pnma1: paraneoplastic antigen MA1

Ppara: peroxisome proliferator-activated receptor alpha

Ppargc1b: peroxisome proliferator-activated receptor gamma, coactivator 1 beta

ppfibp2: PTPRF interacting protein, binding protein 2 (liprin beta 2)

Ppia: peptidylprolyl isomerase A (cyclophilin A)

Ppm2c: pyruvate dehydrogenase phosphatase catalytic subunit 1

Ppp1r14b: protein phosphatase 1, regulatory (inhibitor) subunit 14B

Ppp1r1a: protein phosphatase 1, regulatory (inhibitor) subunit 1A

Ppp1r9a: protein phosphatase 1, regulatory (inhibitor) subunit 9A

Ppp2r1a: protein phosphatase 2 (formerly 2A), regulatory subunit A, alpha isoform

Ppp3cc: protein phosphatase 3 (formerly 2B), catalytic subunit, gamma isoform

Pqlc1: PQ loop repeat containing 1

Prdx1: peroxiredoxin 1

Prdx6: peroxiredoxin 6

Prg3: proteoglycan 3

Prkaa2: protein kinase, AMP-activated, alpha 2 catalytic subunit

Prkaca: protein kinase, cAMP-dependent, catalytic, alpha

Prkar1a: protein kinase, cAMP-dependent, regulatory, type I, alpha (tissue specific extinguisher 1)

Prkar2a: protein kinase, cAMP-dependent, regulatory, type II, alpha

Prkcd: protein kinase C, delta

PRKCQ: protein kinase C, theta

Prkwnk1: WNK lysine deficient protein kinase 1

Prlh: prolactin releasing hormone

Prmt3: protein arginine methyltransferase 3

Prpsap2: phosphoribosyl pyrophosphate synthetase-associated protein 2

Prrx2: paired related homeobox 2

Prss12: protease, serine, 12 (neurotrypsin, motopsin)

Prss15: lon peptidase 1, mitochondrial

Prx: periaxin

Psap: prosaposin

Pscd2: cytohesin 2

Pscd3: cytohesin 3

Psg4: pregnancy specific beta-1-glycoprotein 4

Psma1: proteasome (prosome, macropain) subunit, alpha type, 1

Psma2: proteasome (prosome, macropain) subunit, alpha type, 2

Psmc4: proteasome (prosome, macropain) 26S subunit, ATPase, 4

Psme2: proteasome (prosome, macropain) activator subunit 2 (PA28 beta)

Ptbp1: polypyrimidine tract binding protein 1

Ptch1: patched homolog 1 (Drosophila)

Pth: parathyroid hormone

Pthr2: parathyroid hormone 2 receptor

Ptk2b: PTK2B protein tyrosine kinase 2 beta

Ptp4a1: protein tyrosine phosphatase type IVA, member 1

Ptpn11: protein tyrosine phosphatase, non-receptor type 11

Ptpn23: protein tyrosine phosphatase, non-receptor type 23

Ptprj: protein tyrosine phosphatase, receptor type, J

Ptprr: protein tyrosine phosphatase, receptor type, R

Ptprv: protein tyrosine phosphatase, receptor type, V (pseudogene)

Pxn: paxillin

Pygl: phosphorylase, glycogen, liver

Qscn6: quiescin Q6 sulfhydryl oxidase 1

Rab10: RAB10, member RAS oncogene family

Rab14: RAB14, member RAS oncogene family

Rab2: RAB2A, member RAS oncogene family

Rab21: RAB21, member RAS oncogene family

Rab35: RAB35, member RAS oncogene family

Rab3il1: RAB3A interacting protein (rabin3)-like 1

Rab4a: RAB4A, member RAS oncogene family

Rab5a: RAB5A, member RAS oncogene family

Rab7: RAB7A, member RAS oncogene family

Rab9: RAB9A, member RAS oncogene family

Rabac1: Rab acceptor 1 (prenylated)

Rabggta: Rab geranylgeranyltransferase, alpha subunit

Rac1: ras-related C3 botulinum toxin substrate 1 (rho family, small GTP binding protein Rac1)

Rala: v-ral simian leukemia viral oncogene homolog A (ras related)

RalB: v-ral simian leukemia viral oncogene homolog B (ras related; GTP binding protein)

Ralb: v-ral simian leukemia viral oncogene homolog B (ras related; GTP binding protein)

Raly: RNA binding protein, autoantigenic (hnRNP associated with lethal yellow homolog (mouse))

RanGap1: Ran GTPase activating protein 1

Rap2b: RAP2B, member of RAS oncogene family

Rbbp6: retinoblastoma binding protein 6

Rbl2: retinoblastoma-like 2 (p130)

Rbm3: RNA binding motif (RNP1, RRM) protein 3

Rcn1: reticulocalbin 1, EF-hand calcium binding domain

Rcvrn: recoverin

Rdh10: retinol dehydrogenase 10 (all-trans)

Rdx: radixin

Rest: RE1-silencing transcription factor

Rgs4: regulator of G-protein signaling 4

Rgs5: regulator of G-protein signaling 5

Rgs7: regulator of G-protein signaling 7

Rhoa: ras homolog gene family, member A

RhoB: ras homolog gene family, member B

Rhoj: ras homolog gene family, member J

Rims1: regulating synaptic membrane exocytosis 1

Rnasel: ribonuclease L (2′,5′-oligoisoadenylate synthetase-dependent)

Rnf36: tripartite motif-containing 69

Rnf40: ring finger protein 40

Robo1: roundabout, axon guidance receptor, homolog 1 (Drosophila)

Robo4: roundabout homolog 4, magic roundabout (Drosophila)

Rock1: Rho-associated, coiled-coil containing protein kinase 1

Rock2: Rho-associated, coiled-coil containing protein kinase 2

rora: RAR-related orphan receptor A

Rpe65: retinal pigment epithelium-specific protein 65 kDa

Rpl13: ribosomal protein L13

Rpl6: ribosomal protein L6

Rplp1: ribosomal protein, large, P1

Rpn2: ribophorin II

Rps15: ribosomal protein S15

Rps16: ribosomal protein S16

Rps6ka2: ribosomal protein S6 kinase, 90 kDa, polypeptide 2

Rtcd1: RNA terminal phosphate cyclase domain 1

Rtkn: rhotekin

Rtn1: reticulon 1

Rtn3: reticulon 3

Rtn4: reticulon 4

Rtn4r: reticulon 4 receptor

Samsn1: SAM domain, SH3 domain and nuclear localization signals 1

Sardh: sarcosine dehydrogenase

Sart1: squamous cell carcinoma antigen recognized by T cells

Sbds: Shwachman-Bodian-Diamond syndrome

Sc4mol: sterol-C4-methyl oxidase-like

Sca10: ataxin 10

Scg2: secretogranin II (chromogranin C)

Scg3: secretogranin III

Scn1a: sodium channel, voltage-gated, type I, alpha subunit

Scn2a1: sodium channel, voltage-gated, type II, alpha subunit

Scn5a: sodium channel, voltage-gated, type V, alpha subunit

Scn8a: sodium channel, voltage gated, type VIII, alpha subunit

Scoc: short coiled-coil protein

Scp2: sterol carrier protein 2

SCYB11: chemokine (C-X-C motif) ligand 11

Scye1: aminoacyl tRNA synthetase complex-interacting multifunctional protein 1

Sdfr1: neuroplastin

Sdpr: serum deprivation response

SH3gl1: SH3-domain GRB2-like 1

SH3glb1: SH3-domain GRB2-like endophilin B1

Shank1: SH3 and multiple ankyrin repeat domains 1

Sirpa: signal-regulatory protein alpha

Skiv2l2: superkiller viralicidic activity 2-like 2 (S. cerevisiae)

Slc12a2: solute carrier family 12 (sodium/potassium/chloride transporters), member 2

Slc12a9: solute carrier family 12 (potassium/chloride transporters), member 9

Slc13a3: solute carrier family 13 (sodium-dependent dicarboxylate transporter), member 3

Slc17a6: solute carrier family 17 (sodium-dependent inorganic phosphate cotransporter), member 6

Slc1a1: solute carrier family 1 (neuronal/epithelial high affinity glutamate transporter, system Xag), member 1

Slc26a4: solute carrier family 26, member 4

Slc27a5: solute carrier family 27 (fatty acid transporter), member 5

Slc30a1: solute carrier family 30 (zinc transporter), member 1

Slc44a4: solute carrier family 44, member 4

Slc5a1: solute carrier family 5 (sodium/glucose cotransporter), member 1

Slc6a8: solute carrier family 6 (neurotransmitter transporter, creatine), member 8

Slc8a1: solute carrier family 8 (sodium/calcium exchanger), member 1

Smad4: SMAD family member 4

Smc1l1: structural maintenance of chromosomes 1A

Smoc1: SPARC related modular calcium binding 1

Snai2: snail homolog 2 (Drosophila)

Snap25: synaptosomal-associated protein, 25 kDa

Snap91: synaptosomal-associated protein, 91 kDa homolog (mouse)

Snca: synuclein, alpha (non A4 component of amyloid precursor)

Sncb: synuclein, beta

Snx3: sorting nexin 3

Snx7: sorting nexin 7

sod1: superoxide dismutase 1, soluble

Sod2: superoxide dismutase 2, mitochondrial

Son: SON DNA binding protein

Sord: sorbitol dehydrogenase

Sox5: SRY (sex determining region Y)-box 5

Sp4: Sp4 transcription factor

Sp7: Sp7 transcription factor

Sqle: squalene epoxidase

Srfbp1: serum response factor binding protein 1

Sst: somatostatin

St6gal2: ST6 beta-galactosamide alpha-2,6-sialyltransferase 2

St7l: suppression of tumorigenicity 7 like

Stard3nl: STARD3 N-terminal like

Stat3: signal transducer and activator of transcription 3 (acute-phase response factor)

Stat5a: signal transducer and activator of transcription 5A

Stip1: stress-induced-phosphoprotein 1

Stk2: NIMA (never in mitosis gene a)-related kinase 4

Stk22a: testis-specific serine kinase 1A pseudogene

Stmn1: stathmin 1

Stmn2: stathmin-like 2

Stmn4: stathmin-like 4

Strbp: spermatid perinuclear RNA binding protein

Stx1a: syntaxin 1A (brain)

Stx1b2: syntaxin 1B

Stx5: syntaxin 5

stxbp1: syntaxin binding protein 1

Stxbp3: syntaxin binding protein 3

Sulf1: sulfatase 1

Svop: SV2 related protein homolog (rat)

SYAP1: synapse associated protein 1, SAP47 homolog (Drosophila)

Sycp1: synaptonemal complex protein 1

Sycp2: synaptonemal complex protein 2

Synj2: synaptojanin 2

Syt3: synaptotagmin III

Syt4: synaptotagmin IV

Tacc2: transforming, acidic coiled-coil containing protein 2

Tacc3: transforming, acidic coiled-coil containing protein 3

Tbx2: T-box 2

Tceb3: transcription elongation factor B (SIII), polypeptide 3 (110 kDa, elongin A)

Tcp1: t-complex 1

Tcp11: t-complex 11 homolog (mouse)

Tdg: thymine-DNA glycosylase

Tdrd7: tudor domain containing 7

Tesk2: testis-specific kinase 2

Tfrc: transferrin receptor (p90, CD71)

Tgfb1: transforming growth factor, beta 1

Thrap3: thyroid hormone receptor associated protein 3

Thrb: thyroid hormone receptor, beta (erythroblastic leukemia viral (v-erb-a) oncogene homolog 2, avian)

Thy1: Thy-1 cell surface antigen

Tinag: tubulointerstitial nephritis antigen

Tkt: transketolase

Tle3: transducin-like enhancer of split 3 (E(sp1) homolog, Drosophila)

Tlr5: toll-like receptor 5

Tm4sf8: tetraspanin 3

Tm9sf2: transmembrane 9 superfamily member 2

Tmeff1: transmembrane protein with EGF-like and two follistatin-like domains 1

Tmem17: transmembrane protein 17

Tmlhe: trimethyllysine hydroxylase, epsilon

Tmod2: tropomodulin 2 (neuronal)

Tmpo: thymopoietin

Tnfrsf14: tumor necrosis factor receptor superfamily, member 14 (herpesvirus entry mediator)

Top1: topoisomerase (DNA) I

Tpd52l2: tumor protein D52-like 2

Tpm4: tropomyosin 4

Tra1: heat shock protein 90kDa beta (Grp94), member 1

Traf4: TNF receptor-associated factor 4

Trib3: tribbles homolog 3 (Drosophila)

Trim10: tripartite motif-containing 10

Trim25: tripartite motif-containing 25

Trim50: tripartite motif-containing 50

Trpa1: transient receptor potential cation channel, subfamily A, member 1

TrpV6: transient receptor potential cation channel, subfamily V, member 6

Tsc1: tuberous sclerosis 1

Tsga10: testis specific, 10

Tshr: thyroid stimulating hormone receptor

Ttc1: tetratricopeptide repeat domain 1

Ttn: titin

Tub: tubby homolog (mouse)

Tubb: tubulin, beta

Tubb2: tubulin, beta 2A

Txn: thioredoxin

U2af2: U2 small nuclear RNA auxiliary factor 2

Ubc: ubiquitin C

Ube2l3: ubiquitin-conjugating enzyme E2L 3

Ubqln1: ubiquilin 1

Uchl1: ubiquitin carboxyl-terminal esterase L1 (ubiquitin thiolesterase)

Ugcgl1: UDP-glucose glycoprotein glucosyltransferase 1

Uhrf1: ubiquitin-like with PHD and ring finger domains 1

Unc13: unc-13 homolog B (C. elegans)

Unc13a: unc-13 homolog A (C. elegans)

Unc13d: unc-13 homolog D (C. elegans)

Uqcrfs1: ubiquinol-cytochrome c reductase, Rieske iron-sulfur polypeptide 1

Usp14: ubiquitin specific peptidase 14 (tRNA-guanine transglycosylase)

Usp15: ubiquitin specific peptidase 15

Vamp2: vesicle-associated membrane protein 2 (synaptobrevin 2)

Vangl2: vang-like 2 (van gogh, Drosophila)

Vapa: VAMP (vesicle-associated membrane protein)-associated protein A, 33 kDa

Vapb: VAMP (vesicle-associated membrane protein)-associated protein B and C

Vav1: vav 1 guanine nucleotide exchange factor

Vcp: valosin-containing protein

Vdac2: voltage-dependent anion channel 2

Vegfa: vascular endothelial growth factor A

Vgf: VGF nerve growth factor inducible

Viaat: solute carrier family 32 (GABA vesicular transporter), member 1

Vim: vimentin

Vldlr: very low density lipoprotein receptor

Vps4a: vacuolar protein sorting 4 homolog A (S. cerevisiae)

Vps52: vacuolar protein sorting 52 homolog (S. cerevisiae)

Vps54: vacuolar protein sorting 54 homolog (S. cerevisiae)

Vsnl1: visinin-like 1

Vti1a: vesicle transport through interaction with t-SNAREs homolog 1A (yeast)

Vtn: vitronectin

Wbp11: WW domain binding protein 11

Wbscr1: eukaryotic translation initiation factor 4H

Whsc2: Wolf-Hirschhorn syndrome candidate 2

Wif1: WNT inhibitory factor 1

Wnk4: WNK lysine deficient protein kinase 4

Wrnip1: Werner helicase interacting protein 1

Xpo7: exportin 7

Xrcc5: X-ray repair complementing defective repair in Chinese hamster cells 5

Ybx1: Y box binding protein 1

yes1: v-yes-1 Yamaguchi sarcoma viral oncogene homolog 1

Ywhah: tyrosine 3-monooxygenase/tryptophan 5-monooxygenase activation protein, eta polypeptide

Ywhaq: tyrosine 3-monooxygenase/tryptophan 5-monooxygenase activation protein, theta polypeptide

Zbtb7a: zinc finger and BTB domain containing 7A

Zeb1: zinc finger E-box binding homeobox 1

Zfhx2: zinc finger homeobox 2

Zfp57: zinc finger protein 57 homolog (mouse)

Zmynd19: zinc finger, MYND-type containing 19

Znf219: zinc finger protein 219

Znf291: S-phase cyclin A-associated protein in the ER

Znf292: zinc finger protein 292

Znf382: zinc finger protein 382.

C.

Cellular signaling pathway clusters of extracted proteins from primary cortical tissue. Specific cellular signaling pathway clusters generated in an un-biased manner using Ingenuity Pathway Analysis (v. 8.5). The relative score generated for the degree of pathway population by proteins from the respective input sets (control or 3xTgAD) is shown in bold. The following are different types of signaling pathways.

C.1. ERK/MAPK Signaling (Enrichment Ratio $-\log 10(p)$).*

*Control Protein (**1.32502**).* PPP2R2A, CRK, PPP1R14B, DUSP2, PTK2, SHC1, PAK1, PPP1R10, PPP1R7, PIK3CG, STAT1, PRKCA, ETS1, SRC, PAK2, YWHAB, CRKL, PRKAR2A, STAT3, PLA2G4C, FOS, PPP2CB, PPP2R1A, PRKAR2B, PRKCI, PAK3, PPP2R2B, PRKACA, PPP2R5E, ELK1, PPP2R1B, PRKAR1A, PRKCB.

*3xTgAD Protein (**0.1537**).* PXN, YWHAH, PTK2B, RAC1, PRKAR2A, PLA2G2A, STAT3, MYC, YWHAQ (includes EG:10971), PPP2R1A, PAK3, PIK3C3, PRKCD, PRKACA, PIK3CB, PIK3R2, ELK1, FYN, PRKAR1A.

C.2. Inositol Phosphate Metabolism (Enrichment Ratio $-\log 10(p)$*).*

*Control Protein (**0.86424**).* PDIA3, OCRL, PAK1, PIK3CG, PRKAA2, PLCB1, PLCL1, PI4KA, PMPCA, ATM, GRK4, PRKCQ, PAK2, CDK7, CDK6, PLK1, GRK5, ITPKA, SYNJ2, PIP5K1A, PAK3, SYNJ1, PIP5K1C, GRK6, PIP4K2A, PIP4K2C, CDK2.

*3xTgAD Protein (**0.15355**).* PLK1, INPP5D, SYNJ2, INPP4A, INPP4B, INPP4B, PAK3, PIM1, PRKCD, PIK3C3, PRKAA2, PIK3CB, PIK3R2, PIP4K2A, PLCD4, PI4KA, ATM.

C.3. Wnt/β-Catenin Signaling (Enrichment Ratio $-\log 10(p)$*).*

*Control Protein (**0.5609**).* PPP2R2A, SOX10, CSNK1E, WIF1, WNT7A, TGFB1, SMO, CSNK2A1, CSNK2B, CTNNB1, SRC, SFRP4, GJA1, CSNK1G2, DVL1, FZD9, PPP2CB, CDH2, CDH1, PPP2R1A, PPP2R2B, TLE3, PPP2R5E, UBC, PPP2R1B, WNT5A.

*3xTgAD Protein (**0.12772**).* CSNK1G1, CSNK1G3, DVL1, ACVR1, APC, MYC, CSNK1E, PPP2R1A, CDH2, CDH1, WIF1, TGFB1, GNAO1, TLE3, UBC, CTNNB1, SOX5 (includes EG:6660).

C.4. Calcium Signaling (Enrichment Ratio $-\log 10(p)$*).*

*Control Protein (**0.33825**).* TRPC2, GRIN2A, TNNI2, GRIA1, RCAN2, CALM2, CHRNB4, TRPC5, TNNT3, RYR3, GRIK1, GRIN2B, PRKAR2A, TRPC4, PPP3CC, TRPC7, CHRNG, PRKAR2B, TPM3, CAMKK1, PRKACA, TNNI1, CHRNB3, CAMKK2, PRKAR1A.

*3xTgAD Protein (**0.110875**).* RAP2B, MYH10, CALR, MYH6, ATP2B1, PRKAR2A, TPM4, PPP3CC, ATP2B2, HDAC6, TRPV6, HTR3A, CAMKK1, PRKACA, MYH9, SLC8A1, ACTA1, PRKAR1A.

C.5. Tight Junction Signaling (Enrichment Ratio $-\log 10(p)$*).*

*Control Protein (**0.4147**).* TJP2, CDC42, TJP1, PPP2R2A, CLDN19, VAPA, PRKAR2A, PRKCZ, FOS, PPP2CB, PPP2R1A, PRKCI, PRKAR2B, CLDN4, CLDN1, TGFB1, PPP2R2B, PRKACA, PPP2R5E, STX4, CTNNB1, PPP2R1B, PRKAR1A.

*3xTgAD Protein (**0.24514**).* MYH10, MYH6, CDC42, ACTB, HSF1, CLDN18, VAPA, RAC1, PRKAR2A, MPDZ, PPP2R1A, TGFB1, RHOA, CEBPA, PRKACA, MYH9, CTNNB1, ACTA1, PRKAR1A.

C.6. NF-κB Signaling (Enrichment Ratio $-\log 10(p)$*).*

*Control Protein (**0.12096**).* PRKCQ, EGF, PRKCZ, TLR9, TLR4, TLR5, PIK3CG, TLR6, PRKACA, CSNK2A1, PDGFRA, TLR3, CSNK2B, PRKCB, EGFR.

*3xTgAD Protein (**0.0190128**). IL1R2, TLR5, BCL10, PIK3C3, PRKACA, IL1B, PIK3CB, PIK3R2, NFKB1, EGFR.*

C.7. PTEN Signaling (Enrichment Ratio $-\log 10(p)$*).*

*Control Protein (**0.1368**).* PTK2, SHC1, CDC42, PIK3CG, CSNK2A1, PDGFRA, CSNK2B, CDKN1B, PRKCZ, FASLG, EGFR.

*3xTgAD Protein (**0.1199**).* CDC42, YWHAH, RAC1, PIK3CB, PIK3R2, CDKN1B, NFKB1, INPP5D, EGFR, MAGI3.

C.8. SAPK/JNK Signaling (Enrichment Ratio $-\log 10(p)$*).*

*Control Protein (**0.0544984**).* SHC1, CDC42, GADD45A, CRKL, PIK3CG, CRK, ELK1, GNG7.

*3xTgAD Protein (**0.0717288**).* CDC42, GADD45A, IRS1, PIK3C3, RAC1, PIK3CB, PIK3R2, ELK1, HNRNPK.

C.9. PI3K/AKT Signaling (Enrichment Ratio $-\log 10(p)$*).*

*Control Protein (**0.15481**).* TSC1, PPP2R2A, YWHAB, PRKCZ, PPP2CB, SHC1, PPP2R1A, PIK3CG, TSC2, PPP2R2B, PPP2R5E, CDKN1B, CTNNB1, PPP2R1B.

*3xTgAD Protein (**0.19323**).* TSC1, JAK1, YWHAH, JAK2, NOS3, INPP5D, YWHAQ (includes EG:10971), MTOR, PPP2R1A, HSP90AB1, PIK3CB, PIK3R2, CDKN1B, CTNNB1.

C.10. p38 MAPK Signaling (Enrichment Ratio $-\log 10(p)$*).*

*Control Protein (**0**).*

*3xTgAD Protein (**0.0630702**).* IL1R2, MYC, TGFB1, MAP3K7IP2, IL1B, PLA2G2A, EEF2K, MAPKAPK2, ELK1.

C.11. p53 Signaling (Enrichment Ratio $-\log 10(p)$*).*

*Control Protein (**0.037996**).* GADD45A, FASN, PIK3CG, SNAI2, CTNNB1, CDK2, ATM, SERPINE2.

*3xTgAD Protein (**0.12075**).* CCND2, GADD45A, PIK3C3, SNAI2, CABC1, PIK3CB, PIK3R2, BAX, CTNNB1, ATM.

C.12. JAK/Stat Signaling (Enrichment Ratio $-\log 10(p)$*).*

*Control Protein (**0.051714**).* SHC1, SOCS1, PTPN11, PIK3CG, STAT3, STAT1.

*3xTgAD Protein (**0.25857**).* STAT5A, MTOR, JAK1, PTPN11, PIK3C3, PIK3CB, STAT3, PIK3R2, JAK2.

D.

Neuronal function pathway clusters of extracted proteins from primary cortical tissue. Specific neuronal function pathway clusters generated in an un-biased manner using Ingenuity Pathway Analysis (v. 8.5). The relative score generated for the degree of pathway population by proteins from the respective input sets (control or 3xTgAD) is shown in bold. The following are different types of signaling pathways.

D.1. Synaptic Long-Term Potentiation (Enrichment Ratio $-\log 10(p)$*).*

*Control Protein (**1.27872**).* GRIN2B, GRIN2A, PRKCQ, PPP1R1A, GRIA1, PRKAR2A, CALM2, CACNA1C, PPP3CC, GRM4, PPP1R14B, PRKCZ, GRM5, PRKCI, PRKAR2B, PPP1R10, PPP1R7, PPP1R14D, PRKACA, PLCB1, PRKD1, PRKCA, PRKAR1A, PRKCB

*3xTgAD Protein (**0**).*

D.2. Axonal Guidance Signaling (Enrichment Ratio $-\log 10(p)$*).*

*Control Protein (**0.69525**).* NOS1, GUCY1B2, PRKCQ, GUCY1A3, GUCY2D, PPP2R2A, GRID2, GRIA1, GRM4, PRKCZ, GRM5, PPP2CB, PPP2R1A, PRKCI, PPP2R2B, RYR3, GUCY1A2, PLCB1, PPP2R5E, PPP2R1B, PRKD1, PRKCA, PRKCB.

*3xTgAD Protein (**0.1918**).* NOS1, GUCY2D, GNAI1, PLA2G2A, GNAZ, NOS3, PRDX6, GNAI2, PPP2R1A, PRKCD, GNAO1, IGF1R, GUCY2F, ADCY8, NPR2.

D.3. Synaptic Long-Term Depression (Enrichment Ratio $-\log 10(p)$*).*

*Control Protein (**0.47428**).* NOS1, GUCY1B2, PRKCQ, GUCY1A3, GUCY2D, PPP2R2A, GRID2, GRIA1, GRM4, PRKCZ, GRM5, PPP2CB, PPP2R1A, PRKCI, PPP2R2B, RYR3, GUCY1A2, PLCB1, PPP2R5E, PPP2R1B, PRKD1, PRKCA, PRKCB.

*3xTgAD Protein (**0.11112**).* NOS1, GUCY2D, GNAI1, PLA2G2A, GNAZ, NOS3, PRDX6, GNAI2, PPP2R1A, PRKCD, GNAO1, IGF1R, GUCY2F, ADCY8, NPR2.

D.4. Parkinson's Signaling (Enrichment Ratio $-\log 10(p)$*).*

*Control Protein (**0.168256**).* UCHL1, PARK7, SNCA.

*3xTgAD Protein (**0.18656**).* UCHL1, PARK7, SNCA.

D.5. Huntington's Disease Signaling (Enrichment Ratio $-\log 10(p)$*).*

*Control Protein (**0.20048**).* EGF, GNG7, PRKCZ, TGM2, CTSD, SHC1, PIK3CG, VAMP3, PLCB1, PRKD1, PRKCA, EGFR, SDHA, GRIN2B, PRKCQ, YKT6, SH3GL3, STX1A, SNAP25, TAF9B, GRM5, PRKCI, UBC, GOSR2, SNCA, PRKCB.

*3xTgAD Protein (**0.36179**).* VTI1A, HSPA14, REST, GNB2L1, HDAC6, NSF, MTOR, PIK3C3, IGF1R, PIK3R2, EGFR, CAPN5, CAPN6, CLTC, BAX, STX1A, SNAP25, DNM1, DNAJC5, ATP5B, CAPN1, PRKCD, HAP1, DCTN1, PIK3CB, UBC, SNCA, CASP7.

D.6. Regulation of Actin-Based Motility by Rho (Enrichment Ratio $-\log 10(p)$*).*

*Control Protein (**0.1476**).* PIP5K1A, WIPF1, PAK1, PAK2, CDC42, CFL1, PAK3, PIP5K1C, PIP4K2A, PIP4K2C, PI4KA.

*3xTgAD Protein (**0.3243**).* CDC42, CFL1, ACTB, RAC1, RHOJ, ROCK1, PAK3, RHOB, RHOA, ARHGDIA, PIP4K2A, ACTA1, PI4KA.

D.7. Amyotrophic Lateral Sclerosis Signaling (Enrichment Ratio $-\log 10(p)$*).*

*Control Protein (**0.23184**).* NOS1, GRIN2B, GRIN2A, SOD1, GRIA1, PGF, VEGFA, PAK1, GRIK4, PIK3CG, CAT, GLUL, SSR4.

*3xTgAD Protein (**0.55955**).* NOS1, CAPN5, CAPN6, SOD1, RAB5A, RAC1, NEFH, BAX, CCS, VEGFA, CAPN1, PIK3C3, NEFM, PIK3CB, PIK3R2, CASP7.

D.8. Actin Cytoskeleton Signaling (Enrichment Ratio $-\log 10(p)$*).*

*Control Protein (**0.0763861**).* PAK2, CFL1, CDC42, CRKL, EGF, CRK, TTN, PTK2, SHC1, PAK1, PIP5K1A, PAK3,

PIP5K1C, FGF18, PIK3CG, EZR, FGF23, PIP4K2A, PIP4K2C, GIT1.

*3xTgAD Protein (**0.44928**).* MYH10, MYH6, CDC42, ROCK2, PIK3C3, EZR, PIK3R2, LBP, ACTA1, PXN, ARHGEF12, CFL1, ACTB, RAC1, RDX, APC, TTN, ROCK1, PAK3, RHOA, ARHGEF6, MYH9, VAV1, PIK3CB, ACTN4, PIP4K2A, MSN.

D.9. Amyloid Processing (Enrichment Ratio $-\log 10(p)$*).*

*Control Protein (**0.20636**).* CSNK1E, PRKAR2B, CSNK2A, PRKAR2A, PRKACA, NCSTN, CSNK2B, PRKAR1A.

*3xTgAD Protein (**0.66144**).* CSNK1E, CAPN5, CAPN6, CAPN1, MARK1, PRKAR2A, PRKACA, NCSTN, BACE1, APP, PRKAR1A.

E.

Energy regulation/Metabolism pathway clusters of extracted proteins from primary cortical tissue. Specific energy regulation/metabolism pathway clusters generated in an unbiased manner using Ingenuity Pathway Analysis (v. 8.5). The relative score generated for the degree of pathway population by proteins from the respective input sets (control or 3xTgAD) is shown in bold. The following are different types of signaling pathways.

E.1. Amino Sugars Metabolism (Enrichment Ratio $-\log 10(p)$*).*

*Control Protein (**0.61425**).* FMO3, PDE7A, PDE10A, GM2A, CYB5R1, PDE4A, PDE4B, PDE1A, PDE4D, GFPT2, PDE1C, PDE7B, GALK1, CYB5R3.

*3xTgAD Protein (**0.0471409**).* HK1, CYB5R4, PDE10A, GALK1, CYB5R3, PDE4B.

E.2. Pentose Phosphate Pathway (Enrichment Ratio $-\log 10(p)$*).*

*Control Protein (**0.48608**).* GPI, PGD, TKT, TALDO1, PRPSAP1, PGM1, PRPSAP2, PFKP, PFKL, PDHB, PFKM.

*3xTgAD Protein (**0.0245154**).* GPI, TKT, PRPSAP2, PFKL.

E.3. Glutamate Metabolism (Enrichment Ratio $-\log 10(p)$*).*

*Control Protein (**0.31165**).* FMO3, GPT, GLUL, GCLC, GLUD1, GOT1, GOT2, GFPT2, EPRS.

*3xTgAD Protein (**0**).*

E.4. Pantothenate and CoA Biosynthesis (Enrichment Ratio $-\log 10(p)$*).*

*Control Protein (**0.34188**).* ENPP3, CRMP1, BCAT1, DPYD, DPYSL3, ENPP5, ENPP2.

*3xTgAD Protein (**0.0348908**).* CRMP1, DPYD, ENPP2.

E.5. Glycolysis/Gluconeogenesis (Enrichment Ratio $-\log 10(p)$*).*

*Control Protein (**0.28363**).* PKM2, PGK1, ENO3, ENO2, GAPDH (includes EG:2597), PGM1, ALDH1L1, PFKP, PFKL, PDHB, PFKM, GPI, GALK1, DLAT, PGAM1, DLD.

*3xTgAD Protein (**0.0610449**).* PKM2, HK1, ADH1A, GPI, ALDH1A3, DLAT, GALK1, ENO2, PFKL, ACSL1.

E.6. Citrate Cycle (Enrichment Ratio $-\log 10(p)$*).*

*Control Protein (**0.1581**).* SDHA, PC, CS, SUCLG1, DLD, PCK1.

*3xTgAD Protein (**0**).*

E.7. Galactose Metabolism.

*Control Protein (**0.104958**).* GLA, GALT, GALK1, GAA, PGM1, PFKP, PFKL, PFKM.

*3xTgAD Protein (**0.0486688**).* HK1, GLA, GALK1, GAA, PFKL, AKR1B1.

E.8. Glycosphingolipid Biosynthesis—Globoseries (Enrichment Ratio $-\log 10(p)$*).*

*Control Protein (**0.0411384**).* GLA, ST3GAL1, GM2A.

*3xTgAD Protein (**0**).*

E.9. Glycosphingolipid Biosynthesis—Ganglioseries (Enrichment Ratio $-\log 10(p)$*).*

*Control Protein (**0.008832**).* ST3GAL1, GM2A.

*3xTgAD Protein (**0**).*

E.10. N-Glycan Biosynthesis (Enrichment Ratio $-\log 10(p)$*).*

*Control Protein (**0**).*

*3xTgAD Protein (**0.015272**).* RPN2, ST6GAL2, MGAT5, MGAT1.

E.11. Pentose and Glucuronate Interconversions (Enrichment Ratio* $-\log 10(p)$*).*

*Control Protein (**0**).*

*3xTgAD Protein (**0.0184464**).* UCHL1, B3GAT1, HPSE, DCXR, AKR1B1.

E.12. Fatty Acid Elongation in Mitochondria (Enrichment Ratio* $-\log 10(p)$*).*

*Control Protein (**0**).*

*3xTgAD Protein (**0.0206016**).* ECHS1, PECR.

E.13. Glycerophospholipid Metabolism (Enrichment Ratio* $-\log 10(p)$*).*

*Control Protein (**0.0232106**).* GPAM, PCYT1B, PLD3, CDS1, PDIA3, GNPAT, DGKB, DGKG, PLCB1, PLCL1.

*3xTgAD Protein (**0.048204**).* AGPAT4, CDS1, GNPAT, CHKA, AGPAT1, DGKG, PLA2G2A, CLCF1, PHKA1, PLCD4, PRDX6.

E.14. Fatty Acid Biosynthesis (Enrichment Ratio* $-\log 10(p)$*).*

*Control Protein (**0**).*

*3xTgAD Protein (**0.0329256**).* ACACB, ACACA.

E.15. Purine Metabolism (Enrichment Ratio* $-\log 10(p)$*).*

*Control Protein (**0.08616**).* ENTPD8, PDE7A, PDE4A, DNTT, PDE1A, PDE4D, PSMC5, PDE7B, VCP, DHX16, ENPP2, PRPSAP2, PKM2, TJP2, GUCY1B2, GUCY1A3, GUCY2D, PDE10A, ENPP5, PDE4B, PDE1C, ENPP3, PSMC1, ENTPD2, PRPSAP1, GUCY1A2, PDE5A, DDX1, GMPR2, PSMC3.

*3xTgAD Protein (**0.124932**).* MYH6, ENTPD8, NME2, DNTT, WRNIP1, ABCC1, VCP, KATNA1, ATP5H (includes EG:10476), ENPP2, PRPSAP2, ADCY8, ATP5F1, ATP5I, ATP5J, PKM2, ATP1B1, GUCY2D, PDE10A, AMPD1, ATP5A1, AK3, PSMC4, PDE4B, DDX19B, ATP5B, GUCY2F, MYH9, DDX1, NPR2.

E.16. Pyruvate Metabolism (Enrichment Ratio* $-\log 10(p)$*).*

*Control Protein (**0.0214935**).* PKM2, PC, DLAT, DLD, PCK1, PDHB, GLO1.

*3xTgAD Protein (**0.070173**).* PKM2, ACACB, ALDH1A3, DLAT, ACAT1, ACACA, MDH1, AKR1B1, ACSL1.

E.17. Butanoate Metabolism (Enrichment Ratio* $-\log 10(p)$*).*

*Control Protein (**0**).*

*3xTgAD Protein (**0.0523452**).* ECHS1, ALDH1A3, AACS, ACAT1, MYO5B, DCXR, HMGCS1.

E.18. Synthesis and Degradation of Ketone Bodies (Enrichment Ratio* $-\log 10(p)$*).*

*Control Protein (**0**).*

*3xTgAD Protein (**0.071505**).* ACAT1, HMGCS1.

F.

Cellular stress/damage pathway clusters of extracted proteins from primary cortical tissue. Specific energy cellular stress/damage pathway clusters generated in an un-biased manner using Ingenuity Pathway Analysis (v. 8.5). The relative score generated for the degree of pathway population by proteins from the respective input sets (control or 3xTgAD) is shown in bold. The following are different types of signaling pathways.

F.1. NRF2-mediated Oxidative Stress Response (Enrichment Ratio* $-\log 10(p)$*).*

*Control Protein (**0.44064**).* PRDX1, PPIB, GCLC, PRKCZ, GSTM2, SOD2, PIK3CG, VCP, DNAJA2, TXN, FKBP5, PRKD1, CBR1, PRKCA, GSTK1, SOD1, PRKCQ, TXNRD1, GSTO1, FOS, PRKCI, ERP29, STIP1, CAT, PRKCB, EPHX1.

*3xTgAD Protein (**0.23751**).* USP14, SOD1, PRDX1, ACTB, GSTM3 (includes EG:2947), JUNB, DNAJC5, GSTM2, SOD2, ERP29, STIP1, PIK3C3, PRKCD, ABCC1, VCP, PIK3CB, FOSL1, PIK3R2, TXN, EIF2AK3, ACTA1.

F.2. Ceramide Signaling (Enrichment Ratio* $-\log 10(p)$*).*

*Control Protein (**0.15748**).* CTSD, PPP2CB, FOS, PPP2R1A, PPP2R2A, PIK3CG, PPP2R2B, PPP2R5E, PPP2R1B.

*3xTgAD Protein (**0**).*

F.3. Glutathione Metabolism (Enrichment Ratio* $-\log 10(p)$*).*

*Control Protein (**0.094285**).* OPLAH, PGD, GSTM2, GGT5, GCLC, GGT1, GSTO1, GSTK1, GGT7.

*3xTgAD Protein (**0**).*

F.4. LPS/IL-1 Mediated Inhibition of RXR Function (Enrichment Ratio* $-\log 10(p)$*).*

*Control Protein (**0.19071**).* SULT1C2, FMO3, CPT1A, CHST7, ALDH1L1, NR1H3, GSTO1, SULT4A1, GSTM2, NR1I2, SREBF1, SULT1A1, CAT, CPT2, FABP4, XPO1, FABP1, FABP7, SULT1E1, FABP3, GSTK1, TLR4, FABP2.

*3xTgAD Protein (**0.13872**).* PPARA, GSTM3 (includes EG:2947), ABCA1, IL1R2, ABCC2, SLC27A5, GSTM2, ALDH1A3, NR1I2, CPT2, ACSL4, FABP1, IL1B, NR5A2, CHST10, LBP, ABCC4, HMGCS1, ACSL1, MAOA.

F.5. Fatty Acid Elongation in Mitochondria (Enrichment Ratio $-\log 10(p)$*).*

*Control Protein (**0**).*

*3xTgAD Protein (**0.0206016**).* ECHS1, PECR

F.6. Endoplasmic Reticulum Stress Pathway (Enrichment Ratio $-\log 10(p)$*).*

*Control Protein (**0**).*

*3xTgAD Protein (**0.047841**).* EIF2AK3, CASP7.

F.7. Apoptosis Signaling (Enrichment Ratio $-\log 10(p)$*).*

*Control Protein (**0**).*

*3xTgAD Protein (**0.059156**).* ACIN1, ROCK1, CAPN5, CAPN6, CAPN1, BAX, CASP7, PARP1.

F.8. Hypoxia Signaling (Enrichment Ratio $-\log 10(p)$*).*

*Control protein (**0**).*

*3xTgAD Protein (**0.111983**).* VEGFA, P4HB, HSP90AB1, UBE2L3, NOS3, UBC, ARNT, ATM.

F.9. PPARα/RXRα Activation (Enrichment Ratio $-\log 10(p)$*).*

*Control Protein (**0.0315615**).* PDIA3, PRKAR2A, NR2C2, SHC1, PRKAR2B, TGFB1, FASN, PRKACA, PLCB1, GOT2, PLCL1, PRKCB, PRKCA, PRKAR1A.

*3xTgAD Protein (**0.14586**).* PPARA, ACVR1, PRKAR2A, CD36, IL6, JAK2, ABCA1, IL1R2, ACADL, HSP90AB1, TGFB1, IRS1, PRKACA, SMAD4, IL1B, ADCY8, PLCD4, PRKAR1A.

G.

Receptor signaling pathway clusters of extracted proteins from primary cortical tissue. Specific receptor signaling pathway clusters generated in an un-biased manner using Ingenuity Pathway Analysis (v. 8.5). The relative score generated for the degree of pathway population by proteins from the respective input sets (control or 3xTgAD) is shown in bold. The following are different types of signaling pathways.

G.1. Dopamine Receptor Signaling.

*Control Protein (**0.65824**).* PPP2R2A, PRKAR2A, PPP1R14B, PPP2CB, PPP2R1A, PRKAR2B, PPP1R10, PPP1R14D, PPP1R7, PPP2R2B, PRKACA, FREQ, PPP2R5E, PPP2R1B, PRKAR1A, CALY.

*3xTgAD Protein (**0.071199**).* PPP2R1A, FREQ, PRKAR2A, PRKACA, ADCY8, CALY, MAOA, PRKAR1A.

G.2. PDGF Signaling.

*Control Protein (**0.73892**).* SRC, CRKL, CRK, STAT3, FOS, SHC1, PIK3CG, CSNK2A1, PDGFRA, CAV1, CSNK2B, ELK1, STAT1, PRKCB, PRKCA.

*3xTgAD Protein (**0.15738**).* MYC, JAK1, PIK3C3, STAT3, PIK3R2, JAK2, ELK1, INPP5D.

G.3. EGF Signaling.

*Control Protein (**0.7956**).* SHC1, FOS, PIK3CG, CSNK2A1, EGF, CSNK2B, STAT3, STAT1, ELK1, PRKCA, EGFR.

*3xTgAD Protein (**0.22499**).* JAK1, PIK3C3, PIK3CB, STAT3, PIK3R2, ELK1, EGFR.

G.4. Neuregulin Signaling.

*Control Protein (**0.68068**).* SRC, PRKCQ, CRKL, EGF, CRK, ERBB3, PRKCZ, SHC1, PRKCI, PTPN11, ERBB4, CDKN1B, ELK1, PRKD1, PRKCB, EGFR, PRKCA.

*3xTgAD Protein (**0.1276**).* MYC, STAT5A, MTOR, PTPN11, HSP90AB1, PRKCD, PIK3R2, CDKN1B, ELK1, EGFR.

G.5. Glutamate Receptor Signaling.

*Control Protein (**0.53342**).* GRM5, GRIN2B, GRIN2A, GRIK4, GRIA1, GRID2, CALM2, GLUL, GRIP1, GRM4, GNG7, GRIK1.

*3xTgAD Protein (**0**).*

G.6. Sonic Hedgehog Signaling.

*Control Protein (**0.73272**).* SHH, CCNB1, PRKAR2B, PRKAR2A, PRKACA, SMO, GLI1, PRKAR1A.

*3xTgAD Protein (**0.20769**).* ADRBK1, PTCH1, PRKAR2A, PRKACA, PRKAR1A.

G.7. TR/RXR Activation.

*Control Protein (**0.5481**).* UCP2, RCAN2, UCP1, THRA, GRIP1, PFKP, PCK1, KLF9, SREBF1, DIO1, FASN, PIK3CG, STRBP, THRB, FGA, SYT12.

*3xTgAD Protein (**0.0321142**).* MTOR, PIK3C3, STRBP, ACACA, PIK3CB, PIK3R2, THRB.

G.8. Ephrin Receptor Signaling.

*Control Protein (**0.62472**).* GRIN2A, CDC42, EGF, CRK, GNG7, PGF, VEGFA, PTK2, SHC1, PAK1, SDC2, PIK3CG, EFNB1, EPHA7, GRIN2B, SRC, PAK2, CFL1, CRKL, EPHA3, STAT3, WIPF1, SDCBP, PTPN11, PAK3, EPHA5, EPHB3.

*3xTgAD Protein (**0.21037**).* FYN, PXN, CFL1, CDC42, KALRN, GNB2L1, GNAI1, RAC1, JAK2, STAT3, GNAZ, ROCK1, VEGFA, GNAI2, ROCK2, ABI1, PTPN11, PAK3, RHOA, GNAO1.

G.9. G-Protein Coupled Receptor Signaling.

*Control Protein (**0.3808**).* PDE7A, PDE4A, PDE1A, PDE4D, SHC1, SYNGAP1, PDE7B, PIK3CG, PLCB1, PRKCA, SRC, GRK4, EDNRB, PDE10A, PRKAR2A, PDE4B, STAT3, GRM4, PDE1C, CHRM5, GRM5, OPRD1, PRKAR2B, PRKACA, PRKCB, PRKAR1A.

*3xTgAD Protein (**0.13938**).* FYN, PTK2B, HTR4, ADRBK1, PDE10A, RGS7, PRKAR2A, GNAI1, RGS4, STAT3, PDE4B, GNAI2, HTR2C, PIK3C3, GNAO1, PRKACA, PIK3CB, PIK3R2, ADCY8, PRKAR1A.

G.10. Chemokine Signaling.

*Control Protein (**0.23961**).* PTK2, NOX1, SRC, FOS, CCL4, CFL1, PIK3CG, CALM2, PLCB1, PRKCA, PRKCB.

*3xTgAD Protein (**0.03232**).* ROCK2, GNAI2, CFL1, PTK2B, RHOA, GNAI1.

G.11. Ceramide Signaling.

*Control Protein (**0.15748**).* CTSD, PPP2CB, FOS, PPP2R1A, PPP2R2A, PIK3CG, PPP2R2B, PPP2R5E, PPP2R1B, PRKCZ.

*3xTgAD protein (**0**).*

G.12. FGF (Fibroblast Growth Factor) Signaling.

*Control Protein (**0.17423**).* FGFR3, PTPN11, FGF18, CRKL, PIK3CG, FGFR1, FGF23, FGFR2, CRK, STAT3, PRKCA.

*3xTgAD Protein (**0.0667352**).* PTPN11, PIK3C3, HGF, RAC1, PIK3CB, STAT3, PIK3R2, MAPKAPK2.

G.13. Toll-like Receptor Signaling.

*Control Protein (**0.1644**).* TLR4, FOS, TLR5, TLR6, TLR3, ELK1, TLR9.

*3xTgAD Protein (**0.065562**).* PPARA, TLR5, MAP3K7IP2, LBP, ELK1.

G.14. Nitric Oxide Signaling.

*Control Protein (**0.41157**).* GUCY1B2, GUCY1A3, GUCY2D, CALM2, PRKAR2A, PGF, VEGFA, PRKAR2B, PIK3CG, GUCY1A2, CAV1, PRKACA, PRKAR1A.

*3xTgAD Protein (**0.36801**).* VEGFA, HSP90AB1, GUCY2D, PRKCD, PIK3C3, GUCY2F, PRKAR2A, PRKACA, PIK3CB, PIK3R2, NOS3, PRKAR1A.

G.15. cAMP-Mediated Signaling.

*Control Protein (**0.39295**).* GRK4, SRC, CNGA4, PDE7A, PDE10A, PRKAR2A, CALM2, PDE4A, PPP3CC, STAT3, PDE4B, GRM4, PDE1A, PDE4D, CNGA1, PDE1C, CHRM5, OPRD1, PRKAR2B, PDE7B, PRKACA, PKIA, PRKAR1A.

*3xTgAD Protein (**0.40848**).* AKAP12, HTR4, ADRBK1, PDE10A, RGS7, PRKAR2A, GNAI1, RGS4, AKAP3, PPP3CC, STAT3, PDE4B, CNGA1, GNAI2, AKAP4, GNAO1, PRKACA, CNGB1, PKIA, ADCY8, AKAP9, PRKAR1A.

G.16. TGF-β Signaling.

*Control protein (**0**).*

*3xTgAD Protein (**0.0236421**).* TGFB1, ACVR1, SMAD4, HNF4A, UBC, INHBC.

G.17. Neurotrophin/TRK Signaling.

*Control Protein (**0.016851**).* SHC1, FOS, CDC42, PTPN11, PIK3CG.

*3xTgAD Protein (**0.0440592**).* NTRK2, CDC42, PTPN11, PIK3C3, PIK3CB, PIK3R2.

G.18. IGF-1 Signaling.

*Control Protein (**0.49715**).* PRKAR2A, PTK2, SHC1, FOS, PRKAR2B, PTPN11, PIK3CG, PRKACA, CSNK2A1, CSNK2B, ELK1, PRKAR1A.

*3xTgAD Protein (**0.52722**).* PXN, YWHAH, PRKAR2A, NEDD4, YWHAQ, PTPN11, IRS1, PIK3C3, PRKACA, IGF1R, IRS2, PIK3CB, PIK3R2, ELK1, PRKAR1A.

G.19. Serotonin Receptor Signaling.

*Control protein (**0**).*

*3xTgAD Protein (**0.059769**).* HTR2C, HTR4, HTR3A, MAOA.

G.20. Glucocorticoid Receptor Signaling.

*Control protein (**0**).*

*3xTgAD Protein (**0.066**).* STAT5A, JAK1, YWHAH, HSPA14, RAC1, IL6, PPP3CC, STAT3, JAK2, NFKB1, MNAT1, IL1R2, HSP90AB1, TGFB1, PIK3C3, CEBPA, PRKACA, SMAD4, IL1B, PIK3CB, PIK3R2, ELK1.

G.21. Aryl Hydrocarbon Receptor Signaling.

*Control Protein (**0.1218**).* SRC, CDK6, ALDH1L1, GSTO1, TGM2, CTSD, FOS, GSTM2, TGFB1, FASN, CDKN1B, ESR2, CDK2, FASLG, ATM, GSTK1.

*3xTgAD Protein (**0.31125**).* CYP1A1, NFIX, GSTM3, IL6, BAX, NFKB1, ARNT, MYC, AHRR, GSTM2, CCND2, HSP90AB1, TGFB1, ALDH1A3, IL1B, CDKN1B, AHR, MCM7, ATM.

G.22. Insulin Receptor Signaling.

*Control Protein (**0.28288**).* TSC1, TRIP10, CRKL, PRKAR2A, CRK, VAMP2, PPP1R14B, PRKCZ, SHC1, PRKCI, PPP1R10, PTPN11, PIK3CG, TSC2, PRKACA.

*3xTgAD Protein (**0.5056**).* TSC1, FYN, JAK1, PRKAR2A, JAK2, VAMP2, INPP5D, MTOR, PTPN11, IRS1, PIK3C3, PRKACA, EIF2B1, PIK3CB, IRS2, PIK3R2, PRKAR1A.

G.23. Notch Signaling.

*Control Protein (**0.0437248**).* DLL1, CNTN1, NCSTN, DLL3.

*3xTgAD Protein (**0.30609**).* NOTCH4, DLL1, NOTCH2, NCSTN, JAG1, NOTCH1, HEY1.

G.24. GABA Receptor Signaling.

*Control Protein (**0.099214**).* GABRG2, UBQLN1, GABBR1, GABARAP, UBC, GABRA3.

*3xTgAD Protein (**0.4216**).* DNM1, NSF, SLC32A1, UBQLN1, GABBR1, MYO5B, GABRE, UBC, GABRA3.

G.25. VEGF Signaling.

*Control Protein (**0.0252652**).* VEGFA, PTK2, SHC1, PIK3CG, PGF, PRKCA, PRKCB.

*3xTgAD Protein (**0.53464**).* EIF2S2, PXN, PTK2B, ACTB, NOS3, ARNT, ROCK2, VEGFA, ROCK1, PIK3C3, EIF2B1, PIK3CB, PIK3R2, ACTN4, ACTA1.

G.26. Integrin Signaling.

*Control protein (**0**).*

*3xTgAD Protein (**0.54604**).* RAP2B, FYN, RALA, CDC42, TSPAN3, ARF6, RHOB, PIK3C3, ARF4, PIK3R2, ACTA1, CAPN5, CAPN6, PXN, ACTB, RALB, RAC1, ITGA6, RHOJ.

H.

Heatmap Protein Position Key. The individual position numbers are correlated to the specific multidimensional proteins represented by colored blocks in Figure 6. The following are the symbols of the proteins (the numbers between brackets refer to the position).

(1) adcyap1: adenylate cyclase activating polypeptide 1 (pituitary)

(2) adcyap1r1: adenylate cyclase activating polypeptide 1 (pituitary) receptor type I

(3) hap1: huntingtin-associated protein 1

(4) htr4: 5-hydroxytryptamine (serotonin) receptor 4

(5) ntrk2: neurotrophic tyrosine kinase, receptor, type 2

(6) Kalrn: kalirin, RhoGEF kinase

(7) klc1: kinesin light chain 1

(8) adrbk1: adrenergic, beta, receptor kinase 1

(9) agrn: agrin

(10) apod: apolipoprotein D

(11) app: amyloid beta (A4) precursor protein

(12) arhgef11: Rho guanine nucleotide exchange factor (GEF) 11

(13) arpp19: cAMP-regulated phosphoprotein, 19 kDa

(14) bace1: beta-site APP-cleaving enzyme 1

(15) ccs: copper chaperone for superoxide dismutase

(16) chgb: chromogranin B (secretogranin 1)

(17) flot1: flotillin 1

(18) flot2: flotillin 2

(19) gnb2l1: guanine nucleotide binding protein (G protein), beta polypeptide 2-like 1

(20) hyou1: hypoxia up-regulated 1

(21) lphn1: latrophilin 1

(22) lphn2: latrophilin 2

(23) magi3: membrane associated guanylate kinase, WW and PDZ domain containing 3

(24) nefh: neurofilament, heavy polypeptide

(25) prdx6: peroxiredoxin 6

(26) pscd2: cytohesin 2

(27) rtn3: reticulon 3

(28) rtn4r: reticulon 4 receptor

(29) slc44a4: solute carrier family 44, member 4

(30) stxbp1: syntaxin binding protein 1

(31) abca1: ATP-binding cassette, sub-family A (ABC1), member 1

(32) abi1: abl-interactor 1

(33) adcy1: adenylate cyclase 1 (brain)

(34) adcy5: adenylate cyclase 5

(35) akap9: A kinase (PRKA) anchor protein 9

(36) aldh1a3: aldehyde dehydrogenase 1 family, member A3

(37) alox5: arachidonate 5-lipoxygenase

(38) arf6: ADP-ribosylation factor 6

(39) arhgef12: Rho guanine nucleotide exchange factor (GEF) 12

(40) atcay: ataxia, cerebellar, Cayman type

(41) atp2b1: ATPase, Ca++ transporting, plasma membrane 1

(42) atxn3: ataxin 3

(43) begain: brain-enriched guanylate kinase-associated homolog (rat)

(44) cabc1: chaperone, ABC1 activity of bc1 complex homolog (S. pombe)

(45) capn1: calpain 1, (mu/l) large subunit

(46) caskin1: CASK interacting protein 1

(47) casp7: caspase 7, apoptosis-related cysteine peptidase

(48) cd36: CD36 molecule (thrombospondin receptor)

(49) cfd: complement factor D (adipsin)

(50) clu: clusterin

(51) cpa2: carboxypeptidase A2 (pancreatic)

(52) cript: cysteine-rich PDZ-binding protein

(53) dpp6: dipeptidyl-peptidase 6

(54) espn: espin

(55) fdps: farnesyl diphosphate synthase

(56) filip1: filamin A interacting protein 1

(57) gna11: guanine nucleotide binding protein (G protein), alpha 11 (Gq class)

(58) gnai2: guanine nucleotide binding protein (G protein), alpha inhibiting activity polypeptide 2

(59) gnao1: guanine nucleotide binding protein (G protein), alpha activating activity polypeptide O

(60) gnaq: guanine nucleotide binding protein (G protein), q polypeptide

(61) gnaz: guanine nucleotide binding protein (G protein), alpha z polypeptide

(62) gpr56: G protein-coupled receptor 56

(63) hip1r: huntingtin interacting protein 1 related

(64) hmgcr: 3-hydroxy-3-methylglutaryl-Coenzyme A reductase

(65) hsf1: heat shock transcription factor 1

(66) htr2c: 5-hydroxytryptamine (serotonin) receptor 2C

(67) itm2c: integral membrane protein 2C

(68) itpr3: inositol 1,4,5-triphosphate receptor, type 3

(69) lsamp: limbic system-associated membrane protein

(70) maoa: monoamine oxidase A

(71) map1lc3a: microtubule-associated protein 1 light chain 3 alpha

(72) mapkapk2: mitogen-activated protein kinase-activated protein kinase 2

(73) mark1: MAP/microtubule affinity-regulating kinase 1

(74) mdga2: MAM domain containing glycosylphosphatidylinositol anchor 2

(75) mpdz: multiple PDZ domain protein

(76) mpo: myeloperoxidase

(77) mpp7: membrane protein, palmitoylated 7 (MAGUK p55 subfamily member 7)

(78) ncam1: neural cell adhesion molecule 1

(79) ncam2: neural cell adhesion molecule 2

(80) ncdn: neurochondrin

(81) ndufs1: NADH dehydrogenase (ubiquinone) Fe-S protein 1, 75 kDa (NADH-coenzyme Q reductase)

(82) ndufs7: NADH dehydrogenase (ubiquinone) Fe-S protein 7, 20 kDa (NADH-coenzyme Q reductase)

(83) nes: nestin

(84) nlgn2: neuroligin 2

(85) nlgn3: neuroligin 3

(86) npc2: Niemann-Pick disease, type C2

(87) npdc1: neural proliferation, differentiation and control, 1

(88) npy5r: neuropeptide Y receptor Y5

(89) nsf: N-ethylmaleimide-sensitive factor

(90) padi2: peptidyl arginine deiminase, type II
(91) plcb4: phospholipase C, beta 4
(92) pxn: paxillin
(93) rab5a: RAB5A, member RAS oncogene family
(94) rgs4: regulator of G-protein signaling 4
(95) rgs7: regulator of G-protein signaling 7
(96) rims1: regulating synaptic membrane exocytosis 1
(97) rora: RAR-related orphan receptor A
(98) sh3gl1: SH3-domain GRB2-like 1
(99) sod2: superoxide dismutase 2, mitochondrial
(100) sst: somatostatin
(101) vldlr: very low density lipoprotein receptor
(102) camkk1: calcium/calmodulin-dependent protein kinase kinase 1, alpha
(103) cacna2d2: calcium channel, voltage-dependent, alpha 2/delta subunit 2
(104) vcp: valosin-containing protein
(105) stx1a: syntaxin 1A (brain)
(106) vgf: VGF nerve growth factor inducible
(107) calb2: calbindin 2
(108) prdx1: peroxiredoxin 1
(109) stmn2: stathmin-like 2
(110) vsnl1: visinin-like 1
(111) cdh2: cadherin 2, type 1, N-cadherin (neuronal)
(112) dbn1: drebrin 1
(113) oxr1: oxidation resistance 1
(114) gpsm1: G-protein signaling modulator 1 (AGS3-like, C. elegans)
(115) gmfb: glia maturation factor, beta
(116) cd2ap: CD2-associated protein
(117) centa1: ArfGAP with dual PH domains 1
(118) ncstn: nicastrin
(119) pak3: p21 protein (Cdc42/Rac)-activated kinase 3
(120) sncb: synuclein, beta
(121) calb1: calbindin 1
(122) cnr1: cannabinoid receptor 1 (brain)
(123) disc1: disrupted in schizophrenia 1
(124) dlgap2: discs, large (Drosophila) homolog-associated protein 2
(125) dlgap4: discs, large (Drosophila) homolog-associated protein 4
(126) dtnb: dystrobrevin, beta
(127) dvl1: dishevelled, dsh homolog 1 (Drosophila)
(128) exoc7: exocyst complex component 7
(129) gabbr1: gamma-aminobutyric acid (GABA) B receptor, 1
(130) panx1: pannexin 1
(131) pclo: piccolo (presynaptic cytomatrix protein)
(132) phactr3: phosphatase and actin regulator 3
(133) picalm: phosphatidylinositol binding clathrin assembly protein
(134) shank1: SH3 and multiple ankyrin repeat domains 1
(135) snap91: synaptosomal-associated protein, 91 kDa homolog (mouse)
(136) stmn4: stathmin-like 4
(137) sod1: superoxide dismutase 1, soluble
(138) synj2: synaptojanin 2
(139) tub: tubby homolog (mouse)
(140) snca: synuclein, alpha (non A4 component of amyloid precursor)
(141) park7: Parkinson disease (autosomal recessive, early onset) 7
(142) pcsk1n: proprotein convertase subtilisin/kexin type 1 inhibitor
(143) palm: Paralemmin
(144) vapb: VAMP (vesicle-associated membrane protein)-associated protein B and C
(145) cttn: cortactin
(146) cacna1a: calcium channel, voltage-dependent, P/Q type, alpha 1A subunit
(147) celsr3: cadherin, EGF LAG seven-pass G-type receptor 3 (flamingo homolog, Drosophila)
(148) chl1: cell adhesion molecule with homology to L1CAM (close homolog of L1)
(149) chrm5: cholinergic receptor, muscarinic 5
(150) cnksr2: connector enhancer of kinase suppressor of Ras 2
(151) cnp: 2′,3′-cyclic nucleotide 3′ phosphodiesterase
(152) cntfr: ciliary neurotrophic factor receptor
(153) cntn1: contactin 1
(154) cplx1: complexin 1
(155) dag1: dystroglycan 1 (dystrophin-associated glycoprotein 1)
(156) dbndd2: dysbindin (dystrobrevin binding protein 1) domain containing 2
(157) dbnl: drebrin-like
(158) dclk2: doublecortin-like kinase 2
(159) dlgap1: discs, large (Drosophila) homolog-associated protein 1
(160) dscam: Down syndrome cell adhesion molecule
(161) ecel1: endothelin converting enzyme-like 1
(162) efnb1: ephrin-B1
(163) eml5: echinoderm microtubule associated protein like 5

(164) epha3: EPH receptor A3

(165) epha5: EPH receptor A5

(166) epha7: EPH receptor A7

(167) ephb3: EPH receptor B3

(168) erbb4: v-erb-a erythroblastic leukemia viral oncogene homolog 4 (avian)

(169) evl: Enah/Vasp-like

(170) exoc5: exocyst complex component 5

(171) fzd9: frizzled homolog 9 (Drosophila)

(172) GABARAP: GABA(A) receptor-associated protein

(173) gabarapl2: GABA(A) receptor-associated protein-like 2

(174) gabrr3: gamma-aminobutyric acid (GABA) A receptor, alpha 3

(175) gcgr: glucagon receptor

(176) gng7: guanine nucleotide binding protein (G protein), gamma 7

(177) got1: glutamic-oxaloacetic transaminase 1, soluble (aspartate aminotransferase 1)

(178) got2: glutamic-oxaloacetic transaminase 2, mitochondrial (aspartate aminotransferase 2)

(179) gprc6a: G protein-coupled receptor, family C, group 6, member A

(180) gria1: glutamate receptor, ionotropic, AMPA 1

(181) grid2: glutamate receptor, ionotropic, delta 2

(182) grik4: glutamate receptor, ionotropic, kainate 4

(183) grin2a: glutamate receptor, ionotropic, N-methyl D-aspartate 2A

(184) grip1: glutamate receptor interacting protein 1

(185) gripap1: GRIP1 associated protein 1

(186) grk6: G protein-coupled receptor kinase 6

(187) opa1: optic atrophy 1 (autosomal dominant)

(188) pak1: p21 protein (Cdc42/Rac)-activated kinase 1

(189) pak2: p21 protein (Cdc42/Rac)-activated kinase 2

(190) pawr: PRKC, apoptosis, WT1, regulator

(191) phactr1: phosphatase and actin regulator 1

(192) pip5k1c: phosphatidylinositol-4-phosphate 5-kinase, type I, gamma

(193) plcb1: phospholipase C, beta 1 (phosphoinositide-specific)

(194) pld3: phospholipase D family, member 3

(195) ppfia3: protein tyrosine phosphatase, receptor type, f polypeptide (PTPRF), interacting protein (liprin), alpha 3

(196) ppid: peptidylprolyl isomerase D

(197) ppp2cb: protein phosphatase 2 (formerly 2A), catalytic subunit, beta isoform

(198) ppp2r2a: protein phosphatase 2 (formerly 2A), regulatory subunit B, alpha isoform

(199) prkar2b: protein kinase, cAMP-dependent, regulatory, type II, beta

(200) prnp: prion protein

(201) ptk2: PTK2 protein tyrosine kinase 2

(202) ptn: pleiotrophin

(203) ryr3: ryanodine receptor 3

(204) sdcbp: syndecan binding protein (syntenin)

(205) sh3gl3: SH3-domain GRB2-like 3

(206) shank2: SH3 and multiple ankyrin repeat domains 2

(207) sirt2: sirtuin (silent mating type information regulation 2 homolog) 2 (S. cerevisiae)

(208) smu1: smu-1 suppressor of mec-8 and unc-52 homolog (C. elegans)

(209) soat1: sterol O-acyltransferase 1

(210) sstr2: somatostatin receptor 2

(211) ssx2ip: synovial sarcoma, X breakpoint 2 interacting protein

(212) stau1: staufen, RNA binding protein, homolog 1 (Drosophila)

(213) stmn3: stathmin-like 3

(214) strn: striatin, calmodulin binding protein

(215) syn1: synapsin I

(216) syngap1: synaptic Ras GTPase activating protein 1 homolog (rat)

(217) synj2bp: synaptojanin 2 binding protein

(218) synpo: synaptopodin

(219) syt11: synaptotagmin XI

(220) trap1: TNF receptor-associated protein 1

(221) trpc2: transient receptor potential cation channel, subfamily C, member 2 (pseudogene)

(222) trpc4: transient receptor potential cation channel, subfamily C, member 4

(223) trpc5: transient receptor potential cation channel, subfamily C, member 5

(224) wnt7a: wingless-type MMTV integration site family, member 7A

(225) tuba1a: tubulin, alpha 1a

(226) vipr2: vasoactive intestinal peptide receptor 2

(227) trak2: trafficking protein, kinesin binding 2

(228) snx17: sorting nexin 17

(229) psd: pleckstrin and Sec7 domain containing

(230) ppp2r2b: protein phosphatase 2 (formerly 2A), regulatory subunit B, beta isoform

(231) ppp1r9b: protein phosphatase 1, regulatory (inhibitor) subunit 9B

(232) grm5: glutamate receptor, metabotropic 5

(233) grk5: G protein-coupled receptor kinase 5

(234) grin2b: glutamate receptor, ionotropic, N-methyl D-aspartate 2B

(235) grik1: glutamate receptor, ionotropic, kainate 1

(236) grasp: GRP1 (general receptor for phosphoinositides 1)-associated scaffold protein

(237) gipc1: GIPC PDZ domain containing family, member 1

(238) dpysl4: dihydropyrimidinase-like 4

(239) dpysl3: dihydropyrimidinase-like 3

(240) dgkb: diacylglycerol kinase, beta 90 kDa

(241) ddn: dendrin

(242) cit: citron (rho-interacting, serine/threonine kinase 21)

(243) grm4: glutamate receptor, metabotropic 4

(244) ctnnd2: catenin (cadherin-associated protein), delta 2 (neural plakophilin-related arm-repeat protein).

I.

Receptor-specific protein interaction networks in lipid raft extracts from control animals. IPA-generated receptor-specific protein lists from control lipid raft samples were clustered into coherent functional interaction networks. Focus molecules (**BOLD** in "molecules in network") denote the proteins that are present in the predicted reaction network as well as the experimental input protein set. The following are different types of interaction networks.

(1) Control: *cell signaling, nucleic acid metabolism, small molecule biochemistry;* score: 32; focus molecule: 15; molecules in network: ADCY, Akt, Beta-Arrestin, **CD4**, **CHRM5**, **CNTFR**, Creb, **EDNRB**, ERK1/2, **FSHR**, **GABBR1**, **GCGR**, Gpcr, GPR3, GPR12, GPR20, GPR34, GPR65, GPR161, **GRM5**, hCG, Mapk, **OPRD1**, OVGP1, P2RY6, P2RY11, PDGF BB, PI3K, Pkc(s), **PTGER2**, **SFRP4**, **SSTR2**, **THBD**, **UNC5B**, **VIPR2**.

(2) Control: *infectious disease, antigen presentation, antimicrobial response;* score: 31; focus molecule: 15; molecules in network: Ap1, **CHRNB3**, **CHRNB4**, **CHRNG**, **CLDN4**, **CNR1**, **CXADR**, G alphai, Ifn, IFN Beta, IFN TYPE 1, IgG, IKK (complex), IL-1R/TLR, IL12 (complex), Il12 (family), Interferon alpha, IRAK, IRF, NFkB (complex), NRG, **OSMR**, P38 MAPK, **SMO**, **TACR1**, Tlr, **TLR3**, **TLR4**, **TLR5**, **TLR6**, **TLR9**, **TSHR**, Ubiquitin.

(3) Control: *cellular development tumor morphology, cell death;* score: 18; focus molecule: 10; molecules in network: APOL5, ARR3, ARTN, ASB16, Cadherin (E,N,P,VE), **CELSR2**, **CELSR3**, CTNNB1, CTNNβ-CDHE/N, **DAG1**, EVX1, **FZD9**, GDNF, **GFRA1**, **GFRA3**, GLTSCR1, **GPRC6A**, GRB2, **GRM4**, HRH4, KCNN1, **OPN1LW**, OPN1SW, PALM2-AKAP2, PHACTR2, PRICKLE3, **PTH2R**, SAG, SEPN1, SHROOM2, SRC.

(4) Control: *carbohydrate metabolism;* score: 2; focus molecule: 1; molecules in network: **CLEC4A**, IL13.

(5) Control: *cell-to-cell signaling and interaction, nervous system development and function;* score: 2; focus molecule: 1; molecules in network: **PRPH2**, ROM1.

(6) Control: *protein synthesis, molecular transport, protein trafficking;* score: 2; focus molecule: 1; molecules in network: **GABRR3**, PRKCZ, SQSTM1.

J.

Receptor-specific protein interaction networks in lipid raft extracts from 3xTgAD animals. IPA-generated receptor-specific protein lists from 3xTgAD lipid raft samples were clustered into coherent functional interaction networks. Focus molecules (BOLD in "molecules in network") denote the proteins that are present in the predicted reaction network as well as the experimental input protein set. The following are different types of interaction networks.

(1) 3xTgAD: *metabolic disease, endocrine system disorders, cell signaling;* score: 45; focus molecule: 18; molecules in network: **ADCYAP1R1**, Ap1, **CD36**, **CD86**, **CNR1**, Creb, CREB-NFkB, **CXADR**, ERK, ERK1/2, **GABBR1**, **GPR56**, hCG, **HTR4**, **HTR2C**, **IGF1R**, **IGF2R**, IgG, IL12 (complex), **IL1R2**, Insulin, Jnk, LDL, **LIFR**, **LRPAP1**, Mapk, MIP1, NFkB (complex), **NPR2**, OVGP1, P38 MAPK, Pkc(s), **TLR5**, **TNFRSF14**, **TSHR**.

(2) 3xTgAD: *cell signaling, nucleic acid metabolism, small molecule biochemistry;* score: 13; focus molecule: 7; molecules in network: AATK, ABR, AKR1A1, BPI, CACNG5, CRYM, cyclic AMP, CYP26B1, DHRS3, DLG4, GH1, Histone h3, HSD17B11, KCTD11, KIF3C, LAP3, **LPHN1**, **LPHN2**, **OPN1LW**, OPN1SW, P2RY11, **PTCH1**, **PTH2R**, RLN3, RN5S, **ROBO1**, ROS1, **RXFP1**, RXFP2, SERPINB8, TMEM49, TNF, USP3.

(3) 3xTgAD: *cell signaling, cellular function and maintenance, molecular transport;* score: 2; focus molecule: 1; molecules in network: CFTR, FREQ, **IL1RAPL1**, MYD88.

(4) 3xTgAD: *cell-to-cell signaling and interaction, cellular function and maintenance, cellular movement;* score: 2; focus molecule: 1; molecules in network: **GPR1**, PAX3, PRDM5.

(5) 3xTgAD: *behavior, digestive system development and function, cell morphology;* score: 2; focus molecule: 1; molecules in network: NPY, **NPY5R**, PPY, PYY, SSB.

(6) 3xTgAD: *cancer, reproductive system disease, gene expression;* score: 2; focus molecule: 1; molecules in network: FOS, MIR103-1, MIR103-2, MIR107, MIRLET7G, MYC, **OMG**, RHOA, RTN4R.

Acknowledgments

This work was carried out with the support of the Intramural Research Program of the National Institute on Aging, National Institutes of Health. The authors thank Dr. LaFerla for kindly donating 3xTgAD breeding pairs to the National Institute on Aging.

References

[1] J. W. Ashford, "APOE genotype effects on Alzheimer's disease onset and epidemiology," *Journal of Molecular Neuroscience*, vol. 23, no. 3, pp. 157–165, 2004.

[2] M. P. Mattson, S. Maudsley, and B. Martin, "BDNF and 5-HT: a dynamic duo in age-related neuronal plasticity and neurodegenerative disorders," *Trends in Neurosciences*, vol. 27, no. 10, pp. 589–594, 2004.

[3] J. Hardy, K. Duff, K. G. Hardy, J. Perez-Tur, and M. Hutton, "Genetic dissection of Alzheimer's disease and related dementias: amyloid and its relationship to tau," *Nature Neuroscience*, vol. 1, no. 5, pp. 355–358, 1998.

[4] J. Hardy and D. J. Selkoe, "The amyloid hypothesis of Alzheimer's disease: progress and problems on the road to therapeutics," *Science*, vol. 297, no. 5580, pp. 353–356, 2002.

[5] S. Maudsley and M. P. Mattson, "Protein twists and turns in Alzheimer disease," *Nature Medicine*, vol. 12, no. 4, pp. 392–393, 2006.

[6] R. W. Mahley, "Apolipoprotein E: cholesterol transport protein with expanding role in cell biology," *Science*, vol. 240, no. 4852, pp. 622–630, 1988.

[7] W. J. Strittmatter, A. M. Saunders, D. Schmechel et al., "Apolipoprotein E: high-avidity binding to β-amyloid and increased frequency of type 4 allele in late-onset familial Alzheimer disease," *Proceedings of the National Academy of Sciences of the United States of America*, vol. 90, no. 5, pp. 1977–1981, 1993.

[8] C.-L. Schengrund, "Lipid rafts: keys to neurodegeneration," *Brain Research Bulletin*, vol. 82, no. 1-2, pp. 7–17, 2010.

[9] D. Lingwood and K. Simons, "Lipid rafts as a membrane-organizing principle," *Science*, vol. 327, no. 5961, pp. 46–50, 2010.

[10] G. P. Gellermann, T. R. Appel, A. Tannert et al., "Raft lipids as common components of human extracellular amyloid fibrils," *Proceedings of the National Academy of Sciences of the United States of America*, vol. 102, no. 18, pp. 6297–6302, 2005.

[11] S.-I. Kubo, V. M. Nemani, R. J. Chalkley et al., "A combinatorial code for the interaction of α-synuclein with membranes," *Journal of Biological Chemistry*, vol. 280, no. 36, pp. 31664–31672, 2005.

[12] R. J. Morris, C. J. Parkyn, and A. Jen, "Traffic of prion protein between different compartments on the neuronal surface, and the propagation of prion disease," *FEBS Letters*, vol. 580, no. 23, pp. 5565–5571, 2006.

[13] D. R. Riddell, G. Christie, I. Hussain, and C. Dingwall, "Compartmentalization of β-secretase (Asp2) into low-buoyant density, noncaveolar lipid rafts," *Current Biology*, vol. 11, no. 16, pp. 1288–1293, 2001.

[14] M. O. W. Grimm, H. S. Grimm, I. Tomic, K. Beyreuther, T. Hartmann, and C. Bergmann, "Independent inhibition of Alzheimer disease β- and γ-secretase cleavage by lowered cholesterol levels," *Journal of Biological Chemistry*, vol. 283, no. 17, pp. 11302–11311, 2008.

[15] L. Kalvodova, N. Kahya, P. Schwille et al., "Lipids as modulators of proteolytic activity of BACE: involvement of cholesterol, glycosphingolipids, and anionic phospholipids in vitro," *Journal of Biological Chemistry*, vol. 280, no. 44, pp. 36815–36823, 2005.

[16] N. Yamamoto, Y. Hirabayashi, M. Amari et al., "Assembly of hereditary amyloid β-protein variants in the presence of favorable gangliosides," *FEBS Letters*, vol. 579, no. 10, pp. 2185–2190, 2005.

[17] N. Yamamoto, K. Matsuzaki, and K. Yanagisawa, "Cross-seeding of wild-type and hereditary variant-type amyloid β-proteins in the presence of gangliosides," *Journal of Neurochemistry*, vol. 95, no. 4, pp. 1167–1176, 2005.

[18] T. Ariga, M. P. McDonald, and R. K. Yu, "Role of ganglioside metabolism in the pathogenesis of Alzheimer's disease—a review," *Journal of Lipid Research*, vol. 49, no. 6, pp. 1157–1175, 2008.

[19] R. Williamson, A. Usardi, D. P. Hanger, and B. H. Anderton, "Membrane-bound β-amyloid oligomers are recruited into lipid rafts by a fyn-dependent mechanism," *FASEB Journal*, vol. 22, no. 5, pp. 1552–1559, 2008.

[20] K. Bhaskar, S.-H. Yen, and G. Lee, "Disease-related modifications in tau affect the interaction between Fyn and tau," *Journal of Biological Chemistry*, vol. 280, no. 42, pp. 35119–35125, 2005.

[21] T. A. Fulga, I. Elson-Schwab, V. Khurana et al., "Abnormal bundling and accumulation of F-actin mediates tau-induced neuronal degeneration in vivo," *Nature Cell Biology*, vol. 9, no. 2, pp. 139–148, 2007.

[22] S. Oddo, A. Caccamo, J. D. Shepherd et al., "Triple-transgenic model of Alzheimer's Disease with plaques and tangles: intracellular Aβ and synaptic dysfunction," *Neuron*, vol. 39, no. 3, pp. 409–421, 2003.

[23] R. L. Nelson, Z. Guo, V. M. Halagappa et al., "Prophylactic treatment with paroxetine ameliorates behavioral deficits and retards the development of amyloid and tau pathologies in 3xTgAD mice," *Experimental Neurology*, vol. 205, no. 1, pp. 166–176, 2007.

[24] B. Martin, R. Brenneman, K. G. Becker, M. Gucek, R. N. Cole, and S. Maudsley, "iTRAQ analysis of complex proteome alterations in 3xTgAD Alzheimer's mice: understanding the interface between physiology and disease," *PLoS ONE*, vol. 3, no. 7, article e2750, 2008.

[25] A. M. Stranahan, K. Lee, K. G. Becker et al., "Hippocampal gene expression patterns underlying the enhancement of memory by running in aged mice," *Neurobiology of Aging*, vol. 31, no. 11, pp. 1937–1949, 2010.

[26] S. Maudsley, K. L. Pierce, A. M. Zamah et al., "The β2-adrenergic receptor mediates extracellular signal-regulated kinase activation via assembly of a multi-receptor complex with the epidermal growth factor receptor," *Journal of Biological Chemistry*, vol. 275, no. 13, pp. 9572–9580, 2000.

[27] S. E. Calvano, W. Xiao, D. R. Richards et al., "A network-based analysis of systemic inflammation in humans," *Nature*, vol. 437, no. 7061, pp. 1032–1037, 2005.

[28] B. Martin, M. P. Mattson, and S. Maudsley, "Caloric restriction and intermittent fasting: two potential diets for successful brain aging," *Ageing Research Reviews*, vol. 5, no. 3, pp. 332–353, 2006.

[29] J. Murray and R. A. Capaldi, "Screening for the metabolic basis of neurodegeneration: developing a focused proteomic approach," *Annals of the New York Academy of Sciences*, vol. 1147, pp. 348–357, 2008.

[30] G. J. Brewer, "Epigenetic oxidative redox shift (EORS) theory of aging unifies the free radical and insulin signaling theories," *Experimental Gerontology*, vol. 45, no. 3, pp. 173–179, 2010.

[31] J. A. Allen, R. A. Halverson-Tamboli, and M. M. Rasenick, "Lipid raft microdomains and neurotransmitter signalling," *Nature Reviews Neuroscience*, vol. 8, no. 2, pp. 128–140, 2007.

[32] S. L. Petersen, S. Krishnan, and E. D. Hudgens, "The aryl hydrocarbon receptor pathway and sexual differentiation of neuroendocrine functions," *Endocrinology*, vol. 147, no. 6, pp. S33–S42, 2006.

[33] J. Caltagarone, Z. Jing, and R. Bowser, "Focal adhesions regulate Aβ signaling and cell death in Alzheimer's disease," *Biochimica et Biophysica Acta*, vol. 1772, no. 4, pp. 438–445, 2007.

[34] S. Maudsley, B. Martin, and L. M. Luttrell, "G protein-coupled receptor signaling complexity in neuronal tissue: implications for novel therapeutics," *Current Alzheimer Research*, vol. 4, no. 1, pp. 3–19, 2007.

[35] S. Maudsley, B. Martin, and L. M. Luttrell, "The origins of diversity and specificity in G protein-coupled receptor signaling," *Journal of Pharmacology and Experimental Therapeutics*, vol. 314, no. 2, pp. 485–494, 2005.

[36] N. C. Inestrosa and E. Arenas, "Emerging roles of Wnts in the adult nervous system," *Nature Reviews Neuroscience*, vol. 11, no. 2, pp. 77–86, 2010.

[37] J. A. Johnson, D. A. Johnson, A. D. Kraft et al., "The Nrf2-ARE pathway: an indicator and modulator of oxidative stress in neurodegeneration," *Annals of the New York Academy of Sciences*, vol. 1147, pp. 61–69, 2008.

[38] M. W. Marlatt and P. J. Lucassen, "Neurogenesis and Alzheimer's disease: biology and pathophysiology in mice and men," *Current Alzheimer Research*, vol. 7, no. 2, pp. 113–125, 2010.

[39] E. Cohen, J. F. Paulsson, P. Blinder et al., "Reduced IGF-1 signaling delays age-associated proteotoxicity in mice," *Cell*, vol. 139, no. 6, pp. 1157–1169, 2009.

[40] S. Freude, K. Schilbach, and M. Schubert, "The role of IGF-1 receptor and insulin receptor signaling for the pathogenesis of Alzheimer's disease: from model organisms to human disease," *Current Alzheimer Research*, vol. 6, no. 3, pp. 213–223, 2009.

[41] W. Araki, H. Kume, A. Oda, A. Tamaoka, and F. Kametani, "IGF-1 promotes β-amyloid production by a secretase-independent mechanism," *Biochemical and Biophysical Research Communications*, vol. 380, no. 1, pp. 111–114, 2009.

[42] B. Martin, R. Brenneman, E. Golden et al., "Growth factor signals in neural cells: coherent patterns of interaction control multiple levels of molecular and phenotypic responses," *Journal of Biological Chemistry*, vol. 284, no. 4, pp. 2493–2511, 2009.

[43] Y. A. Ushkaryov, A. Rohou, and S. Sugita, "alpha-Latrotoxin and its receptors," *Handbook of Experimental Pharmacology*, vol. 184, pp. 171–206, 2008.

[44] J. O. Reilly, I. D. Karavanova, K. P. Williams, N. K. Mahanthappa, and K. L. Allendoerfer, "Cooperative effects of Sonic hedgehog and NGF on basal forebrain cholinergic neurons," *Molecular and Cellular Neuroscience*, vol. 19, no. 1, pp. 88–96, 2002.

[45] A. Thathiah and B. De Strooper, "G protein-coupled receptors, cholinergic dysfunction, and Aβ toxicity in Alzheimer's disease," *Science Signaling*, vol. 2, no. 93, p. re8, 2009.

SAGE-Hindawi Access to Research
International Journal of Alzheimer's Disease
Volume 2010, Article ID 528474, 11 pages
doi:10.4061/2010/528474

Review Article

Neuronal Models for Studying Tau Pathology

Thorsten Koechling,[1,2] Filip Lim,[3] Felix Hernandez,[1,3] and Jesus Avila[1,2]

[1] *Centro de Biología Molecular "Severo Ochoa" (C.S.I.C.-U.A.M.), Facultad de Ciencias, Universidad Autónoma de Madrid, 28049 Madrid, Spain*
[2] *CIBERNED, Centro de Investigación Biomédica en Red de Enfermedades Neurodegenerativas, 28031 Madrid, Spain*
[3] *Departamento de Biología Molecular, Universidad Autónoma de Madrid, 28049 Madrid, Spain*

Correspondence should be addressed to Jesus Avila, javila@cbm.uam.es

Received 10 May 2010; Accepted 17 June 2010

Academic Editor: Gemma Casadesus

Alzheimer's disease (AD) is the most frequent neurodegenerative disorder leading to dementia in the aged human population. It is characterized by the presence of two main pathological hallmarks in the brain: senile plaques containing β-amyloid peptide and neurofibrillary tangles (NFTs), consisting of fibrillar polymers of abnormally phosphorylated tau protein. Both of these histological characteristics of the disease have been simulated in genetically modified animals, which today include numerous mouse, fish, worm, and fly models of AD. The objective of this review is to present some of the main animal models that exist for reproducing symptoms of the disorder and their advantages and shortcomings as suitable models of the pathological processes. Moreover, we will discuss the results and conclusions which have been drawn from the use of these models so far and their contribution to the development of therapeutic applications for AD.

1. Introduction: Alzheimer's Disease, Neuropathology, and Clinical Characteristics

Senile plaques and neurofibrillary tangles are the two main histopathological characteristics of Alzheimer's disease. They were described for the first time by Alois Alzheimer in 1907, who discovered both structures in the autopsy of a brain from a patient who had exhibited severe cognitive impairment and memory loss. Although these hallmarks of the disease were established as long as a hundred years ago, the illness was not fully recognized as such due to the social dismissal of dementia as a normal part of the human ageing process [1]. From the late 1970s onwards however, extensive neurobiological research has been in progress to understand the disease and to develop therapeutic approaches.

Today it is widely accepted that the basis for AD is biological and that senile plaques and neurofibrillary tangles are responsible for the inception of the disorder and also that especially the number of NFTs is proportionally related to the severity of the accompanying symptoms, such as memory loss, confusion, and cognitive failure. Plaques and tangles can be found *post mortem* mainly in the hippocampus and cerebral cortex but also in other areas of the brain important for cognitive functioning.

Early and late onset AD as well as familial and sporadic AD are distinguished based on the time in life of the patient when symptoms first occur and the involvement of gene mutations or chromosomal aberrations that can be related to the disease, respectively. Nevertheless, in all cases the development of histopathological and behavioral symptoms is similar to indistinguishable. Several genetic factors have been described in relation with early and late onset familial AD, though their involvement is not *per se* essential for development of the disorder, given that only about 1% of all cases of Alzheimer's are familial.

However, studying how these genetic influences may be able to induce the symptoms characteristic for AD could be a step towards understanding the mechanisms of the disease and lead scientists towards future clinical therapeutic approaches. Late onset familial AD may involve various susceptibility genes [2, 3]. The most studied is the APOE e4 allele of the gene coding for Apolipoprotein E. Though the underlying mechanism is still unknown, proof exists that

this allele causes a shift in age of onset towards a younger age [4]. In early onset familial AD, mutations have been described in three genes involved in senile plaque formation, namely APP, PSEN1, and PSEN2 which encode the proteins Amyloid precursor protein, presenilin-1, and presenilin-2, respectively. The presenilins are integral membrane proteins that form part of the γ-secretase complex that, after β-secretase cleavage of the Amyloid precursor protein, generates the amyloid β (Aβ) fragment. Mutations in PSEN1 and PSEN2 are believed to possibly contribute to an increase in Aβ, especially the more neurotoxic form comprised of 42 amino acids, Aβ_{42}. Mutated forms of human APP have been expressed in a variety of transgenic animal models to further the understanding of plaque formation.

Other contributing factors to the pathogenesis of AD are being addressed in various studies, and today lifestyle choices, adequate nutrition, psychological well being, and intellectual stimulation are proven to exert important influence on susceptibility to AD and other forms of dementia [5, 6]. The understanding and distribution of this information may not provide a cure but help to prevent the development or lower the severity of AD symptoms in many cases.

1.1. Senile Plaques. Senile plaques are formed via the aggregation of amyloid β outside neuronal cells. While Aβ is a naturally occurring 4 kDa polypeptide in the brain, it becomes neurotoxic in excess quantities or when it fails to be degraded so that polymerization occurs. Extracellular plaques developing in this manner act as synaptotoxins blocking the communication between neurons.

Plaques are formed mostly from Aβ derived from amyloid precursor protein (APP) which is an integral membrane protein type I of unknown function which occurs in different isoforms. The most common isoform which is expressed exclusively in neurons is APP695, comprised of 695 amino acids. APP contains various domains: a single transmembrane domain, an extramembranous N-terminal domain, and a cytoplasmic region at its C-terminus as well as a signal sequence. The neurotoxic effects of APP are believed to be mediated by proteolytic processing of APP which gives rise to Aβ [7]. β-secretase (BACE1, cleaving enzyme of the β-site of APP) liberates the amino terminal fragment of Aβ while the subsequent cleavage by γ-secretase of the resulting C-terminal fragment determines the overall length of the amyloid peptide, giving rise to Aβ_{40}, and the less common but more neurotoxic form Aβ_{42}. α-secretase cleavage of APP does not contribute to plaque formation due to the fact that this cleavage takes place inside the Aβ region of APP. Aβ is believed to be one of the principal factors which causes neurodegeneration in Alzheimer's disease by forming oligomeric aggregates leading to accumulation of these structures in the brain [8]. Aβ_{42} is considered to be more prone to aggregation and probably acts as a catalyst for the aggregation of Aβ_{40} [8].

1.2. Neurofibrillary Tangles. Neurofibrillary tangles (NFT) are the second histopathological hallmark found in brains affected by AD. These intraneuronal lesions consist principally of aberrant filaments, the principal proportion (95%) being paired helical filaments (PHFs), and the rest being straight filaments (SFs). PHFs are bundles made up of twisted filaments, which like SFs, are composed of aberrantly hyperphosphorylated tau protein [9, 10]. The diameter range of PHFs is 8–20 nm and they exhibit periodic repeats of 80 nm along their length while straight filaments do not show this periodicity and have a diameter of 15 nm [11]. PHFs are also the components of the neuropil threads, which appear independently of plaques and tangles and may be observed in an array of dystrophic neurites. Not all neuronal cell types appear to develop neurofibrillary tangles. In the cerebral cortex, all cells containing NFTs are pyramidal neurons, while in the subcortical nuclei the most affected cells are the ones with extremely long axons, consistent with the observation of thin long neurites being especially vulnerable to AD-related cytoskeletal changes [12].

NFTs also appear independently from the presence of senile plaques in other neurodegenerative disorders such as Pick's disease, Progressive supranuclear palsy [13], frontotemporal dementia and parkinsonism linked to chromosome 17 [14], meningioangiomatosis [15], or subacute sclerosing panencephalitis [16].

Under normal physiological conditions however, tau is a phosphoprotein that plays an important role in a variety of processes. Besides its crucial role in tubulin assembly and microtubule stabilization [17, 18], it is also important for the outgrowth of neurites from the cell body [19]. Recently, tau has also been observed to be involved in the migration of new neurons [20]. The authors detected phosphorylated tau protein in newly generated neurons in two well-known regions of adult neurogenesis, the subventricular zone associated with the lateral ventricles and the subgranular zone of the hippocampus. In these zones, phosphorylated tau was colocalized with doublecortin, a cytoskeletal protein that serves as a marker for neuronal migration, while tau knockout mice showed similar numbers of doublecortin-expressing cells but also a significant decrease in migration of these cells. The obtained results suggest a function for tau in the migration of newborn neurons in adult neurogenesis.

The modification of the tau protein by phosphorylation can alter the way it interacts with microtubules, as is the case with AD. There, hyperphosphorylation induces tau to dissociate from the microtubules which depolymerize while the concentration of soluble tau in the cells increases. This effect contributes to the assembly of filaments and the creation of PHFs from the soluble pool of tau. As neurofibrillary tangles are composed mainly of PHFs and their number in the brain has been described to be proportional to the severity of symptoms of dementia, phosphorylation of tau appears to play a major role in the pathogenesis of AD.

Given these observations, it would be of great interest to determine the enzymes that phosphorylate tau in the brain. One of them has been identified as the kinase GSK-3. As an example, in a *Drosophila melanogaster* model, tau phosphorylation via its GSK-3 homologue Shaggy has been described to facilitate its aggregation to filamentous structures [21].

For an extensive explanation of tau and its role under physiological and pathological conditions, see the review published by our group [22].

An alternative interpretation of the role of phosphorylated tau protein has been promoted by the group of Mark A. Smith [23]. These authors question the concept that phospho-tau is inherently toxic because of its presence in neurofibrillary tangles and must therefore be a direct mediator of the disease. Instead, tau aggregation could be a response to the disease, and actually play the role of a protective shield against neurotoxic agents rather than leading to neurodegeneration. In support of this model Castellani and coworkers point out that NFTs, (a) are found in viable neuronal cells even in late stages of AD, (b) exist in the neuronal cytoplasm for decades, (c) can be observed, sometimes at high concentrations, in the brains of elderly persons who showed no signs of dementia throughout their lifetime, and (d) are present in neurons which contain normal amounts of structurally intact microtubules [24].

2. Animal Models for AD and Related Tauopathies

Several animal models of AD have been created in order to emulate specific features of the disease, such as its histopathological, biochemical, and behavioral characteristics. These models were designed to probe the pathological and biochemical changes that take place in affected organisms throughout the progression of the disorder and to test for possible therapeutic measures to be applied in the future in human patients.

The usefulness of an animal model depends on its capability of faithfully replicating the physiological processes that take part in the progress of the disease in human patients so that it leads to a better comprehension of the pathogenesis and finally allows developing an efficient therapeutic approach.

Since no other natural species spontaneously produce all of the histopathological, cognitive, and behavioral symptoms that characterize Alzheimer's, there was a need for the development of transgenic animal models or of dietary manipulation of test animals which would allow reproduction of the hallmarks of AD. From a practical viewpoint, it is of great importance to choose animals with a short lifespan and fast rates of ageing in order to be able to observe, in a reasonable time window, processes which take from 50 to 80 years in humans to appear and develop.

Each animal model has its limitations and advantages, as to date, none are able to express the whole set of characteristics needed to resemble full-blown AD pathology (Table 1). The contribution of each model to the understanding of this devastating disease, however, is immeasurable and has permitted the scientific community to establish an extensive base of knowledge on AD and the mechanics of the disorder. In the following, we will present the different animal models which have been established so far, discuss their characteristics, advantages, and pitfalls as well as take a look at the latest developments in this field of research.

2.1. Lower Eukaryote Models. Different invertebrate models have been created for studying Alzheimer's disease, the most commonly used organism being the fruit fly *Drosophila melanogaster*. Besides being easy to breed, manipulate, and genetically modify, *D. melanogaster* presents the advantage of having an extremely short development time spanning only 12 days from a fertilized egg to an adult fly, so the generation of large numbers of offspring is very easy. In one model, transgenic *Drosophila* expressed human wild type and R406 mutant tau [25]. Although overexpression of either tau form led to the premature death of the flies, symptoms of progressive neurodegeneration were more pronounced in the strain carrying the mutant gene. Intriguingly, the symptoms of neurodegeneration were not accompanied by the formation of neurofibrillary tangles. However, when flies which expressed wild type tau were induced to also overexpress the *Drosophila* GSK-3 homologue shaggy, neurofibrillary lesions could be observed. These findings indicate that higher levels of tau phosphorylation cause its aggregation into filaments and thus indicate an important role for GSK-3 in contributing to the formation of neurofibrillary tangles in AD. Drosophila was also used to investigate the neurotoxicity of human wild type and mutant tau in the early stages of embryonic development [26]. These experiments revealed that in spite of the pan-neuronal expression of tau in these transgenic lines, different anatomical patterns of toxicity in the CNS of these flies could be observed depending on whether the expressed isoform was wild type or mutant. While human WT tau was observed to be hyperphosphorylated at specific sites and caused severe abnormalities in the development of the mushroom body (MB) of the animals, the FTDP17 mutant isoform led to significantly less severe aberrations in MB development. The data from these experiments in *D. melanogaster* suggest that not only high levels of phosphorylation are required to mediate tau toxicity but also that modification has to take place at specific phosphorylation sites, and that tau toxicity is cell type-dependent. Another study points in the same direction, coming to the conclusion that specific phosphorylations at various sites modulate tau toxicity in a synergistic manner [27].

Modeling of Aβ plaque formation in *D. melanogaster* has been another objective of animal studies. The transgenic expression of human WT or mutant APP led to neuronal death in the brain already at the larval stage of development [28]. The severity of the symptoms was proportional to the concentration of Aβ and the C-terminal fragment of APP. Clues exist that the different forms of Aβ as soluble, oligomeric, and insoluble plaque deposits exhibit different toxicities towards cells. This fly model together with the recently generated specific antibodies against the different types of Aβ-aggregates [29, 30] could be used to address this question. *D. melanogaster* has also been successfully employed in the study of the influence of oxidative stress on the pathology of Alzheimer's disease. Lowering the antioxidant defenses of animals which expressed R406 mutant human tau increased tau toxicity while the antioxidant α-tocopherol (vitamin E) was able to alleviate the effects of tau toxicity [31].

Table 1: *Overview of the most widely used models for studying Alzheimer's disease.*

Model	Advantages	Drawbacks
Mus musculus (mouse)	(i) Highly evolved organism, brain anatomy, and metabolism close to humans, results often extrapolatable to humans (ii) Cognitive symptoms of neurodegeneration can be assessed (iii) Generation of conditional transgenic models possible	(i) Relatively long breeding/development time (ii) Ethical concerns (iii) Not suitable for drug screening (iv) Expensive
Danio rerio (zebrafish)	(i) Ex-utero development in transparent capsule allows for live imaging of neurodegenerative processes (ii) Short life cycle (iii) Genetic manipulation tools available	(i) Brain anatomy and genetic setup distinct from humans (ii) Behavior not sufficiently studied, difficult to evaluate cognitive deficits
Caenorhabditis elegans (nematode)	(i) Simple anatomy, (ii) Easy laboratory culture, short life cycle (iii) Genetic manipulation tools highly advanced	(i) Brain anatomy and genetics distinct from humans (ii) Cognitive/behavioral deficits difficult to assess
Drosophila melanogaster (fruit fly)	(i) Reference model for genetic studies (ii) Suitable for drug screening (iii) Short generation times, low maintenance costs (iv) genetic manipulation tools highly advanced	(i) Brain anatomy and genetics distinct from humans (ii) Cognitive/behavioral deficits difficult to assess
In vitro cell culture models	(i) Direct monitoring of parameters over time possible (ii) Extremely valuable for high-throughput screening for therapeutic drugs (iii) Easy handling, economic	(i) Organ structure not conserved, environmental cues/interaction with other organs are not taken into account (ii) Ethical considerations in the case of human embryonic/fetal tissue as source material

Another application of the fruit fly with direct clinical relevance is that of a model organism for first round drug screening in AD. Given its extremely short development period, being an organism which is cheap and easy to manipulate even in large numbers and the low ethical restrictions when working with flies, *D. melanogaster* presents an overall advantageous choice. In a very recent study, a *Drosophila* model was described using the fly's notal bristles as a tool for assessing tau-induced toxicity [32]. The authors propose the use of this model for the screening of possible drugs for use in AD therapy. While the fruit fly presents a number of advantages as a suitable animal model for AD, there are also certain pitfalls. One major restriction when trying to extrapolate experimental data gained with *D. melanogaster* is its significantly different brain structure from humans, as it does not possess a hippocampus for example. Due to its small size the *Drosophila* brain is also difficult to analyse using stains for identification of distinct regional expression of histopathological markers. Last, memory impairment and cognitive deficits in such a phylogenetically distant organism are difficult to extrapolate to compare with human conditions.

To widen the understanding of the cellular mechanisms involved in AD and to aid in the search for pharmacological compounds that could be in the benefit of therapeutic interventions for tauopathies, other lower organisms are being employed as models for the disease. Two of the most widely used animal models at the time are the roundworm *Caenorhabditis elegans* and the zebrafish (*Danio rerio*). The advances that these models provided have been summarized in recent literature reviews [33, 34] for *C. elegans* and [35, 36] for *D. rerio,* respectively. *C. elegans* is a small organism with a short life span that allows for high throughput manipulation and drug screening applications, while the zebrafish, another well-suited organism for studying neurodegeneration, presents the advantage of being completely transparent in its larval development state, allowing continuous in vivo observation of processes taking place in its exposed nervous system. Paquet and coworkers [37] generated a fluorescently labeled tau transgenic zebrafish model. Using this animal, the authors were able for the first time to trace directly neurodegenerative processes taking place in the fluorescently stained larvae and to visualize the resulting neuronal cell death via time lapse microscopy in vivo. In addition, they employed this novel model as a tool for drug screening of GSK-3 inhibitors and have validated one promising compound termed AR-534.

2.2. Mouse Models. Choosing a neuroanatomy which more closely resembles the human brain, several mouse models of AD and other tauopathies have been developed in the last fifteen years. Earlier models fell into two main groups, according to the AD hallmark lesion (amyloid plaques or neurofibrillary tangles) mimicked in each model, but more recent approaches have generated models exhibiting both features simultaneously.

2.2.1. APP/Aβ Modeling. Several transgenic mouse lines have been generated which express one of the mutant forms of

APP. Most of these transgenic lines exhibited senile plaques as Aβ depositions and also the characteristic behavioral deficits reminiscent of AD in animal models. The first of the transgenic animals expressed the human mutant V717F APP form driven by the platelet-derived growth factor (PDGF) mini promoter [38]. Aβ plaque formation was observed in the test animals as well as memory impairment, especially related to spatial learning. When compared to wild type mice, the transgenic animals showed a significantly more severe decline in memory as assessed by a modification of the Morris water maze experiment. Another model expressed a different mutant APP form, the APP^{SW} (Swedish) double mutation inserted into a hamster prion protein (PrP) cosmid vector [39]. The animals presented memory and spatial learning deficits at 9 months of age. β-amyloid concentrations increased fivefold in $A\beta_{40}$ and 14-fold in $A\beta_{42}$, and the deposits could be stained with Congo red especially in the cortical and limbic regions of the brain. In a third model that overexpressed APP sevenfold, amyloid plaques appeared as soon as at six months of age in the tested mice. In contrast to the other two cited studies, these mice showed significant neuronal cell death besides the plaque deposits, specifically of pyramidal neurons in the CA1 region of the hippocampus, with the plaques seemingly affecting cell integrity in the adjacent neurons. Several experiments in transgenic mice have shown that amyloid plaque formation can promote tau pathology [40, 41]. When crossing human APP transgenic mice with tau expressing strains, or administering $A\beta_{42}$ intracerebrally, tau phosphorylation was enhanced and NFT depositions increased in concentration. Interestingly however, when hAPP mice were crossed with tau knockout animals, no memory or learning deficits could be detected in spite of the massive deposition of plaques in these mice [42]. These findings underscore the importance of the presence of tau protein for the induction of the disease as in this animal model amyloid-mediated toxicity was nullified by the absence of tau. The level of neurotoxicity exerted by Aβ also depends on its length as was revealed in a transgenic mouse study carried out by McGowan and coworkers [43], as transgenic mice which express only $A\beta_{40}$ did not develop any senile plaques while $A\beta_{42}$-expressing animals did.

A different mechanism of proteolytic modification of the Amyloid precursor protein is the cleavage at aspartate residue 664 (D664) by caspases. Previous studies suggested that this cleavage, alternative to the described catalytic mechanisms involving secretases, could play a key role in the pathogenesis of AD [44, 45]. To address this question, Harris and coworkers used two transgenic mouse lines carrying the APP gene with (B254) and without (J20) the caspase-specific cleavage site and studied the possible implication of the resulting products, the C31 and Jcasp fragments, in AD [46]. Although these products had been described before to cause cell death in vitro, in these in vivo experiments, histological and behavioral assessment of the test animals did not reveal significant differences between the B254 and J20 mice. The authors came to the conclusion that caspase cleavage of APP does not play a critical role in the generation of AD-related abnormalities in these transgenic mice, and that therefore the D664 cleavage site of APP would not be a suitable target for the development of therapeutic interventions.

Recently, the differential toxicity of soluble Aβ oligomers and fibrillary Aβ plaques has been discussed [47]. In a study with mice, animals which overexpressed the "Arctic" mutation were compared to mice overexpressing wildtype Aβ [48]. While the mutant Aβ (AβE22G) led to the marked formation of amyloid plaques, it also lowered the concentration of a specific nonfibrillar Aβ-assembly (Aβ*56). Remarkably, both strains showed similar behavioral and neuronal deterioration when normalized for Aβ*56 levels, while the number of plaques was very different. The authors of the study concluded that Aβ*56 concentrations are a more suitable marker for AD-related functional deficits than the amount of Aβ deposited in the form of plaques. Therapeutic approaches that lead to the breakdown of fibrillary Aβ but possibly increase the levels of soluble oligomers could therefore be counterproductive.

In view of these data, therapeutic interventions which block the production of Aβ monomers and soluble oligomers should be explored. This could be achieved by inhibiting the secretases involved in APP processing. These enzymes however are involved in other physiological processes as well, and it may therefore be detrimental to indiscriminately reduce their activity. Recent strategies avoid this problem, as in the case of some nonsteroidal anti-inflammatory drugs (NSAIDs) which do not alter secretase activity but alter its cleavage site specificity resulting in the generation of the less toxic 38 residue Aβ instead of the highly amyloidogenic Aβ42 [49]. The introduction of immunotherapeutic treatments could also lead to the specific elimination of Aβ oligomers and might prevent their formation. Positive effects of this approach have been described in a transgenic mouse model [50] and were also assessed in humans in a small cohort of AD patients [51].

2.2.2. NFT Modeling. Transgenic mice carrying cDNAs which encode either the largest or the smallest human tau isoform have been generated. Later, mouse models which express the mutant isoform of tau found in FTDP-17 patients were also developed, as well as mice that model the disease via the overexpression of certain kinases which play a key role in the hyperphosphorylation of tau in AD and related disorders.

The first transgenic mouse which expressed the longest tau isoform under control of the human Thy-1 promoter showed tau phosphorylation at sites which are usually found to be modified in PHFs and presented localization of human tau in neuronal soma, axons, and dendrites. These mice exhibit modest expression of human tau protein (approximately 10% of total tau in the animals) and did not exhibit neurofibrillary tangles [52]. However, the histopathology observed in these animals reflects an early stage of AD prior to the formation of neurofibrillary tangles, in which hyperphosphorylated forms of tau are localized in the soma and dendrites of neuronal cells. In another mouse model in which the shortest human tau isoform was overexpressed [53] under the murine HMG CoA reductase promoter, transgenic tau could be detected in the somatodendritic compartment, although again no NFT formation was observed. Subsequent

transgenic mouse models were designed using stronger promoters, resulting in increased expression of human tau in these animals until eventually brain tau aggregates could be detected, although the formation of NFTs still remained elusive [54, 55]. These models showed not only AD-like symptoms in brain cells but also exhibited spheroidal tau aggregates in the spinal cord resulting in motor symptoms in the animals characteristic more of amyotrophy [56]. While transgenic mice with excessive overexpression of human tau are not viable, lines that overexpress tau less than tenfold have been generated and tau inclusions have been observed in cortical, brain stem, and spinal cord neurons, accompanied by other symptoms such as axon degeneration, decrease of microtubules, and motor deficits. Staining of the inclusions with the AD pathology-specific dyes Congo red and Thioflavin S revealed increasing insolubility of the aggregates over time and NFT-like inclusions could be detected in old animals (18 to 20 months) [57]. Other models with the tau gene under the control of the PrP promoter led to the expression of high levels in certain types of neurons and glial cells. Here, fibrillary structures could be detected in glial cells (oligodendrocytes) as well as neurons [40]. The phenotype however was still not severe. In a mouse model expressing three isoforms of human tau simultaneously, structures were observed which were similar to the astrocytic plaques that characteristically appear in the gray matter in cases of Corticobasal Degeneration (CBD), although neuronal cells were not equally affected, as they did not show any fibrillary lesions [58].

While to this day no mutations have been found in the tau-encoding MAPT gene in AD patients, molecular analysis of another tauopathy, frontotemporal dementia with parkinsonism linked to chromosome 17 (FTDP-17), has revealed characteristic mutations in this gene. Some of them like the P301L or the R406W mutations have been observed to lower tau's potential to promote microtubule stability [59]. In mouse models expressing a human tau isoform containing the P301L mutation [60], reviewed in [61], it was found that this mutation reduces the affinity of tau for microtubules. In one study, the mice showed NFTs in the brain as well as in the spinal cord alongside with a substantial reduction in the number of motor neurons [60]. Furthermore, the animals developed severe behavioral deficits which emulate neurological symptoms of the disease in humans. In another study also employing mice overexpressing human tau with the P301L mutation [40], short tau filaments were isolated from the brains of the test animals. Interestingly, one study revealed that when the expression of mutant P301L tau was suppressed after a period of overexpression, the behavioral symptoms in these mice could be reversed, while the insoluble NFTs were not removed but continued to accumulate. This result hints at the possibility that soluble tau rather than its fibrillary deposits is the cause of neuronal cell death in Alzheimer's disease [62]. A triple transgenic mouse model expressing the mutant transgenes PS1 (M146V), APP^{SW}, and P301L tau was generated by the group of LaFerla to examine the interactions between beta-amyloid, neuronal dysfunction and neurofibrillary tangles [63]. These 3xTg-AD mice developed both of the classical hallmarks of Alzheimer's in human patients, senile plaques and neurofibrillary tangles, and furthermore, synaptic plasticity and neuronal long-term potentiation were impaired in these animals in a manner which could be related to Aβ formation.

In 2002, a transgenic mouse was created that expressed tau bearing the P301S mutation. This mutation is responsible in humans for an early onset of the pathological signs of FTDP-17 [64]. In this model, numerous PHFs consisting of tau filaments could be detected in the brains and spinal cords of the animals. Another observation was that motor neurons were the cell type where the highest concentrations of tau could be detected. Consistent with the findings in human patients where the P301S mutation is related with an earlier onset of FTDP-17 as compared to the P301L mutation, neuronal cell death was highly elevated (49%) in mice which overexpressed human P301S tau. Colocalization of hyperphosphorylated tau deposits and MAP kinases hinted at the possible implication of these enzymes in tau modification. In another study which compared the development of neurodegenerative signs in P301S mutant transgenic and wild type mice, neurofibrillary lesions could be detected in the transgenic animals at the age of 9 to 12 months, accompanied by the massive loss of hippocampal and cortical neurons [65]. Interestingly, synapse loss in the hippocampus and deficits in synaptic function could be observed long before the formation of NFTs, at about three months of age. Given that early microglial activation was also observed and that tau pathology could to some extent be reverted by administration of the immunosuppressive drug FK506, the authors of the study established a link between neuroinflammation and the early stages in the development of tauopathies.

The implication of an improperly controlled cell cycle in neurodegenerative diseases has also been described in the literature [66]. In degenerating neurons elevated concentrations of proteins associated with the cell cycle such as cyclins, cyclin-dependent kinases, and the products of proto-oncogenes such as c-myc, can often be detected. Two studies investigate the effects of cell cycle reentry mediated by transduction with c-myc, using an in vitro cell culture model [67] as well as a transgenic mouse model [68]. Induced cell cycle reentry led to the death of neurons, gliosis, and cognitive impairment in the mouse model, thus indicating that this loss of control in mature, postmitotic neurons may contribute to the pathogenesis of diseases like Alzheimer's. Interestingly, forced cell cycle re-entry led to the phosphorylation of tau and to the formation of tangle-like structures in the in vitro model, providing further evidence for a possible causal connection between the cell cycle and AD.

Another interesting study addresses the possible contribution of insulin to the pathogenesis of AD [69]. As insulin has been described to be involved in the metabolism of both Aβ and tau, the researcher studied the possible effect of artificially induced Diabetes mellitus (DM) on the brain cells of pR5 transgenic mice which expressed the P301L human mutant tau and produced neurofibrillary tangles. After drug induced-insulin depletion, tau phosphorylation increased in both wild type controls and transgenic mice,

though remarkably only the transgenic animals produced massive deposits of nonsoluble hyperphosphorylated tau protein. The authors came to the conclusion that DM is capable of triggering an earlier onset of a preexisting tau pathology in susceptible animals and that diabetes might cause an abnormal phosphorylation of tau via the elevation of glucose levels. Given the high rates of comorbidity of AD and DM in the human population, this line of research deserves further investigation as it might unveil new insights on the pathogenesis of AD.

In a complex yet very elegant survey, a genome wide search strategy employing lentivectors led to the identification of a retroposed gene in mouse [70]. This Rps23r1 gene normally encodes for the ribosomal protein S23 but in the retroposed form is transcribed in the reversed sense, expressing a functional protein which is localized integrated in cell membranes of the cerebral cortex and hippocampus. Intriguingly, overexpression of Rps23r1 reduced levels of Aβ, GSK-3 activity, and tau phosphorylation. The proposed mechanism of this effect consists of an initial interaction with adenylate cyclases upregulating cellular cAMP levels, which in turn activates protein kinase A (PKA). This activation results in the inhibition of GSK-3, a kinase that is involved in tau phosphorylation and Aβ generation.

Given that these aberrant phosphorylations of tau play a key role in the development of Alzheimer's disease, another important strategic approach is to identify the phosphorylation sites that are connected to the formation of aggregates and to identify the responsible enzymes and pathways for these tau modifying reactions, namely, the kinases and phosphatases.

The first generation of transgenic mice expressing GSK-3β, a kinase involved in many physiological pathways, was generated using both ubiquitous or CNS-specific promoters [71]. In all cases however, though slight increases in the phosphorylation levels of tau could be observed, no overexpression of the enzyme took place. This is probably due to the narrow window of concentrations in which GSK-3 can be expressed in cells, below and above which the lack or excess of GSK-3 activity proves lethal.

Considering the narrow concentration range of GSK-3 that permits cell viability, a model was created with GSK-3 gene expression adjustable by means of a conditional tetracycline regulated system under the control of the CaM kinase II α-promoter [72]. The advantage of animal models employing the tetracycline regulation system lies in the possibility to carry out reversible studies [73]. In this mouse model, GSK-3β overexpression was confined to a particular set of cortical and hippocampal neurons. The overexpression of the kinase led to hyperphosphorylation of tau as detected by specific antibodies and showed how tau phosphorylation lowers its affinity for microtubule binding. Behavioral deficits related to Alzheimer's disease however, could be observed in this animal model by applying the Morris water maze test [74]. In spite of these findings, the correlated deposition of insoluble tau neurofibrillary tangles could not be observed. The shutdown of GSK-3 overexpression in turn leads to normal GSK-3 activity, normal phospho-tau levels, diminished neuronal death, and the suppression of the cognitive deficits. These findings further support the potential of GSK-3 inhibitors in the treatment of AD [75].

To further study the involvement of GSK-3, transgenic mice that overexpress GSK-3β were crossed with FTDP-17 mutant tau mice [75]. This AD animal model, termed GSK-3/VLW, shows tau hyperphosphorylation in CA1 hippocampal neurons, the region where the expression patterns of both transgenes overlap. Tau filaments with a PHF-like structure were found in GSK-3/VLW mice but not in single transgenic mice expressing either GSK-3β or FTDP-17 tau alone. PHF-like filament formation in GSK-3/VLW mice was accompanied by thioflavin-S staining, indicating the presence of senile plaques. All these data suggest that there is a synergistic contribution of both types of tau modification, hyperphosphorylation and missense mutations, to induce aberrant tau aggregation.

The same animal model has been utilized to study the possible effects of lithium, a GSK-3 inhibitor used for treating affective disorders with well-documented effects in humans [76]. Two questions were addressed: first, whether chronic lithium treatment is able to prevent the formation of aberrant tau aggregates (formed by overexpression of FTDP-17 tau and GSK-3β); and second, whether lithium can revert already formed tau aggregates and NFTs to achieve their clearance in aged animals. The results indicated that lithium is capable of preventing the development of tau pathology when administered early in disease progression. On the other hand, if lithium administration is initiated at late stages, tau hyperphosphorylation is reduced but tau aggregation cannot be reversed. The data supports studies describing novel GSK-3 inhibitors as new pharmacological treatments of this kind of neurodegenerative disorders, as reviewed byAvila and Hernández [77].

A second transgenic animal expressing a constitutively active form of the kinase, GSK-3β(S9A), has been cross-bred with transgenic mice that overexpress the longest human tau isoform [55]. The number of axonal enlargements present and the motor impairment typical for these tau transgenic animals were reduced in the double transgenic mice [78]. Thus, taking into account all these data it seems that GSK-3 could have different functions in different neurons and in different regions of the brain, while the hippocampal dentate gyrus seems to be more susceptible to degeneration in transgenic mice overexpressing GSK-3β [75]. A recent publication examines the possible role of GSK-3 in tau phosphorylation in the dentate gyrus [79]. Previously generated transgenic mice which overexpress GSK-3 in the dentate gyrus were crossed with a tau knockout strain in order to verify if GSK-3 mediated phosphorylation of tau is the cause of neurodegeneration in the dentate gyrus. When compared to tau-expressing control animals, the authors observed that the signs of neurodegenerative damage were significantly attenuated in the absence of tau. Therefore, hyperphosphorylation of tau is proposed to be a causal factor of the histopathological lesions found in the animals.

Very recently, the role of caspases in AD was reevaluated in a study by Calignon and coworkers [80]. Using the transgenic Tg4510 mouse strain, the researchers observed

that tangle free cells which showed caspase activation formed NFTs within 24 hours. Furthermore, administration of wild type tau into wild type animals led to caspase activation and eventually to tangle formation. The data from this study suggest that caspase activation of tau could be a direct cause of tangle formation, and as has been pointed out in various recent articles, that the AD typical neurofibrillary deposits are the final histological outcome of a neurodegenerative process, rather than the cause of it.

3. Cell Culture Models

While research models in animals allow studies in the whole organism within a reasonable time, there also exists a need for the possibility to investigate disease-related processes in human cells. Live human neuronal cells however are difficult to access for study. Therefore, recently cell culture-based approaches are being developed, relying on the derivation and propagation of neuronal cells from different types of human tissue.

One widely employed model for neuronal cells in culture is the human neuroblastoma line SHSY5Y, which was used to elucidate the role of leptin in Alzheimer's disease. Leptin has recently been proposed as another factor related to the susceptibility of contracting AD. It is an endocrine hormone with implications in food intake regulation as well as processes of learning and memory, for example, in long-term potentiation (LTP) [81]. Epidemiological data from human populations suggest a significantly lower risk of developing AD for people with higher leptin blood levels [82]. The mechanism of action is probably the same as one described for the physiologically closely related peptide insulin. Experiments with differentiated SHSY5Y human neuroblastoma cells indicate that both compounds are capable of reducing the level of tau phosphorylation via inactivation of GSK3-β [83]. Another study revealed a possible protective effect of leptin on neuronal cells against β-amyloid toxicity [84]. In as SHSY5Y cell culture model as well as in a transgenic mouse model, leptin was found to reduce toxic Aβ levels. Leptin reduces the activity of β-secretase, one of the enzymes that cleaves APP, which could probably be the underlying mechanism of the Aβ reducing effect of leptin.

Recently, the applicability of cell culture models has been vastly improved by the possibility of deriving patient-specific cell lines that can be propagated in vitro. Patient-specific fibroblasts for example, can be reprogrammed to induced pluripotent stem (iPS) cells and then differentiated into neuronal cell types similar to those found in the hippocampus or cerebral cortex. This allows the generation of cell models that reproduce certain disease-specific features in vitro, without ethical concerns and which are easily accessible for analysis and manipulation [85].

The groundbreaking work in iPS generation was conducted by the group of Yamanaka, who succeeded in creating pluripotent stem cells first by transducing mouse embryonic fibroblasts with a set of four genes encoding the factors Oct3/4, Sox2, c-Myc, and Klf4. When grown under culture conditions for embryonic stem (ES) cells, these iPS cells showed the morphological traits, growth potential, and immunomarkers of ES cells [86]. Later, the authors were able to generate iPS cells from adult human dermal fibroblasts using the same four factors [87]. Today, several cell lines specific for various neurodegenerative diseases have been generated with the objective of creating human in vitro models. Examples are Amyotrophic lateral sclerosis (ALS) [88], Parkinson disease (PD), and Huntington disease (HD), reviewed in [89]. In the case of ALS, Dimos and coworkers [88] were able to derive iPS cells from fibroblasts of an 82-year-old patient suffering from the disease and subsequently differentiate these iPS cells into motor neurons, the cell type affected by ALS. To date, the generation of Alzheimer's specific iPS cells has not been published, but their generation and differentiation to neuronal types involved in disease progression hopefully will be accomplished soon, offering a novel tool to study the pathological processes, such as tau phosphorylation and tangle formation, which so far have not been completely recapitulated in animal models.

Another strategy is the use of fetal human neural stem cells (hNSC) to create cell models by differentiation of these cells to neuronal types of interest. We have established a method for the differentiation of hNSC to postmitotic neurons which express the neuronal markers tau and βIII-tubulin. These neurons were derived from human fetal forebrain tissue [90] and are viable in cell culture for weeks. This model permits the study of effects of candidate therapeutic drugs on tau expression or phosphorylation state. Furthermore, these cells can be transduced with viral vectors to overexpress AD-related genes, such as those encoding tau or GSK-3 allowing the study of the consequent alterations, including the formation of tangles and plaques.

Additionally, the effect of tau-overexpression on neural stem cells (in their undifferentiated state) is an interesting topic, as brains affected by AD show high levels of tau phosphorylation in regions, such as the hippocampus, where neural stem cells reside and are involved in adult neurogenesis. As research in neural stem cells and neurodifferentiation continues to make technological leaps, further contributions to Alzheimer research can be expected soon by means of creation of human cell models that imitate specific aspects of the disease.

4. Conclusion

In summary, a variety of animal models have been generated which reproduce either the Aβ or tau histopathological hallmark lesions of AD as well as transgenic animals which exhibit both features simultaneously. Some of these models reproduce the lesions as well as the related behavioral impairments, while suggesting that both plaques and tangles may have synergistic effects in driving the disorder rather than developing independently from each other. This observation is strengthened by the notion that the transgenic mouse models most successfully reproducing AD-like pathology are the ones which combine overexpression of tau and APP, like the 3xTg-AD mice [63]. The animal models shed light on mechanisms of progression of tauopathies and their application as drug screening systems pave the way for the development of future treatments of dementia. Due to

the additional need for human models combined with the impossibility of conducting basic research in humans in vivo, the use of iPS cells and neural stem cell cultures derived from human fetal and adult tissue is being established as an alternative and complementary route. While this approach does not hold the advantages of conserving the integrity of the biological system under study, they do allow the study of molecular interaction and biochemical pathways in an all-human system, a point of high relevance due to the human specificity of many aspects of AD.

References

[1] N. S. Whaley, *Senility, confusion, debate, fear: conceptualizing Alzheimer's disease and the history of senile dementia*, Thesis, Drew University, Madison, NJ, USA, 2002.

[2] A. Serretti, P. Artioli, R. Quartesan, and D. De Ronchi, "Genes involved in Alzheimer's disease, a survey of possible candidates," *Journal of Alzheimer's Disease*, vol. 7, no. 4, pp. 331–353, 2005.

[3] A. D. Roses and A. M. Saunders, "Perspective on a pathogenesis and treatment of Alzheimer's disease," *Alzheimer's and Dementia*, vol. 2, no. 2, pp. 59–70, 2006.

[4] A. S. Khachaturian, C. D. Corcoran, L. S. Mayer, P. P. Zandi, and J. C. S. Breitner, "Apolipoprotein E $\varepsilon 4$ count affects age at onset of Alzheimer disease, but not lifetime susceptibility: the Cache County Study," *Archives of General Psychiatry*, vol. 61, no. 5, pp. 518–524, 2004.

[5] S. L. Tyas, D. A. Snowdon, M. F. Desrosiers, K. P. Riley, and W. R. Markesbery, "Healthy ageing in the Nun Study: definition and neuropathologic correlates," *Age and Ageing*, vol. 36, no. 6, pp. 650–655, 2007.

[6] J. Götz and L. M. Ittner, "Animal models of Alzheimer's disease and frontotemporal dementia," *Nature Reviews Neuroscience*, vol. 9, no. 7, pp. 532–544, 2008.

[7] J. Nunan and D. H. Small, "Regulation of APP cleavage by α-, β- and γ-secretases," *FEBS Letters*, vol. 483, no. 1, pp. 6–10, 2000.

[8] J. T. Jarrett and P. T. Lansbury Jr., "Seeding "one-dimensional crystallization" of amyloid: a pathogenic mechanism in Alzheimer's disease and scrapie?" *Cell*, vol. 73, no. 6, pp. 1055–1058, 1993.

[9] K. S. Kosik, C. L. Joachim, and D. J. Selkoe, "Microtubule-associated protein tau (τ) is a major antigenic component of paired helical filaments in Alzheimer disease," *Proceedings of the National Academy of Sciences of the United States of America*, vol. 83, no. 11, pp. 4044–4048, 1986.

[10] R. A. Crowther, "Structural aspects of pathology in Alzheimer's disease," *Biochimica et Biophysica Acta*, vol. 1096, no. 1, pp. 1–9, 1991.

[11] M. Goedert, M. G. Spillantini, N. J. Cairns, and R. A. Crowther, "Tau proteins of Alzheimer paired helical filaments: abnormal phosphorylation of all six brain isoforms," *Neuron*, vol. 8, no. 1, pp. 159–168, 1992.

[12] E. Braak, K. Griffing, K. Arai, J. Bohl, H. Bratzke, and H. Braak, "Neuropathology of Alzheimer's disease: what is new since A. Alzheimer?" *European Archives of Psychiatry and Clinical Neuroscience*, vol. 249, no. 3, pp. III14–III22, 1999.

[13] D. R. Williams and A. J. Lees, "Progressive supranuclear palsy: clinicopathological concepts and diagnostic challenges," *The Lancet Neurology*, vol. 8, no. 3, pp. 270–279, 2009.

[14] D. J. Selkoe and M. B. Podlisny, "Deciphering the genetic basis of Alzheimer's disease," *Annual Review of Genomics and Human Genetics*, vol. 3, pp. 67–99, 2002.

[15] J. Halper, B. W. Scheithauer, H. Okazaki, and E. R. Laws Jr., "Meningio-angiomatosis: a report of six cases with special reference to the occurrence of neurofibrillary tangles," *Journal of Neuropathology and Experimental Neurology*, vol. 45, no. 4, pp. 426–446, 1986.

[16] M. M. Paula-Barbosa, R. Brito, C. A. Silva, R. Faria, and C. Cruz, "Neurofibrillary changes in the cerebral cortex of a patient with subacute sclerosing panencephalitis (SSPE)," *Acta Neuropathologica*, vol. 48, no. 2, pp. 157–160, 1979.

[17] M. D. Weingarten, A. H. Lockwood, S. Y. Hwo, and M. W. Kirschner, "A protein factor essential for microtubule assembly," *Proceedings of the National Academy of Sciences of the United States of America*, vol. 72, no. 5, pp. 1858–1862, 1975.

[18] R. Takemura, S. Okabe, T. Umeyama, Y. Kanai, N. J. Cowan, and N. Hirokawa, "Increased microtubule stability and alpha tubulin acetylation in cells transfected with microtubule-associated proteins MAP1B, MAP2 or tau," *Journal of Cell Science*, vol. 103, no. 4, pp. 953–964, 1992.

[19] C.-W. A. Liu, G. Lee, and D. G. Jay, "Tau is required for neurite outgrowth and growth cone motility of chick sensory neurons," *Cell Motility and the Cytoskeleton*, vol. 43, no. 3, pp. 232–242, 1999.

[20] A. Fuster-Matanzo, E. G. de Barreda, H. N. Dawson, M. P. Vitek, J. Avila, and F. Hernández, "Function of tau protein in adult newborn neurons," *FEBS Letters*, vol. 583, no. 18, pp. 3063–3068, 2009.

[21] G. R. Jackson, M. Wiedau-Pazos, T.-K. Sang et al., "Human wild-type tau interacts with wingless pathway components and produces neurofibrillary pathology in Drosophila," *Neuron*, vol. 34, no. 4, pp. 509–519, 2002.

[22] J. Avila, J. J. Lucas, M. Pérez, and F. Hernández, "Role of tau protein in both physiological and pathological conditions," *Physiological Reviews*, vol. 84, no. 2, pp. 361–384, 2004.

[23] H.-G. Lee, G. Perry, P. I. Moreira et al., "Tau phosphorylation in Alzheimer's disease: pathogen or protector?" *Trends in Molecular Medicine*, vol. 11, no. 4, pp. 164–169, 2005.

[24] R. J. Castellani, A. Nunomura, H.-G. Lee, G. Perry, and M. A. Smith, "Phosphorylated tau: toxic, protective, or none of the above," *Journal of Alzheimer's Disease*, vol. 14, no. 4, pp. 377–383, 2008.

[25] C. W. Wittmann, M. F. Wszolek, J. M. Shulman et al., "Tauopathy in Drosophila: neurodegeneration without neurofibrillary tangles," *Science*, vol. 293, no. 5530, pp. 711–714, 2001.

[26] S. Kosmidis, S. Grammenoudi, K. Papanikolopoulou, and E. M. C. Skoulakis, "Differential effects of tau on the integrity and function of neurons essential for learning in Drosophila," *Journal of Neuroscience*, vol. 30, no. 2, pp. 464–477, 2010.

[27] M. L. Steinhilb, D. Dias-Santagata, T. A. Fulga, D. L. Felch, and M. B. Feany, "Tau phosphorylation sites work in concert to promote neurotoxicity in vivo," *Molecular Biology of the Cell*, vol. 18, no. 12, pp. 5060–5068, 2007.

[28] A. Fossgreen, B. Brückner, C. Czech, C. L. Masters, K. Beyreuther, and R. Paro, "Transgenic Drosophila expressing human amyloid precursor protein show γ-secretase activity and a blistered-wing phenotype," *Proceedings of the National Academy of Sciences of the United States of America*, vol. 95, no. 23, pp. 13703–13708, 1998.

[29] B. O'Nuallain and R. Wetzel, "Conformational Abs recognizing a generic amyloid fibril epitope," *Proceedings of the National Academy of Sciences of the United States of America*, vol. 99, no. 3, pp. 1485–1490, 2002.

[30] G. Habicht, C. Haupt, R. P. Friedrich et al., "Directed selection of a conformational antibody domain that prevents mature amyloid fibril formation by stabilizing Aβ protofibrils," *Proceedings of the National Academy of Sciences of the United States of America*, vol. 104, no. 49, pp. 19232–19237, 2007.

[31] D. Dias-Santagata, T. A. Fulga, A. Duttaroy, and M. B. Feany, "Oxidative stress mediates tau-induced neurodegeneration in Drosophila," *Journal of Clinical Investigation*, vol. 117, no. 1, pp. 236–245, 2007.

[32] P.-A. Yeh, J.-Y. Chien, C.-C. Chou et al., "Drosophila notal bristle as a novel assessment tool for pathogenic study of Tau toxicity and screening of therapeutic compounds," *Biochemical and Biophysical Research Communications*, vol. 391, no. 1, pp. 510–516, 2010.

[33] M. Morcos and H. Hutter, "The model Caenorhabditis elegans in diabetes mellitus and Alzheimer's disease," *Journal of Alzheimer's Disease*, vol. 16, no. 4, pp. 897–908, 2009.

[34] Y. Wu and Y. Luo, "Transgenic C. elegans as a model in Alzheimer's research," *Current Alzheimer Research*, vol. 2, no. 1, pp. 37–45, 2005.

[35] J. J. Sager, Q. Bai, and E. A. Burton, "Transgenic zebrafish models of neurodegenerative diseases," *Brain Structure and Function*, vol. 214, no. 2-3, pp. 285–302, 2010.

[36] D. Paquet, B. Schmid, and C. Haass, "Transgenic zebrafish as a novel animal model to study tauopathies and other neurodegenerative disorders in vivo," *Neurodegenerative Diseases*, vol. 7, no. 1–3, pp. 99–102, 2010.

[37] D. Paquet, R. Bhat, A. Sydow et al., "A zebrafish model of tauopathy allows in vivo imaging of neuronal cell death and drug evaluation," *Journal of Clinical Investigation*, vol. 119, no. 5, pp. 1382–1395, 2009.

[38] D. Games, D. Adams, R. Alessandrini et al., "Alzheimer-type neuropathology in transgenic mice overexpressing V717F β-amyloid precursor protein," *Nature*, vol. 373, no. 6514, pp. 523–527, 1995.

[39] K. Hsiao, P. Chapman, S. Nilsen et al., "Correlative memory deficits, Aβ elevation, and amyloid plaques in transgenic mice," *Science*, vol. 274, no. 5284, pp. 99–102, 1996.

[40] J. Götz, M. Tolnay, R. Barmettler et al., "Human tau transgenic mice: towards an animal model for neuro- and glialfibrillary lesion formation," *Advances in Experimental Medicine and Biology*, vol. 487, pp. 71–83, 2001.

[41] J. Lewis, D. W. Dickson, W.-L. Lin et al., "Enhanced neurofibrillary degeneration in transgenic mice expressing mutant tau and APP," *Science*, vol. 293, no. 5534, pp. 1487–1491, 2001.

[42] E. D. Roberson, K. Scearce-Levie, J. J. Palop et al., "Reducing endogenous tau ameliorates amyloid β-induced deficits in an Alzheimer's disease mouse model," *Science*, vol. 316, no. 5825, pp. 750–754, 2007.

[43] E. McGowan, F. Pickford, J. Kim et al., "Aβ42 is essential for parenchymal and vascular amyloid deposition in mice," *Neuron*, vol. 47, no. 2, pp. 191–199, 2005.

[44] F. G. Gervais, D. Xu, G. S. Robertson et al., "Involvement of caspases in proteolytic cleavage of Alzheimer's amyloid-β precursor protein and amyloidogenic Aβ peptide formation," *Cell*, vol. 97, no. 3, pp. 395–406, 1999.

[45] D. C. Lu, S. Rabizadeh, S. Chandra et al., "A second cytotoxic proteolytic peptide derived from amyloid β-protein precursor," *Nature Medicine*, vol. 6, no. 4, pp. 397–404, 2000.

[46] J. A. Harris, N. Devidze, B. Halabisky et al., "Many neuronal and behavioral impairments in transgenic mouse models of Alzheimer's disease are independent of caspase cleavage of the amyloid precursor protein," *Journal of Neuroscience*, vol. 30, no. 1, pp. 372–381, 2010.

[47] L. Mucke, E. Masliah, G.-Q. Yu et al., "High-level neuronal expression of Aβ(1-42) in wild-type human amyloid protein precursor transgenic mice: synaptotoxicity without plaque formation," *Journal of Neuroscience*, vol. 20, no. 11, pp. 4050–4058, 2000.

[48] I. H. Cheng, K. Scearce-Levie, J. Legleiter et al., "Accelerating amyloid-β fibrillization reduces oligomer levels and functional deficits in Alzheimer disease mouse models," *The Journal of Biological Chemistry*, vol. 282, no. 33, pp. 23818–23828, 2007.

[49] C. Haass and D. J. Selkoe, "Soluble protein oligomers in neurodegeneration: lessons from the Alzheimer's amyloid β-peptide," *Nature Reviews Molecular Cell Biology*, vol. 8, no. 2, pp. 101–112, 2007.

[50] D. Schenk, R. Barbour, W. Dunn et al., "Immunization with amyloid-β attenuates Alzheimer disease-like pathology in the PDAPP mouse," *Nature*, vol. 400, no. 6740, pp. 173–177, 1999.

[51] C. Hock, U. Konietzko, J. R. Streffer et al., "Antibodies against β-amyloid slow cognitive decline in Alzheimer's disease," *Neuron*, vol. 38, no. 4, pp. 547–554, 2003.

[52] J. Gotz, A. Probst, M. G. Spillantini et al., "Somatodendritic localization and hyperphosphorylation of tau protein in transgenic mice expressing the longest human brain tau isoform," *EMBO Journal*, vol. 14, no. 7, pp. 1304–1313, 1995.

[53] J.-P. Brion, G. Tremp, and J.-N. Octave, "Transgenic expression of the shortest human tau affects its compartmentalization and its phosphorylation as in the pretangle stage of Alzheimer's disease," *American Journal of Pathology*, vol. 154, no. 1, pp. 255–270, 1999.

[54] T. Ishihara, M. Hong, B. Zhang et al., "Age-dependent emergence and progression of a tauopathy in transgenic mice overexpressing the shortest human tau isoform," *Neuron*, vol. 24, no. 3, pp. 751–762, 1999.

[55] K. Spittaels, C. Van den Haute, J. Van Dorpe et al., "Prominent axonopathy in the brain and spinal cord of transgenic mice overexpressing four-repeat human tau protein," *American Journal of Pathology*, vol. 155, no. 6, pp. 2153–2165, 1999.

[56] A. Probst, M. Tolnay, C. Mistl et al., "Axonopathy and amyotrophy in mice transgenic for human four-repeat tau protein," *Acta Neuropathologica*, vol. 99, no. 5, pp. 469–481, 2000.

[57] T. Ishihara, B. Zhang, M. Higuchi, Y. Yoshiyama, J. Q. Trojanowski, and V. M.-Y. Lee, "Age-dependent induction of congophilic neurofibrillary tau inclusions in tau transgenic mice," *American Journal of Pathology*, vol. 158, no. 2, pp. 555–562, 2001.

[58] M. Higuchi, T. Ishihara, B. Zhang et al., "Transgenic mouse model of tauopathies with glial pathology and nervous system degeneration," *Neuron*, vol. 35, no. 3, pp. 433–446, 2002.

[59] M. Hasegawa, M. J. Smith, and M. Goedert, "Tau proteins with FTDP-17 mutations have a reduced ability to promote microtubule assembly," *FEBS Letters*, vol. 437, no. 3, pp. 207–210, 1998.

[60] J. Lewis, E. McGowan, J. Rockwood et al., "Neurofibrillary tangles, amyotrophy and progressive motor disturbance in mice expressing mutant (P301L)tau protein," *Nature Genetics*, vol. 25, no. 4, pp. 402–405, 2000.

[61] J. Götz, J. R. Streffer, D. David et al., "Transgenic animal models of Alzheimer's disease and related disorders: histopathology, behavior and therapy," *Molecular Psychiatry*, vol. 9, no. 7, pp. 664–683, 2004.

[62] K. Santacruz, J. Lewis, T. Spires et al., "Medicine: tau suppression in a neurodegenerative mouse model improves memory function," *Science*, vol. 309, no. 5733, pp. 476–481, 2005.

[63] S. Oddo, A. Caccamo, J. D. Shepherd et al., "Triple-transgenic model of Alzheimer's disease with plaques and tangles: intracellular Aβ and synaptic dysfunction," *Neuron*, vol. 39, no. 3, pp. 409–421, 2003.

[64] B. Allen, E. Ingram, M. Takao et al., "Abundant tau filaments and nonapoptotic neurodegeneration in transgenic mice expressing human P301s tau protein," *Journal of Neuroscience*, vol. 22, no. 21, pp. 9340–9351, 2002.

[65] Y. Yoshiyama, M. Higuchi, B. Zhang et al., "Synapse loss and microglial activation precede tangles in a P301S tauopathy mouse model," *Neuron*, vol. 53, no. 3, pp. 337–351, 2007.

[66] X. Zhu, H.-G. Lee, G. Perry, and M. A. Smith, "Alzheimer disease, the two-hit hypothesis: an update," *Biochimica et Biophysica Acta*, vol. 1772, no. 4, pp. 494–502, 2007.

[67] A. McShea, H.-G. Lee, R. B. Petersen et al., "Neuronal cell cycle re-entry mediates Alzheimer disease-type changes," *Biochimica et Biophysica Acta*, vol. 1772, no. 4, pp. 467–472, 2007.

[68] H.-G. Lee, G. Casadesus, A. Nunomura et al., "The neuronal expression of MYC causes a neurodegenerative phenotype in a novel transgenic mouse," *American Journal of Pathology*, vol. 174, no. 3, pp. 891–897, 2009.

[69] Y. D. Ke, F. Delerue, A. Gladbach, J. Götz, and L. M. Ittner, "Experimental diabetes mellitus exacerbates Tau pathology in a transgenic mouse model of Alzheimer's disease," *PLoS ONE*, vol. 4, no. 11, Article ID e7917, 2009.

[70] Y.-W. Zhang, S. Liu, X. Zhang et al., "A functional mouse retroposed gene Rps23r1 reduces Alzheimer's β-amyloid levels and tau phosphorylation," *Neuron*, vol. 64, no. 3, pp. 328–340, 2009.

[71] J. Brownlees, N. G. Irving, J.-P. Brion et al., "Tau phosphorylation in transgenic mice expressing glycogen synthase kinase-3β transgenes," *NeuroReport*, vol. 8, no. 15, pp. 3251–3255, 1997.

[72] J. J. Lucas, F. Hernández, P. Gómez-Ramos, M. A. Morán, R. Hen, and J. Avila, "Decreased nuclear β-catenin, tau hyperphosphorylation and neurodegeneration in GSK-3β conditional transgenic mice," *EMBO Journal*, vol. 20, no. 1-2, pp. 27–39, 2001.

[73] A. Yamamoto, J. J. Lucas, and R. Hen, "Reversal of neuropathology and motor dysfunction in a conditional model of Huntington's disease," *Cell*, vol. 101, no. 1, pp. 57–66, 2000.

[74] F. Hernández, J. Borrell, C. Guaza, J. Avila, and J. J. Lucas, "Spatial learning deficit in transgenic mice that conditionally over-express GSK-3β in the brain but do not form tau filaments," *Journal of Neurochemistry*, vol. 83, no. 6, pp. 1529–1533, 2002.

[75] T. Engel, F. Hernández, J. Avila, and J. J. Lucas, "Full reversal of Alzheimer's disease-like phenotype in a mouse model with conditional overexpression of glycogen synthase kinase-3," *Journal of Neuroscience*, vol. 26, no. 19, pp. 5083–5090, 2006.

[76] T. Engel, P. Goñi-Oliver, J. J. Lucas, J. Avila, and F. Hernández, "Chronic lithium administration to FTDP-17 tau and GSK-3β overexpressing mice prevents tau hyperphosphorylation and neurofibrillary tangle formation, but pre-formed neurofibrillary tangles do not revert," *Journal of Neurochemistry*, vol. 99, no. 6, pp. 1445–1455, 2006.

[77] J. Avila and F. Hernández, "GSK-3 inhibitors for Alzheimer's disease," *Expert Review of Neurotherapeutics*, vol. 7, no. 11, pp. 1527–1533, 2007.

[78] K. Spittaels, C. Van den Haute, J. Van Dorpe et al., "Glycogen synthase kinase-3β phosphorylates protein tau and rescues the axonopathy in the central nervous system of human four-repeat tau transgenic mice," *The Journal of Biological Chemistry*, vol. 275, no. 52, pp. 41340–41349, 2000.

[79] E. G. de Barreda, M. Pérez, P. G. Ramos et al., "Tau-knockout mice show reduced GSK3-induced hippocampal degeneration and learning deficits," *Neurobiology of Disease*, vol. 37, no. 3, pp. 622–629, 2010.

[80] A. de Calignon, L. M. Fox, R. Pitstick et al., "Caspase activation precedes and leads to tangles," *Nature*, vol. 464, no. 7292, pp. 1201–1204, 2010.

[81] J. Harvey, "Leptin: the missing link in Alzheimer disease?" *Clinical Chemistry*, vol. 56, no. 5, pp. 696–697, 2010.

[82] W. Lieb, A. S. Beiser, R. S. Vasan et al., "Association of plasma leptin levels with incident Alzheimer disease and MRI measures of brain aging," *Journal of the American Medical Association*, vol. 302, no. 23, pp. 2565–2572, 2009.

[83] S. J. Greco, S. Sarkar, G. Casadesus et al., "Leptin inhibits glycogen synthase kinase-3β to prevent tau phosphorylation in neuronal cells," *Neuroscience Letters*, vol. 455, no. 3, pp. 191–194, 2009.

[84] D. C. Fewlass, K. Noboa, F. X. Pi-Sunyer, J. M. Johnston, S. D. Yan, and N. Tezapsidis, "Obesity-related leptin regulates Alzheimer's Aβ," *FASEB Journal*, vol. 18, no. 15, pp. 1870–1878, 2004.

[85] S. J. Chamberlain, X.-J. Li, and M. Lalande, "Induced pluripotent stem (iPS) cells as in vitro models of human neurogenetic disorders," *Neurogenetics*, vol. 9, no. 4, pp. 227–235, 2008.

[86] K. Takahashi and S. Yamanaka, "Induction of pluripotent stem cells from mouse embryonic and adult fibroblast cultures by defined factors," *Cell*, vol. 126, no. 4, pp. 663–676, 2006.

[87] K. Takahashi, K. Tanabe, M. Ohnuki et al., "Induction of pluripotent stem cells from adult human fibroblasts by defined factors," *Cell*, vol. 131, no. 5, pp. 861–872, 2007.

[88] J. T. Dimos, K. T. Rodolfa, K. K. Niakan et al., "Induced pluripotent stem cells generated from patients with ALS can be differentiated into motor neurons," *Science*, vol. 321, no. 5893, pp. 1218–1221, 2008.

[89] I.-H. Park, N. Arora, H. Huo et al., "Disease-specific induced pluripotent stem cells," *Cell*, vol. 134, no. 5, pp. 877–886, 2008.

[90] E. Åkesson, J.-H. Piao, E.-B. Samuelsson et al., "Long-term culture and neuronal survival after intraspinal transplantation of human spinal cord-derived neurospheres," *Physiology and Behavior*, vol. 92, no. 1-2, pp. 60–66, 2007.

SAGE-Hindawi Access to Research
International Journal of Alzheimer's Disease
Volume 2010, Article ID 573138, 10 pages
doi:10.4061/2010/573138

Review Article

Modeling of Tau-Mediated Synaptic and Neuronal Degeneration in Alzheimer's Disease

Tomasz Jaworski,[1] Sebastian Kügler,[2] and Fred Van Leuven[1]

[1] *Experimental Genetics Group, Department of Human Genetics, KULeuven-Campus Gasthuisberg ON1-06.602, Herestraat 49, 3000 Leuven, Belgium*
[2] *Center of Molecular Physiology of the Brain (CMPB), Department of Neurology, University Medicine Göttingen, Waldweg 33, 37073 Göttingen, Germany*

Correspondence should be addressed to Fred Van Leuven, fred.vanleuven@med.kuleuven.be

Received 18 May 2010; Accepted 9 July 2010

Academic Editor: Gemma Casadesus

Patients suffering from Alzheimer's disease (AD) are typified and diagnosed postmortem by the combined accumulations of extracellular amyloid plaques and of intracellular tauopathy, consisting of neuropil treads and neurofibrillary tangles in the somata. Both hallmarks are inseparable and remain diagnostic as described by Alois Alzheimer more than a century ago. Nevertheless, these pathological features are largely abandoned as being the actual pathogenic or neurotoxic factors. The previous, almost exclusive experimental attention on amyloid has shifted over the last 10 years in two directions. Firstly, from the "concrete" deposits of amyloid plaques to less well-defined soluble or pseudosoluble oligomers of the amyloid peptides, ranging from dimers to dodecamers and even larger aggregates. A second shift in research focus is from amyloid to tauopathy, and to their mutual relation. The role of Tau in the pathogenesis and disease progression is appreciated as leading to synaptic and neuronal loss, causing cognitive deficits and dementia. Both trends are incorporated in a modified amyloid cascade hypothesis, briefly discussed in this paper that is mainly concerned with the second aspect, that is, protein Tau and its associated fundamental questions.

1. Background

1.1. The Amyloid Problem. Amyloid peptides are derived from the amyloid precursor protein (APP) by sequential proteolytic cleavages by β- and γ-secretases [1, 2]. Amyloid peptides, particularly the longer Aβ42 species, aggregate into various and different chemical or physical entities, which are now considered the primary pathological agents in AD. Controversial experimental data leave nevertheless many questions open with regards to the exact composition and size of the amyloid oligomers in vivo [3–5]. Moreover, the precise molecular actions of the amyloid peptides and their aggregates remain unknown and enigmatic, largely because their molecular targets, or their specific receptors remain undefined. This issue raises more fundamental questions. For one, while the proteolytic enzymes and their mechanisms responsible for the generation of the amyloid peptides become well-known and understood at the molecular level, the eventual physiological function of the peptides is still questioned—and remains questionable.

The original pathological importance ascribed to amyloid plaques was weakened, if not eliminated based on information gathered in transgenic models expressing mutant APP. We have advocated this hypothesis since we discovered early defects in cognition and LTP in APP.V717I mice [6–11]. Matters are, however, complicated further by recent data originating from several clinical trials that identified a large fraction of individuals in the control groups with considerable brain amyloid load using PET-imaging [12–14]. Obviously, this means that high-amyloid concentration in the brain is not per se incompatible with normal cognitive functioning in old age. This calls for other factors to be at least coresponsible for the cognitive demise in AD-forwarding protein Tau as the most obvious candidate.

1.2. Tauopathy: Not Primary but Secondary in AD. Primary Tauopathy is recognized in a vast and still increasing number of CNS-disorders. The pathology is visualized postmortem as intraneuronal aggregates of protein Tau, known as neuropil treads and neurofibrillary tangles. These are similar if not identical to those observed in AD brain and mostly present without other associated pathological hallmarks, except inflammation markers. The large clinical variability among the primary Tauopathies stems from the presence of the Tau pathology in different types of neurons and in different brain-regions [15–18].

Biochemically, all Tauopathies consist of smaller and larger aggregates and fibrils that become intertwined to form larger tangles in the soma as well as in axons and dendrites of affected neurons. The aggregates consist almost exclusively of protein Tau, albeit as different isoforms in different diseases, that is, either Tau.3R or Tau.4R or as a variable admixture. Their widely different grading of phosphorylation is usually referred to as hyperphosphorylated Tau, denoted here as hP-Tau. Importantly, no accurate definition based on either the level or the specific phosphorylated residues can typify any Tauopathy exactly, because of the large variability with each primary disease.

Most primary Tauopathies are sporadic. Rare familial cases of frontotemporal dementia (FTD) are linked to exonic and intronic mutations in the MAPT gene coding for protein Tau (chromosome 17). Although rare, their identification marked a major breakthrough and boosted interest in Tauopathy, because of the evident implication that Tauopathy itself is sufficient to cause cognitive decline and dementia [15, 16, 18–21].

Both intronic and exonic mutations have important mechanistical implications: (i) most expressed mutations are in the microtubule binding domain of Tau; (ii) intronic mutations promote or hinder splicing of exon 10 coding for the second repeat domain in the microtubule binding domain, skewing expression of isoforms to either Tau3R or Tau4R, but both with normal sequences and consequently normal binding-affinity for microtubules.

The pathology resulting from intronic mutations in the MAPT gene can only be explained by effects on RNA splicing, eventually resulting in changes in absolute or relative levels of Tau isoforms that otherwise have normal wild-type protein sequences. The overexpression or overrepresentation of one or the other Tau isoform can then be extrapolated to the primary Tauopathies that are sporadic, as well as to sporadic AD as the most prominent secondary Tauopathy involving normal, wild-type Tau-isoforms.

1.3. The Obligate Amyloid-Tau Relation. The major unresolved problem in AD is the mechanistic relation of amyloid and Tau pathology. Amyloid oligomers are proposed to precede, and eventually trigger the intracellular Tauopathy, likely by increasing the phosphorylation of protein Tau [11, 15, 17, 22]. While this hypothesis remains at this moment in time impossible to prove in sporadic AD cases, it is supported by extrapolation of observations in familial AD cases. Indeed, even in the most early onset familial AD that are caused by mutant Presenilin or mutant APP, and therefore by definition are "amyloid-triggered", Tauopathy is always evident and codiagnostic. Experimentally, double and triple transgenic mouse models with combined amyloid and Tau-pathology prove the same intimate relation [23–26].

The genetic data imply that deranged Tau-microtubule interactions, caused either directly by the mutation, by phosphorylation, by increased absolute or by disturbed relative concentrations of Tau, all can contribute or even be sufficient to cause neurodegeneration in primary Tauopathies, that is, in the absence of amyloid pathology. Importantly, experimental decrease of the level of Tau in amyloid transgenic mice can actually ameliorate several clinical symptoms and defects [27]. The combined data further corroborate the hypothesis that protein Tau is essentially contributing to amyloid-induced cognitive defects.

Not resolved are the identity and exact nature of the receptors and associated signaling pathways that lead from amyloid to Tau. These pathways obligatory involve kinases such as GSK3 [25, 26] that contribute, directly or indirectly to the phosphorylation of Tau at residues that affect its binding to microtubuli. This is thought, but not proven, to instigate its eventual aggregation into fibrils that are deposited locally as neuropil treads or transported to the soma and form the neurofibrillary tangles, and both types of aggregates occur in the same neurons. Nevertheless, Tauopathy does not per se cause immediate or even delayed neuronal death, as tangled and Tau-loaded neurons are observed in humans as well as in experimental models, that is, transgenic mice, zebra-fish, and flies [26, 28, 29].

The pertinent question to be answered then is: what chemical or physical form of protein Tau causes synapto- and neurodegeneration?

2. Transgenic and Adeno-Associated Virus Models

Invaluable insight in the problems that we are concerned with, have resulted from analyzing different transgenic mouse models. Our research-group generated, characterized, and validated many different transgenic mouse strains and their bigenic combinations as preclinical models over the last two decades. So far none of the models recapitulates robustly the evident neurodegeneration observed in the brain of AD patients.

We explored and reported on additional models to increase our understanding of this aspect of the pathogenesis of AD [11, 30]. Here, we review data and insights obtained with adeno-associated viral vectors that were engineered to express wild-type or mutant APP or protein Tau in pyramidal neurons of the hippocampus of wild-type mice. Thereby, we aimed to recapitulate aspects of AD pathology and related features that are not attainable in transgenic mice, particularly neurodegeneration.

Among the different viral vectors available, we selected AAV because these have been demonstrated as excellent and safe tools for gene delivery into the CNS. Recent technical advances have improved AAV-based vectors as

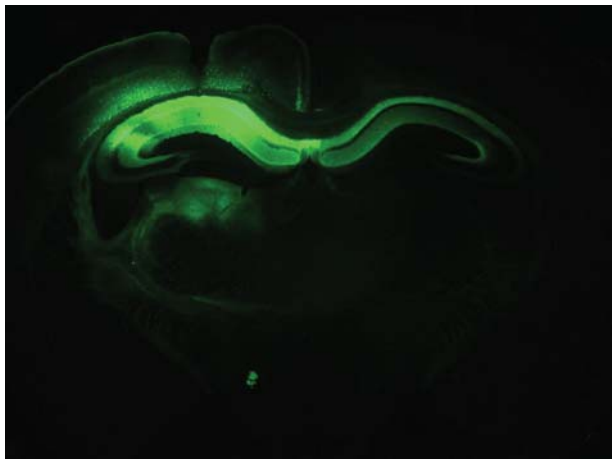

Figure 1: *Expression of EGFP following hippocampal injection of AAV1/2.EGFP is long-lasting.* Six months following intracerebral injection of the AAV.EGFP vector, the transgene remained expressed in the CA1/2 subfields of the hippocampus and in the deeper layers of the cortex. Expression of EGFP is also evident in and likely propagates along axonal projections of the fornix.

tools in neuronal research [31, 32]. The expression of the human transgenes used in our studies was controlled by the human Synapsin1 gene promoter, with constructs packed in chimeric capsids AAV1/2, expressing efficiently in pyramidal neurons of the CA1/2 subfield of the hippocampus (Figure 1). Control AAV vectors expressed EGFP in the designated neurons and areas that persisted for months without negative signs or symptoms (Figure 1) and [31, 32].

2.1. Amyloid Pathology without Neurodegeneration. We first constructed AAV vectors to recapitulate the amyloid pathology in the limbic region of wild-type mice. The constructs contained APP695 as the most abundant neuronal isoform, either as wild type sequence or as the engineered triple mutant (denoted APP.SLA). The incorporated Swedish, London and Austrian mutations are each associated with familial forms of AD [33–35].

Following intracerebral injection into wild-type mice, the APP.SLA mutant produced a gradual accumulation of APP and amyloid peptides in pyramidal neurons in the hippocampal CA1/2-region, as well as in the deeper layers of the neighboring cortex. Similar expression of wild-type human APP695 failed to produce any deposition of amyloid or of the related effects observed with mutant APP.SLA [30].

Initially, from 3 weeks to 3 months postinjection (p.i.), amyloid immunoreactivity appeared as intracellular inclusions or vacuolar bodies inside pyramidal neurons. At 6 months p.i., amyloid plaques developed as immunoreactive and thioflavinS positive deposits in the hippocampus and cortex (Figure 2). At this late time-point, we also observed increased phosphorylation of endogenous mouse protein Tau, particularly at residues T181 and T231, both known to be substrate for GSK3. These phosphoepitopes, defined by antibodies AT270 and AT180 were differentially expressed, that is, in hippocampal pyramidal neurons (T231) and in dystrophic neurites around amyloid plaques (T181).

In contrast, Intracerebral injection of AAV-APP.SLA not in wild-type but in Tau.P301L mice led to the formation of neurofibrillary tangles (NFT), demonstrating that the viral assault did not prevent protein Tau from forming tangles (Figure 2). Moreover, the combination demonstrated that besides the primary hit, also the receiving genetic background is of utmost importance. Most interesting for the interpretation of the data obtained with protein Tau, discussed in the next section, was the observation that at 6 months p.i. the phosphorylation of endogenous mouse Tau was increased and coincided with a minor but significant reduction in the number of neurons in the CA1 region of AAV-APP.SLA injected mice [30].

2.2. Tau-Mediated Pyramidal Neurodegeneration without Tauopathy. In second instance, we similarly expressed either wild-type Tau.4R or mutant Tau.P301L by AAV-vectors in wild-type mouse brain. In sharp contrast to APP-SLA, AAV-mediated expression of protein Tau resulted already at 3 weeks p.i. in marked neurodegeneration of pyramidal neurons in CA and adjacent cortical layers [30]. These findings were rather unexpected and we analyzed them in different directions, yielding novel and important insight into the mechanisms causing neuronal death by protein Tau.

Most remarkably, we could not detect any major form of aggregates of protein Tau in pyramidal neurons that expressed either wild-type or mutant protein Tau. Extensive analysis by histochemistry and immunohistochemistry with a panel of indicator compounds and monoclonal antibodies to protein Tau, did not reveal any appreciable signs of formation of intraneuronal Tau-aggregates, either before or during or after the pyramidal neurons in CA1/2 succumbed [30].

The observed neurodegeneration was not due to massive overexpression of human protein Tau. The actual levels in hippocampal extracts were near-physiological and only about twice those of endogenous mouse Tau4R. Note that also in the AAV-APP.SLA model described in the previous section, the hippocampal levels of human APP.SLA were only about twice those of endogenous murine APP. In addition, expression of EGFP by the same AAV-type vectors proved harmless to pyramidal neurons over long time-periods (Figure 1) and [30, 31].

Intracerebral injection of 3- and 10-fold less AAV-Tau, with consequently less expression of human protein Tau, produced a graded, lesser loss of hippocampal neurons [30]. The AAV-Tau-induced neurodegeneration is thereby further demonstrated to be directly caused by and proportional to the near-physiological levels of protein Tau.

Consequently, the observed pyramidal cell-death is qualified as specific for human protein Tau. This conclusion holds up for wild-type Tau.4R and for mutant Tau.P301L, making the model at least conform the observations in familial FTD. Indeed, as discussed above, intronic and exonic mutations yield very similar clinical outcome, despite the expression of mutant or wild-type Tau4R, respectively. The actual

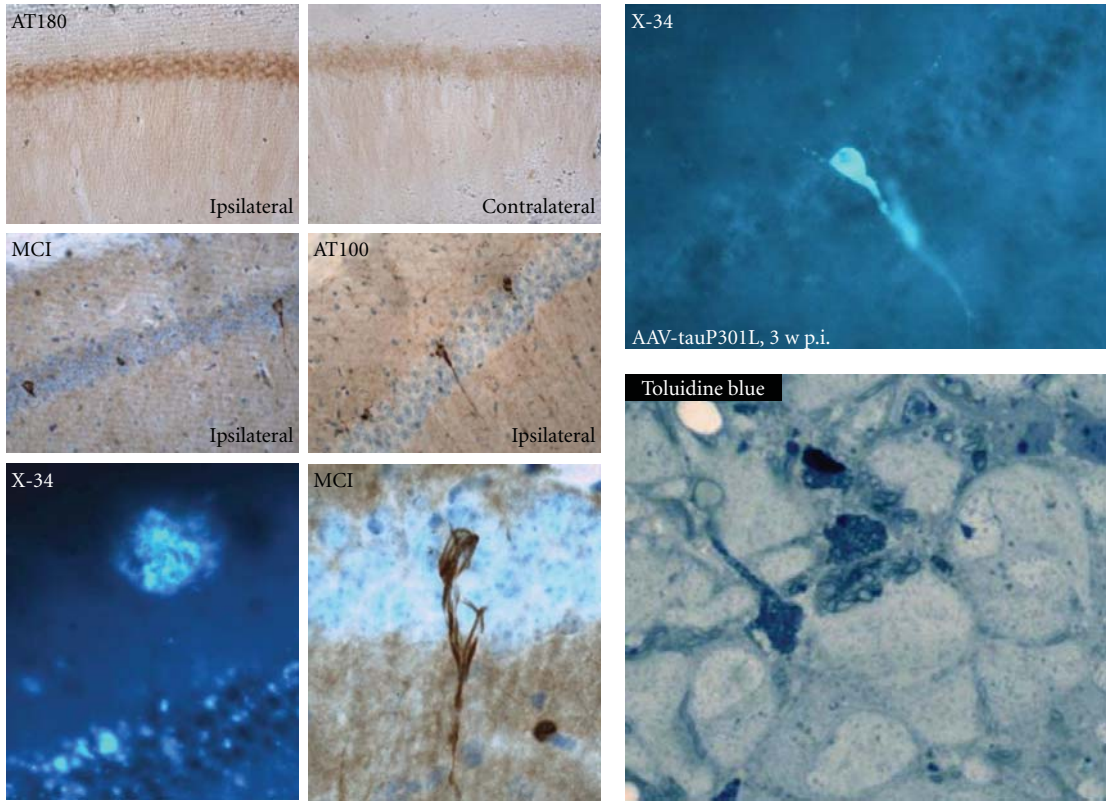

Figure 2: *Protein Tau is activated by and therefore downstream of amyloid pathology.* (a) Tau.P301L transgenic mice [36] were injected intracerebrally at age 1.5 months with either AAV-APP.SLA vector (10e8 tu) or with AAV-EGFP as control. At 6 months p.i. the expression of APP.SLA, unlike EGFP, led to formation of amyloid aggregates and plaques, as shown by histochemical staining with X34 (lower left panel). The mutant APP.SLA also strongly increased the phosphorylation of transgenic Tau.P301L resulting in the formation of neurofibrillary tangles already at this age of the Tau.P301L mice in pyramidal neurons of CA1: immunohistochemistry with Mab AT180 specific for phospho-T231-Tau (upper panels), Mab MC1 (conformational Tau-epitope) (middle panel left) and Mab AT100 (phospho-S212/T214) (middle panel right). Remarkably, the amyloid plaques and Tau pathological aggregates coexist in AAV-APP.SLA-injected Tau.P301L mice without causing appreciable neurodegeneration. (b) Intracerebral injection of AAV-Tau.P301L (10e8 tu) in wild-type mice produced extensive neurodegeneration of CA1 pyramidal neurons as shown before [11]. Aggregates of Tau or tangles were very rare although they can form in these neurons in the experimental conditions, as shown histochemically with compound X34 as sensitive probe for β-sheeted aggregated protein [12, 14]. Clearly, the paucity of tangles cannot explain the extensive neuronal cell death. Degenerating neurons share morphological features of necrosis and autophagy, with extensive vacuolization as demonstrated histochemically by toluidin blue staining (bottom panel).

contribution of the mutation to the mechanism underlying the pathogenesis requires a rational explanation in human FTD patients, as well as in the AAV-models.

3. Mechanisms Underlying Tau-Mediated Pyramidal Neurodegeneration

Extensive analysis to define the mechanisms that underlie the observed Tau-mediated pyramidal neurodegeneration are described, summarizing reported data and preliminary data of work in progress.

Similar AAV-mediated expression of a truncated version of protein Tau.4R, lacking the microtubule binding C-terminal domain, proved completely harmless and did not cause any neurodegeneration over similar time-periods [30]. The inherent conclusion must be that microtubule binding of protein Tau is essentially involved in the neurotoxic degenerative mechanism. Consequently, we must orient further analysis to mechanisms that involve axonal and dendritic transport over microtubuli, which is of paramount importance for all cells but especially for neurons with their intricate branching.

Of note, microgliosis was observed to be intense, and spatially and temporally closely associated with AAV-Tau induced degenerating neurons [30]. This was most recently also reported in a similar model based on AAV vectors but in rats and for a different pathology in a different brain-region [38]. Previously, we have observed a similar relation of microgliosis to neurodegeneration in an unrelated model for

hippocampal sclerosis, caused by conditional expression of p25, the truncated activator of cdk5 [39]. Also, in that model, intense neurodegeneration was not marked by aggregation of protein Tau, further strengthening our conclusion that cdk5 is not a major Tau-kinase in vivo [39–41].

The data originating from the AAV-models led us to conclude that not large aggregates of protein Tau cause neurodegeneration [30]. This confirms our observations in transgenic mice that show aggregation of Tau leading to Tauopathy in somata and neuropil, but not accompanied by marked neurodegeneration [25, 26, 36].

We proposed that neurons affected by Tauopathy can either engage in aggregation of Tau and thereby try to decrease the toxic species and hope to survive, or to enter the "path to death" by failing to aggregate protein Tau [11]. Clearly, the viral models comply with the transgenic models that aggregation of Tau and neurodegeneration are not closely linked. Thereby, questions are raised that are addressed in more detail in the next sections.

3.1. What is the Neurotoxic Tau-Species?

The classic concept that Tau-fibrils or tangles are neurotoxic in Tauopathies can be abandoned. We advocate that neurofibrillary tangles, like amyloid plaques are the final pathological hallmarks, but not the neurotoxic agents. The outcome fits independent observations that the extent of neuronal loss exceeds the number of NFT in patients with AD [42, 43]. In inducible Tg4510 mice, memory decline and neuronal loss are dissociated from tangle formation in time and brain region [44, 45].

In the AAV-Tau injected mice, phosphorylation of Tau was evident at many pathological epitopes, including those defined by antibodies AT8, AT100, AT180, and AT270 [30]. Despite the increased phosphorylation no aggregates of protein Tau were deposited in degenerating pyramidal neurons, analyzed histochemically or immunohistochemically. Biochemical analysis indicated the formation of low molecular weight aggregates [30] which need and deserve further analysis.

Intriguingly, experiments whereby AAV-APP.SLA was injected intracerebrally not in wild-type mice but in transgenic Tau.P301L mice, produced not only amyloid plaques but also intracellular Tau aggregates. Nevertheless, no substantial neuronal loss was evident, substantiating our previous data of absence of marked neurodegeneration in Tau.P301L mice and Tau.P301LxGSK3b bigenic mice (biGT), despite extensive or even dramatic Tauopathy [26, 36].

The combined results from our experimental models and from a Drosophila model of Tauopathy [46] consolidates the thesis that neurotoxicity is not exerted by large aggregates of protein Tau but rather by Tau-species that are intermediate between normally phosphorylated protein Tau and the hyper-phosphorylated fibrils. The identity of the toxic Tau species, which we have termed "Tau-P*" [11, 30] remains to be defined—a challenge equaling that of the identification of the amyloid receptor.

It must be remembered that Tau is subject to other posttranslational modifications, besides phosphorylation. Indeed, Tau can be ubiquitinated, truncated, glycosylated, glycated, oxidized, and, moreover, undergoes isomerization at proline residues. At any given moment protein Tau is present in various molecular forms, which most likely differ subtly in properties of binding to microtubuli, interaction with other proteins, binding to membranes, being transported for normal duty or for degradation.

The decision whether neurons will enter the cell death path or protect itself by forming Tauopathy, must depend on the actual levels of protein Tau and on its modifications. The rapid accumulation of Tau-P* will lead to cell death, while more gradual accumulation of Tau-P* would result in formation of aggregates. Both pathways will be affected by various external factors, for example, inflammation, amyloid, stress, and so forth. In this concept, the aggregation of Tau acts as the "escape from cell death pathway". Evidence from patients, whereby CA1 hippocampal neurons survive for decades despite neurofibrillary tangles [47] and experimental animals show tangle bearing neurons survive [26], even with lost membrane integrity [48].

3.2. Protein Aggregation, Impaired Clearance?

Two major pathways are responsible for removal of damaged, unfolded, or aggregated cellular proteins: the ubiquitin/proteasome system and the autophagy/lysosomal system that also can remove aged or damaged organelles. Malfunction of autophagy can result in accumulation of protein aggregates that may contribute to the disease pathology in AD and other neurodegenerative disorders [49–52]. Stimulating autophagy pharmacologically, for example, by inhibition of mTOR, ameliorates cognitive deficits and reduces amyloid and Tau pathology in the 3xTg mouse model for AD [53]. Autophagosomes form in a stepwise process that requires transport over the microtubular network, which is known to be affected by protein Tau, a major microtubule-associated protein.

In our mouse models, we did however not detect clear indications for problems with autophagy. Degenerating neurons in the AAV-Tau.P301L injected mice displayed as dark neurons with extensive vacuolization that could be taken to indicate a defective autophagic process. A similar facet of neurons we observed in an unrelated mouse model, that is, the p25 inducible mice that recapitulate hippocampal sclerosis [39]. The combined data do lend more support to the hypothesis that vacuolization is a correlate or consequence of the degenerative process, as an intrinsic mechanism needed to clean up defective organelles, protein aggregates or even entire dead or dying neurons. Consistent with this view is our observation in the AAV-Tau.P301L mice that vacuoles do not form early in the disease process but only after the neurons are already degenerating [11, 30]. Finally, we searched but did not find biochemical evidence for the conversion of LC3-I to LC3-II, which is generally accepted as the necessary step in and read-out of the increased formation of autophagosomes.

3.3. Cell Cycle Reentry, or Not?

After differentiation from neuronal precursors, neurons enter their post-mitotic state, while attempts to reenter the cell cycle is considered pathological and eventually result in cell death. In AD and other Tauopathies, cell-cycle related events have been suggested to be directly related to neurodegeneration.

We tested this hypothesis in the AAV-Tau model by examining cell cycle-related markers. Various markers were increased, that is, CyclinD2, phosphorylated Retinoblastoma protein, proliferating cell nuclear antigen (PCNA), cyclin B1 [30]. However, intracerebral injection of AAV-Tau in cyclinD2 deficient mice showed no extra effect on neurodegeneration, suggesting that cell cycle reentry is not a prerequisite for neuronal death [30].

3.4. Microtubular Transport. The only physiological function for protein Tau is binding to and stabilization of microtubules. Microtubules ensure cell shape and constitute roads of transport, a feature prominent in neurons with the most complex architecture of all cells. Microtubule dependent transport is ensured by families of motor proteins dyneins and kinesins, respectively for retrograde transport from distal processes towards soma and as plus-end directed motor for anterograde transport.

The effect of protein Tau on transport appears to be dual. First, mutant Tau and hP-Tau can cause it to detach from the microtubules and decrease its ability to control microtubule dynamics. On the other hand, increased levels of protein Tau can saturate microtubules and hinder the "foot-stepping" of the motor proteins needed for axonal and dendritic transport. Both aspects of Tau-related transport deficits have been observed and both can fit into a model leading to "starving synapses" that eventually culminates in neuronal death. In this hypothesis, Tau-mediated neurodegeneration is likely to start in distal neuronal processes, that is, axons and apical dendrites, which degenerate progressively towards the cell soma [54].

Synaptic pathology could be an early defect in neurodegenerative Tauopathies [55] as proper functioning of distal synapses is totally dependent on adequate transport of essential cargos and uninterrupted provision of energy. Impaired oxidative phosphorylation and mitochondrial dysfunction has been observed in mouse models expressing mutant Tau, which was potentiated by mutant APP and Presenilin1 [56, 57].

In Tau.4R transgenic mice, we previously documented axonopathy and motor deficits that were rescued by coexpression of constitutively active GSK3b [37, 58]. The data explain how excess Tau in first instance blocks transport by covering microtubuli, while GSK3 acting as major Tau-kinase I phosphorylates Tau to detach it from the microtubules and relieves the transport blockade [37]. Interestingly, treatment of Tau.4R mice with lithium salts significantly increased the axonopathy, an effect that can be ascribed to its inhibition of GSK3b [59].

As discussed above, AAV-mediated expression of truncated Tau, lacking the microtubule binding domain did not cause neurodegeneration, in marked contrast to full length protein Tau (Figures 3 and 4) and [30]. The combined data from various approaches allow us to conclude that Tau mediated pathology is, at least in part, mediated by its microtubule binding properties.

3.5. Inflammation. Chronic inflammation is evident in brain of AD patients and proposed to contribute essentially to the "vicious circle" leading eventually to neuronal death, brain atrophy and severe dementia. CNS-related features of the immune system remain hardly understood, and supposed to be "janus-faced", that is, providing protection as well as causing damage, steered by complex mostly unknown control mechanisms [60, 61]. Protection could be impaired in AD, fueled by—and fueling—debates on possible prevention or therapeutic benefits of antioxidants, radical scavengers, nonsteroidal anti-inflammatory drugs (NSAID), and so forth, although clinical trials do not substantiate the claims.

Microglia are immunocompetent cells that enter brain during developing as immature macrophages. They react rapidly to brain damage, including amyloid pathology in AD. Amyloid deposits attract microglia in a phagosomal attempt of their elimination, but activated microglia release proinflammatory cytokines, chemokines, reactive oxygen species, prostaglandins, and other mediators that harm neurons. Much attention has been paid to neurotoxicity mediated by free radicals, both reactive oxygen and nitrogen species, released by microglia.

Astrocytes are the most common cell-type in the brain, involved in many functions and increasingly appreciated also in synaptic signaling and integrity. Astrocytes co-localize with microglia at damage-sites, but remain to be explored in detail in AD. Strictly speaking, neurons must also be considered when discussing neuroinflammation because they (can) produce active factors, that is, complement, interleukins, tumor necrosis factor, acute-phase proteins.

We observed and discussed that degenerating neurons were temporally and spatially closely associated with activated microglia in two independent models, that is, the AAV-Tau viral model and the p25 transgenic model [30, 39].

Too many "unknowns" prevent us from answering the question how Tau-mediated damage can lead to neurodegeneration by involving activation of microglia. We maintain the most straightforward hypothesis, that is, that the expression of protein Tau, either wild-type or mutant by the viral vectors, is imposing stress on the pyramidal neurons that cannot adapt rapidly enough to produce Tau-aggregates as a means of temporarily detoxification. The impact on various neuronal functions is evident, including disturbances in post-mitotic state and cell-cycle control, as well as disturbing microtubule-mediated transport. The latter is most destructive in axons and larger dendrites, compromising the major synapses that become dys- or non-functional. Secreted neuronal proteins then activate nearby microglia that counter-react by secreting proinflammatory and potentially neurotoxic factors, fueling the viscous cycle that eventually leads to neuronal death.

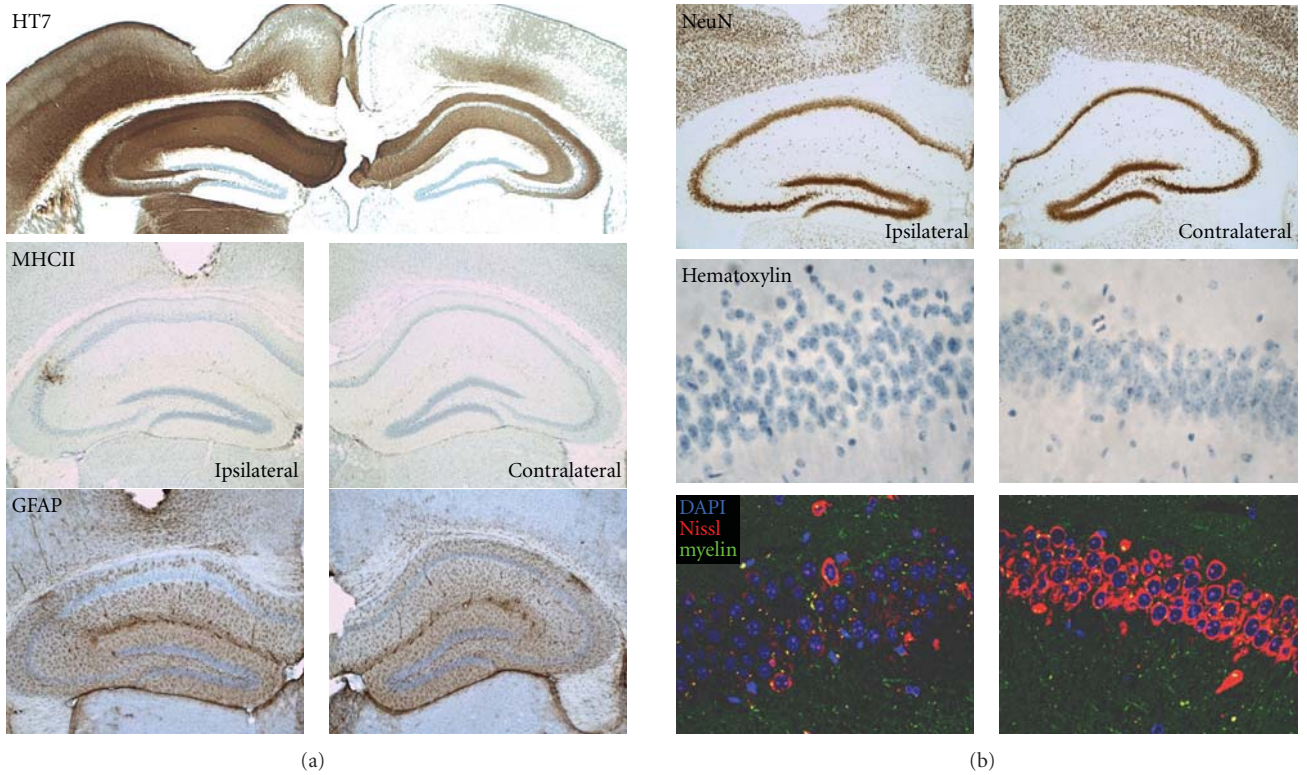

Figure 3: *Tau-mediated toxicity depends on the microtubule binding domain.* Intracerebral injection of AAV-Tau.255 (10e8 tu) into wild-type mice to express a truncated form of protein Tau devoid of the microtubule binding and C-terminal domains, did not cause appreciable neurodegeneration nor inflammation. Shown are immunohistochemical stainings at 3 months p.i. for human Tau (HT7), GFAP, and MHCII as indicators of astrogliosis and microgliosis, respectively [30]. Neurons expressing truncated protein Tau still maintain neuronal nuclei (NeuN) despite changes in nuclear morphology (hematoxylin) and in content of Nissl substance (lower panels).

4. Conclusions

Based on the combination of transgenic and viral models, and taking into account pathological and clinical data from human patients, we defend the thesis that neurodegeneration is not caused by a single defect but by—at least—dual actions (Figure 4).

The first is proposed to be intrinsically neuronal, for example, damage by accumulation of endogenous proteins in various molecular forms. In the case discussed here, protein Tau is the cause in primary Tauopathies. In AD, the upstream triggers are the amyloid peptides that accumulate because of mutations or other imposed defects in the proteolytic machinery that controls their formation and turnover.

The second factor is also essential, and can be neuronal or microglial in origin, related to any type of stress the brain can experience or has to endure, that is, partial hypoxia, glucose overload or shortage, problems with lipid or cholesterol, or other essential metabolites. The thesis is supported by clinical, but mainly experimental observations. For one, all available data convinced us that the "macro" protein-aggregates, that is, plaques and tangles, are not the most essential in causing cognitive defects and dementia. The challenge to define the neurotoxic Tau-species and its mode of action does nevertheless become not less complicated.

The combination of transgenic and viral models illustrates eloquently the power of the approach as well as its weaknesses. We still have more modeling to do, taking into account the data and indications that are provided by ongoing clinical studies, because only the human patient can eventually confirm any hypothesis based on experimental models.

Acknowledgments

The investigations were made possible by funding and support from the Fonds voor Wetenschappelijk Onderzoek-Vlaanderen (FWO-Vlaanderen), the Instituut voor Wetenschap en Techniek (IWT), the EEC-6th and 7th Framework Programs, the Rooms-fund, the KULeuven-Research Fund (BOF), and KULeuven-Research&Development. The authors sincerely thank many collaborators and scientists for technical assistance, advice, materials, and scientific or moral support. T. Jaworski was the recipient of EU-Marie Curie doctoral Fellowship (MEST-CT-2005-020589—EURON PhD School for Neurosciences).

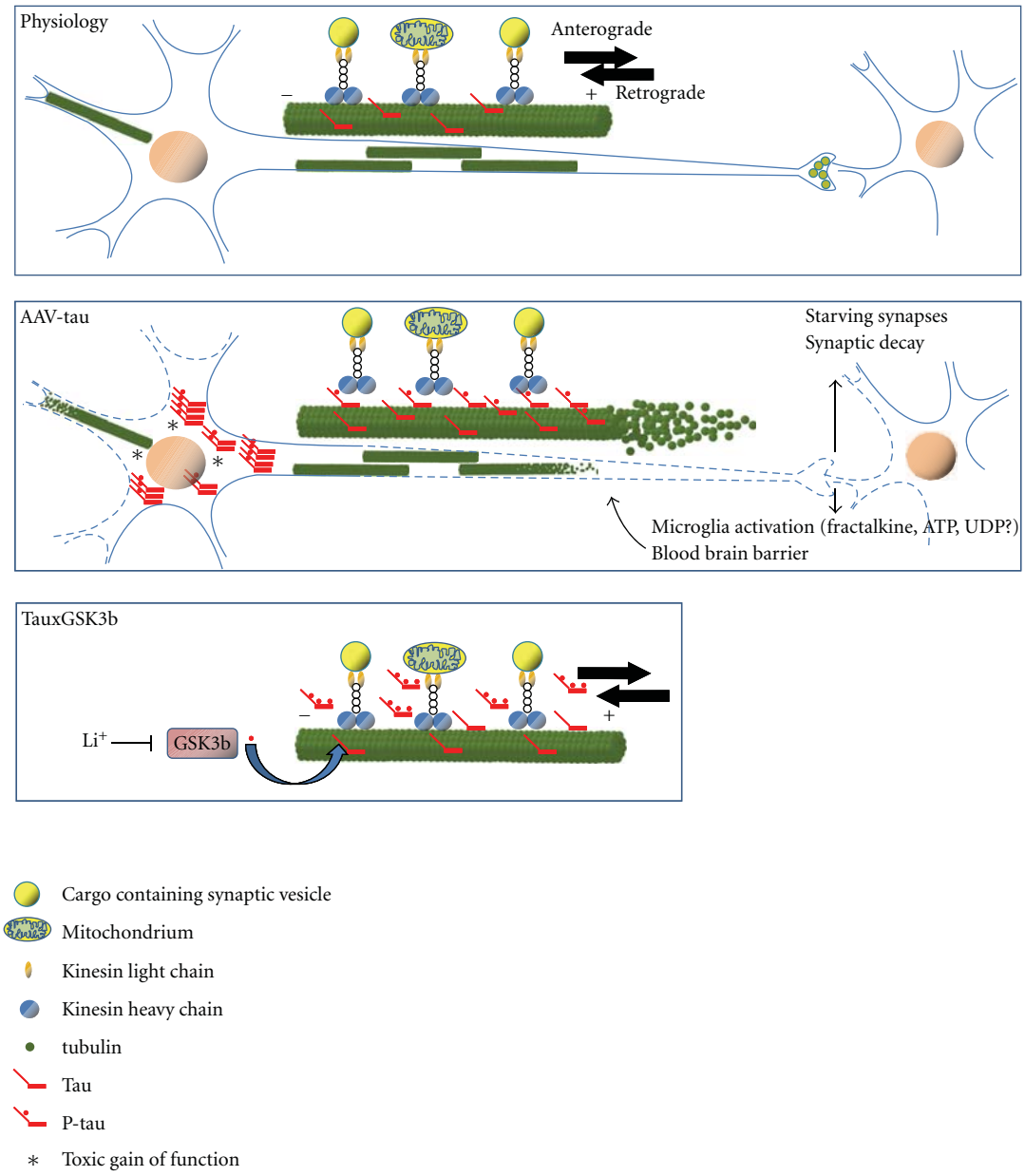

Figure 4: *Model for Tau-mediated neurodegeneration.* In normal conditions, protein Tau is regulated tightly at different levels: isoform expression, phosphorylation, microtubule binding, turnover, all needed to ensure normal transport along microtubules in axons and dendrites (upper panel). Increased expression of protein Tau, either genetically or pathologically in humans or experimentally in animal models will increase the amount of protein Tau bound to microtubules, thereby competing for and blocking the binding-sites needed for the motor proteins that carry out transport (middle panel). The resulting impairment in transport of any cargo, from synaptic vesicles and mitochondria to proteins, will impair any transport and energy-dependent processes at the synapses, which will extend and evolve into degenerating neuronal processes, and eventually lead to neuronal death. Defective synaptic transmission is then expected to be an early indication or symptom. Initially, small and loose aggregates or oligomers of protein Tau collect onto the microtubules, causing them to disintegrate or collapse. We also propose that the injured neuronal processes release proteins and factors, purposely or accidental that contribute to the activation of microglia and astroglia. The activated inflammatory cells secrete then factors that affect not only neurons but also other cells that constitute the unit blood-brain-barrier, provoking higher permeability, which further negatively affects neurons [11, 30]. Interesting is the connection to increased activity of GSK3, which rescued the axonopathy of Tau4R mice and the premature death of Tau.P301L mice by phosphorylating protein Tau and thereby detach it from the microtubuli to restore normal transport by motor proteins (lower panel) [26, 37]. Likewise, neither cell-death nor inflammation is provoked by AAV-Tau.255, devoid of the microtubule binding domain. The transgenic and viral models thereby underscore the microtubule binding of protein Tau as the common mechanism of action whereby protein Tau is causing neuronal demise and eventually neurodegeneration.

References

[1] I. Dewachter and F. Van Leuven, "Secretases as targets for the treatment of Alzheimer's disease: the prospects," *Lancet Neurology*, vol. 1, no. 7, pp. 409–416, 2002.

[2] C. Haass, "Take five—BACE and the γ-secretase quartet conduct Alzheimer's amyloid β-peptide generation," *EMBO Journal*, vol. 23, no. 3, pp. 483–488, 2004.

[3] D. M. Walsh and D. J. Selkoe, "Deciphering the molecular basis of memory failure in Alzheimer's disease," *Neuron*, vol. 44, no. 1, pp. 181–193, 2004.

[4] C. G. Glabe and R. Kayed, "Common structure and toxic function of amyloid oligomers implies a common mechanism of pathogenesis," *Neurology*, vol. 66, no. 2, pp. S74–S78, 2006.

[5] S. Lesné, M. T. Koh, L. Kotilinek et al., "A specific amyloid-β protein assembly in the brain impairs memory," *Nature*, vol. 440, no. 7082, pp. 352–357, 2006.

[6] D. Moechars, I. Dewachter, K. Lorent et al., "Early phenotypic changes in transgenic mice that overexpress different mutants of amyloid precursor protein in brain," *Journal of Biological Chemistry*, vol. 274, no. 10, pp. 6483–6492, 1999.

[7] F. Van Leuven, "Single and multiple transgenic mice as models for Alzheimer's disease," *Progress in Neurobiology*, vol. 61, no. 3, pp. 305–312, 2000.

[8] I. Dewachter, D. Moechars, J. Van Dorpe et al., "Modelling Alzheimer's disease in multiple transgenic mice," *Biochemical Society Symposium*, vol. 67, pp. 203–210, 2001.

[9] D. Terwel, I. Dewachter, and F. Van Leuven, "Axonal transport, tau protein, and neurodegeneration in Alzheimer's disease," *NeuroMolecular Medicine*, vol. 2, no. 2, pp. 151–165, 2002.

[10] T. Van Dooren, I. Dewachter, P. Borghgraef, and F. Van Leuven, "Transgenic mouse models for APP processing and Alzheimer's disease: early and late defects," *Sub-Cellular Biochemistry*, vol. 38, pp. 45–63, 2005.

[11] T. Jaworski, I. Dewachter, C. M. Seymour et al., "Alzheimer's disease: old problem, new views from transgenic and viral models," *Biochimica et Biophysica Acta*. In press.

[12] M. A. Mintun, G. N. Larossa, Y. I. Sheline et al., "[^{11}C]PIB in a nondemented population: potential antecedent marker of Alzheimer disease," *Neurology*, vol. 67, no. 3, pp. 446–452, 2006.

[13] A. Nordberg, "Amyloid plaque imaging in vivo: current achievement and future prospects," *European Journal of Nuclear Medicine and Molecular Imaging*, vol. 35, no. 1, pp. S46–S50, 2008.

[14] W. E. Klunk and C. A. Mathis, "The future of amyloid-beta imaging: a tale of radionuclides and tracer proliferation," *Current Opinion in Neurology*, vol. 21, no. 6, pp. 683–687, 2008.

[15] A. Delacourte and L. Buee, "Tau pathology: a marker of neurodegenerative disorders," *Current Opinion in Neurology*, vol. 13, no. 4, pp. 371–376, 2000.

[16] V. M.-Y. Lee, M. Goedert, and J. Q. Trojanowski, "Neurodegenerative tauopathies," *Annual Review of Neuroscience*, vol. 24, pp. 1121–1159, 2001.

[17] C. Duyckaerts, B. Delatour, and M.-C. Potier, "Classification and basic pathology of Alzheimer disease," *Acta Neuropathologica*, vol. 118, no. 1, pp. 5–36, 2009.

[18] A. C. Ludolph, J. Kassubek, B. G. Landwehrmeyer et al., "Tauopathies with parkinsonism: clinical spectrum, neuropathologic basis, biological markers, and treatment options," *European Journal of Neurology*, vol. 16, no. 3, pp. 297–309, 2009.

[19] P. Heutink, "Untangling tau-related dementia," *Human Molecular Genetics*, vol. 9, no. 6, pp. 979–986, 2000.

[20] E. M. Ingram and M. G. Spillantini, "Tau gene mutations: dissecting the pathogenesis of FTDP-17," *Trends in Molecular Medicine*, vol. 8, no. 12, pp. 555–562, 2002.

[21] D. H. Geschwind, "Tau phosphorylation, tangles, and neurodegeneration: the chicken or the egg?" *Neuron*, vol. 40, no. 3, pp. 457–460, 2003.

[22] J. Hardy and D. Allsop, "Amyloid deposition as the central event in the aetiology of Alzheimer's disease," *Trends in Pharmacological Sciences*, vol. 12, no. 10, pp. 383–388, 1991.

[23] J. Lewis, D. W. Dickson, W.-L. Lin et al., "Enhanced neurofibrillary degeneration in transgenic mice expressing mutant tau and APP," *Science*, vol. 293, no. 5534, pp. 1487–1491, 2001.

[24] S. Oddo, A. Caccamo, J. D. Shepherd et al., "Triple-transgenic model of Alzheimer's disease with plaques and tangles: intracellular Aβ and synaptic dysfunction," *Neuron*, vol. 39, no. 3, pp. 409–421, 2003.

[25] D. Muyllaert, D. Terwel, P. Borghgraef, H. Devijver, I. Dewachter, and F. Van Leuven, "Transgenic mouse models for Alzheimer's disease: the role of GSK-3β in combined amyloid and tau-pathology," *Revue Neurologique*, vol. 162, no. 10, pp. 903–907, 2006.

[26] D. Terwel, D. Muyllaert, I. Dewachter et al., "Amyloid activates GSK-3β to aggravate neuronal tauopathy in bigenic mice," *American Journal of Pathology*, vol. 172, no. 3, pp. 786–798, 2008.

[27] E. D. Roberson, K. Scearce-Levie, J. J. Palop et al., "Reducing endogenous tau ameliorates amyloid β-induced deficits in an Alzheimer's disease mouse model," *Science*, vol. 316, no. 5825, pp. 750–754, 2007.

[28] D. Paquet, B. Schmid, and C. Haass, "Transgenic zebrafish as a novel animal model to study tauopathies and other neurodegenerative disorders in vivo," *Neurodegenerative Diseases*, vol. 7, no. 1–3, pp. 99–102, 2010.

[29] V. Khurana, "Modeling tauopathy in the fruit fly Drosophila melanogaster," *Journal of Alzheimer's Disease*, vol. 15, no. 4, pp. 541–553, 2008.

[30] T. Jaworski, I. Dewachter, B. Lechat et al., "AAV-tau mediates pyramidal neurodegeneration by cell-cycle re-entry without neurofibrillary tangle formation in wild-type mice," *PLoS One*, vol. 4, no. 10, Article ID e7280, 2009.

[31] Z. Shevtsova, J. M. I. Malik, U. Michel, M. Bähr, and S. Kügler, "Promoters and serotypes: targeting of adeno-associated virus vectors for gene transfer in the rat central nervous system in vitro and in vivo," *Experimental Physiology*, vol. 90, no. 1, pp. 53–59, 2005.

[32] S. Kügler, R. Hahnewald, M. Garrido, and J. Reiss, "Long-term rescue of a lethal inherited disease by adeno-associated virus-mediated gene transfer in a mouse model of molybdenum-cofactor deficiency," *American Journal of Human Genetics*, vol. 80, no. 2, pp. 291–297, 2007.

[33] A. Goate, M.-C. Chartier-Harlin, M. Mullan et al., "Segregation of a missense mutation in the amyloid precursor protein gene with familial Alzheimer's disease," *Nature*, vol. 349, no. 6311, pp. 704–706, 1991.

[34] S. Kumar-Singh, C. De Jonghe, M. Cruts et al., "Nonfibrillar diffuse amyloid deposition due to a γ42-secretase site mutation points to an essential role for N-truncated Aβ42 in Alzheimer's disease," *Human Molecular Genetics*, vol. 9, no. 18, pp. 2589–2598, 2000.

[35] M. Citron, T. Oltersdorf, C. Haass et al., "Mutation of the β-amyloid precursor protein in familial Alzheimer's disease increases β-protein production," *Nature*, vol. 360, no. 6405, pp. 672–674, 1992.

[36] D. Terwel, R. Lasrado, J. Snauwaert et al., "Changed conformation of mutant tau-P301L underlies the moribund tauopathy, absent in progressive, nonlethal axonopathy of tau-4R/2N transgenic mice," *Journal of Biological Chemistry*, vol. 280, no. 5, pp. 3963–3973, 2005.

[37] K. Spittaels, C. Van Den Haute, J. Van Dorpe et al., "Glycogen synthase kinase-3β phosphorylates protein tau and rescues the axonopathy in the central nervous system of human four-repeat tau transgenic mice," *Journal of Biological Chemistry*, vol. 275, no. 52, pp. 41340–41349, 2000.

[38] R. L. Klein, R. D. Dayton, C. G. Diaczynsky, and D. B. Wang, "Pronounced microgliosis and neurodegeneration in aged rats after tau gene transfer," *Neurobiology of Aging*. In press.

[39] D. Muyllaert, D. Terwel, A. Kremer et al., "Neurodegeneration and neuroinflammation in cdk5/p25-inducible mice: a model for hippocampal sclerosis and neocortical degeneration," *American Journal of Pathology*, vol. 172, no. 2, pp. 470–485, 2008.

[40] C. Van den Haute, K. Spittaels, J. Van Dorpe et al., "Coexpression of human cdk5 and its activator p35 with human protein tau in neurons in brain of triple transgenic mice," *Neurobiology of Disease*, vol. 8, no. 1, pp. 32–44, 2001.

[41] T. Vandebroek, D. Terwel, T. Vanhelmont et al., "Microtubule binding and clustering of human Tau-4R and Tau-P301L proteins isolated from yeast deficient in orthologues of glycogen synthase kinase-3β or cdk5," *Journal of Biological Chemistry*, vol. 281, no. 35, pp. 25388–25397, 2006.

[42] T. Gómez-Isla, R. Hollister, H. West et al., "Neuronal loss correlates with but exceeds neurofibrillary tangles in Alzheimer's disease," *Annals of Neurology*, vol. 41, no. 1, pp. 17–24, 1997.

[43] J. J. Kril, S. Patel, A. J. Harding, and G. M. Halliday, "Neuron loss from the hippocampus of Alzheimer's disease exceeds extracellular neurofibrillary tangle formation," *Acta Neuropathologica*, vol. 103, no. 4, pp. 370–376, 2002.

[44] K. Santacruz, J. Lewis, T. Spires et al., "Tau suppression in a neurodegenerative mouse model improves memory function," *Science*, vol. 309, no. 5733, pp. 476–481, 2005.

[45] T. L. Spires, J. D. Orne, K. SantaCruz et al., "Region-specific dissociation of neuronal loss and neurofibrillary pathology in a mouse model of tauopathy," *American Journal of Pathology*, vol. 168, no. 5, pp. 1598–1607, 2006.

[46] S. Feuillette, L. Miguel, T. Frébourg, D. Campion, and M. Lecourtois, "Drosophila models of human tauopathies indicate that Tau protein toxicity in vivo is mediated by soluble cytosolic phosphorylated forms of the protein," *Journal of Neurochemistry*, vol. 113, no. 4, pp. 895–903, 2010.

[47] R. Morsch, W. Simon, and P. D. Coleman, "Neurons may live for decades with neurofibrillary tangles," *Journal of Neuropathology and Experimental Neurology*, vol. 58, no. 2, pp. 188–197, 1999.

[48] A. de Calignon, T. L. Spires-Jones, R. Pitstick, G. A. Carlson, and B. T. Hyman, "Tangle-bearing neurons survive despite disruption of membrane integrity in a mouse model of tauopathy," *Journal of Neuropathology and Experimental Neurology*, vol. 68, no. 7, pp. 757–761, 2009.

[49] W. H. Yu, A. M. Cuervo, A. Kumar et al., "Macroautophagy—a novel β-amyloid peptide-generating pathway activated in Alzheimer's disease," *Journal of Cell Biology*, vol. 171, no. 1, pp. 87–98, 2005.

[50] Y. Wang, M. Martinez-Vicente, U. Krüger et al., "Tau fragmentation, aggregation and clearance: the dual role of lysosomal processing," *Human Molecular Genetics*, vol. 18, no. 21, pp. 4153–4170, 2009.

[51] L. Li, X. Zhang, and W. Le, "Autophagy dysfunction in Alzheimer's disease," *Neurodegenerative Diseases*, vol. 7, no. 4, pp. 265–271, 2010.

[52] M. García-Arencibia, W. E. Hochfeld, P. P. C. Toh, and D. C. Rubinsztein, "Autophagy, a guardian against neurodegeneration," *Seminars in Cell and Developmental Biology*. In press.

[53] A. Caccamo, S. Majumder, A. Richardson, R. Strong, and S. Oddo, "Molecular interplay between mammalian target of rapamycin (mTOR), amyloid-β, and Tau: effects on cognitive impairments," *Journal of Biological Chemistry*, vol. 285, no. 17, pp. 13107–13120, 2010.

[54] E. Braak and H. Braak, "Alzheimer's disease: transiently developing dendritic changes in pyramidal cells of sector CA1 of the Ammon's horn," *Acta Neuropathologica*, vol. 93, no. 4, pp. 323–325, 1997.

[55] Y. Yoshiyama, M. Higuchi, B. Zhang et al., "Synapse loss and microglial activation precede tangles in a P301S tauopathy mouse model," *Neuron*, vol. 53, no. 3, pp. 337–351, 2007.

[56] D. C. David, S. Hauptmann, I. Scherping et al., "Proteomic and functional analyses reveal a mitochondrial dysfunction in P301L tau transgenic mice," *Journal of Biological Chemistry*, vol. 280, no. 25, pp. 23802–23814, 2005.

[57] V. Rhein, X. Song, A. Wiesner et al., "Amyloid-β and tau synergistically impair the oxidative phosphorylation system in triple transgenic Alzheimer's disease mice," *Proceedings of the National Academy of Sciences of the United States of America*, vol. 106, no. 47, pp. 20057–20062, 2010.

[58] K. Spittaels, C. Van den Haute, J. Van Dorpe et al., "Prominent axonopathy in the brain and spinal cord of transgenic mice overexpressing four-repeat human tau protein," *American Journal of Pathology*, vol. 155, no. 6, pp. 2153–2165, 1999.

[59] D. Muyllaert, A. Kremer, T. Jaworski et al., "Glycogen synthase kinase-3β, or a link between amyloid and tau pathology?" *Genes, Brain and Behavior*, vol. 7, no. 1, pp. 57–66, 2008.

[60] L. Arnaud, N. K. Robakis, and M. E. Figueiredo-Pereira, "It may take inflammation, phosphorylation and ubiquitination to 'tangle' in Alzheimer's disease," *Neurodegenerative Diseases*, vol. 3, no. 6, pp. 313–319, 2007.

[61] K. M. Lucin and T. Wyss-Coray, "Immune activation in brain aging and neurodegeneration: too much or too little?" *Neuron*, vol. 64, no. 1, pp. 110–122, 2009.

SAGE-Hindawi Access to Research
International Journal of Alzheimer's Disease
Volume 2010, Article ID 576357, 5 pages
doi:10.4061/2010/576357

Research Article

Grape-Seed Polyphenolic Extract Improves the Eye Phenotype in a *Drosophila* Model of Tauopathy

Cathie M. Pfleger,[1] Jun Wang,[2] Lauren Friedman,[2] Roselle Vittorino,[2] Lindsay M. Conley,[2] Lap Ho,[2] Hayley C. Fivecoat,[2] and Giulio M. Pasinetti[2,3]

[1] *Department of Oncological Sciences, Mount Sinai School of Medicine, One Gustave L. Levy Place, NY 10029, USA*
[2] *Department of Neurology, The Mount Sinai School of Medicine, One Gustave L. Levy Place, NY 10029, USA*
[3] *James J. Peters Veteran Affairs Medical Center, 130 West Kingsbridge Road, Bronx, NY 10468, USA*

Correspondence should be addressed to Giulio M. Pasinetti, giulio.pasinetti@mssm.edu

Received 8 April 2010; Revised 24 June 2010; Accepted 9 July 2010

Academic Editor: Gemma Casadesus

Drosophila models of tauopathies have been developed by transgenically overexpressing the disease-associated forms of *tau*. In this paper we report for the first time that a recently developed Grape-Seed Polyphenolic Extract (GSPE) improves the eye phenotype of a *Drosophila* eye model of *R406W tau*. GSPE-mediated improvements in this distinct *in vivo* neurodegeneration model for protein misfolding/aggregation suggest that GSPE may have therapeutic value in disorders involving aberrant protein aggregation.

1. Introduction

Abnormal protein conformations resulting in misfolded and/or abnormally aggregated protein species are a characteristic feature of several neurodegenerative disorders. For example, the microtubule-associated protein tau adopts abnormal conformations resulting in protein helical filament/immunopositive neurofibrillary tangles (NFTs) and is a characteristic neuropathological feature in Alzheimer's Disease (AD), Pick's disease, progressive supranuclear palsy, and corticobasal ganglionic degeneration (CBD). Tau mutations cause frontotemporal dementia with Parkinsonism- (FTDP-) 17, proving that tau dysfunction can directly promote neurodegeneration [1].

Drosophila models using the transgenic Gal4/UAS system [2] to overexpress disease-associated aggregation-prone proteins have modeled aspects of tauopathy by overexpressing *R406W* mutant tau [3, 4] and Huntington's disease (HD) by overexpressing *Q93httexon1* [5–7] (for review, see [8]). Overexpressing *R406W* in cells that form the eye (*ey* > *R406W*) leads to dramatic reduction in or complete absence of the eye. Eyes that do form demonstrate abnormal morphology [4]; for review, see [8].

We previously reported that moderate consumption of the red wine, Cabernet Sauvignon (*Vitis vinifera*), prevented abnormal β-amyloid (Aβ) oligomerization coincidental with a significant attenuation of spatial memory impairment in a mouse model of AD-type amyloid neuropathology [9]. Most importantly, we identified a polyphenolic compound highly concentrated in grape-seed polyphenolic extract (GSPE) as potentially responsible for the beneficial role of moderate consumption of red wine *(Vitis vinifera)* [10, 11].

More recently, Ho et al. reported that, using an *in vitro* aggregation assay, GSPE can significantly inhibit tau peptide Ac(306)VQIVYK(311) aggregation. Moreover, GSPE can also disaggregate preexisting aggregated tau peptides [12]. These results strongly suggest that GSPE might provide beneficial disease-modifying activity in tau-associated neurodegenerative disorders by modulating tau-mediated neuropathologic mechanisms. In this paper, we use the eye phenotype of a Drosophila model of mutant R406W tau to further evaluate the beneficial role of GSPE in tau-mediated neuropathology *in vivo*. We report for the first time that treatment with GSPE significantly benefits *Drosophila* phenotypes carrying mutant tau (*R406W)*, further supporting the potential use *in vivo* of GSPE in abnormal tau aggregation, as previously demonstrated *in vitro* [12].

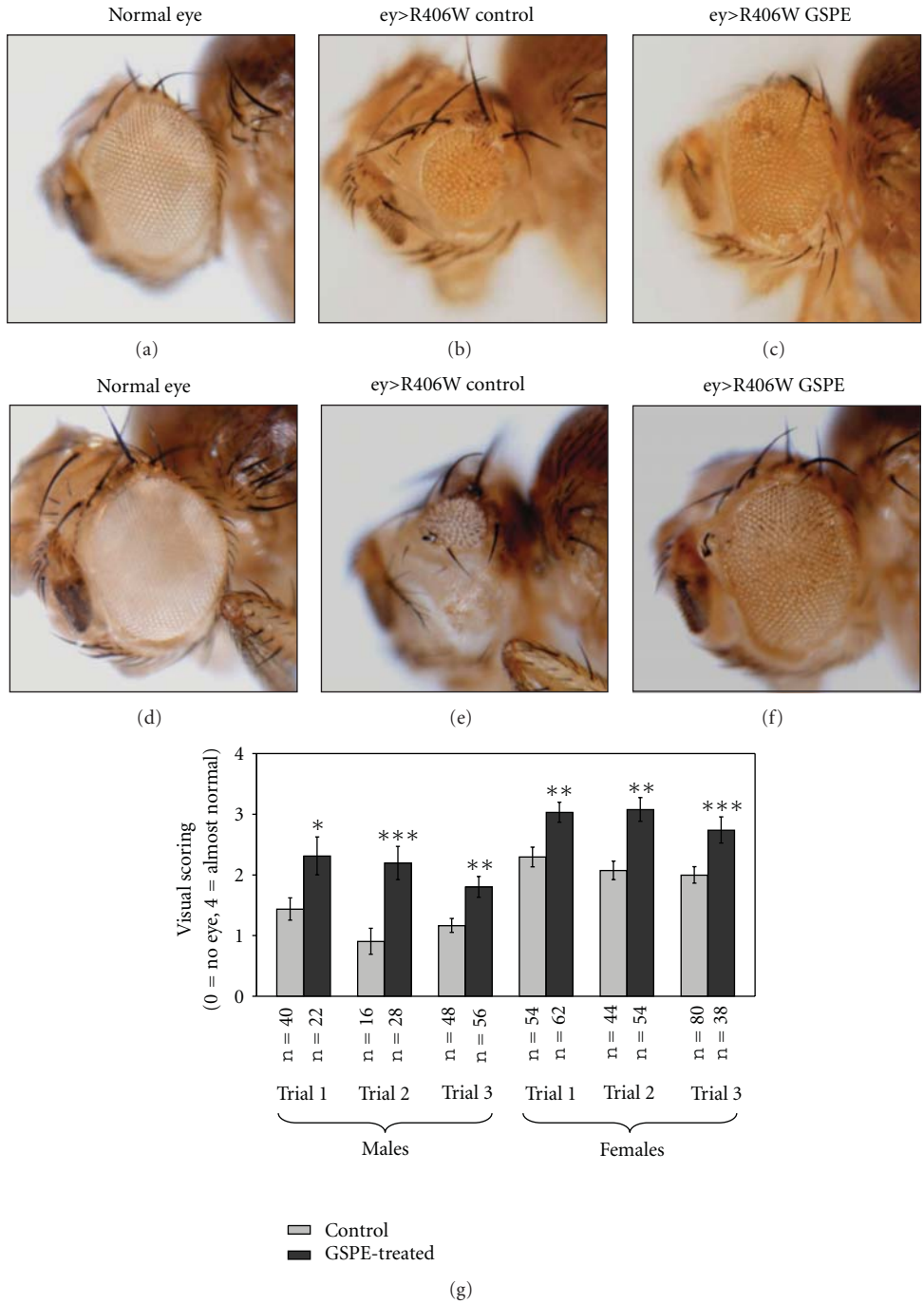

Figure 1: *GSPE attenuates R406W tau overexpression in the fly eye*. Male and female eye size differs; male eyes are shown in (a)–(c), and female eyes are shown in (d)–(f). Overexpression of *R406W* early in eye development results in a small or no eye ((b), (e)). Eyes that do not overexpress *R406W* are shown in (a), (d) for comparison. GSPE treatment ameliorates the reduction in eye size (representative eyes shown in (c), (f)). GSPE treatment does not affect normal-eye development (not shown). (g) The range of *ey > R406W* phenotypes varies between trials, so treatment comparisons were made within experiments. The average visual score (0 = no eye, 4 = almost normal eye) ± SEM of male and female eyes is shown for three independent trials for males and three independent trials for females. The number of flies (n) and P value calculated using a paired t-test on GraphPad online software are indicated beneath each trial. Flies were collected within 5 days of eclosion. Statistically significant improvement ($P < .05$) was observed in multiple independent experiments. * indicates $P < .05$, ** indicates $P < .01$, and *** indicates $P < .001$. (An excerpt of these images has been presented without data in a review manuscript by the author.)

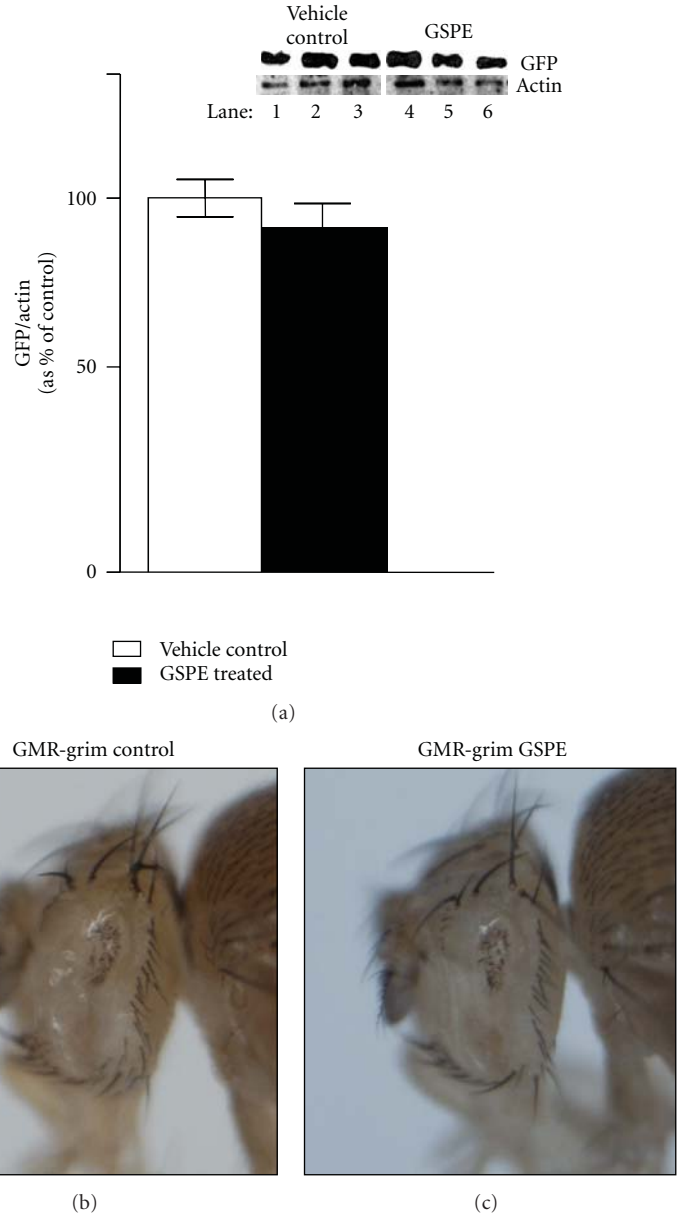

Figure 2: *GSPE does not inhibit Gal4-mediated expression of GFP*. (a) Western-blot analysis of lysates from *TubGal4 > GFP* flies (created by crossing *TubGal4* flies to *UAS-GFP* flies) reared from egg deposition either on food supplemented with water (vehicle control) (Lanes 1–3) or reared on GSPE food (lanes 4–6). Each lysate was prepared from 6 fly heads, and three independent groups of 6 flies per group (lane) are shown. The same immunoblot was probed first with antibodies raised against GFP (upper panel) and then immunoblots were stripped and reprobed with antiactin antibodies (lower panel). (b) *GMR-grim* flies have very small, almost absent eyes when reared on control food. (c) Eye size is not affected when *GMR-grim* flies are reared on GSPE food.

2. Materials and Methods

In this study, MegaNatural grape-seed polyphenolic extract (*GSPE*) was provided by Polyphenolics, Inc. (Madera, CA), as highly purified (>97% total polyphenols) water-soluble polyphenolic preparation from *Vitis vinifera* seeds.

2.1. Drosophila Strains. w; *eygal4/SM6-TM6B* and *GMR-grim* flies were obtained from the lab of IK Hariharan; *w*; *UAS R406W* and *w; Tubgal4* (FlyBase ID = FBti0012687) and *UAS green fluorescent protein (GFP)* (FlyBase ID FBti0012686) elements were obtained from the Bloomington Stock Center.

2.2. R406W Tau Experiments and Visual Scoring of Eye Abnormality. eygal4/SM6-TM6B flies were crossed to *UAS R406W* flies to generate *ey > R406W* flies. *ey > R406W* eggs were laid in and reared on instant fly medium formula 4–24 supplemented with 2.8 μg/mL GSPE ("GSPE food"), the

concentration used in our previous study [13], or control food supplemented with an equivalent volume of water (GSPE solvent, vehicle control).

Flies of the indicated genotypes were examined side by side under a dissecting scope. Eye regions which formed no ommatidia (therefore lacked eye tissue completely) were considered "0 = no eye" and required no comparison. For eye areas which did form obvious ommatidia/eye tissue, wild-type control flies were examined at the same time to establish the "4 = almost wild-type" eye size, shape, and pattern upper limit. Eyes that formed but did not reach the "4 = almost wild-type" category were lined up under the scope by size and grouped into categories based on the amount of eye tissue present. Because eyes were grouped side by side under the microscope, relative sizes were easy to establish. When additional conditions or repeated experiments were examined, representative eyes of each category from the previous experiments were examined again in parallel to ensure that the same designations/scoring were maintained.

2.3. Statistical Analyses. The distribution of eye sizes was reviewed and found to have negative kurtosis, indicating a distribution that was more uniform over the range from 0 to 4 than a normal distribution. Negative kurtosis does not substantially impair analysis of variance.

In addition to overall analysis of variance (with trials nested within gender and crossed by treatment), separate *t*-tests were performed for each trial tested.

3. Results

3.1. GSPE Treatment Improves the Eye Phenotype of ey > R406W Flies. *ey > R406W* flies show a range of phenotypes from no eye to small, abnormal eyes. The reduced size and abnormal morphology of *ey > R406W* eyes were improved by GSPE ($F(1,531) = 57.29$; $P < .0005$). The incidence of the worst outcomes (visual score of 0 or 1) decreased upon GSPE treatment in each trial while the incidence of the best outcomes (visual score of 3 or 4) increased upon GSPE treatment in each trial. There were also differences in the size of male and female eyes ($F(1,531) = 58.62$; $P < .0005$). Representative eyes are shown in Figures 1(a)–1(f) ((a)–(c) male; (d)–(f) female). Nonetheless, there was no interaction between gender and treatment ($F(1,531) = 0.30$; $P = .59$); the difference between treated and untreated flies was similar in male and female flies. Separate *t*-tests showed that each of the six trials had a statistical difference with GSPE treatment characterized by increased visual scoring relative to untreated controls (Figure 1(g)). However, within the combinations of gender and treatment, the trials did not differ significantly ($F(4,531) = 1.90$; $P < .11$).

3.2. GSPE Effects on Gal4/UAS-Mediated Protein Expression. To address the concern that GSPE could disrupt the production of the toxic proteins by the Gal4/UAS system, we performed control experiments using the Gal4/UAS system to determine whether GSPE treatment prevents expression of GFP using a *UAS-GFP* transgene and *TubGal4* (constitutively expressed as Gal4). We found no detectable alteration in the production of GFP both by fluorescent imaging of GFP (not shown) and by Western analysis (Figure 2(a)).

3.3. GSPE Does Not Affect the Small-Eye Phenotype Caused by Overexpression of the Proapoptotic Gene Grim. To investigate if GSPE acts on cell death pathways directly, we examined the effects of GSPE treatment on flies overexpressing the pro-apoptotic gene *grim* in differentiating cells in the eye (which causes a very small eye). *GMR-grim* flies (which overexpress the pro-apoptotic gene *grim* in differentiating cells in the eye) laid eggs on control food or GSPE food. *GMR-grim* flies reared entirely on GSPE food showed no effect of reduced eye size (Figures 2(b)-2(c)).

4. Discussion

We have demonstrated that GSPE treatment benefits a distinct *Drosophila* model of neurodegeneration involving aggregation *in vivo* (Figures 1 and 2). GSPE showed no effect on Gal4-mediated expression of GFP (Figure 2(a)), indicating that GSPE does not block Gal4/UAS-dependent gene expression. GSPE had no effect on eye size in *GMR-grim* flies (which overexpress in the eye the pro-apoptotic gene *grim* which activates caspases and severely reduces eye size [14]) (Figures 2(b)-2(c)). Thus, although the mechanism remains unknown, GSPE-mediated improvements in the *Drosophila* eye model likely occur subsequent to production of the toxic protein but upstream of caspase activation.

Presently there is no treatment for the devastating progressive neurodegenerative disorders involving tau abnormalities. Continuing investigations suggest that oligomeric forms of these misfolded proteins may play a seminal role in disease etiology. Results from our studies show that GSPE may rescue abnormal tau phenotype in a Drosophila model of tauopathy. This study is consistent with our previous study, which provided evidence that GSPE could inhibit tau peptide aggregation [12] and prevent oligomerization of Aβ peptides into high molecular weight species in models of AD-amyloid neuropathology [10, 11]. The study supports further investigations of GSPE in models of tauopathies, for example, frontotemporal dementia and CBD, among others.

Acknowledgments

This paper was generously supported in part by NIH P01 80004511 and Polyphenolics, Inc. (Madera, CA), to G.M. Pasinetti. Drs. Pasinetti, Wang, and Ho are named inventors of a pending patent application filed by Mount Sinai School of Medicine (MSSM) for grape-seed polyphenolic extract. In the event that the pending or issued patent is licensed, Drs. Pasinetti, Wang, and Ho would be entitled to a share of any proceeds MSSM receives from the license.

References

[1] M. Hutton, "Missense and splicing mutations in Tau associated with FTDP-17: multiple pathogenic mechanisms," *NeuroScience News*, vol. 2, no. 3-4, pp. 73–82, 1999.

[2] A. H. Brand and N. Perrimon, "Targeted gene expression as a means of altering cell fates and generating dominant phenotypes," *Development*, vol. 118, no. 2, pp. 401–415, 1993.

[3] C. W. Wittmann, M. F. Wszolek, J. M. Shulman et al., "Tauopathy in *Drosophila*: neurodegeneration without neurofibrillary tangles," *Science*, vol. 293, no. 5530, pp. 711–714, 2001.

[4] Z. Berger, B. Ravikumar, F. M. Menzies et al., "Rapamycin alleviates toxicity of different aggregate-prone proteins," *Human Molecular Genetics*, vol. 15, no. 3, pp. 433–442, 2006.

[5] N. Agrawal, J. Pallos, N. Slepko et al., "Identification of combinatorial drug regimens for treatment of Huntington's disease using *Drosophila*," *Proceedings of the National Academy of Sciences of the United States of America*, vol. 102, no. 10, pp. 3777–3781, 2005.

[6] J. S. Steffan, A. Kazantsev, O. Spasic-Boskovic et al., "The Huntington's disease protein interacts with p53 and CREB-binding protein and represses transcription," *Proceedings of the National Academy of Sciences of the United States of America*, vol. 97, no. 12, pp. 6763–6768, 2000.

[7] W. J. Wolfgang, T. W. Miller, J. M. Webster et al., "Suppression of Huntington's disease pathology in *Drosophila* by human single-chain Fv antibodies," *Proceedings of the National Academy of Sciences of the United States of America*, vol. 102, no. 32, pp. 11563–11568, 2005.

[8] T.-K. Sang and G. R. Jackson, "*Drosophila* models of neurodegenerative disease," *NeuroRx*, vol. 2, no. 3, pp. 438–446, 2005.

[9] J. Wang, L. Ho, Z. Zhao et al., "Moderate consumption of Cabernet Sauvignon attenuates Aβ neuropathology in a mouse model of Alzheimer's disease," *The FASEB Journal*, vol. 20, no. 13, pp. 2313–2320, 2006.

[10] K. Ono, M. M. Condron, L. Ho et al., "Effects of grape seed-derived polyphenols on amyloid β-protein self-assembly and cytotoxicity," *The Journal of Biological Chemistry*, vol. 283, no. 47, pp. 32176–32187, 2008.

[11] J. Wang, L. Ho, W. Zhao et al., "Grape-derived polyphenolics prevent Aβ oligomerization and attenuate cognitive deterioration in a mouse model of Alzheimer's disease," *Journal of Neuroscience*, vol. 28, no. 25, pp. 6388–6392, 2008.

[12] L. Ho, S. Yemul, J. Wang, et al., "Grape seed polyphenolic extract (GSE) as a novel therapeutic reagent in tau-mediated neurodegenerative disorders," *Journal of Alzheimer's Disease*, vol. 16, pp. 433–439, 2009.

[13] J. Wang, C. Pfleger, L. Friedman, et al., "Potential application of grape derived polyphenols in Huntington's disease," *Translational Neuroscience*. In press.

[14] P. Chen, W. Nordstrom, B. Gish, and J. M. Abrams, "grim, a novel cell death gene in *Drosophila*," *Genes and Development*, vol. 10, no. 14, pp. 1773–1782, 1996.

SAGE-Hindawi Access to Research
International Journal of Alzheimer's Disease
Volume 2010, Article ID 128354, 17 pages
doi:10.4061/2010/128354

Research Article

Gender-Specific Neuroimmunoendocrine Response to Treadmill Exercise in 3xTg-AD Mice

Lydia Giménez-Llort,[1] Yoelvis García,[2] Karla Buccieri,[1] Susana Revilla,[2] Cristina Suñol,[2] Rosa Cristofol,[2] and Coral Sanfeliu[2]

[1] *Medical Psychology Unit, Department of Psychiatry and Forensic Medicine, Institute of Neuroscience, Autonomous University of Barcelona, Bellaterra, 08193 Barcelona, Spain*
[2] *Institute of Biomedical Research of Barcelona (IIBB), CSIC-IDIBAPS, 08036 Barcelona, Spain*

Correspondence should be addressed to Lydia Giménez-Llort, lidia.gimenez@uab.cat

Received 16 May 2010; Accepted 9 August 2010

Academic Editor: Gemma Casadesus

The 3xTg-AD mouse develops a progressive Alzheimer's disease- (AD-) like brain pathology that causes cognitive- and neuropsychiatric-like symptoms of dementia. Since its neuroimmunoendocrine axis is likewise impaired, this mouse is also useful for modelling complex age-related neurodegeneration. This study analyzed behavioral, physiological, neurochemical, pathological and immunoendocrine alterations in male and female 3xTg-AD mice and assayed the effects of a short therapy of forced physical exercise at the moderate pathology stage of 6 months of age. Gender effects were observed in most AD-related pathology and dysfunctions. Five weeks of treadmill training produced beneficial effects, such as the reduction of brain oxidative stress and GABA-A receptor dysfunction in males and improvement of sensorimotor function in females. In both sexes, exercise decreased the brain amyloid β 42/40 ratio levels. The results highlight the importance of analyzing experimental therapies in both mouse model genders in order to improve our understanding of the disease and develop more appropriate therapies.

1. Introduction

Alzheimer's disease (AD) is the leading cause of dementia in people over 65, and it affects more than 20 million people worldwide [1]. No cure has yet been found, and current pharmacological therapy only temporarily ameliorates the symptoms [2]. Recent research has focused on preventive strategies derived from a healthier lifestyle, which may decrease the incidence of AD in the population [3]. One such strategy is physical exercise. Regular physical exercise enhances brain functionality and protects against neurodegeneration through multiple pathways. Regular exercise can attenuate oxidative damage in brain by reducing the ROS production and increasing the antioxidant systems [4]. These effects indicate that exercise could be a preventive tool against neurodegeneration-associated oxidative challenge. Also in brain, exercise can upregulate the expression of growth factors, such as BDNF, VEGF, FGF-2, NGF, and IGF-1 that regulate synaptic plasticity, learning, neurogenesis, and angiogenesis indicating an involvement of exercise in these cerebral processes [5]. On the other hand, exercise is suggested to reduce Aβ accumulation in cortical areas of AD transgenic mouse by increasing proteolytic degradation by proteasome [6]. The exact molecular mechanisms underlying these favorable effects of exercise in brain are not well known, but the MAPK, PI3K, and PI/Akt signaling pathways and the transcription factor CREB have been involved at the molecular level [5]. Exercise also can change the function of glutamatergic systems, increasing both NR2A and NR2B subtypes of the NMDA receptor in the hippocampus [7], which are crucial in learning and memory processes.

The health and psychological benefits elicited by regular physical activity in older adults contribute to healthy aging [8, 9]. Therefore, physical exercise is a potential intervention to preserve or ameliorate cognitive function and behavior in AD. Indeed, exercise is associated with a reduced incidence of AD in the at-risk population [10]. Moreover, improved cognition through exercise has been described in older adults

at risk for AD [11]. Physical exercise programs ameliorate mood [12] and symptoms of depression [13, 14] in AD patients. However, the timing and duration of the exercise required to be effective against disease symptoms, as well as the underlying mechanisms, are not known. Anticipated low adherence of AD patients to exercise regimes could be an obstacle for clinical studies, although this can be overcome, at least in part, by experimental studies. Transgenic mouse models of AD are useful and reliable experimental models for testing anti-AD therapies. Several studies have reported some pathology amelioration in AD transgenic mice as a result of physical exercise, either assaying voluntary exercise with a freely available running wheel [15, 16] or forced exercise with a treadmill [16–19]. However, more studies are needed to understand the effects and consequences of physical exercise intervention on the pathological cascade of AD neurodegeneration. Gender differences have not been extensively explored in the literature yet. In parallel, more studies are also needed to find out differential gender responses both in normal and mutant animals.

This study used the mandatory treadmill exercise paradigm in AD triple transgenic mice (3xTg-AD) [20]. These mice develop age-dependent and progressive neuropathology that includes plaque and tangle pathology [21]. Their associated behavioral disturbances include cognitive and noncognitive symptoms (i.e., Behavioral and psychological symptoms of dementia, BPSD) and other neuronal symptoms that mimic AD dementia [22]. In addition, these mice present a gender-related progression of AD changes [23, 24]. Therefore, 3xTg-AD is a valuable model for preclinical intervention studies. As few as 2–5 weeks of moderate intensity, treadmill running has been demonstrated to promote nerve cell regeneration and improve learning and memory in rodents [25–27]. However, some previous studies of treadmill effects in AD transgenic mice were extended to 12 weeks [17, 19] or 16 weeks [18, 28]. This study evaluates the effects of just 5 weeks of treadmill exercise on the brain and peripheral organ function of 3xTg-AD mice at several levels of study, namely the cellular (oxidative stress), neurochemical (GABA function), physiological (body weight curve, glucose homeostasis), immunoendocrine (involution of thymus, plasma levels of glucocorticoids), behavioral (BPSD-like and cognition impairments), and neuropathological (presence of amyloid and tau pathologies). The effects of exercise on physical functions were evaluated by means of sensorimotor tasks, including muscular strength and coordination. Emphasis was placed on the differential AD-like pathology severity present in male and female 3xTg-AD, which underlines the importance of translating the findings of therapeutic studies in this animal model to AD.

2. Materials and Methods

2.1. Animals. 3xTg-AD mice harboring PS1/M146V, APP-Swe, and tauP301L transgenes were genetically engineered at the University of California Irvine, as previously described [20]. Six-month-old male and female 3xTg-AD mice from the Spanish colony of homozygous 3xTg-AD mice established in the Medical Psychology Unit, Autonomous University of Barcelona [22, 29] were used in this study. Genotypes were confirmed by PCR analysis of DNA obtained from tail biopsies. Three to five littermates of the same genotype and sex were maintained (Makrolon, $35 \times 35 \times 25$ cm) under standard laboratory conditions (food and water *ad lib*, $22 + 2^{\circ}$C, 12 h light: dark starting at 08:00).

Thirty-six 3xTg-AD mice were subjected to five weeks of exercise on a treadmill (see below), after which their behavior was assessed on a series of tests used to screen for behavioral abnormalities in mutant mice [22, 30]: physical condition by body weight and sensorimotor tasks (SMT); BPSD-like behaviors, including the corner test (CT), open-field (OF), dark-light box (DLB), and T-maze (TM); several tasks to assess spatial learning and memory in the Morris water maze (MWM). Behavior was evaluated using both direct observation and a video-computerized tracking system (SMART, Panlab S.A.) by two independent observers who were unaware of the animal's genotype. Eighteen nontransgenic (non-Tg) mice with the same genetic background were used as a reference group. Experiments were performed under dim white-light conditions (16–20 lux) from 10:00 to 13:00 and in accordance with Spanish legislation on "Protection of Animals Used for Experimental and Other Scientific Purposes" and the European Communities Council Directive (86/609/EEC) on this subject.

2.2. Administration of Exercise on the Treadmill. The animals were divided into two sets according to their gender (males/females) and thereafter randomly assigned to one of two treatment groups (exercise, EXE; no exercise or sedentary, SED). Treatments were administered from Monday to Friday, between 9:00 and 19:00 in a soundproof room under dim light. The experimental design was counterbalanced by gender each day (starting with males in the morning and females in the afternoon, and vice-versa on the next day) and per treatment. The sedentary group (without exercise) was placed on the treadmill running apparatus (Scientific Instruments L18706) for the same amount of time as the animals doing exercise. Animals were constantly monitored, and the training of exercise group was slowly increased over time and by speed, that is, from minimum (15 min/day, 5 cm/s) to moderate exercise (30 min/day, 7 cm/s). The treadmill was carefully cleaned between animals, including a 30-min rest period without animals when starting the set of animals of the opposite gender.

2.3. Physical and Behavioral Profile of 3xTg-AD. Two days after the end of the administration of exercise, several physical, physiological, and neuroimmunoendocrine parameters were studied and compared to those of non-Tg mice.

2.3.1. Physical Conditions: Weight and Sensorimotor Functions. The body weight of animals was monitored every day before and after the treatments. The weight of intra-abdominal white adipose tissue (WAT) was measured. The contribution of WAT to total body weight was calculated as the percentage of the weight of WAT versus the total body weight.

Reflexes (*visual reflex* and *posterior legs extension reflex tests*) were measured three times by holding the animal by his tail and slowly lowering to a black surface. The motor coordination and equilibrium were assessed by the distance covered and the latency to fall off a horizontal *wooden rod* (1.3 cm wide) on two consecutive 20 s trials, respectively. In order to increase the difficulty of the task, the test was repeated on a metal *wire rod* (1 cm diameter). Prehensility and motor coordination were measured as the distance covered on the *wire hang test*, which consisted in allowing the animal to cling from the middle of a horizontal wire (diameter: 2 mm, length: 40 cm, divided into eight 5 cm segments) with its forepaws for two trials of 5 s and a third 60 s trial. Muscle strength was measured as the time until falling off the wire in the 60 s trial. All the apparatus were suspended 40 cm above a padded table.

2.3.2. Corner Test. Neophobia to a new home-cage was assessed by introducing the animal into the center of the standard cage (Makrolon, $35 \times 35 \times 25$ cm) and counting the number of visited corners and rearings during a period of 30 s. Latency of the first rearing was also recorded.

2.3.3. Open-Field Test. Mice were placed in the centre of the apparatus (home-made, wooden, white, $55 \times 55 \times 25$ cm high) and observed for 5 min. Horizontal (crossings of 5×5 cm squares) and vertical (rearings) locomotor activities were recorded for each minute of the test. We also recorded the latency of the sequence of the following behavioral events: initial freezing (latency of initial movement), thigmotaxis or discrimination of unprotected/protected areas in the test (latency of leaving the central 5×5 cm square and that of entering in the peripheral ring 5 cm to the walls), and self-grooming behavior (latency, number, and duration of groomings). Defecation was also measured.

2.3.4. Dark-Light Box Test. Anxiety-like behavior was also measured in the dark-light box (Panlab, S.L., Barcelona, Spain). The apparatus consisted of two compartments (black, $27 \times 18 \times 27$ cm; white, $27 \times 27 \times 27$ cm; lit with a 20 W white bulb) connected by an opening (7×7 cm). The mice were introduced into the black compartment and observed for 5 min. Latency to enter (all four paws) the lit compartment, the time spent in the lit compartment, and the horizontal (crossings of 3×3 cm) and vertical (rearings) activities developed once they were recorded.

2.3.5. Morris Water Maze Tests. Animals were tested for spatial learning and memory in the MWM [31] consisting of four trials of place learning for spatial reference memory followed by one probe trial and one day of cue learning. In the *place-learning task*, mice were trained to locate a platform (7 cm diameter, 1.5 cm below the water surface) in a circular pool (Intex Recreation Corp. CA, USA; 91 cm diameter, 40 cm height, 25°C opaque water) located in a test room with distal visual cues. The acquisition task consisted of four trial sessions per day, with trials spaced 15 min apart. In each trial, the mouse was gently released (facing the wall) from one randomly selected starting point (N, S, E, or W) and allowed to swim until escaped onto the platform (always in the middle of the SE quadrant). Mice that failed to find the platform within 60 s were placed on it for 20 s, the same period as was allowed for the successful animals. In session 4, one and a half hour after the fourth trial of place learning, the platform was removed from the maze and the mice performed a *probe trial test* of 60 s. On the following day, the animals were tested for *the cue learning* of a visual platform consisting of four trials in one single day. The platform was elevated 1 cm above the water level with its new position (NW) indicated by a visible striped flag (5×8 cm), and the distal cues were removed.

During each trial of the learning tasks the escape latency, the distance traveled, and the mean speed were measured by means of the computerized tracking system (SMART, Panlab S.A., Barcelona, Spain). The number of annulus crossings during the probe trial was also measured.

2.3.6. T-Maze Test. The spontaneous exploratory behavior of mice was tested in a T-shaped maze (with arms 25 cm in length). Animals were placed inside the "vertical" arm of the maze with its head facing the end wall. The performance was evaluated by determining with a chronometer the time elapsed until the animal crossed (four paws criteria) the intersection of the three arms [32].

2.4. Intraperitoneal Glucose Tolerance Test. Three days after the end of the behavioral assessment, mice were assayed for glucose tolerance with the intraperitoneal glucose tolerance test (IPGTT) [33]. Baseline glucose was measured from tail vein blood in mice fasted overnight. Mice were then loaded by intraperitoneal injection with a solution of 2 g glucose/kg body weight. Blood samples were subsequently collected 15, 30, and 60 min after glucose administration using a standardized glucometer. Results are expressed as mg/dL.

2.5. Glucocorticoid Analysis. Mice were sacrificed by decapitation. Samples of about 1 mL of whole trunk blood were collected at the time of sacrifice into heparinized tubes and centrifuged immediately at 10,000 ×g for 2 min. The plasma obtained was stored at –20°C. Corticosterone content (ng/mL) was analyzed using a commercial kit (Corticosterone EIA Immunodiagnostic Systems Ltd, Boldon, UK) and ELISA EMS Reader MF V.2.9-0.

2.6. Target Samples. Brain was dissected to obtain hippocampus, cerebral cortex, and cerebellum. Tissue samples were stored at −80°C for further biochemical analysis (see below). The size (weight in mg) and relative size (% versus body weight) of the thymus were recorded as an indirect measure of the putative impairment (involution) of the peripheral immunological system [24].

2.7. Immunohistochemistry. The hemibrain of four animals per group was fixed by immersion in 4% paraformaldehyde for 48 h. Paraffin-embedded brain sections were cut at

8 mm. Sections were autoclaved in citrate buffer pH 6 for 10 min to expose the epitopes. The endogenous peroxidase activity was quenched for 15 min in 1% H_2O_2. Sections were immunostained with antiamyloid β (Aβ), clone 4G8 (Covance, Emeryvlle, CA, USA) or anti-paired helical filament tau (PHF-tau), clone AT180 (Thermo Scientific, Rockford, IL) at dilutions of 1 : 50 and 1 : 100, respectively, both overnight at 4°C. After subsequent washes to remove primary antibody excess, sections were incubated with the appropriate biotin-conjugate secondary antibody for 1 h at room temperature. Sections were developed with diaminobenzidine (DAB) substrate using the avidin-biotin horseradish peroxidase system (Vector Laboratories, Inc.).

2.8. Amyloid β ELISA. Cerebral cortex was homogenized in a buffer containing 50 mM Tris, 400 mM NaCl, 2 mM EDTA, 0.1% triton X-100, 2% bovine serumalbumin, and a cocktail of protease inhibitors (Complete, Calbiochem). Samples were centrifuged at 12,000 ×g for 7 min at 4°C, and supernatants were collected and used to detect Aβ by ELISA. Both Aβ40 and Aβ42 soluble levels were measured by sandwich ELISA [34]. Antibody clone 6E10 against Aβ1–17 (Chemicon, Temecula, CA, USA) was used as a capture antibody and rabbit polyclonal anti-Aβ40 and anti-Aβ42 (Chemicon) as detection antibodies. After incubation for 3 h, wells were washed, and a horseradish peroxidase-conjugated antirabbit (GE Healthcare, UK) was added. Wells were washed with phosphate-buffered saline (PBS), and Quantablue reagent (Pierce, Rockford, IL, USA) was added. Samples were then measured at 320 nm using a plate reader (iEMS Reader MF; Labsystems, Vantaa, Finland).

2.9. [^{3}H] Flunitrazepam Binding Assay. Synaptic membrane preparations were obtained from mice cerebral cortices that had been stored frozen at −80°C. Brain samples were thawed and homogenized in 50 volumes (w/v) of Tris-HCl buffer (50 mM, pH 7.4) and then centrifuged at 20,000 ×g, at 4°C, 20 min. The pellet was resuspended in 1.5 mL of the same buffer and again centrifuged at 20,000 ×g, at 4°C, 20 min. This procedure was repeated five times. The last suspension was frozen at −80°C for at least one day. For the binding assays, the samples were thawed and centrifuged, and the membranes were then resuspended in 1 mL of 50 mM Tris-HCl buffer/NaCl 200 mM. Proteins were measured in 200 μL following the Bradford method. Membranes were then incubated with 1 nM [^{3}H] flunitrazepam for 30 min at 25°C. Binding obtained in the presence of 20 μM diazepam was considered to be nonspecific. After incubation the suspensions were rapidly filtered in a Brandel (Gaithersburg, MD, USA) and washed through Whatman GF/B filters (435 μm). The amount of bound radioactivity was determined following the addition of 2 mL of OptiPhase "Hisafe" scintillation cocktail in a Wallac 1414 Winspectral liquid scintillation counter (Perkin Elmer, Waltham, MA). Radioligand binding data were subjected to Scatchard analysis in order to obtain the neurochemical variables for binding site density (Bmax, in pmol/mg protein) and binding affinity (Kd, in nM).

2.10. Lipid Peroxidation, Glutathione Peroxidase, and Superoxide Dismutase Assays. For lipid peroxidation and enzymatic assays, 100 mg of cerebral cortex tissue was sonicated for 30 s in 1 mL of ice-cold 50 mM potassium phosphate buffer containing 1 mM EDTA pH 7.4 and before being centrifuged at 12,000 ×g for 30 min at 4°C. The supernatants were collected and stored at −80°C until assay. Enzymatic activities and lipid peroxidation were determined as described previously [35]. Peroxidation of lipids was measured by determining malondialdehyde and 4-hydroxyalkenal (MDA + 4-HAD) using a Lipid Peroxidation Assay Kit from Calbiochem (EMD Biosciences Inc., Darmstadt, Germany). Glutathione peroxidase (GPx) activity was determined by measuring spectrophotometrically the rate of NADPH oxidation in the presence of hydrogen peroxide. Superoxide dismutase (SOD) activity was measured using the SOD assay kit Ransod (Randox Laboratories Ltd, Crumlin, UK), based on the xanthinexanthine oxidase system. After total SOD (Cu/Zn SOD and Mn SOD) was determined, samples were again analyzed in the presence of 500 μM KCN to inhibit CuZn SOD and to obtain Mn SOD activity. SODCuZn activity was obtained by subtracting Mn SOD activity. Proteins were measured in 10 μL of supernatants following the Bradford method.

2.11. Reduced Glutathione and Oxidized Glutathione Assays. For reduced glutathione (GSH) and oxidized glutathione disulphide (GSSG) assays, 200 mg of cerebral cortical tissue was sonicated in 1 mL of 3.3% sulphosalicylic acid. Acid homogenates were centrifuged at 12,000 ×g for 30 min at 4°C, and supernatant fractions were collected and stored at −80°C until assay. The levels of GSH and GSSG were determined using an enzymatic assay [36] that is essentially a modification of Tietze's recycling method. Samples for GSSG determination were previously incubated at room temperature with 2 μL of 2-vinyl pyridine per 100 μL sample in order to conjugate any GSH present in the sample, such that only GSSG was recycled to GSH. Both GSH and GSSG samples were then neutralized by the addition of 6 μL of triethanolamine. For total glutathione determination, 50 μL of each sample was mixed with 100 μL of 100 mM sodium phosphate/1 mM EDTA buffer containing 1 mM dithiobisnitrobenzoate, 20 U/mL glutathione reductase, and 1 mM β-nicotinamide adenine dinucleotide phosphate (NADPH). The kinetics of the formation of 5-thio-2-nitrobenzoic acid was immediately recorded at 30°C and 405 nm, every 15 s over a 5-min period.

2.12. Statistics. Statistical analyses were performed using SPSS 12.0 software. Two-way ANOVA was performed using gender and treatment as the independent variables for detecting the respective effects. Post hoc comparisons were carried out using a post hoc Duncan's test, unless otherwise stated. Temporal courses were analyzed using repeated-measures ANOVA (RMA), and when comparing two time points, paired t-test was used.

Table 1

(a) The treadmill exercise exerted beneficial effects on the sensorimotor function which were more relevant in females

	M non-Tg ($n = 8$)	M TgSED ($n = 10$)	M TgEXE ($n = 10$)	F non-Tg ($n = 8$)	F TgSED ($n = 8$)	F TgEXE ($n = 8$)
Body weight						
Weight curve						
Start of week 1 (g)	34.4 ± 0.7	36.0 ± 0.8	39.2 ± 1.8	24.7 ± 1.2	32.3 ± 1.2	32.0 ± 1.4
End of week 5 (g)	34.4 ± 0.4	37.0 ± 0.7	38.4 ± 1.6*	23.8 ± 0.3*	28.8 ± 1.0#	29.7 ± 1.2#
WAT (% versus body weight)	See Figure 1					
Sensorimotor function						
Reflex tests						
Incidence of both reflexes	8/8	10/10	10/10	8/8	8/8	8/8
Wooden rod test						
Equilibrium (mean latency to fall, s)	8.3 ± 2.2	17.5 ± 1.4	19.2 ± 0.5	14.5 ± 2.1	20.0 ± 0.0	20.0 ± 0.0
Coordination (mean distance, cm)	2.5 + 1.5	3.2 ± 2.0	5.7 ± 2.5	1.4 ± 0.7#	5.3 ± 4.3#	39.7 ± 8.4#
Wire rod test						
Equilibrium (mean latency to fall, s)	3.0 ± 0.5	9.4 ± 1.9	9.8 ± 1.7	3.5 ± 0.8#	15.4 ± 1.6#	16.7 ± 1.6#
Coordination (mean distance, cm)	0 ± 0	0 ± 0	5.3 ± 4.0	0 ± 0#	0.9 ± 0.9#	19.7 ± 6.6#
Wire hang test (2 trials 5 s)						
Strength (mean latency to fall, s)	0.9 ± 0.1	4.1 ± 0.4*	4.2 ± 0.3*	0.9 ± 0.3	4.5 ± 0.2*	5.0 ± 0.0*
Coordination (mean distance, cm)	0 ± 0	0.5 ± 0.3	0.6 ± 0.4	0 ± 0	0.3 ± 0.3	1.1 ± 0.3
Elements of support (n)	1.1 ± 0	1.5 ± 0.4	1.2 ± 0.3	0.8 ± 0.1	1.25 ± 0.4	2.3 ± 0.4
Wire hang test (1 trial 60 s)						
Strength (mean latency to fall, s)	4.0 ± 2.6	34.1 ± 7.6*	33.4 ± 6.4*	1.0 ± 0.1	55.7 ± 4.2#,*	55.0 ± 5.0#,*
Coordination (mean distance, cm)	0.3 ± 0.3	2.4 ± 0.6*	3.1 ± 0.5*	0 ± 0	5.0 ± 1.7*	6.7 ± 1.1#,*
Elements of support (n)	1.7 ± 0.3	2.4 ± 0.3	2.4 ± 0.3	1.1 ± 0	2.8 ± 0.2	3.0 ± 0.0#,*

Note: non-Tg, nontransgenic mice; TgSED, 3xTgAD mice not exercised; TgEXE, 3xTg-AD mice submitted to a daily treadmill running for five weeks. The body weight, fat composition, and sensorimotor function of 3xTg-AD mice differed from that of non-Tg mice. The treadmill exercise exerted beneficial effects on the sensorimotor function which were more relevant in females. Results are the mean ± SEM, $n = 8$–10 as indicated. Statistics: $^*P < .05$ compared to non-Tg; $^\#P < .01$ compared to TgSED.

(b) BPSD-like behaviors are characteristic of 3xTg-AD mice at early stages of the disease and show an important gender component

	M non-Tg ($n = 8$)	M TgSED ($n = 10$)	M TgEXE ($n = 10$)	F non-Tg ($n = 8$)	F TgSED ($n = 8$)	F TgEXE ($n = 8$)
Corner test						
Vertical activity (latency, s)	5.0 ± 1.5	16.3 ± 7.4*	19.6 ± 7.9*	8.9 ± 4.7	5.3 ± 1.7	10.5 ± 4.1
Open-field test						
Initial movement (latency, s)	7.2 ± 1.3	3.3 ± 1	1.9 ± 0.6*	13.6 ± 6.7	4.2 ± 1.7	3.0 ± 0.9

(b) Continued.

	M non-Tg ($n = 8$)	M TgSED ($n = 10$)	M TgEXE ($n = 10$)	F non-Tg ($n = 8$)	F TgSED ($n = 8$)	F TgEXE ($n = 8$)
Open-field test						
Exit of the center (latency, s)	14.2 ± 2.3	10.7 ± 2	5.2 ± 1.1*	30.4 ± 13.7	7.6 ± 2.3	4.4 ± 1.0*
Entrance to periphery (latency, s)	17.0 ± 5.3	21.7 ± 8	10.7 ± 2.5	57.6 ± 16.9#	10.6 ± 3.2*	7.8 ± 2.8*
Vertical activity (latency, s)	49.2 ± 6.9	75.0 ± 14	119.7 ± 31.2*	87.5 ± 17.7	29.5 ± 5.3#*	34.2 ± 6.4#*
Self-grooming (latency, s)	173.0 ± 57.0	172.3 ± 18	172.1 ± 18.3	127.8 ± 11.6	136.9 ± 23.5	183.0 ± 21.0
Total self-grooming duration (s)	3.2 ± 1.6	3.9 ± 1.0	6.7 ± 1.3*	4.4 ± 0.9	5.6 ± 1.0	3.0 ± 0.9
Defecation boli (n)	2.0 ± 0.3	2.7 ± 0.7	2.8 ± 0.4	3.2 ± 0.5	4.4 ± 0.5	2.9 ± 0.6
Dark-light box test						
Latency to enter into the lit area (s)	16.2 ± 2.4	25.5 ± 5.9	47.4 ± 28.2	39.4 ± 12.3	11.5 ± 2.3*	16.1 ± 5.9
Defecation boli (n)	0.2 ± 0.2	4.3 ± 0.7*	4.2 ± 0.5*	2.4 ± 0.4	4.0 ± 1.3	4.4 ± 0.7
Morris water maze tasks						
Place learning task						
Mean speed on day 1 (cm/s)	18.9 ± 0.8	21.6 ± 0.9	20.9 ± 0.7	19.3 ± 0.8	22.7 ± 0.7	22.7 ± 1.2
Mean speed on day 2 (cm/s)	20.6 ± 0.6	23.4 ± 1.2	22.7 ± 0.7	19.4 ± 1.1	23.8 ± 0.7	24.0 ± 1.3
Mean speed on day 3 (cm/s)	22.0 ± 0.5	21.4 ± 1.6	23.7 ± 0.7	19.2 ± 1.5	23.3 ± 0.3	23.3 ± 1.4
Mean speed on day 4 (cm/s)	21.7 ± 1.2	20.9 ± 0.8	19.9 ± 1.1	18.0 ± 2.0	23.3 ± 0.7	23.4 ± 1.3
Mean speed (cm/s)	20.8 ± 0.7	21.8 ± 1.0	21.8 ± 0.6	19.0 ± 1.1#	23.2 ± 0.4*	23.4 ± 1.2*
Probe trial						
Annulus crossings (n)	8.0 ± 1.41	8.4 ± 1.5	10.1 ± 1.0	5.6 ± 0.8	6.3 ± 1.1	6.9 ± 0.7
Cue learning task						
Mean distance covered (cm)	567.0 ± 62.5	138.2 ± 42.4	399.7 ± 149.9	235.9 ± 71.0#	312.8 ± 162.6	293.7 ± 96.6
Mean speed (cm/s)	19.1 ± 0.5	19.3 ± 1.3	20.4 ± 0.7	14.8±1.6#P	18.8 ± 1.1P	19.0 ± 1.4P
T-maze						
Performance (latency, s)	8.7 ± 1.2	12.9 ± 1.7	11.3 ± 1.3	20.0 ± 5.9#	9.9 ± 1.2*	7.8 ± 1.0*

Note: non-Tg, nontransgenic mice; TgSED, 3xTgAD mice not exercised; TgEXE, 3xTg-AD mice submitted to a daily treadmill running for five weeks. The 3xTg-AD mice exhibited several behavioral changes indicative of increased neofobia, emotionality, anxiety-like behavior, hyperactivity, and impulsivity, which were mainly observed in females. The exercise did not induce major changes but showed gender-dependent effects. Results are the mean ± SEM, $n = 8$–10 as indicated. Statistics: *$P < .05$ compared to non-Tg; #$P < .01$ compared to TgSED, Pcompared to mean speed on place learning task $P < .05$.

3. Results

3.1. Physical and Behavioral Profile of 3xTg-AD. Tables 1(a) and 1(b), Figures 1 and 2(c) summarize the results obtained in the physical and behavioral assessments of 3xTg-AD mice.

3.1.1. Weight. On a general basis, clear body weight differences could be observed among the different groups with higher weight recorded in males than females in both non-Tg and 3xTg-AD mice, while the transgenic genotype involved a significant increase of weight (see Table 1(a), ANOVA, $F(5,46) = 29.37$, $P < .001$, post hoc Duncan's test, $P < .05$) which was independent of the gender or treatment. The contribution of WAT to total body weight in the non-Tg mice was smaller in females (0.3 ± 0.0 g) than in males (0.8 ± 0.0 g). This gender-dependent effect was completely lost when genotype was considered, as the weight of WAT was exactly the same in both genders of 3xTg-AD mice (M TgSED: 1.0 ± 0.1 g, F TgSED: 1.0 ± 0.0 g, M TgEXE: 1.1 ± 0.2, F TgEXE: 1.0 ± 0.2 g) independent of the treatment. As illustrated in Figure 2(c), the contribution of WAT to total body weight (% versus total weight) was similar in all males independent of genotype or treatment but significantly higher in both groups of females as compared to the non-Tg female group [ANOVA, $F(5,46) = 5.09$, $P < .001$].

When the weight curve was considered, the repeated-measures ANOVA indicated a global effect of the "day" factor ($F(24,32) = 7.521$, $P < .001$) which was dependent on gender ("gender" and "day × gender" interaction effects, $F(1,32) = 25.163$, $P < .001$ and $F(24,32) = 5.979$, $P < .001$, resp.) with a 9.3% statistically significant reduction of weight in females across the test (paired t-test, $t = 5.774$, df 15, $P < .001$). However, there was no influence of the "exercise" factor on weight ($F(24,32) = 0.939$, *n.s.*).

3.1.2. Sensorimotor Tasks. Two-way ANOVA showed gender-dependent differences on most of the tasks (gender, all F's$(1, 35) > 4,488$, $P < .05$) and a clear beneficial

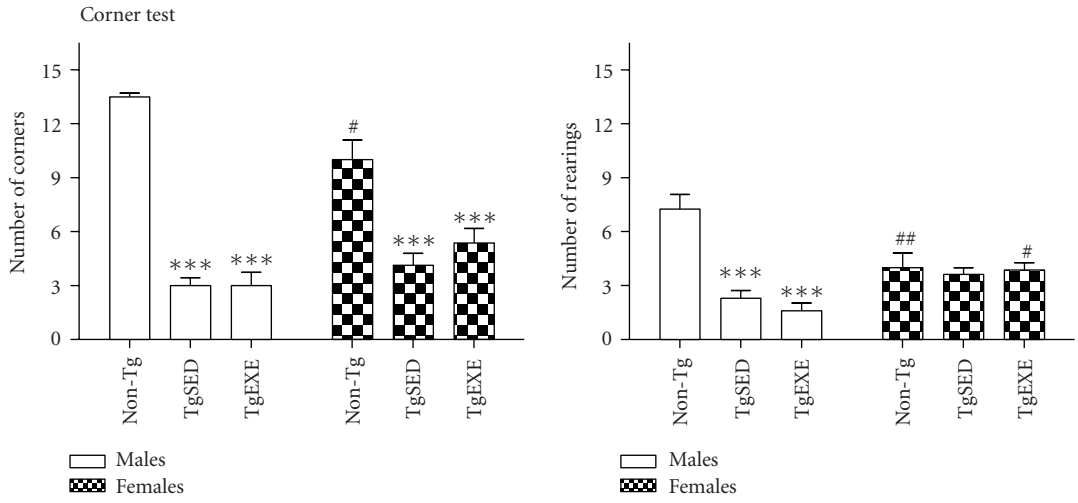

(a)

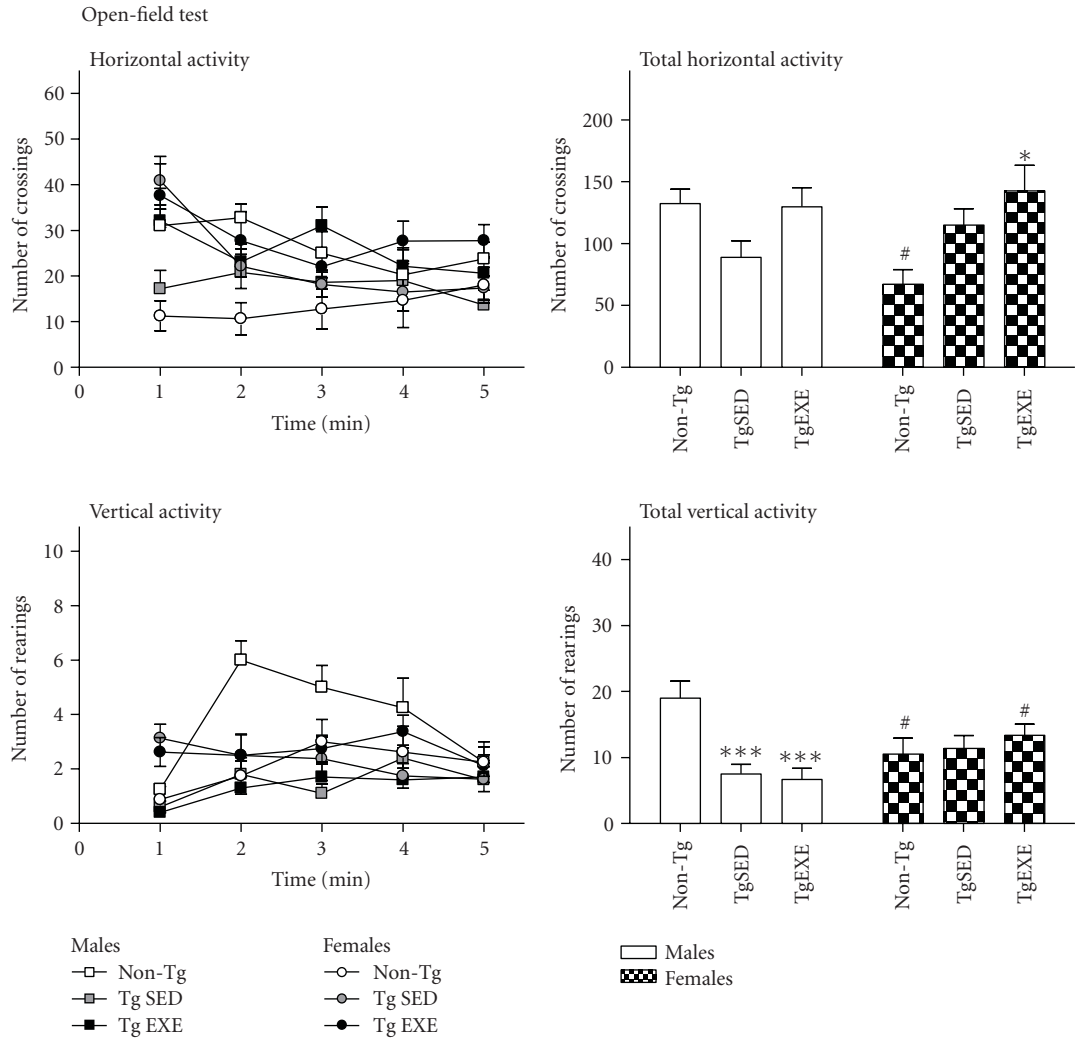

(b)

Figure 1: Continued.

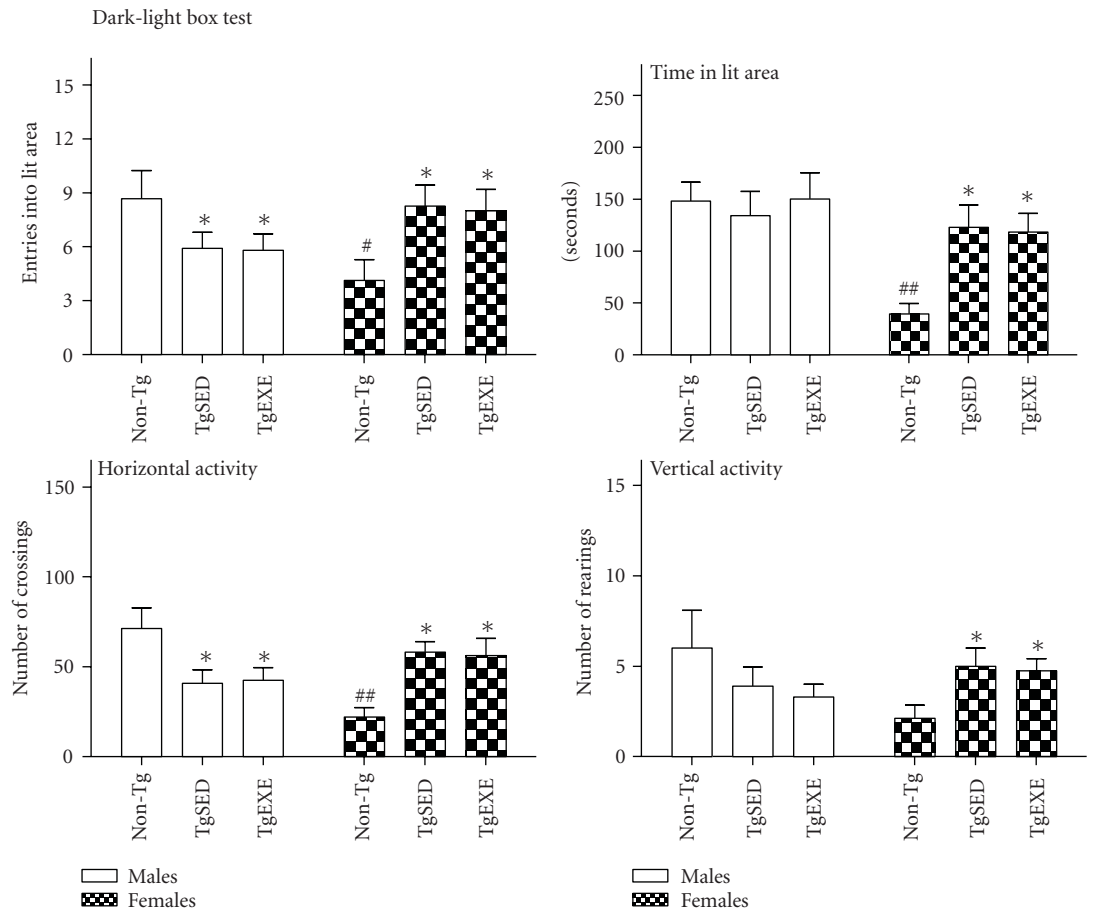

(c)

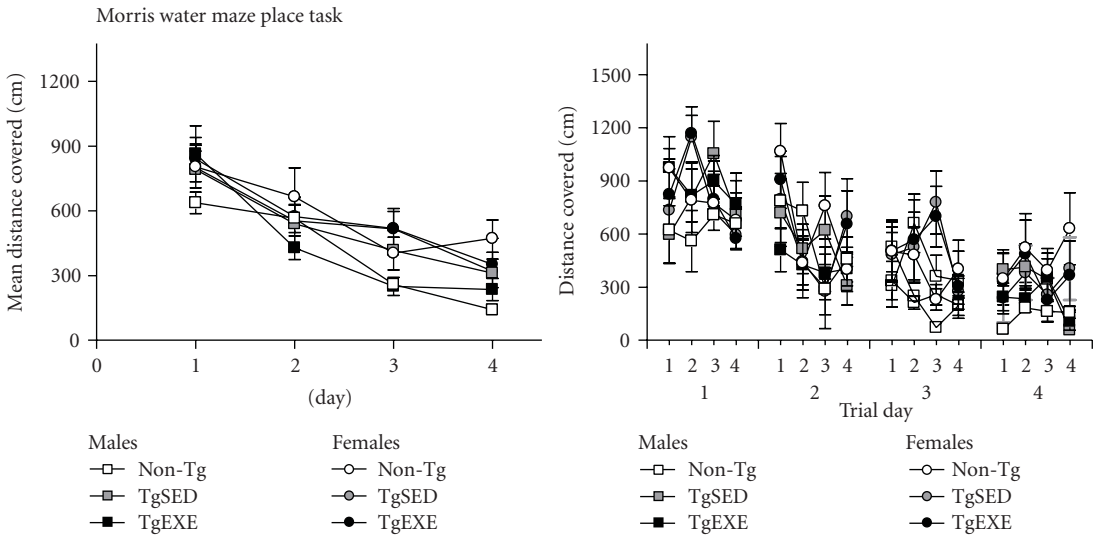

(d)

Figure 1: All the behavioral tests do consistently refer to presence of BPSD-like symptoms as a characteristic of early stages of the disease in 3xTg-AD mice, with an important gender component. The effects of exercise are gender dependent. (a) The neophobia in the corner test was increased in both male and female 3xTg-AD mice. (b and c) The anxious profile could be also observed in several variables measured by the open-field test and dark-light box. (d) In the Morris water maze, changes in the swim speed and motivation could be recorded and were mainly important in females (see complementary data in Tables 1(a) and 1(b)). Values are the mean ± SEM, $n = 8$–10. Statistics: $^{*}P < .05$, $^{**}P < .01$, and $^{***}P < .001$ compared to the corresponding non-Tg; $^{\#}P < .05$, $^{\#\#}P < .01$ compared to the corresponding TgSED.

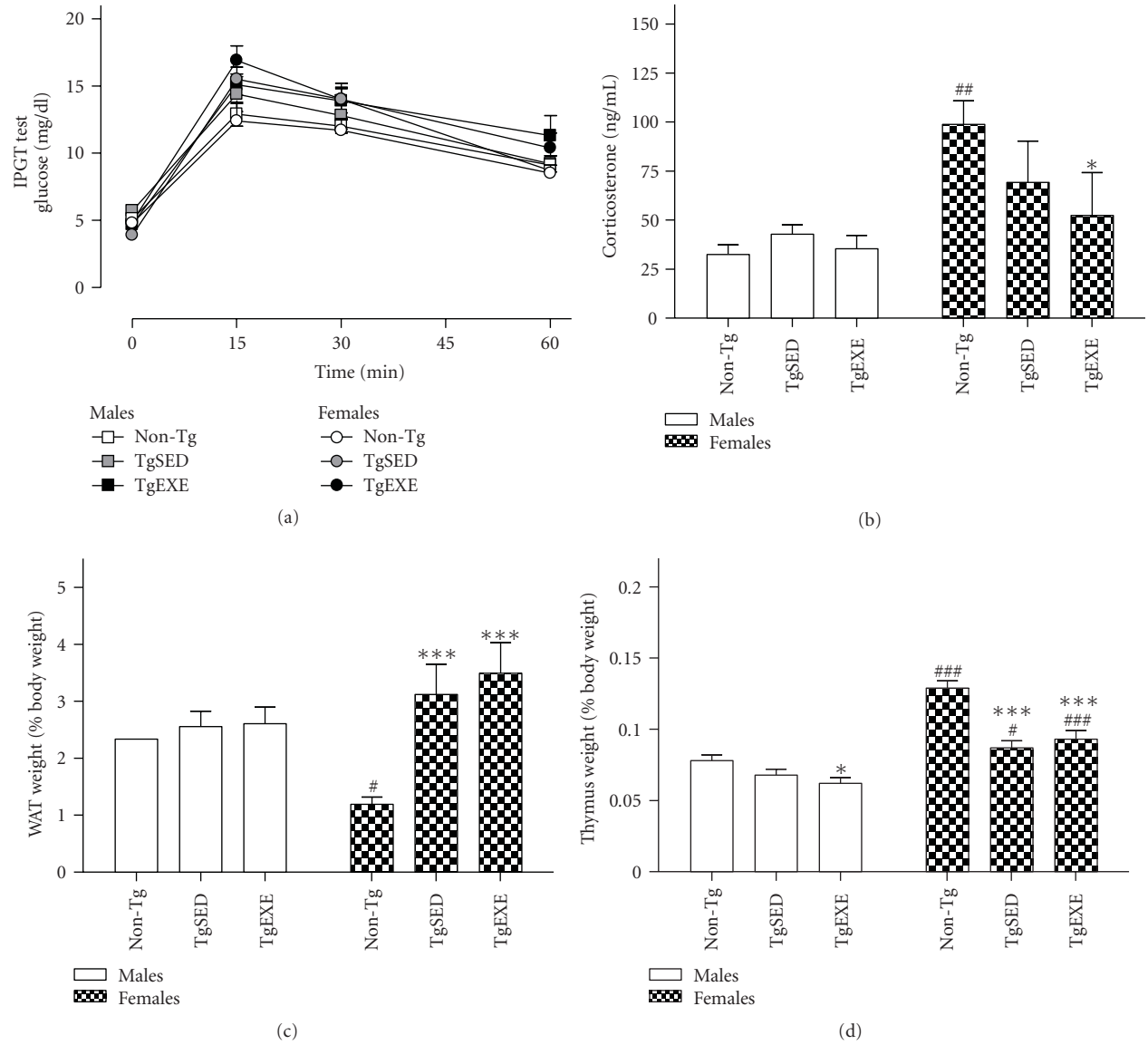

Figure 2: Peripheral physiological-immunoendocrine function is differentially impaired in male and female 3xTg-AD mice and is not ameliorated by treadmill exercise. (a) The IPGT test, indicating plasma glucose levels after an ip injection of glucose, denoted lower tolerance in female 3xTg-AD (see text for statistics). (b–d) Immunoendocrine function as measured by corticosterone plasma levels (b), white adipose tissue (WAT) weight (c), and thymus weight (d) was better in females than in males. Values are the mean ± SEM, $n = 8$–10. Statistics: $^{*}P < .05$ and $^{***}P < .001$ compared to the corresponding non-Tg; $^{\#}P < .05$, $^{\#\#}P < .01$, and $^{\#\#\#}P < .001$ compared to the corresponding TgSED.

effect of exercise ("exercise," all F's$(1, 35) > 4,313$) on the distance covered on both rod tests (coordination), with "gender x exercise" interaction effects ("gender × exercise," all F's$(1, 35) > 5,088$). The post hoc Duncan's test revealed that all females exhibited longer latencies to fall (equilibrium) than did males when the complexity of the task was increased (metal rod test) as well as longer latencies to fall (strength) and more distance covered (coordination and equilibrium) on the 60 s trial of the hanging test. The benefit of exercise had a strong gender component, with the group of treated females showing statistically significant differences with respect to the other three groups in terms of the distance covered on the rod tests (coordination and equilibrium).

3.1.3. Corner Test. As illustrated in Figure 1(a), the normal behavioral pattern exhibited by NTg mice clearly differed between genders, with females being more neophobic than males. On the other hand, two-way ANOVA also showed gender effects in both horizontal (number of corners) and vertical activities (number) (all F's$(1, 35) > 6.145$, $P < .01$). Latency of rearings (see Table 1(a)) was influenced by all factors (genotype, gender, treatment, and gender × treatment

interaction effects; all F's$(1, 35) > 4.846$, $P < .05$ and $F(3,34) = 9.752$, $P < .001$, resp.). Exercise did not induce modifications on the total number of these behaviors but modified its onset (as mentioned above) and showed interaction effects with gender in the number and latency of rearings (all F's$(3, 34) > 6.082$, $P < .01$).

3.1.4. Open-Field Test. Figure 1(b) shows the time course and total activity developed in the open-field test, while in Table 1(b), the sequence of behavioral events is indicated.

In the non-Tg mice males and females mainly differed in the initial horizontal and vertical activities developed in the test, the latency to reach the peripheral area. Overall, that also resulted in a total higher activity in males than females (all $P < .05$). No differences in self-grooming or defecation were recorded.

When the genotype was considered, it was observed that the behavioral sequence of events was faster developed by 3xTg-AD mice, reaching the statistical significance in most of the studied variables in the groups with exercise (see Table 1(b) and Figure 1(b)). Accordingly, the first minute of the test was the most sensitive to show gender (all F's$(1, 25) > 5.104$, $P < .05$) and genotype differences, with TgSED and TgEXE animals being more active than their non-Tg counterparts (males, all F's$(2, 21) > 5.375$, $P < .01$; females, all F's$(2, 25) > 3.750$, $P < .01$). Also, the horizontal and vertical activities developed during the first minute of the test was different between males and females. However, when the total activity developed during the test was considered, a genotype × gender interaction effect (all F's$(3, 34) > 3.125$, $P < .05$) was found. Thus, genotype differences were maintained in the female groups (TgSED and TgEXE) but were inversed (vertical activity) in the male groups (TgSED and TgEXE). Exercise increased self-grooming behavior was observed in male TgEXE.

3.1.5. Dark-Light Box Test. As in the previous tests (see Table 1(b) and Figure 1(c)) gender-dependent differences between non-Tg males and females were observed and then disappeared in the 3xTg-AD genotype. TgSED and TgEXE males exhibited reduced number of entries into the lit area, and once there they developed less locomotor activity and increased the number of defecations (all F's$(2, 25) > 3.750$, $P < .05$). Oppositely, female TgSED and TgEXE increased their presence in the lit area as it was consistently shown in all the variables measured in the test (all F's$(2, 21) > 3.508$, $P < .05$).

3.1.6. Morris Water Maze Tests. Figure 1(d) illustrates the "day-by-day" and "trial-by-trial" acquisition curves. Results are expressed in distances because we found gender, genotype, and gender × genotype differences in the swim speed (see Table 1(b)). In the non-Tg mice, mean speed of females was slower than males, oppositely of what was found in 3xTg-AD mice. Besides, mean speed of 3xTg-AD was higher than that of non-Tg counterparts ($F(5,46) = 3.18$, $P < .05$), mainly in females (see Table 1(b)).

All the animals exhibited a similar acquisition curve (day effect, $F(3,152) = 31.0$, $P < .001$), but in the males the reduction of the mean distance covered to find the platform along the four days of the test was faster than in females ($F(5,152) = 2.483$, $P < .05$). Still, no differences could be found in the annulus crossing during the probe trial, except for a general gender effect ($F(3,35) = 31$, $P < .001$).

In the cue learning task gender differences in the non-Tg groups were also found in the mean distance covered and the speed, with non-Tg males taking longer and being faster than non-Tg females (see Table 1(b), t-test, 14 df, $P < .05$ in both cases). This gender effect was not observed among the 3xTg-AD groups.

3.1.7. T-Maze. Differences in the latency to reach the intersection of the T-maze were found ($F(5,46) = 2.31$, $P < .05$) with the highest values spent by non-Tg females as compared with their male non-Tg and female 3xTg-AD counterparts. No differences were due to exercise.

3.2. Glucose Tolerance. Results of the IPGTT test are shown in Figure 2(a). Female 3xTg-AD mice showed decreased glucose tolerance as related to non-Tg mice. ANOVA showed an effect for female glucose curves ($F(2,84) = 6.764$, $P < .005$) with the peak of glucose levels (15 min of the IPGTT test) in female 3xTg-AD mice, both sedentary and exercised groups, being higher than those measured in non-Tg female mice ($P < .05$). On parallel both groups of male 3xTg-AD mice showed a trend to impaired glucose tolerance albeit it did not reach statistical significance.

3.3. Immunoendocrine Status. Corticosterone plasma levels are shown in Figure 2(b). Weight of WAT and thymus are shown in Figures 2(c) and 2(d). Other weighed organs did not show any significant differences between the experimental groups. There was a "gender" effect on corticosterone levels ($F(1,52) = 1.18$, $P < .005$) and thymus weight ($F(1,46) = 78.02$, $P < .001$). There was a "genotype" effect on thymus weight ($F(2,46) = 20.68$, $P < .001$) and WAT weight ($F(2,46) = 8.051$, $P < .001$), with "genotype × gender" interaction effects in both weights ($F(2,46) = 5.996$, $P < .005$ and $F(2,46) = 5.042$, $P < .01$, resp.). non-Tg females showed higher corticosterone and thymus weight and lower fat than did males. 3xTg-AD females showed a decrease in corticosterone and thymus weight and an increase in fat as compared to non-Tg females. However, 3xTg-AD females showed a better immunoendocrine status than did the corresponding males, as shown by thymus weight. Treadmill exercise had a minimal effect on these parameters.

3.4. Brain Amyloid Pathology. In order to assess AD pathology, we performed Aβ and PHF-tau immunostaining in sections of male and female 3xTg-AD mice that had been maintained under sedentary or forced exercise conditions (Figure 3(a)). Immunoreactivity of 4G8 and AT180 was evident in hippocampus and amygdala neurons. Treadmill exercise did not decrease 4G8 and AT180 immunoreactivity in any of the 3xTg-AD sex groups. Further, we measured soluble Aβ40 and Aβ42 levels in cerebral cortex of male and female 3xTg-AD mice (with and without exercise) by

Table 2: Treadmill exercise recovers the [^{3}H] flunitrazepam binding parameters of cerebral cortical tissue of 3xTgAD mice.

		non-Tg	TgSED	TgEXE
Males	Bmax (pmol/mg prot)	1.77 ± 0.32	1.85 ± 0.36	1.58 ± 0.43
	Kd (nM)	3.85 ± 0.73	6.46 ± 0.69*	3.64 ± 0.69#
Females	Bmax (pmol/mg prot)	1.21 ± 0.43	1.45 ± 0.65	1.27 ± 0.30
	Kd (nM)	3.46 ± 1.61	4.03 ± 2.80	3.20 ± 1.08

Note: non-Tg, nontransgenic mice; TgSED, 3xTgAD mice not exercised; TgEXE, 3xTg-AD mice submitted to a daily treadmill running for five weeks. Exercise protected against the decrease of the affinity of [^{3}H] flunitrazepam for its binding site in the GABA-A receptor, as showed by a low Kd. Results are the mean ± SEM, $n = 3$. Statistics: $^*P < .05$ compared to non-Tg; $^\#P < .01$ compared to TgSED.

using sandwich ELISA (Figure 3(b)). Both peptides showed higher levels in females than in males. Two-way ANOVA analyses showed a significant effect of "gender" on Aβ40 ($F(1,9) = 64.97$, $P < .005$) and Aβ42 ($F(1,9) = 8.159$, $P = .05$). Exercise induced an increase in Aβ40 level and a decrease in the Aβ42/Aβ40 relationship in female mice. Two-way ANOVA showed a significant effect of "exercise" on the Aβ42/Aβ40 ratio ($F(1,19) = 10.17$, $P < .05$), but no "gender" effect. We therefore analyzed all animals together using a two-tailed Student's t-test, which confirmed that treadmill exercise decreased the Aβ42/Aβ40 ratio in 3xTg-AD (last graph in Figure 3(b)).

3.5. GABA Function Alteration. The effects of treadmill exercise on GABA-A receptor functionality were assayed by measuring [^{3}H] flunitrazepam binding parameters in male and female non-Tg mice, 3xTg-AD without exercise and 3xTg-AD with treadmill exercise (Table 2). We observed that the density of the [^{3}H] flunitrazepam binding sites (Bmax) was unchanged in both male and female 3xTg-AD compared to non-Tg.In relation to the dissociation constant (Kd), there were no binding affinity changes among any of the three groups of female mice. In contrast, 3xTg-AD males that had not practiced exercise showed a lower Kd of flunitrazepam than did non-Tg mice (Kd increased 2.15-fold in 3xTg-AD versus non-Tg), whereas those subjected to one month of forced exercise had recovered control affinity levels.

3.6. Oxidative Stress. The effects of exercise on the disturbed redox homeostasis of 3xTg-AD were studied by analyzing brain cortex lipid peroxidation levels and the status of the main antioxidant cell systems. Lipid peroxidation levels (Figure 4(a)) were increased in 3xTg-AD males as compared to non-Tg, but this was not the case in females. Exercise significantly reduced male lipid peroxidation. GSH and GSSG levels (Figures 4(b) and 4(c)) were significantly increased in 3xTg-AD males as compared to non-Tg, and these alterations were not changed by treadmill exercise. non-Tg females had higher glutathione levels than did males. Levels were also high in 3xTg-AD females, but significantly reduced by exercise. GPx activity (Figure 4(d)) was significantly decreased in 3xTg-AD males as compared to non-Tg, and this was not changed by exercise. non-Tg females had lower GPx levels than did males. SOD-CuZn activity (Figure 4(e)) was not changed among the several groups of male and female mice, but there was increased SOD-Mn activity (Figure 4(f)) in 3xTg-AD exercised males compared to non-Tg.

A two-way ANOVA for 3xTg-AD animals indicated an effect of "gender" in SOD-Mn ($F(1,16) = 13.13$, $P < .005$), GSH ($F(1,16) = 90.70$, $P < .001$), GSSG ($F(1,18) = 46.80$, $P < .001$), and GPx ($F(1,18) = 23.93$, $P < .001$) as well a "gender × exercise" interaction with respect to GSH ($F(1,16) = 5.479$, $P < .05$). Accordingly, there was a difference between 3xTg-AD sedentary males and females in SOD-Mn ($P < .05$), GSH ($P < .001$), GSSG ($P < .001$), and GPx ($P < .05$), but in exercised male and female 3xTg-AD the difference was only observed for GSH ($P < .001$), GSSG ($P < .001$), and GPx ($P < .001$). In contrast, there were no differences between nontransgenic males and females in any of the redox parameters analyzed. The correlation analysis showed a direct relationship between SOD-Mn activity and both GSH and GSSG levels as well as a negative relationship between SOD-Mn activity and lipid peroxidation levels and GPx activity.

4. Discussion

In this work we have performed a wide screening in both genders of 3xTg-AD mice at early stages of the disease and non-Tg mice. Several levels of study have been considered from cellular to behavioral ones, including new areas of interest such as physical condition, glucose homeostasis, immunoendocrine function, and oxidative stress. The main interest of the present results has been the description of differences of gender, specific for both genotypes, as well as the beneficial effects that even a short training with forced exercise can have. Also, the results indicate that interaction effects between gender, genotype, and treatment should be always taken into consideration when assessing the outcome of preventive and/or therapeutic interventions.

The first studies focused on the physical condition. Expected gender differences on weight between males and females were found in both genotypes. The results do also confirm that the overweight reported from early stages of the disease in male 3xTg-AD mice of the Spanish colony [22] is observed in both genders and that females seem to be more sensitive to some etiological-causal and related factors. Thus, in this strain background (C57BL/6 x 129S non-Tg mice) WAT had a statistically significant smaller contribution to the total body weight in females as compared to males. However, in the 3xTg-AD mice the total amount of WAT was equal in both genders, and both the total amount and the relative contribution of WAT exhibited a three-fold increase with the triple-transgenic genotype, an effect restricted to females. Since overweight and glucose metabolism are closely related, we also studied both basal glycemia and glucose tolerance. Although the overweight animals did not show altered basal glucose levels, the increased peak of glucose observed in both genders of 3xTg-AD confirmed our recent

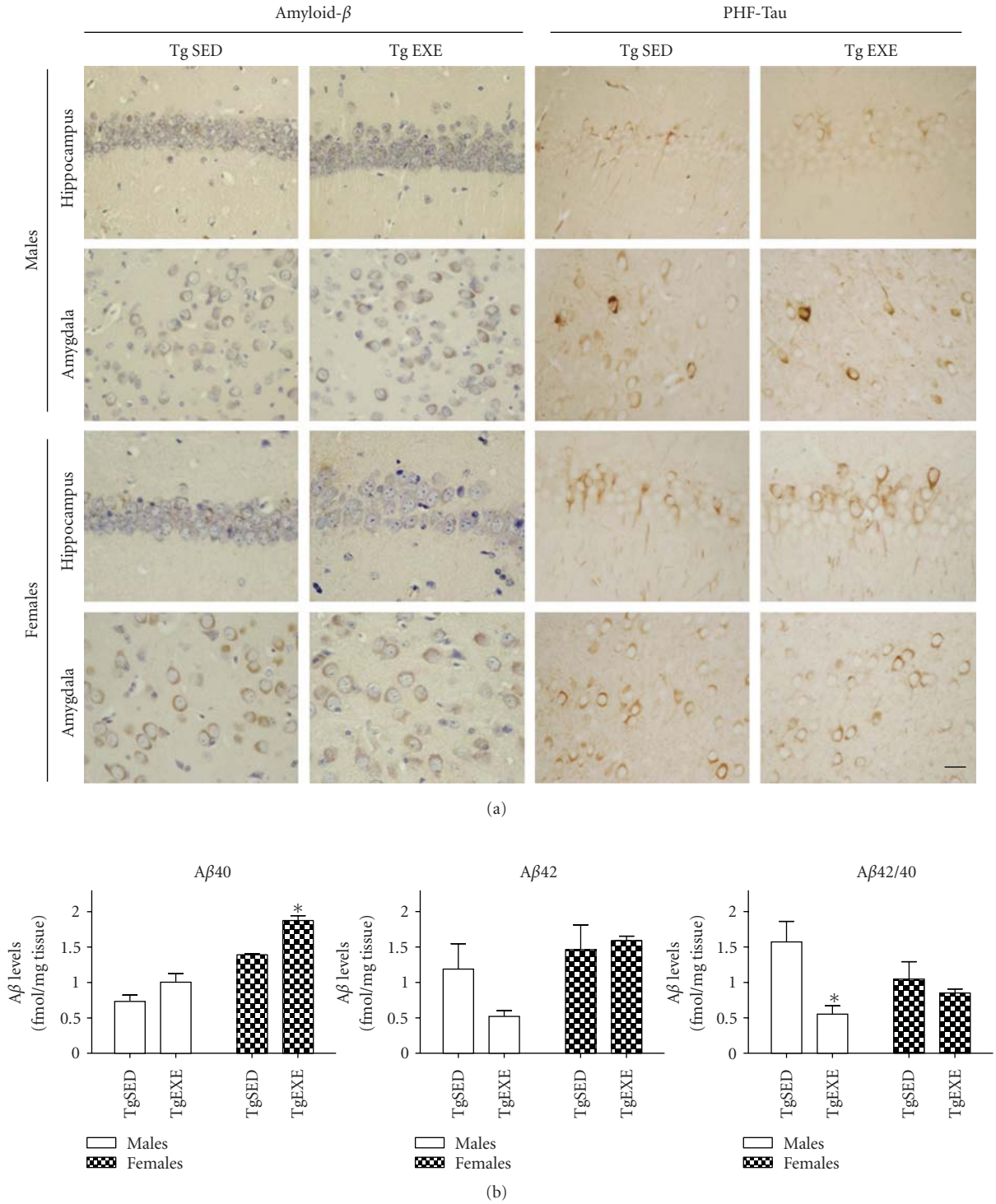

Figure 3: Brain pathology in male and female 3xTg-AD sedentary mice (TgEXE) is partially protected against by treadmill running exercise (TgSED). (a) Representative microphotographs of hippocampus CA1 and basolateral amygdala showing amyloid-β and PHF-tau immunoreactivity using antibodies 4G8 and AT180, respectively. 4G8 reacts against amino acids 1–17 of amyloid β. AT180 detects phosphorylated tau at the threonine 321 residue. No changes in intraneuronal amyloid β or PHF-tau were induced by exercise. Scale bar = 20 μm. (b) Levels of soluble amyloid β 40 (Aβ40) and amyloid-β42 (Aβ42) in cerebral cortex as determined by sandwich ELISA. Treadmill exercise induced a protective change by decreasing the Aβ42/Aβ40 ratio (Aβ42/40) (ANOVA, $P = .0110$). Values are the mean ± SEM, n = 3-4. Statistics: $^*P < .05$.

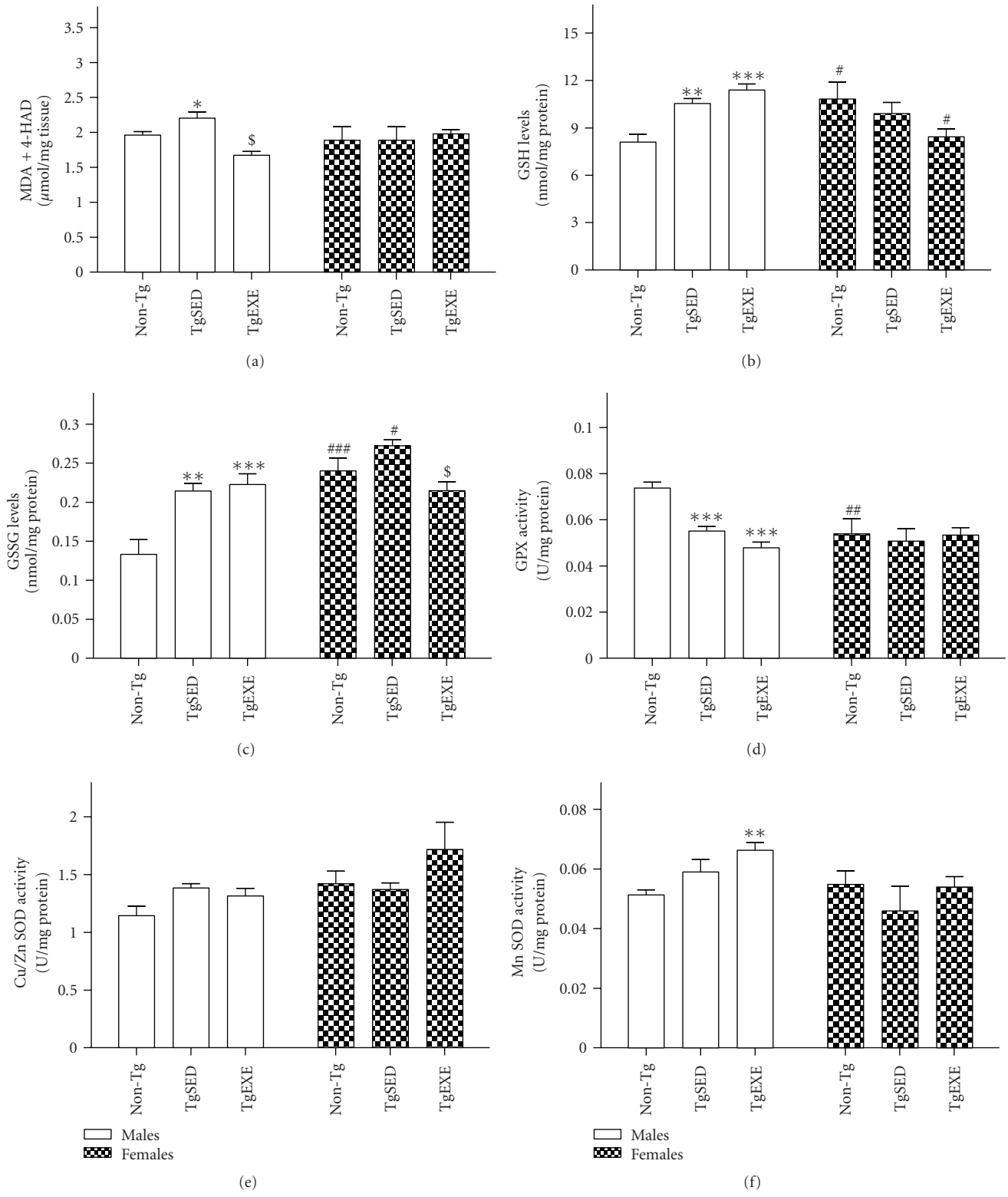

Figure 4: Oxidative stress in the cerebral cortex of sedentary male 3xTg-AD mice (TgSED) is partially ameliorated by treadmill running exercise (TgEXE), whereas 3xTg-AD females show less alteration. Tissue of sedentary nontransgenic mice (non-Tg) was analyzed as a reference. (a) Lipid peroxidation levels expressed as malondialdehyde (MDA) plus 4-hydroxyalkenal (4-HAD). (b) Levels of reduced glutathione (GSH). (c) Levels of oxidized glutathione (GSSG). (d) Glutathione peroxidase (GPx) enzymatic activity. (e) SOD-CuZn enzymatic activity. (f) SOD-Mn activity. Data represent the mean ± SEM of 4–8 animals, tested in duplicate. Statistics: $^{*}P < .05$, $^{**}P < .01$, and $^{***}P < .001$ compared to non-Tg; $^{\#}P < .05$ compared to TgSED.

findings suggesting that glucose homeostasis is compromised in 3xTgAD mice from early stages of the disease [37]. The results also suggest that females may be more sensitive than males (statistical significance was only reached in females). In addition, other metabolism derangements can be involved in the increased relative WAT levels in females and the generally increased body weight in 3xTg-AD mice. For instance, leptin-related pathways were reported to be impaired with mice models of AD and leptin treatment ameliorated cognitive loss [38]. The weight of females was also more sensitive to repeated handling or exposure to the apparatus itself, independent of the administration of the treatment, as a decline in the curve of weight was only observed in this gender but not in male mice. We cannot assert to which extent the loss of weight can be related to emotional reactivity as, on general, blood corticosterone levels did not differ between both groups of 3xTg-AD females, and, in any case, the corticosterone levels were lower than that recorded on non-Tg females. Overall, the results indicate a poorer ability to maintain weight and glucose homeostasis in female 3xTg-AD mice already at early stages of the disease. The lack of effects of exercise on weight or glucose tolerance may be explained by the fact that the profile exhibited by animals submitted to exercise could be classified as that of "low runners" and therefore is not enough for such expected beneficial effects. In fact, the physical condition of both male and female 3xTg-AD was observed to be lower than that expected for animals of its age as other strains of mice can be successfully trained in three different treadmill exercise conditions from minimum (15 min/day, 5 $cm \cdot s^{-1}$, 0° slope) to moderate exercise (60 min/day, 10 $cm \cdot s^{-1}$, 0° slope) to exhaustive exercise (60 min/day, 25 $cm \cdot s^{-1}$, 20° slope). Here, no slope, low initial speed, and a slow increase of speed and duration of exercise had to be used to avoid animals to get physically exhausted. Moreover, it was observed that animals only run when approaching the electric foot-shock panel, but once reaching the opposite side of the apparatus they stopped. The pause persisted until arriving to the proximity of the panel when they felt encouraged again to run to avoid the negative reinforce. Thus, the 3xTg-AD mice could be classified as "low or nonrunners" according to the "pause number" criterion [38].

The behavioral profile which was aimed to assess not only cognitive but also BPSD-like behaviors which we have described can be already observed from early stages of the disease in 3xTg-AD male mice [22, 29]. All the results obtained in the different behavioral tests (corner, OF, and DLB) consistently indicated gender-dependent differences in anxiety-like behaviors in non-Tg mice; that is, non-Tg females showed increased anxiety as measured by reduced number of horizontal and vertical activities in the three tests, increased latencies of some behavioral events in the open field, and reduced entrance and time spent in the lit area of the dark-light box as compared to non-Tg males.

The results also showed that the transgenic behavioral phenotype was characterized by increased BPSD-like behaviors. Thus, both male and female 3xTg-AD mice exhibited a strong increase of neophobia in the corner test which was nicely observed in the horizontal component (corners), while the vertical activity levels of 3xTg-AD mice did not differ from that shown by non-Tg females. The results in the open field do confirm the increase of anxiety-like behaviors which imply a faster sequence of events related to thigmotaxis or preference for protected areas in the test (leaving the central square to enter in the peripheral ring) and increased horizontal activity (hyperactivity in females). In contrast, the vertical activity in the three groups of both males and females found a strong parallelism with that exhibited in the corner tests and that to be observed in the dark-light box on the next day. In the DLB, the BPSD-like behaviors exhibited by both groups of 3xTg-AD mice were gender dependent. Disinhibitory behavior was observed in TgSED and TgEXE females as compared to non-Tg females. The BPSD-like behavior in males was manifested as increased anxiety (reduction in the number of entries and therefore of horizontal and vertical activities, increased defecatory behavior) although in previous works we have also been able to observe the disinhibitory effect in males [22].

When the animals were tested for spatial learning and memory in the different paradigms of MWM, no differences could be found on their learning and memory abilities. However, the main finding was an increased speed during all the days of the tests in the female groups (TgSED and TgEXE), although in current investigations we have found this effect also in 3xTg-AD males. The speed was reduced in the cue learning task albeit only reached statistical significance in non-Tg mice and 3xTgAD females (TgSED and TgEXE), but it is indicative of genotype and genotype-dependent differences in motivation or emotionality, in agreement with the increase of BPSD-like behaviors observed in the other tests. Genotype-dependent differences in thermoregulation [22] could also account for the observed differences in swimming speed. These results are also aware about the relevance of analysing the trajectories on parallel to the traditional latency measurement.

In a previous study [24] we have described gender-dependent neuroimmunoendocrine disfunction in 3xTg-AD at advanced stages of the disease (15 month of age). In this work, the weight of thymus was used as an indirect indicator of immunological functional state, with involution of thymus showing a correlation with differences in immunological function [39] and immunological aging [40]. As expected, the total weight of thymus was higher in females than in males, and this gender difference was more obvious when its relative weight was considered, suggesting a better immune function in the female gender. Interestingly, although this gender-dependent protection was still persistent in 3xTg-AD females, it was strongly reduced as compared to the one exhibited by non-Tg females. Also in males, the transgenic phenotype resulted in involution of the weight of thymus albeit it only reached statistical significance in one of the transgenic groups. Therefore, the present results show an involution of thymus in adult 3xTg-AD mice and suggest that the gender-dependent neuroimmunoendocrine disfunction described in old 3xTg-AD mice [24] may find a clear correlation with impaired immunological function at early stages of the disease, a subject which is under current investigations. Related to this, female 3xTg-AD mice were

very fast to reach the intersection of the T-maze as compared to the non-Tg females. This fast performance could be more fight counterpart to the flight copying with stress strategy (slow performance) than has been related to premature accelerated neuroimmunoendocrine system in mice [32].

When considering neuropathological aspects, it is known that at six month of age, 3xTg-AD mice develop intraneuronal Aβ as a characteristic pathological feature of this AD mouse model [20, 21]. Aβ deposits appeared slightly larger in females than in males, in agreement with previous observations in this mouse [41]. These mice showed intraneuronal PHF-tau. At this early age the phosphorylation at Thr321 in intraneuronal tau can be added to that previously described for Thr212, Ser214, and Ser262 in soluble tau [42]. The exercise paradigm used (forced treadmill running) did not ameliorate Aβ deposits or PHF-tau pathology. Other authors also reported no plaque reduction with a similarly short exercise treatment in a freely available wheel [43, 44]. Brain levels of soluble Aβ40 and Aβ42 at 7 months of age were low in comparison to levels of more than 100 fmol/mg reported at 13 months [20]. Interestingly, the two-way ANOVA showed that Aβ levels were, overall, higher in females than in males. Therefore, this increased level may cause the greater behavioral alterations observed in young adult females compared with males (this study, [41]).

In the neurochemical approach, we considered underlying mechanisms of BSPD-like symptoms that model noncognitive AD deterioration which are yet needed to be further explored in these mice. The GABAergic system is considered to be involved in depressive symptoms in AD [45], and the lowered affinity for flunitrazepam binding found in 3xTg-AD males paralleled that reported in the temporal cortex of AD patients [45]. The GABAergic system is less sensitive to the neurodegeneration process than are other neurotransmitter receptors, and GABA-A receptors are relatively well preserved in AD. However, particular receptor subunits may be altered, leading to compensatory changes or physiological disturbances [46, 47]. Forced exercise reversed the flunitrazepam binding affinity to non-Tg values, although it barely ameliorated the anxiety and depression-like behaviors, as discussed above. Therefore, there is gender dualism in the mechanisms underlying noncognitive behaviors in these AD mice, and BPSD are probably derived from disturbances in several neurotransmitter systems and the subsequent imbalance that is caused [45, 48].

Finally, although conclusive evidence is still lacking, the oxidative stress hypothesis of AD may help to explain the triggering of AD neurodegeneration by environmental or genetic factors [49]. Indeed, AD brain shows an elevation of markers for oxidative damage [50–53], and the prevalence of these markers is higher in initial than later stages of the disease, suggesting an involvement of oxidative stress in AD etiology [54, 55]. Therefore, treatments that help to restore redox homeostasis may delay or ameliorate AD pathology. The presence of brain oxidative stress in 3xTg-AD mice at an early age of 3–5 months (females) has been previously reported [56]. In this study, older mice aged 7 months showed fewer changes in oxidative stress. The main effect found was an increased lipid peroxidation and a derangement of the glutathione system in males. The latter disturbance is consistent with the glutathione metabolism gender alteration in AD male patients [57]. One of the mechanisms involved in physical exercise is the regulation of redox homeostasis. Chronic nonstrenuous exercise decreases oxidative damage and increases antioxidant defenses in brain [4]. Accordingly, 3xTg-AD male rats submitted to treadmill exercise showed a decreased level of lipid peroxidation. Exercise also increased the activity level of SOD-Mn, the first line of defense against mitochondrial oxidative damage. No amelioration of the glutathione system changes was obtained in males, but a decreased oxidization of glutathione was observed in females.

5. Conclusions

Physical exercise is a promising intervention against AD, and the use of a good model such as the 3xTg-AD mice will enable the best exercise strategies to be defined. Five weeks of forced treadmill exercise partially protected 3xTg-AD mice against AD-like pathology. However, the results differed according to gender, this being due to the differential pathological phenotype of 3xTg-AD males and females, in agreement with previous reports [19, 20, 58]. Specifically, we found that males showed more homeostasis redox derangement than did females, while females showed greater brain AD pathology compared with males. Peripheral immunoendocrine status was better in females than in males, even though 3xTg-AD females were impaired with respect to non-Tg females. Therefore, the 3xTg-AD mouse models human gender differences in the progression and expression of the disease. The results of this study corroborate the beneficial effects of a short burst of physical exercise at a moderate stage of AD neurodegeneration (7 months of age), even though these effects were rather modest. Studies with voluntary exercise are ongoing [41], as this might induce greater neuroprotective effects than does forced exercise [59]. We speculate that over a short training period the stress associated with the mandatory treadmill exercise may partially interfere with the beneficial aerobic effects.

Acknowledgments

This work received financial support from Fundació La Marató de TV3 2006-062930 and 2006-062931; Red Envejecimiento y Fragilidad, RD06/0013/0003 and RD06/0013/1004 from ISCIII; SAF2006-13642 and SAF2009-13093-C02-02 from MICINN. Yoelvis García and Karla Buccieri acknowledge support from Fundació La Marató de TV3. The authors thank Mónica De la Fuente for her kind support offering the treadmill apparatus as well as Dung Van Nguyen, Santi Solé, and Jèssica López Regal for technical assistance. The animals used in this study are from the colonies of homozygous 3xTg-AD and wild-type non-Tg mice established at UAB by Lydia Giménez-Llort from progenitors kindly provided by Prof. Frank M. LaFerla, Department of Neurobiology and Behavior, University of California Irvine, CA, USA.

References

[1] R. Brookmeyer, E. Johnson, K. Ziegler-Graham, and H. M. Arrighi, "Forecasting the global burden of Alzheimer's disease," *Alzheimer's and Dementia*, vol. 3, no. 3, pp. 186–191, 2007.

[2] M. N. Sabbagh, "Drug development for Alzheimer's disease: where are we now and where are we headed?" *American Journal Geriatric Pharmacotherapy*, vol. 7, no. 3, pp. 167–185, 2009.

[3] S. K. Pope, V. M. Shue, and C. Beck, "Will a healthy lifestyle help prevent Alzheimer's disease?" *Annual Review of Public Health*, vol. 24, pp. 111–132, 2003.

[4] Z. Radak, H. Y. Chung, and S. Goto, "Systemic adaptation to oxidative challenge induced by regular exercise," *Free Radical Biology and Medicine*, vol. 44, no. 2, pp. 153–159, 2008.

[5] C. W. Cotman, N. C. Berchtold, and L.-A. Christie, "Exercise builds brain health: key roles of growth factor cascades and inflammation," *Trends in Neurosciences*, vol. 30, no. 9, pp. 464–472, 2007.

[6] Z. Radak, N. Hart, L. Sarga, et al., "Exercise plays a preventive role against Alzheimer's disease," *Journal of Alzheimer's Disease*, vol. 20, no. 3, pp. 777–783, 2010.

[7] H. van Praag, "Exercise and the brain: something to chew on," *Trends in Neurosciences*, vol. 32, no. 5, pp. 283–290, 2009.

[8] D. E. R. Warburton, C. W. Nicol, and S. S. D. Bredin, "Health benefits of physical activity: the evidence," *Canadian Medical Association Journal*, vol. 174, no. 6, pp. 801–809, 2006.

[9] K. A. Barbour and J. A. Blumenthal, "Exercise training and depression in older adults," *Neurobiology of Aging*, vol. 26, supplement 1, pp. S119–S123, 2005.

[10] E. B. Larson, L. Wang, J. D. Bowen et al., "Exercise is associated with reduced risk for incident dementia among persons 65 years of age and older," *Annals of Internal Medicine*, vol. 144, no. 2, pp. 73–81, 2006.

[11] N. T. Lautenschlager, K. L. Cox, L. Flicker et al., "Effect of physical activity on cognitive function in older adults at risk for Alzheimer disease: a randomized trial," *Journal of the American Medical Association*, vol. 300, no. 9, pp. 1027–1037, 2008.

[12] C. L. Williams and R. M. Tappen, "Effect of exercise on mood in nursing home residents with Alzheimer's disease," *American Journal of Alzheimer's Disease and other Dementias*, vol. 22, no. 5, pp. 389–397, 2007.

[13] L. Teri, L. E. Gibbons, S. M. McCurry et al., "Exercise plus behavioral management in patients with Alzheimer disease: a randomized controlled trial," *Journal of the American Medical Association*, vol. 290, no. 15, pp. 2015–2022, 2003.

[14] C. L. Williams and R. M. Tappen, "Exercise training for depressed older adults with Alzheimer's disease," *Aging and Mental Health*, vol. 12, no. 1, pp. 72–80, 2008.

[15] P. A. Adlard, V. M. Perreau, V. Pop, and C. W. Cotman, "Voluntary exercise decreases amyloid load in a transgenic model of Alzheimer's disease," *Journal of Neuroscience*, vol. 25, no. 17, pp. 4217–4221, 2005.

[16] C. M. Yuede, S. D. Zimmerman, H. Dong et al., "Effects of voluntary and forced exercise on plaque deposition, hippocampal volume, and behavior in the Tg2576 mouse model of Alzheimer's disease," *Neurobiology of Disease*, vol. 35, no. 3, pp. 426–432, 2009.

[17] J. Y. Cho, D. Y. Hwang, T. S. Kang et al., "Use of NSE/PS2m-transgenic mice in the study of the protective effect of exercise on Alzheimer's disease," *Journal of Sports Sciences*, vol. 21, no. 11, pp. 943–951, 2003.

[18] H. S. Um, E. B. Kang, Y. H. Leem et al., "Exercise training acts as a therapeutic strategy for reduction of the pathogenic phonetypes for Alzheimer's disease in an NSE/APPSw-transgenic model," *International Journal of Molecular Medicine*, vol. 22, no. 4, pp. 529–539, 2008.

[19] Y.-H. Leem, H.-J. Lim, S.-B. Shim, J.-Y. Cho, B.-S. Kim, and P.-L. Han, "Repression of tau hyperphosphorylation by chronic endurance exercise in aged transgenic mouse model of tauopathies," *Journal of Neuroscience Research*, vol. 87, no. 11, pp. 2561–2570, 2009.

[20] S. Oddo, A. Caccamo, J. D. Shepherd et al., "Triple-transgenic model of Alzheimer's disease with plaques and tangles: intracellular Aβ and synaptic dysfunction," *Neuron*, vol. 39, no. 3, pp. 409–421, 2003.

[21] S. Oddo, A. Caccamo, M. Kitazawa, B. P. Tseng, and F. M. LaFerla, "Amyloid deposition precedes tangle formation in a triple transgenic model of Alzheimer's disease," *Neurobiology of Aging*, vol. 24, no. 8, pp. 1063–1070, 2003.

[22] L. Giménez-Llort, G. Blázquez, T. Cañete et al., "Modeling behavioral and neuronal symptoms of Alzheimer's disease in mice: a role for intraneuronal amyloid," *Neuroscience and Biobehavioral Reviews*, vol. 31, no. 1, pp. 125–147, 2007.

[23] L. K. Clinton, L. M. Billings, K. N. Green et al., "Age-dependent sexual dimorphism in cognition and stress response in the 3xTg-AD mice," *Neurobiology of Disease*, vol. 28, no. 1, pp. 76–82, 2007.

[24] L. Giménez-Llort, L. Arranz, I. Maté, and M. De La Fuente, "Gender-specific neuroimmunoendocrine aging in a triple-transgenic 3×Tg-AD mouse model for Alzheimer's disease and its relation with longevity," *NeuroImmunoModulation*, vol. 15, no. 4–6, pp. 331–343, 2008.

[25] C.-W. Wu, Y.-C. Chen, L. Yu et al., "Treadmill exercise counteracts the suppressive effects of peripheral lipopolysaccharide on hippocampal neurogenesis and learning and memory," *Journal of Neurochemistry*, vol. 103, no. 6, pp. 2471–2481, 2007.

[26] Y.-F. Liu, H.-I. Chen, L. Yu et al., "Upregulation of hippocampal TrkB and synaptotagmin is involved in treadmill exercise-enhanced aversive memory in mice," *Neurobiology of Learning and Memory*, vol. 90, no. 1, pp. 81–89, 2008.

[27] M. J. Sabatier, N. Redmon, G. Schwartz, and A. W. English, "Treadmill training promotes axon regeneration in injured peripheral nerves," *Experimental Neurology*, vol. 211, no. 2, pp. 489–493, 2008.

[28] Y. García, S. Revilla, R. Cristòfol, et al., "Voluntary exercise ameliorates both cognitive and noncognitive symptoms in the 3xTgAD mouse," *Alzheimer's and Dementia*, vol. 5, no. 4, p. P443, 2009.

[29] L. Giménez-Llort, G. Blázquez, T. Cañete, et al., "Modeling neuropsychiatric symptoms of Alzheimer's disease dementia in 3xTg-AD mice," in *Alzheimer's Disease: New Advances*, K. Iqbal, B. Winblad, and J. Avila, Eds., pp. 513–516, Medimond, Englewood, NJ, USA, 2006.

[30] L. Giménez-Llort, A. Fernández-Teruel, R. M. Escorihuela et al., "Mice lacking the adenosine A1 receptor are anxious and aggressive, but are normal learners with reduced muscle strength and survival rate," *European Journal of Neuroscience*, vol. 16, no. 3, pp. 547–550, 2002.

[31] R. Morris, "Developments of a water-maze procedure for studying spatial learning in the rat," *Journal of Neuroscience Methods*, vol. 11, no. 1, pp. 47–60, 1984.

[32] N. Guayerbas, A. I. Sánchez, A. Gamallo, and M. De la Fuente, "Mouse performance in an exploratory activity test

as a longevity biomarker," in *Animal Research Welfare: A Partnership*, J. A. TurMari and J. M. Orellana-Muriana, Eds., pp. 159–161, Laboratory Animals, London, UK, 2000.

[33] L. C. Solberg, W. Valdar, D. Gauguier et al., "A protocol for high-throughput phenotyping, suitable for quantitative trait analysis in mice," *Mammalian Genome*, vol. 17, no. 2, pp. 129–146, 2006.

[34] C. Guardia-Laguarta, M. Coma, M. Pera et al., "Mild cholesterol depletion reduces amyloid-β production by impairing APP trafficking to the cell surface," *Journal of Neurochemistry*, vol. 110, no. 1, pp. 220–230, 2009.

[35] J. Sebastià, R. Cristòfol, M. Pertusa et al., "Down's syndrome astrocytes have greater antioxidant capacity than euploid astrocytes," *European Journal of Neuroscience*, vol. 20, no. 9, pp. 2355–2366, 2004.

[36] I. Rahman, A. Kode, and S. K. Biswas, "Assay for quantitative determination of glutathione and glutathione disulfide levels using enzymatic recycling method," *Nature Protocols*, vol. 1, no. 6, pp. 3159–3165, 2006.

[37] L. Giménez-Llort, E. K. Oghagbon, T. Cañete, and A. Bosch, "Glucose homeostasis in triple-transgenic 3xTg-AD mice is disrupted at early stages of the disease," *Alzheimer's & Dementia*, vol. 4, no. 4, supplement 1, pp. T689–T690, 2008.

[38] S. J. Greco, K. J. Bryan, S. Sarkar et al., "Leptin reduces pathology and improves memory in a transgenic mouse model of Alzheimer's disease," *Journal of Alzheimer's Disease*, vol. 19, no. 4, pp. 1155–1167, 2010.

[39] M. D. Ferrández, M. De la Fuente, E. Fernández, and R. Manso, "Anabolic steroids and lymphocyte function in sedentary and exercise-trained rats," *Journal of Steroid Biochemistry and Molecular Biology*, vol. 59, no. 2, pp. 225–232, 1996.

[40] M. De la Fuente and L. Gimenez-Llort, "Models of aging of neuroimmunomodulation: strategies for its improvement," *NeuroImmunoModulation*, vol. 17, no. 3, pp. 213–216, 2010.

[41] S. Pietropaolo, Y. Sun, R. Li, C. Brana, J. Feldon, and B. K. Yee, "The impact of voluntary exercise on mental health in rodents: a neuroplasticity perspective," *Behavioural Brain Research*, vol. 192, no. 1, pp. 42–60, 2008.

[42] S. Oddo, A. Caccamo, D. Cheng, B. Jouleh, R. Torp, and F. M. LaFerla, "Genetically augmenting tau levels does not modulate the onset or progression of Aβ pathology in transgenic mice," *Journal of Neurochemistry*, vol. 102, no. 4, pp. 1053–1063, 2007.

[43] S. Mirochnic, S. Wolf, M. Staufenbiel, and G. Kempermann, "Age effects on the regulation of adult hippocampal neurogenesis by physical activity and environmental enrichment in the APP23 mouse model of Alzheimer disease," *Hippocampus*, vol. 19, no. 10, pp. 1008–1018, 2009.

[44] H. Richter, O. Ambrée, L. Lewejohann et al., "Wheel-running in a transgenic mouse model of Alzheimer's disease: protection or symptom?" *Behavioural Brain Research*, vol. 190, no. 1, pp. 74–84, 2008.

[45] M. Garcia-Alloza, S. W. Tsang, F. J. Gil-Bea et al., "Involvement of the GABAergic system in depressive symptoms of Alzheimer's disease," *Neurobiology of Aging*, vol. 27, no. 8, pp. 1110–1117, 2006.

[46] O. Howell, J. R. Atack, D. Dewar, R. M. McKernan, and C. Sur, "Density and pharmacology of α5 subunit-containing GABA(A) receptors are preserved in hippocampus of Alzheimer's disease patients," *Neuroscience*, vol. 98, no. 4, pp. 669–675, 2000.

[47] R. A. Rissman, A. L. De Blas, and D. M. Armstrong, "$GABA_A$ receptors in aging and Alzheimer's disease," *Journal of Neurochemistry*, vol. 103, no. 4, pp. 1285–1292, 2007.

[48] M. M. Esiri, "The basis for behavioural disturbances in dementia," *Journal of Neurology Neurosurgery and Psychiatry*, vol. 61, no. 2, pp. 127–130, 1996.

[49] D. Praticò, "Oxidative stress hypothesis in Alzheimer's disease: a reappraisal," *Trends in Pharmacological Sciences*, vol. 29, no. 12, pp. 609–615, 2008.

[50] K. V. Subbarao, J. S. Richardson, and L. S. Ang, "Autopsy samples of Alzheimer's cortex show increased peroxidation in vitro," *Journal of Neurochemistry*, vol. 55, no. 1, pp. 342–345, 1990.

[51] C. D. Smith, J. M. Carney, P. E. Starke-Reed et al., "Excess brain protein oxidation and enzyme dysfunction in normal aging and in Alzheimer disease," *Proceedings of the National Academy of Sciences of the United States of America*, vol. 88, no. 23, pp. 10540–10543, 1991.

[52] P. Mecocci, U. MacGarvey, and M. F. Beal, "Oxidative damage to mitochondrial DNA is increased in Alzheimer's disease," *Annals of Neurology*, vol. 36, no. 5, pp. 747–751, 1994.

[53] D. Praticò, V. M.-Y. Lee, J. Q. Trojanowski, J. Rokach, and G. A. Fitzgerald, "Increased F2-isoprostanes in Alzheimer's disease: evidence for enhanced lipid peroxidation in vivo," *FASEB Journal*, vol. 12, no. 15, pp. 1777–1783, 1998.

[54] L. M. Sayre, G. Perry, and M. A. Smith, "Oxidative stress and neurotoxicity," *Chemical Research in Toxicology*, vol. 21, no. 1, pp. 172–188, 2008.

[55] S. García-Matas, N. de Vera, A. Ortega-Aznar, et al., "In vitro and in vivo activation of astrocytes by amyloid-beta is potentiated by pro-oxidant agents," *Journal of Alzheimer's Disease*, vol. 20, no. 1, pp. 229–245, 2010.

[56] R. Resende, P. I. Moreira, T. Proença et al., "Brain oxidative stress in a triple-transgenic mouse model of Alzheimer disease," *Free Radical Biology and Medicine*, vol. 44, no. 12, pp. 2051–2057, 2008.

[57] H. Liu, L. E. Harrell, S. Shenvi, T. Hagen, and R.-M. Liu, "Gender differences in glutathione metabolism in Alzheimer's disease," *Journal of Neuroscience Research*, vol. 79, no. 6, pp. 861–867, 2005.

[58] S. A. Wolf, G. Kronenberg, K. Lehmann et al., "Cognitive and physical activity differently modulate disease progression in the amyloid precursor protein (APP)-23 model of Alzheimer's disease," *Biological Psychiatry*, vol. 60, no. 12, pp. 1314–1323, 2006.

[59] A. Parachikova, K. E. Nichol, and C. W. Cotman, "Short-term exercise in aged Tg2576 mice alters neuroinflammation and improves cognition," *Neurobiology of Disease*, vol. 30, no. 1, pp. 121–129, 2008.

SAGE-Hindawi Access to Research
International Journal of Alzheimer's Disease
Volume 2010, Article ID 180734, 10 pages
doi:10.4061/2010/180734

Review Article

The Chick as a Model for the Study of the Cellular Mechanisms and Potential Therapies for Alzheimer's Disease

Radmila Mileusnic and Steven Rose

Department of Life Sciences, Faculty of Sciences, The Open University, Milton Keynes, MK7 6AA, UK

Correspondence should be addressed to Radmila Mileusnic, r.mileusnic@open.ac.uk

Received 5 May 2010; Accepted 17 June 2010

Academic Editor: Gemma Casadesus

While animal experiments have contributed much to our understanding of the mechanisms of Alzheimer's disease (AD), their value in predicting the effectiveness of treatment strategies in clinical trials has remained controversial. The disparity between the results obtained in animal models and clinical trials may in part be explained by limitations of the models and species-specific differences. We propose that one trial passive avoidance in the day-old chick is a useful system to study AD because of the close sequence homologies of chick and human amyloid precursor protein (APP). In the chick, APP is essential for memory consolidation, and disrupting its synthesis or structure results in amnesia. RER, a tripeptide sequence corresponding to part of the growth domain of APP, can restore memory loss and act as a cognitive enhancer. We suggest that RER and its homologues may form the basis for potential pharmacological protection against memory loss in AD.

1. Introduction

At first, the day-old chick does not seem a likely model system in which to study the molecular processes involved in a degenerative disease that primarily affects brain function in ageing humans. Before proceeding to argue the case for including the chick amongst such models, however, we should consider more carefully what we mean by, and expect from, an "animal model" of a human disease.

What does one want from an animal model? By an animal model we mean a nonhuman organism that displays some or all of the features of the human condition we wish to understand. These may include some or all of the genetic, molecular, physiological, anatomical, or behavioural features of the human condition or acceptable analogues thereof. To be of utility, such an organism must be readily amenable to experimental manipulation in one or more of these biological/behavioural levels. As the manifestation of the disease or disorder is likely to be species-typical, especially when we are dealing with neurological or psychiatric diagnoses, inferences as to the relevance of any animal analogue are always going to be problematic, as much of the literature on animal models of depression and schizophrenia has demonstrated [1–5].

Alzheimer's disease (AD) manifests itself in humans in terms of behaviour—initially memory loss and confusion, with progressive decline in other faculties. Neurologically, there is accumulation of amyloid plaques and tangles, neuronal death, notably of cholinergic cells in the hippocampus, and brain shrinkage [6–9]. However, there is no known naturally occurring animal equivalent of these features either behaviourally or neurologically, apart from some partial resemblances such as plaque accumulation in aged captive apes. Thus, animal models have been directed towards mimicking the neurological and/or biochemical features of the disease, primarily in rodents, including transgenics, and examining the behavioural consequences in terms of impaired performance on standard memory tasks [10–12].

2. Choice of Task

The measure of neurological deficit commonly chosen as an indicator of an animal model's relevance for AD is an impairment in learning or memory retention in a standard task. Such impairment is taken as analogous to, or better, homologous with, that in human memory in conditions

such as AD. Standard laboratory tasks may be aversive or appetitive, single or multiple trial. For rodents, they include passive avoidance and fear conditioning (both single trial) and versions of the Morris water maze (multiple trial). The merit of one trial tasks is that they are sharply timed; the brevity of the training trial allows for a separation of events surrounding the training experience from the processes that occur during memory consolidation. However, single trial learning is not typical of learning in general, because many instances of animal and human learning are based on the acquisition of experience in a number of repeated trials, involving processes such as generalisation, categorisation, and discrimination. Furthermore, the memory expressed in such animal models is procedural rather than declarative, and procedural memory is the last, not the first, to be lost during the degeneration typical of the progression of AD. While it is a necessary assumption for such studies that the biochemical and pharmacological processes explored in the context of animal memory have their parallels in the human case, the repeated failure of agents which act as cognitive enhancers in well-controlled animal experiments to affect human cognition in clinical trials is a salutary warning that the assumption remains-just that.

3. The APP and AD

The amyloid precursor protein (APP) is a multifunctional transmembrane glycoprotein involved in diverse and opposing cellular functions such as: synapse formation and maintenance [13–16], memory formation [17–23], regulation of transcription, and neurotoxicity [13, 14]. It is extensively processed posttranslationally by specific proteolytic cleavage [13–15]. Like APP, the APP-derived fragments initiate or execute a variety of cellular functions. Most of the evidence that APP is implicated in memory consolidation is based on the effects of intracerebral or intraventricular injections of exogenous APP, its proteolytic fragments, or antibodies and antisense oligodeoxynucleotides. For example, smaller soluble fragments of β-amyloid (Aβ) and structurally mimetic nonpeptidic substances injected centrally antagonise the binding of Aβ protein and produce amnesia [24] as well as a decrease of K^+-evoked acetylcholine release from hippocampus [25, 26]. Centrally administered amyloid β peptides (Aβ) impair retention in the Y-maze, passive avoidance and place-learning in the water maze [26] and cause amnesia for footshock active avoidance in mice [24]. Multiple bilateral injections of $A\beta_{1-40}$ into the dorsal hippocampus produce performance decrements in short-term working memory [27]. In contrast to the effects of Aβ, the secreted form of APP (sAPP) is neurotrophic and neuroprotective and when administered intracerebroventricularly, shows potent memory-enhancing effects [26]; amongst other effects it prevents the learning deficits induced by scopolamine in an object recognition task and improves spatial recognition memory [28–30].

APP is generally accepted to be directly involved in AD and consequently has been extensively studied in a number of different mammalian and nonmammalian systems [13, 14]. Thus, attention has been focussed on enzymes such as the alpha, beta, and gamma secretases associated with the misprocessing of APP leading to accumulation of senile plaques and methods for clearing or diminishing plaque load. Animal models for AD such as mice transgenic for the mutant forms of human APP are therefore in principle directed towards any of these processes and events [11]. However, a major weakness of such studies, although very understandable in the earlier days of AD research, has been that the striking appearance of the plaques and the early death of cholinergic cells has focussed excessive attention on these end-products of the biochemical chain of events leading to the disease, on the assumption that they are both proximal causes of the condition and likely therapeutic targets. An alternative hypothesis would be that the primary lesion in the disease is the disruption of neural processes that require the normal functioning of APP and are essential for cognitive functions such as memory. It is towards this hypothesis that our studies in the chick have proceeded, and which in turn has resulted in uncovering a molecular mechanism that could be of therapeutic significance.

4. Avian APP

Although birds and mammals diverged about 270 million years ago, and consequently are very different in morphology, behaviour, lifespan, and in the age-dependent repression of a broad-spectrum of neuronal genes, the chick may be a better experimental model to study APP than mice because its APP gene sequence and the enzymatic machinery for processing APP are almost identical to that of humans and closer than those in mice [31–38].

Chicken APP expression parallels mammalian APP expression both temporally and topographically. Furthermore, the chick embryo expresses the genes that encode the main proteases implicated in the production of APP, including BACE-1, BACE-2, presenilin-1, presenilin-2, and nicastrin as well as Neprilysin, the main Aβ-degrading enzyme, and ADAM-17, a protease implicated in the non-amyloidogenic processing of APP. Importantly, the level of the APP gene expression is related to the strength of learning in day-old chicks [19]. That makes the chick a useful natural model in which to study the cell biology and functions of APP and a potential "assay system" for drugs that regulate APP processing.

The degree of evolutionary conservation of APP is very high. The chick APP gene sequence, similar to that of the mouse, has 93% amino acid identity and 96% similarity with the human sequence (Figure 1). However, it is important to stress that avian Aβ has 100% sequence similarity with the human Aβ sequence in contrast to rodent Aβ which is lacking residues Arg, Tyr, and His in the Aβ domain, shown to be crucial for amyloidogenesis. In addition, the rodent 5′upstream regulatory region of the APP gene is only 82% homologous to the corresponding region of the human APP gene [39]. These differences may be functionally related to the fact that Aβ plaques do not accumulate in aged memory impaired rodents. Another important difference between rodents and humans is related to the sequence of the last 101 C-terminal amino acids of the human APP

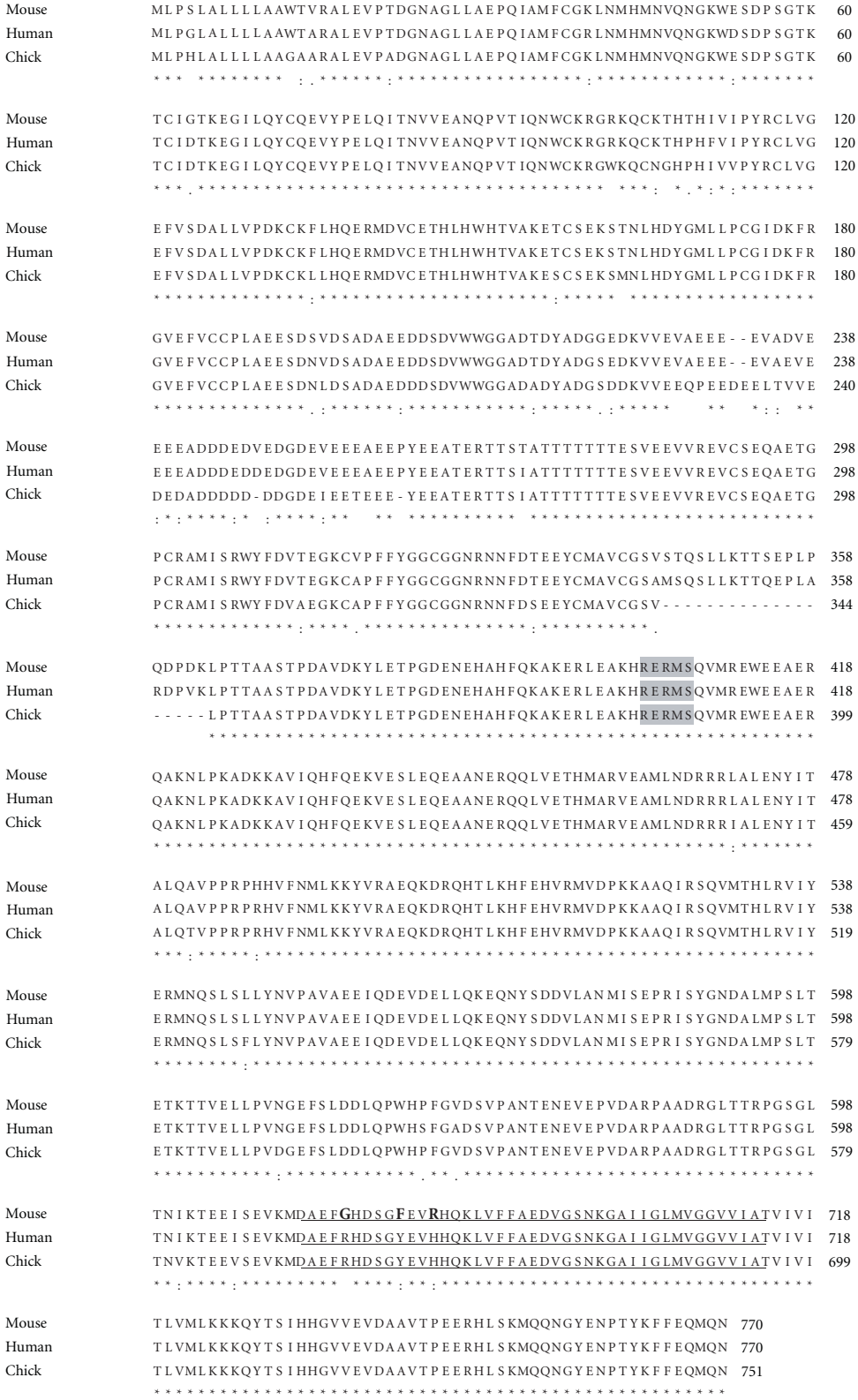

Figure 1: *Alignment of the amino acid sequences of human, mouse, and chick APP.* The numbering refers to the human APP sequence. The RERMS sequence is in gray. Amino acid sequences of Aβ domain are underlined. Residues implicated in amyloidogenesis are indicated in bold. The human (P05067), chicken (Q9DGJ7) and mouse (P12023) APP sequences were obtained from the EMBL database (CLUSTAL 2.0.12 multiple sequence alignment).

sequence (corresponding to the Aβ, transmembrane and intracytoplasmic domains). In contrast to mouse and rat, chick and human sequence are identical. That makes the chick a useful natural model in which to study regulation of APP gene expression and the amyloidogenic characteristics of Aβ.

In contrast to many transgenic models wild type heterozygous chicks do not carry a burden of genetic background which might be a possible confounding factor with regard to crucial aspects of AD [40, 41]. Although sophisticated and precise molecular genetic tools are applied to transgenic animals in order to study the pathophysiology of AD [11, 42, 43], animal performance in the behavioural tests used to assess learning and memory is often affected by variables apparently unrelated to memory function, as shown in an extensive study analysing data from 3003 mice tested in the Morris water maze [44]. This meta-analysis showed that genetic background and environmental differences between laboratories in rearing and handling procedures alone can produce sufficient variation to span the range of most, if not all, behavioural variables and can thus easily mask or fake mutational effects. In addition, disparity attributable to evolutionary divergence between humans and rodents, brings about another type of problem: the strong but incomplete homology between human and mouse APP sequences and the weaker but still considerable homology between APP and APP-like protein (APLP2), compromise accurate measurements of total APP transcript levels in humanised APP transgenic mice and make assessment of the neuropathogenic potential of human APP gene products rather difficult [42, 45, 46].

5. The Chick as an Animal Model for the Study of Memory

Our route towards research on AD led through our lab's interest, over many years, in the molecular mechanisms involved in memory storage, on which we have worked extensively with the young chick. The suitability of the chick as a model system for such studies is well documented. Chicks are precocial birds, and need actively to explore and learn about their environment from the moment they hatch. Thus, they learn very rapidly to identify their mother on the basis of visual, olfactory and auditory cues (imprinting), to distinguish edible from inedible or distasteful food, and to navigate complex routes. Training paradigms that exploit these species-specific tasks work with the grain of the animal's biology, and because such learning is a significant event in the young chick's life the experiences involved may be expected to result in readily measurable brain changes. Chicks have large and well-developed brains and soft unossified skulls, making localised cerebral injections of drugs easy without the use of implanted cannulae or anaesthesia. The virtual lack of any blood-brain barrier in these young animals also ensures rapid entry into the brain of peripherally injected agents (for review see [47]).

The training task that we employ is one trial passive avoidance, in which chicks learn to avoid pecking at a small bead coated in the bitter, distasteful, but nontoxic methylanthranilate (MeA). The task has the merits of being rapid and sharply timed (chicks peck a bead within 10 seconds) and as many as 60 chicks can be trained in a single session. Table 1 compares this chick task with those commonly used in rodents. In the standard version of the task in our lab, day-old chicks are held in pairs in small pens, pretrained by being offered a small dry white bead, and those that peck trained with a larger (4 mm dia) chrome or coloured bead coated with MeA. Chicks that peck such a bead show a disgust reaction (backing away, shaking their heads and wiping their bills) and will avoid a similar but dry bead for at least 48 hours subsequently. However, they continue to discriminate, as shown by pecking at control beads of other colours. Chicks trained on the bitter bead are matched with controls which have pecked at a water-coated or dry bead, and which peck the dry bead on test. Generally some 80% of chicks in any hatch group can be successfully trained and tested on this protocol. Each chick is usually trained and tested only once. Because the pecking response requires a positive, accurate act by the bird, it also controls for effects on attentional, visual, and motor processes [47, 48].

The training task has two variants: strong, and weak. In the strong version, the aversive substance used to coat the beads is 100% MeA and it produces high and persisting levels of avoidance. However, if the MeA is diluted to 10%, the high level of avoidance for the training bead persists only up 8 hours; long term memories are not formed. In its strong form, the task can be used to identify the molecular cascade involved in memory formation and the interventions that impair consolidation; in its weak form the task can be used to explore potential memory enhancing agents.

These features make the young chick a highly suitable model for the analysis of the biochemical (and in our hands morphological and physiological) correlates of memory consolidation. Table 1 compares the passive avoidance task in the chick with commonly used tasks in the mouse.

6. The Biochemical Cascade of Memory Consolidation in the Chick

Over the past decades a combination of correlative and interventive experimental strategies has enabled us to identify a biochemical cascade that is associated with memory consolidation in the minutes to hours following training. These have been fully reviewed elsewhere [47] so only a brief summary will be given here. In the minutes following training on this task, there is upregulation of N-methyl-D-aspartate receptor activity, phosphorylation of the presynaptic membrane protein B50, and genomic activation of the immediate early genes c-fos and c-jun. During the next hours after training, increased incorporation of fucose into brain glycoproteins occurs. During this time, memory for the passive avoidance task can be impaired by inhibitors of protein and glycoprotein synthesis injected around the time of training. Two regions of the chick brain are involved specifically in the biochemical responses to the learning experience. These are the intermediate medial mesopallium

Table 1: Comparison of training tasks in chicks and mice.

	Chicks	Mice
Training paradigm	Passive avoidance	Passive avoidance Fear conditioning Water maze (multiple trials)
Timing	10 secends training time	Passive avoidance - Brief Fear conditioning - Brief Water maze - multiple trials
Suitable for biochemical analysis	Yes	Passive avoidance - yes Fear conditioning - yes Water maze - unsuitable
Sex	Natural distribution of males and females in the hatch. (Sex determined post hoc by inspection of gonads)	Generally males only
Group size	Large (20 chicks/group)	Small
Intracranial injections	Anaesthesia not required	Anaesthesia required
BBB	Not fully developed	Fully developed
Genome	Sequenced in 2004	Sequenced in 2002
Transgenic model	No	Yes, many (for review see Crews et al., 2010; [11])

(IMMP), an association "cortical" area, and the medial striatum (MS), a basal ganglia homologue. The chick brain is strongly lateralized and many, but not all, of the molecular events we observe are confined to the left IMMP.

All these events depend on de novo protein synthesis and insertion of a variety of proteins, especially glycoproteins, into pre- and postsynaptic membranes. Cell adhesion or cell recognition molecules constitute a major group amongst these glycoproteins. They are expressed both pre- and post-synaptically and involved in the process that allows information about synaptic activity to be simultaneously communicated to both side of the synapse. Our early work identified two such adhesion molecule, L1 and NCAM, which are recruited into this cascade of cellular events at different periods posttraining. Injection of inhibitors of protein and glycoprotein synthesis (anisomycin and 2-deoxy-galactose resp.) at times corresponds to these periods of recruitment (Figure 2) result in amnesia for the task [47].

This and related data on the effects of application of protein synthesis inhibitors on memory retention led us to propose that there were two waves of protein synthesis occurring following a learning experience, the first within an hour of the experience and involving the synthesis of proteins expressed by immediate early genes, and the second, some 4–6 hours later, involving structural proteins such as the adhesion molecules. Both are necessary for consolidation of long-term memory.

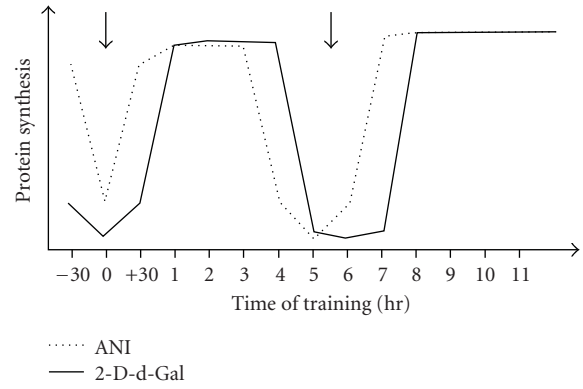

Figure 2: Two time-windows when protein synthesis is sensitive to inhibitors of protein synthesis, such as anisomycin (ANI) and glycoprotein synthesis, such as 2-d-Galactose (2-d-Gal).

7. APP and Memory Consolidation in the Chick

APP is an important member of the family of cell adhesion molecules, and having identified a role for NCAM and L1 [51–53] in the consolidation cascade, it seemed logical to explore the role of APP itself. Chick APP cross-reacts with the mouse monoclonal antibody raised against human APP. Therefore, we tested the effect of anti-APP antibody on memory. The residence time for the anti-APP corresponds to the relatively rapid turnover time for membrane-bound APP. When injected pre-training, anti-APP did not interfere with the chicks pecking and learning the avoidance task; however, it did result in amnesia in birds tested 30 minutes later. Amnesia persisted for at least the subsequent 24 hours and was not apparent if the antibody was injected just posttraining or 5.5 hours after training [17, 49].

This finding indicated that APP might be required at an early phase and not continually during memory consolidation. Given that blocking APP function by use of specific antibodies outside of a specific time window

Table 2: Effect of anti-APP and APP antisense on memory retention.

	Time of injection	Memory retention (% Avoidance)	Time of injection	Memory retention (% Avoidance)
Control (Saline, non-immune sera)	30 minutes pre-training	78–95	5.5 hours Posttraining	78–95
Anti APP	30 minutes pre training	28–35**	5.5 hours Posttraining	78–95
Control (SC)	6 hours pre-training	78–95	30 minutes pre-training	78–95
AS	6 hours pre-training	32–37*	30 minutes pre-training	7 8–95

$N = 18–25$; $^{*}P < .05$; $^{**}P < .01$.
Anti APP: monoclonal human antibody mAb22C11 [17]; AS: 16-mer end-protected phosphodiester oligodeoxynucleotide, 5′ CXC GAG GAC TGA XCC A 3′, designed to correspond to the transcription start sites −146 and AUG1786 of the βAPP mRNA, immediately upstream of a ribozyme binding site [17]; SC: Scrambled AS sequence [17]; For further details see [18, 49, 50].

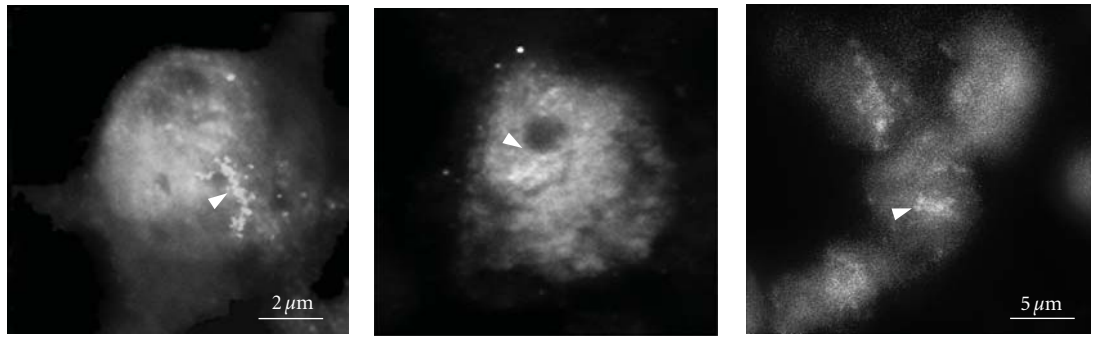

(a) (b) (c)

Figure 3: *RER binding detected on chick, human and mouse neuronal cells*. Specific binding of the biotinylated RER (arrows) to chick (a), human (b) and mouse neuronal (c) cell. Location of the chick neuronal cells is in the IMMP area; Human and mouse neuronal cells are located in the CA1 are in hippocampus.

was without effect, we compromised APP gene expression using antisense oligodeoxynucleotides (AS) designed to correspond to the −146 and to AUG1786 transcription start site of APP [17]. The antisense oligodeoxynucleotides (AS ODNs) were injected intracerebrally at 6 hours or 30 minutes pre-training and chicks were tested at different times posttraining. Injection at 6 hours pre-training was aimed to suppress APP synthesis during the first wave of protein synthesis while the injection made at 30 minutes pre-training was aimed at the second wave (Table 2). Thus, in both groups the AS was present for 6 hours before training. Controls were treated with scrambled (SC) ODNs or saline and trained and tested as the AS ODNs treated groups.

The results showed that APP-antisense both decreased APP gene expression and affected memory formation. The time-window of onset of amnesia relative to time of injection of ODNs and to time of training confirmed our previous finding that APP exerts its function during an early phase of memory formation and appears to be a necessary factor in the biochemical cascade involved in the transition between short- and long-term memory. Our findings on the importance of APP in learning were supported by reports [19] that APP gene expression in the young chick is related to the strength of memory retention for an imprinting task.

8. APP-Related Peptides as a Tool to Study Memory

Studies conducted on the physiological activity of APP [54–58] resulted in the identification of a small stretch of amino acids containing the RERMS sequence C-terminal to the KPI insertion site of sAPP-695 as the active domain responsible for growth promotion and neurite extension, neuronal survival, and for sAPP's ability to interfere with the deleterious effects of Aβ on neurons. A synthetic peptide homologous to the RERMS sequence, APP 328–332, was identified as the shortest active peptide to exhibit trophic activity through cell-surface binding and induction of inositol polyphosphate accumulation. Such observations suggested that the RERMS peptide might substitute for sAPP during memory formation and thereby reverse or protect against the blockade resulting from antibody or antisense.

We first assessed the effects of RERMS on memory in chicks rendered amnesic by APP-antisense and APP-antibody treatment [17, 49]. In the series of experiments which followed, we studied the time window in which injection of RERMS might affect amnesia and showed that if injected either before or just after training on the task, the pepide protected against the memory loss. As a control for the behavioural effect of RERMS, we used the reversed

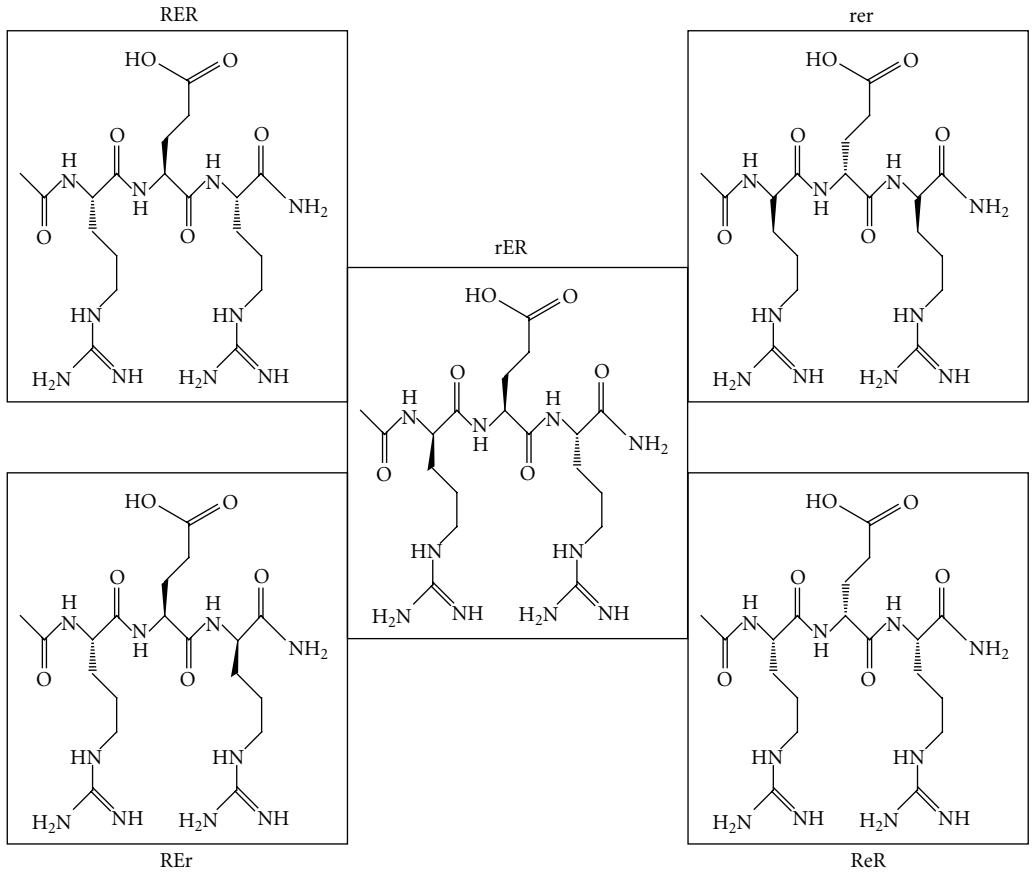

Figure 4: Structure of D/L tripeptides included in the study.

peptide sequence SMRER, but to our surprise SMRER was as effective in relieving the memory block as RERMS. However, a different control peptide, RSAER, was without effect. Analysis of these experiments led to two principal observations: first, that the APP-derived peptide might exert its action by compensating for the low presence of APP. According to the proposed amyloid hypothesis, the faulty processing of APP and accumulation of the amyloid fragments might be one of the factors leading to neurotoxicity. Therefore, we tested whether the RERMS peptide might also have a potential protective effect against the memory deficit induced by Aβ. Amyloid-beta, injected into the IMMP bilaterally at a dose of 2 μg/hemisphere, 30 minutes prior to training, resulted in amnesia for the task in chicks tested 24 hours subsequently. However, administration of 1 μg/hemisphere of RERMS 10 minutes after Aβ injection prevented the memory deficit caused by Aβ. Conversely, if the injection is delayed to 5.5 hours posttraining, there is no subsequent amnesia.

The second observation came from analysis of the amino acid sequence of the peptides used in this study [17, 49]. Both the forward and reverse sequences contain the tripeptide palindrome RER. The next step was therefore to investigate the ability of RER to relieve memory block under the same conditions used for testing RERMS. The RER tripeptide, when injected around the time of training, showed the same potential as the RERMS pentapeptide and rescued memory in animals rendered amnesic by pretreatment with Aβ. We concluded that the RER sequence acts as a core domain of the growth promoting region of APP in the chick because it appears able to substitute for sAPP. The protection against the amnestic effects of Aβ may also result from RER's ability to initiate receptor-mediated processes. This interpretation is strengthened by the evidence that RER binds to two neuronal cell membrane proteins, of ~66 and 110 kDa, respectively. In experiments aimed at identifying specific neuronal binding partners, using a combination of biotinylated tripeptide and cell-specific antibodies, bound RER was localised in chick and human brain sections (Figure 3), suggesting that it might also be active in humans, and could play an important role in the memory formation process which is deficient in the early stages of AD. Moreover, the distribution of biotinylated RER binding suggested membrane binding. In the chick, binding is displaced by longer peptides derived from APP's external domain, but not by Aβ, suggesting that RER competes with sAPP for a putative receptor [17, 49].

To overcome the problem of the short half-life of RER we protected it by N-acylation, and showed that Ac-RER is as effective as RER in protecting against memory loss. More importantly, Ac-RER crosses the partially formed blood brain barrier of the one-day old chicks, enabling the peptide to be injected intraperitoneally [17]. The immediate implication of these findings is that it is possible to introduce

Table 3: Summary of peptides and their effects on memory reported in this study.

Peptide	Injection route		Effective dose		Rescue of amnesia induced with:			Enhances weak training	Crossing BBB	$t1/2$ hour
	Ic	ip	Ic μg/brain	Ip mg/kg bw	Anti APP	AS	Aβ			Up to
RERMS	Y	Y	4	20–25	Y	Y	Y	Y	Y	2
SMRER	Y	Y	4	20–25	Y	Y	Y	Y	Y	2
RSAER	N	N	4	/	N	N	N	N	Y	/
RER	Y	Y	4	20–25	Y	Y	Y	Y	Y	/
Ac-RER	Y	Y	16	20–25	Y	/	Y	Y	Y	6
Ac-RRE	N	N	16	/	/	/	N	N	/	/
Ac-rER	Y	Y	16	20–25	Y	/	Y	Y	Y	>12
Ac-REr	N	N	16	/	N	/	N	N	/	/
Ac-ReR	N	N	16	/	N	/	N	N	/	/
Ac-rer	Y	Y	16	20–25	N	/	N	N	/	/

Y: yes, there is an effect on memory; N: No, there is no effect on memory; Anti-APP: monoclonal antibody, clone mAb22C11 [17]; AS: 16-mer end-protected phosphodiester oligodeoxynucleotide, 5′ CXC GAG GAC TGA XCC A 3′, designed to correspond to the transcription start sites −146 and AUG1786 of the βAPP mRNA, immediately upstream of a ribozyme binding site [17]; Aβ: amyloid-beta. For further details see [18, 49, 50].

a behaviourally effective form of RER peripherally by N-terminal acylation, hence protecting the peptide against rapid degradation.

If the RER sequence acts as a substitute for sAPP than the question to ask is whether it might act as a cognitive enhancer in the weak version of the passive avoidance task discussed above. The weak training protocol is an ideal paradigm to test this hypothesis as memory for the task is not retained beyond an early phase, presumably because the mild aversant does not provide a sufficient signal for the release of sAPP. Under these conditions, tripeptide injected peripherally was as effective as memory enhancer as when injected intracerebrally, meaning that even in the weak training task, in the presence of the tripeptide peptide, memory persists for at least 24 hours.

All our results point to the short APP-related peptides used in our experiments as both powerful tools in studying the structure and function of APP and as of potential therapeutic interest in AD. We have therefore begun to explore the effectiveness of a number of compounds structurally related to RER. Of particular interest have been the optically isomeric D- or diasteromeric (D/L) forms of the peptide, which are more resistant to proteolysis than their L-equivalents. The diasteromeric forms have begun lately to attract increasing interest as potential immunogens, diagnostic and therapeutic agents [59].

Our results using different D/L forms (shown in Figure 4) demonstrated that substitution of C-terminal L-arginine with the D-isomer essentially abolished the memory retention-enhancing effect of the peptide. This finding pointed to the crucial role of C-terminal L-arginine, in its normal L-conformation, in binding to the peptide's putative receptors.

Moreover, these experiments clearly show that Ac-rER is a longer lasting and more stable form of the putative memory enhancer than the RER. In addition, it is taken up into the brain from peripheral administration, and is active behaviourally for at least 12 hours following such administration. The fact that there was no difference in the magnitude of the effect of the L- and L/D tripeptide on behaviour suggested that they engage the same biochemical processes [50]. These results are summarised in Table 3.

What is now required is to determine the identity of the RER binding proteins, the specific second messenger systems activated and the genes controlled by RER. Our currently unpublished experiments go some way towards answering these questions, which may be central to understanding the peptide's effects both in memory enhancement and, potentially, in neuroprotection.

9. Concluding Remarks

Although it remains important to demonstrate that the peptide or its related structures is effective in other learning tasks and in mammals, we propose that the chick is a useful animal model in which to study AD, and that Ac-rER is a molecule which might form the basis for a potential therapeutic agent in the early stages of AD. Even though some specific details of protein-protein interactions can vary between birds and human, the degree of functional conservation seems to be of particular relevance for the AD field. This animal model, like many other natural model-systems, often appears to suffer from publication bias towards transgenic animal models, which may account for substantial under-representation of avian model system in the experimental literature related to neurodegenerative diseases such as AD.

Acknowledgment

The authors acknowledge K. Evans, S.W. Walters, and C.L. Lancashire for technical support, Dr. J. Clark the Babraham Institute, Cambridge, UK for discussions. The authors are named as inventors of the tripeptides described in this paper in UK Patent no. GB2391548. (The Open University). This work was partially supported by EUSA Pharma.

References

[1] R. D. Porsolt, "Animal models of depression: utility for transgenic research," *Reviews in the Neurosciences*, vol. 11, no. 1, pp. 53–58, 2000.

[2] A. V. Kalueff, M. Wheaton, and D. L. Murphy, "What's wrong with my mouse model? Advances and strategies in animal modeling of anxiety and depression," *Behavioural Brain Research*, vol. 179, no. 1, pp. 1–18, 2007.

[3] T. Fujii and H. Kunugi, "p75NTR as a therapeutic target for neuropsychiatric diseases," *Current Molecular Pharmacology*, vol. 2, no. 1, pp. 70–76, 2009.

[4] M. P. Moisan and A. Ramos, "Rat genomics applied to psychiatric research," *Methods in Molecular Biology*, vol. 597, pp. 357–388, 2010.

[5] P. C. Hart, C. L. Bergner, A. N. Smolinsky et al., "Experimental models of anxiety for drug discovery and brain research," *Methods in Molecular Biology*, vol. 602, pp. 299–321, 2010.

[6] S. E. Arnold, B. T. Hyman, J. Flory, A. R. Damasio, and G. W. Van Hoesen, "The topographical and neuroanatomical distribution of neurofibrillary tangles and neuritic plaques in the cerebral cortex of patients with Alzheimer's disease," *Cerebral Cortex*, vol. 1, no. 1, pp. 103–116, 1991.

[7] J. S. Snowden, D. Bathgate, A. Varma, A. Blackshaw, Z. C. Gibbons, and D. Neary, "Distinct behavioural profiles in frontotemporal dementia and semantic dementia," *Journal of Neurology Neurosurgery and Psychiatry*, vol. 70, no. 3, pp. 323–332, 2001.

[8] N. D. Weder, R. Aziz, K. Wilkins, and R. R. Tampi, "Frontotemporal dementias: a review," *Annals of General Psychiatry*, vol. 6, article no. 15, 2007.

[9] D. J. Selkoe, "Alzheimer's disease is a synaptic failure," *Science*, vol. 298, no. 5594, pp. 789–791, 2002.

[10] J. Götz and L. M. Ittner, "Animal models of Alzheimer's disease and frontotemporal dementia," *Nature Reviews Neuroscience*, vol. 9, no. 7, pp. 532–544, 2008.

[11] L. Crews, E. Rockenstein, and E. Masliah, "APP transgenic modeling of Alzheimer's disease: mechanisms of neurodegeneration and aberrant neurogenesis," *Brain Structure and Function*, vol. 214, no. 2-3, pp. 111–126, 2010.

[12] H. Bart van der Worp, D. W. Howells, E. S. Sena et al., "Can animal models of disease reliably inform human studies?" *PLoS Medicine*, vol. 7, no. 3, Article ID e1000245, 8 pages, 2010.

[13] D. J. Selkoe, "Normal and abnormal biology of the β-amyloid precursor protein," *Annual Review of Neuroscience*, vol. 17, pp. 489–517, 1994.

[14] P. R. Turner, K. O'Connor, W. P. Tate, and W. C. Abraham, "Roles of amyloid precursor protein and its fragments in regulating neural activity, plasticity and memory," *Progress in Neurobiology*, vol. 70, no. 1, pp. 1–32, 2003.

[15] C. Reinhard, S. S. Hébert, and B. De Strooper, "The amyloid-β precursor protein: integrating structure with biological function," *The EMBO Journal*, vol. 24, no. 23, pp. 3996–4006, 2005.

[16] L. Mucke, "Neuroscience: Alzheimer's disease," *Nature*, vol. 461, no. 7266, pp. 895–897, 2009.

[17] R. Mileusnic, C. L. Lancashire, A. N. B. Johnston, and S. P. R. Rose, "APP is required during an early phase of memory formation," *European Journal of Neuroscience*, vol. 12, no. 12, pp. 4487–4495, 2000.

[18] R. Mileusnic, C. L. Lancashire, and S. R. R. Rose, "The peptide sequence Arg-Glu-Arg, present in the amyloid precursor protein, protects against memory loss caused by Aβ and acts as a cognitive enhancer," *European Journal of Neuroscience*, vol. 19, no. 7, pp. 1933–1938, 2004.

[19] R. O. Solomonia, K. Morgan, A. Kotorashvili, B. J. McCabe, A. P. Jackson, and G. Horn, "Analysis of differential gene expression supports a role for amyloid precursor protein and a protein kinase C substrate (MARCKS) in long-term memory," *European Journal of Neuroscience*, vol. 17, no. 5, pp. 1073–1081, 2003.

[20] E. Doyle, M. T. Bruce, K. C. Breen, D. C. Smith, B. Anderton, and C. M. Regan, "Intraventricular infusions of antibodies to amyloid β-protein precursor impair the acquisition of a passive avoidance response in the rat," *Neuroscience Letters*, vol. 115, no. 1, pp. 97–102, 1990.

[21] G. Huber, Y. Bailly, J. R. Martin, J. Mariani, and B. Brugg, "Synaptic β-amyloid precursor proteins increase with learning capacity in rats," *Neuroscience*, vol. 80, no. 2, pp. 313–320, 1997.

[22] U. Müller, N. Cristina, Z.-W. Li et al., "Behavioral and anatomical deficits in mice homozygous for a modified β-amyloid precursor protein gene," *Cell*, vol. 79, no. 5, pp. 755–765, 1994.

[23] H. Zheng, M. Jiang, M. E. Trumbauer et al., "β-amyloid precursor protein-deficient mice show reactive gliosis and decreased locomotor activity," *Cell*, vol. 81, no. 4, pp. 525–531, 1995.

[24] J. F. Flood, J. E. Morley, and E. Roberts, "Amnestic effects in mice of four synthetic peptides homologous to amyloid β protein from patients with Alzheimer disease," *Proceedings of the National Academy of Sciences of the United States of America*, vol. 88, no. 8, pp. 3363–3366, 1991.

[25] E. Abe, F. Casamenti, L. Giovannelli, C. Scali, and G. Pepeu, "Administration of amyloid β-peptides into the medial septum of rats decreases acetylcholine release from hippocampus in vivo," *Brain Research*, vol. 636, no. 1, pp. 162–164, 1994.

[26] T. Maurice, B. P. Lockhart, and A. Privat, "Amnesia induced in mice by centrally administered β-amyloid peptides involves cholinergic dysfunction," *Brain Research*, vol. 706, no. 2, pp. 181–193, 1996.

[27] J. Cleary, J. M. Hittner, M. Semotuk, P. Mantyh, and E. O'Hare, "Beta-amyloid(1–40) effects on behavioral and memory," *Brain Research*, vol. 682, no. 1-2, pp. 69–74, 1995.

[28] H. Meziane, J.-C. Dodart, C. Mathis et al., "Memory-enhancing effects of secreted forms of the β-amyloid precursor protein in normal and amnestic mice," *Proceedings of the National Academy of Sciences of the United States of America*, vol. 95, no. 21, pp. 12683–12688, 1998.

[29] A. Bour, S. Little, J.-C. Dodart, C. Kelche, and C. Mathis, "A secreted form of the β-amyloid precursor protein (sAPP 695) improves spatial recognition memory in OF1 mice," *Neurobiology of Learning and Memory*, vol. 81, no. 1, pp. 27–38, 2004.

[30] S. Ring, S. W. Weyer, S. B. Kilian et al., "The secreted β-amyloid precursor protein ectodomain APPsα is sufficient to rescue the anatomical, behavioral, and electrophysiological abnormalities of APP-deficient mice," *Journal of Neuroscience*, vol. 27, no. 29, pp. 7817–7826, 2007.

[31] E. J. Coulson, K. Paliga, K. Beyreuther, and C. L. Masters, "What the evolution of the amyloid protein precursor supergene family tells us about its function," *Neurochemistry International*, vol. 36, no. 3, pp. 175–184, 2000.

[32] J. A. Carrodeguas, A. Rodolosse, M. V. Garza et al., "The chick embryo appears as a natural model for research in beta-amyloid precursor protein processing," *Neuroscience*, vol. 134, no. 4, pp. 1285–1300, 2005.

[33] M. Sarasa and P. Pesini, "Natural non-trasgenic animal models for research in Alzheimer's disease," *Current Alzheimer Research*, vol. 6, no. 2, pp. 171–178, 2009.

[34] B. D. Shivers, C. Hilbich, G. Multhaup, M. Salbaum, K. Beyreuther, and P. H. Seeburg, "Alzheimer's disease amyloidogenic glycoprotein: expression pattern in rat brain suggests a role in cell contact," *The EMBO Journal*, vol. 7, no. 5, pp. 1365–1370, 1988.

[35] T. Yamada, H. Sasaki, H. Furuya, T. Miyata, I. Goto, and Y. Sakaki, "Complementary DNA for the mouse homolog of the human amyloid beta protein precursor," *Biochemical and Biophysical Research Communications*, vol. 149, no. 2, pp. 665–671, 1987.

[36] T. Yamada, H. Sasaki, K. Dohura, I. Goto, and Y. Sakaki, "Structure and expression of the alternatively-spliced forms of mRNA for the mouse homolog of Alzheimer's disease amyloid beta protein precursor," *Biochemical and Biophysical Research Communications*, vol. 158, no. 3, pp. 906–912, 1989.

[37] J. Kang and B. Muller-Hill, "The sequence of the two extra exons in rat preA4," *Nucleic Acids Research*, vol. 17, no. 5, p. 2130, 1989.

[38] D. A. Kirschner, H. Inouye, L. K. Duffy, A. Sinclair, M. Lind, and D. J. Selkoe, "Synthetic peptide homologous to beta protein from Alzheimer disease forms amyloid-like fibrils in vitro," *Proceedings of the National Academy of Sciences of the United States of America*, vol. 84, no. 19, pp. 6953–6957, 1987.

[39] J. M. Chernak, "Structural features of the 5′ upstream regulatory region of the gene encoding rat amyloid precursor protein," *Gene*, vol. 133, no. 2, pp. 255–260, 1993.

[40] C. J. Maynard, R. Cappai, I. Volitakis et al., "Gender and genetic background effects on brain metal levels in APP transgenic and normal mice: implications for Alzheimer β-amyloid pathology," *Journal of Inorganic Biochemistry*, vol. 100, no. 5-6, pp. 952–962, 2006.

[41] D. P. Wolfer, U. Müller, M. Stagliar, and H.-P. Lipp, "Assessing the effects of the 129/Sv genetic background on swimming navigation learning in transgenic mutants: a study using mice with a modified β-amyloid precursor protein gene," *Brain Research*, vol. 771, no. 1, pp. 1–13, 1997.

[42] S. Heber, J. Herms, V. Gajic et al., "Mice with combined gene knock-outs reveal essential and partially redundant functions of amyloid precursor protein family members," *Journal of Neuroscience*, vol. 20, no. 21, pp. 7951–7963, 2000.

[43] T. A. Kokjohn and A. E. Roher, "Amyloid precursor protein transgenic mouse models and Alzheimer's disease: understanding the paradigms, limitations, and contributions," *Alzheimer's and Dementia*, vol. 5, no. 4, pp. 340–347, 2009.

[44] D. P. Wolfer and H.-P. Lipp, "Dissecting the behaviour of transgenic mice: is it the mutation, the genetic background, or the environment?" *Experimental Physiology*, vol. 85, no. 6, pp. 627–634, 2000.

[45] P. Du, K. M. Wood, M. H. Rosner, D. Cunningham, B. Tate, and K. F. Geoghegan, "Dominance of amyloid precursor protein sequence over host cell secretases in determining β-amyloid profiles studies of interspecies variation and drug action by internally standardized immunoprecipitation/mass spectrometry," *The Journal of Pharmacology and Experimental Therapeutics*, vol. 320, no. 3, pp. 1144–1152, 2007.

[46] E. M. Rockenstein, L. McConlogue, H. Tan, M. Power, E. Masliah, and L. Mucke, "Levels and alternative splicing of amyloid β protein precursor (APP) transcripts in brains of APP transgenic mice and humans with Alzheimer's disease," *The Journal of Biological Chemistry*, vol. 270, no. 47, pp. 28257–28267, 1995.

[47] S. P. R. Rose, "God's organism? The chick as a model system for memory studies," *Learning & Memory*, vol. 7, no. 1, pp. 1–17, 2000.

[48] M. E. Gibbs, A. N. B. Johnston, R. Mileusnic, and S. F. Crowe, "A comparison of protocols for passive and discriminative avoidance learning tasks in the domestic chick," *Brain Research Bulletin*, vol. 76, no. 3, pp. 198–207, 2008.

[49] R. Mileusnic, C. L. Lancashire, and S. P. R. Rose, "Amyloid precursor protein: from synaptic plasticity to Alzheimer's disease," *Annals of the New York Academy of Sciences*, vol. 1048, pp. 149–165, 2005.

[50] R. Mileusnic, C. Lancashire, J. Clark, and S. P. R. Rose, "Protection against Aβ-induced memory loss by tripeptide D-Arg-L-Glu-L-Arg," *Behavioural Pharmacology*, vol. 18, no. 3, pp. 231–238, 2007.

[51] A. B. Scholey, R. Mileusnic, M. Schachner, and S. P. Rose, "A role for a chicken homolog of the neural cell adhesion molecule L1 in consolidation of memory for a passive avoidance task in the chick," *Learning & Memory*, vol. 2, no. 1, pp. 17–25, 1995.

[52] R. Mileusnic, S. P. R. Rose, C. Lancashire, and S. Bullock, "Characterisation of antibodies specific for chick brain neural cell adhesion molecules which cause amnesia for a passive avoidance task," *Journal of Neurochemistry*, vol. 64, no. 6, pp. 2598–2606, 1995.

[53] R. Mileusnic, C. Lancashire, and S. P. R. Rose, "Sequence-specific impairment of memory formation by NCAM antisense oligonucleotides," *Learning & Memory*, vol. 6, no. 2, pp. 120–127, 1999.

[54] I. Ohsawa, C. Takamura, and S. Kohsaka, "The amino-terminal region of amyloid precursor protein is responsible for neurite outgrowth in rat neocortical explant culture," *Biochemical and Biophysical Research Communications*, vol. 236, no. 1, pp. 59–65, 1997.

[55] H. L. Li, J.-M. Roch, M. Sundsmo et al., "Defective neurite extension is caused by a mutation in amyloid β/A4 (Aβ) protein precursor found in familial Alzheimer's disease," *Journal of Neurobiology*, vol. 32, no. 5, pp. 469–480, 1997.

[56] L.-W. Jin, H. Ninomiya, J.-M. Roch et al., "Peptides containing the RERMS sequence of amyloid β/A4 protein precursor bind cell surface and promote neurite extension," *Journal of Neuroscience*, vol. 14, no. 9, pp. 5461–5470, 1994.

[57] K. Yamamoto, T. Miyoshi, T. Yae et al., "The survival of rat cerebral cortical neurons in the presence of trophic APP peptides," *Journal of Neurobiology*, vol. 25, no. 5, pp. 585–594, 1994.

[58] H. Ninomiya, J.-M. Roch, M. P. Sundsmo, D. A. C. Otero, and T. Saitoh, "Amino acid sequence RERMS represents the active domain of amyloid β/A4 protein precursor that promotes fibroblast growth," *Journal of Cell Biology*, vol. 121, no. 4, pp. 879–886, 1993.

[59] N. Fujii, "D-amino acids in living higher organisms," *Origins of Life and Evolution of the Biosphere*, vol. 32, no. 2, pp. 103–127, 2002.

SAGE-Hindawi Access to Research
International Journal of Alzheimer's Disease
Volume 2010, Article ID 749061, 8 pages
doi:10.4061/2010/749061

Research Article

Behavioral Impact of the Regulation of the Brain 2-Oxoglutarate Dehydrogenase Complex by Synthetic Phosphonate Analog of 2-Oxoglutarate: Implications into the Role of the Complex in Neurodegenerative Diseases

L. Trofimova,[1] M. Lovat,[2] A. Groznaya,[2] E. Efimova,[2] T. Dunaeva,[2] M. Maslova,[2] A. Graf,[2] and V. Bunik[3]

[1] *Departments of Biophysics, Biology Faculty, Lomonosov Moscow State University, Moscow 119992, Russia*
[2] *Departments of Physiology, Biology Faculty, Lomonosov Moscow State University, Moscow 119992, Russia*
[3] *Belozersky Institute of Physico-Chemical Biology, Lomonosov Moscow State University, Moscow 119992, Russia*

Correspondence should be addressed to V. Bunik, bunik@belozersky.msu.ru

Received 15 May 2010; Revised 5 July 2010; Accepted 30 September 2010

Academic Editor: Gemma Casadesus

Decreased activity of the mitochondrial 2-oxoglutarate dehydrogenase complex (OGDHC) in brain accompanies neurodegenerative diseases. To reveal molecular mechanisms of this association, we treated rats with a specific inhibitor of OGDHC, succinyl phosphonate, or exposed them to hypoxic stress. In males treated with succinyl phosphonate and in pregnancy-sensitized females experiencing acute hypobaric hypoxia, we revealed upregulation of brain OGDHC (within 24 hours), with the activity increase presumably representing the compensatory response of brain to the OGDHC inhibition. This up-regulation of brain OGDHC was accompanied by an increase in exploratory activity and a decrease in anxiety of the experimental animals. Remarkably, the hypoxia-induced elevation of brain OGDHC and most of the associated behavioral changes were abrogated by succinyl phosphonate. The antagonistic action of hypoxia and succinyl phosphonate demonstrates potential therapeutic significance of the OGDHC regulation by the phosphonate analogs of 2-oxoglutarate.

1. Introduction

A number of inborn [1–5] and acquired [6–13] neuropathologies are associated with impaired function of the mitochondrial 2-oxoglutarate dehydrogenase multienzyme complex (OGDHC). OGDHC comprises multiple copies of the three catalytic components: the thiamine diphosphate-dependent 2-oxoglutarate dehydrogenase (E1o), the lipoyl-bearing dihydrolipoamide succinyl transferase (E2o), and the FAD-binding dihydrolipoamide dehydrogenase (E3). Coupled action of the components is required for an important regulatory step in the mitochondrial tricarboxylic acid cycle, the oxidative decarboxylation of 2-oxoglutarate (Reaction 1, where R = $-CH_2-CH_2-COOH$) generating energy in the form of NADH, and macroergic compound succinyl-CoA [14]:

$$\begin{aligned} &\mathrm{HOOC-C(=O)(R)-HS-CoA + NAD^+} \longrightarrow \\ &\mathrm{O=C(R)\sim S-CoA + CO_2 + NADH + H^+} \end{aligned} \quad (1)$$

To reveal molecular mechanisms of the association between neuropathologies and OGDHC function, we introduced specific inhibitors of OGDHC [15], which have been successfully applied in recent years for cellular [16–19], tissue [20], and animal [21] studies. Having the

phosphonate residue instead of the leaving carboxyl group of 2-oxoglutarate, these synthetic inhibitors target the starting and rate-limiting E1o component of OGDHC in a highly specific manner, imitating transition state of the E1o-catalyzed step [15, 22]. Hence, application of such phosphonate analogs of 2-oxoglutarate allows modeling the states when a decrease in the OGDHC activity is observed. In particular, such a decrease occurs in brains of patients with neurodegenerative diseases, including Alzheimer's [9, 10, 13] and Parkinson's [6, 11] diseases, Wernicke-Korsakoff syndrome [12], and progressive supranuclear palsy [8]. It is important to note that 2-oxoglutarate is the glutamate precursor in the glutamate synthesis from glucose *de novo*. In view of this, the irreversible degradation of 2-oxoglutarate by OGDHC (Reaction 1) is intimately related to the synthesis/degradation of excitatory (glutamate) and inhibitory (GABA) neurotransmitters. Indeed, the perturbed flux through the complex was shown to affect the amino acid levels [23], which may explain the developmental impact of the OGDHC regulation, shown in our previous paper [21]. In the present work, we apply the OGDHC inhibitor succinyl phosphonate to study the behavioral impact of the OGDHC function in adult rats. We show a compensatory response of cortex and striatum to the OGDHC inhibition, which correlates with behavioral changes. Increasing the inhibition or combining the inhibition with hypoxia may abrogate the response. The antagonistic action on OGDHC of the hypoxic stress and synthetic inhibitor is of potential therapeutic significance.

2. Methods

2.1. Animal Experiments. All experiments were performed with consent to Helsinki Declaration on the Guide for the Care and Use of Laboratory Animals, defining the conduct of ethical research on laboratory and other animals. Animals were kept at 21 ± 2°C on standard ration and 12/12 h light/dark cycle. Wistar rats of about 200 g (males) or 250–300 g (females) were used in the experiment. Pregnant rats were exposed to hypobaric hypoxia at day 9–10 of pregnancy by placing in a decompression (altitude) chamber of 3.3 L volume, with a vacuum pump "Mez Mohelnice" (Mohelnice, Czech Republic). Acute hypoxia was achieved by decreasing the atmospheric pressure in 1 min to 145 mm Hg, correspondent to 11500 m altitude [24]. SP was introduced to animals at 5 and 25 mg/kg by intranasal application of the water solution of the trisodium salt, with the physiologic solution substituting for SP in all reference groups. In the study of the SP influence on hypoxic effects, the compound was introduced 45–50 min before hypoxic treatment. Experimental groups comprised 6–15 animals.

2.2. Behavioral Parameters. They were estimated in the standard tests: open-field [25], elevated plus maze [26]; light-dark chamber [27], and closed plus maze [28]. Video-recording and ≪Easy Track≫ program [29] were used to follow behavior. To increase the assessment power, the data from different behavioral tests were analyzed. Different tests were also employed to exclude the animal adaptation to experimental conditions when the time dependence of the behavioral changes was studied. The parameters presented in figures correspond to those which showed statistically significant changes ($P < .05$) and the changes at the level of trends ($P < .1$). The latter provided additional support for the statistically significant changes, thus increasing the conclusion accuracy.

2.3. Tissue Samples and Enzyme Assay. After physiological monitoring has been performed, the animals were sacrificed by decapitation; cortex and striatum were excised on ice quickly, frozen in liquid nitrogen, and stored at −70°C until assay. OGDHC activity was extracted and assayed as described earlier [21]. Each sample corresponded to one animal, with the OGDHC assay in a sample repeated 3-4 times at three different protein concentrations. This was done to ensure that the activity is estimated in the interval where the dependence of the reaction rate on the catalyst concentration is linear. Preservation of the linearity at low and high protein concentrations attests to the absence of the multienzyme complex dissociation upon dilution and of the interfering activities consuming the produced NADH, respectively. The OGDHC activity is expressed as μmol/min per g of wet tissue.

2.4. Reagents. Succinyl phosphonate was synthesized and purified according to published conditions [15]. Halt Protease Inhibitor Single-Use Cocktail was from "Pierce;" CoA was from "Gerbu", Germany, and other chemicals were from "Sigma," USA.

2.4.1. Statistical Analysis. It was performed using Statistica 6.0 Software, Inc.. Values are expressed as means ± SEM. Dispersion of the ratios of the affected to control values (%) was calculated by taking into account experimental errors in determination of both values as in [30]. Statistical significance of the differences in the parameter mean values was tested by one-way analysis of variance (ANOVA) followed the Student-Newman-Keuls post hoc test. Statistical significance of the differences in the animal stratification by the resistance to hypoxia was assessed by the Fisher's exact test.

3. Results

3.1. OGDHC Inhibitor SP Induces Behavioral Changes Concomitantly with Up-Regulation of the Brain OGDHC in Male Rats. Behavior was assessed within 4 h (Figure 1) and the next day (Figure 2) after application of SP. All together, the results of the open field, elevated plus maze and closed plus maze tests pointed to increased exploratory activity and decreased anxiety, resulting from the SP application. An increase in exploratory activity was obvious from statistically significant elevations in the hole inspections (Figure 1(a)), coming out into light (Figure 1(b)), rearing and crossing the center (Figure 2). Visits and time per a round in the closed plus maze showed a trend to decrease (Figure 2), suggesting improved orientation ability and inspection efficiency [28]. Along with the mentioned above increase in the coming out

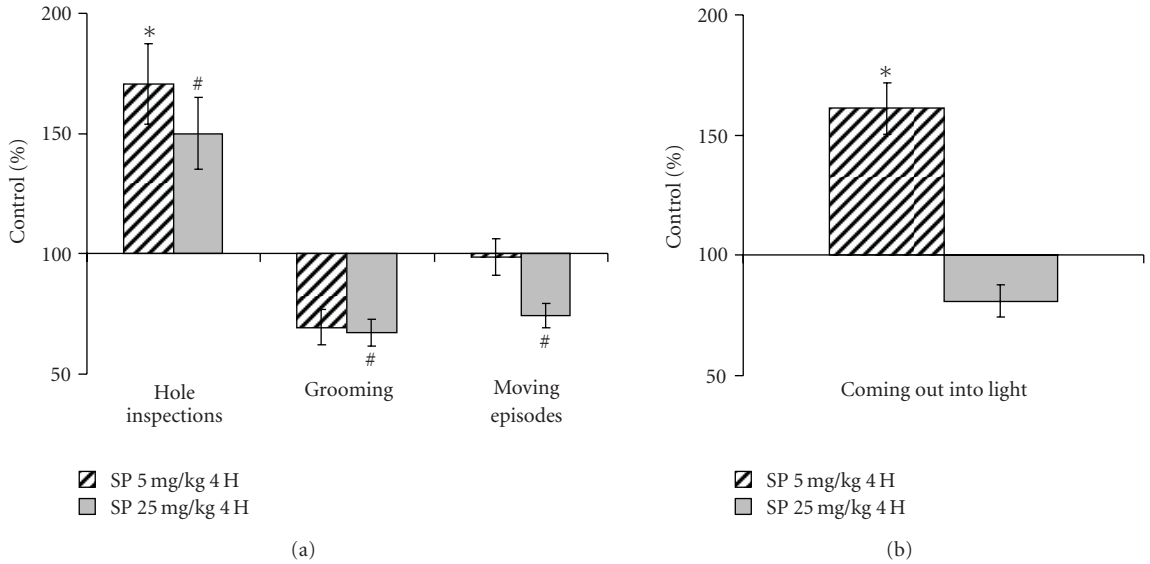

Figure 1: Changed behavioral parameters of male rats tested in the open field (a) and elevated plus maze (b) 4 hours after the treatment with 5 and 25 mg/kg SP. Statistical significance: $^{*}P < .05$; $^{\#}P \leq .1$.

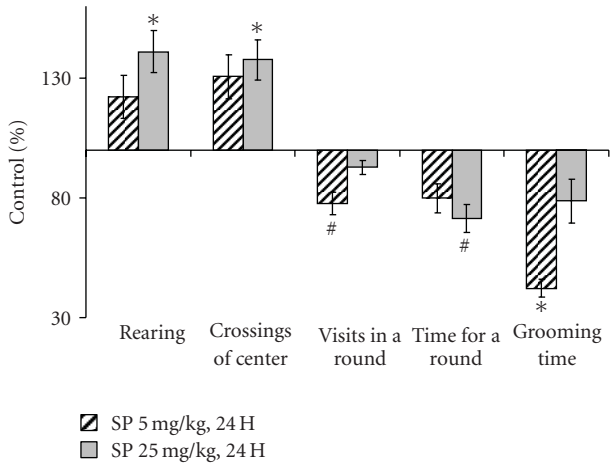

Figure 2: Changed behavioral parameters of male rats tested in the closed plus maze 24 hours after the treatment with 5 and 25 mg/kg SP. Statistical significance: $^{*}P < .05$; $^{\#}P \leq .1$.

into light (Figure 1), the shorter grooming times (Figures 1(a) and 2) pointed to decreased anxiety. It is noteworthy, that these effects were not pronounced when the SP-treated animals were imposed to stress. That is, under stressful conditions of the light-dark chamber, no statistically significant changes in the exploratory activity and anxiety were detected 24 h after the treatment (data not shown). Thus, the SP-induced increases in exploratory activity and risk behavior do not persist under potentially dangerous conditions when animal is challenged with a bright light. The difference of the animal response to the SP treatment, revealed under comfortable and stressful conditions, is indicative of a certain adequacy of the response, supporting its behavioral rather than motoric origin.

Remarkably, increasing SP to 25 mg/kg did not always increase the behavioral effect of 5 mg/kg SP, often even alleviating effects of the low dose (Figures 1 and 2). At the same time, elevating SP tended to decrease the moving episodes (Figure 1(a)) and muscle force (data not shown). It thus appears that at 25 mg/kg the systemic action of SP increases, with the muscle OGDHC inhibition obviously causing energetic impairment and muscular weakness. This may complicate interpretation of behavioral changes assessed by the animal movements. Thus, there is a specific window of the SP doze where the OGDHC inhibitor increases the exploratory activity and decreases anxiety of experimental animals.

After the behavioral parameters were assessed, the animals were sacrificed and the OGDHC activity in the extracts of cortex and striatum determined (Figure 3). The cortex activity was increased at 5 mg/kg SP, returning to the control level at 25 mg/kg SP (Figure 3(a)). SP also increased the OGDHC activity in striatum (Figure 3(b)), with the maximal effect achieved already at a low doze. Thus, increases in the OGDHC activity of cortex and striatum correlate with the increased exploratory activity and decreased anxiety of the animals, as observed under comfortable conditions in the open field, elevated plus maze and closed plus maze tests.

3.2. Protective Action of the SP Preconditioning upon Acute Hypoxia. In neurodegenerative diseases, the metabolic stress is often increased by hypoxia, in which damaging action is associated with the elevated ROS and glutamate excitotoxicity. In cellular experiments, SP was shown to protect from the glutamate-induced ROS [18] and excitotoxicity [16, 17, 21]. Owing to this, we tested if SP would show a protective action on the behavioral and biochemical changes induced by hypoxia. We used the previously established model, in which acute hypoxia was created in a decompression chamber with

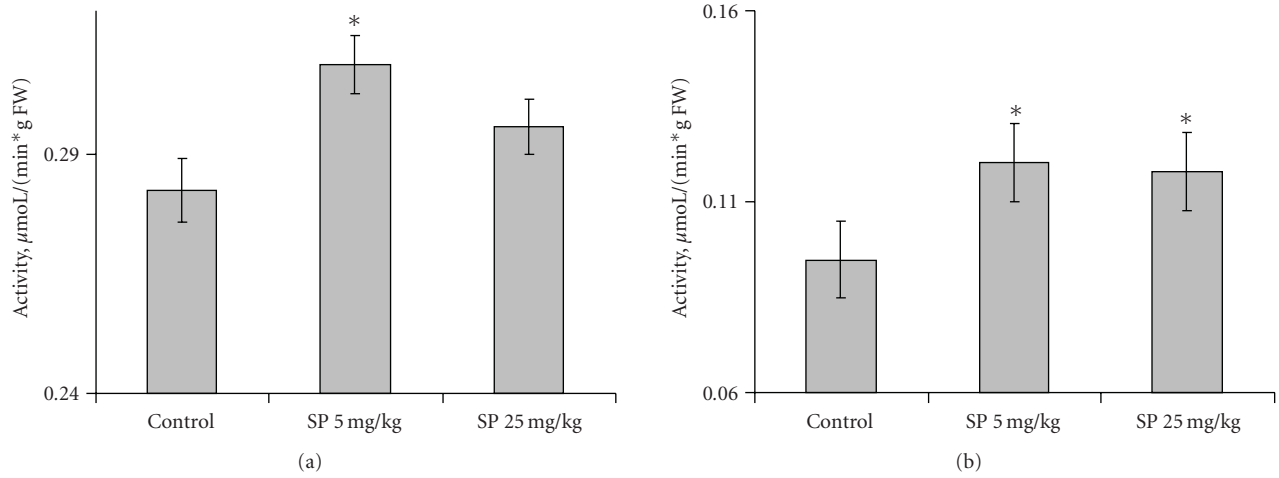

Figure 3: Influence of the SP treatment (5 and 25 mg/kg) on the cortex (a) and striatum (b) activity of OGDHC in male rats. Statistical significance: $^*P < .05$.

female rats sensitized to the insult by pregnancy [21, 24, 31]. Protective action of SP was observed already during the acute hypoxia in decompression chamber. Within an animal group, the resistance to hypoxia assessed by both physiological and behavioral parameters is known to vary, defined as low, medium, or high when the time before collapsing under hypoxic conditions is less than 5 minutes, between 5 and 10 minutes, and 10 minutes and more, respectively [24, 32]. Figure 4 shows that pre-conditioning with a low doze of SP (5 mg/kg) increased the percentage of the highly resistant animals at the expense of the medium resistant group. The SP-induced increase in the number of animals highly resistant to hypoxic conditions exhibits the protective effect of the pretreatment with the OGDHC effector upon acute hypoxia.

The behavioral effects were determined in the most reactive low resistant rats 24 hours after recovery from the hypoxia-induced collapse. Compared to the males assessed at the same time after the SP treatment (Figure 2), pregnant females showed more resistance to the action of SP *per se* (Figures 5 and 6). That is, SP alone did not significantly influence the behavioral parameters in the open field or elevated plus maze tests. Only the grooming time was significantly decreased by the low SP doze in both females (2-fold, Figure 6) and males (3-fold, Figure 2), indicative of the sex-independent anxiolytic effect of SP on animals. Remarkably, not only SP, but also hypoxia *per se* showed an anxiolytic effect. However, the latter was expressed in the rat sensitivity to light rather than grooming. That is, hypoxia caused the statistically significant increase in the looking out into light (Figure 6), with the freezing time tending to decrease (Figure 5), but did not change the grooming time (Figure 6). Thus, a certain degree of similarity in the action of both SP and hypoxia was revealed, although the common anxiolytic effect was expressed in different behavioral parameters, such as grooming or light sensitivity in the SP or hypoxia treatments, respectively. Noteworthy, the SP pre-treatment abrogated the hypoxia effects, exposing the

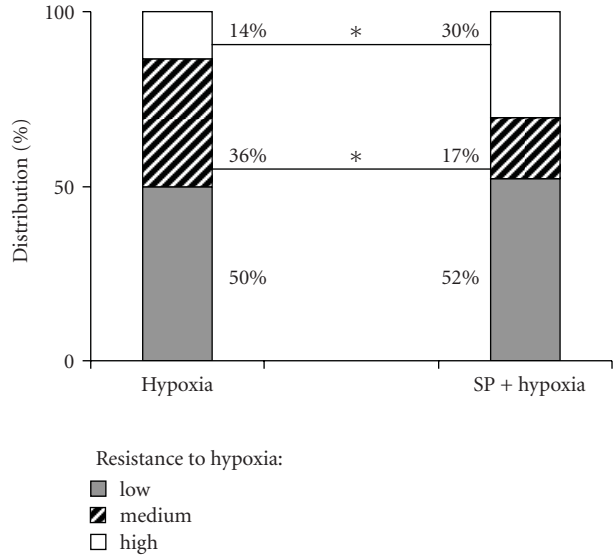

Figure 4: Influence of the pre-treatment with 5 mg/kg SP on the resistance of pregnant rats to acute hypobaric hypoxia. Statistical significance: $^*P < .05$.

protective action of SP upon hypoxia. That is, the hypoxia-induced changes in the locomotor activity and freezing time were abolished in the SP-treated animals (Figure 5), as was the statistically significant increase in the looking out into light (Figure 6). Analysis of the OGDHC activity in cortex of pregnant females provided further evidence on the SP-induced protection from the hypoxic effects. As seen from Figure 7, hypoxia increased the OGDHC activity in cortex, whereas pre-treatment with SP returned the OGDHC activity to the control level. The data of Figure 7 also support the conclusion that the OGDHC activity level correlates with behavioral parameters. That is, the hypoxia-induced behavioral effects (Figures 5 and 6) were accompanied by the up-regulation of the cortex OGDHC, with the combined

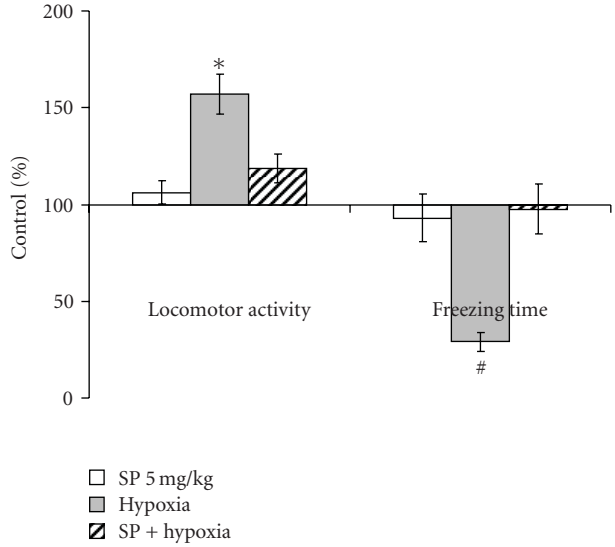

Figure 5: Influence of the pre-treatment with 5 mg/kg SP on the behavioral effects of the acute hypobaric hypoxia of pregnant rats with low resistance to hypoxia in the open field test 24 hours after hypoxia. Statistical significance: $^{*}P < .05$; $^{\#}P \leq .1$.

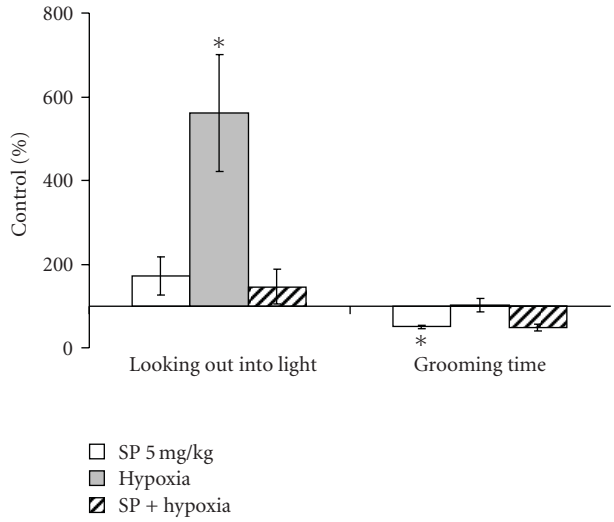

Figure 6: Influence of the pre-treatment with 5 mg/kg SP on the behavioral effects of the acute hypobaric hypoxia of pregnant rats with low resistance to hypoxia in the elevated plus maze test 24 hours after hypoxia. Statistical significance: $^{*}P < .05$.

action of hypoxia and SP returning both the OGDHC activity (Figure 7) and behavioral parameters (Figures 5 and 6) close to the norm.

Thus, the pre-treatment with a low SP doze (5 mg/kg) normalized the hypoxia-induced changes in the cortex OGDHC activity (Figure 7) and behavioral parameters (Figures 5 and 6), increasing the proportion of rats exhibiting the high resistance to hypoxia (Figure 4). This means that the SP pre-treatment protected from hypoxia on biochemical, behavioral, and physiological levels.

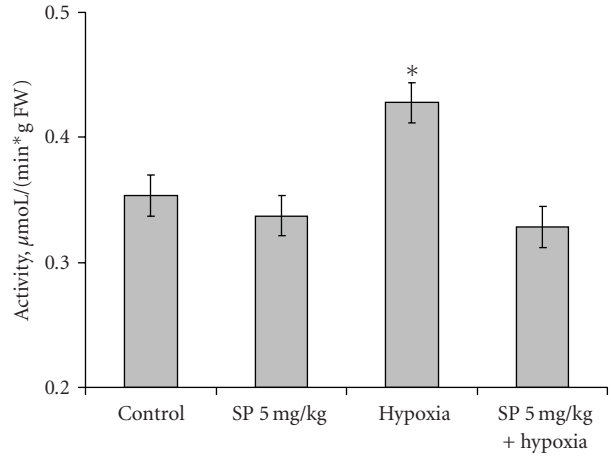

Figure 7: Influence of 5 mg/kg SP on the elevation in the cortex activity of OGDHC, induced by acute hypoxia in pregnant rats. Statistical significance: $^{*}P < .05$.

4. Discussion

In male rats treated with the OGDHC inhibitor SP, we revealed increased exploratory activity and decreased anxiety (Figures 1 and 2) concomitant with increases in the OGDHC activity in cortex and striatum (Figure 3). This result complements the known correlation found in human subjects. That is, the impaired cognition in patients with neurodegenerative diseases was observed along with the decreased OGDHC activity in their brains [7], whereas in animal model we observe increased exploratory activity with the orientation and inspection efficiency tending to improve (Figures 1 and 2), when the brain OGDHC activity is elevated (Figure 3).

It should be kept in mind that the OGDHC activity assayed in brain extracts under standard test conditions is not equal to the flux through OGDHC inside brain cells. The flux may differ dependent on the cell type, being determined, in particular, by the substrate concentrations within the cellular mitochondria, which are most probably different from those in the standard assay system *in vitro*. However, the activity assays do show that (i) application of SP induces the brain response at the level of the OGDHC regulation, and (ii) the response is to up-regulate OGDHC, obviously compensating for the enzyme inhibition by SP. The compensatory response of brain to the OGDHC inhibition by SP (Figure 3) may occur through activation of internal mechanisms of the OGDHC stimulation, for example, by protein-protein interactions, posttranslational modifications, increased synthesis. In particular, increased synthesis of the first component of OGDHC, E1o, was observed in response to the acute ethanol-induced stress [33]. Besides, in addition to its action as the reversible OGDHC inhibitor [15], SP is a protector of OGDHC from an irreversible inactivation occurring in the course of catalysis [16, 17]. During a certain time period, this protective effect may manifest itself as an apparent increase in the OGDHC activity compared to the control value with the unprotected enzyme (Figure 3). It cannot, however, be the only reason for the increase, as the latter may

be observed in the absence of SP as well. That is, the OGDHC activity of cortex increases also as a result of acute hypoxia in pregnant rats (Figure 7). Worth noting, also in this case the elevation of the OGDHC activity in cortex is accompanied by increased exploratory activity and decreased anxiety (Figures 5 and 6).

In our earlier work on the developmental impact of the brain OGDHC activity, we observed the sex-determined differences in the brain OGDHC expression and reactivity to SP [21]. The present study confirms dependence of the behavioral impact of the OGDHC regulation on the animal physiology, as behavior of pregnant females is less responsive to SP than that of males. Nevertheless, the sex-independent anxiolytic effect of SP was also observed, with the low doze of SP decreasing the grooming time in both males (Figures 1(a) and 2) and females (Figure 6).

Remarkably, both earlier [21] and here, the SP action exhibited an interplay with different stresses. For instance, in males, the SP-induced increase in exploratory activity and decrease in anxiety were pronounced only under comfortable test conditions (Figures 1 and 2), but not under the stress conditions of the light-dark chamber (data not shown). Likewise, in pregnant rats exposed to hypoxia, the SP pretreatment abrogated most of the hypoxia-induced behavioral changes (Figures 5 and 6). Combination of the hypoxic stress with SP also reduced the brain OGDHC activity elevated by hypoxia (Figure 7). Our data thus point to the antagonistic action of stress and SP at both biochemical and behavioral levels. This antagonism could be used to protect from the negative effects of the metabolic stress. In particular, we show the protection in the hypoxic model, where SP not only normalized the behavioral parameters (Figures 5 and 6) and OGDHC activity in cortex (Figure 7), but also increased the proportion of rats highly resistant to hypoxia (Figure 4).

Earlier, we suggested that metabolic stress accompanying the onset of neurodegeneration increases an irreversible inactivation of OGDHC [34, 35], which may also lead in appearance of aberrant enzyme forms with an elevated ability to catalyze hazardous side reactions [36]. This irreversible damage of the OGDHC function occurring in neurodegenerative diseases [7, 36] may be alleviated through the reversible inhibition of OGDHC by SP due to several reasons. First of all, the inhibition by SP may induce compensatory effects up-regulating OGDHC (Figure 3). Furthermore, as shown earlier, SP binding to the active site protects the essential groups of enzyme from irreversible modifications causing inactivation [16, 17]. The SP binding also prevents the enzyme from catalysis of the side reactions, including production of ROS and enzyme-bound radicals irreversibly damaging OGDHC [18]. The work presented here extends our previous *in vitro* and *in situ* studies to animal experiments, showing that reversible inhibition of OGDHC under conditions of metabolic stress may indeed normalize both the behavior (Figures 5 and 6) and brain OGDHC activity level (Figure 7). It is probable that up-regulation of OGDHC occurs also in response to its irreversible inactivation upon initial stages of the neurodegenerative diseases. However, when the inactivatory conditions persist with the up-regulated OGDHC not protected, the cellular compensatory ability is exhausted, eventually resulting in the increasing damage of the brain mitochondrial metabolism. In contrast, the protective effects of SP described above would allow cells to combine the OGDHC up-regulation with the enzyme protection, which may underlie cellular ability to overcome metabolic stress.

5. Conclusions

Up-regulation of the brain OGDHC activity correlates with increased exploratory activity and decreased anxiety. Compensatory response of brain to metabolic stress may include up-regulation of OGDHC. The up-regulation under metabolic stress may be adjusted by reversible inhibition of OGDHC, normalizing the biochemical and behavioral deviations.

Abbreviations

E1o: 2-oxoglutarate dehydrogenase;
E2o: Dhydrolipoamide succinyl transferase;
E3: Dihydrolipoamide dehydrogenase;
OGDHC: 2-oxoglutarate dehydrogenase complex;
ROS: Reactive oxygen species;
SP: Succinyl phosphonate.

Acknowledgments

This paper is supported by Grants from the Russian Foundation of Basic Research (09-04-90473 and 10-04-90007) and Alexander von Humboldt Foundation (RUS-1003594).

References

[1] M. H. Odièvre, D. Chretien, A. Munnich et al., "A novel mutation in the dihydrolipoamide dehydrogenase E3 subunit gene (DLD) resulting in an atypical form of alpha-ketoglutarate dehydrogenase deficiency," *Human Mutation*, vol. 25, no. 3, pp. 323–324, 2005.

[2] A. Amsterdam, R. M. Nissen, Z. Sun, E. C. Swindell, S. Farrington, and N. Hopkins, "Identification of 315 genes essential for early zebrafish development," *Proceedings of the National Academy of Sciences of the United States of America*, vol. 101, no. 35, pp. 12792–12797, 2004.

[3] R. J. Dunckelmann, F. Ebinger, A. Schulze, R. J. A. Wanders, D. Rating, and E. Mayatepek, "2-Ketoglutarate dehydrogenase deficiency with intermittent 2-ketoglutaric aciduria," *Neuropediatrics*, vol. 31, no. 1, pp. 35–38, 2000.

[4] N. Guffon, C. Lopez-Mediavilla, R. Dumoulin et al., "2-Ketoglutarate dehydrogenase deficiency, a rare cause of primary hyperlactataemia: report of a new case," *Journal of Inherited Metabolic Disease*, vol. 16, no. 5, pp. 821–830, 1993.

[5] J.-P. Bonnefont, D. Chretien, P. Rustin et al., "Alpha-ketoglutarate dehydrogenase deficiency presenting as congenital lactic acidosis," *Journal of Pediatrics*, vol. 121, no. 2, pp. 255–258, 1992.

[6] G. E. Gibson, A. E. Kingsbury, H. Xu et al., "Deficits in a tricarboxylic acid cycle enzyme in brains from patients with Parkinson's disease," *Neurochemistry International*, vol. 43, no. 2, pp. 129–135, 2003.

[7] G. E. Gibson, J. P. Blass, M. F. Beal, and V. Bunik, "The α-ketoglutarate-dehydrogenase complex: a mediator between mitochondria and oxidative stress in neurodegeneration," *Molecular Neurobiology*, vol. 31, no. 1–3, pp. 43–63, 2005.

[8] L. C. H. Park, D. S. Albers, H. Xu, J. G. Lindsay, M. F. Beal, and G. E. Gibson, "Mitochondrial impairment in the cerebellum of the patients with progressive supranuclear palsy," *Journal of Neuroscience Research*, vol. 66, no. 5, pp. 1028–1034, 2001.

[9] L.-W. Ko, K.-F. R. Sheu, H. T. Thaler, W. R. Markesbery, and J. P. Blass, "Selective loss of KGDHC-enriched neurons in Alzheimer temporal cortex: does mitochondrial variation contribute to selective vulnerability?" *Journal of Molecular Neuroscience*, vol. 17, no. 3, pp. 361–369, 2001.

[10] F. Mastrogiacomo, J. G. Lindsay, L. Bettendorff, J. Rice, and S. J. Kish, "Brain protein and α-ketoglutarate dehydrogenase complex activity in Alzheimer's disease," *Annals of Neurology*, vol. 39, no. 5, pp. 592–598, 1996.

[11] Y. Mizuno, S. Matuda, H. Yoshino, H. Mori, N. Hattori, and S.-I. Ikebe, "An immunohistochemical study on α-ketoglutarate dehydrogenase complex in Parkinson's disease," *Annals of Neurology*, vol. 35, no. 2, pp. 204–210, 1994.

[12] R. F. Butterworth, J. J. Kril, and C. G. Harper, "Thiamine-dependent enzyme changes in the brains of alcoholics: relationship to the Wernicke-Korsakoff Syndrome," *Alcoholism: Clinical and Experimental Research*, vol. 17, no. 5, pp. 1084–1088, 1993.

[13] G. E. Gibson, K.-F. R. Sheu, J. P. Blass et al., "Reduced activities of thiamine-dependent enzymes in the brains and peripheral tissues of patients with Alzheimer's disease," *Archives of Neurology*, vol. 45, no. 8, pp. 836–840, 1988.

[14] V. I. Bunik and S. Strumilo, "Regulation of catalysis within cellular network: metabolic and signaling implications of the 2-oxoglutarate oxidative decarboxylation," *Current Chemical Biology*, vol. 3, no. 3, pp. 279–290, 2009.

[15] V. I. Bunik, T. T. Denton, H. Xu, C. M. Thompson, A. J. L. Cooper, and G. E. Gibson, "Phosphonate analogues of α-ketoglutarate inhibit the activity of the α-ketoglutarate dehydrogenase complex isolated from brain and in cultured cells," *Biochemistry*, vol. 44, no. 31, pp. 10552–10561, 2005.

[16] V. I. Bunik, M. S. Kabysheva, E. I. Klimuk, T. P. Storozhevykh, and V. G. Pinelis, "Phosphono analogues of 2-oxoglutarate protect cerebellar granule neurons upon glutamate excitotoxicity," *Annals of the New York Academy of Sciences*, vol. 1171, no. 1, pp. 521–529, 2009.

[17] M. S. Kabysheva, T. P. Storozhevykh, V. G. Pinelis, and V. I. Bunik, "Synthetic regulators of the 2-oxoglutarate oxidative decarboxylation alleviate the glutamate excitotoxicity in cerebellar granule neurons," *Biochemical Pharmacology*, vol. 77, no. 9, pp. 1531–1540, 2009.

[18] G. Zündorf, S. Kahlert, V. I. Bunik, and G. Reiser, "α-ketoglutarate dehydrogenase contributes to production of reactive oxygen species in glutamate-stimulated hippocampal neurons in situ," *Neuroscience*, vol. 158, no. 2, pp. 610–616, 2009.

[19] S. S. Santos, G. E. Gibson, A. J. L. Cooper et al., "Inhibitors of the α-ketoglutarate dehydrogenase complex alter [1^{13}C]glucose and [U^{13}C]glutamate metabolism in cerebellar granule neurons," *Journal of Neuroscience Research*, vol. 83, no. 3, pp. 450–458, 2006.

[20] W. L. Araújo, A. Nunes-Nesi, S. Trenkamp, V. I. Bunik, and A. R. Fernie, "Inhibition of 2-oxoglutarate dehydrogenase in potato tuber suggests the enzyme is limiting for respiration and confirms its importance in nitrogen assimilation," *Plant Physiology*, vol. 148, no. 4, pp. 1782–1796, 2008.

[21] A. Graf, M. Kabysheva, E. Klimuk et al., "Role of 2-oxoglutarate dehydrogenase in brain pathologies involving glutamate neurotoxicity," *Journal of Molecular Catalysis B*, vol. 61, no. 1-2, pp. 80–87, 2009.

[22] V. I. Bunik, A. I. Biryukov, and Y. N. Zhukov, "Inhibition of pigeon breast muscle α-ketoglutarate dehydrogenase by phosphonate analogues of α-ketoglutarate," *FEBS Letters*, vol. 303, no. 2-3, pp. 197–201, 1992.

[23] V. I. Bunik and A. R. Fernie, "Metabolic control exerted by the 2-oxoglutarate dehydrogenase reaction: a cross-kingdom comparison of the crossroad between energy production and nitrogen assimilation," *Biochemical Journal*, vol. 422, no. 3, pp. 405–421, 2009.

[24] M. V. Maslova, A. V. Graf, A. S. Maklakova, Y. V. Krushinskaya, N. A. Sokolova, and V. B. Koshelev, "Acute hypoxia during organogenesis affects cardiac autonomic balance in pregnant rats," *Bulletin of Experimental Biology and Medicine*, vol. 139, no. 2, pp. 180–182, 2005.

[25] H. F. Jackson and P. L. Broadhurst, "The effects of parachlorophenylalanine and stimulus intensity on open-field test measures in rats," *Neuropharmacology*, vol. 21, no. 12, pp. 1279–1282, 1982.

[26] S. Pellow and S. E. File, "Anxiolytic and anxiogenic drug effects on exploratory activity in an elevated plus-maze: a novel test of anxiety in the rat," *Pharmacology Biochemistry and Behavior*, vol. 24, no. 3, pp. 525–529, 1986.

[27] J. N. Crawley, "Neuropharmacologic specificity of a simple animal model for the behavioral actions of benzodiazepines," *Pharmacology Biochemistry and Behavior*, vol. 15, no. 5, pp. 695–699, 1981.

[28] R. M. Salimov, W. J. Mcbride, J. D. Sinclair, L. Lumeng, and T.-K. Li, "Performance in the cross-maze and slip funnel tests of four pairs of rat lines selectively bred for divergent alcohol drinking behavior," *Addiction Biology*, vol. 1, no. 3, pp. 273–280, 1996.

[29] P. A. Kuptsov, M. G. Pleskacheva, and K. V. Anokhin, "Spatial memory in bank voles (Clethrionomys Glareolus schreb) assessed in the cue-controlled open field with the place of refuge," *Zhurnal Vysshei Nervnoi Deyatelnosti Imeni I. P. Pavlova*, vol. 56, no. 3, pp. 349–354, 2006.

[30] V. Bunik, G. Raddatz, S. Lemaire, Y. Meyer, J.-P. Jacquot, and H. Bisswanger, "Interaction of thioredoxins with target proteins: Role of particular structural elements and electrostatic properties of thioredoxins in their interplay with 2-oxoacid dehydrogenase complexes," *Protein Science*, vol. 8, no. 1, pp. 65–74, 1999.

[31] T. Yu. Dunaeva, L. K. Trofimova, A. V. Graf et al., "Transgeneration effects of antenatal acute hypoxia during early organogenesis," *Bulletin of Experimental Biology and Medicine*, vol. 146, no. 4, pp. 385–387, 2008.

[32] N. A. Bondarenko, E. L. Germanova, and L. D. Luk'yanova, "Behavioral peculiarities and reactions of brain dopaminergic systems in rats with different resistance to acute hypobaric hypoxia," *Bulletin of Experimental Biology and Medicine*, vol. 130, no. 9, pp. 849–851, 2000.

[33] A. Venkatraman, A. Landar, A. J. Davis et al., "Modification of the mitochondrial proteome in response to the stress of ethanol-dependent hepatotoxicity," *Journal of Biological Chemistry*, vol. 279, no. 21, pp. 22092–22101, 2004.

[34] V. I. Bunik, "2-Oxo acid dehydrogenase complexes in redox regulation: role of the lipoate residues and thioredoxin," *European Journal of Biochemistry*, vol. 270, no. 6, pp. 1036–1042, 2003.

[35] V. I. Bunik and C. Sievers, "Inactivation of the 2-oxo acid dehydrogenase complexes upon generation of intrinsic radical species," *European Journal of Biochemistry*, vol. 269, no. 20, pp. 5004–5015, 2002.

[36] V. I. Bunik, J. V. Schloss, J. T. Pinto, G. E. Gibson, and A. J. L. Cooper, "Enzyme-catalyzed side reactions with molecular oxygen may contribute to cell signaling and neurodegenerative diseases," *Neurochemical Research*, vol. 32, no. 4-5, pp. 871–891, 2007.

SAGE-Hindawi Access to Research
International Journal of Alzheimer's Disease
Volume 2010, Article ID 954589, 17 pages
doi:10.4061/2010/954589

Research Article

Chronic Cerebral Ischaemia Forms New Cholinergic Mechanisms of Learning and Memory

E. I. Zakharova,[1] Z. I. Storozheva,[2] A. M. Dudchenko,[1] and A. A. Kubatiev[1]

[1] *Institute of General Pathology and Pathophysiology, RAMS, Baltic street 8, Moscow 125315, Russia*
[2] *P.K. Anokhin' Institute of Normal Physiology, RAMS, Baltic street 8, Moscow 125315, Russia*

Correspondence should be addressed to E. I. Zakharova, zakharova-ei@yandex.ru

Received 16 May 2010; Revised 10 August 2010; Accepted 2 November 2010

Academic Editor: Gemma Casadesus

The purpose of this research was a comparative analysis of cholinergic synaptic organization following learning and memory in normal and chronic cerebral ischaemic rats in the Morris water maze model. Choline acetyltransferase and protein content were determined in subpopulations of presynapses of "light" and "heavy" synaptosomal fractions of the cortex and the hippocampus, and the cholinergic projective and intrinsic systems of the brain structures were taken into consideration. We found a strong involvement of cholinergic systems, both projective and intrinsic, in all forms of cognition. Each form of cognition had an individual cholinergic molecular profile and the cholinergic synaptic compositions in the ischaemic rat brains differed significantly from normal ones. Our data demonstrated that under ischaemic conditions, instead of damaged connections new key synaptic relationships, which were stable against pathological influences and able to restore damaged cognitive functions, arose. The plasticity of neurochemical links in the individual organization of certain types of cognition gave a new input into brain pathology and can be used in the future for alternative corrections of vascular and other degenerative dementias.

1. Introduction

Vascular dementia sometimes can precede or accompany Alzheimer's disease, and in these cases the development of Alzheimer's disease becomes more dramatic. The dementia of ischaemic type and Alzheimer's disease is synergistic or additive in the earliest stages of Alzheimer's disease, although the interactive mechanisms are not known [1, 2]. Both types of dementia are neurodegenerative diseases and for both the dysfunction and degeneration of cholinergic projective systems in the cortex and the hippocampus from the forebrain nuclei are critical [3–8]. A number of studies on animal models demonstrated a possible trigger role of cholinergic projective neurons in brain ischaemia. The early activation of cholinergic projective neurons was found to occur simultaneously with glutamatergic activation in the cortex and the hippocampus [9–12]. Correlations between the development of cholinergic dysfunctions and the destruction of pyramidal neurons in the hippocampus [6, 13, 14], and also damage to the cognitive functions of animals [4–8, 10], led to the presumption that a dysfunction in cholinergic afferents plays a major role in the development of ischaemic pathologies [9, 12, 14, 15].

Modern electrophysiology accumulated numerous data that interneurons of the cortex and the hippocampus actively participate in the modulation of neuronal activity including the hippocampal pyramidal neurons [16–18]. It was revealed that the cholinergic effects on the interneurons of the cortex and the hippocampus was substantially mediated through nicotinic receptors (nAChRs) [16–21]. On the other hand the role of the cholinergic interneurons in behavioural, and neurodegenerative mechanisms is still unknown.

Our investigations on the "light" and "heavy" synaptosomal fractions of the cortex and the hippocampus allowed the study of the major cholinergic projection systems of the cortex and the hippocampus and their minor intrinsic systems of cholinergic interneurons. According to immunochemical data, both the cortex and the hippocampus have two basic sources of cholinergic innervations. The first major sources are the neuronal projections from the forebrain nuclei basalis magnocellularis into the cortex (precursor of the Meynert nucleus in primates and humans) and projections

from the forebrain medial septal nuclei and vertical limb nuclei of the diagonal band of Broca into the hippocampus. The second minor source is the interneurons (intrinsic neurons) [22–28]. The synaptosomes are presynaptic parts of synapses with their junction complexes; these shall be termed presynapses in the present study. We previously showed that for both the cortex and the hippocampus the cholinergic presynapses from different sources are isolated in different synaptosomal fractions during preparation in the sucrose density gradient. The presynapses of cholinergic projections from the forebrain nuclei are accumulated mainly in the light synaptosomal fractions whereas the presynapses of cholinergic interneurons are accumulated mainly in the heavy synaptosomal fractions [29–31]. It is probable that the heavy synaptosomal fraction of the hippocampus may also accumulate a small part of the cholinergic projective presynapses (lateral projection pathway into the hippocampus [32]) [31]. Our studies on the cortical synaptosomal fractions of cats allowed suggest the involvement of the cholinergic interneurons in cognitive functions [29]. In the studies on the cortical and hippocampal synaptosomal fractions of rat we revealed that during the first three hours of chronic brain ischaemia the cholinergic projective neurons were reactive, as were the interneurons of the cortex and the hippocampus as well [33].

At present, the molecular, genetic and neurochemical mechanisms of cognitive functions are widely investigated in different behavioural models and widely discussed as well. Some among these data induce to revise generally conception that memory formation involves an irreversible passage via labile phases, such as working and short-term memory to the stable form of long-term memory. Thus it was shown, that several drugs inhibited short-term memory without altering long-term memory [34] and that working, short-term, and long-term memory were differentially regulated in the various brain regions by the various neurotransmitter systems, including cholinergic one [34–37]. The authors concluded that different types of memory had the separate mechanisms, various neurotransmitter systems, and regions. These data demanded an individual approach for the restoration of cognitive abilities.

The basis of our investigation is importance of the cholinergic systems in human and animal cognition, and also the existence of general mechanisms in the development of dementias of different aetiologies. In the present study, the cholinergic synaptic organization of different forms of learning and memory in rats with normal and chronic ischaemic brains was investigated using spatial contextual and spatial cued models in the Morris water maze. A marker of cholinergic neurons, enzyme of acetylcholine synthesis choline acetyltransferase (ChAT; EC 2.3.1.6) was used for estimation of the cholinergic systems. ChAT activity and also protein contents (total synaptic parameters) were measured in subfractions of the synaptic membranes and the synaptoplasm isolated from "light" and "heavy" synaptosomal fractions of the cortex and the hippocampus. Thus, the participation of projective and intrinsic cholinergic systems of the cortex and hippocampus in mechanisms of learning and memory under normal and ischaemic conditions was researched. In addition, the regulation of learning performance under prolonged action of selective agonist of $\alpha 4\beta 2$ subtype of nAChR metanicotine (RJR) and selective antagonist of non$\alpha 7$ subtypes of nAChR mecamlamine was studied.

2. Materials and Methods

2.1. Animals. Outbred white adult male rats (220–270 g) were supplied from the animal's nursery "Light mountains" (Russia) and then kept in the vivarium of our Institute of General Pathology and Pathophysiology. The rats were housed in a temperature-controlled room (20–24°C) with free access to food and water and kept on a 12 h light/dark cycle according to the National Institutes of Health Animal Care and the "Principles of Laboratory Animal Care" guidelines and the study was approved by the Ethical Committees of the Institutes. All animals were allocated to experimental groups randomly, using random numbers.

2.2. Chronic Ischaemia Model (Two-Vessel Occlusion). Chronic rat ischaemia was induced by permanent occlusion of the common carotid arteries (two-vessel occlusion, 2VO) by ligation. The bilateral common carotid arteries were tied with silk threads whilst the rats were under an appropriate level of pentobarbital anaesthesia. The common carotid arteries were separated from the cervical sympathetic and vagal nerves through a ventral cervical incision. The sham-operated animals (control groups) underwent a similar surgery but vessel ligation was excluded.

2.3. Behaviour Tests. Behaviour was studied in spatial contextual (noncued) or spatial cued models of learning and memory in the Morris water maze following standard procedures [38]. The experimental apparatus consisted of a circular water pool (diameter, 120 cm; height, 60 cm) filled with milk-clouded water at 24°C to a depth of 40 cm. A Plexiglas hidden platform (10 × 10 cm) was submerged 2 cm below the water surface and was placed at the midpoint of one quadrant.

Rat training started 6, 7, or 8 days after the surgery. The rats were trained during three daily sessions in the contextual (sham-operated/2VO rats) or the cued learning models. In both learning models the rats were given four daily attempts to find the hidden platform in a 60 s time interval and the estimated swim time for platform achievement (latency time) was recorded. Rats which failed to find the platform within 60 s were considered unable to solve the task and were softly guided there by the investigator with 60 s scored. The other rats remained on the platform for 30 s and were returned to their home cage during the intertrial interval (60 s).

In the contextual model the location of the hidden platform remained the same throughout the training period. The pool was located in a test room containing no prominent visual marks. At the start of all trials, the rats were placed in the pool at one of four starting positions. In the cued model a prominent visual mark (cue) was placed on the maze wall over the hidden platform to help the animal locate

the platform. In this model the rats had the same starting position but the hidden platform with its cue was moved to four different positions during the session.

The following forms of cognitive functions were observed and investigated: the inherited abilities (the first noncasual attempts at decision making in the task, that is, 1s1 trial in the cued model and 1s2 trial in the contextual model); working memory in the first session (1s2–4 and 1s3-4 averaged out over the following trials, resp.); learning in the second and the third sessions (2s2–4 and 3s2–4 averaged trials, resp.); and long-term memory on the days after the first and the second sessions of training (2s1 and 3s1 trials, resp.).

All behavioural experiments were carried out by investigators who had no knowledge of the experimental groups.

2.4. Drug Administration. Metanicotine (RJR 2304, Tocris), a selective agonist of $\alpha 4\beta 2$ subtype of nAChR and mecamilamine (Sigma), a selective antagonist of non-$\alpha 7$ subtypes of nAChR, were used. The preparations were subchronically administered (i.p.) three times daily in doses of 26 and 3.9 nmoles/kg, respectively. Both the sham-operated and the ischaemic rats received the first injection of the preparations immediately after the end of narcosis (1.5–3 hours after surgical intervention). The control group of the sham-operated animals received saline. The rats were tested 6–10 days after 2VO.

2.5. Brain Tissue Preparation. Some of animals were decapitated for biochemical analysis 3-4 days after the third session of training. It means, the rats which trained from 6 day after the surgery were decapitated at 11 or 12 days after the surgery and so on. The biochemical group included the control/2VO animals trained in the contextual model (contextual biochemical subgroup) or the cued model (cued biochemical subgroup).

All preparative procedures were carried out at 2–4°C. Briefly, the brain, cortex and hippocampus were removed, separated and homogenized. From each sample the light and heavy synaptosomal fractions were isolated, with further separation of the subfractions of the synaptic membranes and the synaptoplasm, following preparative and the disruptive procedures and the discontinued gradients of sucrose density as described previously [30, 39]. The fractions of the synaptosomes were obtained from the rough mitochondrial fraction by centrifugation using a bucket rotor (84,000 g × 120 min, 2–4°C) in layers between 1.0–1.2 M sucrose densities (the light synaptosomes) and between 1.2–1.4 M sucrose densities (the heavy synaptosomes) [40]. The synaptosomes were disrupted by combined shock procedures: the synaptosome pellets were suspended in hypo-osmotic solution containing 6 mM Tris-NCl buffer, pH 8.1 [41] (100 mg tissue/ml) and they were then exposed by freeze-thawing. The synaptoplasm subfractions were obtained as supernatants by centrifugation from the disrupted synaptosomal fractions (14,000 g × 30 min, 2–4°C). The pellets were suspended in the hypo-osmotic solution and stratified on discontinued gradients again. The synaptic membrane subfractions were obtained by centrifugation using the bucket rotor (130,000 g × 120 min, 2–4°C) in layers between 0.6–1.2 M sucrose densities. The clean synaptic membrane subfractions were free from glial, mitochondrial and synaptic vesicle contamination [39]. All samples were stored at −70°C until the day of the assay.

2.6. Analytical Methods. The activity of ChAT in subfractions of synaptic membranes and synaptoplasm of the cortex and the hippocampus was determined by the radiometric method of Fonnum [42] and the protein contents were determined by the method of Lowry et al. [43]. Accordingly, the membrane-bound mChAT activity and m-protein contents were determined in the synaptic membrane subfractions, and the water-soluble cChAT activity and c-protein contents were estimated in synaptoplasm subfractions. Moreover, both the light and the heavy synaptosomal fractions include presynapses of different sizes [38]. Small and large presynapses have different relationships with synaptic membranes and synaptoplasm mass. This is the reason why changes in mChAT activity could be exposed and changes in cChAT activity could be masked in the small presynapses, whereas changes in cChAT activity, but not in mChAT activity, could be exposed in the large presynapses. Therefore, estimations of mChAT and cChAT activities (as well as m- and c-protein contents) could give additional information on the characteristics of changes caused by ischaemia.

2.6.1. Choline Acetyltransferase Assay. The reactive solution was prepared at the day of experiment. The enzymatic reaction was started by mixing subfraction samples with the reactive solution. The reactive mixture contained a final concentration of 0.2 mM acetyl CoASA (Fluka) and [1-^{14}C]-acetyl CoASA (Amersham Pharmacia Bioscience) with SPA 5 mCi/mmol, 300 mM NaCl, 3 mM $MgCl_2$, 0.2 mM physostigmine salicylate (Sigma), 10 mM choline chloride (Serva), 0.5% Triton X-100 (Serva), 0.5 mg/ml albumin from bull serum (Koch-Light), 10 mM sodium phosphate buffer/1 mM EDTA-Na_2, pH 7.8 and the subfraction samples (near 3.5 mg of protein) at a common volume of 0.05–0.1 ml. The reactive mixture was incubated in a water shaker at 37°C for 30–60 min. The reaction was stopped by adding 2 ml of ice-cold stop solution (0.2 mM acetylcholine in 10 mM sodium phosphate buffer/1 mM EDTA-Na_2, pH 7.8) and by placing the mixture in an ice bath. Then, a 1 ml solution of sodium tetraphenylborate (Sigma) in butyl acetate (15 mg/ml) was added and quickly subjected to intensive mixing in a shaker (500 turns/min, 4 min, room temperature). The organic phase was separated from the inorganic phase by centrifugation (1000 g × 15 min, 2–4°C). The organic phase with acetylcholine (0.5–0.7 ml) was placed into scintillation liquid for organic solutions and the radioactively synthesized acetylcholine (DPM) was quantified with a Beta counter.

2.6.2. Protein Assay. Reactive solution (Biuret reagent) was prepared at the day of experiment by mixing 0.5 ml of 1% cupric sulfate with 0.5 ml of 2% sodium potassium tartrate, followed by the addition of 50 ml of 2% sodium carbonate in 0.1 N NaOH. A standard curve was prepared as follows.

Bovine serum albumin (BSA) powder was dissolved in distilled water and diluted to a concentration of 1000 μg/ml. A series of dilutions of the basic BSA solution (50, 100, 200, 400 and 500 μg/ml) was made by mixed thoroughly of the aliquots of basic BSA solution and water with repeated pipeting. Samples were within the BSA standard range (1–20 μg in assay volume). Reaction was started by intensive mixed of 0.02/0.04 ml of BSA or subfractions samples with 1 ml of the reactive solution. The mixture was then allowed to incubate at room temperature for 10–15 min prior to the addition of 0.1 ml per tube of 1.0 N Folin & Ciocalteu's reagent. Samples were mixed immediately. Color was allowed to develop for 2 hours in dark at room temperature and the absorbance of the reduced Folin reagent measured at 750 nm and blanked on the water only control. After then the reaction was found to be stable for up to an hour at room temperature and kept in refrigerator at 5–8°C for up to 1-2 days.

2.7. Statistical Analysis. The behavioural results were expressed in terms of time taken to swim to the hidden platform (s) and the biochemical results were expressed in terms of ChAT activity (nmoles acetylcholine/min) or protein content (mg) in 1 g wet weight of cortex and hippocampus tissue, respectively. The data were calculated using the nonparametric Fisher's Exact Test and the r-criterion of the Pearson's correlative test in Microsoft Excel with a glance of adjusting formula for small number of observations [44]. Differences were considered to be statistically significant if $P < .05$.

3. Results

3.1. Behavioural Performance under 2VO Conditions: Total the Contextual and the Cued Groups. The period of 6–10 days of chronic brain ischaemia led to a strong decline in training efficiency in the Morris water maze. Learning and long-term memory were impaired in both the contextual and cued models (Figure 1). Learning in 2s2–4 and 3s2–4 were impaired in a similar manner in both of the behavioural models, whereas impairment of the long-term memory had the specificity in each model. In the contextual model (Figure 1, top), impairment of long-term memory developed gradually and only 3s1 was significantly impaired. In the cued model (Figure 2, bottom), long-memory 2s1 was impaired and 3s1 was the same as the control. Working memory and inherited abilities were intact in both behavioural models.

It can be noted that although the investigated cognitive functions were impaired, they were still performed in ischaemic rats. From all of the investigated animals ($n = 27$), only two rats could not solve the tasks in our experimental conditions (in the contextual model). As a rule, the prolongation of solving tasks and/or the delay in learning (successful solving of the task only occurred in the third session) was observed.

3.2. ChAT Activity and Protein Content under 2VO Conditions. Total Biochemical Group. The period of 11–14 days of chronic ischaemia resulted in significant changes in ChAT activity and protein content in the investigated subfractions of the synaptosomes, both of the cortex and the hippocampus (Figure 2-all rats). In the cortical light synaptosomal fraction, mChAT activity and m-protein content were increased, and these changes were positively correlated amongst themselves ($r = +0.770$, $n = 18$, total control and 2VO groups data, $P < .001$; in the control group $r = +0.788$, $n = 9$, $P < .02$). The cChAT activity did not significantly vary or correlate with mChAT activity but it was positively correlated with increasing c-protein content ($r = +0.669$, $n = 9$, $P < .05$; in the control group $r = +0.305$, $n = 9$, $P > .05$). This indicated a reorganization of the synaptic pool in more than one synaptic population of the cholinergic projective neurons in the cortex.

The activity of mChAT activity was only increased in the cortical heavy synaptosomal fraction. But mChAT activation was accompanied by a reinforcement in the positive correlation between its values and the m-protein content ($r = +0.694$, $n = 9$, $P < .05$; in the control group $r = +0.291$, $n = 9$, $P > .05$). Also, a reinforcement of the positive correlation between the values of cChAT activity and c-protein content was observed ($r = +0.835$, $n = 9$, $P < .01$; in the control group $r = +0.633$, $n = 9$, $P > .05$).

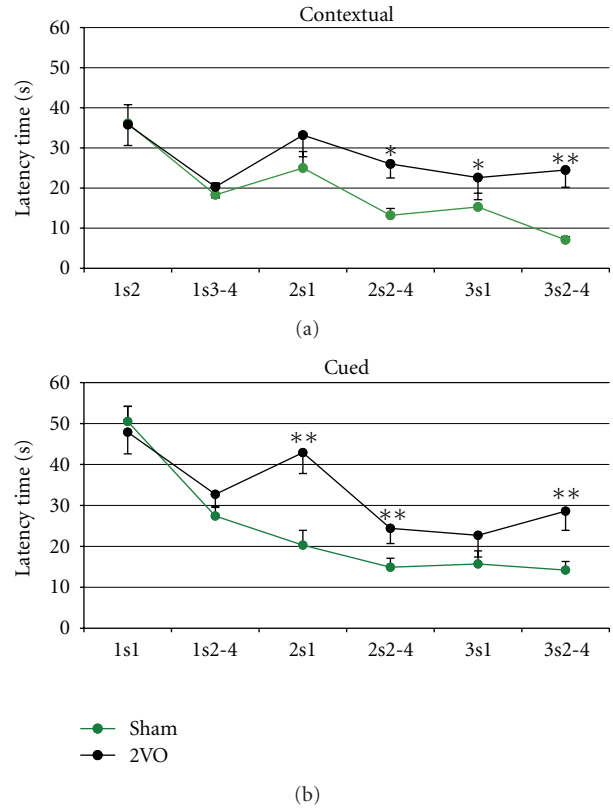

Figure 1: Behavioural performance of control and ischaemic rats in the Morris water maze. Graphs represent the swim latency time (sec, mean ± SEM) of the hidden platform achievement (behavioural criterion) by control (sham-operated, green curve) and ischaemic (2VO-operated, black curve) rats in spatial contextual (on the top) and spatial cured (on the bottom) behavioural conditions.

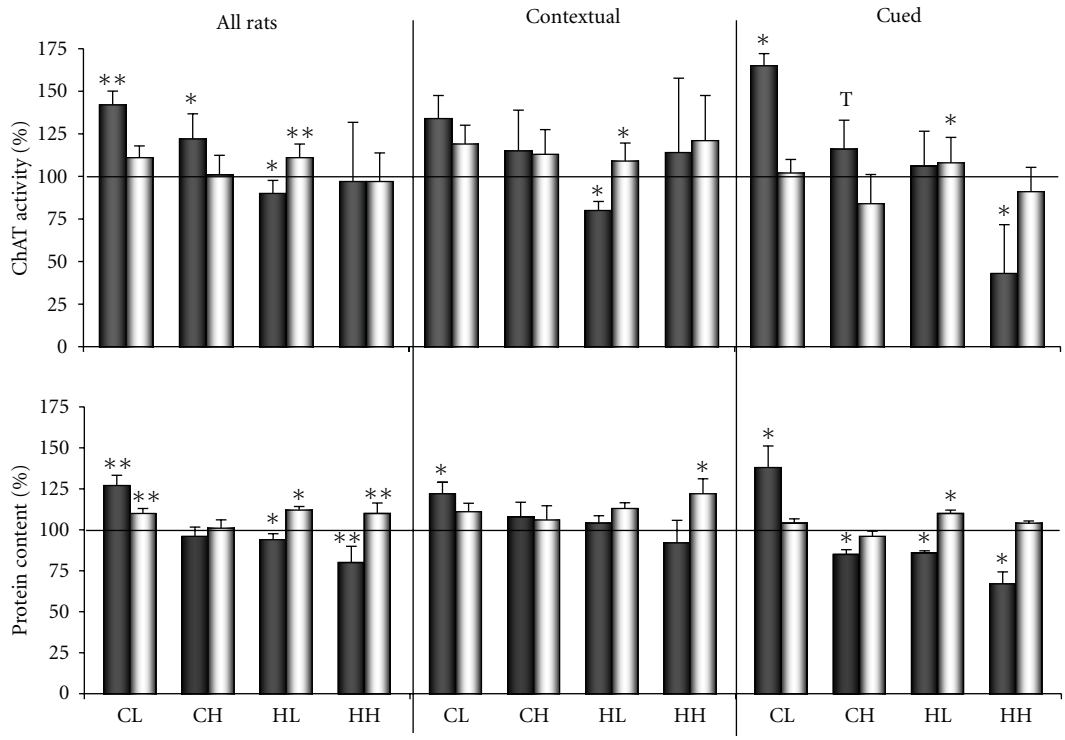

Figure 2: ChAT activity (top row of bars) and protein content (bottom row of bars) in the subfractions of the synaptic membranes and synaptoplasm of the light and heavy synaptosomes of the cortex and the hippocampus under 2VO conditions. Over the bars: All Rats, whole rat biochemical groups ($n = 9$ for control and 2VO rats); Contextual: the spatial contextual biochemical rat's subgroup ($n = 5$ per group); Cued: the spatial cued biochemical rat's subgroup ($n = 4$ per group). All values were expressed as percentage of enzyme activity or protein content in comparison to their control values (100%). For each pair of bars: dark bar represents synaptic membrane subfraction; light bar: synaptoplasm subfraction. CL: the subfractions of the light synaptosomal cortical fraction; CH: the subfractions of the heavy synaptosomal cortical fraction; HL: the subfractions of the light synaptosomal hippocampal fraction; HH: the subfractions of the heavy synaptosomal hippocampal fraction. *,**, significant differences from control ($P < .05$ and $P < .025$, resp.) by the Fisher's Exact test. Comments and r-criterion values of the significant correlations by the Pearson's test between ChAT activity and protein content or of the significant correlations between m- and c-parameters in own synaptosomal fractions see in Section 3.

At the same time, the correlation between the activity of mChAT and the activity of cChAT became weaker than in the control ($r = +0.579$, $n = 9$, $P > .05$; in the control group $r = +0.754$, $n = 9$, $P < .02$). This indicated a reorganization of the synaptic pool in more than one synaptic population of the cholinergic interneurons in the cortex.

In the hippocampal light synaptosomal fraction, mChAT activity decreased and cChAT activity increased. The protein content showed similar changes. However, significant correlations between the values of mChAT and cChAT activity, and between the values of ChAT activity and protein content, were absent. This indicated a reorganization of the synaptic pool in more than one synaptic population in the hippocampus, in both the cholinergic systems and some noncholinergic systems.

In the hippocampal heavy synaptosomal fraction, m-protein content decreased and c-protein content increased. Changes in the m-protein content did not correlate with ChAT activity and thus reflected reorganization of noncholinergic presynapses in the hippocampus. The activities of mChAT and cChAT did not differ from the controls although at the same time a positive correlation arose between their values ($r = +0.802$, $n = 8$, $P < .02$; in the control group $r = -0.300$, $n = 9$, $P > .05$). Also, the positive correlations between values of c-protein content and mChAT activity ($r = +0.927$, $n = 8$, $P < .01$; in the control group $r = +0.265$, $n = 9$, $P > .05$) and cChAT activity ($r = +0.844$, $n = 8$, $P < .01$; in the control group $r = +0.091$, $n = 9$, $P > .05$) were reinforced. This indicated a reorganization of the presynapses of the cholinergic interneurons/lateral pathway projective neurons in the hippocampus. It seems that the unchanged values of ChAT activity reflected parallel processes of activation and inactivation of ChAT in different synaptic populations of this fraction.

3.3. ChAT Activity and Protein Content in the Contextual and Cued Biochemical Subgroups. Also, the biochemical data of the contextual biochemical subgroup were compared with the cued biochemical subgroup. Analysis of the biochemical parameters in the control biochemical subgroups did not reveal significant changes between the subgroups (Table 1). Only the values of mChAT activity were lower in the cortical heavy and in the hippocampal light synaptosomal subfractions in the cued biochemical subgroup of rats as compared with the contextual one.

Table 1: ChAT activity and protein content in the subfractions of the synaptic membranes and the synaptoplasm of light and heavy synaptosomes of the cortex and the hippocampus in the spatial contextual (I, Contextual) and the spatial cued (II, Cued) biochemical subgroups of rats under the normal conditions. CL: the cortical light synaptosomes fraction; CH: the cortical heavy synaptosomes fraction; HL: the hippocampal light synaptosomes fraction; HH: the hippocampal heavy synaptosomes fraction; sm and Sp: the synaptic membranes and the synaptoplasm subfractions, respectively. The values of ChAT activity (nmoles acetylcholine/min) and protein content (mg) were expressed in 1 g of wet weight of tissue. In the contextual/cued biochemical subgroups $n = 5/4$, respectively. $P < .05$, significant differences between the contextual and cued biochemical subgroups by the Fisher's Exact test.

(a)

		I, Contextual		II, Cued		II/I%	P
ChAT Activity		mean	SEM	mean	SEM		
CL	sm	1.16	0.18	0.91	0.12	78%	>.05
	Sp	5.57	0.36	5.97	0.46	107%	>.05
CH	sm	0.054	0.008	0.048	0.004	**89**%	<.05
	Sp	0.367	0.037	0.352	0.021	96%	>.05
HL	sm	0.395	0.024	0.320	0.013	**81**%	<.05
	Sp	4.34	0.129	4.21	0.129	97%	>.05
HH	sm	0.022	0.004	0.017	0.003	77%	>.05
	Sp	0.410	0.038	0.415	0.040	101%	>.05

(b)

		I, Contextual		II, Cued		II/I%	P
Protein content		mean	SEM	mean	SEM		
CL	sm	5.69	0.55	5.00	0.45	88%	>.05
	Sp	4.01	0.14	4.34	0.11	108%	>.05
CH	sm	0.629	0.054	0.677	0.086	108%	>.05
	Sp	2.150	0.054	2.13	0.055	99%	>.05
HL	sm	7.10	0.304	7.49	0.304	105%	>.05
	Sp	2.90	0.195	2.95	0.139	102%	>.05
HH	sm	3.07	0.432	3.45	0.214	112%	>.05
	Sp	2.72	0.104	2.62	0.077	96%	>.05

Analysis of the biochemical parameters in the 2VO biochemical subgroups confirmed our observations about the reorganization of the synaptic pool. In the cortical light synaptosomal fraction in the contextual biochemical subgroup (Figure 2-contextual), independent correlations were detected between the values of mChAT activity and m-protein content ($r = +0.765$, $n = 10$, total control and 2VO contextual biochemical subgroups data, $P < .01$; in the control contextual biochemical subgroup $r = +0.774$, $n = 5$, $P > .05$) and between the values of cChAT activity and c-protein content ($r = +0.987$, $n = 5$, $P < .01$; in the control contextual biochemical subgroup $r = +0.441$, $n = 5$, $P > .05$). In the cued subgroup (Figure 2-cued), a correlation was only detected between mChAT activity and m-protein content ($r = +0.783$, $n = 8$, total control and 2VO cued biochemical subgroups data, $P < .05$; in the control cued biochemical subgroup $r = +0.622$, $n = 4$, $P > .05$) and a correlation was revealed between mChAT and cChAT activities ($r = +0.995$, $n = 4$, $P < .01$; in the control biochemical cued biochemical subgroups $r = -0.404$, $n = 4$, $P > .05$).

In the cortical heavy synaptosomal fraction in the contextual biochemical subgroup, independent correlations were detected between mChAT activity and m-protein content ($r = +0.981$, $n = 5$, $P < .01$) and between the values of cChAT activity and c-protein content ($r = +0.966$, $n = 5$, $P < .01$), whereas there was no correlation between the activities of mChAT and cChAT among themselves ($r = +0.652$, $n = 5$, $P > .05$). In the cued biochemical subgroup, an increase in mChAT activity was detected (a tendency) whereas a decrease in m-protein content was revealed. The decrease in m-protein content allows to suppose the changes in noncholinergic presynapses.

In the hippocampal light synaptosomal fraction in the contextual biochemical subgroup, an independent decrease in mChAT activity and an increase in cChAT activity only, and in the cued biochemical subgroup an increase in cChAT activity only, and a decrease in m-protein content and an increase in c-protein content were detected.

In the hippocampal heavy synaptosomal fraction in the contextual biochemical subgroup, positive correlations were detected between the increased values of c-protein content and mChAT activity ($r = +0.922$, $n = 5$, $P < .01$) and cChAT activitiy ($r = +0.919$, $n = 5$, $P < .05$), and between mChAT and cChAT activities ($r = +0.910$, $n = 5$, $P < .05$; in the control contextual biochemical subgroup $r = -0.266$, $n = 5$, $P > .05$). However, in the cued biochemical subgroup, a decrease in mChAT activity and

m-protein content was revealed and these changes did not correlate among themselves. This indicated a reorganization of the presynapses of the cholinergic interneurons/lateral pathway projective neurons and noncholinergic neurons in the hippocampus.

3.4. Comparison of the Behavioural Performance and ChAT Activity in the Control Rats of the Biochemical Subgroups. Differentiation of the rats into biochemical subgroups, tested in the contextual and cued models, permit to compare the behavioural performance and ChAT activity in these rats. Under the normal conditions, each form had individual cholinergic composition (Table 2: sham-contextual, Figure 3-I: sham). The inherited ability 1s2 cholinergic composition included large presynapses of projective cortical neurons (positive correlation with cChAT activity) and presynapses of hippocampal interneurons/lateral pathway projective neurons (negative correlation with mChAT and cChAT activities). The same cholinergic structures associated with the long-term memory 3s1, but with inverse symbols of *r*-criterions. The long-term memory 2s1 had composition other than 3s1 which involved small presynapses of the projective hippocampal neurons (negative correlation with mChAT activity) and some populations of hippocampal interneurons (positive correlations with mChAT and cChAT activities). The composition of the working memory 1s3-4 involved small presynapses (positive correlation with mChAT activity) and large presynapses (negative correlation with cChAT activity) of the projective hippocampal neurons. The composition of learning 2s2–4 and 3s2–4 was identical and involved small presynapses of the projective cortical neurons (positive correlation with mChAT activity in both forms of learning) and the hippocampal interneurons/lateral pathway projective neurons (positive correlations with mChAT activity).

The similar analysis in the cued biochemical subgroup revealed other individual cholinergic compositions of learning and memory (Table 2: sham-cued, Figure 3-II: sham). According to our data, the cholinergic systems did not participate in realization of inherited abilities 1s1. Working memory 1s2–4 composition involved small presynapses of both cortical cholinergic systems (negative correlation with mChAT activity) and of the hippocampal interneurons/lateral pathway projective neurons (positive correlation with mChAT activity). The composition of learning 2s2–4 and 3s2–4 was identical and comprised large presynapses of cortical interneurons and projective hippocampal neurons (positive correlations with cChAT activity in both cases). The long-term memory composition in 2s1 involved large presynapses of the cortical interneurons and small presynapses of projective hippocampal neurons (in both cases, there were positive correlations with cChAT or mChAT activities). And the long-term memory composition in 3s1 involved large presynapses of the cortical projective neurons (positive correlations with cChAT activity).

3.5. Comparison of the Behavioural Performance and ChAT Activity in the Ischemic Rats of the Biochemical Subgroups. Chronic brain ischaemia had considerable effects on the cholinergic organization of the investigated cognitive functions. In the contextual model (Table 2: 2VO-contextual, Figure 3-I: 2VO), inherited abilities 1s2, learning 2s2–4 and long-term memory 3s1 completely lost correlations with the cholinergic populations and all forms of cognition lost correlations with the cortical cholinergic populations. The composition of working memory 1s3-4 only kept negative connections with the large presynapses of projective hippocampal neurons. The positive connections of learning 3s2–4 with the small presynapses of the hippocampal interneurons/lateral pathway projective neurons inversed to negative ones. The long-term memory composition 2s1 consisted of only new, positive connections with large presynapses of the projective hippocampal neurons.

In the cued model (Table 2:2VO-cued, Figure 3-II: 2VO), long-term memory 2s1 and 3s1 completely lost correlations with the cholinergic populations and all forms of cognition lost correlations with the hippocampal cholinergic influences. The working memory 1s2–4 lost its negative connections with the small presynapses of cortical projective neurons and its negative connections with the small presynapses of cortical interneurons inversed to positive ones. The composition of learning 2s2–4 included a reversal to negative connections with the large presynapses of cortical interneurons, new negative connections with presynapses of cortical projective neurons and new negative connections with the small presynapses of cortical interneurons. The learning composition 3s2–4 kept its connections with the large presynapses of cortical interneurons and added new negative connections with presynapses of the cortical projective neurons.

So, under 2VO conditions as in the contextual and in the cued biochemical subgroup quantity of the cholinergic connections with the cognitive functions significantly reduced and some new links arose. Each form of cognition as resulting had 2VO cholinergic synaptic composition organized differently from normal ones.

3.6. Analysis of Correspondence between 2VO Induced Changes in Behavioral Performance and ChAT Activity in the Key Cholinergic Populations in the Biochemical Subgroups. We attempted to analyze the dependence of impairment of the investigated cognitive functions in 2VO conditions from the reorganization of key cholinergic systems. It seems, in the contextual biochemical subgroup only preservation of the inherited abilities 1s2 from damage could be explaned by preservation of the key cholinergic populations, revealed in the normal conditions (Figure 4, middle row). But long-term memory 3s1 had the same cholinergic composition with inverse symbols of *r*-criterions. In this case it would be expected that 3s1 would also be protected; however, this did not take place. Moreover, according to the cholinergic organization under normal conditions, working memory 1s3-4 would be considerably impaired, whereas long-term memory 2s1 and learning 2s2–4 and 3s2–4 would be considerably improved; however, these did not occur either.

On the other hand, the new cholinergic composition in 2VO conditions had accordance between reinforcement

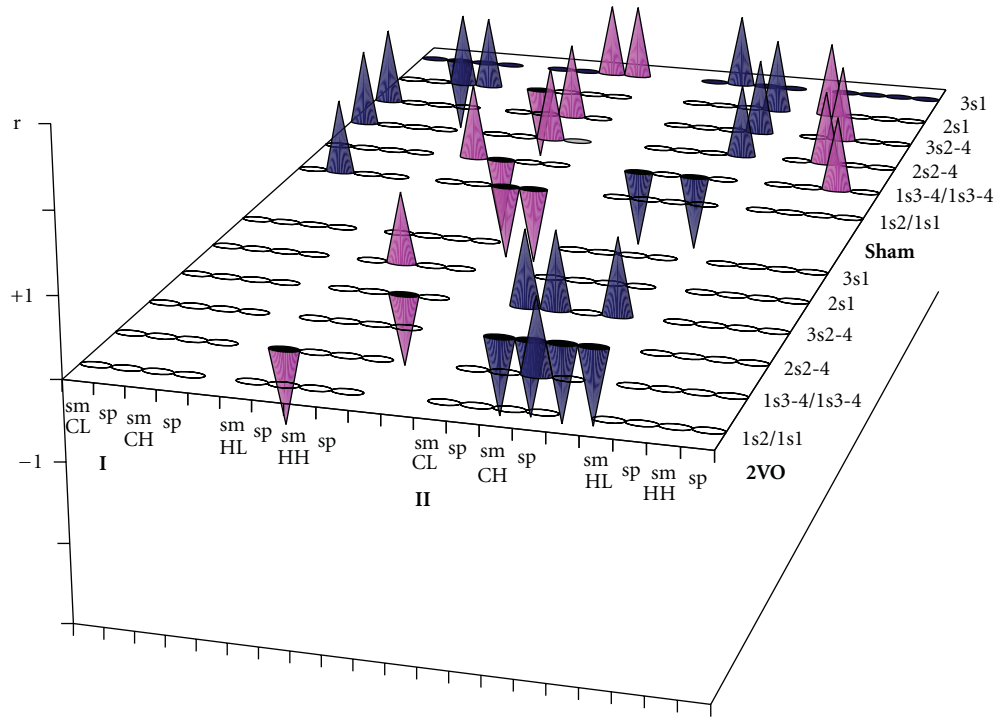

FIGURE 3: Significant r-criterion values (by the Pearson's test) of behavioural performance and ChAT activity in rats in the Morris water maze in the spatial contextual (I) and the spatial cued (II) behavioural models under control (sham) and ischaemic (2VO) conditions. 1s2/1s1, 1s3-4/1s2–4, 2s2–4, 3s2–4, 2s1, 3s1 are the same as in Figure 1; sm and Sp, subfractions of the synaptic membranes and the synaptoplasm, respectively, of the cortical light (CL) and heavy synaptosomes (CH) and hippocampal light (HL) and heavy synaptosomes (HH) as in Table 1. In the spatial contextual biochemical subgroup $n = 5$ for control and 2VO rats; in spatial cued biochemical subgroup $n = 4$ for control and 2VO rats.

of the negative influence of the hippocampal interneurons/lateral pathway projective neurons on learning 3s2–4 and impairment of this function (Figure 4, bottom row). But reinforcement of new negative and positive influences of projective hippocampal neurons was not reflected in the performance of either working memory 1s3-4 or long-term memory 2s1.

In the cued biochemical subgroup, only the preservation of long-term memory 3s1 could be explained by the resistance to ischaemia of the key synaptic population revealed in normal conditions (Figure 5, middle row). At the same time, working memory 1s2–4 would be considerably impaired, learning 2s2–4 and 3s2–4 would be equally improved or otherwise unchanged and long-term memory 2s1 would be unchanged, but these were not observed.

On the other hand, the absence of 1s2–4 impairment could also be explained by the new, weakly expressed positive cholinergic influence (tendency) of the large presynapses of cortical interneurons (Figure 4, bottom row). Then the distinctions in learning 2s2–4 and 3s2–4 performance in 2VO conditions would be explained by their new cholinergic compositions if we suppose more considerable influence of the large presynapses of the cortical interneurons on these functions in comparison with the influence of the other new key synaptic populations. Such supposition is in accordance with the data regarding long-term memory 2s1. The impairment of 2s1 also would be explained by the reduction of the link with this key synaptic population under the normal conditions.

So, it seems that performance of the cognitive functions as in the contextual and in the cued model under 2VO conditions, as a rule, did not depend on their cholinergic organization, revealed in normal conditions. Contrary, new cholinergic organization, revealed in 2VO conditions showed more significant correlations with changes in behavioral performance.

3.7. Regulation of the Learning Performance in the Normal and 2VO Conditions by Selective nAChR Agonist RJR and Antagonist Mecamilamine. Whereas, the contextual and cued learning 2s2–4 and 3s2–4 revealed cholinergic synaptic compositions identical for normal conditions and different ones, revealed in 2VO conditions, it was investigated prolonged action on the learning performance of the selective agonist of $\alpha 4\beta 2$ subtype of nAChR RJR and the selective antagonist of non-$\alpha 7$ subtypes of nAChR mecamilamine.

In the contextual model under normal conditions, both the agonist RJR and the antagonist mecamilamine did not influence on learning as 2s2–4 and 3s2–4 performance. It seems, this fact indicate that non-$\alpha 7$ subtypes of nAChR did not participate in the regulation of ones (Figure 6, contextual learning). under the 2VO conditions, effects of RJR on both learning performance was absent similar whereas mecamilamine potentiated effect of 2VO on learning

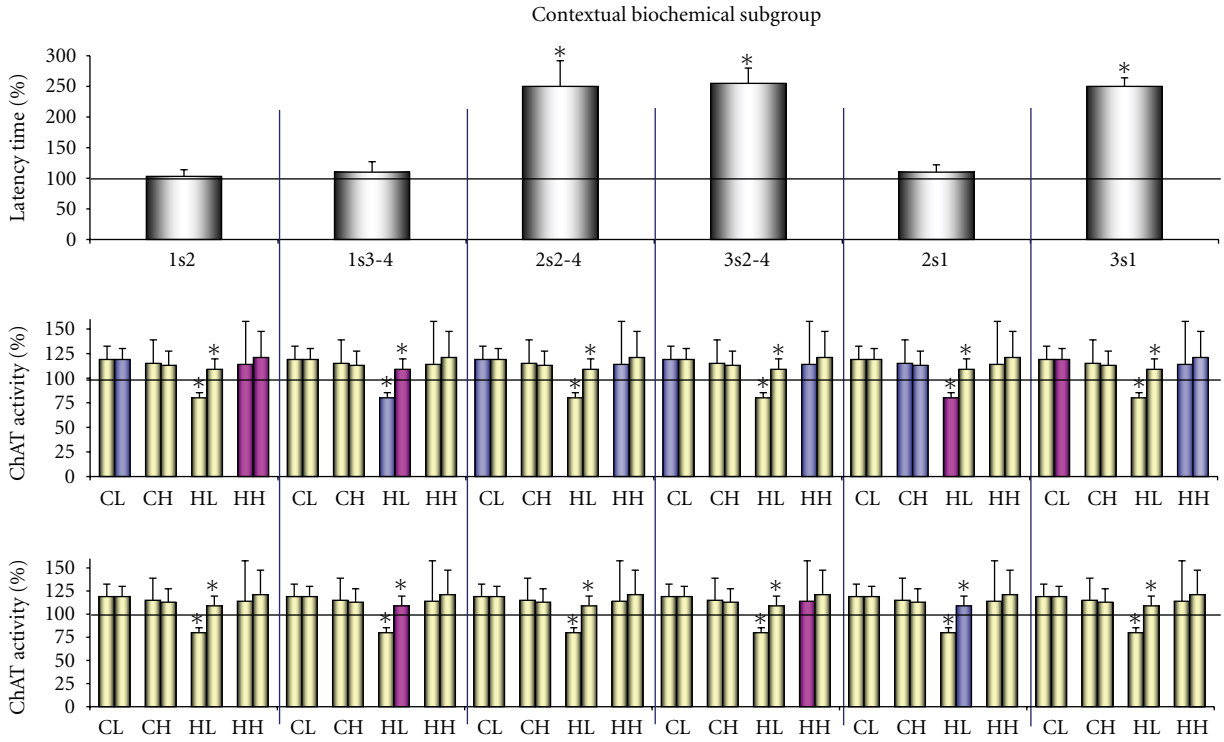

Figure 4: 2VO induced changes in behavioral performance and ChAT activity in the key cholinergic populations in the spatial contextual biochemical subgroup ($n = 5$). 1s2, 1s3-4, 2s2–4, 3s2–4, 2s1 and 3s1, the same forms of cognition as in Figure 1. Behavioral performance was expressed as percentage of latency time compared to their control values (100%). CL, CH, HL, HH, the same pairs of the subfractions as in Figure 2. Values of ChAT activity in the subfractions are identical to ones in Figure 2-contextual, and they were duplicated under the each form of cognition. Blue bars, the values of ChAT activity had positive significant correlations with corresponding forms of cognition; violet bars, the values of ChAT activity had negative significant correlations with corresponding forms of cognition. In the middle row were marked correlations between behavioral performance and ChAT activity in the control rats (correlations correspond to Table 2, Sham-Contextual). In the bottom row were marked correlations between behavioral performance and ChAT activity in 2VO rats (correlations correspond to Table 2, 2VO—Contextual). *, $P < .05$ by the Fisher's exact test. See comments in Section 3.6.

3s2–4. Evidently, the $\alpha4\beta2$ subtype did not participate in the regulation of the contextual learning, as before, while some non-$\alpha7$ and non-$\alpha4\beta2$ subtypes participated with negative influences on learning 3s2–4.

In the cued model under normal conditions, the agonist RJR impaired learning 2s2–4 and did not affect learning 3s2–4 (Figure 6, cued learning). The antagonist mecamilamine impaired learning 2s2–4 and improved learning 3c2–4. The negative effect of the agonist on learning in 2s2–4 was significantly greater than that of the antagonist ($P < .05$). The difference between the agonistic and antagonistic actions on learning in 3s2–4 at were also significant ($P < .05$). It follows that the $\alpha4\beta2$ subtype (negative influence) and some non-$\alpha7$ and non-$\alpha4\beta2$ subtypes of nAChR (positive but weak influence) participated in the regulation of learning in 2s2–4. At the same time, the $\alpha4\beta2$ subtype did not participate in the regulation of learning 3s2–4, while some non-$\alpha7$ and non-$\alpha4\beta2$ subtypes participated with negative influences. under the 2VO conditions, RJR did not correct the impaired functions 2s2–4 and 3s2–4, and mecamilamine did not correct learning 2s2–4 but resulted in normal learning 3s2–4 performance. It seems, non-$\alpha7$ subtypes of were removed from the receptor composition of learning 2s2–4. At the same time, the importance of some non-$\alpha7$ and non-$\alpha4\beta2$ subtypes of nAChR was reinforced or new connections arose in the receptor organization of learning 3s2–4 (negative influence).

So, in the contextual learning 2s2–4 and 3s2–4, nAChR were absent in normal and were acquired in 2VO receptor composition (3s2–4). Then, the cued learning 2s2–4 and 3s2–4, with identical cholinergic synaptic compositions in the norm, had differences in receptor compositions. Moreover, the cued learning 2s2–4 and 3s2–4 had also differences in 2VO receptor compositions via another means.

4. Discussion

4.1. Characteristic of the Chronic 2VO Brain Ischaemia Influence on the Rat's Behavioural Performance in the Morris Water Maze and the Cortical and Hippocampal Cholinergic Synaptic Pool. This research showed that the chronic 2VO brain ischaemia model was an efficient model of neurodegenerative disorders, which was the first purpose of our investigation. The period of 6–10 days of 2VO ischaemia provoked typical attributes of vascular dementias such as impairment of learning and long-term memory in both

Table 2: r-criterion values by the Pearson's test between behavioural performance and ChAT activity in rats in the Morris water maze in the spatial contextual (Contextual) and spatial cued (Cued) behavioural models in the control (Sham) and ischaemic (2VO) conditions. 1s2/1s1, 1s3-4/1s2–4, 2s2–4, 3s2–4, 2s1, 3s1, the abbreviations of the forms of cognition are the same as in Figure 1; sm and Sp, respectively subfractions of the synaptic membranes and the synaptoplasm of the cortical light (CL) and heavy synaptosomes (CH) and hippocampal light (HL) and eavy synaptosomes (HH) as in Table 1. The signs of correlations were placed as plus and minus for the purpose of direct reflection of correlations between performance of the cognitive functions and ChAT activity in the subfractions. The positive (plus) sign of value reflects the positive influence on cognitive function of the corresponding synaptic population and the negative (minus) sign of value reflects accordingly the negative influence on the function of the corresponding synaptic population. In the control and 2VO spatial contextual biochemical rat subgroups $n = 5$ per group; in the control and 2VO spatial cued biochemical rat subgroups $n = 4$ per group. *,**, ***, significant r-criterion values of correlations between behavioural performance and ChAT activity ($P < .05$, $P < .01$, $P < .001$, resp.) by the Pearson's test. Significant r-criterion values were marked in bold values.

		Contextual						Cued					
sham		1s2	1s3-4	2s2–4	3s2–4	2s1	3s1	1s1	1s2–4	2s2–4	3s2–4	2s1	3s1
CL	Sm	+0.487	−0.359	**+0.994*****	**+1*****	+0.295	+0.575	+0.405	**− 1*****	−0.196	+0.409	−0.234	−0.808
	Sp	**+0.961***	−0.242	−0.729	−0.396	+0.689	**− 1*****	+0.673	+0.515	+0.425	−0.429	+0.249	**+0.966***
CH	sm	+0.776	−0.268	−0.441	−0.246	**+0.980***	−0.596	+0.617	**− 0.982***	−0.617	−0.023	−0.501	−0.503
	Sp	+0.388	−0.343	+0.145	+0.145	**+0.965***	−0.219	−0.041	−0.052	**+0.958***	**+0.997****	**+0.978***	−0.369
HL	sm	+0.106	**+0.997*****	−0.292	−0.263	**− 0.967***	+0.207	−0.187	+0.667	+0.759	+0.475	**+0.993****	+0.340
	Sp	−0.614	**− 0.988***	+0.645	+0.591	+0.460	+0.317	−0.276	−0.249	**+0.974***	**+1*****	+0.658	_0.640
HH	sm	**− 0.967***	−0.288	**+0.985***	**+0.998*****	−0.120	**+0.979***	−0.413	**+0.971***	+0.684	+0.202	+0.730	+0.501
	Sp	**− 0.992*****	+0.079	+0.601	+0.549	−0.720	**+0.993*****	+0.644	−0.565	+0.127	+0.689	+0.466	−0.448
2VO		1s2	1s3-4	2s2–4	3s2–4	2s1	3s1	1s1	1s2–4	2s2–4	3s2–4	2s1	3s1
CL	sm	−0.464	−0.270	+0.548	+0.006	+0.242	+0.450	+0.400	+0.321	**− 0.981***	**+0.986***	−0.677	−0.139
	Sp	−0.656	−0.153	−0.326	−0.797	+0.198	−0.510	+0.577	+0.047	**− 0.954***	**+0.998****	−0.752	−0.377
CH	sm	+0.082	+0.477	−0.403	−0.750	−0.482	−0.110	−0.307	**+0.955***	**− 0.995****	+0.403	−0.784	+0.553
	Sp	−0.328	−0.004	−0.231	−0.350	−0.022	+0.304	+0.356	+0.373	**− 0.982***	**+0.978***	−0.655	−0.095
HL	sm	−0.162	−0.518	−0.302	−0.387	+0.426	+0.375	+0.160	+0.419	−0.782	+0.637	−0.843	+0.133
	Sp	−0.765	**− 0.928***	+0.169	−0.119	**− 0.908***	+0.145	+0.264	+0.319	−0.756	+0.691	−0.727	+0.027
HH	sm	−0.709	−0.434	−0.454	**− 0.905***	+0.448	−0.411	+0.711	−0.346	−0.559	+0.779	−0.634	−0.606
	Sp	−0.497	−0.408	−0.382	−0.753	+0.372	−0.027	−0.604	+0.780	−0.632	+0.050	−0.558	+0.680

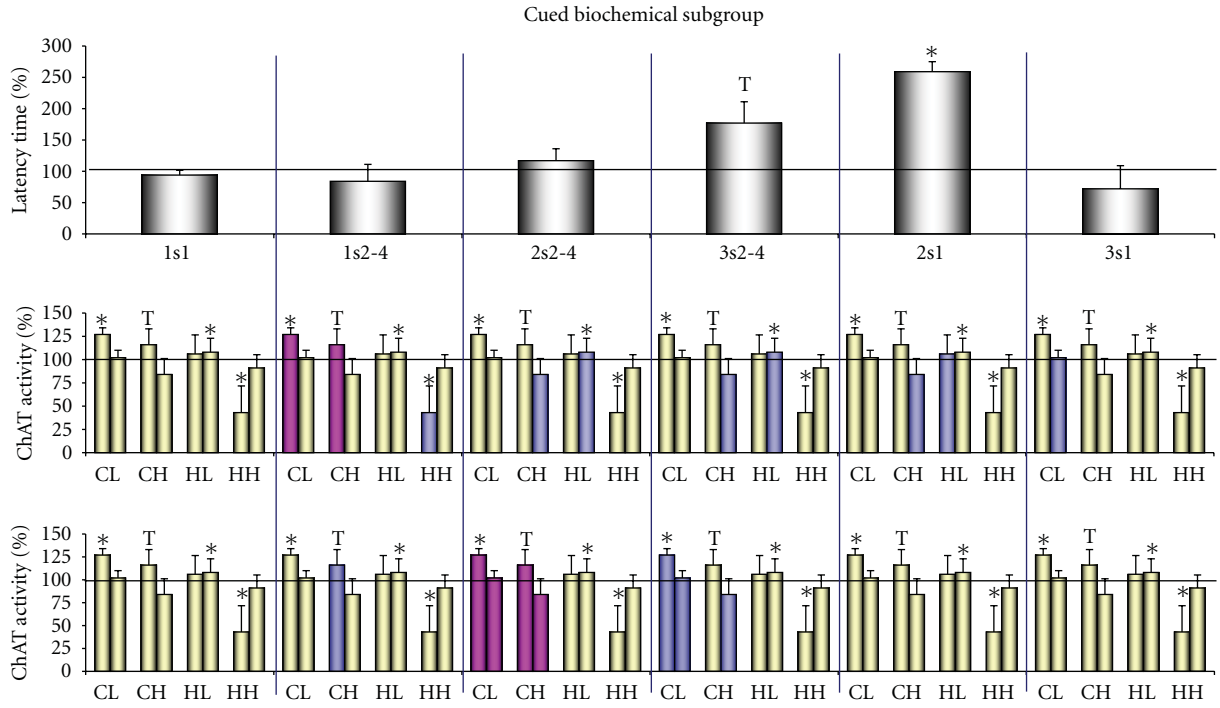

Figure 5: 2VO induced changes in behavioral performance and ChAT activity in the key cholinergic populations in the spatial cued biochemical subgroup ($n = 4$). 1s2, 1s3-4, 2s2–4, 3s2–4, 2s1 and 3s1, the same forms of cognition as in Figure 1. Behavioral performance was expressed as percentage of latency time compared to their control values (100%) as in Figure 4. CL, CH, HL, HH, the same pairs of the subfractions as in Figure 2. Values of ChAT activity in the subfractions are identical to ones in Figure 2-cued, and were duplicated under the each form of cognition as in Figure 4. Blue and violet bars the same as in Figure 4. In the middle row were marked correlations between behavioral performance and ChAT activity in the control rats (correlations correspond to Table 2, Sham-Cued). In the bottom row were marked correlations between behavioral performance and ChAT activity in 2VO rats (correlations correspond to Table 2, 2VO—Cued). *, $P < .05$ by the Fisher's Exact test. See comments in Section 3.6.

spatial-contextual and spatial-cued models of behaviour in the Morris water maze. The inherited abilities and working memory remained intact, and damage to the cued long-term memory was transient in this ischaemic period. A considerable reorganization of the synaptic pool of all investigated cholinergic systems in the cortex and the hippocampus was revealed in these same 2VO rats 11–14 days after the surgery. A decrease in mChAT or cChAT activity in one synaptosomal fraction and an increase in another were obtained as result of the 2VO influence, but not of the training, whereas the biochemical parameters did not reveal similar changes between the control contextual and cued biochemical subgroups except one. It is possible that decrease in mChAT activity in the hippocampal heavy synaptosomal fraction in the cued biochemical subgroup was result of the training (see Table 1 and Figure 2-cued).

The decrease in mChAT and cChAT activity reflected cholinergic hypofunction or a degeneration of the cholinergic presynapses. Neurodegeneration was observed in different brain ischaemia models starting from the second day up to half a year of ischaemia [45, 46]. Dysfunction of ChAT in the projective fibres in the hippocampus (representing 80–90% of the total activity of this enzyme, [30] and see Table 1) was described at 7–14 days of ischaemia [6, 13, 14, 47, 48]. It was shown in vitro that the activity of mChAT was selectively suppressed when the exchange of acetylcholine was damaged by inhibition of the vesicular acetylcholine transporter [49] or the high affinity transport of choline [50]. The function of the vesicular acetylcholine transporter depends on the proton gradient, which in turn is disturbed due to falling ATP levels (inhibition of the proton ATPase) or acidosis [49]. The chronic ischaemia/hypoxia provokes both these factors [51–53]. One effect of the degenerative process is a decrease in protein content. We did not reveal a decrease in protein content correlated with ChAT activity in our research. But we did suppose that the correlation between ChAT activity and protein content could be masked because of the complex opposing processes that took place in some of the synaptosomal fractions.

At the same time, according to data in the literature, sprouting and destruction with the swelling of neurons and their terminals predominates in late brain ischaemia or postischaemic reoxygenation (in days and months) [3, 48, 53, 54]. In our research, activation of ChAT was also observed in the majority of the synaptic subfractions, and it could have reflected cholinergic hyperfunction or synaptogenesis (sprouting). It is known that synaptic hyperfunction is accompanied with an enhanced structuring of proteins from the synaptoplasm. Under these conditions, the m-protein content will increase and the c-protein content

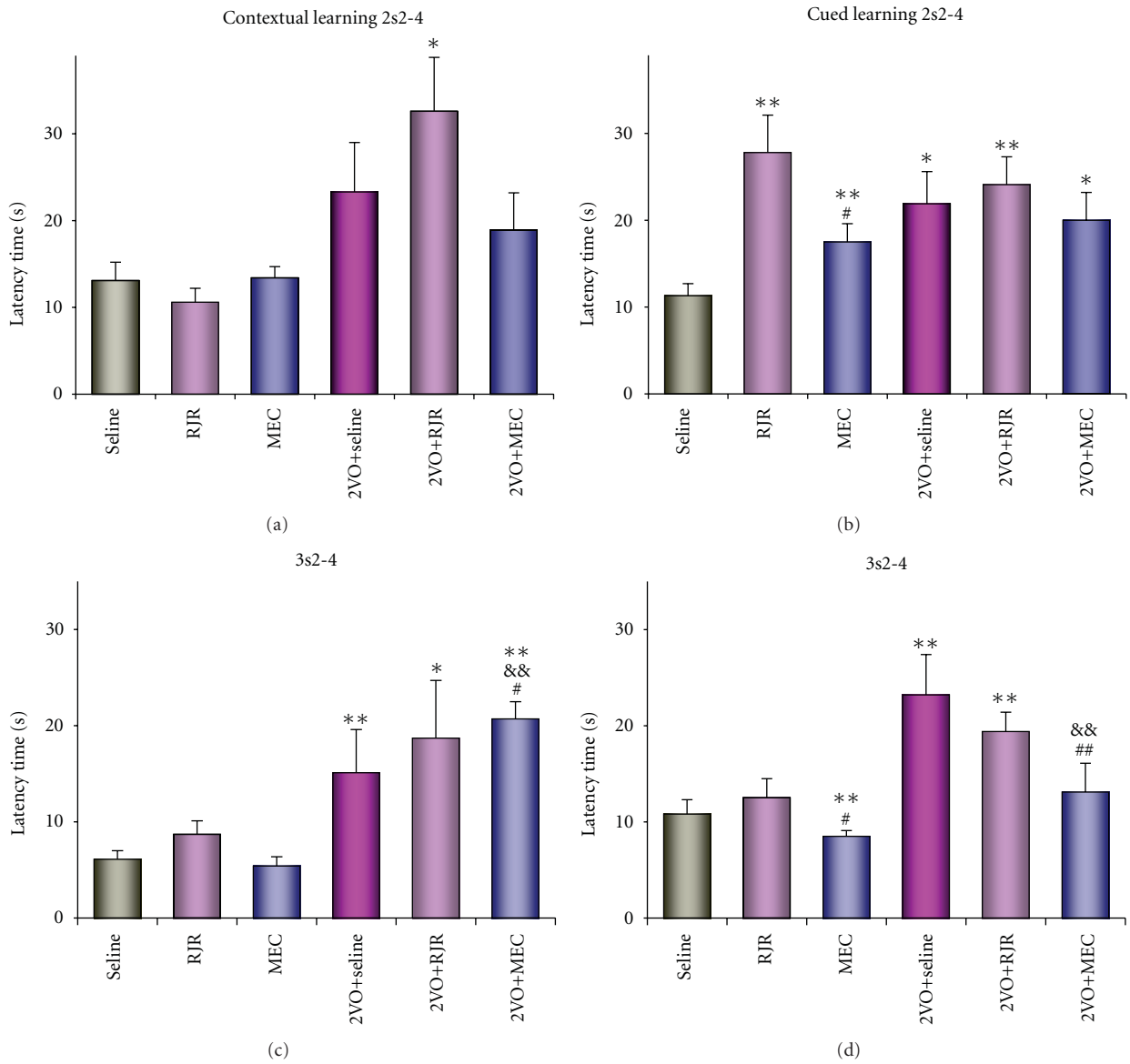

Figure 6: Influence of the agonist of $\alpha 4\beta 2$ subtype of nAChR RJR and the antagonist of non-$\alpha 7$ subtype of nAChR mecamilamine (MEC) on learning 2s2–4 (top row of figures) and 3s2–4 (bottom row of figures) in rats in the Morris water maze in the spatial contextual and the spatial cued models under control and 2VO conditions. The learning performance is presented as latency time (sec). Seline, control rat's groups ($n = 12$ for learning as 2s2–4 and 3s2–4 in the contextual model; $n = 13$ for the ones in the cued model); RJR, MEC, groups of rats with RJR or MEC administered under the normal conditions ($n = 6$ for both groups for learning as 2s2–4 and 3s2–4 in the contextual model; $n = 7$, 11 for learning 2s2–4 in RJR, MEC groups, respectively, and $n = 10$, 11 for learning 3s2–4 in ones in the cued model); 2VO + seline, the 2VO rat's group ($n = 9$ for learning as 2s2–4 and 3s2–4 in the contextual model; $n = 7$ for the ones in the cued model); 2VO + RJR, 2VO + MEC, groups of rats with RJR or MEC administered under the 2VO conditions (resp., $n = 9$, 10 for learning as 2s2–4 and 3s2–4 in the contextual model; $n = 8$, 9 for the ones in the cued model). *, **, significant differences from control rat's group ($P < .05$ and $P < .025$, resp.); #,##, significant differences between RJR and MEC or 2VO + RJR and 2VO + MEC rat's groups ($P < .05$ and $P < .025$, resp.); &&, significant differences between 2VO and 2VO + MEC rat's groups ($P < .025$) by the Fisher's Exact test.

will decrease. Therefore, the correlated increase between mChAT activity and m-protein content will be reflected as cholinergic hyperfunction and synaptogenesis (cortical light synaptosomes in the biochemical total group and both subgroups), whereas the correlated increase between cChAT/mChAT activity and the c-protein contect will only reflect synaptogenesis (cortical light synaptosomes in the biochemical total group and the contextual subgroup, hippocampal heavy synaptosomes in the total group and the cued subgroup). Selective activation of mChAT in vitro was shown under conditions of impaired ionic balance such as an accumulation of $[Ca^{2+}]_i$ and $[Zn^{2+}]_i$ [55, 56]. It was revealed that $[Zn^{2+}]_i$ precedes $[Ca^{2+}]_i$ accumulation [56] and $[Ca^{2+}]_i$ in turn results in the functional hyperactivation

and swelling of synapses [53, 57, 58]. According to data in vitro activation of cChAT reflect cholinergic hyperfunction under normal ionic and metabolic conditions [49, 59, 60]. cChAT activation under ischemic pathology did not describe in the literature. Therefore, we suppose that the activation of cChAT reflected synaptogenesis, in agreement with other researchers [3].

Thus, chronic brain ischaemia for 11–14 days resulted in a complex reorganization of the cortical and hippocampal synaptic pool which involved synaptogenesis or hyperfunctions in the unbalanced ionic conditions of one of the cholinergic synaptic populations and degeneration or dysfunction of the others. We supposed that all of the cholinergic processes revealed under 2VO conditions were present in both cholinergic subgroups of the rats but with different intensities (see Figure 2-all rats, contextual and cued). We also supposed that the variety of cholinergic reactions was revealed by the phenotypical variety of the outbred rats and it was useful for understanding some of the principles of the organization of different forms of cognition.

4.2. Cholinergic Composition of the Forms of Cognition in the Normal and 2VO Conditions. The second purpose of our research was a comparative analysis of the behavioural and biochemical parameters for identification of the cholinergic composition of the investigated cognitive functions under normal and 2VO conditions. In the first place it is necessary to note that the results of this research confirmed and expanded the knowledge about cholinergic mechanisms of cognitive functions under normal brain conditions. Our data showed the active involvement of cholinergic projective systems and also regional ones of the cortex and the hippocampus in cognitive processes. Cholinergic synaptic connections with the investigated cognitive functions revealed under normal conditions indicate that each form of cognition has an individual cholinergic synaptic and probably receptor compositions. This conclusion is conformed to the results of investigations, obtained in the Morris water maze and some other behavioural models [34–37].

Then, the data showed the participation of the cholinergic systems not only in mechanisms of learning and working memory, which was repeatedly observed in previous studies [3–5, 45, 61], but also in mechanisms of the inherited abilities and long-term memory.

Our "inherited abilities" in the contextual task in the Morris water maze was firstly detected by R G Morris and U Frey as a distinct type of memory and termed as "rapid one-trial memory" [62, 63]. We suppose that this function can be inherited. It seems the problem of future discussions. Our data, concerning individual cholinergic organisation of function support contextual inherited abilities as a distinct form of cognition. Morris and Frey observed that allocentric spatial learning can sometimes occur in one trial. Our data concerning the same cholinergic structures associated with inherited abilities 1s2 and long-term memory 3s1 also testify to possible tight interaction between these two forms of cognition.

The involvement of cholinergic projective systems in mechanisms of the long-term memory is usually denied [64–67], and was only discussed in a few studies [36, 68, 69]. Our data confirmed that synaptic populations of cholinergic projective neurons and of the interneurons of the cortex and the hippocampus can have positive and negative connections with cognitive functions. A negative dependence of cognitive functions on cholinergic cortical efficiency was also revealed earlier in cats using a similar methodology for researching the cholinergic synaptic organization of cognitive functions [29]. Therefore, our data demonstrate that the cholinergic mechanisms of learning and memory are more complex than currently perceived. It is evident that this can complicate the detection of cholinergic effects on some cognitive functions by means of nonselective influences on cholinergic efficiency. For example, according to our data in the contextual model, the nonselective pharmacological cholinergic means as well as use of different methods of degeneration of the cholinergic projective systems would certainly have revealed the participation of the cholinergic projective systems in learning 2s2–4 and 3s2–4, but it would probably have concealed a cholinergic participation in the mechanisms of the inherited abilities, the long-term and the working memory. Such results would correspond to the data in the literature [62, 63, 68, 70].

From the numerous data in the literature, preservation of the cholinergic projective systems is critical for the success of cognitive processes, and it was thought that cholinergic dysfunction or degeneration results in the impairment of memory in neurodegenerative diseases of different aetiologies. Therefore, we analyzed the connections between reorganization of the cholinergic synaptic pool and impairment of learning and memory under 2VO conditions. The comparative analysis showed that the connections between the functional and cholinergic parameters revealed under normal conditions were practically lost in the ischemic rats. In our research, only impairment of cued long-term memory 2s1 was really dependent on degeneration of the key synaptic population of the cholinergic cortical interneurons, and also, probably, the intact cued memory 3s1 by the unchanged key synaptic population of the cholinergic cortical projective neurons. At the same time, our data also showed different cholinergic compositions of the cognitive functions under 2VO and under normal conditions in as the spatial contextual and the spatial cued models. Under 2VO conditions, most connections of the investigated functions with cholinergic synaptic populations revealed under normal conditions disappeared and new connections with other cholinergic synaptic populations arose. The quantity of cholinergic synaptic populations, involving in mechanisms of the investigated cognitive functions, was considerable reduced. Furthermore, cholinergic connections in general disappeared from the mechanisms of the following forms of cognition: inherited abilities 1s2, learning 2s2–4 and long-term memory 3s1 in the contextual model, and long-term memory 2s1 and 3s1 in the cued model. Moreover, brain region specializations of both the contextual and the cued functions were changed. Cortical cholinergic influences had been completely removed from the contextual functions and hippocampal ones from the cued functions. All considerable differences between cholinergic organisation of the cognitive

functions in the normal and 2VO conditions stated above are clear demonstrated in Figure 3. It is important that a consistency between the performances of cognitive functions and their new key cholinergic synaptic populations was found in the majority of the remaining cholinergic-dependent functions under 2VO conditions (from four to six functions).

Thus, according to our data, we suggest that the normal cholinergic synaptic connections in learning and memory were progressively reduced and changed during chronic ischaemia. It seems that any neurodegenerative pathology undergoes the same processes. It is known that anticholinesterase drugs are only effective in the early stages of Alzheimer's disease (early and mild Alzheimer's disease). It can be noted that the new cholinergic connections with the cognitive functions were not necessarily a consequence of degeneration or dysfunctions in the key cholinergic synaptic populations (it was evident for contextual learning in 3s2–4 and long-term memory in 2s1, that is, these new links could arise by other, indirect reasons). The dependence on the inclusion of cholinergic links in the realization of cognitive functions from the functional background of neuronal environments was recently revealed [64]. This corresponds with the theory by D. A. Sakharov about the nonsynaptic transfer of chemical information [71, 72]. According to this theory, any change in any functional system results in a change in all systems as a result of the change in neuroactive compounds of intercellular environments (the matrix). The changes in the matrix determine the activation of one or another neuronal ensemble which finally determines the behavioural act. From all of these viewpoints, it seems that the main value for cognitive functions is its receptor composition and its change in neurodegenerative pathology. Our data concerning the different consequences on the learning performance under normal and 2VO conditions by the action of RJR and mecamilamine on the same subtypes of nAChR testify to this version.

5. Conclusions

It seems that the reasons for changes in the cholinergic organization of cognitive functions in an ischaemic pathology can be any neurodegenerative or, on the contrary, reparative process (sprouting) of cholinergic and noncholinergic synaptic populations. In spite of the brain reparative potentials, the cholinergic and the whole neurochemical organization of cognitive functions under the chronic actions of pathological factors will be formed as optimally as possible under the new conditions. Pathological conditions essentially differ from natural ones. A new organization of cognitive functions will be constructed on neuronal elements which are stable against pathological influences. This new organization can provide an optimum realization of some cognitive functions but not of others. In any case, the study of new key neurochemical links in the organization of cognitive functions may be promising. The plasticity of neurochemical links in the individual organization of certain types of cognition can be used in the future for alternative corrections of vascular and other degenerative dementia.

Acknowledgments

The authors would like to thank RFBR for support at sources of this research (the Grants [1]98-04-48959 and 01-04-49286). Also the authors thank Dr. M.V. Rayevskaya (Independent Scientific Researcher/Consultant, Philadelphia, PA, USA) for careful reading, revision, and constructive suggestions.

References

[1] G. C. Román and R. N. Kalaria, "Vascular determinants of cholinergic deficits in Alzheimer disease and vascular dementia," *Neurobiology of Aging*, vol. 27, no. 12, pp. 1769–1785, 2006.

[2] G. M. McKhann and O. A. Selnes, "Vascular cognitive change: perspective from neurology," *Alzheimer's and Dementia*, vol. 3, no. 2, pp. S23–S29, 2007.

[3] E. J. Mufson, S. E. Counts, S. E. Perez, and S. D. Ginsberg, "Cholinergic system during the progression of Alzheimer's disease: therapeutic implications," *Expert Review of Neurotherapeutics*, vol. 8, no. 11, pp. 1703–1718, 2008.

[4] J. W. Ni, K. Matsumoto, H. B. Li, Y. Murakami, and H. Watanabe, "Neuronal damage and decrease of central acetylcholine level following permanent occlusion of bilateral common carotid arteries in rat," *Brain Research*, vol. 673, no. 2, pp. 290–296, 1995.

[5] H. Watanabe, J. -W. Ni, Y. Sakai, K. Matsumoto, Y. Murakami, and M. Tohda, "Permanent occlusion of bilateral internal carotid arteries produces cognitive deficits in two learning behavior tasks," *Nihon Shinkei Seishin Yakurigaku Zasshi*, vol. 16, no. 1, pp. 19–24, 1996.

[6] K. I. Tanaka, N. Wada, K. Hori, M. Asanuma, M. Nomura, and N. Ogawa, "Chronic cerebral hypoperfusion disrupts discriminative behavior in acquired-learning rats," *Journal of Neuroscience Methods*, vol. 84, no. 1-2, pp. 63–68, 1998.

[7] T. Watanabe, K. Iwasaki, S. Ishikane et al., "Spatial memory impairment without apoptosis induced by the combination of beta-amyloid oligomers and cerebral ischemia is related to decreased acetylcholine release in rats," *Journal of Pharmacological Sciences*, vol. 106, no. 1, pp. 84–91, 2008.

[8] Z. I. Storozheva, A. T. Proshin, V. V. Sherstnev et al., "Dicholine salt of succinic acid, a neuronal insulin sensitizer, ameliorates cognitive deficits in rodent models of normal aging, chronic cerebral hypoperfusion, and beta-amyloid peptide-(25-35)-induced amnesia," *BMC Pharmacology*, vol. 8, article no. 1, 2008.

[9] N. Ogawa, K. Haba, M. Asanuma, K. Mizukava, and A. Mori, "Super-delayed changes of muscarinic acetylcholine receptors in the gerbil hippocampus following transient ischemia," in *Neuroreceptor Mechanisms in Brain*, S e.a. Kito, Ed., pp. 343–347, Plenum Press, New York, NY, USA, 1991.

[10] K. Iwasaki, Y. Kitamura, Y. Ohgami, K. Mishima, and M. Fujiwara, "The disruption of spatial cognition and changes in brain amino acid, monoamine and acetylcholine in rats with transient cerebral ischemia," *Brain Research*, vol. 709, no. 2, pp. 163–172, 1996.

[11] P. Lipton, "Ischemic cell death in brain neurons," *Physiological Reviews*, vol. 79, no. 4, pp. 1431–1568, 1999.

[12] M. W. Riepe, "Cholinergic treatment: what are the early neuropathological targets?" *European Journal of Neurology*, vol. 12, supplement 3, pp. 3–9, 2005.

[13] M. O'Neill, M. Canney, B. Earley, J. L. Junien, and B. E. Leonard, "The novel σ ligand JO 1994 protects against ischaemia-induced behavioural changes, cell death and receptor dysfunction in the gerbil," *Neurochemistry International*, vol. 28, no. 2, pp. 193–207, 1996.

[14] H. Ishimaru, A. Takahashi, Y. Ikarashi, and Y. Maruyama, "NGF delays rather than prevents the cholinergic terminal damage and delayed neuronal death in the hippocampus after ischemia," *Brain Research*, vol. 789, no. 2, pp. 194–200, 1998.

[15] H. Onodera, G. Sato, and K. Kogure, "Quantitative autoradiographic analysis of muscarinic cholinergic and adenosine A_1 binding sites after transient forebrain ischemia in the gerbil," *Brain Research*, vol. 415, no. 2, pp. 309–322, 1987.

[16] D. Ji and J. A. Dani, "Inhibition and disinhibition of pyramidal neurons by activation of nicotinic receptors on hippocampal interneurons," *Journal of Neurophysiology*, vol. 83, no. 5, pp. 2682–2690, 2000.

[17] M. Alkondon and E. X. Albuquerque, "Nicotinic acetylcholine receptor $\alpha 7$ and $\alpha 4\beta 2$ subtypes differentially control GABAergic input to CA1 neurons in rat hippocampus," *Journal of Neurophysiology*, vol. 86, no. 6, pp. 3043–3055, 2001.

[18] E. X. Albuquerque, E. F. R. Pereira, M. Alkondon, and S. W. Rogers, "Mammalian nicotinic acetylcholine receptors: from structure to function," *Physiological Reviews*, vol. 89, no. 1, pp. 73–120, 2009.

[19] A. V. Buhler and T. V. Dunwiddie, "$\alpha 7$ nicotinic acetylcholine receptors on GABAergic interneurons evoke dendritic and somatic inhibition of hippocampal neurons," *Journal of Neurophysiology*, vol. 87, no. 1, pp. 548–557, 2002.

[20] J. T. Porter, B. Cauli, K. Tsuzuki, B. Lambolez, J. Rossier, and E. Audinat, "Selective excitation of subtypes of neocortical interneurons by nicotinic receptors," *Journal of Neuroscience*, vol. 19, no. 13, pp. 5228–5235, 1999.

[21] S. N. Sudweeks and J. L. Yakel, "Functional and molecular characterization of neuronal nicotinic ACh receptors in rat CA1 hippocampal neurons," *Journal of Physiology*, vol. 527, no. 3, pp. 515–528, 2000.

[22] K. J. Anderson, R. B. Gibbs, P. M. Salvaterra, and C. W. Cotman, "Ultrastructural characterization of identified cholinergic neurons transplanted to the hippocampal formation of the rat," *Journal of Comparative Neurology*, vol. 249, no. 2, pp. 279–292, 1986.

[23] P. E. Batchelor, D. M. Armstrong, S. N. Blaker, and F. H. Gage, "Nerve growth factor receptor and choline acetyltransferase colocalization in neurons within the rat forebrain: response to fimbria-fornix transection," *Journal of Comparative Neurology*, vol. 284, no. 2, pp. 187–204, 1989.

[24] F. P. Eckenstein, R. W. Baughman, and J. Quinn, "An anatomical study of cholinergic innervation in rat cerebral cortex," *Neuroscience*, vol. 25, no. 2, pp. 457–474, 1988.

[25] M. Frotscher, I. Vida, and R. Bender, "Evidence for the existence of non-GABAergic, cholinergic interneurons in the rodent hippocampus," *Neuroscience*, vol. 96, no. 1, pp. 27–31, 2000.

[26] C. R. Houser, G. D. Crawford, P. M. Salvaterra, and J. E. Vaughn, "Immunocytochemical localization of choline acetyltransferase in rat cerebral cortex: a study of cholinergic neurons and synapses," *Journal of Comparative Neurology*, vol. 234, no. 1, pp. 17–34, 1985.

[27] N. J. Woolf, "Cholinergic systems in mammalian brain and spinal cord," *Progress in Neurobiology*, vol. 37, no. 6, pp. 475–524, 1991.

[28] M. N. Rossor, C. Svendsen, and S. P. Hunt, "The substantia innominata in Alzheimer's disease: an histochemical study of cholinergic marker enzymes," *Neuroscience Letters*, vol. 28, no. 2, pp. 217–222, 1982.

[29] E. I. Mukhin, E. I. Zakharova, and E. A. Kikteva, "Comparison of the cholinergic system in neocortical field Ep in cats with strong and weak cognitive abilities," *Neuroscience and Behavioral Physiology*, vol. 32, no. 4, pp. 379–387, 2002.

[30] E. I. Zakharova, A. M. Dudchenko, M. M. Svinov, D. S. Ivanov, and I. V. Ignatiev, "Comparative characteristics of the cholinergic systems in the brain of rats with the low and high resistance to the oxygen deficient," *Neurokhimia (Mosk)*, vol. 18, no. 2, pp. 119–131, 2001 (Russian).

[31] E. I. Zakharova, A. M. Dudchenko, M. M. Svinov, M. M. Fedorova, and E. L. Germanova, "Cholinergic systems of the rat brain and neuronal reorganization under conditions of acute hypoxia," *Neurochemical Journal*, vol. 4, no. 4, pp. 290–303, 2010.

[32] C. B. Saper, "Organization of cerebral cortical afferent systems in the rat. II. Magnocellular basal nucleus," *Journal of Comparative Neurology*, vol. 222, no. 3, pp. 313–342, 1984.

[33] E. I. Zakharova, Z. I. Storojeva, E. L. Germanova et al., "Characteristics of cholinergic and cognitive functions in rats with individual resistance to the cerebral ischemia," in *Adaptation Biology and Medicine*, L. Lukyanova, N. Takeda, and P. K. Singal, Eds., vol. 5 of *Health Potentials*, pp. 121–141, Narosa Publishing House, New Delhi, India, 2008.

[34] I. Izquierdo, J. H. Medina, L. A. Izquierdo, D. M. Barros, M. M. de Souza, and T. Mello e Souza, "Short- and long-term memory are differentially regulated by monoaminergic systems in the rat brain," *Neurobiology of Learning and Memory*, vol. 69, no. 3, pp. 219–224, 1998.

[35] I. Izquierdo, L. A. Izquierdo, D. M. Barros et al., "Differential involvement of cortical receptor mechanisms in working, short-term and long-term memory," *Behavioural Pharmacology*, vol. 9, no. 5-6, pp. 421–427, 1998.

[36] D. M. Barros, P. Pereira, J. H. Medina, and I. Izquierdo, "Modulation of working memory and of long- but not short-term memory by cholinergic mechanisms in the basolateral amygdala," *Behavioural Pharmacology*, vol. 13, no. 2, pp. 163–167, 2002.

[37] R. W. Brown, K. S. Beale, and G. D. Jay Frye, "Mecamylamine blocks enhancement of reference memory but not working memory produced by post-training injection of nicotine in rats tested on the radial arm maze," *Behavioural Brain Research*, vol. 134, no. 1-2, pp. 259–265, 2002.

[38] R. Morris, "Developments of a water-maze procedure for studying spatial learning in the rat," *Journal of Neuroscience Methods*, vol. 11, no. 1, pp. 47–60, 1984.

[39] N. N. Bogolepov, E. L. Dovedova, E. I. Orlova, and N. I. Yakovleva, "Ultrastructural and biochemical characterization of the subfractions of synaptic membranes isolated from light and heavy synaptosomes of the brain," *Arkhiv Anatomii*, vol. 89, no. 11, pp. 88–94, 1985 (Russian).

[40] E. De Robertis, A. Pellegrino De Iraldi, G. Rodrigues De Lores Arnaiz, and L. Salganicoff, "Cholinergic and non-cholinergic nerve endings in rat brain. I. Isolation and subcellular distribution of acetylcholine and acetylcholinesterase," *Journal of Neurochemistry*, vol. 9, pp. 23–35, 1962.

[41] C. W. Cotman and D. A. Matthews, "Synaptic plasma membranes from rat brain synaptosomes: Isolation and partial characterization," *Biochimica et Biophysica Acta*, vol. 249, no. 2, pp. 380–394, 1971.

[42] F. Fonnum, "Radiochemical micro assays for the determination of choline acetyltransferase and acetylcholinesterase activities," *Biochemical Journal*, vol. 115, no. 3, pp. 465–472, 1969.

[43] O. H. Lowry, N. J. Rosenbrough, A. L. Farr, and R. J. Randall, "Protein measurement with the Folin phenol reagent," *The Journal of Biological Chemistry*, vol. 193, no. 1, pp. 265–275, 1951.

[44] A. I. Kobzar', *Applied Mathematical Statistics. For Engineers and Scientists*, Physmatlit, Moscow, Russia, 2006.

[45] H. Higashi, J. R. Meno, A. S. Marwaha, and H. R. Winn, "Hippocampal injury and neurobehavioral deficits following hyperglycemic cerebral ischemia: effect of theophylline and ZM 241385," *Journal of Neurosurgery*, vol. 96, no. 1, pp. 117–126, 2002.

[46] M. Amano, T. Hasegawa, and T. Nabeshima, "Characteristics of transient cerebral ischemia-induced deficits on various learning and memory tasks in male Mongolian gerbils," *Japanese Journal of Pharmacology*, vol. 63, no. 4, pp. 469–477, 1993.

[47] T. Taguchi, N. Takagi, K. Miyake et al., "Effects of naftidrofuryl oxalate on microsphere-induced changes in acetylcholine and amino acid content of rat brain regions," *Experimental Brain Research*, vol. 99, no. 1, pp. 7–16, 1994.

[48] T. Bueters, M. von Euler, O. Bendel, and G. von Euler, "Degeneration of newly formed CA1 neurons following global ischemia in the rat," *Experimental Neurology*, vol. 209, no. 1, pp. 114–124, 2008.

[49] DI. Sha, H. Jin, R. D. Kopke, and J. Y. Wu, "Choline acetyltransferase: regulation and coupling with protein kinase and vesicular acetylcholine transporter on synaptic vesicles," *Neurochemical Research*, vol. 29, no. 1, pp. 199–207, 2004.

[50] R. J. Rylett, "Synaptosomal "membrane-bound" choline acetyltransferase is most sensitive to inhibition by choline mustard," *Journal of Neurochemistry*, vol. 52, no. 3, pp. 869–875, 1989.

[51] E. I. Maevsky, A. S. Rozenfeld, E. V. Grishina, and M. N. Kondrashova, *Correction of the Metabolic Acidose by Maintenance of the Mitochondrial Functions*, ONTI, Pushino, Russia, 2001.

[52] V. V. Belousova, A. M. Dudchenko, and L. D. Lukyanova, "Relationship between energy consumption and synthesis in rat hepatocytes in various O2-deficiency regimens," *Biulleten Eksperimentalnoi Biologii I Meditsiny*, vol. 114, no. 12, pp. 588–590, 1992 (Russian).

[53] V. V. Semchenko, N. N. Bogolepov, S. S. Stepanov, S. V. Maksimishin, and A. S. Khizhnyak, "Synaptic plasticity of the neocortex of white rats with diffuse-focal brain injuries," *Neuroscience and Behavioral Physiology*, vol. 36, no. 6, pp. 613–618, 2006.

[54] M. K. Sun, J. Hongpaisan, T. J. Nelson, and D. L. Alkon, "Poststroke neuronal rescue and synaptogenesis mediated in vivo by protein kinase C in adult brains," *Proceedings of the National Academy of Sciences of the United States of America*, vol. 105, no. 36, pp. 13620–13625, 2008.

[55] L. K. Smith and P. T. Carroll, "Membrane-bound choline-O-acetyltransferase in rat hippocampal tissue is anchored by glycosyl-phosphatidylinositol," *Brain Research*, vol. 605, no. 1, pp. 155–163, 1993.

[56] Y. V. Medvedeva, B. Lin, C. W. Shuttleworth, and J. H. Weiss, "Intracellular Zn^{2+} accumulation contributes to synaptic failure, mitochondrial depolarization, and cell death in an acute slice oxygen-glucose deprivation model of ischemia," *Journal of Neuroscience*, vol. 29, no. 4, pp. 1105–1114, 2009.

[57] D. Uematsu, J. H. Greenberg, M. Reivich, and A. Karp, "In vivo measurement of cytosolic free calcium during cerebral ischemia and reperfusion," *Annals of Neurology*, vol. 24, no. 3, pp. 420–428, 1988.

[58] N. R. Sims, "Calcium, energy metabolism and the development of selective neuronal loss following short-term cerebral ischemia," *Metabolic Brain Disease*, vol. 10, no. 3, pp. 191–217, 1995.

[59] T. Dobransky, W. L. Davis, G. H. Xiao, and R. J. Rylett, "Expression, purification and characterization of recombinant human choline acetyltransferase: phosphorylation of the enzyme regulates catalytic activity," *Biochemical Journal*, vol. 349, no. 1, pp. 141–151, 2000.

[60] T. Dobransky, W. L. Davis, and R. J. Rylett, "Functional characterization of phosphorylation of 69-kDa human choline acetyltransferase at serine 440 by protein kinase C," *Journal of Biological Chemistry*, vol. 276, no. 25, pp. 22244–22250, 2001.

[61] D. C. Rogers and A. J. Hunter, "Photothrombotic lesions of the rat cortex impair acquisition of the water maze," *Pharmacology Biochemistry and Behavior*, vol. 56, no. 4, pp. 747–754, 1997.

[62] R. G. M. Morris, "Hippocampal synaptic plasticity: role in spatial learning or the automatic recording of attended experience?" *Philosophical Transactions of the Royal Society B*, vol. 352, no. 1360, pp. 1489–1503, 1997.

[63] L. A. Feldman, M. L. Shapiro, and J. Nalbantoglu, "A novel, rapidly acquired, and persistent spatial memory task that induces immediate early gene expression," *Behavioral and Brain Functions*, vol. 6, article 35, 2010.

[64] L. A. B. Wisman, G. Sahin, M. Maingay, G. Leanza, and D. Kirik, "Functional convergence of dopaminergic and cholinergic input is critical for hippocampus-dependent working memory," *Journal of Neuroscience*, vol. 28, no. 31, pp. 7797–7807, 2008.

[65] B. Lee, I. Shim, H. Lee, and D. H. Hahm, "Effect of Bupleurum falcatum on the stress-induced impairment of spatial working memory in rats," *Biological and Pharmaceutical Bulletin*, vol. 32, no. 8, pp. 1392–1398, 2009.

[66] F. Casamenti, L. Bracco, L. Bartolini, and G. Pepeu, "Effects of ganglioside treatment in rats with a lesion of the cholinergic forebrain nuclei," *Brain Research*, vol. 338, no. 1, pp. 45–52, 1985.

[67] G. Wenk, J. Sweeney, and D. Hughey, "Cholinergic function and memory: extensive inhibition of choline acetyltransferase fails to impair radial maze performance in rats," *Pharmacology Biochemistry and Behavior*, vol. 25, no. 3, pp. 521–526, 1986.

[68] J. A. Vuckovich, M. F. Semel, and M. G. Baxter, "Extensive lesions of cholinergic basal forebrain neurons do not impair spatial working memory," *Learning and Memory*, vol. 11, no. 1, pp. 87–94, 2004.

[69] B Lee, E. J. Choi, E. J. Lee et al., "The neuroprotective effect of methanol extract of gagamjungjihwan and fructus euodiae on ischemia-induced neuronal and cognitive impairment in the rat," *Evidence-Based Complementary and Alternative Medicine*. In press.

[70] B. M. De Castro, G. S. Pereira, V. Magalhães et al., "Reduced expression of the vesicular acetylcholine transporter causes learning deficits in mice," *Genes, Brain and Behavior*, vol. 8, no. 1, pp. 23–35, 2009.

[71] D. A. Sakharov, "The multiplicity of neurotransmitters: the functional significance," *Zhurnal Evolyutsionnoi Biokhimii i Fiziologii*, vol. 26, no. 5, pp. 733–741, 1990 (Russian).

[72] V. E. Dyakonova, I. A. Chistopolsky, T. L. Dyakonova, D. D. Vorontsov, and D. A. Sakharov, "Direct and decarboxylation-dependent effects of neurotransmitter precursors on firing of isolated monoaminergic neurons," *Journal of Comparative Physiology A*, vol. 195, no. 6, pp. 515–527, 2009.

SAGE-Hindawi Access to Research
International Journal of Alzheimer's Disease
Volume 2010, Article ID 864625, 13 pages
doi:10.4061/2010/864625

Research Article

Ablation of the Locus Coeruleus Increases Oxidative Stress in Tg-2576 Transgenic but Not Wild-Type Mice

Orest Hurko,[1,2] Kurt Boudonck,[3,4] Cathleen Gonzales,[5] Zoe A. Hughes,[5] J. Steve Jacobsen,[6] Peter H. Reinhart,[6,7] and Daniel Crowther[8]

[1] *Biologics Consulting Group, Inc., 400 N. Washington Street, Suite 100, Alexandria, VA 22314, USA*
[2] *Department of Medicine, Nursing, and Dentistry, University of Dundee, Nethergate, Dundee DD1 4HN, UK*
[3] *Metabolon Inc., 800 Capitola Drive, Suite 1, Durham, NC 27713-4385, USA*
[4] *Bayer Cropscience, 3500 Paramount Parkway Morrisville, NC 27560-7218, USA*
[5] *Pfizer, 558 Eastern Point Road Groton, CT 06340-5196, USA*
[6] *Proteostasis Therapeutics, 200 Technology Square, Suite 402, Boston, MA 02139, USA*
[7] *Department of Neuroscience, Duke University, Durham, NC 27708, USA*
[8] *Pfizer, Translational Medicine Research Collaboration, Dundee DD1 9SY, UK*

Correspondence should be addressed to Orest Hurko, orest.hurko@gmail.com

Received 24 May 2010; Revised 23 August 2010; Accepted 3 September 2010

Academic Editor: Gemma Casadesus

Mice transgenic for production of excessive or mutant forms of beta-amyloid differ from patients with Alzheimer's disease in the degree of inflammation, oxidative damage, and alteration of intermediary metabolism, as well as the paucity or absence of neuronal atrophy and cognitive impairment. Previous observers have suggested that differences in inflammatory response reflect a discrepancy in the state of the locus coeruleus (LC), loss of which is an early change in Alzheimer's disease but which is preserved in the transgenic mice. In this paper, we extend these observations by examining the effects of the LC on markers of oxidative stress and intermediary metabolism. We compare four groups: wild-type or Tg2576 Aβ transgenic mice injected with DSP4 or vehicle. Of greatest interest were metabolites different between ablated and intact transgenics, but not between ablated and intact wild-type animals. The Tg2576_DSP4 mice were distinguished from the other three groups by oxidative stress and altered energy metabolism. These observations provide further support for the hypothesis that Tg2576 Aβ transgenic mice with this ablation may be a more congruent model of Alzheimer's disease than are transgenics with an intact LC.

1. Introduction

The degree of congruence between animal models and human disease is likely to be a measure of how faithfully preclinical compound validation will translate into efficacy in the clinic. Both academic and industrial laboratories have made major investments in investigations of putative disease-modifying treatments for Alzheimer's disease, relying on various mouse models transgenic for structural variants or elevated quantities of beta-amyloid. Among them are the Tg2576 mice which express the Swedish mutation of APP ($APP_{K670N, M671L}$) [1], which is the focus of this study. This mutation causes increases in secreted Aβ1-40 and Aβ1-42 [2, 3]. Although this and other transgenic models reproducibly lead to pathological accumulations of beta-amyloid, they poorly mimic several key pathologic features of human Alzheimer's disease: gross brain atrophy and profound dementia [4]. This incongruence may compromise their utility for validation for putative disease-modifying treatments, particularly those directed not on amyloid accumulation, but on downstream pathophysiology.

Several lines of evidence indicate that features other than amyloid may also play critical roles in the pathological cascade leading to the severe brain atrophy and progressive dementia that are the ultimate clinical concern in nonmendelian Senile Dementia of the Alzheimer Type (SDAT), which in the last decade has come to be called Alzheimer disease (AD), as it will be referred to in this

paper. The most compelling come from two independent prospective observational studies: the Religious Orders study in Kentucky and the adjacent Midwest [5, 6] and the similar, MRC Cognitive Function and Ageing Study (CFAS) [7]. In both studies, subjects were assessed periodically for cognitive ability and after death, their brains were examined. In both studies, the relationship between amyloid burden and cognitive impairment was complex. There were many individuals whose total burden of amyloid pathology was incongruent with their normal cognitive status, even when all pathologies were considered in a multivariable model of dementia risk factors. These observations suggested that a congruent rodent model of AD also requires more than just alterations of amyloid.

Although not understood completely, two biochemical features of AD are oxidative damage [8–22] and inflammation [23]. Although these are prominent in AD, they are variable in amyloid transgenic mice [24–29]. Another change in human AD—but also absent or minor in transgenic rodents—is early degeneration of the locus coeruleus (LC) [30–41]. Work by Heneka et al. [42–45] suggested that there may be a link between loss of the noradrenergic LC and inflammatory changes in AD. The purpose of the experiments described in this paper was to determine if there is a similar link with oxidative stress and other metabolic changes.

The LC is a midline brainstem nucleus that is the origin of a widely projecting noradrenergic system, the major site of norepinephrine synthesis in the brain that projects widely to the neocortex and the hippocampus with terminals on neurons, glia, and blood vessels [46]. Loss of noradrenergic cells of the LC is an early event in human AD, comparable to the more widely recognized loss of cells from the cholinergic midline projection system originating in the substantia innominata [40].

Heneka et al. [42] injected wild-type adult rats with DSP4 [47, 48] to eliminate noradrenergic LC neurons and then challenged with intracortical injections of Aβ. The ablated rats showed greater induction of inflammatory nitric oxide synthase, interleukin 1β, and IL-6 expression in response to injection with Aβ than did control animals in which the LC had been left intact. This demonstrated that LC loss in the rats augments inflammatory responses to Aβ. In a followup study, APP23 transgenic mice overexpressing Aβ were injected with DSP4 to selectively destroy noradrenergic neurons in the LC as a model for Alzheimer's disease [45], with similar increases in inflammatory response. These observations invited our hypothesis that LC loss in AD might be permissive not only for increased inflammation but also for potentiation of oxidative stress.

The specific goals of the current study were to determine if the same ablative procedure of the LC with DSP4 in Tg2576 mice would significantly alter other metabolic pathways that are not affected by transgenesis for amyloid in mice with an intact LC and to determine if such alterations are typical of human AD. Furthermore, we were interested in determining only those metabolic changes resulting from this ablation that were also dependent on transgenesis for amyloid and were not simply nonspecific consequences of treatment with DSP4 in control wild-type mice.

To ensure a comprehensive unbiased survey, we chose to perform a metabolomic analysis. Metabolomics has attracted increasing interest in the field of disease research, since it has proven to be a fast and reproducible method directly reflecting biological events. Metabolomics involves the determination of changes in the levels of endogenous or exogenous metabolites in biological samples, in response to a perturbation such as disease, drug, or toxin. In the present study, we used a combination of gas chromatography/mass spectrometry (GC/MS) and liquid chromatography/mass spectrometry (LC/MS) to monitor the biochemical changes associated with a transgenic murine model system for Alzheimer's disease. This global metabolite profiling allows the measurement of low molecular weight biochemicals including lipids, sugars, nucleotides, organic acids, amino acids, vitamins, cofactors, small peptides, and xenobiotics.

2. Materials and Methods

2.1. Neurochemical Analysis of Brain Tissue. DSP4 (50 mg/kg in PBS, $N = 5$) or PBS (vehicle, $N = 5$) was administered intraperitoneally to C57BL/6SJL mice on days 1 and 7. Mice were sacrificed 7 days following the second injection (day 14). Mice were euthanized by exposure to CO_2 and the brains removed. Frontal cortex tissue was dissected on ice and frozen on dry ice for subsequent analysis of monoamine concentration. Frozen tissue samples were weighed and perchloric acid (0.4 M) added at 10 μL/mg tissue. Samples were made homogeneous using a sonicating probe. Samples were then centrifuged at 15 000 rpm for 20 min and the supernatant removed. The supernatant was then centrifuged in a filtered tube at 3000 rpm for 5 min. This supernatant was then diluted 1 in 100 for measurement of dopamine and 1 in 10 for measurement of DOPAC and HVA. Supernatant was analyzed for neurochemical content using HPLC-ECD. Chromatographic separations were performed using reverse phase HPLC (C18 ODS3 column, 150 × 3.0 mm, Metachem, Torrance, CA, USA). The mobile phase comprised: 0.15 M NaH_2PO_4, 0.25 mM EDTA, 1.75 mM 1-octane sulphonic acid, 2% isopropanol and 4% methanol, pH = 4.6 and delivered at 0.5 mL/min at 30°C. Dopamine and metabolites were detected using an electrochemical amperometric detector (Decade, Antec-Leyden, NL) with a working electrode set at +650 mV versus Ag/AgCl reference electrode.

2.2. Preparation of Mice for Spectroscopic Analyses. A total of 120 samples from mice were used in this study, comprising 4 sets of 23 week old animals ($n = 10$/group): either wild-type or Tg2576 Aβ transgenics which express the Swedish mutation ($APP_{K670N, M671L}$) of the amyloid protein precursor (APP) [1]. Each 23 week-old animal was injected intraperitoneally on day 1, (5 weeks prior to harvest) with either vehicle (PBS) or DSP4 (N-(2-chloroethyl)-N-ethyl-2-bromobenzylamine, Sigma C-8417), a selective neurotoxin for noradrenergic neurons [47, 48] dissolved in PBS. Each animal was injected intraperitoneally with a volume of

5 mL/kg. An identical injection was given to each animal 7 days later (on day 8) when animals were 24 weeks old. Four weeks after the second injection, the mice were anesthetized with 3% isoflurane and plasma, CSF, and brains (40 samples each) were harvested for metabolite profiling, as described below.

2.3. Sample Collection for Spectroscopic Analyses. Approximately 7 microliters of CSF was collected from each mouse *via* the cisterna magna and visually inspected for the presence of blood. Any sample that was contaminated with blood was removed from the study. The collected CSF was immediately frozen on dry ice. For the collection of plasma, the chest cavity was opened and approximately 0.3 mL of blood was collected via cardiac puncture into EDTA tubes and the mice were euthanized by exsanguination. The blood samples were centrifuged to separate plasma. The plasma was collected and immediately frozen on dry ice. Brains were extracted from the skull and frozen on dry ice. For these brain samples, the cerebellum was left intact.

The plasma (100 μL), CSF (approximately 7 μL) and brain samples (half brain, 150 mg) were extracted according to Metabolon's standard protocol, which uses a series of proprietary solvent extractions designed to remove protein and dislodge any small molecules bound to protein or physically trapped in the precipitated protein matrix. Each solvent extraction step was performed by shaking for two minutes in the presence of glass beads using a Glen Mills Genogrinder 2000. After each extraction the sample was centrifuged and the supernatant removed using the MicroLab STAR robotics system, followed by re-extraction of the pellet in subsequent steps. The multiple extract supernatants were pooled and then split into equal parts for analysis on the GC/MS and LC/MS platforms. Further details on Metabolon's extraction procedures and metabolic profiling platform can be found in Boudonck et al. [49, 50] and Evans et al. [51].

2.4. Data Collection and Quality Control. The data were collected over two platform day runs each for plasma, CSF, and brain matrix. Each day consisted of 19 or 20 study samples, with samples from the different treatment groups equally distributed among the days, then randomized. Two brain samples did not pass QC inspection and were omitted from the study. Approximately 30% of process samples were dedicated to QC. In addition to the study samples, pooled samples of homogenized plasma, CSF, and brain tissue were extracted four independent times per day. These samples (CMTRX) served as technical replicates throughout the data set to assess process variability. Also, 100 μL of water was extracted five independent times per day to serve as process blanks. Every sample analyzed was spiked with standards to monitor and evaluate instrument and extraction performance [49].

2.5. Data Normalization. Raw area counts for each metabolite in each sample were normalized to correct for variation resulting from instrument interday tuning differences [49]. For each metabolite, the area counts were divided by its median value for each run day, therefore setting the medians equal to 1 for each day's run. This correctly preserves all of the variation between the samples yet allows metabolites of widely different raw peak areas to be compared directly on a similar graphical scale. Missing values were assumed to result from areas falling below the limits of detection. For each metabolite, the missing values were imputed with the observed minimum after the normalization step. Additional normalization steps were added to correct for the volume differences between samples in the different matrices. For plasma, several samples had volumes lower than 100 μL and to those samples a correction factor was applied. For CSF, sample volumes varied between 5 and 10 μL. Therefore, a correction factor was applied to each sample based on the total ion count for all metabolites present in the sample. For brain samples a correction factor based on the total ion count for all metabolites present in the sample was applied as well, as in the case for CSF.

2.6. Statistical Analysis. Individual contrast analyses were performed between various groups of the study. The following comparisons were made: Tg2576_DSP4 versus wild type_DSP4, Tg2576_vehicle versus wild-type_vehicle, Tg2576_DSP4 versus Tg2576_vehicle, and wild-type_DSP4 versus wild-type_vehicle. In addition, a two-way (factorial) ANOVA analysis was performed to test whether the mean difference between genotype depends on the drug (or vice-versa). Data were log-transformed for all tests. A conservative P-value cutoff of .01 was used for this study. To account for multiple testing, false discovery rates (FDRs) were computed for each comparison [52]. The FDRs were estimated using the Q value method [53]. The Q value is a measure of each metabolite's significance that takes into account the hundreds of comparisons that we are making simultaneously in our analysis. The Q value, which is an extension of the FDR, is similar to the more familiar P value, which is a measure of the false positive rate. We use it in our univariate analyses to minimize the occurrence of potentially misleading false positives that would be otherwise expected with the performance of this many simultaneous comparisons.

2.7. Principal Component Analysis (PCA) and Partial Least Squares-Discriminant Analysis (PLS-DA). Principal components analysis (PCA) is a dimension reduction method that uses a linear transformation of a sample of points to exhibit the properties of the sample most clearly along the coordinate axes [54]. This analysis is now routinely used in the analysis of genome scale data sets, for example, [55]. The principal components (PCs) are displayed as a set of "scores", which highlight clustering or outliers, and a set of "loadings", which highlight the influence of input variables on t. PCA and PLS-DA analysis were completed in SIMCA P v12.0 (Umetrics AB) on a desktop PC running Windows XP Professional with 3 Gb RAM. For the PCA, a separate model was built for each tissue; three models in total—one for serum, one for CSF and one for brain tissue. The metabolite intensity data was mean centered and scaled to unit variance and the models were fitted using the autofit function. For

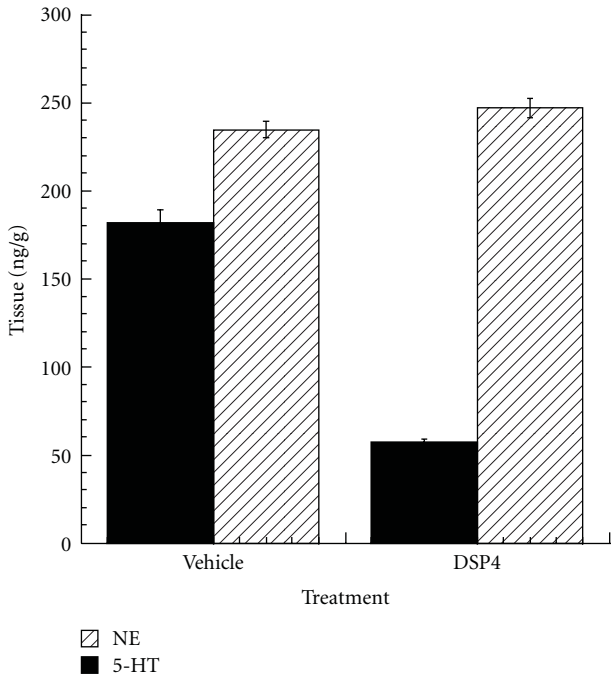

Figure 1: Effects of treatment with DSP4 on monoamine neurotransmitter levels. DSP4 (50 mg/kg in PBS, $N = 5$) or PBS (vehicle, $N = 5$) was administered intraperitoneally to C57BL/6SJL mice on days 1 and 7. Mice were sacrificed 7 days following the second injection (day 14). Brain was harvested and frontal cortex dissected for analysis of monoamine concentrations, demonstrating a 68% reduction of NE levels but no effect on serotonin.

the brain samples, PLS-DA model was fitted using the autofit function on mean centered unit variance scaled data.

3. Results

3.1. Effect of DSP4 Pretreatment on Monoamine Levels in Brain Tissue. Analyses of neurotransmitters in frontal cortices dissected from C57BL/6SJL mice on day 14, after treatment with DSP4 or vehicle on days 1 and 7, demonstrated a 68% reduction in the levels of norepinephrine, but no detectable effect on levels of serotonin (Figure 1).

3.2. Platform QC and Study Precision. The quality control data for this study can be summarized as follows: for plasma samples, standards ($n = 20$) in CMTRX yielded a median relative standard deviation (RSD) of 6.5%, nonstandards ($n = 326$) in CMTRX yielded a median RSD of 17%; for CSF samples, standards ($n = 20$) in CMTRX yielded a median RSD of 6.5%, nonstandards ($n = 68$) in CMTRX yielded a median RSD of 17%; for brain samples, standards ($n = 20$) in CMTRX yielded a median RSD of 11%, nonstandards ($n = 194$) in CMTRX yielded a median RSD of 23%. Results of this analysis indicated that the platform performed well within Metabolon's QC specifications for both plasma and CSF matrices. The brain RSD is higher because of the significant presence of lipids in brain tissue.

3.3. Metabolite Summary. Full data curation of the plasma samples yielded 487 chemical entities. 152 of these corresponded to identifiable chemical compounds and the remaining represented currently unnamed compounds. The CSF samples yielded 115 chemical entities, which is a little less than is typically seen due to the smaller sample volume of mouse CSF. 61 of these corresponded to identifiable chemical compounds and the remaining represented unnamed compounds. The brain tissue samples yielded 232 chemical entities. 115 of these corresponded to identifiable chemical compounds, and the remaining represented unnamed compounds. Results for individual metabolites are shown as Whisker plots demarcating upper and lower quartiles and further annotated with mean and median values.

3.4. Principal Component Analysis (PCA) and Partial Least Squares-Discriminant Analysis (PLS-DA). For the plasma specimens, autofit function generated a model containing 6 principal components that captured 56% of the total variance. The principal components do not correspond with experimental factors and the experimental groups do not segregate clearly. For the CSF specimens, autofit function generated a model containing 3 principal components that captured 57% of the total variance. The scores plot highlighted mouse Veh 11 as a potential outlier sample. The principal components did not correspond with experimental factors and the experimental groups did not clearly segregate. In contrast, for the brain specimens, autofit generated a model containing 7 principal components that captured 48% of the total variance. The majority of principal components did not correspond to a specific experimental factor but a combination of PC3 and PC6 gave a separation of the wild type and transgenic samples of brain metabolites. This observation was confirmed using PLS-DA, using the wild type and Tg2576 animals as groups. The Variable Importance in Projection (VIP) plot highlighted the carbohydrate and oxidative stress metabolites as the most significant in driving the separation between the wild-type and Tg2576 data sets in the PLS-DA analysis (Figure 2).

3.5. Overview of Biochemical Findings. Statistically significant differences ($P \leq .05$) were detected from amyloid transgenesis alone (i.e., differences between transgenics and the appropriate control group of wild-type animals, as matched with respect to treatment with DSP4 or vehicle), and from LC ablation alone (i.e., differences between DSP4-treated animals and the appropriate control group of vehicle animals, as matched with respect to transgenesis). However, of greatest interest were those changes that required both amyloid transgenesis and also ablation of the LC, that is, those in which Tg2576_DSP4 versus Tg2576_VEH showed statistically significant changes but WT_DSP4 versus WT_VEH did not. We will restrict the analysis in this paper to those changes observed in the brain as a result of LC ablation in Tg2576 transgenic animals, but not observed in wild-type animals, at a more stringent P-value of $\leq .01$ (Table 1). In this latter group the major biochemical

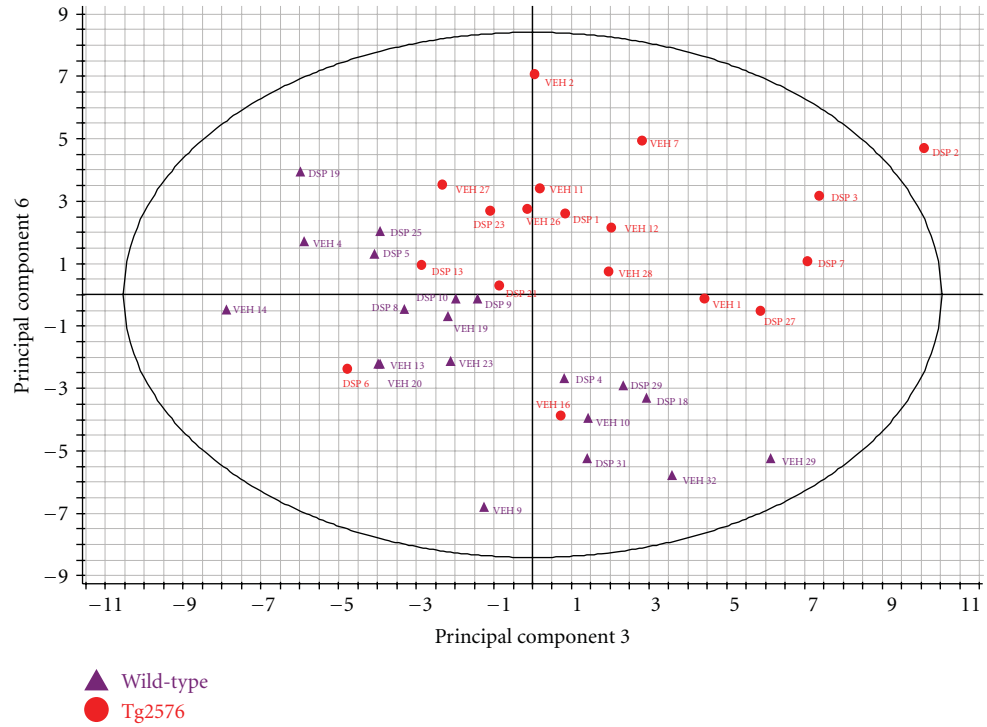

Figure 2: Principal components analysis. From an autofit model that yielded 7 principal components, a combination of PC3 and PC6 gives a separation of the wild type and transgenic samples of brain metabolites. This figure shows the scores plot, derived by principal components analysis, as a combination of Principal Component (PC) 3 on the x-axis and PC 6 on the y-axis. Each transgenic animal is represented by a red circle, each wild type by a purple triangle. Each point is labeled either with VEH for vehicle treatment or DSP for drug treatment followed by the number assigned to an individual mouse after assignment to a treatment group, but before any experimental procedure. The clustering observed in this plot indicates separation of the wild-type and transgenic samples based on the global profile of all of the brain metabolites detected in our analysis.

findings are: (1) The Tg2576_DSP4 mice already show signs of oxidative stress at 28 weeks of age, as demonstrated by decreased levels of several antioxidants such as glutathione (Figure 3) and increases of oxidative stress metabolite, ascorbate (Figure 4); (2) the Tg2576_DSP4 group shows an overall decrease of carbohydrates in the glycolysis/gluconeogenesis and pentose phosphate pathways, as well as minimal alterations of lactate, which varied between the three tissue compartments (Figure 5). This is consistent with decreased glucose turnover described in the literature on AD; (3) changes in brain lipids, modest increases in cholesterol and octadecanoic (stearic) acid (Figure 6) in transgenics in which the LC was ablated, in comparison to wild-type animals with the same LC ablation.

3.6. Comparisons of Specific Biochemical Pathways

3.6.1. Oxidative Stress. Many small molecules involved in the metabolism of glutathione, the major nonenzymatic cellular antioxidant, showed significant changes in the brain tissue of the Tg2576_DSP4 group (Figure 3 and Table 1). Of all the metabolic comparisons performed in this study, the most statistically significant is the decrease of oxidized glutathione in brain tissue of lesioned transgenic mice (Tg2576_DSP4) to that in wild-type mice with the same lesion (wt_DSP4). This comparison is significant at P-value of <.0005 and a Q-value of 0.006. This appears to depend on both the presence of amyloid and the absence of the LC inasmuch as it is not seen in the comparison of wild-type animals with transgenics in which the LC had been left intact. Comparison of levels of oxidized glutathione in Tg2576_VEH to wt_VEH only yields differences with nonsignificant $P = .536$ and $Q = 0.697$. The same comparison with reduced glutathione in the brain yields a $P = .005$, albeit with a marginal Q-value of 0.078. Similarly, this effect also requires both amyloid and the absence of the LC, since there is no difference in reduced glutathione levels between wild-type and transgenic animals in which the LC was left intact ($P = .829$, $Q = 0.752$) (Table 1).

There were also changes in the Tg2576_DSP4 brain levels of all examined γ-glutamyl-peptides, which are produced by γ-glutamyl transpeptidase- (GGT-) catalyzed cleavage of γ-glutamyl residues from glutathione and transfer to amino acids [56–59]. Of these, the most significant comparison is that of γ-glutamyl-leucine which is increased in Tg2576_DSP4 brains to 1.23-fold the levels seen in wt_DSP4 brains, with $P = .006$ and $Q = 0.081$. As in the case for oxidized and reduced glutathione, comparison of transgenic and wild-type animals does not demonstrate a difference in the presence of an intact LC (Table 1). Similar

Table 1: The 10 most statistically significant metabolic differences in brain tissue, associated with transgenesis for Tg2576 that were observed after ablation of the locus coeruleus with DSP4 but not in animals in which the locus coeruleus had been left intact. The *P*-value describes the false positive rate, the *Q*-value the false discovery rate.

Compound	Locus coeruleus ablated: Tg/wt		Locus coeruleus intact: Tg/wt		Tg-ablated/wt-ablated (Ratio of means)	Tg-intact/wt-intact (Ratio of means)
	P	*Q*	*P*	*Q*		
Glutathione, oxidized	.000	0.006	.536	0.697	0.41	0.80
Glucose-6-phosphate	.001	0.051	.121	0.458	0.78	0.88
D-arabitol	.001	0.051	.193	0.505	0.69	1.12
Cholesterol	.002	0.051	.853	0.752	1.51	0.95
Lactate	.002	0.051	.135	0.461	0.84	1.06
Ascorbic acid	.003	0.051	.251	0.530	0.73	0.92
Glutathione, reduced	.005	0.078	.829	0.752	0.68	1.03
γ-glutamyl-leucine	.006	0.081	.968	0.777	1.23	0.99
Octadecanoic acid	.009	0.101	.058	0.423	1.12	1.07
Uric acid	.010	0.101	.576	0.715	2.91	0.63

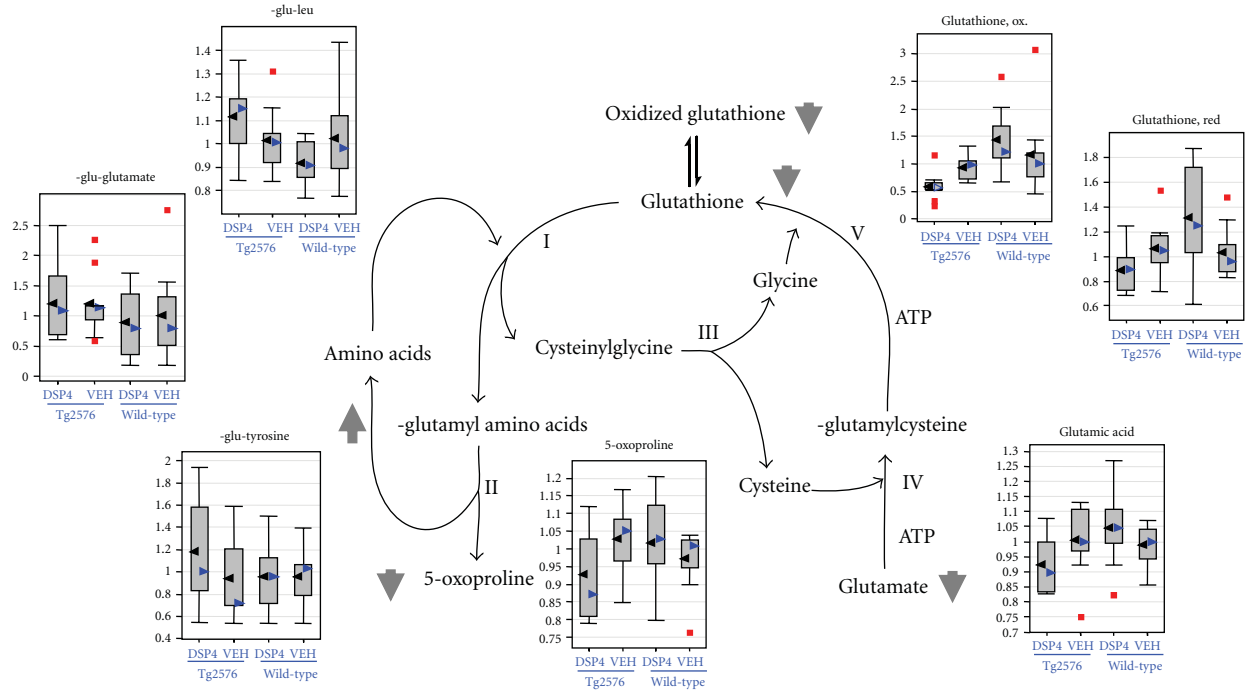

Figure 3: Glutathione metabolism. Glutathione metabolism and gamma-glutamyl-dipeptide formation are altered in the brains of the Tg2576_DSP4 group. For each metabolite, the distribution of values within each of the four cohorts is represented as a Whisker plot, with the relative normalized intensity as the abscissa. Mean values represented by the black arrowheads, median values by blue arrowheads. Detailed statistical comparisons of oxidized glutathione, reduced glutathione, and γ-glutamine-leucine are given in Table 1. Glutamic acid was omitted from the table even though the *P*-value for the comparison of ablated transgenics to ablated wild-types was .0109, the *Q*-value exceeded our threshold at a value of 0.154.

trends were seen for the other γ-glutamyl peptides, albeit not at statistically significant levels (Figure 3). γ-glutamyl transpeptidase- (GGT-) catalyzed cleavage plays important roles in glutathione metabolism, amino acid transfer and metabolism of toxic compounds [56–59]. Therefore, the altered levels of γ-glutamyl dipeptides in the Tg2576_DSP4 group (Figure 3) are another indication of increased stress conditions in this group.

Ascorbic acid levels (Figure 4) were severely reduced in Tg2576_DSP4 brains (Table 1; $P = .003$, $Q = 0.051$) consistent with reports that levels of ascorbate are altered in AD [17]. As in the case of the glutathione pathway, there is no significant difference in brain ascorbate levels in transgenic and wild-type animals in which the LC remained intact (Table 1). Paradoxically, there was an almost three-fold increase in the uric acid level in the brains of the Tg2576_DSP4

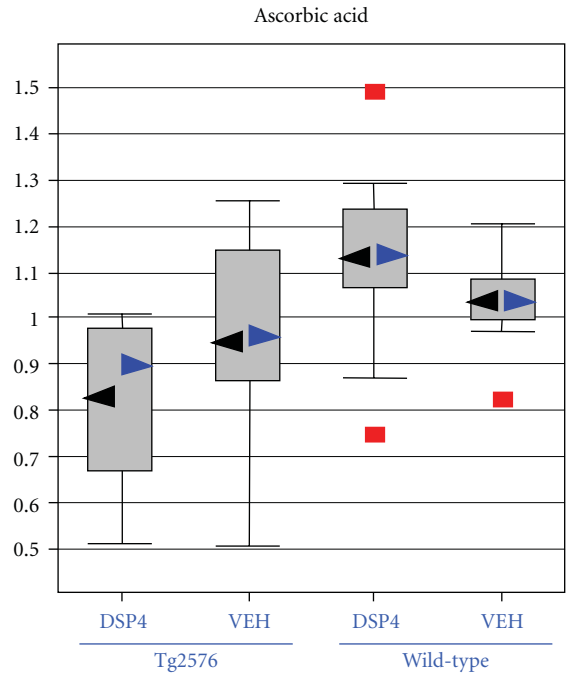

Figure 4: Ascorbic acid, another marker of oxidative stress. Box plots for levels of ascorbic acid in the brain, displaying the distribution of values within each of the four cohorts represented as a Whisker plot, with the relative normalized intensity as the abscissa. Mean values represented by the black arrowheads, median values by blue arrowheads. Detailed statistical comparisons of ascorbate in the four cohorts are given in Table 1.

group in comparison to the wt_DSP4 group whereas the amount of uric acid in the transgenic animals was 63% that of wild type when the LC was left intact (Table 1). In summary, the significant changes of antioxidants and oxidative stress markers in the Tg2576_DSP4 group support the model that transgenic Tg2576 mice, injected with DSP4, show increased levels of oxidative stress as is seen in AD.

3.6.2. Energy Metabolism. We observed an overall decrease of carbohydrates involved in glycolysis, gluconeogenesis, and the pentose phosphate pathway in Tg2576_DSP4 mice. The most significant change was a decrease of the brain levels of glucose-6-phosphate in Tg2576_DSP4 brains compared to wt_DSP4 brains ($P = .001$, $Q = 0.051$) (Table 1 and Figure 5), a difference not observed between brains of unlesioned animals. Another possible indication of activation of the pentose phosphate pathway is the equally significant lowering of brain levels of D-arabitol, a naturally occurring polyol with antioxidant properties that is synthesized in the brain [57]. As is the case for the other antioxidant metabolites described in earlier paragraphs, it is exclusively altered in the brains of transgenic mice in whom the LC has been lesioned (Tg2576_DSP4) with $P = .001$, $Q = 0.051$ (Table 1 and Figure 5). In the presence of an intact LC, transgenic mice do not have a detectable difference in brain levels of d-arabitol from wild-type mice. The third significant alteration relating to energy metabolism in the brains of Tg2576_DSP4 mice is a minimal decrease in lactate levels ($P = .002$, $Q = 0.051$) (Table 1 and Figure 5).

Nearly all metabolites of the tricarboxylic acid (TCA) cycle showed significant changes between wild-type and Tg2576 transgenic mice, and between DSP4 and vehicle mice. The TCA cycle intermediates are significantly increased in Tg2576_vehicle mice compared to wild-type vehicle mice. However, treatment with DSP4 reduced the TCA intermediates in both wild type and transgenic mice backgrounds. Some TCA metabolites show rather minor changes in the wild-type_DSP4 versus wild-type_VEH group, but a significant change in the Tg2576_DSP4 versus Tg2576_VEH comparison. The most statistically significant change was for malic acid levels in the brains of Tg2576_DSP4 which were shown to be minimally altered at 0.89-fold the level in wt_DSP4 brains, at a $P = .032$, $Q = 0.212$. However, there was an even more significant alteration ($P = .007$, $Q = 0.206$) comparing wild type and transgenic mice in whom the LC was intact, albeit in the opposite direction. In summary, the Tg2576_DSP4 mice showed reductions in carbohydrates involved in the glycolysis, gluconeogenesis and pentose phosphate pathways compared to wild type controls.

3.6.3. Free Fatty Acids and Lipids. A diverse array of changes in free fatty acids (FFA) and lipids were observed in this study. However, only the change in octadecanoic (stearic) acid was found to approach statistical significance ($P = .009$, $Q = 0.101$) comparing Tg2576_DSP4 to wt_DSP4 mice (Table 1 and Figure 6). Brain cholesterol showed the same trend. However, several other lipid-derived brain metabolites showed a decrease in the Tg2576_DSP4 group compared to the other treatment groups.

4. Discussion

The PCA analysis identified group differences between the metabolic profiles in the brains of wild type and Tg2576 animals. These differences are subtle in that they are not highlighted in the first principal components and the sum of the variance of the principal components is only 11% of the total variance. The PLS-DA analysis allows us to identify the metabolites which contribute most to the separation of the wild type and Tg2576 animal groups. These metabolites are involved in carbohydrate metabolism and oxidative stress response, which corresponds to the metabolites identified as significantly differentially expressed in the univariate analysis of the metabolite data. These changes also correspond with known changes in the brain in AD where, it has been long established that glucose metabolism is impaired in AD [12, 60]. The multivariate analysis of the metabolite data does not reveal much significance over and above the univariate analysis. With the exception of the genotype differences in the brain samples, the other models fail to capture more than 60% of the total variance. The majority of single or pairs of principal components do not correspond to either

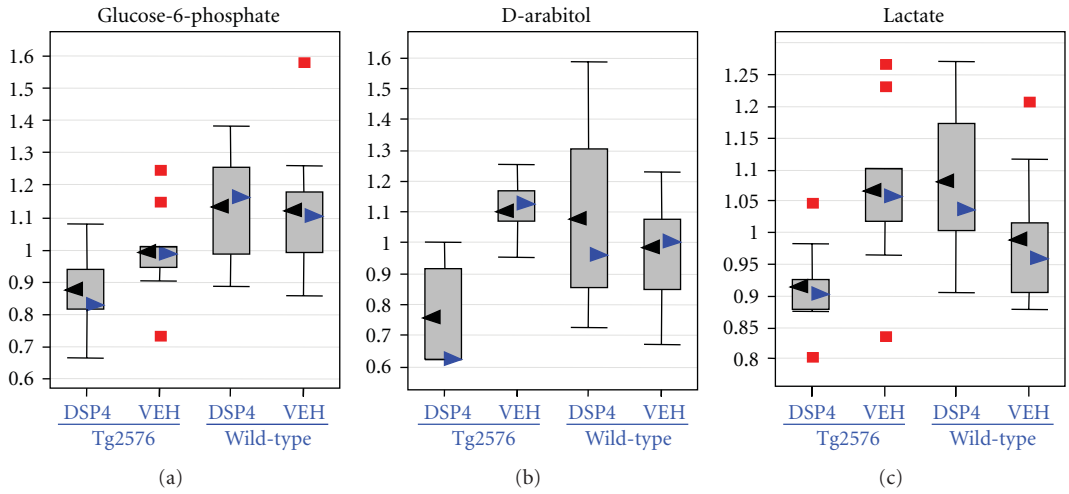

FIGURE 5: Carbohydrate metabolism. Box plots demonstrating selective depressions in the brains of glucose-6-phosphate (an early intermediary of anaerobic glycolysis as well as the pentose monophosphate shunt), lactate the end product of anaerobic glycolysis, and D-arabitol, a polyol with antioxidant properties which is thought to be a product of the pentose phosphate pathway. For each metabolite, the distribution of values within each of the four cohorts is represented as a Whisker plot, with the relative normalized intensity as the abscissa. Mean values represented by the black arrowheads, median values by blue arrowheads. Detailed statistical comparisons of each of the pictured metabolites in the four cohorts are given in Table 1.

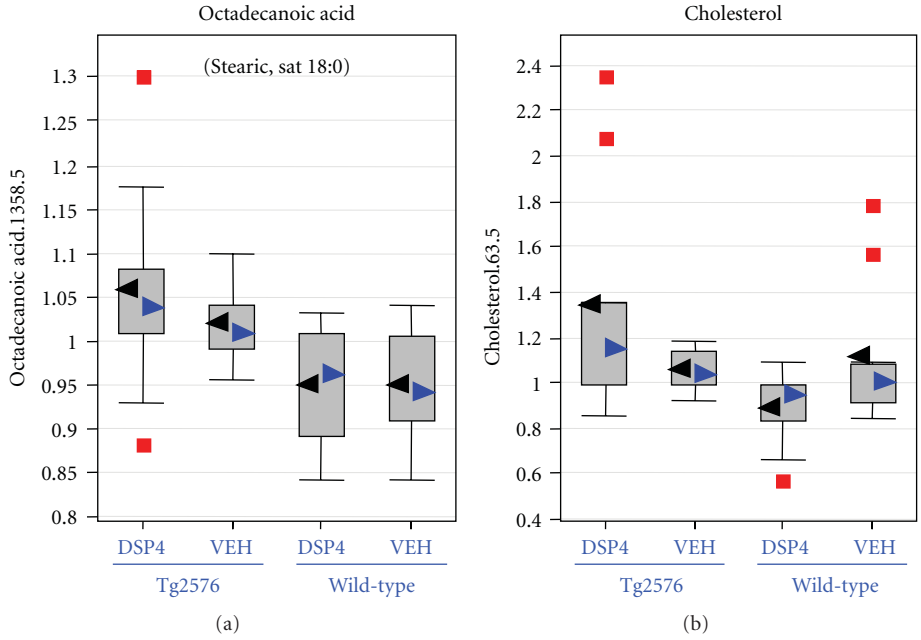

FIGURE 6: Lipids: Octadecanoic (stearic) acid and cholesterol. Box plots describing the modest elevations of octadecanoic acid and cholesterol in the brains of transgenic animals in which the locus coeruleus had been ablated. For each metabolite, the distribution of values within each of the four cohorts is represented as a Whisker plot, with the relative normalized intensity as the abscissa. Mean values represented by the black arrowheads, median values by blue arrowheads. Detailed statistical comparisons of both of these metabolites in the four cohorts are given in Table 1.

the drug or genotype experimental factors in the plasma or the CSF. For this reason, we chose to limit this analysis to the brain, even though multiple metabolites in plasma and CSF did show apparently significant differences in individual comparisons.

Mindful of the hazards attendant to multiple comparisons, we chose to focus on those brain metabolites that demonstrated differences with a more restrictive nominal P-value of $\leq .01$ (Table 1). In this set of 10 metabolites, six fell effectively within the conventional cutoff value for False Discovery Rate of $Q \leq 0.05$ and the remaining four within the range $0.05 < Q \leq 0.10$, indicating trends. Eight of these 10 most significantly altered metabolites relate to oxidative stress.

4.1. Oxidative Stress. The most significant change was in the levels of glutathione, the major antioxidant protecting cells from toxins such as free radicals. Glutathione is found almost exclusively in its reduced form, since the enzyme which reverts it from its oxidized form is constitutively active and inducible upon oxidative stress. The severe depletion of glutathione and its metabolites in the Tg2576_DSP4 brains is consistent with the presence of increased oxidative stress in these mice. This is an important finding since previous studies examining the relationship between glutathione and AD have been inconclusive [61, 62]. It is of interest that both reduced and oxidized forms of glutathione were lowered, indicating decreased synthesis or increased degradation. Whatever the mechanism, these indicate a decreased capacity to scavenge free radicals. Further support for the significance of the observed differences in the glutathione cycle come from the analysis of concordant trends in the γ-glutamyl peptides, of which the alteration of γ-glutamyl-leucine approached statistical significance (Table 1).

In addition to changes directly related to the glutathione cycle, there was a statistically significant reduction of ascorbic acid in the brains of transgenic animals in whom the LC was ablated ($P = .003$, $Q = 0.051$) whereas no difference was observed when the LC had been left intact (Table 1). Reduced levels of ascorbate had been observed in AD [17]. Surprisingly, we also observed an apparently discordant result in the elevation of uric acid levels in the brain of Tg2756_DSP4 mice, instead of the expected reduction, which was observed in the unlesioned transgenics. Uric acid is a scavenger of ROS, about as effective as vitamin C. Tohgi et al. [63] found that uric acid and xanthine are much lower in AD CSF presumably because of impaired brain metabolism. The increase of uric acid in our experimental animals appears robust but unexplained. Similarly, there were equivocal differences seen in levels of tocopherol. Kontush and Schekatolina [64] have shown that vitamin E levels in AD subjects vary widely depending on the study. Furthermore, it is possible that some antioxidants show significant changes in this study while others do not show the same extent of changes because of only partial depletion of norepinephrine (63%) or the relatively young age (23 weeks) of the transgenic mice used in this study. Kawarabayashi et al. [65] have previously shown that the accumulation of amyloid β plaques in the Tg2576 mouse model only reach the levels seen in AD brain between 15 and 23 months of age.

4.2. Energy Metabolism. Less direct but nevertheless compelling evidence of increased oxidative stress in the brains of Tg2756_DSP4 animals derives from our observations of significantly altered levels of glucose-6-phosphate and of the polyol D-arabitol (Table 1) [66–69]. Glucose-6-phosphate can undergo a number of metabolic transformations. Besides being an intermediate in the Embden-Meyerhof pathway, where it is reversibly isomerized to D-fructose-6-phosphate by phosphoglucose isomerase, it can also be irreversibly metabolized by NADP-linked glucose-6-phosphate dehydrogenase in the first step of the oxidative pentose phosphate pathway, or by phosphoglucomutase in the first step of the glucuronic acid pathway [66]. Glucose-6-phosphate dehydrogenase plays a pivotal role in homeostatic redox control by providing reducing equivalents to glutathione. Thus, lower levels of glucose-6-phosphate in the brains of transgenic animals in which the LC has been ablated could indicate either decreased glucose uptake or increased flux through the pentose monophosphate shunt, which has been shown to be induced in AD [67], presumably to provide reductive compensation to oxidative stress. Furthermore, the striking alteration in the levels of D-arabitol, a little-studied polyol that is believed to be derived from sugar phosphates in the pentose monophosphate pathway, further supports alteration of this pathway. However, the metabolic pathways for these and other brain derived polyols have not yet been fully determined [68], so that our interpretation must be considered speculative.

There is extensive literature documenting altered metabolism of carbohydrates in AD [12, 60, 70]. Our claim of greater concordance of LC-lesioned transgenic mice with human AD is consistent with the general consensus in the literature that glucose and carbohydrate metabolism, and therefore the formation of cellular energy is reduced severely in AD. Bigl et al. [71] observed a lowered glucose metabolism in Tg2576 mice as well, but only at 24 months of age were reductions in the key enzymes in the glycolysis and gluconeogenesis pathway detected.

Several metabolites in the TCA cycle demonstrated an interaction effect between the genotype and drug (data not shown), most notably malate. However, malate was also significantly altered in comparisons of transgenics and wild type animals in which the LC had been left intact. TCA cycle proteins prone to reactive oxygen species (ROS) damage include aconitase, pyruvate dehydrogenase and alpha-ketoglutarate dehydrogenase, all of which have been shown to be significantly reduced in AD [72–75].

4.3. Free Fatty Acids and Lipids. The remaining two of the ten most statistically significant contrasts in the Tg2756_DSP4 brains relate to lipid metabolism, neither of which can we relate readily to oxidative stress. There is a statistically significant elevation in cholesterol in lesioned transgenic animals, but no difference from wild-type in transgenic animals with an intact LC (Table 1). The relationship of cholesterol to autopsy findings in AD is complex, depending on one's use of the historical or the currently accepted definition of AD. Up to this point in our discussion, we have used the term AD exclusively to refer to sporadic, senile onset Alzheimer's disease, as it is referred to in the current literature, but which had previously been referred to as SDAT, Senile Dementia of the Alzheimer Type. This distinction is germane to considerations of cholesterol metabolism. Two independent autopsy studies have demonstrated a decrease in cholesterol in the cerebral white matter in autopsies of patients with Alzheimer's disease as defined historically—that is, autosomal dominant presenile dementia as described by Alois Alzheimer [76]—in comparison with age-matched controls or patients with SDAT. In contrast, cholesterol and

certain other lipids were reduced in the frontal centrum semiovale of patients with SDAT in comparison to age-matched controls or patients with presenile dementia—referred to by the authors of that report as "true Alzheimer's disease" [77]. It is of further interest that cholesterol loading was found to modulate Aβ toxicity through depletion of mitochondrial stores of glutathione, possibly furnishing an indirect link to oxidative stress [78]. Be that as it may, we cannot offer a meaningful interpretation of this statistically significant difference in cholesterol. Similarly, we do not understand the modest elevation of octadecanoic (stearic) acid in the brains of Tg2756_DSP4 mice, but note its concordance with observations in autopsy studies of Alzheimer's disease [79] as well as to a report of its ability to induce hyperphosphorylation of tau in an experimental system [80].

5. Conclusion

This data provides further support to the original hypothesis by Heneka et al. [42, 43], that loss of the widely projecting noradrenergic LC is not just an incidental finding but may contribute to key pathophysiological features of human Alzheimer's disease. Furthermore, it extends this hypothesis from inflammation to oxidative stress and altered carbohydrate metabolism. It is an interesting historical note that after an extensive body of work on the role of the noradrenergic LC in Alzheimer's disease [30–41, 81], most investigators shifted their focus to the cholinergic substantia innominata, in which cell loss is not as extensive [40]. Perhaps this deserves reappraisal.

If the importance of the loss of the LC is corroborated by studies of other markers of oxidative damage, such as 8-hydroxyguanosine [82], 4-hydroxy-2-nonenal (HNE), isoprostanes [83] and nitrotyrosine [84], this may have practical consequences in the development of animal models more congruent with the human disease. An important test of this extended hypothesis will be comparison of cell loss and cognitive function in amyloid transgenics in which the LC has been ablated. If confirmed, not only would this have practical consequences in the design of animal models, but would also provide an experimental test of the hypothesis that free radicals are the rate limiting step in this as well as other neurodegenerative disorders [22].

Acknowledgments

This work was performed in the laboratories of Wyeth Research, of which O. Hurko, C. Gonzales, Z. Hughes, S. Jacobsen, P. Reinhart, and D. Crowther had been employees and the laboratories of Metabolon, where K. Boudonck had been an employee.

References

[1] K. Hsiao, P. Chapman, S. Nilsen et al., "Correlative memory deficits, Aβ elevation, and amyloid plaques in transgenic mice," *Science*, vol. 274, no. 5284, pp. 99–102, 1996.

[2] X.-D. Cai, T. E. Golde, and S. G. Younkin, "Release of excess amyloid β protein from a mutant amyloid β protein precursor," *Science*, vol. 259, no. 5094, pp. 514–516, 1993.

[3] X.-D. Cai, T. E. Golde, and S. G. Younkin, "Release of excess amyloid β protein from a mutant amyloid β protein precursor," *Science*, vol. 259, no. 5094, pp. 514–516, 1993.

[4] K. Hsiao, P. Chapman, S. Nilsen et al., "Correlative memory deficits, Aβ elevation, and amyloid plaques in transgenic mice," *Science*, vol. 274, no. 5284, pp. 99–102, 1996.

[5] K. P. Riley, D. A. Snowdon, M. F. Desrosiers, and W. R. Markesbery, "Early life linguistic ability, late life cognitive function, and neuropathology: findings from the Nun Study," *Neurobiology of Aging*, vol. 26, no. 3, pp. 341–347, 2005.

[6] D. Iacono, W. R. Markesbery, M. Gross et al., "The nun study: clinically silent AD, neuronal hypertrophy, and linguistic skills in early life," *Neurology*, vol. 73, no. 9, pp. 665–673, 2009.

[7] M. S. Fernando and P. G. Ince, "Vascular pathologies and cognition in a population-based cohort of elderly people," *Journal of the Neurological Sciences*, vol. 226, no. 1-2, pp. 13–17, 2004.

[8] J. K. Andersen, "Oxidative stress in neurodegeneration: cause or consequence?" *Nature Medicine*, vol. 10, pp. S18–S25, 2004.

[9] I. Baldeiras, I. Santana, M. T. Proença et al., "Peripheral oxidative damage in mild cognitive impairment and mild Alzheimer's disease," *Journal of Alzheimer's Disease*, vol. 15, no. 1, pp. 117–128, 2008.

[10] S. M. De La Monte and J. R. Wands, "Molecular indices of oxidative stress and mitochondrial dysfunction occur early and often progress with severity of Alzheimer's disease," *Journal of Alzheimer's Disease*, vol. 9, no. 2, pp. 167–181, 2006.

[11] J. N. Keller, "Interplay between oxidative damage, protein synthesis, and protein degradation in Alzheimer's disease," *Journal of Biomedicine and Biotechnology*, vol. 2006, Article ID 12129, 2006.

[12] S. Hoyer, "Oxidative metabolism deficiencies in brains of patients with Alzheimer's disease," *Acta Neurologica Scandinavica, Supplement*, vol. 93, no. 165, pp. 18–24, 1996.

[13] T.-S. Kim, C.-U. Pae, S.-J. Yoon et al., "Decreased plasma antioxidants in patients with Alzheimer's disease," *International Journal of Geriatric Psychiatry*, vol. 21, no. 4, pp. 344–348, 2006.

[14] M. A. Lovell and W. R. Markesbery, "Oxidative DNA damage in mild cognitive impairment and late-stage Alzheimer's disease," *Nucleic Acids Research*, vol. 35, no. 22, pp. 7497–7504, 2007.

[15] M. A. Lovell and W. R. Markesbery, "Oxidative damage in mild cognitive impairment and early Alzheimer's disease," *Journal of Neuroscience Research*, vol. 85, no. 14, pp. 3036–3040, 2007.

[16] W. R. Markesbery and M. A. Lovell, "Damage to lipids, proteins, DNA, and RNA in mild cognitive impairment," *Archives of Neurology*, vol. 64, no. 7, pp. 954–956, 2007.

[17] P. Mecocci, "Oxidative stress in mild cognitive impairment and Alzheimer disease: a continuum," *Journal of Alzheimer's Disease*, vol. 6, no. 2, pp. 159–163, 2004.

[18] L. Mosconi, A. Pupi, and M. J. De Leon, "Brain glucose hypometabolism and oxidative stress in preclinical Alzheimer's disease," *Annals of the New York Academy of Sciences*, vol. 1147, pp. 180–195, 2008.

[19] R. B. Petersen, A. Nunomura, H.-G. Lee et al., "Signal transduction cascades associated with oxidative stress in Alzheimer's disease," *Journal of Alzheimer's Disease*, vol. 11, no. 2, pp. 143–152, 2007.

[20] J. B. Schulz, J. Lindenau, J. Seyfried, and J. Dichgans, "Glutathione, oxidative stress and neurodegeneration," *European*

Journal of Biochemistry, vol. 267, no. 16, pp. 4904–4911, 2000.

[21] B. Su, X. Wang, A. Nunomura et al., "Oxidative stress signaling in Alzheimer's disease," *Current Alzheimer Research*, vol. 5, no. 6, pp. 525–532, 2008.

[22] A. F. Wright, S. G. Jacobson, A. V. Cideciyan et al., "Lifespan and mitochondrial control of neurodegeneration," *Nature Genetics*, vol. 36, no. 11, pp. 1153–1158, 2004.

[23] H. Akiyama, S. Barger, S. Barnum et al., "Inflammation and Alzheimer's disease," *Neurobiology of Aging*, vol. 21, no. 3, pp. 383–421, 2000.

[24] Y. Yao, C. Chinnici, H. Tang, J. Q. Trojanowski, V. M. Y. Lee, and D. Praticò, "Brain inflammation and oxidative stress in a transgenic mouse model of Alzheimer-like brain amyloidosis," *Journal of Neuroinflammation*, vol. 1, 2004.

[25] S. S. Karuppagounder, H. Xu, Q. Shi et al., "Thiamine deficiency induces oxidative stress and exacerbates the plaque pathology in Alzheimer's mouse model," *Neurobiology of Aging*, vol. 30, no. 10, pp. 1587–1600, 2009.

[26] R. Resende, P. I. Moreira, T. Proença et al., "Brain oxidative stress in a triple-transgenic mouse model of Alzheimer disease," *Free Radical Biology and Medicine*, vol. 44, no. 12, pp. 2051–2057, 2008.

[27] K.-W. Lee, J.-B. Kim, J.-S. Seo et al., "Behavioral stress accelerates plaque pathogenesis in the brain of Tg2576 mice via generation of metabolic oxidative stress," *Journal of Neurochemistry*, vol. 108, no. 1, pp. 165–175, 2009.

[28] M. Dumont, E. Wille, C. Stack, N. Y. Calingasan, M. F. Beal, and M. T. Lin, "Reduction of oxidative stress, amyloid deposition, and memory deficit by manganese superoxide dismutase overexpression in a transgenic mouse model of Alzheimer's disease," *The FASEB Journal*, vol. 23, no. 8, pp. 2459–2466, 2009.

[29] D. A. Butterfield, V. Galvan, M. B. Lange et al., "In vivo oxidative stress in brain of Alzheimer disease transgenic mice: requirement for methionine 35 in amyloid β-peptide of APP," *Free Radical Biology and Medicine*, vol. 48, no. 1, pp. 136–144, 2009.

[30] D. M. A. Mann, J. Lincoln, and P. O. Yates, "Changes in the monoamine containing neurones of the human CNS in senile dementia," *British Journal of Psychiatry*, vol. 136, no. 6, pp. 533–541, 1980.

[31] B. E. Tomlinson, D. Irving, and G. Blessed, "Cell loss in the locus coeruleus in senile dementia of Alzheimer type," *Journal of the Neurological Sciences*, vol. 49, no. 3, pp. 419–428, 1981.

[32] D. M. A. Mann, P. O. Yates, and J. Hawkes, "The pathology of the human locus ceruleus," *Clinical Neuropathology*, vol. 2, no. 1, pp. 1–7, 1983.

[33] D. M. A. Mann, P. O. Yates, and B. Marcyniuk, "A comparison of changes in the nucleus basalis and locus caeruleus in Alzheimer's disease," *Journal of Neurology Neurosurgery and Psychiatry*, vol. 47, no. 2, pp. 201–203, 1984.

[34] W. Bondareff, C. Q. Mountjoy, and M. Roth, "Loss of neurons of origin of the adrenergic projection to cerebral cortex (nucleus locus ceruleus) in senile dementia," *Neurology*, vol. 32, no. 2, pp. 164–168, 1982.

[35] Y. Ichimiya, H. Arai, K. Kosaka, and R. Iizuka, "Morphological and biochemical changes in the cholinergic and monoaminergic systems in Alzheimer-type dementia," *Acta Neuropathologica*, vol. 70, no. 2, pp. 112–116, 1986.

[36] V. Chan-Palay and E. Asan, "Alterations in catecholamine neurons of the locus coeruleus in senile dementia of the Alzheimer type and Parkinson's disease with and without dementia and depression," *Journal of Comparative Neurology*, vol. 287, no. 3, pp. 373–392, 1989.

[37] V. Chan-Palay, "Alterations in the locus coeruleus in dementias of Alzheimer's and Parkinson's disease," *Progress in Brain Research*, vol. 88, pp. 625–630, 1991.

[38] D. C. German, K. F. Manaye, C. L. White III et al., "Disease-specific patterns of locus coeruleus cell loss," *Annals of Neurology*, vol. 32, no. 5, pp. 667–676, 1992.

[39] A. J. Nazarali and G. P. Reynolds, "Monoamine neurotransmitters and their metabolites in brain regions in Alzheimer's disease: a postmortem study," *Cellular and Molecular Neurobiology*, vol. 12, no. 6, pp. 581–587, 1992.

[40] C. Zarow, S. A. Lyness, J. A. Mortimer, and H. C. Chui, "Neuronal loss is greater in the locus coeruleus than nucleus basalis and substantia nigra in Alzheimer and Parkinson diseases," *Archives of Neurology*, vol. 60, no. 3, pp. 337–341, 2003.

[41] R. Adolfsson, C. G. Gottfries, B. E. Roos, and B. Winblad, "Changes in the brain catecholamines in patients with dementia of Alzheimer type," *British Journal of Psychiatry*, vol. 135, no. 3, pp. 216–223, 1979.

[42] M. T. Heneka, E. Galea, V. Gavriluyk et al., "Noradrenergic depletion potentiates β-amyloid-induced cortical inflammation: implications for Alzheimer's disease," *Journal of Neuroscience*, vol. 22, no. 7, pp. 2434–2442, 2002.

[43] D. L. Feinstein, M. T. Heneka, V. Gavrilyuk, C. Dello Russo, G. Weinberg, and E. Galea, "Noradrenergic regulation of inflammatory gene expression in brain," *Neurochemistry International*, vol. 41, no. 5, pp. 357–365, 2002.

[44] M. T. Heneka, V. Gavrilyuk, G. E. Landreth, M. K. O'Banion, G. Weinberg, and D. L. Feinstein, "Noradrenergic depletion increases inflammatory responses in brain: effects on IκB and HSP70 expression," *Journal of Neurochemistry*, vol. 85, no. 2, pp. 387–398, 2003.

[45] M. T. Heneka, M. Ramanathan, A. H. Jacobs et al., "Locus ceruleus degeneration promotes Alzheimer pathogenesis in amyloid precursor protein 23 transgenic mice," *Journal of Neuroscience*, vol. 26, no. 5, pp. 1343–1354, 2006.

[46] R. N. Kalaria, C. A. Stockmeier, and S. I. Harik, "Brain microvessels are innervated by locus ceruleus noradrenergic neurons," *Neuroscience Letters*, vol. 97, no. 1-2, pp. 203–208, 1989.

[47] G. Jonnson, H. Hallman, F. Fonzio, and S. Ross, "DSP4 (N-(2-chloroethyl)-N-(ethyl-2-bromobenzylamine)—a useful denervation tool for central and peripheral noradrenalin neurons," *European Journal of Pharmacology*, vol. 72, no. 2-3, pp. 173–188, 1981.

[48] M. E. Landa, M. C. Rubio, and G. Jaim-Etcheverry, "The neurotoxic compound N-(2-chloroethyl)-N-ethyl-2-bromobenzylamine hydrochloride (DSP4) depletes endogenous norepinephrine and enhances release of [*3H*]norepinephrine from rat cortical slices," *Journal of Pharmacology and Experimental Therapeutics*, vol. 231, no. 1, pp. 131–136, 1984.

[49] K. J. Boudonck, M. W. Mitchell, L. Német et al., "Discovery of metabolomics biomarkers for early detection of nephrotoxicity," *Toxicologic Pathology*, vol. 37, no. 3, pp. 280–292, 2009.

[50] K. J. Boudonck, D. J. Rose, E. D. Karoly, D. P. Lee, K. A. Lawton, and P. J. Lapinskas, "Metabolomics for early detection of drug-induced kidney injury: review of current status," *Bioanalysis*, vol. 1, pp. 1645–1663, 2009.

[51] A. M. Evans, C. D. DeHaven, T. Barrett, M. Mitchell, and E. Milgram, "Integrated, nontargeted ultrahigh performance liquid chromatography/electrospray ionization tandem mass spectrometry platform for the identification and relative

quantification of the small-molecule complement of biological systems," *Analytical Chemistry*, vol. 81, no. 16, pp. 6656–6667, 2009.

[52] Y. Benjamini and Y. Hochberg, "Controlling the false discovery rate: a practical and powerful approach to multiple testing," *Journal of the Royal Statistical Society: Series B*, vol. 57, pp. 289–300, 1995.

[53] J. D. Storey and R. Tibshirani, "Statistical significance for genomewide studies," *Proceedings of the National Academy of Sciences of the United States of America*, vol. 100, no. 16, pp. 9440–9445, 2003.

[54] K. Pearson, "On lines and planes of closest fit to systems of points in space," *Philosophical Magazine*, vol. 2, pp. 559–572, 1901.

[55] J. Gottfries, M. Sjögren, B. Holmberg, L. Rosengren, P. Davidsson, and K. Blennow, "Proteomics for drug target discovery," *Chemometrics and Intelligent Laboratory Systems*, vol. 73, no. 1, pp. 47–53, 2004.

[56] A. G. Palekar, S. S. Tate, and A. Meister, "Formation of 5 oxoproline from glutathione in erythrocytes by the γ glutamyltranspeptidase cyclotransferase pathway," *Proceedings of the National Academy of Sciences of the United States of America*, vol. 71, no. 2, pp. 293–297, 1974.

[57] W. Wang and N. Ballatori, "Endogenous glutathione conjugates: occurrence and biological functions," *Pharmacological Reviews*, vol. 50, no. 3, pp. 335–355, 1998.

[58] A. Visvikis, C. Thioudellet, T. Oster, S. Fournel-Gigleux, M. Wellman, and G. Siest, "High-level expression of enzymatically active mature human γ-glutamyltransferase in transgenic V79 Chinese hamster cells," *Proceedings of the National Academy of Sciences of the United States of America*, vol. 88, no. 16, pp. 7361–7365, 1991.

[59] M. W. Lieberman, A. L. Wiseman, Z.-Z. Shi et al., "Growth retardation and cysteine deficiency in γ-glutamyl transpeptidase-deficient mice," *Proceedings of the National Academy of Sciences of the United States of America*, vol. 93, no. 15, pp. 7923–7926, 1996.

[60] U. Lying-Tunell, B. S. Lindblad, H. O. Malmlund, and B. Persson, "Cerebral blood flow and metabolic rate of oxygen, glucose, lactate, pyruvate, ketone bodies and amino acids. II. Presenile dementia and normal-pressure hydrocephalus," *Acta Neurologica Scandinavica*, vol. 63, no. 6, pp. 337–350, 1981.

[61] J. B. Schulz, J. Lindenau, J. Seyfried, and J. Dichgans, "Glutathione, oxidative stress and neurodegeneration," *European Journal of Biochemistry*, vol. 267, no. 16, pp. 4904–4911, 2000.

[62] V. Vitvitsky, M. Thomas, A. Ghorpade, H. E. Gendelman, and R. Banerjee, "A functional transsulfuration pathway in the brain links to glutathione homeostasis," *Journal of Biological Chemistry*, vol. 281, no. 47, pp. 35785–35793, 2006.

[63] H. Tohgi, T. Abe, S. Takahashi, and T. Kikuchi, "The urate and xanthine concentrations in the cerebrospinal fluid in patients with vascular dementia of the Binswanger type, Alzheimer type dementia, and Parkinson's disease," *Journal of Neural Transmission: Parkinson's Disease and Dementia Section*, vol. 6, no. 2, pp. 119–126, 1993.

[64] A. Kontush and S. Schekatolina, "Vitamin E in neurodegenerative disorders: Alzheimer's disease," *Annals of the New York Academy of Sciences*, vol. 1031, pp. 249–262, 2004.

[65] T. Kawarabayashi, L. H. Younkin, T. C. Saido, M. Shoji, K. H. Ashe, and S. G. Younkin, "Age-dependent changes in brain, CSF, and plasma amyloid β protein in the Tg2576 transgenic mouse model of Alzheimer's disease," *Journal of Neuroscience*, vol. 21, no. 2, pp. 372–381, 2001.

[66] M. M. C. Wamelink, E. A. Struys, and C. Jakobs, "The biochemistry, metabolism and inherited defects of the pentose phosphate pathway: a review," *Journal of Inherited Metabolic Disease*, vol. 31, no. 6, pp. 703–717, 2008.

[67] R. L. Russell, S. L. Siedlak, A. K. Raina, J. M. Bautista, M. A. Smith, and G. Perry, "Increased neuronal glucose-6-phosphate dehydrogenase and sulfhydryl levels indicate reductive compensation to oxidative stress in Alzheimer disease," *Archives of Biochemistry and Biophysics*, vol. 370, no. 2, pp. 236–239, 1999.

[68] J. Kusmierz, J. J. DeGeorge, D. Sweeney, C. May, and S. I. Rapoport, "Quantitative analysis of polyols in human plasma and cerebrospinal fluid," *Journal of Chromatography: Biomedical Applications*, vol. 497, pp. 39–48, 1989.

[69] A. M. Palmer, "The activity of the pentose phosphate pathway is increased in response to oxidative stress in Alzheimer's disease," *Journal of Neural Transmission*, vol. 106, no. 3-4, pp. 317–328, 1999.

[70] W. Meier-Ruge and C. Bertoni-Freddari, "The significance of glucose turnover in the brain in the pathogenetic mechanisms of Alzheimer's disease," *Reviews in the Neurosciences*, vol. 7, no. 1, pp. 1–19, 1996.

[71] M. Bigl, J. Apelt, K. Eschrich, and R. Schliebs, "Cortical glucose metabolism is altered in aged transgenic Tg2576 mice that demonstrate Alzheimer plaque pathology," *Journal of Neural Transmission*, vol. 110, no. 1, pp. 77–94, 2003.

[72] F. Mastrogiacomo, C. Bergeron, and S. J. Kish, "Brain α-ketoglutarate dehydrogenase complex activity in Alzheimer's disease," *Journal of Neurochemistry*, vol. 61, no. 6, pp. 2007–2014, 1993.

[73] G. E. Gibson, J. P. Blass, M. F. Beal, and V. Bunik, "The α-ketoglutarate-dehydrogenase complex: a mediator between mitochondria and oxidative stress in neurodegeneration," *Molecular Neurobiology*, vol. 31, no. 1–3, pp. 43–63, 2005.

[74] G. E. Gibson, H. Zhang, K. F.-R. Sheu et al., "α-ketoglutarate dehydrogenase in Alzheimer brains bearing the APP670/671 mutation," *Annals of Neurology*, vol. 44, no. 4, pp. 676–681, 1998.

[75] P. Bubber, V. Haroutunian, G. Fisch, J. P. Blass, and G. E. Gibson, "Mitochondrial abnormalities in Alzheimer brain: mechanistic implications," *Annals of Neurology*, vol. 57, no. 5, pp. 695–703, 2005.

[76] A. Wallin, C. G. Gottfries, I. Karlsson, and L. Svennerholm, "Decreased myelin lipids in Alzheimer's disease and vascular dementia," *Acta Neurologica Scandinavica*, vol. 80, no. 4, pp. 319–323, 1989.

[77] C.-G. Gottfries, I. Karlsson, and L. Svennerholm, "Membrane components separate early-onset Alzheimer's disease from senile dementia of the Alzheimer type," *International Psychogeriatrics*, vol. 8, no. 3, pp. 365–372, 1996.

[78] A. Fernández, L. Llacuna, J. C. Fernández-Checa, and A. Colell, "Mitochondrial cholesterol loading exacerbates amyloid β peptide-induced inflammation and neurotoxicity," *Journal of Neuroscience*, vol. 29, no. 20, pp. 6394–6405, 2009.

[79] M. R. Prasad, M. A. Lovell, M. Yatin, H. Dhillon, and W. R. Markesbery, "Regional membrane phospholipid alterations in Alzheimer's disease," *Neurochemical Research*, vol. 23, no. 1, pp. 81–88, 1998.

[80] S. Patil and C. Chan, "Palmitic and stearic fatty acids induce Alzheimer-like hyperphosphorylation of tau in primary rat cortical neurons," *Neuroscience Letters*, vol. 384, no. 3, pp. 288–293, 2005.

[81] H. Braak and E. Braak, "Neuropathological stageing of Alzheimer-related changes," *Acta Neuropathologica*, vol. 82, no. 4, pp. 239–259, 1991.

[82] P. I. Moreira, L. M. Sayre, X. Zhu, A. Nunomura, M. A. Smith, and G. Perry, "Detection and localization of markers of oxidative stress by in situ methods: application in the study of Alzheimer disease," *Methods in Molecular Biology*, vol. 610, pp. 419–434, 2010.

[83] M. C. Irizarry, Y. Yao, B. T. Hyman, J. H. Growdon, and D. Praticò, "Plasma F2A isoprostane levels in Alzheimer's and Parkinson's disease," *Neurodegenerative Diseases*, vol. 4, no. 6, pp. 403–405, 2007.

[84] D. A. Butterfield, T. T. Reed, M. Perluigi et al., "Elevated levels of 3-nitrotyrosine in brain from subjects with amnestic mild cognitive impairment: implications for the role of nitration in the progression of Alzheimer's disease," *Brain Research*, vol. 1148, no. 1, pp. 243–248, 2007.